To the Graduate Council:

I am submitting herewith a thesis written by Stephen C. Kelley entitled "Stress Rupture Behavior of PWHT 2-1/4Cr-1Mo Weld Metal." I have examined the final copy of this thesis for form and content and recommend that it be accepted in partial fulfillment of the requirements for the degree of Master of Science, with a major in Metallurgical Engineering.

Carl D. Lundin, Major Professor

We have read this thesis
and recommend its acceptance:

Charlie R. Brooks

E. E. Hanstorp

Accepted for the Council:

Vice Provost
and Dean of the Graduate School

2

STATEMENT OF PERMISSION TO USE

In presenting this thesis in partial fulfillment of the requirements for a Master's degree at the University of Tennessee, Knoxville, I agree that the Library shall make it available to borrowers under rules of the Library. Brief quotations from this thesis are allowable without special permission, provided that accurate acknowledgment of the source is made.

Permission for extensive quotation from or reproduction of this thesis may be granted by my major professor, or in his absence, by the Head of Interlibray Services when, in the opinion of either, the proposed use of the material is for scholarly purposes. Any copying or use of the material in this thesis for financial gain shall not be allowed without my written permission.

Signature Stephen C Kelley

Date 11/1/85

STRESS RUPTURE BEHAVIOR OF PWHT 2-1/4CR-1MO WELD METAL

A Thesis

Presented for the

Master of Science

Degree

The University of Tennessee, Knoxville

Stephen C. Kelley

December 1985

DEDICATION

This thesis is dedicated to my wife, Susan. Without her support and sacrifice, its completion would not have been possible.

ACKNOWLEDGEMENTS

The author would like to thank the following people:

a. Dr. Carl Lundin for his sponsorship and guidance.

b. The Pressure Vessel Research Committee of the Welding Research Council for their monetary support of this research program.

c. Doctors Charlie Brooks and E. E. Stansbury for their efforts as thesis committee members.

d. Doctors Odette, Lucas, and Chung of U. C. Santa Barbara for their assistance in the performance of the STEM carbide studies.

e. Dr. Joseph Pepe of General Electric for his Manson MCM computer programs.

f. Mr. Blaine Roberts of Combustion Engineering for his advice in performing rupture data analysis.

g. Mr. Bob McGill for his guidance in the operation of the AMR 900 scanning electron microscope.

h. Mr. Mike Neal for his assistance in modifying and maintaining the creep laboratory.

The assistance of those listed above was considerable. Without their aid, the research herein described could not have been performed.

ABSTRACT

The goal of this program was to investigate the effect of carbon content and post-weld heat treatment (PWHT) on the stress rupture strength of 2-1/4Cr-1Mo weld metal. In order to establish the correlation between carbon level and rupture strength, rupture testing of weld metals with carbon contents in the range of 0.02 to 0.13 weight percent was conducted. For this phase of the study, the PWHT selected was 1300°F/25 hrs. Secondly, the effect of PWHT on rupture strength was evaluated by rupture testing 0.08-0.09 carbon weld metal PWHT 1175°F/25.5 hrs. and comparing the results to those obtained for the same material PWHT 1300°F/25 hrs.

To gain further insight into the relationship between the rupture strength of 2-1/4Cr-1Mo weld metal and both carbon content and PWHT, additional rupture data were collected from the literature with the restriction that only data from tests of 100 percent weld metal specimens in the PWHT condition be considered. The resulting data base, consisting of data from this program as well as from the literature, was partitioned by both temper parameter and carbon content and analyzed using three separate techniques.

The results of the analysis indicated that the 100,000 hour rupture strength of 2-1/4Cr-1Mo weld metal increases as the temper parameter which characterizes the PWHT decreases. This effect is particularly pronounced for weld metal PWHT with $P<32.0$ which, at 750°F, has a 100,000 hour rupture strength 40 to 45 KSI higher than that of weld metal PWHT with $32.0<P<36.2$. However this strength

advantage diminishes rapidly with increasing temperature and becomes insignificant at approximately 900°F.

The effect of carbon content on rupture strength depends on the PWHT given the material. For weld metal PWHT with P<37.5, the 100,000 hour rupture strength increases with carbon level over the entire range of carbon contents typical of 2-1/4Cr-1Mo steel. In contrast, the 100,000 hour rupture strength of weld metal given a more extensive PWHT (P>37.5) appears to increase with carbon content only for levels up to about 0.05 weight percent. Weld metals having higher carbon contents have similar rupture strengths. It should be noted, however, that the strengthening effect of carbon diminishes as the temperature increases.

In support of the rupture testing effort, extensive microstructural examination of the above weld metals in the as-welded, PWHT, and rupture tested condition was performed using the SEM and STEM. This microstructural work was aimed at characterizing the microstructure as a function of carbon content and PWHT with the ultimate goal of correlating the microstructure with the stress rupture properties. SEM examination of the weld metals revealed the dependence of microconstituent morphology on prior material history. Furthermore, to obtain information on the type, size, morphology, distribution, and composition of the alloy carbides present, STEM examination of carbide extraction replicas taken from weld metal specimens was also conducted.

Efforts to correlate the weld metal microstructure with observed rupture behavior were successful. Microstructural analysis indicated

that the superior rupture strength of the 0.08-0.09 carbon weld metal PWHT 1175°F/25.5 hrs. is primarily a consequence of the strengthening effect of the fine acicular M_2C carbides present within the matrix. In contrast, the rupture behavior of weld metal PWHT 1300°F/25 hrs. is determined primarily by the major constituents present in the microstructure. The 0.02-0.03 carbon weld metal has a fully ferritic structure and also has the lowest rupture strength. The higher carbon materials (0.04-0.05, 0.08-0.09, and 0.12-0.13 weight percent) have a tempered bainite structure and have similar rupture strengths despite the variations in carbon content.

Weld metal specimens were thermally cycled on the Gleeble using a variety of thermal cycles designed to simulate the thermal history occurring in the coarse-grained region of the weld metal HAZ during welding. Cooling conditions were chosen to span the normal range of weld energy inputs characteristic of welds in heavy-section Cr-Mo materials. A dilatometric technique was employed to detect the weld metal transformation during cycling and the data obtained used to construct CCT diagrams. SEM examination of the resulting microstructures was then performed to determine the microconstituents produced as a consequence of the thermal history.

Both the dilatometric studies and the microstructural analyses indicated that the as-transformed microstructure of the 0.08-0.09 and 0.12-0.13 carbon weld metals is fully bainitic except in the material thermally cycled 150 KJ/IN (2400°F peak temperature, 400°F preheat, 2 inch plate) which contain traces of polygonal ferrite. The bainite morphologies observed include lath-like, granular, and massive. The

lath bainite predominates at faster cooling rates and is gradually replaced by granular bainite as the cooling rate decreases. Some massive bainite is present at all cooling rates. Comparison of the as-transformed microstructures of the 0.08-0.09 and 0.12-0.13 carbon weld metals indicated that increasing the carbon content lowers the bainite start and finish temperatures and thus results in a finer bainitic structure.

TABLE OF CONTENTS

CHAPTER		PAGE
1.	INTRODUCTION	1
	History and Applications	1
	Properties	2
	Creep Strengthening Mechanisms in Low Alloy Ferritic Steels	5
	Availability	11
	Welding Processes	11
2.	LITERATURE REVIEW	18
	Microstructure - Base Metal and Weld Metal	18
	Microstructural Effects on Creep Strength	27
	Alloying Element Effects on Creep Strength	37
	Stress Rupture Data Analysis	69
	Summary	72
3.	MATERIALS AND EXPERIMENTAL PROCEDURE	77
	Materials	78
	Stress Rupture Testing	80
	Tensile Testing	88
	Metallographic Preparation	88
	Transformation Studies	90
4.	RESULTS AND DISCUSSION	94
	Stress Rupture Data Analysis	94
	Comparison of Data Analysis Techniques	198
	Tensile Testing	201
	Microstructural Analysis	207
5.	CONCLUSIONS	263
LIST OF REFERENCES		271
APPENDICES		281
APPENDIX A.	Comprehensive Data Analysis Presentations	282
APPENDIX B.	Stress Rupture Data	379
VITA		394

LIST OF TABLES

TABLE		PAGE
1.	Nominal composition of 2-1/4Cr-1Mo steel per ASTM A 387	3
2.	Comparison of the properties of 2-1/4Cr-1Mo plate, ASTM A 387 vs. ASTM A 542	12
3.	Chemical composition of base metals and weld metals employed in the study	79
4.	Welding procedure and parameters employed in fabrication of the 2-1/4Cr-1Mo SMA weldments	81
5.	Stress for 100,000 hour rupture as a function of test temperature and temper parameter determined by Larson-Miller analysis of 2-1/4Cr-1Mo weld metal literature data	108
6.	Stress for 100,000 hour rupture as a function of test temperature, carbon content, and temper parameter determined by Larson-Miller analysis of 2-1/4Cr-1Mo weld metal literature data considered independent of deposition process	109
7.	Stress for 100,000 hour rupture as a function of test temperature, carbon content, and temper parameter determined by Larson-Miller analysis of 2-1/4Cr-1Mo SMA weld metal literature data	110
8.	Stress for 100,000 hour rupture as a function of test temperature and PWHT determined by Larson-Miller analysis of UTK 2-1/4Cr-1Mo SMA weld metal data	117
9.	Stress for 100,000 hour rupture as a function of test temperature and carbon content for 2-1/4Cr-1Mo SMA weld metal PWHT 1300^{o}F/25 hrs. determined by Larson-Miller analysis of UTK data	118
10.	Stress for 100,000 hour rupture of 2-1/4Cr-1Mo SMA weld metal as a function of test temperature and temper parameter determined by Larson-Miller analysis of combined literature and UTK data	123

TABLE PAGE

11. Stress for 100,000 hour rupture of 2-1/4Cr-1Mo SMA weld metal as a function of test temperature, temper parameter, and carbon content determined by Larson-Miller analysis of combined literature and UTK data 124

12. Stress for 100,000 hour rupture as a function of test temperature and temper parameter determined by log stress/log rupture time analysis of 2-1/4Cr-1Mo SMA weld metal literature data 134

13. Stress for 100,000 hour rupture as a function of test temperature, carbon content, and temper parameter determined by log stress/log rupture time analysis of 2-1/4Cr-1Mo SMA weld metal literature data 136

14. Stress for 100,000 hour rupture as a function of test temperature and carbon content determined by log stress/log rupture time analysis of Cl. 2 UTK data 147

15. Stress for 100,000 hour rupture of 2-1/4Cr-1Mo SMA weld metal as a function of temperature and PWHT determined by log stress/log rupture time analysis of UTK data 148

16. Stress for 100,000 hour rupture of 2-1/4Cr-1Mo weld metal as a function of test temperature and temper parameter determined by log stress/log rupture time analysis of combined literature and UTK data 158

17. Stress for 100,000 hour rupture of 2-1/4Cr-1Mo SMA weld metal as a function of test temperature, carbon content, and temper parameter determined by log stress/log rupture time analysis of combined literature and UTK data 159

18. Stress for 100,000 hour rupture of 2-1/4Cr-1Mo SMA weld metal as a function of test temperature and temper parameter determined by Manson MCM analysis of literature data 166

19. Stress for 100,000 hour rupture of 2-1/4Cr-1Mo SMA weld metal as a function of test temperature, carbon content, and temper parameter determined by Manson MCM analysis of literature data 174

TABLE PAGE

20. Stress for 100,000 hour rupture of 2-1/4Cr-1Mo weld metal as a function of test temperature and PWHT determined by Manson MCM analysis of UTK data 179

21. Stress for 100,000 hour rupture of 2-1/4Cr-1Mo Class 2 SMA weld metal as a function of test temperature and carbon content determined by Manson MCM analysis of UTK data 184

22. Stress for 100,000 hour rupture of 2-1/4Cr-1Mo SMA weld metal as a function of test temperature and temper parameter determined by Manson MCM analysis of combined literature and UTK data 188

23. Stress for 100,000 hour rupture of 2-1/4Cr-1Mo SMA weld metal as a function of test temperature, carbon content, and temper parameter determined by Manson MCM analysis of combined literature and UTK data 195

24. Stress for 100,000 hour rupture of 2-1/4Cr-1Mo SMA weld metal as a function of test temperature and temper parameter determined by analysis of combined literature and UTK data 199

25. Tensile test results for 2-1/4Cr-1Mo weld metal PWHT 1300°F/25 hrs. 202

26. Comparison of stress allowables from ASME Boiler and Pressure Vessel Code and tensile test results for 2-1/4Cr-1Mo weld metal PWHT 1300°F/25 hrs. 203

27. Tensile test results for 0.08-0.09 carbon 2-1/4Cr-1Mo weld metal as a function of condition 205

28. The occurrence of various alloy carbides in 2-1/4Cr-1Mo weld metal as a function of carbon content and PWHT . . . 233

29. Time/temperature equivalence between rupture test condition and PWHT 252

LIST OF FIGURES

FIGURE		PAGE
1.	Illustration of the "sub-vert" welding process	16
2.	CCT diagram for 0.1 percent carbon 2-1/4Cr-1Mo steel	19
3.	Carbide evolutionary sequence for 2-1/4Cr-1Mo steel	22
4.	Diagrams showing carbides present in 2-1/4Cr-1Mo steel as a function of tempering time and temperature for quenched and normalized material	24
5.	The variation in the relative amounts of carbides present in 2-1/4Cr-1Mo steel at 700°C as a function of carbon content and tempering time	26
6.	Carbide sequence for 2-1/4Cr-1Mo steel having typical weld metal composition	28
7.	Correlation between creep rupture strength and room temperature tensile strength as a function of test temperature	31
8.	Stress-rupture time as a function of bainite content for 2-1/4Cr-1Mo steel tested at 565°C (1050°F) at a stress of 17.8 KSI	34
9.	Effect of chromium content on the room temperature tensile strength of Cr-Mo-V-Ti-B steel	39
10.	Effect of chromium content on the 1000 hour rupture strength of Cr-1Mo steel at 550°C	41
11.	Effect of molybdenum and chromium content on the creep strength of Cr-Mo steel at 1000°F	43
12.	Effect of molybdenum content on the room temperature properties of 3Cr-Mo-V-Ti-B steel	45
13.	Effect of molybdenum content on the rupture time (for a fixed stress) of 3Cr-Mo steel at 538°C	46
14.	Effect of changing levels of various alloying additions on the 1000 hour rupture strength of 3 Cr steel	47

FIGURE PAGE

15. Effect of molybdenum content on the rupture strength of 2-1/4Cr-1Mo-1/4V steel at 550°C 49

16. Effect of carbon content on the creep and rupture strength of 2-1/4Cr-1Mo steel 52

17. Effect of vanadium content on the room temperature yield and tensile strength of 3Cr-1Mo-V-Ti-B steel for three different tempering treatments 54

18. Minimum creep rate and rupture life as a function of applied stress for a titanium-free and a titanium-modified 0.09 percent carbon 2-1/4Cr-1Mo steel 57

19. The variation in minimum creep rate for titanium-modified 2-1/4Cr-1Mo steel in response to changes in the carbon content 58

20. Comparison of Larson-Miller parameter curves for a low silicon (0.08% Si) 2-1/4Cr-1Mo steel and steels of the same type having "typical" 2-1/4Cr silicon levels (0.42%, 0.43% Si) 63

21. Comparison of creep curves for normalized and tempered 2-1/4Cr-1Mo steel with and without a tin addition (0.1% vs. 0.002% Sn) 65

22. Comparison of creep curves for 2-1/4Cr-1Mo with and without a phosphorus addition (0.05% vs. 0.005% P) 66

23. Stress-rupture test specimen 82

24. Schematic of creep frame with specimen in place 84

25. Gleeble thermal cycles employed in transformation determinations 93

26. Stress rupture behavior of 2-1/4Cr-1Mo weld metal as a function of temper parameter determined by analysis of literature data for weld metal deposited by a variety of welding processes 100

27. Stress rupture behavior of 2-1/4Cr-1Mo SMA weld metal as a function of temper parameter determined by analysis of literature data 101

FIGURE PAGE

28. Stress rupture behavior of PWHT 2-1/4Cr-1Mo weld metal (32.0<P<36.2) as a function of carbon content determined by analysis of literature data for weld metal deposited by a variety of welding processes 102

29. Stress rupture behavior of PWHT 2-1/4Cr-1Mo SMA weld metal (32.0<P<36.2) as a function of carbon content determined by analysis of literature data 103

30. Stress rupture behavior of PWHT 2-1/4Cr-1Mo weld metal (36.2<P<37.5) as a function of carbon content determined by analysis of literature data for weld metal deposited by a variety of welding processes 104

31. Stress rupture behavior of PWHT 2-1/4Cr-1Mo SMA weld metal (36.2<P<37.5) as a function of carbon content determined by analysis of literature data 105

32. Stress rupture behavior of PWHT 2-1/4Cr-1Mo weld metal (P>37.5) as a function of carbon content determined by analysis of literature data for weld metal deposited by a variety of welding processes 106

33. Stress rupture behavior of PWHT 2-1/4Cr-1Mo SMA weld metal (P>37.5) as a function of carbon content determined by analysis of literature data 107

34. Stress rupture behavior of 2-1/4Cr-1Mo SMA weld metal as a function of temper parameter determined by analysis of UTK data 114

35. Stress rupture behavior of 2-1/4Cr-1Mo SMA weld metal PWHT 1300°F/25 hrs. as a function of carbon content determined by analysis of UTK data 115

36. Stress rupture behavior of 0.02-0.03 and 0.04-0.13 carbon 2-1/4Cr-1Mo SMA weld metal PWHT 1300°F/25 hrs. as a function of carbon content determined by analysis of UTK data 116

37. Stress rupture behavior of 2-1/4Cr-1Mo SMA weld metal as a function of temper parameter determined by analysis of combined literature and UTK data 120

38. Stress rupture behavior of PWHT 2-1/4Cr-1Mo SMA weld metal (32.0<P<36.2) as a function of carbon content determined by analysis of combined literature and UTK data 121

FIGURE PAGE

39. Stress rupture behavior of PWHT 2-1/4Cr-1Mo SMA weld metal (P>37.5) as a function of carbon content determined by analysis of combined literature and UTK data 122

40. Stress rupture behavior of PWHT 2-1/4Cr-1Mo SMA weld metal (P<32.0) as a function of test temperature determined by analysis of literature data 128

41. Stress rupture behavior of PWHT 2-1/4Cr-1Mo SMA weld metal (32.0<P<36.2) as a function of test temperature determined by analysis of literature data 129

42. Stress rupture behavior of PWHT 2-1/4Cr-1Mo SMA weld metal (36.2<P<37.5) as a function of test temperature determined by analysis of literature data 130

43. Stress rupture behavior of PWHT 2-1/4Cr-1Mo SMA weld metal (P>37.5) as a function of test temperature determined by analysis of literature data 131

44. Stress rupture behavior of PWHT 2-1/4Cr-1Mo weld metal (32.0<P<36.2) at 1068^{o}F as a function of carbon content determined by analysis of literature data 132

45. Stress rupture behavior of PWHT 2-1/4Cr-1Mo weld metal (32.0<P<36.2) at 1100^{o}F as a function of carbon content determined by analysis of literature data 133

46. Stress rupture behavior of 2-1/4Cr-1Mo SMA weld metal (PWHT 1300^{o}F/25 hrs.) at 850^{o}F as a function of carbon content determined by analysis of UTK data . . 137

47. Stress rupture behavior of 2-1/4Cr-1Mo SMA weld metal (PWHT 1300^{o}F/25 hrs.) at 950^{o}F as a function of carbon content determined by analysis of UTK data . . 138

48. Stress rupture behavior of 2-1/4Cr-1Mo SMA weld metal (PWHT 1300^{o}F/25 hrs.) at 1050^{o}F as a function of carbon content determined by analysis of UTK data . . 139

FIGURE PAGE

49. Stress rupture behavior of 0.02-0.03 and 0.04-0.13 carbon 2-1/4Cr-1Mo SMA weld metal (PWHT 1300°F/25 hrs.) at 850°F as a function of carbon content determined by analysis of UTK data 140

50. Stress rupture behavior of 0.02-0.03 and 0.04-0.13 carbon 2-1/4Cr-1Mo SMA weld metal (PWHT 1300°F/25 hrs.) at 950°F as a function of carbon content determined by analysis of UTK data 141

51. Stress rupture behavior of 0.02-0.03 and 0.04-0.13 carbon 2-1/4Cr-1Mo SMA weld metal (PWHT 1300°F/25 hrs.) at 1050°F as a function of carbon content determined by analysis of UTK data 142

52. Stress rupture behavior of 2-1/4Cr-1Mo SMA weld metal at 950°F as a function of PWHT determined by analysis of UTK data 143

53. Stress rupture behavior of 2-1/4Cr-1Mo SMA weld metal at 1050°F as a function of PWHT determined by analysis of UTK data 144

54. Stress rupture behavior of 0.08-0.09 carbon 2-1/4Cr-1Mo SMA weld metal at 950°F as a function of PWHT determined by analysis of UTK data 145

55. Stress rupture behavior of 0.08-0.09 carbon 2-1/4Cr-1Mo SMA weld metal at 1050°F as a function of PWHT determined by analysis of UTK data 146

56. Stress rupture behavior of PWHT 2-1/4Cr-1Mo SMA weld metal ($32.0<P<36.2$) as a function of test temperature determined by analysis of combined literature and UTK data 150

57. Stress rupture behavior of PWHT 2-1/4Cr-1Mo SMA weld metal ($P>37.5$) as a function of test temperature determined by analysis of combined literature and UTK data 151

58. Stress rupture behavior of PWHT 2-1/4Cr-1Mo SMA weld metal ($32.0<P<36.2$) at 950°F as a function of carbon content determined by analysis of combined literature and UTK data 152

FIGURE PAGE

59. Stress rupture behavior of PWHT 2-1/4Cr-1Mo SMA weld metal (32.0<P<36.2) at 1050°F as a function of carbon content determined by analysis of combined literature and UTK data 153

60. Stress rupture behavior of PWHT 2-1/4Cr-1Mo SMA weld metal (P>37.5) at 850°F as a function of carbon content determined by analysis of combined literature and UTK data 154

61. Stress rupture behavior of PWHT 2-1/4Cr-1Mo SMA weld metal (P>37.5) at 950°F as a function of carbon content determined by analysis of combined literature and UTK data 155

62. Stress rupture behavior of PWHT 2-1/4Cr-1Mo SMA weld metal (P>37.5) at 1050°F as a function of carbon content determined by analysis of combined literature and UTK data 156

63. Stress rupture behavior of PWHT 2-1/4Cr-1Mo SMA weld metal (P<32.0) as a function of test temperature determined by Manson MCM analysis of literature data 161

64. Stress rupture behavior of PWHT 2-1/4Cr-1Mo SMA weld metal (32.0<P<36.2) as a function of test temperature determined by Manson MCM analysis of literature data 162

65. Stress rupture behavior of PWHT 2-1/4Cr-1Mo SMA weld metal (36.2<P<37.5) as a function of test temperature determined by Manson MCM analysis of literature data 163

66. Stress rupture behavior of PWHT 2-1/4Cr-1Mo SMA weld metal (P>37.5) as a function of test temperature determined by Manson MCM analysis of literature data 164

67. Stress rupture behavior of PWHT 2-1/4Cr-1Mo SMA weld metal (32.0<P<36.2) with carbon content in the range of 0.04<C<0.08 determined by analysis of literature data 168

68. Stress rupture behavior of PWHT 2-1/4Cr-1Mo SMA weld metal (32.0<P<36.2) with carbon content in the range of 0.08<C<0.12 determined by analysis of literature data 169

FIGURE PAGE

69. Stress rupture behavior of PWHT 2-1/4Cr-1Mo SMA weld metal (32.0<P<36.2) with carbon content in the range of C>0.12 determined by analysis of literature data 170

70. Stress rupture behavior of PWHT 2-1/4Cr-1Mo SMA weld metal (36.2<P<37.5) with carbon content in the range of 0.04<C<0.08 determined by analysis of literature data 171

71. Stress rupture behavior of PWHT 2-1/4Cr-1Mo SMA weld metal (36.2<P<37.5) with carbon content in the range of 0.08<C<0.12 determined by analysis of literature data 172

72. Stress rupture behavior of 0.08-0.09 carbon 2-1/4Cr-1Mo Class 3 SMA weld metal as a function of test temperature determined by analysis of UTK data 175

73. Stress rupture behavior of 2-1/4Cr-1Mo Class 2 SMA weld metal as a function of test temperature determined by analysis of UTK data 176

74. Stress rupture behavior of all 2-1/4Cr-1Mo Class 2 SMA weld metal except the 0.02-0.03 carbon material as a function of test temperature determined by analysis of UTK data 177

75. Stress rupture behavior of 0.02-0.03 carbon 2-1/4Cr-1Mo Class 2 SMA weld metal as a function of test temperature determined by analysis of UTK data 180

76. Stress rupture behavior of 0.04-0.05 carbon 2-1/4Cr-1Mo Class 2 SMA weld metal as a function of test temperature determined by analysis of UTK data 181

77. Stress rupture behavior of 0.08-0.09 carbon 2-1/4Cr-1Mo Class 2 SMA weld metal as a function of test temperature determined by analysis of UTK data 182

78. Stress rupture behavior of 0.12-0.13 carbon 2-1/4Cr-1Mo Class 2 SMA weld metal as a function of test temperature determined by analysis of UTK data 183

FIGURE PAGE

79. Stress rupture behavior of PWHT 2-1/4Cr-1Mo SMA weld metal (32.0<P<36.2) as a function of test temperature determined by Manson MCM analysis of combined literature and UTK data 186

80. Stress rupture behavior of PWHT 2-1/4Cr-1Mo SMA weld metal (P>37.5) as a function of test temperature determined by Manson MCM analysis of combined literature and UTK data 187

81. Stress rupture behavior of PWHT 2-1/4Cr-1Mo SMA weld metal (32.0<P<36.2) with carbon content in the range of 0.08<C<0.12 determined by analysis of combined literature and UTK data 190

82. Stress rupture behavior of PWHT 2-1/4Cr-1Mo SMA weld metal (P>37.5) with carbon content in the range of 0.02<C<0.04 determined by analysis of combined literature and UTK data 191

83. Stress rupture behavior of PWHT 2-1/4Cr-1Mo SMA weld metal (P>37.5) with carbon content in the range of 0.04<C<0.08 determined by analysis of combined literature and UTK data 192

84. Stress rupture behavior of PWHT 2-1/4Cr-1Mo SMA weld metal (P>37.5) with carbon content in the range of 0.08<C<0.12 determined by analysis of combined literature and UTK data 193

85. Stress rupture behavior of PWHT 2-1/4Cr-1Mo SMA weld metal (P>37.5) with carbon content in the range of C>0.12 determined by analysis of combined literature and UTK data 194

86. Continuous cooling transformation diagram for 0.08-0.09 carbon 2-1/4Cr-1Mo weld metal 210

87. Continuous cooling transformation diagram for 0.12-0.13 carbon 2-1/4Cr-1Mo weld metal 211

88. Lath bainite in 0.08-0.09 carbon 2-1/4Cr-1Mo weld metal thermally cycled 18 KJ/IN, 10000X, SEM 213

89. Granular bainite in 0.08-0.09 carbon 2-1/4Cr-1Mo weld metal thermally cycled 80 KJ/IN, 10000X, SEM 217

90. Massive bainite in 0.08-0.09 carbon 2-1/4Cr-1Mo weld metal thermally cycled 60 KJ/IN, 10000x, SEM 219

FIGURE PAGE

91. Three zones in the intermediate transformation range defined in terms of temperature and cooling time between 800 and 500°C 221

92. Polygonal ferrite at the prior austenite grain boundaries of a granular bainite matrix 222

93. Upper bainite matrix containing a second constituent, possibly lower bainite or auto-tempered martensite 224

94. Comparison of 0.08-0.09 and 0.12-0.13 carbon 2-1/4Cr-1Mo weld metal thermally cycled 60 KJ/IN, 10000X, SEM 226

95. Comparison of the as-welded microstructure of 0.04-0.05, 0.08-0.09, and 0.12-0.13 carbon 2-1/4Cr-1Mo weld metal, 2000X, SEM 228

96. Comparison of the as-welded microstructure of 0.04-0.05, 0.08-0.09, and 0.12-0.13 carbon weld metal, 10000X, SEM 229

97. Polygonal ferrite in lath bainite matrix of as-welded 0.02-0.03 carbon 2-1/4Cr-1Mo weld metal, 2000X, SEM 230

98. Carbide morphology and distribution of as-welded 0.04-0.05, 0.08-0.09, and 0.12-0.13 carbon 2-1/4Cr-1Mo weld metal as shown by carbide extraction replica, 9000X, STEM 232

99. Variation in microstructure of 0.02-0.03 carbon 2-1/4Cr-1Mo weld metal PWHT 1300°F/25 hrs. (Class 2) as a function of location, 2000X, SEM 236

100. Region of 0.02-0.03 carbon 2-1/4Cr-1Mo weld metal PWHT 1300°F/25 hrs. (Class 2) showing grain boundary curvature indicative of grain boundary migration, 10000X, SEM 238

101. Tempered bainite structure of 0.08-0.09 carbon 2-1/4Cr-1Mo weld metal PWHT 1300°F/25 hrs. (Class 2) 239

102. Carbide morphologies in 0.02-0.03 carbon 2-1/4Cr-1Mo weld metal PWHT 1300°F/25 hrs. as shown by carbide extraction replica, 3700X, STEM 243

FIGURE PAGE

103. Similar morphologies of M_7C_3, $M_{23}C_6$, and M_6C carbides in 0.04-0.05 carbon 2-1/4Cr-1Mo weld metal PWHT 1300°F/25 hrs. (Class 2) as shown by carbide extraction replica, 10000X, STEM 245

104. Carbide morphology and distribution in 0.04-0.05, 0.08-0.09, and 0.12-0.13 carbon 2-1/4Cr-1Mo weld metal PWHT 1300°F/25 hrs. (Class 2) as shown by carbide extraction replica, 9000X, SEM 247

105. Microstructure of 0.08-0.09 carbon 2-1/4Cr-1Mo weld metal PWHT 1175°F/25.5 hrs.(Class 3) 248

106. Carbide morphology and distribution in 0.08-0.09 carbon 2-1/4Cr-1Mo weld metal PWHT 1175°F/25.5 hrs. (Class 3) as shown by carbide extraction replica, 10000X, SEM 249

107. Comparison of 0.12-0.13 carbon 2-1/4Cr-1Mo weld metal PWHT 1300°F/25 hrs. (Class 2) before and after rupture testing, 10000X, SEM 251

108. Microstructure Of 0.08-0.09 carbon 2-1/4Cr-1Mo weld metal PWHT 1175°F/25.5 hrs. (Class 3) after rupture testing at 1050°F for 3100 hours, 10000X, SEM 254

109. Microstructure of 0.08-0.09 carbon 2-1/4Cr-1Mo weld metal PWHT 1175°F/25.5 hrs. after aging 1193°F/21.5 hrs. to simulate 100,000 hours at 950°F . . . 257

110. Microstructure of 2-1/4Cr-1Mo pipe weld metal subjected to 1050°F for 15 hears 259

A1. Larson-Miller parameter analysis of PWHT 2-1/4Cr-1Mo weld metal (P<32.0) determined from literature data for weld metal deposited by a variety of welding processes 283

A2. Larson-Miller parameter analysis of PWHT 2-1/4Cr-1Mo weld metal (32.0<P<36.2) determined from literature data for weld metal deposited by a variety of welding processes 284

A3. Larson-Miller parameter analysis of PWHT 2-1/4Cr-1Mo weld metal (36.2<P<37.5) determined from literature data for weld metal deposited by a variety of welding processes 285

FIGURE PAGE

A4. Larson-Miller parameter analysis of PWHT 2-1/4Cr-1Mo weld metal (P>37.5) determined from literature data for weld metal deposited by a variety of welding processes 286

A5. Larson-Miller parameter analysis of PWHT 2-1/4Cr-1Mo weld metal (P<32.0) determined from literature data for SMA weld metal 287

A6. Larson-Miller parameter analysis of PWHT 2-1/4Cr-1Mo SMA weld metal (32.0<P<36.2) determined from literature data 288

A7. Larson-Miller parameter analysis of PWHT 2-1/4Cr-1Mo SMA weld metal (36.2<P<37.5) determined from literature data 289

A8. Larson-Miller parameter analysis of PWHT 2-1/4Cr-1Mo SMA weld metal (P>37.5) determined from literature data 290

A9. Larson-Miller parameter analysis of PWHT 2-1/4Cr-1Mo weld metal (32.0<P<36.2, C<0.02) determined from literature data for weld metal deposited by a variety of welding processes 291

A10. Larson-Miller parameter analysis of PWHT 2-1/4Cr-1Mo weld metal (32.0<P<36.2, 0.02<C<0.04) determined from literature data for weld metal deposited by a variety of welding processes 292

A11. Larson-Miller parameter analysis of PWHT 2-1/4Cr-1Mo weld metal (32.0<P<36.2, 0.04<C<0.08) determined from literature data for weld metal deposited by a variety of welding processes 293

A12. Larson-Miller parameter analysis of PWHT 2-1/4Cr-1Mo weld metal (32.0<P<36.2, 0.08<C<0.12) determined from literature data for weld metal deposited by a variety of welding processes 294

A13. Larson-Miller parameter analysis of PWHT 2-1/4Cr-1Mo weld metal (32.0<P<36.2, C>0.12) determined from literature data for weld metal deposited by a variety of welding processes 295

A14. Larson-Miller parameter analysis of PWHT 2-1/4Cr-1Mo SMA weld metal (32.0<P<36.2, 0.02<C<0.04) determined from literature data 296

FIGURE PAGE

A15. Larson-Miller parameter analysis of PWHT 2-1/4Cr-1Mo SMA weld metal (32.0<P<36.2, 0.04<C<0.08) determined from literature data 297

A16. Larson-Miller parameter analysis of PWHT 2-1/4Cr-1Mo SMA weld metal (32.0<P<36.2, 0.08<C<0.12) determined from literature data 298

A17. Larson-Miller parameter analysis of PWHT 2-1/4Cr-1Mo SMA weld metal (32.0<P<36.2, C>0.12) determined from literature data 299

A18. Larson-Miller parameter analysis of PWHT 2-1/4Cr-1Mo weld metal (36.2<P<37.5, 0.02<C<0.04) determined from literature data for weld metal deposited by a variety of welding processes 300

A19. Larson-Miller parameter analysis of PWHT 2-1/4Cr-1Mo weld metal (36.2<P<37.5, 0.04<C<0.08) determined from literature data for weld metal deposited by a variety of welding processes 301

A20. Larson-Miller parameter analysis of PWHT 2-1/4Cr-1Mo weld metal (36.2<P<37.5, 0.08<C<0.12) determined from literature data for weld metal deposited by a variety of welding processes 302

A21. Larson-Miller parameter analysis of PWHT 2-1/4Cr-1Mo SMA weld metal (36.2<P<37.5, 0.04<C<0.08) determined from literature data 303

A22. Larson-Miller parameter analysis of PWHT 2-1/4Cr-1Mo SMA weld metal (36.2<P<37.5, 0.08<C<0.12) determined from literature data 304

A23. Larson-Miller parameter analysis of PWHT 2-1/4Cr-1Mo weld metal (P>37.5, 0.02<C<0.04) determined from literature data for weld metal deposited by a variety of welding processes 305

A24. Larson-Miller parameter analysis of PWHT 2-1/4Cr-1Mo weld metal (P>37.5, 0.04<C<0.08) determined from literature data for weld metal deposited by a variety of welding processes 306

A25. Larson-Miller parameter analysis of PWHT 2-1/4Cr-1Mo weld metal (P>37.5, 0.08<C<0.12) determined from literature data for weld metal deposited by a variety of welding processes 307

FIGURE PAGE

A26. Larson-Miller parameter analysis of PWHT 2-1/4Cr-1Mo SMA weld metal (P>37.5, 0.02<C<0.04) determined from literature data 308

A27. Larson-Miller parameter analysis of PWHT 2-1/4Cr-1Mo SMA weld metal (P>37.5, 0.04<C<0.08) determined from literature data 309

A28. Larson-Miller parameter analysis of 2-1/4Cr-1Mo SMA weld metal PWHT 1300°F/25 hrs. (Class 2) determined from UTK data 310

A29. Larson-Miller parameter analysis of 2-1/4Cr-1Mo SMA weld metal PWHT 1175°F/25.5 hrs. (Class 3) determined from UTK data 311

A30. Larson-Miller parameter analysis of 2-1/4Cr-1Mo SMA weld metal PWHT 1300°F/25 hrs. (Class 2, 0.02-0.03C) determined from UTK data 312

A31. Larson-Miller parameter analysis of 2-1/4Cr-1Mo SMA weld metal PWHT 1300°F/25 hrs. (Class 2, 0.04-0.05C) determined from UTK data 313

A32. Larson-Miller parameter analysis of 2-1/4Cr-1Mo SMA weld metal PWHT 1300°F/25 hrs. (Class 2, 0.08-0.09C) determined from UTK data 314

A33. Larson-Miller parameter analysis of 2-1/4Cr-1Mo SMA weld metal PWHT 1300°F/25 hrs. (Class 2, 0.12-0.13C) determined from UTK data 315

A34. Larson-Miller parameter analysis of 2-1/4Cr-1Mo SMA weld metal PWHT 1300°F/25 hrs. (Class 2, 0.04-0.13C) determined from UTK data 316

A35. Larson-Miller parameter analysis of PWHT 2-1/4Cr-1Mo SMA weld metal (32.0<P<36.2) determined from combined literature and UTK data 317

A36. Larson-Miller parameter analysis of PWHT 2-1/4Cr-1Mo SMA weld metal (P>37.5) determined from combined literature and UTK data 318

A37. Larson-Miller parameter analysis of PWHT 2-1/4Cr-1Mo SMA weld metal (32.0<P<36.2, 0.08<C<0.12) determined from combined literature and UTK data 319

FIGURE PAGE

A38. Larson-Miller parameter analysis of PWHT 2-1/4Cr-1Mo SMA weld metal (P>37.5, 0.02<C<0.04) determined from combined literature and UTK data 320

A39. Larson-Miller parameter analysis of PWHT 2-1/4Cr-1Mo SMA weld metal (P>37.5, 0.04<C<0.08) determined from combined literature and UTK data 321

A40. Log stress/log rupture time analysis of PWHT 2-1/4Cr-1Mo SMA weld metal (32.0<P<36.2) at 750, 850, 950, 1050, and 1100°F as determined from literature data 322

A41. Log stress/log rupture time analysis of PWHT 2-1/4Cr-1Mo SMA weld metal (32.0<P<36.2) at 1022, 1067, and 1112°F as determined from literature data . . . 323

A42. Log stress/log rupture time analysis of PWHT 2-1/4Cr-1Mo SMA weld metal (32.0<P<36.2) at 1058°F as determined from literature data 324

A43. Log stress/log rupture time analysis of PWHT 2-1/4Cr-1Mo SMA weld metal (36.2<P<37.5) at 900, 1050, 1100, and 1200°F as determined from literature data 325

A44. Log stress/log rupture time analysis of PWHT 2-1/4Cr-1Mo SMA weld metal (36.2<P<37.5) at 1000°F as determined from literature data 326

A45. Log stress/log rupture time analysis of PWHT 2-1/4Cr-1Mo SMA weld metal (36.2<P<37.5) at 1022°F as determined from literature data 327

A46. Log stress/log rupture time analysis of 2-1/4Cr-1Mo SMA weld metal PWHT 1300°F/25 hrs. (Class 2, 0.02-0.03C) at 850, 950, and 1050°F as determined from UTK data 328

A47. Log stress/log rupture time analysis of 2-1/4Cr-1Mo SMA weld metal PWHT 1300°F/25 hrs. (Class 2, 0.04-0.05C) at 850, 950, and 1050°F as determined from UTK data 329

A48. Log stress/log rupture time analysis of 2-1/4Cr-1Mo SMA weld metal PWHT 1300°F/25 hrs. (Class 2, 0.08-0.09C) at 850, 950, and 1050°F as determined from UTK data 330

FIGURE PAGE

A49. Log stress/log rupture time analysis of 2-1/4Cr-1Mo SMA weld metal PWHT 1300°F/25 hrs. (Class 2, 0.12-0.13C) at 850, 950, and 1050°F as determined from UTK data 331

A50. Log stress/log rupture time analysis of 2-1/4Cr-1Mo SMA weld metal PWHT 1300°F/25 hrs. (Class 2, 0.04-0.13C) at 850, 950, and 1050°F as determined from UTK data 332

A51. Log stress/log rupture time analysis of 2-1/4Cr-1Mo SMA weld metal PWHT 1300°F/25 hrs. (Class 2, 0.02-0.13C) at 850, 950, and 1050°F as determined from UTK data 333

A52. Log stress/log rupture time analysis of 2-1/4Cr-1Mo SMA weld metal PWHT 1175°F/25.5 hrs. (Class 3, 0.08-0.09C) at 950, and 1050°F as determined from UTK data 334

A53. Log stress/log rupture time analysis of PWHT 2-1/4Cr-1Mo SMA weld metal (32.0<P<36.2) at 950 and 1050°F as determined from combined literature and UTK data 335

A54. Log stress/log rupture time analysis of PWHT 2-1/4Cr-1Mo SMA weld metal (P>37.5) at 850 and 1050°F as determined from combined literature and UTK data 336

A55. Log stress/log rupture time analysis of PWHT 2-1/4Cr-1Mo SMA weld metal (P>37.5) at 950°F as determined from combined literature and UTK data 337

A56. Log stress/log rupture time analysis of PWHT 2-1/4Cr-1Mo SMA weld metal (P>37.5) at 1022 and 1100°F as determined from combined literature and UTK data 338

A57. Log stress/log rupture time analysis of PWHT 2-1/4Cr-1Mo SMA weld metal (P>37.5, 850°F) with carbon contents of 0.04-0.08 and C>0.12 as determined from combined literature and UTK data 339

A58. Log stress/log rupture time analysis of PWHT 2-1/4Cr-1Mo SMA weld metal (P>37.5, 950°F) with carbon contents of 0.02-0.04 and 0.08-0.12 as determined from combined literature and UTK data 340

FIGURE PAGE

A59. Manson MCM analysis of PWHT 2-1/4Cr-1Mo SMA weld metal (P<32.0) at 850 and 900°F as determined from literature data 341

A60. Manson MCM analysis of PWHT 2-1/4Cr-1Mo SMA weld metal (32.0<P<36.2) at 750, 950, 1050, and 1100°F as determined from literature data 342

A61. Manson MCM analysis of PWHT 2-1/4Cr-1Mo SMA weld metal (32.0<P<36.2) at 850, 1000, 1058, and 1112°F as determined from literature data 343

A62. Manson MCM analysis of PWHT 2-1/4Cr-1Mo SMA weld metal (32.0<P<36.2) at 1022 and 1167°F as determined from literature data 344

A63. Manson MCM analysis of PWHT 2-1/4Cr-1Mo SMA weld metal (36.2<P<37.5) at 900, 1022 and 1100°F as determined from literature data 345

A64. Manson MCM analysis of PWHT 2-1/4Cr-1Mo SMA weld metal (36.2<P<37.5) at 1000, 1050 and 1200°F as determined from literature data 346

A65. Manson MCM analysis of PWHT 2-1/4Cr-1Mo SMA weld metal (P>37.5) at 1022 and 1100°F as determined from literature data 347

A66. Manson MCM analysis of PWHT 2-1/4Cr-1Mo SMA weld metal (32.0<P<36.2, 0.04<C<0.08) at 1000 and 1100°F as determined from literature data 348

A67. Manson MCM analysis of PWHT 2-1/4Cr-1Mo SMA weld metal (32.0<P<36.2, 0.04<C<0.08) at 1022 and 1112°F as determined from literature data 349

A68. Manson MCM analysis of PWHT 2-1/4Cr-1Mo SMA weld metal (32.0<P<36.2, 0.04<C<0.08) at 1050°F as determined from literature data 350

A69. Manson MCM analysis of PWHT 2-1/4Cr-1Mo SMA weld metal (32.0<P<36.2, 0.04<C<0.08) at 1058°F as determined from literature data 351

A70. Manson MCM analysis of PWHT 2-1/4Cr-1Mo SMA weld metal (32.0<P<36.2, 0.04<C<0.08) at 1067°F as determined from literature data 352

FIGURE PAGE

A71. Manson MCM analysis of PWHT 2-1/4Cr-1Mo SMA weld metal (32.0<P<36.2, 0.08<C<0.12) at 1067 and 1100°F as determined from literature data 353

A72. Manson MCM analysis of PWHT 2-1/4Cr-1Mo SMA weld metal (32.0<P<36.2, C>0.12) at 750, 850, and 950°F as determined from literature data 354

A73. Manson MCM analysis of PWHT 2-1/4Cr-1Mo SMA weld metal (36.2<P<37.5, 0.04<C<0.08) at 900, 1022, and 1100°F as determined from literature data 355

A74. Manson MCM analysis of PWHT 2-1/4Cr-1Mo SMA weld metal (36.2<P<37.5, 0.04<C<0.08) at 1000 and 1050°F as determined from literature data 356

A75. Manson MCM analysis of PWHT 2-1/4Cr-1Mo SMA weld metal (36.2<P<37.5, 0.08<C<0.12) at 1000 and 1100°F as determined from literature data 357

A76. Manson MCM analysis of PWHT 2-1/4Cr-1Mo SMA weld metal (36.2<P<37.5, 0.08<C<0.12) at 1050 and 1200°F as determined from literature data 358

A77. Manson MCM analysis of 2-1/4Cr-1Mo SMA weld metal PWHT 1175°F/25.5 hrs. (Class 3, 0.08-0.09C) at 950 and 1050°F as determined from UTK data 359

A78. Manson MCM analysis of 2-1/4Cr-1Mo SMA weld metal PWHT 1300°F/25 hrs. (Class 2, 0.02-0.13C) at 850, 950, and 1050°F as determined from UTK data 360

A79. Manson MCM analysis of 2-1/4Cr-1Mo SMA weld metal PWHT 1300°F/25 hrs. (Class 2, 0.04-0.13C) at 850, 950, and 1050°F as determined from UTK data 361

A80. Manson MCM analysis of 2-1/4Cr-1Mo SMA weld metal PWHT 1300°F/25 hrs. (Class 2, 0.02-0.03C) at 850, 950, and 1050°F as determined from UTK data 362

A81. Manson MCM analysis of 2-1/4Cr-1Mo SMA weld metal PWHT 1300°F/25 hrs. (Class 2, 0.04-0.05C) at 850, 950, and 1050°F as determined from UTK data 363

A82. Manson MCM analysis of 2-1/4Cr-1Mo SMA weld metal PWHT 1300°F/25 hrs. (Class 2, 0.08-0.09C) at 850, 950, and 1050°F as determined from UTK data 364

FIGURE PAGE

A83. Manson MCM analysis of 2-1/4Cr-1Mo SMA weld metal PWHT 1300°F/25 hrs. (Class 2, 0.12-0.13C) at 850, 950, and 1050°F as determined from UTK data 365

A84. Manson MCM analysis of PWHT 2-1/4Cr-1Mo SMA weld metal (32.0<P<36.2) at 750, 950, 1050, and 1100°F as determined from combined literature and UTK data . . . 366

A85. Manson MCM analysis of PWHT 2-1/4Cr-1Mo SMA weld metal (32.0<P<36.2) at 850, 1000, 1058, and 1112°F as determined from combined literature and UTK data . . . 367

A86. Manson MCM analysis of PWHT 2-1/4Cr-1Mo SMA weld metal (32.0<P<36.2) at 1022 and 1067°F as determined from combined literature and UTK data 368

A87. Manson MCM analysis of PWHT 2-1/4Cr-1Mo SMA weld metal (P>37.5) at 850, 1022 and 1100°F as determined from combined literature and UTK data 369

A88. Manson MCM analysis of PWHT 2-1/4Cr-1Mo SMA weld metal (P>37.5) at 950 and 1050°F as determined from combined literature and UTK data 370

A89. Manson MCM analysis of PWHT 2-1/4Cr-1Mo SMA weld metal (P>37.5, 0.02<C<0.04) at 850 and 1050°F as determined from combined literature and UTK data 371

A90. Manson MCM analysis of PWHT 2-1/4Cr-1Mo SMA weld metal (P>37.5, 0.02<C<0.04) at 950 and 1100°F as determined from combined literature and UTK data 372

A91. Manson MCM analysis of PWHT 2-1/4Cr-1Mo SMA weld metal (P>37.5, 0.04<C<0.08) at 850 and 1022°F as determined from combined literature and UTK data 373

A92. Manson MCM analysis of PWHT 2-1/4Cr-1Mo SMA weld metal (P>37.5, 0.04<C<0.08) at 950 and 1050°F as determined from combined literature and UTK data 374

A93. Manson MCM analysis of PWHT 2-1/4Cr-1Mo SMA weld metal (P>37.5, 0.08<C<0.12) at 850, 950, and 1050°F as determined from combined literature and UTK data . . . 375

A94. Manson MCM analysis of PWHT 2-1/4Cr-1Mo SMA weld metal (P>37.5, 0.08<C<0.12) at 950 and 1067°F as determined from combined literature and UTK data 376

FIGURE PAGE

A95. Manson MCM analysis of PWHT 2-1/4Cr-1Mo SMA weld metal (P>37.5, 0.08<C<0.12) at 1050 and 1100°F as determined from combined literature and UTK data 377

A96. Manson MCM analysis of PWHT 2-1/4Cr-1Mo SMA weld metal (P>37.5, C>0.12) at 850, 950, and 1050°F as determined from combined literature and UTK data 378

B1. Example of stress rupture data format 380

B2. Literature stress rupture data 382

B3. UTK stress rupture data 391

CHAPTER 1

INTRODUCTION

1. HISTORY AND APPLICATIONS

Chromium-molybdenum steels have been used in the fabrication of pressure vessels and boiler steam pipes since the 1930's (1). 2-1/4Cr-1Mo steel, one member of this family, was originally formulated for use at elevated temperatures where creep resistance is required (2). This alloy is employed in steam generating and handling equipment on a regular basis where temperatures may reach as high as 1000°F to 1100°F (2,3). In the petrochemical industry, pressure vessels and reactors used in the refining and processing of petroleum are commonly composed of 2-1/4Cr-1Mo steel (4,5). Such processes as thermal reforming, polymerization, alkylation, and hydrocracking are performed in these vessels at high temperatures and pressures (3,6). In the past few years, 2-1/4Cr-1Mo steel has also come to be used in the fabrication of heavy-section well-head equipment because of its resistance to sulfide stress-cracking (4).

2-1/4Cr-1Mo steel is being favorably considered for a number of uses in the alternative energy field. Spurred on by the Arab oil embargo of 1973 and in anticipation of future petroleum shortages resulting from a dwindling supply of a limited resource, research and development in the areas of nuclear energy (fast breeder reactors), coal gasification/liquifaction, and synthetic fuels has continued. Although its use was never fully realized in the ill-fated Clinch

River liquid metal fast breeder reactor (7,8), 2-1/4Cr-1Mo steel has been used in the construction of several European fast breeder reactors as well as for superheaters in the Russian BOR-350 project (9). Coal, a resource which this nation possesses in great supply, is of significant interest as a raw material from which liquid and gaseous products can be made for use as fuels and replacements for some of the petrochemicals employed today. 2-1/4Cr-Mo steel is considered the primary material for the fabrication of the pressure vessels required for these processes. These vessels would operate at 750°F to 900°F at pressures of 1000 to 4000 PSI (10).

2. PROPERTIES

2-1/4Cr-1Mo steel is a low carbon, low alloy ferritic steel with a nominal composition given in Table 1. It is particularly well suited to elevated temperature service because of the following properties. First, 2-1/4Cr-1Mo steel has good high temperature strength (12,13,14) as characterized by elevated temperature tensile strength, creep strength, and rupture strength (14). It has been called the strongest low alloy steel for high temperature service (7) and is second only to austenitic stainless steels in terms of allowable stresses at temperatures exceeding 1050°F as specified by the ASME Boiler and Pressure Vessel Code (12,13). Second, 2-1/4Cr-1Mo steel has good to moderate corrosion and oxidation resistance (7,8,12,14). Zeisloft et al. (7) refer to its good water corrosion resistance while Bynum et al. (12) address its low stress-

Table 1. Nominal composition of 2-1/4Cr-1Mo steel per ASTM A 387 (11)

Element	Composition (Weight Percent)
Carbon	0.15 max.
Manganese	0.30-0.60
Phosphorus	0.035 max.
Sulfur	0.035 max.
Silicon	0.50 max.
Chromium	2.00-2.50
Molybdenum	0.90-1.10

corrosion cracking susceptibility in wetting steam conditions (with properly controlled water chemistry). Once thought to be immune to hydrogen attack (15), more recent studies have found that 2-1/4Cr-1Mo steel does suffer degradation due to the action of pressurized hydrogen at elevated temperatures. Stone et al. (16) have found evidence that methane bubbles nucleate at carbides, particularly at grain boundaries in 2-1/4Cr-1Mo steel exposed to 2000 PSI hydrogen gas at 600^{o}C. Bubble formation, however, appears to be predominantly limited to carbides of low stability such as M_3C. Finally, 2-1/4Cr-1Mo steel has relatively good high temperature microstructural stability (4). Baker and Nutting (17) have described the alloy carbides present in 2-1/4Cr-1Mo steel as a function of heat treatment and thermal exposure. Those carbides which form first are not the equilibrium precipitates. During tempering or elevated temperature service, the carbides change according to a complex evolutionary scheme, each successive carbide more stable than its predecessor. Wada et al. (4) have indicated that the ratio of chromium to molybdenum in 2-1/4Cr-1Mo steel creates a condition in which the driving force for such alloy carbides as M_2C, M_7C_3, and $M_{23}C_6$ to transform to the next precipitate in the evolutionary chain is small. Thus, the transformation is slow, contributing to the overall stability of the steel. Carbide stability can be further improved by overtempering to produce carbides which are in their equilibrium state. It is, in fact, in the overtempered condition that 2-1/4Cr-1Mo has its highest resistance to hydrogen attack (4).

Aside from its elevated temperature properties, 2-1/4Cr-1Mo steel has other properties which are advantageous. It has good formability (7,8) and is weldable if the proper precautions are taken (7,8,13). It is not exceptionally expensive (12) and has a high bainitic hardenability (4,13). The latter indicates that on cooling from austenite, the resulting microstructure is fully bainitic over a wide range of cooling rates (4). Standard composition 2-1/4Cr-1Mo steel plate can be austenitized and water quenched in thicknesses of up to 8 inches and still be bainitic throughout the entire thickness (4). The bainitic microstructure results not only in enhanced strength at room temperature but at elevated temperatures as well (12,13). Emmanuel et al. (13) have indicated that the strengthening benefits of heat treatment are good for service temperatures of at least 850^{o}F. Furthermore, by adding a tempering step subsequent to normalizing or quenching, steels with a range of strengths are attainable.

3. CREEP STRENGTHENING MECHANISMS IN LOW ALLOY FERRITIC STEELS

Metals to be used in components and structures which are to operate in the creep temperature range must be creep resistant in order to avoid failure resulting from elevated temperature deformation. Since deformation occurs by the creation and movement of dislocations, creep resistance may be achieved by creating conditions within the microstructure which will interfere with dislocation mobility (31). This is usually accomplished by adding

alloying elements to the metal which can strengthen the material in a number of ways.

Carbide Dispersion Strengthening

The primary creep strengthening technique employed in low alloy ferritic creep-resisting steels is carbide dispersion hardening. A combination of alloying elements are added to the steel to produce a fine dispersion of precipitates in the matrix which serve as barriers to dislocation movement. The effectiveness of these particulates in strengthening the matrix depends on many variables. First, the shear strength of the particles themselves is important. The precipitates must be strong enough to resist the shearing action of an impinging dislocation. Otherwise, the dislocation can glide through the intended obstacle, leaving the particle permanently sheared (31,32). Second, particle spacing, size, and volume fraction have an effect on the creep strength (33). Using a model consisting of a dislocation passing through a regular array of precipitates, Verhoeven (32) has shown that the strength is proportional to the square root of the precipitate volume fraction divided by the particle radius. Thus strength increases with an increase in the volume fraction and a decrease in the particle size. Furthermore, since particle spacing is inversely related to the volume fraction of precipitate, decreasing the spacing also increases the strength. According to Shoek (34), theory predicts that the effectiveness of a dispersion of particles in interfering with dislocation glide is a maximum for a particle spacing on the order

of 10^{-6} cm. Third, the effectiveness of a precipitate in interacting with dislocations is directly related to the magnitude of the strain field associated with it in the surrounding lattice. Particles which are coherent with the surrounding matrix (particle lattice planes continuous with those of the matrix) generate a significantly larger strain field than those which are not coherent (35), making particle coherency desirable for good creep strength. Unfortunately, at creep temperatures, coherent precipitates are not stable, continuing to grow and eventually losing their coherency with the matrix (35). Finally, the difference in specific volume of the particulate and the surrounding matrix is important. The larger the disparity in the two values, the better the precipitate is as a source of vacancies (31). Since vacancies are required for a dislocation to climb, any dislocations whose movement has been stopped by the presence of the particle will be assisted in climbing over that obstacle by having a source of vacancies close at hand.

Precipitates which are effective creep strengtheners must be stable under service conditions to be of any value (31,33,34,36,37). Stability implies that at the temperature of interest, the particles will not change in size, spacing, or composition with time or will do so at an acceptably slow rate. Precipitate growth or dissolution is made possible by the diffusion of atoms through the matrix to or from the precipitation site. Thus factors which affect the diffusion rate can also influence particle stability. Diffusivity is related to

temperature through an Arrhenius-type equation (38,39) of the form,

$$D=D_o\exp(-Q/RT). \quad (1)$$

Since the diffusivity increases rapidly with temperature, as indicated by the above relation, one expects that increasing the temperature can also result in accelerated precipitate growth or dissolution. The surface energy of the precipitate/matrix interface is also related to the diffusion rate. High interfacial energy encourages diffusion, promoting rapid particle growth (31). The interfacial energy can be reduced by the addition of the proper amounts of suitable alloying elements to the matrix. This, in turn, lowers the rate of solute diffusion and reduces the precipitate growth rate. The composition of a precipitate can affect its stability. Particle growth or dissolution is inhibited if the elements of which it is composed have a low solubility in the matrix at the temperature of interest (36). In addition, if once in solution in the matrix, the diffusivity of that element is low, such growth/dissolution is further hampered (34).

In ferritic low alloy creep-resistant steels, the strengthening particles are alloy carbides. Due to the interplay of the various alloy additions in the composition, the precipitation sequence in these steels is not simple, being described by a complex evolutionary scheme in which a progression of metastable carbides are formed before the equilibrium carbides appear (37). These metastable precipitates can appear in sequence or simultaneously. The carbides which endow the material with good creep resistance are formed in the matrix as a fine dispersion, often homogeneously precipitated.

However, continued exposure to elevated temperatures results in the appearance of other metastable carbides which may coexist with but finally replace the desirable precipitates. The metastable carbides nucleate heterogeneously at grain boundaries and other microstructural defects as well as at carbide/matrix interfaces and grow rapidly. The precipitation of the equilibrium carbides requires extensive aging (33).

Solid Solution Strengthening

Solid solution strengthening in low alloy ferritic steels plays a secondary role to the strengthening effects of carbides. Of the various mechanisms proposed by which solid solution strengthening occurs, in these alloys, it is thought to be primarily due to interactions between interstitial elements (carbon/nitrogen) and carbide/nitride-forming substitutional alloying elements (40,41). This interaction arises because of the affinity these interstitials and substitutionals have for one another. In solid solution, they are drawn together to form loose associations called clusters which are too small to serve as precipitation nuclei. Denoting substitutional atoms by "S" and interstitial atoms by "I", the resulting clusters may be described as "S-I" and "S-I-S." These are in addition to the solute atoms which can be found alone as "S" or paired as "S-S." The association of interstitials with one or more substitutionals greatly reduces the mobility of the interstitials in the lattice.

Considering the attraction that dislocations have for interstitial atoms, two strengthening mechanisms can be envisioned. First, if the affinity between the interstitial and substitutional atoms is stronger than that between interstitials and dislocations, the interstitials remain bound to the substitutional atoms in the lattice and strengthening results from the interaction of the dislocations with the elastic strain fields of the clusters. "S-I" and "S-I-S" clusters are more effective strengthening agents than "S" or "S-S" couples because the strain field around substitutional atoms is basically spherical in shape and can only effectively interact with edge dislocations (42). However, when interstitial atoms which have non-spherical strain fields are coupled with the substitutional atoms, the resulting net field of lattice distortion is also non-spherical. Such a field can interact with both edge and screw dislocations (42). Second, if the interstitial atoms are bound more strongly to dislocations than they are to substitutional atoms, the dislocations carry interstitial solute atmospheres which interact with the less mobile substitutional atoms in the lattice. Thus, strengthening is by the mechanism of solute drag. In the transitional zone where the interstitial/substitutional affinity is comparable to that between interstitials and dislocations, both mechanisms may be in effect, with clusters included in the dislocation solute atmospheres as well as bound in the lattice. In this instance, relative cluster mobility depends on cluster size as well as strain rate.

4. AVAILABILITY

2-1/4Cr-1Mo steel is available in many forms depending on its application. The American Society for Testing and Materials (ASTM) has a minimum of 12 standards which specify 2-1/4Cr-1Mo steel in such forms as plate, forgings, castings, pipe, and seamless tube. Some of these specifications differentiate by application while others do so by heat treatment. In the literature, 2-1/4Cr-1Mo steel is often referred to in its plate form as specified by ASTM A 387 Grade 22 (11) or ASTM A 542 (18). Within each of these standards are subgroups or classes which further differentiate plate by strength. Although the compositions of the plates indicated in both specifications are the same, A 387 specifies plate in the annealed or normalized and tempered condition while A 542 is for quenched and tempered plate. Table 2 compares the properties of plate made to the two specifications.

5. WELDING PROCESSES

The primary fabrication technique employed in the construction of 2-1/4Cr-1Mo pressure vessels is welding. Welding processes commonly used include electroslag (ESW), shielded metal arc (SMAW), and submerged arc (SAW) (19). Furthermore, development is underway to apply the processes of electron beam (EBW) and narrow groove gas metal arc welding (GMAW) to pressure vessel fabrication (19,20,21).

Electroslag welding is a high heat input process which tends to produce an extensive coarse-grained heat-affected zone (HAZ) and a

Table 2. Comparison of the properties of 2-1/4Cr-1Mo Plate, ASTM A 387 vs. ASTM A 542 (11,18).

Standard	Class	Condition	UTS (KSI)	min. YS (KSI)	%El (2")
A 387	1	Annealed	60-85	30	18
	2	Normalized and Tempered	75-100	45	18
A 542	1	Quenched and Tempered	105-125	85	14
	2	"	115-135	100	13
	3	"	95-115	75	20
	4	"	85-105	60	20

fusion zone composed of large columnar grains. Because ESW can be used to weld heavy sections in a single pass, it is an attractive welding process for pressure vessel fabrication. If proper welding procedure and filler metals are used, electroslag welds can have mechanical properties equal to or better than those of the base metal (with the exception of notch toughness) (22). To optimize the impact properties, the ASME Boiler and Pressure Vessel Code requires that ESW-welded vessels with wall thicknesses greater than 1-1/2 inches receive an austenitizing post-weld heat treatment (PWHT) to refine the coarse-grained structure (22). Such a PWHT requires extensive heat treating and quenching facilities making ESW a process limited to shop-fabricated vessels. Those vessels which must be assembled in the field because their size makes shipping impractical (such as proposed synthetic fuel vessels) (20) are therefore not fabricated using this process.

Shielded metal arc welding is, in general, the most widely used process for welding today because of its versatility and the fact that the equipment required is relatively inexpensive and portable (24,25). Weld metal properties can be controlled by the choice of electrode used. Furthermore, the weld metal and HAZ receive grain refinement from each subsequent weld pass. As a result, the completed weldment requires only a sub-critical PWHT, which can be performed in the field. While SMAW is often used in the fabrication of 2-1/4Cr-1Mo pressure vessels, it becomes less economical relative to other processes such as SAW or GMAW as the wall thickness of the vessels increase (24). Since SMAW involves

welding with electrodes typically 9 to 18 inches long which are rapidly consumed and must be discarded on reaching a length of about 2 inches (24), the downtime required to discard the stub and replace it with a new electrode reduces the effective welding time and thus the effective deposition rate. In contrast, SAW and GMAW use a continuous wire electrode fed from a spool by a motor drive, eliminating the repetitive interruptions and increasing the effective deposition rate. Since the volume of weld metal required increases significantly with the member thickness, welding processes which have higher deposition rates (lower overall welding time and labor cost) become increasingly favored.

Relative to SMAW, submerged arc welding is a high deposition rate welding process (20). It can be automated, further increasing the deposition rate, and can be set up to weld joints in the flat and horizontal position. SAW has also been adapted to weld vertically oriented joints in heavy members. This latter technique was introduced in the early 1970's for the fabrication of nuclear reactors and has been termed the "sub-vert" process (20). In the shop, welds in cylindrical vessel sections are made in the flat position both longitudinally and circumferentially with the use of large positioners and turning rolls. In the field where, because of their size, vessels must be fabricated in place, SAW is used to weld circumferential welds in the horizontal position. Equipment has been devised which can make such welds in plates up to 16 inches thick (20). It is in these same large field-fabricated vessels that the sub-vert process is applicable. The weld groove used is of a

simple butt geometry which is cheaper and easier to machine and requires 50 to 70 percent less weld metal than a conventional SMAW groove preparation (20). The weld metal is deposited conventionally in the flat position through the thickness of the vessel wall (see Figure 1). In all instances, the multi-pass nature of the welding process, as in SMAW, results in grain refinement of the HAZ and fusion zone by subsequent weld passes. The as-welded microstructure therefore requires only a sub-critical PWHT which can be done in the field to achieve desirable mechanical properties.

Electron beam welding is being considered as a welding process which can be adapted to welding of heavy members for pressure vessel fabrication (19,20,26). Using a tightly focused beam of high energy electrons as a heating source, EBW requires no filler metal (27,28). The two members to be welded are butted together with no clearance. The beam strikes and fully penetrates the work at the joint, fusing the two members together autogenously. The deep penetrating characteristic of EBW results in a narrow HAZ and fusion zone, eliminating the need for multiple passes. This, in turn, cuts down on the welding time required, leading to cost reductions. The total energy input into the work is less than for conventional welding processes.

These positive factors must be balanced against the disadvantages of using EBW. Due to the narrowness of the electron beam and the high aspect ratio of the resulting fusion zone, beam tracking of the joint is critical, requiring joint preparation and positioning that is precise and highly toleranced. Since the

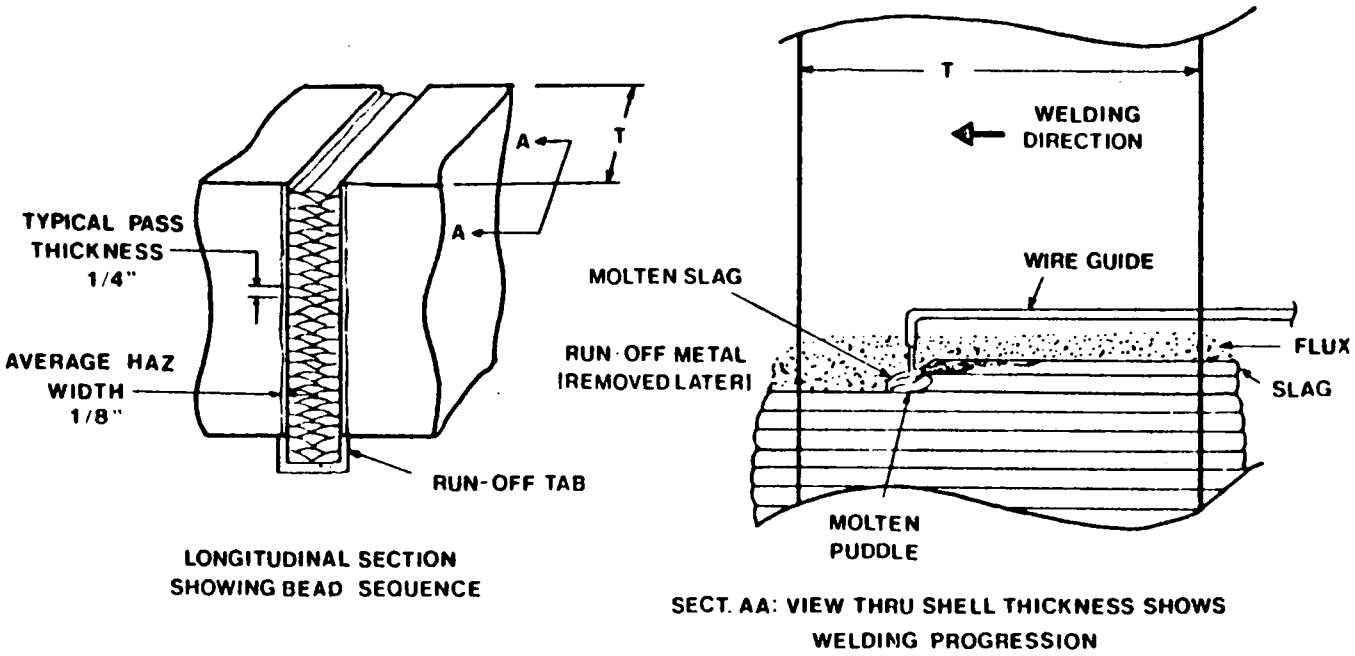


Figure 1. Illustration of the "sub-vert" welding process.

Source: Bonta, J. E. and Sikora, O. G., "Fabrication of Heavy-Wall Pressure Vessels," Application of 2-1/4Cr-1Mo Steel for Thick-Wall Pressure Vessels, ASTM STP 755, ASTM, 255-274 (1982).

collision of beam electrons with gas molecules in the environment leads to scattering and attenuation of the electron beam, welding must be done under a vacuum better than 10^{-3} torr (27,28). Therefore, portable clamp-on vacuum chambers are required (20). EBW machines do exist which can weld with the work at higher pressures (even up to atmospheric) but with a significant loss of weld penetration (27). These are therefore not practical to use in welding thick-wall vessels.

Narrow-groove gas metal arc welding (GMAW), developed for welding narrow weld grooves in thick plate, has been proposed for use in fabricating pressure vessels (20,29). Because the joint geometry used is square or of the "V" type with a small included angle, the volume of filler metal required is less than for a conventional weld groove. This leads to cost savings in terms of man-hours and material (20,29). Narrow-groove GMAW can be fully automated (29,30). However, precise operator control and tight fabrication tolerances must be maintained. Because of the relatively high welding speeds employed, even small errors can result in significant weld defects (20). Furthermore, once in place, the flaws are more difficult to remove due to the narrow confines of the joint which make worker access a problem. Narrow-gap GMAW has been used in some shop applications and is currently being tested for application to pressure vessel fabrication (20).

CHAPTER 2

LITERATURE REVIEW

1. MICROSTRUCTURE - BASE METAL AND WELD METAL

General Microstructure

The room temperature microstructure for any steel formed on cooling from austenite is given by its time-temperature-transformation diagram. Such a diagram for continuous cooling of 0.1 percent carbon 2-1/4Cr-1Mo steel is given in Figure 2 (4). Inspection of the figure indicates that there is an extensive range of cooling rates over which the resulting microstructure will be bainitic.

2-1/4Cr-1Mo steel is used in various conditions including annealed, normalized and tempered, and quenched and tempered. The microstructure of the annealed steel is predominantly ferrite with some gross carbide areas (that sometimes appear pearlitic) and possibly bainite. The exact mix of these microconstituents depends on the carbon content. Klueh (8) has reported observing proeutectoid ferrite with a scattering of carbides in annealed 0.009 carbon 2-1/4Cr-1Mo steel while higher carbon annealed material (0.12 percent carbon) also contains some fine pearlite and small amounts of bainite. Normalized 2-1/4Cr-1Mo steel contains ferrite and bainite with the amount of bainite increasing with carbon to nearly 100 percent of the structure for material with carbon levels greater than about 0.12 percent. Quenched 2-1/4Cr-1Mo steel has the

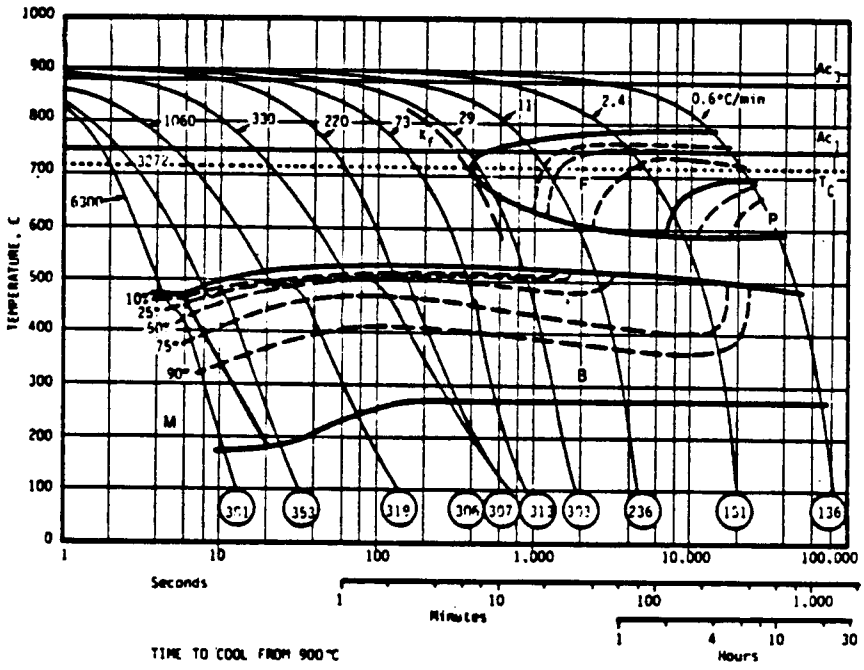


Figure 2. CCT diagram for 0.1 percent carbon 2-1/4Cr-1Mo steel.

Source: Wada, T. and Eldis, G. T., "Transformation Characteristics of 2-1/4Cr-1Mo Steel," Application of 2-1/4Cr-1Mo Steel for Thick-Wall Pressure Vessels, ASTM STP 755, ASTM, 343-362 (1982).

potential to contain martensite. However in most applications, this steel is used in rather thick sections which limits the cooling rate and therefore affects the resulting microstructure. Brown et al. (43) report for quenched 6-1/4 inch thick plate (0.13 percent carbon) a quarter-thickness microstructure of 100 percent bainite. The variation in cooling rate with distance from the plate surface alters the fineness (or coarseness) of the bainitic structure, but no martensite is present. Furthermore, despite the quenching treatment, some proeutectoid ferrite may be found at the half-thickness location.

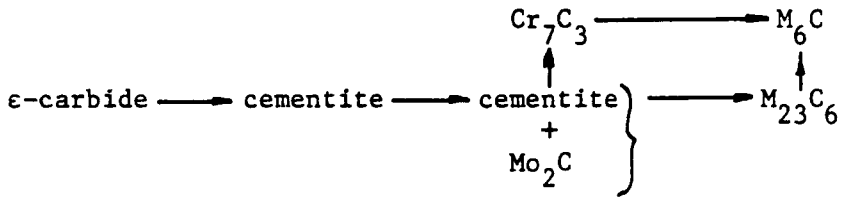
Related to the wide bainitic shelf characteristic of the CCT diagram for 2-1/4Cr-1Mo steel, weld metal is primarily bainitic for most welding processes. Exceptions to this rule are those processes which have unusually high or unusually low energy inputs. Richey (44) has shown that for cooling rates characteristic of electroslag welding, a high heat input process, some proeutectoid ferrite does form (in addition to bainite) in 2-1/4Cr-1Mo steel with a carbon content of 0.12 percent. At the other end of the spectrum, Sims and Fuchs (19) have determined that the microstructure obtained in the fusion zone of electron beam welded 2-1/4Cr-1Mo steel consists predominantly of lath-type martensite, this result stemming from the low heat input and therefore high cooling rate of the weld metal.

Examination of the bainite formed in 2-1/4Cr-1Mo steel using the scanning electron microscope (SEM) sometimes reveals a structure termed "granular" bainite. Klueh (8) has defined granular bainite as islands of a second phase dispersed in a bainitic ferrite matrix with

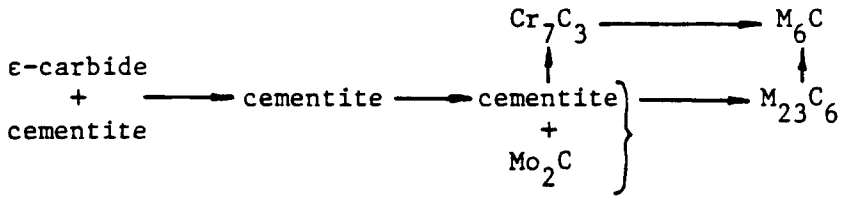
a high dislocation density. Habraken and Economopoulos (45) have determined that these islands consist of a combination of martensite and retained austenite. Wada and Eldis (4) have maintained that the bainite in 2-1/4Cr-1Mo steel with carbon contents less than or equal to about 0.1 percent is all of the granular variety. They indicate that the bainite is essentially free of carbides and contains only islands of martensite/austenite. This statement has been disputed by others including Kar and Todd (46) who report observing only ferrite and conventional bainite in 2-1/4Cr-1Mo steel cooled at rates comparable to those used by Wada and Eldis.

Carbides

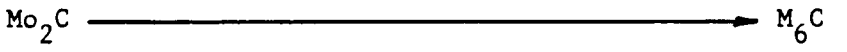
The properties of 2-1/4Cr-1Mo steel depend primarily on the carbide type, size, morphology, and distribution in the microstructure. Baker and Nutting (17) have described the general sequence of carbides formed in both quenched and in normalized 2-1/4Cr-1Mo steel during tempering. They indicate that the carbide sequence which describes the tempering of the acicular martensitic structure formed during quenching is almost identical to that for the portion of the normalized steel that is bainite. This sequence is depicted schematically in Figures 3a and 3b. Prior to tempering, the microstructure contains epsilon carbide which can be described as $Fe_{2.4}C$ (47). This precipitate appears alone in the martensitic structure but is accompanied by cementite (M_3C) in the bainite. This difference probably results from the greater period of time available in the normalizing process for carbide formation to occur (i.e. due



(a) Quenched (martensite)



(b) Normalized (bainite)



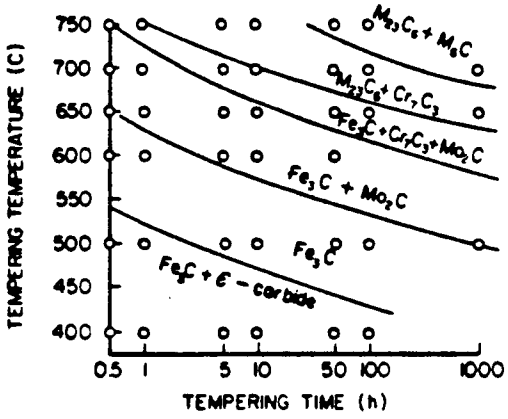
(c) Normalized (ferrite)

Figure 3. Carbide evolutionary sequence for 2-1/4Cr-1Mo steel.

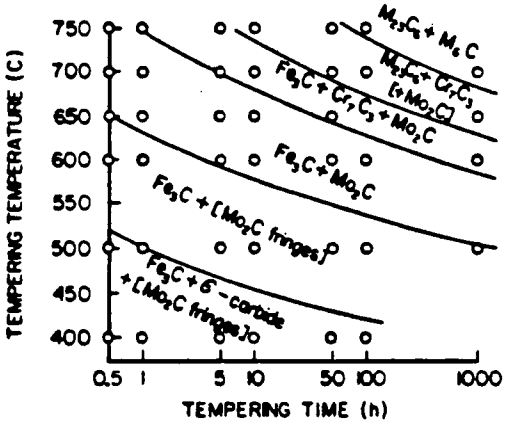
Source: Baker, R. G. and Nutting, J., "The Tempering of 2-1/4Cr-1Mo Steel after Quenching and Normalizing," JISI, 192, 257-268 (1959).

to the slower cooling rate). In either case, the initiation of tempering soon results in the in-situ transformation of any epsilon carbide present to M_3C. On further tempering, Mo_2C appears in the matrix along with the M_3C already in place and seems to precipitate homogeneously from diffuse zones. Mo_2C has considerable solubility for other alloying elements, especially chromium, and should probably be referred to as M_2C (37,48). At this point, the carbide sequence splits with the formation of Cr_7C_3 (generally denoted as M_7C_3) and $M_{23}C_6$. The M_7C_3 probably nucleates at the M_3C/matrix interface while the $M_{23}C_6$ nucleates and grows at grain boundaries as large spheroidal particles. The growth of M_7C_3 and $M_{23}C_6$ is accompanied by a decrease in the number of M_3C and M_2C particles with the latter going back into solution. The last carbide to form, M_6C, grows at the expense of all other carbides and is believed to be the equilibrium precipitate in 2-1/4Cr-1Mo steel. The carbide sequence observed in the ferritic portion of the normalized structure is quite different as shown in Figure 3c. After normalizing, the ferrite is free of any carbides. The first precipitates to appear in the ferrite during tempering are acicular M_2C particles which develop from diffuse zones in the matrix similar to those observed in the bainite. These carbides persist in the ferrite, showing no tendency to transform to any of the other metastable carbides observed in the other micro-constituents. Eventually, M_6C forms in the ferrite and the M_2C begins to dissolve.

The kinetics of these precipitation and transformation reactions are given in Figures 4a and 4b. This information is presented as an



(a) QUENCHED



(b) NORMALIZED

Figure 4. Diagrams showing carbides present in 2-1/4Cr-1Mo steel as a function of tempering time and temperature for quenched and normalized material.

Source: Baker, R. G. and Nutting, J., "The Tempering of 2-1/4Cr-1Mo Steel After Quenching and Normalizing," JISI, 192, 257-268 (1959).

isothermal diagram which plots tempering temperature vs. tempering time. The field is divided up into regions which are identified by the carbides present in that time/temperature regime.

In a more recent program, Pilling and Ridley (49) have studied the effect of carbon content on the tempering behavior at 700°C of 2-1/4Cr-1Mo steel with typical weld metal compositions. They found that in the range of 0.02 to 0.09 percent, the carbon level not only influences the rate at which the carbides evolve but also plays a role in determining what the equilibrium carbides will be. Figures 5a, 5b, and 5c show the variation in relative amounts of M_2C, M_7C_3, $M_{23}C_6$, and M_6C with tempering time and carbon content. Examination of these figures reveals that, in general, the increase in carbon level slows the evolution of the carbides in the microstructure. M_7C_3, which is totally removed from the structure in the 0.018 carbon material in the 12 hour tempering time, remains fairly stable and even increases in quantity slightly in the 0.09 carbon steel. The dissolution of M_2C is complete in the low carbon specimen while, in the high carbon material during the same time interval, tempering removes only 25 percent of the M_2C present. The formation of M_6C, which makes up 85 percent of the carbides in the 0.018 carbon steel after 12 hours at 700°C has barely begun in the 0.09 carbon material. Finally, the effect on the amount of $M_{23}C_6$ present as a function of tempering time is inconsistent and is small relative to that for the other carbides. The net result of the increase in carbon content is to displace the equilibrium structure from M_6C in ferrite to M_6C and M_7C_3 in ferrite. The carbide sequence proposed by Pilling and

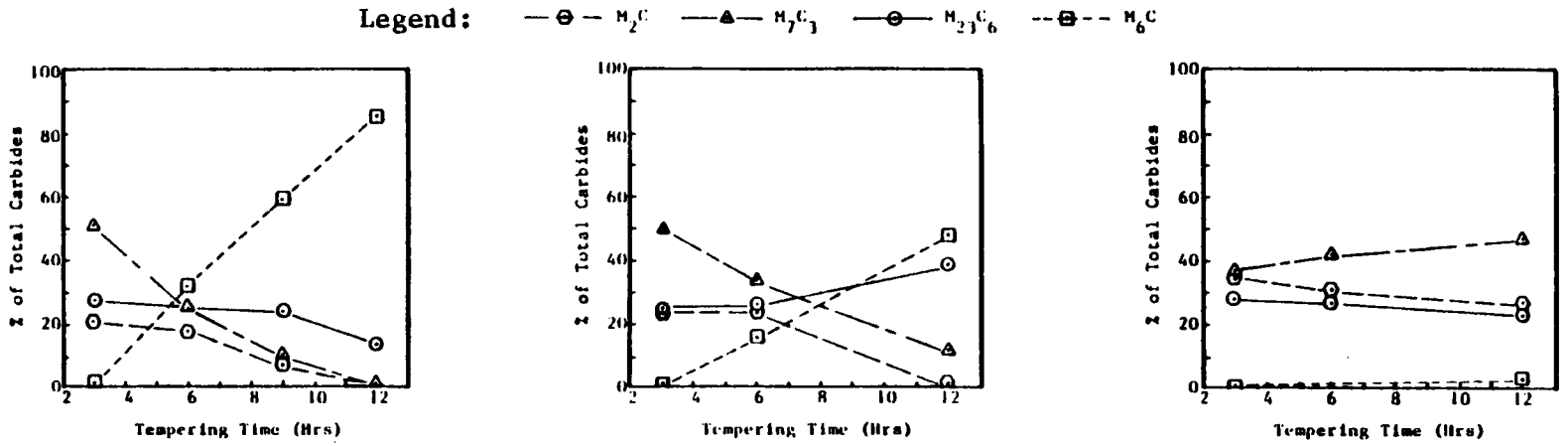


Figure 5. The variation in the relative amounts of carbides present in 2¼Cr-1Mo steel at 700°C as a function of carbon content and tempering time.

Ridley (49) differs from that of Baker and Nutting (17) and is given in Figure 6.

2. MICROSTRUCTURAL EFFECTS ON CREEP STRENGTH

As in any material, the microstructure of 2-1/4Cr-1Mo steel determines its properties, creep strength being no exception. The key to creep resistance in this material is the carbides. Such factors as carbide type, morphology, size, distribution, and volume fraction work together to influence the relative effectiveness of the carbides in conferring creep strength. These factors, in turn, are affected by heat treatment and the microconstituents in which the carbides reside. Finally, solute elements in the ferrite and prior austenite grain size have a less significant effect on creep resistance.

Carbides

Of the various alloy carbides to be found in 2-1/4Cr-1Mo steel, the carbide which is the primary creep strengthener is M_2C (17,37,45,48,50). This molybdenum-rich precipitate is most effective when present as a fine dispersion of acicular particles that have just lost coherency with the matrix (37,45,50). As indicated by Baker and Nutting (17), M_2C forms in tempered martensite, bainite and ferrite. During tempering or elevated temperature service, the M_2C in martensite and/or bainite is an intermediate which is eventually replaced by M_7C_3 or $M_{23}C_6$. However in proeutectoid ferrite (found in annealed or normalized and tempered

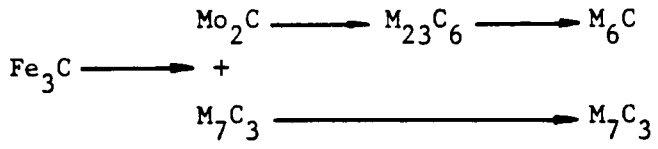


Figure 6. Carbide sequence for 2¼Cr-1Mo steel having typical weld metal composition.

Source: Pilling, J. and Ridley, N., "Tempering of 2.25%Cr-1%Mo Low Carbon Steels," Met. Trans A, 13A(4), 557-563 (1982).

2-1/4Cr-1Mo), the M_2C is the first carbide to form and persists for a much longer time until finally being replaced by M_6C. One means by which M_2C is believed to impart creep strength is by preventing the migration of boundaries and subboundaries during creep (45). Such migration is a known mechanism for the relaxation of creep stresses.

At a rate determined by the starting microstructure (a function of heat treatment), time at elevated temperature causes the carbides to undergo changes. Starting with a microstructure that has been optimized for creep strength through the application of heat treatment, the following may be observed. The acicular precipitates responsible for most of the strength coarsen and then dissolve as they are replaced by more stable carbides (as determined by the carbide sequence for the steel). This occurrence, in itself, is obviously detrimental to the creep resistance. However, considering that the new carbides must have some strengthening effect as well, that influence is further attenuated as the more stable particles coarsen, spheroidize, and agglomerate. Both the growth in size and the increase in spacing (which results from the agglomeration) lower the strength further. This situation can be altered through the addition of such alloying elements as titanium or niobium. These elements are strong carbide formers and produce carbides of the MC type which are much more stable than M_2C and are at least as effective in conferring creep resistance. If enough Ti or Nb is added, the MC precipitates totally displace the M_2C and take over the strengthening role.

Tempering and PWHT

Ignoring the microstructural changes taking place and looking just at the response to tempering and elevated temperature service, one finds that the highest apparent creep strengths (based on short time tests) are obtained in 2-1/4Cr-1Mo steel that has been tempered at relatively low temper parameters (51). Smith (52) has stated that higher room temperature strength can be obtained by tempering at temperatures as low as 1150°F for normalized material and as low as 1050°F for quenched materials. Unfortunately, the microstructures derived in this manner are less stable (51,53,54) than those produced by more conventional heat treatments. As a result, the increased strength may be transitory and may decrease during service (51). Since the rate of microstructural change is temperature dependent, one expects that 2-1/4Cr-1Mo steel with strength enhanced by heat treatment is of use at lower temperature but that the strength advantage diminishes as the service temperature increases. This is, in fact, the case. Various authors have put the cut-off temperature above which there is no strength advantage in the range of 900°F to 1000°F (13,14,43,52,54,55,56). The effect is graphically depicted by Sangdahl and Vorhees (55) in Figure 7 which is a plot of creep rupture strength vs. room temperature tensile strength. The figure shows that the correlation between the tensile strength and the 100,000 hour rupture strength decreases with increasing temperature until, at 1000°F, there is no correlation (rupture strength constant over the tensile strength range). In fact, given a high enough temperature or long enough time, the strength of all 2-1/4Cr-1Mo

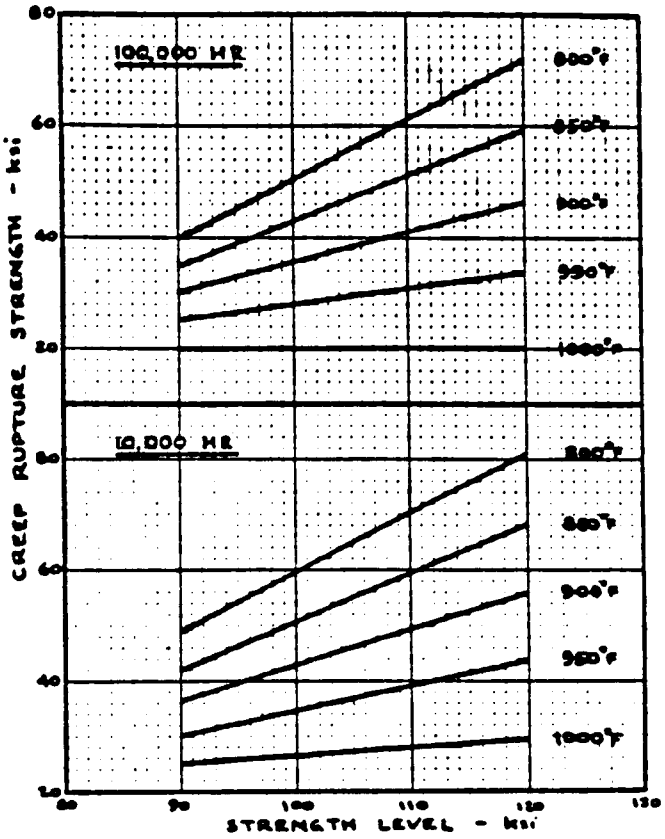


Figure 7. Correlation between creep rupture strength and room temperature tensile strength as a function of test temperature.

Source: Sangdahl, G. S. and Vorhees, H. R., "Quenched and Tempered 2-1/4Cr-1Mo Steel at Elevated Temperatures-Tests and Evaluation," Current Evaluation of 2-1/4 Chrome 1 Molybdenum Steel in Pressure Vessels and Piping, ASME-MPC, New Orleans, LA (1972).

steel approaches a common value (40,57). This results from the evolution of the microstructure to one of overaged equilibrium carbides in a carbon-saturated ferrite matrix (58). In this condition, the carbides are too large to impart any significant creep resistance to the steel and the strength is entirely due to the strength of the ferrite.

Microconstituents

Comparing the relative strengths of quenched, normalized, and annealed 2-1/4Cr-1Mo steel is basically a comparison of the merits of martensite, bainite, and ferrite with respect to creep resistance. The strength of quenched 2-1/4Cr-1Mo steel is mainly derived from the extensive dislocation substructure formed as a result of the shear transformation from austenite to martensite (53). On tempering, this network can become decorated with fine carbides, stabilizing it as long as the carbides remain in an effective condition. It has already been noted however that in the heavy sections usually employed in 2-1/4Cr-1Mo steel applications, quenching 2-1/4Cr-1Mo steel results in a bainitic or bainitic/ferritic microstructure. Bainite/ferrite microstructures also result from normalizing but the morphology differs from that observed in quenched 2-1/4Cr-1Mo steel. The bainite morphology varies with the temperature at which it forms, becoming finer and more acicular as the transformation temperature decreases (faster cooling rates) (45). Viswanathan (59) has indicated that the strength of the bainite increases as the lath-like structure becomes finer. In comparison, ferrite is a much weaker

microconstituent than bainite or martensite. Its effect on the rupture strength of a mixed bainite/ferrite microstructure has not been agreed upon. Both Klueh (60) and Viswanathan (59) maintain that the ferrite is detrimental to creep resistance and should be eliminated by suitable heat treatment or alloying additions. In contrast, Baker and Nutting (17) have alluded to the superiority of normalized and tempered 2-1/4Cr-1Mo steel over the quenched and tempered material at 500°C based on the presence of ferrite in the normalized and tempered steel since the M_2C which precipitates out in the ferrite persists much longer than in the bainite. Moreover, Cane and Fidler (61) have presented data indicating that the rupture strength of 2-1/4Cr-1Mo steel containing a 65 percent bainite-35 percent polygonal ferrite mix is superior to that for a similar material consisting of 100 percent bainite (see Figure 8). Based on the observation that the rupture mode changes from intergranular to transgranular as the bainite content of the microstructure decreases, they have explained the correlation between rupture strength and polygonal ferrite content as follows. In a fully bainitic microstructure, intergranular failure involves the formation and growth of cavities at the prior austenite grain boundaries. However, the introduction of increasing amounts of ferrite into the microstructure reduces the susceptibility to cavitational damage by eliminating more and more of the prior austenite grain boundaries. The softer ferrite accommodates some of the strain which might otherwise contribute to cavity formation.

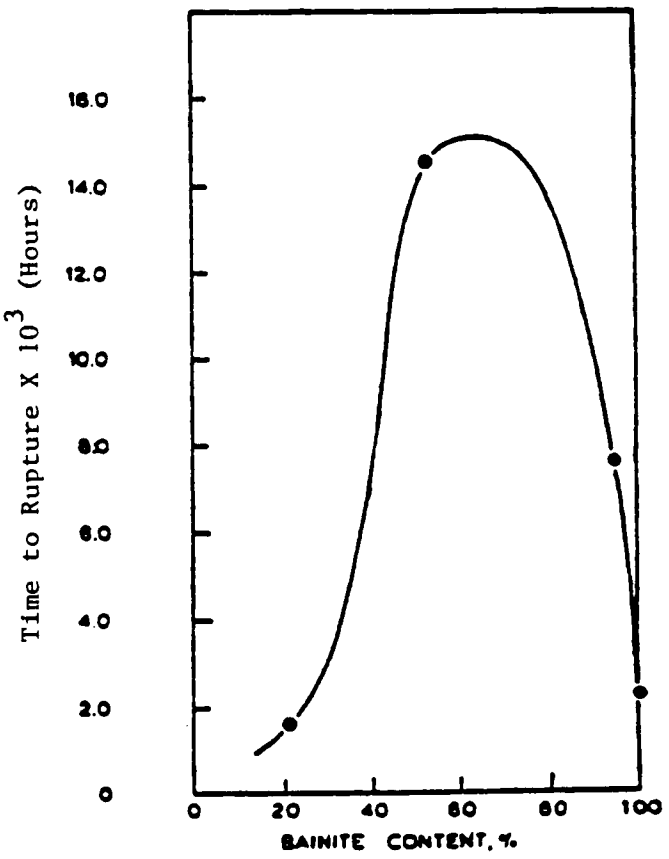


Figure 8. Stress-rupture time as a function of bainite content for 2¼Cr-1Mo steel tested at 565°C (1050°F) at a stress of 17.8 KSI. For bainite contents less than 100 percent, the balance of the microstructure is polygonal ferrite.

Source: Cane, B. J. and Fidler, R. S., "The Effect of Microstructure and Grain Size on the Creep and Rupture Properties of 2-1/4Cr-1Mo and 9Cr1Mo Steels," International Conference on Ferritic Steels for Fast Reactor Steam Generators, British Nuclear Energy Society, London, UK (1977).

In the same study, Cane and Fidler (61) have heat treated a number of fully bainitic 2-1/4Cr-1Mo steel samples to obtain a range of prior austenite grain sizes. They have observed that stress rupture strength increases as the prior austenite grain size decreases. This behavior has been explained as resulting from the increased grain boundary area available to contribute to the overall strain during creep. Furthermore, in a fine grained microstructure, a greater amount of boundary crack interlinking is required to produce a critical crack size which will propagate to produce rupture. However, Cane and Fidler (61) have also noted that the variation in heat treatment required to produce the range of grain sizes also affects the type, size, and distribution of precipitates present in the microstructure. Specifically, the coarse grained specimens contain increased amounts of $M_{23}C_6$ carbide, the formation of which can result in the dissolution of M_2C and lead to reduced rupture strength. In that light, the apparent dependence of rupture strength on prior austenite grain size may be due, at least in part, to other variables.

The strength of ferrite in 2-1/4Cr-1Mo steel, exclusive of the effects of any included carbides, is due to the interaction solid solution hardening effect previously described, with the elements chromium, molybdenum, and carbon playing a significant role (40,41). Comparison of the binding energies of chromium and molybdenum atoms with dislocations and/or carbon atoms indicates that at approximately 1100^{o}F, the molybdenum atoms have about ten times more interaction energy with dislocations than do chromium atoms. At the same time,

the interaction energies for chromium and molybdenum with carbon atoms are comparable (41). Based on this, it is concluded that associations of molybdenum and carbon atoms (clusters) are more effective strengthening agents than chromium-carbon clusters.

The interaction of these molybdenum-carbon clusters with dislocations is thought to be dependent on strain rate. At all strain rates, "Mo-C-Mo" clusters are believed to form and are the main strengthening agent in the solid solution strengthening of 2-1/4Cr-1Mo steel (41). At low strain rates, "Mo-C-Mo" clusters are stationary in the lattice and "Mo-C" couples are mobile enough to diffuse along with moving dislocations. Strengthening is due to the interaction of the dislocations with the "Mo-C-Mo" clusters. As the strain rate increases, dislocation movement becomes increasingly hindered due to the drag of pulling the associated "Mo-C" clusters through the lattice. Eventually, the strain rate is sufficient for the dislocations to break away from the "Mo-C" pairs, greatly reducing the solute drag. Under this condition, strengthening is entirely due to dislocation interactions with stationary "Mo-C-Mo" and "Mo-C" clusters in the lattice.

For the effect of interaction solid solution hardening to be significant, the concentration of solute atoms in the lattice must be above its equilibrium value (40,41). Such supersaturation is achieved by non-equilibrium cooling of the steel from austenitizing temperatures. Because the elements involved are carbide or nitride formers, the amount of solute steadily decreases during elevated temperature exposure as a result of carbide and nitride precipitation

and growth. Thus, under high stresses where failure due to creep occurs in a relatively short time, interaction solid solution hardening plays a significant role. However, at lower stresses and longer rupture times, precipitation and growth robs the matrix of solute elements, and strengthening is mainly due to carbide/nitride-dislocation interactions.

The introduction of strong carbide formers such as titanium, niobium, or vanadium into the low carbon steel results in the formation of carbides of these metals in preference to molybdenum and chromium carbides (50,62). In sufficient quantities, these "stabilizing" elements effectively remove nearly all of the carbon from solution, leaving the molybdenum in solution to interact with moving dislocations and strengthen the matrix. Similarly, if the carbon content of the steel is low enough, insufficient carbon is present to remove all of the molybdenum from solution and solid solution strengthening due to the molybdenum occurs as well (58).

3. ALLOYING ELEMENT EFFECTS ON CREEP STRENGTH

Chromium

One of the major alloying elements in 2-1/4Cr-1Mo steel, chromium contributes to the stress rupture behavior of that alloy by way of one of two mechanisms. First, in solid solution, chromium associates with interstitials in the lattice (particularly the carbon atoms) to form clusters like "Cr-C" and "Cr-C-Cr" (41,53). Depending on the conditions, these clusters can interfere with dislocation movement by a solute drag mechanism or by regular solid solution

hardening. However, since chromium is an excellent carbide former and is, to an extent determined by the carbon content, removed from solution by the formation of chromium carbides (58), solid solution strengthening by chromium atoms is severely limited. This leads to the conclusion that if the carbon level in the steel is kept low, less carbon is available for carbide formation, leaving more chromium in solution to strengthen the steel.

Despite the loss in strength due to carbide precipitation, the presence of carbides in the matrix can be beneficial to the rupture strength, particularly if they are finely dispersed and are of the acicular variety. However, the carbides formed with chromium (M_7C_3,$M_{23}C_6$) (37) are not stable at elevated temperatures, spheroidizing easily and soon grow to become large and blocky. Argent et al. (53) have indicated that at 600°C, chromium carbides soon grow to where their spacing is greater than the elements of the dislocation network in the matrix and thus lower their ability to strengthen the matrix.

In the literature, increasing chromium has traditionally been tied to an observed decrease in strength for alloys with chromium contents in the range of 1 to 3 weight percent. Data published by the Japan Steel Works (63) for Cr-Mo-V-Ti-Nb steels shows that despite variations in austenitizing temperature and tempering time at 690°C, the room temperature tensile strength steadily decreases as the chromium content increases from 2.25 to 3.14 percent (see Figure 9). As far back as 1940, the deleterious effect of increasing chromium content on creep strength has been observed. Miller et

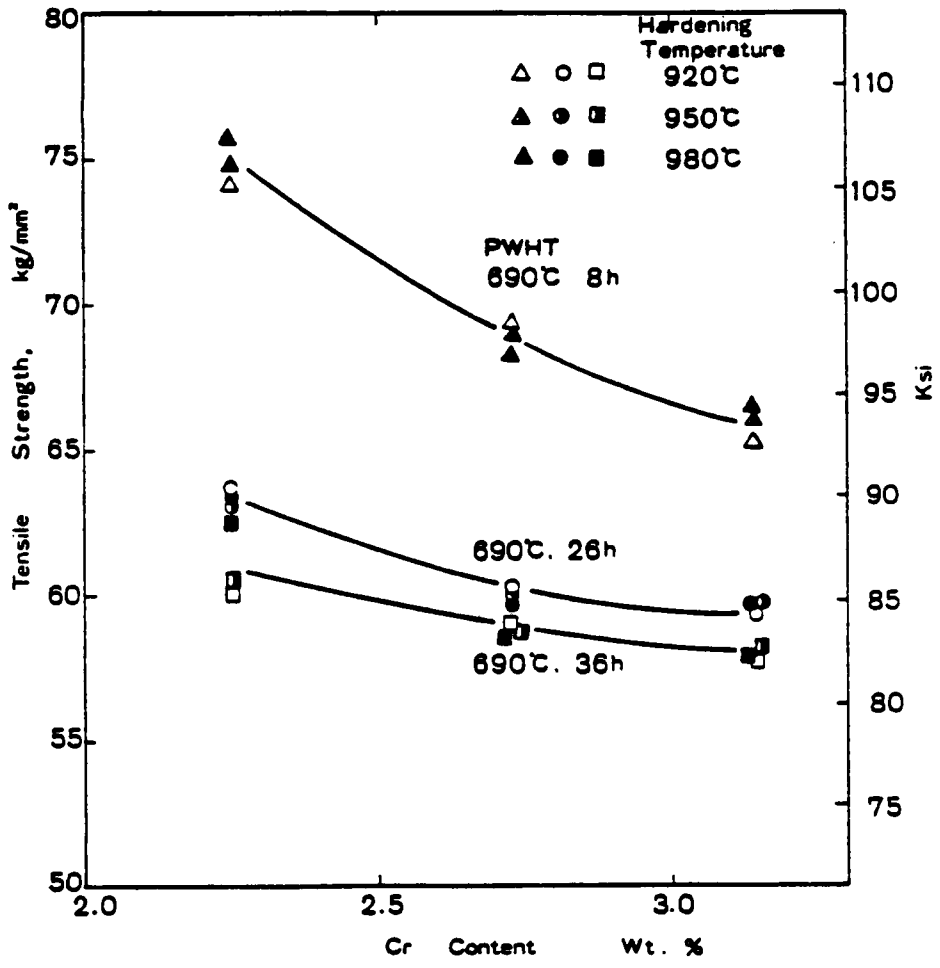


Figure 9. Effect of chromium content on the room temperature tensile strength of Cr-Mo-V-Ti-B steel.

Source: Mechanical and Metallurgical Properties of a 3Cr-1Mo-¼V-Ti-B Pressure Vessel Steel for Coal Liquefaction Reactor, NEDO/JSW Data Sheets, Series No. CLR-C, New Energy Development Organization, The Japan Steel Works Ltd. (1981).

al. (51) have indicated that for Cr-Mo steels containing 1 percent molybdenum, the creep strength at 1000°F falls off for chromium levels greater than 2.25 percent. More recently, preliminary results from Kobe Steel (64) have shown that in the range of 1 to 9 percent chromium, the 1000 hour rupture strength of Cr-1Mo steels falls rapidly for increasing chromium up to 5 percent and then rises slowly for chromium contents greater than that value (64) (see Figure 10).

Molybdenum

Molybdenum is the major element responsible for the creep strength of 2-1/4Cr-1Mo steel (3,51,65). As in the case of chromium, molybdenum increases the creep resistance of steel when it is present either in solid solution (37,41,50,53,58,62,66) or as a carbide precipitate (17,37,65,67).

In solid solution, molybdenum atoms have a stronger affinity for the interstitial alloying elements than do the chromium atoms and thus play a more significant role in the interaction solid solution effect (41). Argent et al. (53) have stated that in ferritic steels, the presence of one weight percent molybdenum in solution is sufficient to saturate the dislocation networks. Thus, the addition of more than 1 percent molybdenum is of no benefit (assuming that all of the molybdenum is in solution). In a similar manner, Jones and Avyle (41) indicate that 0.5 percent molybdenum in iron is enough to decorate 75 percent of the dislocation line. Two effects are possible which can diminish the solid solution strengthening effect. First, in the presence of significant amounts of phosphorus and/or

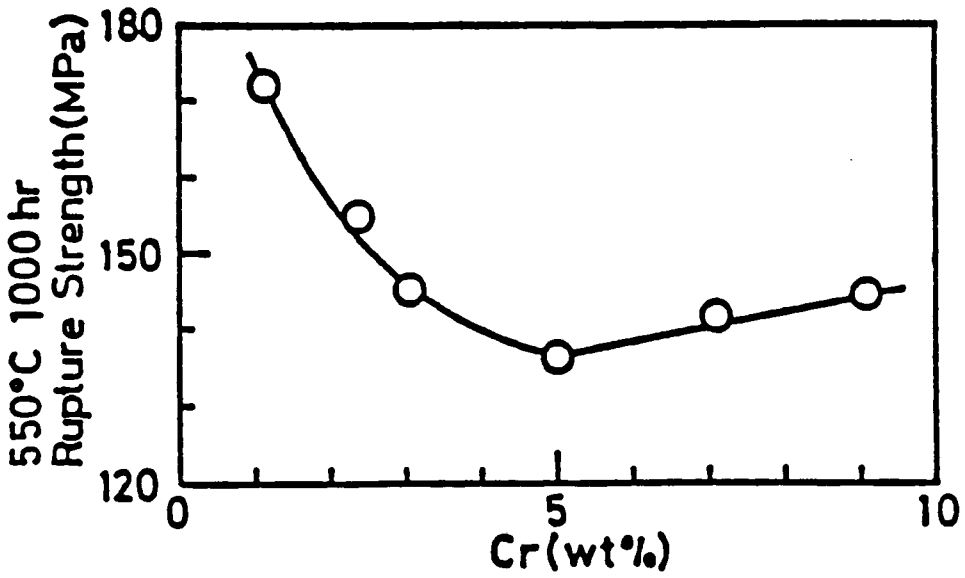


Figure 10. Effect of chromium content on the 1000 hour rupture strength of Cr-1Mo steel at 550°C.

Source: Rawlins, Carl E., Prescott, G. R., Braun, C. F., McGuire, W. J., and Lorentz, R. E., "Report to the American Petroleum Institute on a Program to Study Materials for Pressure Vessel Service with Hydrogen at High Temperatures and Pressures," MPC (1982).

arsenic, the molybdenum cosegregates along with those elements to the grain boundaries, depleting the molybdenum in the matrix and thereby weakening it (62). Second, the precipitation of molybdenum carbides can occur (58). Molybdenum is such a strong carbide former that precipitation is limited only by the amount of carbon in the steel above the equilibrium level. This fact suggests that carbide precipitation (and thus the depletion of molybdenum from the matrix) can be limited by lowering the carbon content of the steel (50). Alternatively, other alloying elements with an even stronger affinity for carbon than molybdenum may be added to the steel such as titanium, niobium, or vanadium (50,62). These tie up the carbon in the steel and leave the bulk of the molybdenum in solution.

Despite its negative effect on solid solution strengthening, the precipitation of molybdenum carbides may increase the stress rupture strength. The carbide which is most effective in this regard is Mo_2C, particularly when present as a fine dispersion of acicular precipitates (37,65,67). Such a morphology has been observed both in ferrite and bainite in 2-1/4Cr-1Mo steel, with the Mo_2C being much more stable at elevated temperatures in the ferrite (17).

Test results from the literature have traditionally indicated that increasing molybdenum in Cr-Mo steels is beneficial to strength. Miller et al. (51) have shown that increasing the molybdenum content from 0.5 to 1.0 percent increases creep strength at $1000^{o}F$ (see Figure 11). The curve for 1.0 percent molybdenum steel is significantly above that for the 0.5 percent molybdenum material. Data from the Japan Steel Works (63) for 3Cr-Mo-V-Ti-B steels reveals

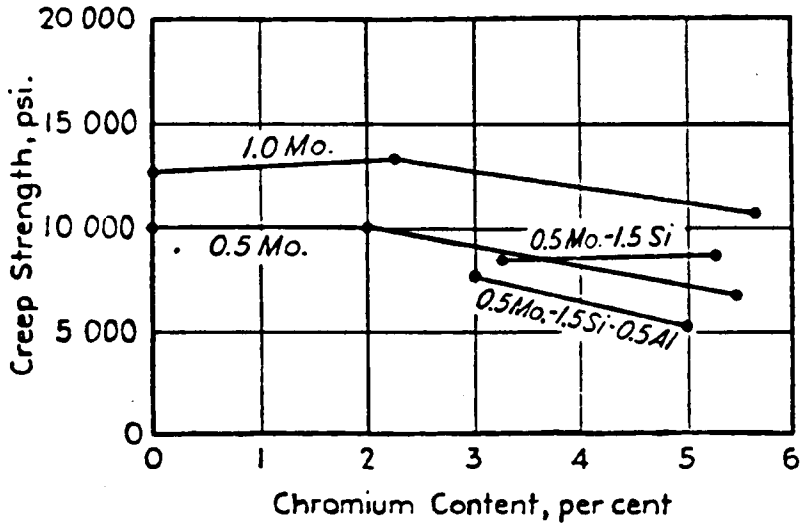


Figure 11. Effect of molybdenum and chromium content on the creep strength of Cr-Mo steel at 1000°F.

Source: Miller, R. F., Benz, W. G., and Unverzagt, W. E., "The Creep Strength of 17 Low Alloy Steels at 1000°F," ASTM Proc., 40, 771-781 (1940).

that for molybdenum contents in the range of 0.5 to 1.5 percent, the room temperature yield and tensile strengths increase continuously with percent molybdenum (see Figure 12).

Results of recent tests on Cr-Mo steels have not been in total agreement with the traditional view. On the positive side, work done by Climax (68) on 3Cr-Mo steel at 1000°F has shown that increasing the molybdenum progressively from 0.8 to 1.6 percent increases both the room temperature and elevated temperature tensile strength as well as the stress rupture strength of these steels (see Figure 13). However, Kobe Steel (68) has found that for 3Cr-Mo steels tested at 550°C, the effect of increasing the molybdenum content from 1.0 to 1.4 percent on the 1000 hour rupture strength depends on the room temperature tensile strength of the material. For tensile strength levels around 90 KSI, increasing the molybdenum content has a beneficial effect on rupture strength while the opposite is true for steels with tensile strengths around 80 KSI. This behavior is illustrated in Figure 14. As indicated in the figure, the difference in strength level is due to a tempering treatment given the lower strength material. Since such a treatment alters the microstructure, particularly the carbides, the observed conflict in response to increases in molybdenum content between the high and low strength 3Cr-Mo steels may be related to these changes. In another study of 2-1/4Cr-Mo-1/4V steels, Kobe has reported that, for the range of 0 to 1.8 percent molybdenum, the rupture strength at 550°C (100 hour and 1000 hour strengths) increases significantly for molybdenum levels up to 0.4 percent but then falls slowly with further increases in

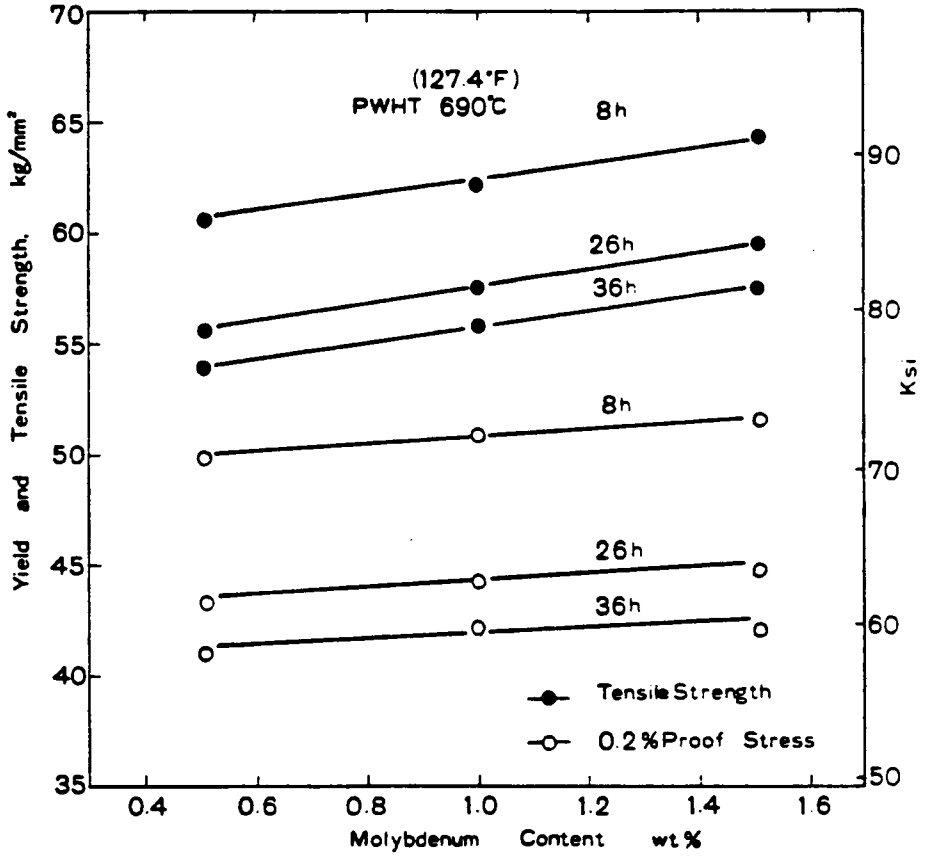


Figure 12. Effect of molybdenum content on the room temperature properties of 3Cr-Mo-V-Ti-B steel.

Source: Mechanical and Metallurgical Properties of a 3Cr-1Mo-¼V-Ti-B Pressure Vessel Steel for Coal Liquefaction Reactor, NEDO/JSW Data Sheets, Series No. CLR-C, New Energy Development Organization, The Japan Steel Works Ltd. (1981).

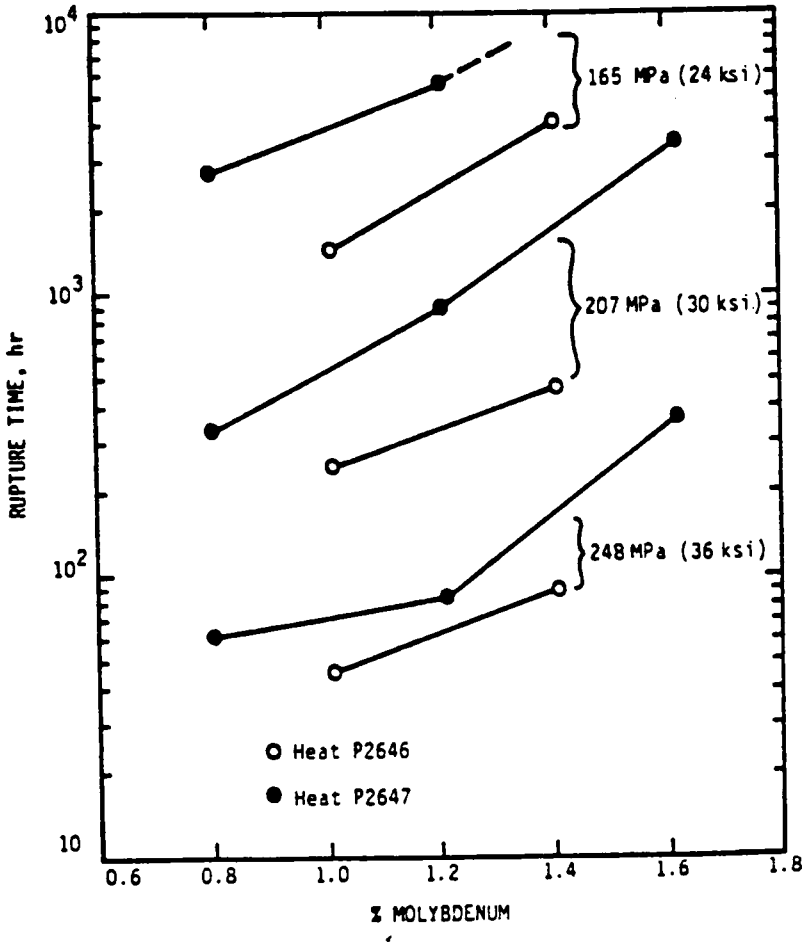


Figure 13. Effect of molybdenum content on the rupture time (for a fixed stress) of 3Cr-Mo steel at 538°C.

Source: Prescott, G. R. and Braun, C. F., "Update on Modified 2-1/4Cr-1Mo and 3Cr-Mo Alloys," MPC, HPV-7 (1983).

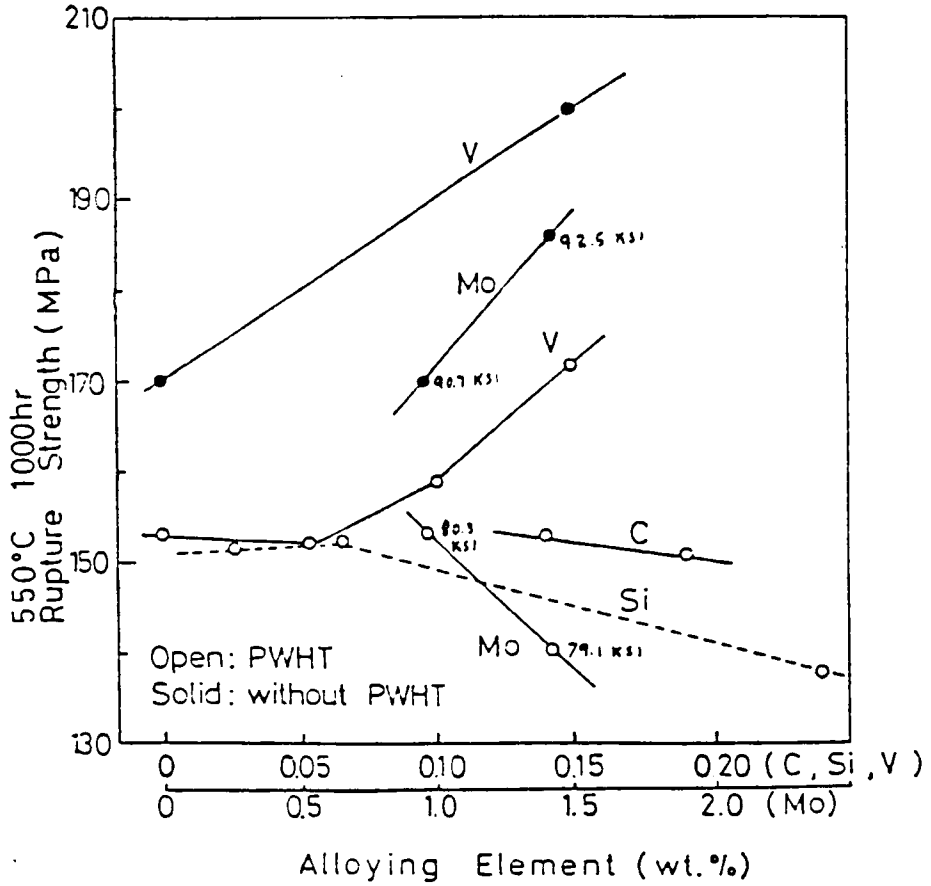


Figure 14. Effect of changing levels of various alloying additions on the 1000 hour rupture strength of 3 Cr steel. Strength levels indicated for the Mo data points are room temperature tensile strength.

Source: Prescott, G. R. and Braun, C. F., "Update on Modified 2-1/4Cr-1Mo and 3Cr-Mo Alloys," MPC, HPV-7 (1983).

molybdenum content (see Figure 15). It has been observed that the steels containing less than 0.4 percent molybdenum have some polygonal ferrite in their microstructures while those with greater molybdenum levels are fully bainitic. Thus, it has been concluded that once enough molybdenum has been added to make the steel fully bainitic, no benefit is to be gained by adding more.

Carbon

Carbon is a strengthening element whose presence distinguishes steel from ordinary iron. Carbon's strengthening effect can be attributed to one or more of the following: (a) its combination with other elements in the steel to produce carbide precipitates, (b) its effect on the transformation kinetics of austenite to lower temperature microconstituents thus determining the microconstituents present for a given heat treatment, and (c) its interaction while in solution with other alloying elements.

Carbon readily combines with many elements to produce carbides. Carbide-forming alloying elements often introduced into creep-resistant ferritic steels include chromium, molybdenum, vanadium, titanium, and niobium. The type, size, distribution, and morphology of carbide precipitates that result are controlled by the amount of carbon and alloying elements added to the steel. Because of the strength loss associated with increased precipitate spacing, it is desirable to produce a large volume fraction of precipitate in the microstructure. Thus, when the carbides grow in response to elevated temperature exposure, the particle-particle spacing grows at a slower

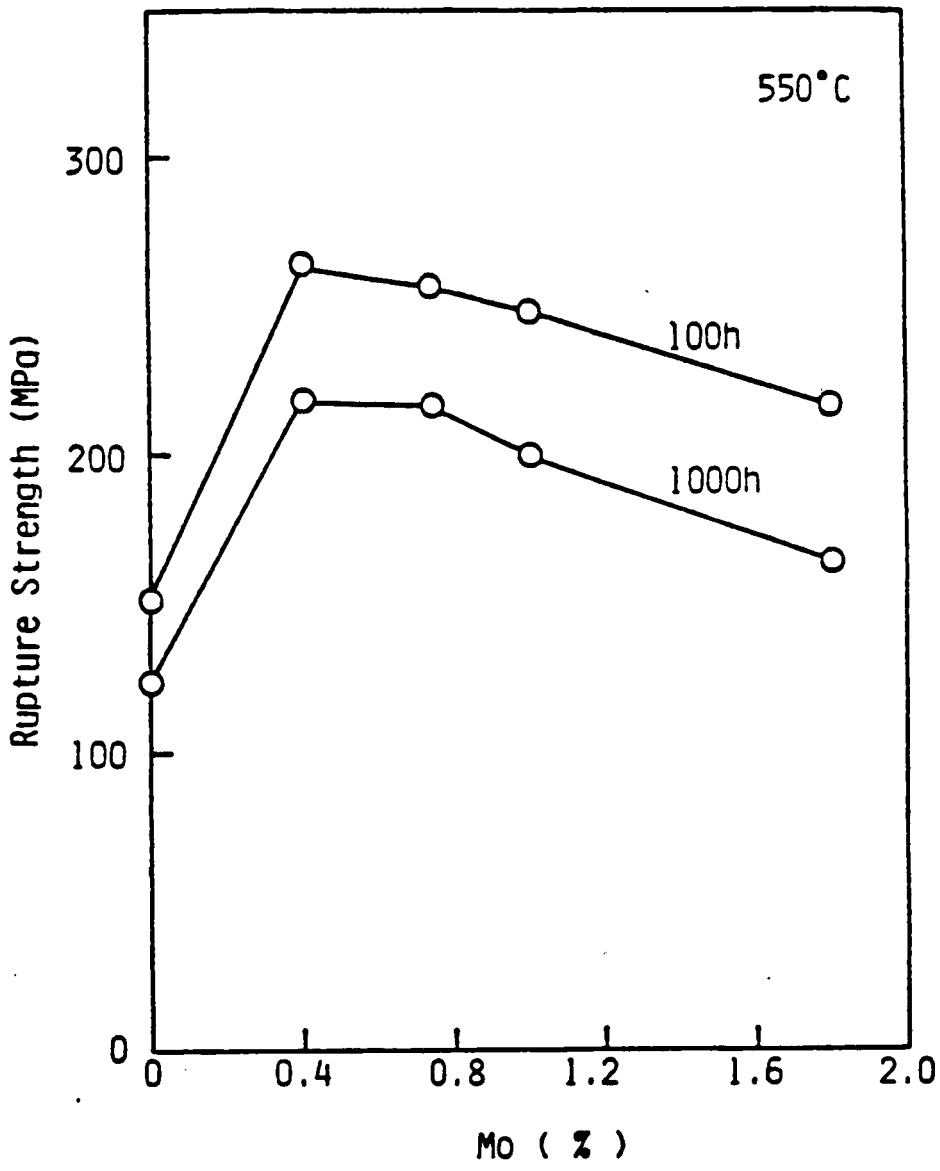


Figure 15. Effect of molybdenum content on the rupture strength of 2¼Cr-1Mo-¼V steel at 550°C.

Source: Prescott, G. R. and Braun, C. F., "Update on Modified 2-1/4Cr-1Mo and 3Cr-Mo Alloys," MPC, HPV-7 (1983).

rate. This argument leads to the conclusion that higher carbon steels should be used to increase the volume fraction of carbides. Analyses have indicated that optimum creep properties are obtained for carbon levels in the range of 0.1 to 0.2 weight percent (37). However, such a practice may lead to a steel with unacceptable ductility, weldability, and impact toughness (37).

Because the carbon level in a steel has a pronounced effect on hardenability (65), it is at least partly responsible for determining the microconstituents present as a function of cooling rate and thus indirectly affects the creep behavior of the steel. In 2-1/4Cr-1Mo steel, the microconstituents normally observed include ferrite and bainite. Martensite is attainable at high cooling rates and may occur in quenched and tempered steel, depending on the thickness. 2-1/4Cr-1Mo weld metal deposited with the SMA or SA process may be fully bainitic or a bainite/ferrite mix depending on such factors as carbon content, preheat/interpass temperature, and energy input. Kotecki (69) reports that for SA welds using 2-1/4Cr-1Mo filler metal with a manganese content below about 0.7 percent and a preheat/interpass temperature of 400^{o}F, some polygonal ferrite may form when the weld metal carbon content is less than 0.08–0.10 percent. A similar effect is observed for SMA welds. However, due to the lower energy inputs characteristic of this welding process, the carbon level below which polygonal ferrite is observed in the microstructure is somewhat lower. Kotecki (69) also indicates that the presence of polygonal ferrite in PWHT 2-1/4Cr-1Mo SA weld metal

leads to significantly inferior impact toughness relative to the fully bainitic materials.

Carbon plays a major role in "interaction" solid solution hardening (41,53), associating with certain alloying elements to form substitutional/interstitial clusters which can impede dislocation movement. In creep resistant ferritic steels with relatively low carbon contents, the carbon can be tied up in the form of alloy carbides and still leave sufficient quantities of carbide forming substitutional alloying elements in solution to contribute to this strengthening effect.

The relationship between carbon level and stress rupture strength has been a source of disagreement for some time. In 1965, Campbell (70) published a paper indicating that carbon content is not related to stress rupture strength in 2-1/4Cr-1Mo weld metal. His testing was done in the temperature range of 1050°F to 1200°F for rupture times up to 1800 hours and carbon contents of 0.04 and 0.10 weight percent. However, ten years later, Klueh and Canonico (58,71) observed both in 2-1/4Cr-1Mo base plate and in weld metal an increase in stress rupture strength with increasing carbon levels. It should be noted however, that their work was done at lower temperatures (850°F to 1050°F) for carbon contents in the range of 0.003 to 0.135 percent. Thus, test temperature appears to affect the strength dependence on carbon level with carbon being of little benefit at temperatures exceeding 1000°F (3). Figure 16 plots strength as a function of carbon content for 2-1/4Cr-1Mo steel (9). Inspection reveals that as the temperature increases, the

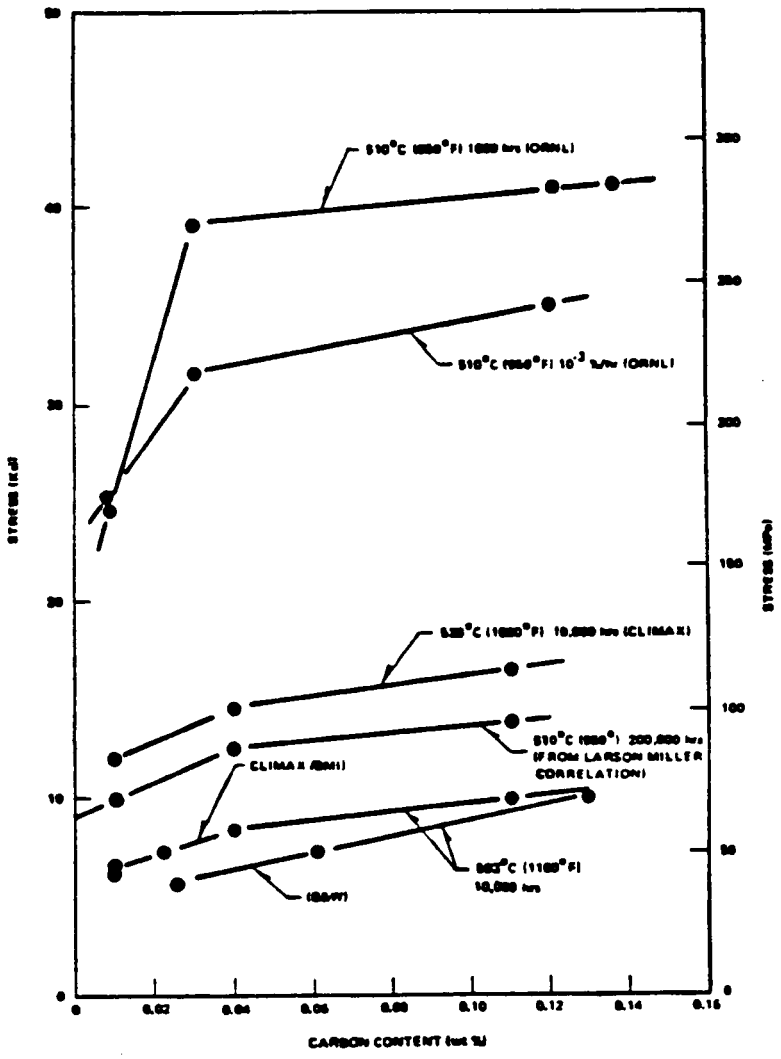


Figure 16. Effect of carbon content on the creep and rupture strength of 2¼Cr-1Mo steel. Each curve is labeled with the test temperature and conditions for which the strength was determined (i.e. creep test or rupture test).

Source: Copeland, J. F. and Licina, G. J., "A Review of 2-1/4Cr-1Mo Steel for LMFBR Steam Generator Applications," Symposium on Structural Materials for Service at Elevated Temperatures in Nuclear Power Generation, ASME, Houston, TX (1975).

strengthening effect of carbon decreases. This dependence may be due to the acceleration of carbide growth and evolution in response to increasing temperature and the accompanying depletion of alloying elements from the matrix to feed that growth.

The limited dependence of stress rupture strength on carbon content at constant temperature has been observed by others. Copeland and Licina (9) (see Figure 16) have stated that the beneficial effect of increasing the carbon level on stress rupture strength holds primarily for carbon contents less than about 0.04 percent. Zeisloft et al. (7) have indicated a similar behavior except with the cut-off at 0.08 percent carbon.

Vanadium

Vanadium is a strong carbide former (3,62) which is added to ferritic steels to improve strength, particularly stress rupture strength (3,64,67,68,72). The carbide formed, V_4C_3, is fine when first precipitated (62,67) and is responsible for much of the strengthening effect (50,67). V_4C_3 is relatively stable (72) at intermediate service temperatures but soon coarsens at 600°C (1112°F) (53). Vanadium has an even greater affinity for carbon than does molybdenum (62) (or chromium) and, as such, can have an additional strengthening effect on the steel by tying up the carbon and leaving the molybdenum in solution to strengthen the matrix.

The strengthening effects of vanadium are illustrated in the following examples taken from recent literature. Figure 17 is a graph of 0.2 percent proof stress (yield) and tensile strength as a

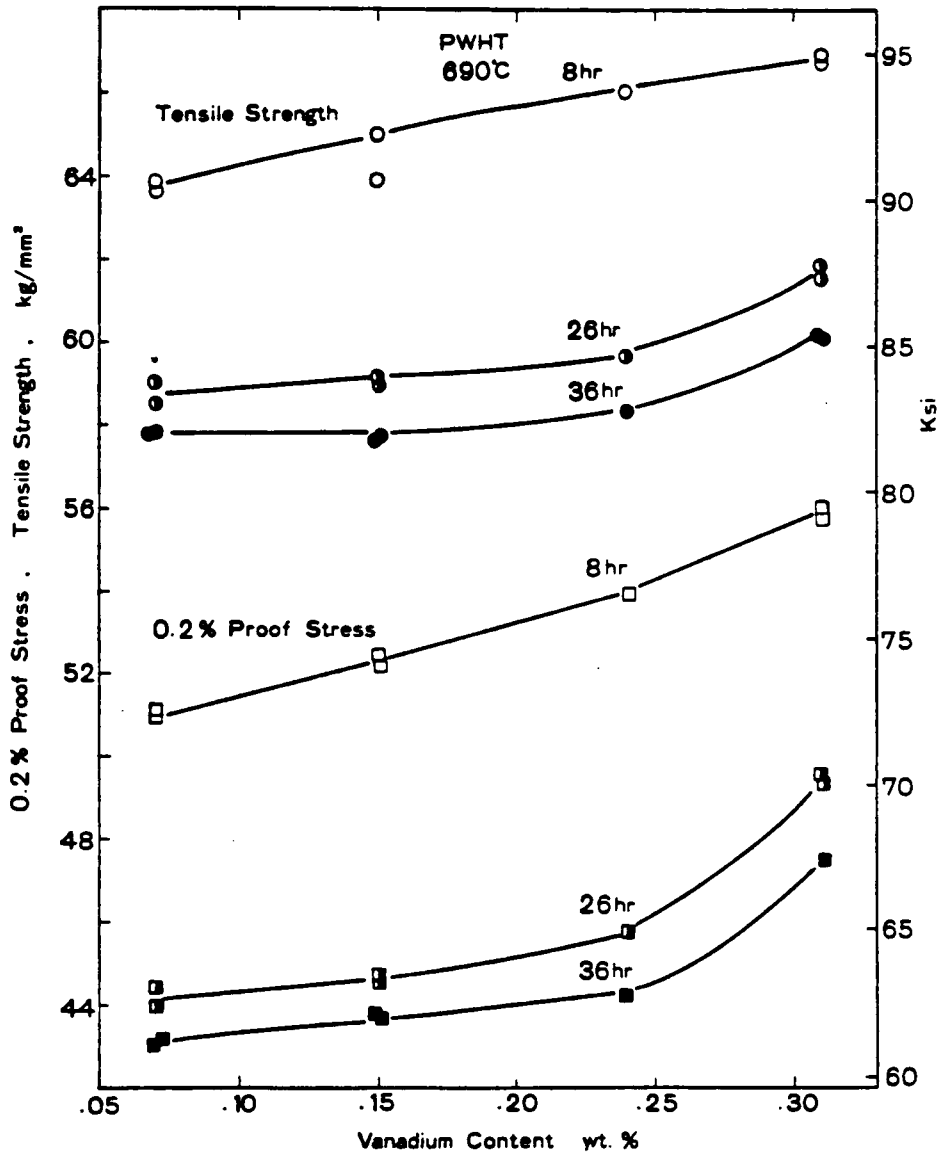


Figure 17. Effect of vanadium content on the room temperature yield and tensile strength of 3Cr-1Mo-V-Ti-B steel for three different tempering treatments.

Source: Mechanical and Metallurgical Properties of a 3Cr-1Mo-¼V-Ti-B Pressure Vessel Steel for Coal Liquefaction Reactor, NEDO/JSW Data Sheet, Sereies CLR-C, New Energy Development Organization, The Japan Steel Works Ltd. (1981).

function of vanadium content for 3Cr-1Mo-V-Ti-B steels (63). The vanadium level ranges from 0.07 to 0.31 percent. The plot shows that these room temperature properties improve continuously with increased vanadium content in this range, with the greatest strengthening seen between 0.24 and 0.31 percent. Kobe Steel has published test results for 3Cr-Mo steels with vanadium levels of 0 to 0.15 percent (68) (see Figure 14, p. 47). This graph of 1000 hour rupture strength at 550°C vs. alloy content indicates that rupture strength increases as the vanadium content is raised from 0.05 to 0.15 percent. The two curves for vanadium shown in Figure 14 are for steels heat treated to two different strength levels. Nippon Kokan (68) has reported that optimum elevated temperature properties and resistance to hydrogen attack are observed for a vanadium content of 0.1 percent vanadium. However, Kawasaki Steel (68) has reported stress-relief cracking problems for similar steels with this composition.

Titanium

Titanium is added to low alloy ferritic steels as a strengthener (particularly for elevated temperatures) (50,51,72,73,74), a stabilizer (50,75), and/or a deoxidizer (73,74). Strengthening by titanium addition results from the formation of fine TiC precipitates (50 to 100 Angstroms) in the matrix (50,72). The stabilizing effect of titanium on the microstructure arises from the resistance of TiC to coarsening at elevated temperatures. The persistence of these carbides as a fine precipitate inhibits degradation of the microstructure during creep, limiting loss of creep strength due to

microstructural change (50). Titanium has been used as a deoxidizer in SMA electrodes. One of these, Suprex B, is used to deposit weld metal with a nominal 2-1/4Cr-1Mo composition. Tests of the deposit indicate that its stress rupture strength is superior to that of other 2-1/4Cr-1Mo SMA electrodes (73,74).

The effect of titanium additions on the creep strength of 2-1/4Cr-1Mo steels has been specifically addressed by Pilling et al. (50) in a recent paper. They found that the addition of only 0.04 percent titanium results in a significant increase in creep strength at 565°C (1049°F). However, the amount of strengthening depends upon the carbon content. For a fixed titanium level and solution treatment temperature, the amount of titanium which goes into solution and is thus available for precipitation during tempering decreases as the carbon content increases.

These effects are substantiated by the following figures. Figure 18 is a dual plot of minimum creep rate and rupture life vs. stress for 0.09 percent carbon 2-1/4Cr-1Mo steel with and without a titanium addition. The benefit of adding titanium is indicated by the increased rupture life and decreased minimum creep rate for steel AF3. Figure 19, a graph of minimum creep rate as a function of carbon content for three steels austenitized at 950°C and containing 0.04 percent titanium, shows that creep rate increases (strength decreases) as the carbon content is elevated. Analysis has revealed that the volume fraction of TiC is greater in the lowest carbon specimen and falls off with increasing carbon level, lowering the creep strength.

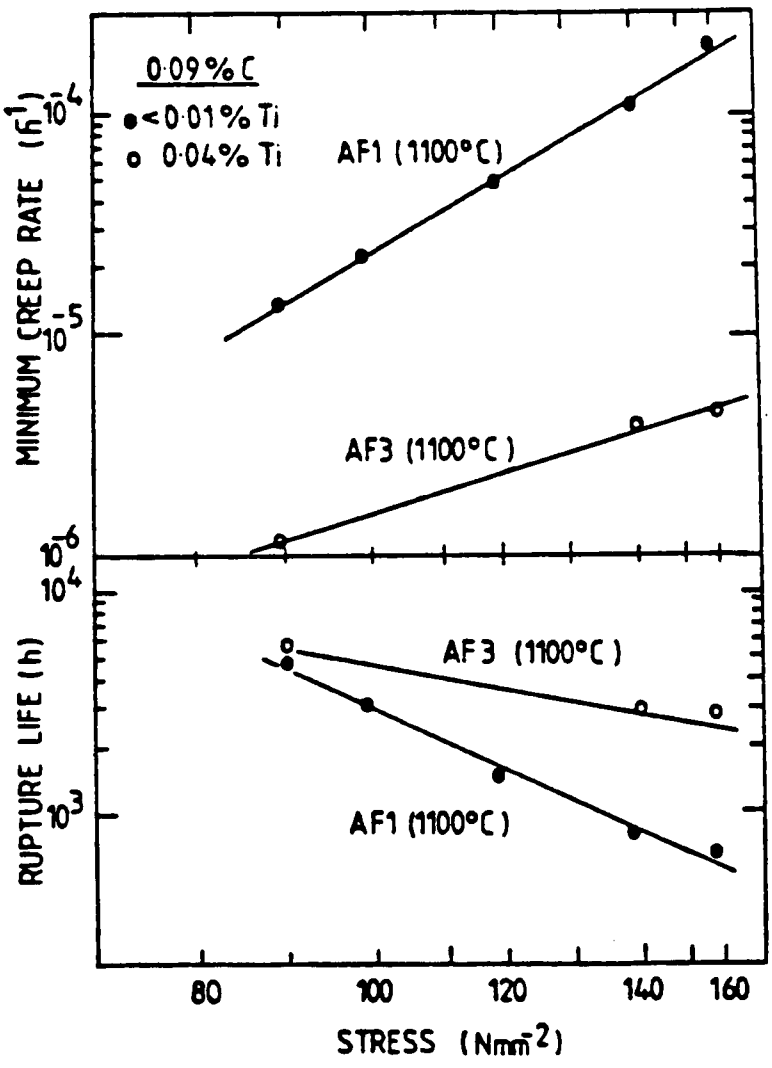


Figure 18. Minimum creep rate and rupture life as a function of applied stress for a titanium-free and a titanium-modified 0.09 percent carbon 2¼Cr-1Mo steel.

Source: Pilling, J., Ridley, N., and Gooch, D. J., "The Effect of Titanium on Creep Strength in 2.25Pct-1PctMo Steels," Met. Trans. A, 14A(7), 1443-1449 (1983).

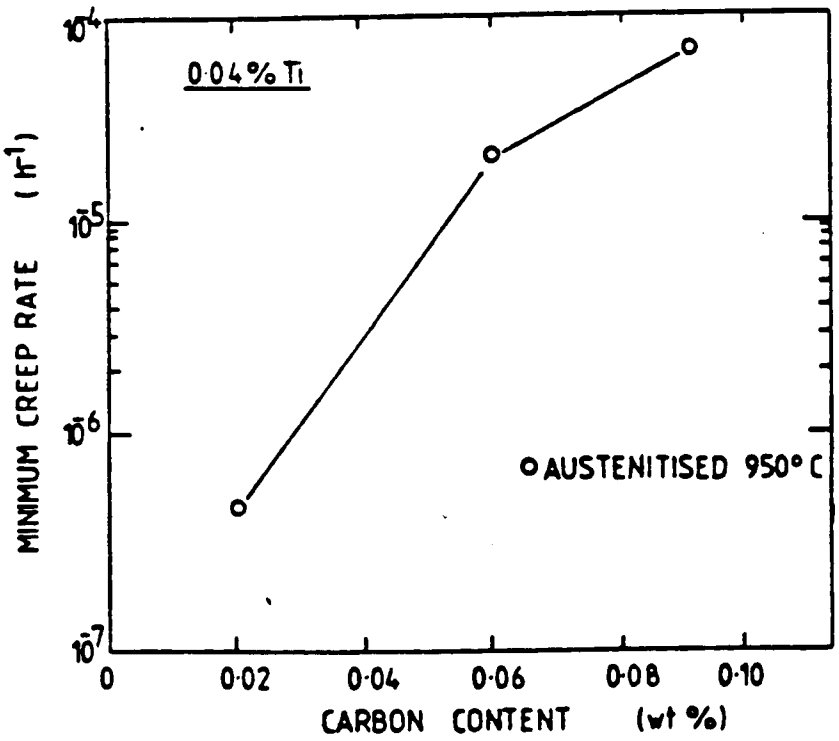


Figure 19. The variation in minimum creep rate for titanium-modified 2¼Cr-1Mo steel in response to changes in the carbon content.

Source: Pilling, J., Ridley, N., and Gooch, D. J., "The Effect of Titanium on Creep Strength in 2.25PctCr-1PctMo Steels," Met. Trans. A, 14A(7), 1443-1449 (1983).

The beneficial influence of titanium on creep strength is related to its effect on carbide stability, composition, and morphology (50). The acicular M_2C carbides normally found in 2-1/4Cr-1Mo steel are partially replaced by fine TiC precipitates in the Ti-modified steel. Furthermore, the M_2C carbides remaining are much smaller than in the titanium-free steel and contain up to 20 atomic percent titanium. The other more coarse Cr-Mo carbides present in the microstructure (M_7C_3,$M_{23}C_6$,M_6C) remain relatively unchanged in type and distribution. The stabilizing effect of titanium on the carbides is evident by the fact that during creep exposure at 565°C, the M_2C carbides in the titanium-free steel dissolve while the TiC and titanium-rich M_2C particles in the titanium-modified 2-1/4Cr-1Mo steel coarsen only slightly.

The benefit to stress rupture strength of titanium additions has been observed to depend on the presence of other alloying elements as well. Viswanathan (59) has stated that for 1-1/4Cr-1/2Mo steel tested at 538°C (1000°F), the addition of 300 ppm of titanium can have either a positive or negative effect on rupture strength depending on the impurity elements present in the steel. When phosphorus is a major impurity (300 ppm) with tin and antimony levels low, titanium has a detrimental effect on rupture strength. However, if the phosphorus content is lowered and the antimony and tin levels raised, titanium increases the strength. Finally, if boron is added (50 ppm), titanium is beneficial independent of the impurity levels.

Niobium

Relative to vanadium and titanium, niobium forms carbides which are the most stable. Austenitizing temperatures as high as 2370°F (76) are required to dissolve the niobium carbides in Nb-stabilized 2-1/4Cr-1Mo steel. The stability of these precipitates at elevated temperatures makes niobium an attractive alloying addition for the purpose of refining grain size (50), stabilizing the microstructure (75,76), and increasing elevated temperature strength (51,53,75,76,77) in low alloy ferritic steels.

To attain stress rupture strength in 2-1/4Cr-1Mo steel, niobium is added to create a fine dispersion of NbC precipitates in the microstructure. According to Argent et al. (53), the strength obtained is proportional to the square root of the volume fraction of NbC precipitated "on dislocations." Because of the stability of the carbides at elevated temperature and their pinning of dislocation networks in the microstructure, microstructural degradation during creep occurs slowly and the rupture strength is maintained well into the life of the specimen. Husselage and Dortland (77) have reported no significant microstructural changes occur in 2-1/4Cr1MoNiNb steel after creep testing for 3100 hours at 650°C. Creep strengthening of 2-1/4Cr-1Mo steel by niobium additions appears to yield superior strength for service temperatures up to about 930°F (76). Tests at 1020°F have shown that after about 5000 hours, the strength advantage over conventional 2-1/4Cr-1Mo steel is lost due to NbC coarsening (76).

Gooch (62) has indicated that the action of vanadium, titanium, and niobium in weld metal may be somewhat different than in base metal. In addition to carbon, these three elements also have a strong affinity for oxygen. Oxide and silicate inclusions in the weld metal absorb these carbide forming elements from the surrounding matrix by virtue of their oxygen content. As a result, in modified 2-1/4Cr-1Mo weld metal, the formation of V_4C_3, TiC, and NbC is suppressed and the carbides formed are more in keeping with those seen in the unmodified steel. In contrast, the inclusion content of base metal is often lower than in the weld metal. Thus, more V/Ti/Nb is left in the matrix to precipitate out as carbides.

Boron

Boron is added to steels to increase their hardenability by retarding the transformation from austenite to ferrite and pearlite (67,68). When used in this capacity, it must be accompanied by sufficient titanium to tie up the nitrogen in the microstructure. Boron's influence on creep and rupture strength is indirect and depends on the type and quantity of other alloying elements in the steel. As indicated in the discussion of titanium's effect on the creep strength of 1-1/4Cr-1/2Mo steel, the addition of 50 to 60 ppm of boron along with 300 ppm of titanium results in improved strength independent of the levels of tramp elements (P,Sb,Sn) (59). In the absence of titanium, adding boron alone to 1-1/4Cr-1/2Mo steel with varying levels of phosphorus, antimony, and tin appears to have an uncertain effect on rupture strength. In steels with relatively

high phosphorus levels (300 ppm), boron additions increase time to rupture (78) but also elevate the minimum creep rate, an apparent inconsistency. Investigation reveals however that the high phosphorus level increases the rupture ductility, allowing greater reduction in area before failure.

Silicon and Aluminum

Silicon and aluminum are typically added to steel during its manufacture as deoxidizers (65). Both elements are considered to have a negative effect on creep strength. Silicon's effect is particularly detrimental at service temperatures in the range of 950°F to 1200°F (3). Recent work aimed at improving the creep behavior of 2-1/4Cr-1Mo and 3Cr-1Mo steels has involved the reduction of silicon levels. Kawasaki Steel's study of 2-1/4Cr-1Mo steel has indicated that there is a noticeable improvement in stress rupture strength when the silicon content is reduced from 0.4 percent to 0.08 percent (79). Graphically illustrated in Figure 20, this effect is thought to be due to a slowing of molybdenum-precipitate coarsening resulting from the silicon reduction. Referring back to page 46, Figure 13 is a graph of 1000 hour rupture strength at 550°C as a function of alloy content for 3Cr-1Mo steel. This plot shows that rupture strength begins to fall once the silicon content is increased beyond about 0.06 percent (68).

The reduction of creep strength by aluminum is thought to stem from two causes. First, the aluminum in its deoxidizing role forms highly stable oxides which have a grain refining effect on the

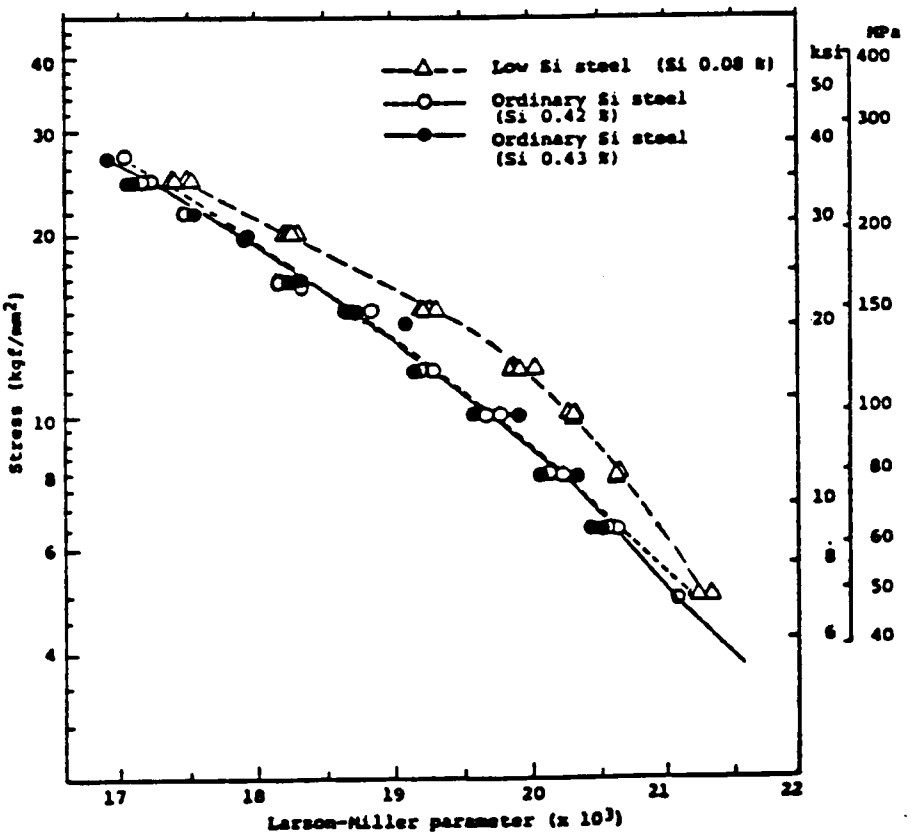


Figure 20. Comparison of Larson-Miller parameter curves for a low silicon (0.08% Si) 2¼Cr-1Mo steel and steels of the same type having "typical" 2¼Cr silicon levels (0.42%, 0.43% Si)

Source: Improvement in High Temperature Properties of Heavy Section 2-1/4Cr-1Mo Steel, Kawasaki Steel Corporation (1982).

microstructure during cooling from temperatures above the A_3 (65,80). Traditionally, creep strength is associated with larger grain size. Thus the grain refining action reduces strength. Second, the aluminum combines with dissolved nitrogen to form nitrides, thus preventing it from combining, along with carbon, with the strengthening elements to form carbonitrides (65).

Tin, Phosphorus, and Antimony

Tin, phosphorus, and antimony are impurity elements in low alloy ferritic steels. Their influence on creep and rupture strength has been studied when present individually or in combination with each other. Hopkin and Jenkinson (81) have investigated the effect of 0.1 percent tin on the creep resistance of 2-1/4Cr-1Mo steel. Figure 21 is a graph of creep strain vs. time for tin-bearing and tin-free steel in the normalized and tempered condition (tempered 1 hour at 700°C). It shows that the tin-bearing 2-1/4/Cr-1Mo steel has a noticeably greater strain rate than the tin-free alloy with the difference greater for higher stresses and test temperature.

Work on the effect of phosphorus level on creep in 2-1/4Cr-1Mo steels with carbon levels of 0.02, 0.06, and 0.09 percent has been done by Pilling et al. (82). They have reported that the addition of 0.05 percent phosphorus increases the minimum creep rate with the magnitude of the increase directly related to the carbon content. Despite this evidence, the rupture life of the steels is not adversely affected except in the case of the 0.09 percent carbon material (which also exhibits greater rupture ductility). Figure 22

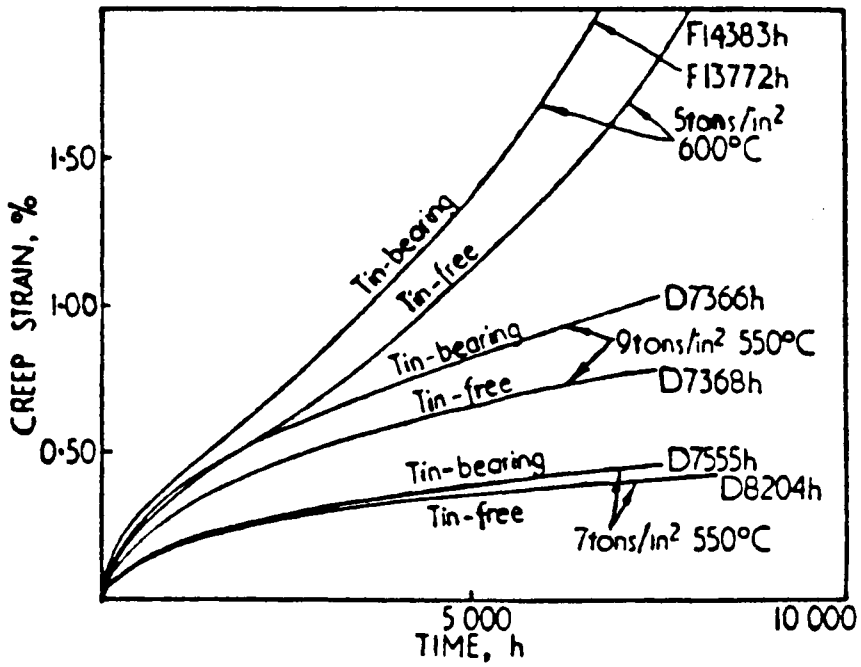


Figure 21. Comparison of creep curves for normalized and tempered 2¼Cr-1Mo steel with and without a tin addition (0.1% vs. 0.002% Sn).

Source: Hopkin, L. N. T. and Jenkinson, E. A., "Creep Resistance and Metallographic Structure of 2-1/4Cr-1Mo Steel with and without a Tin Addition," JISI, 200(5), 356-359 (1962).

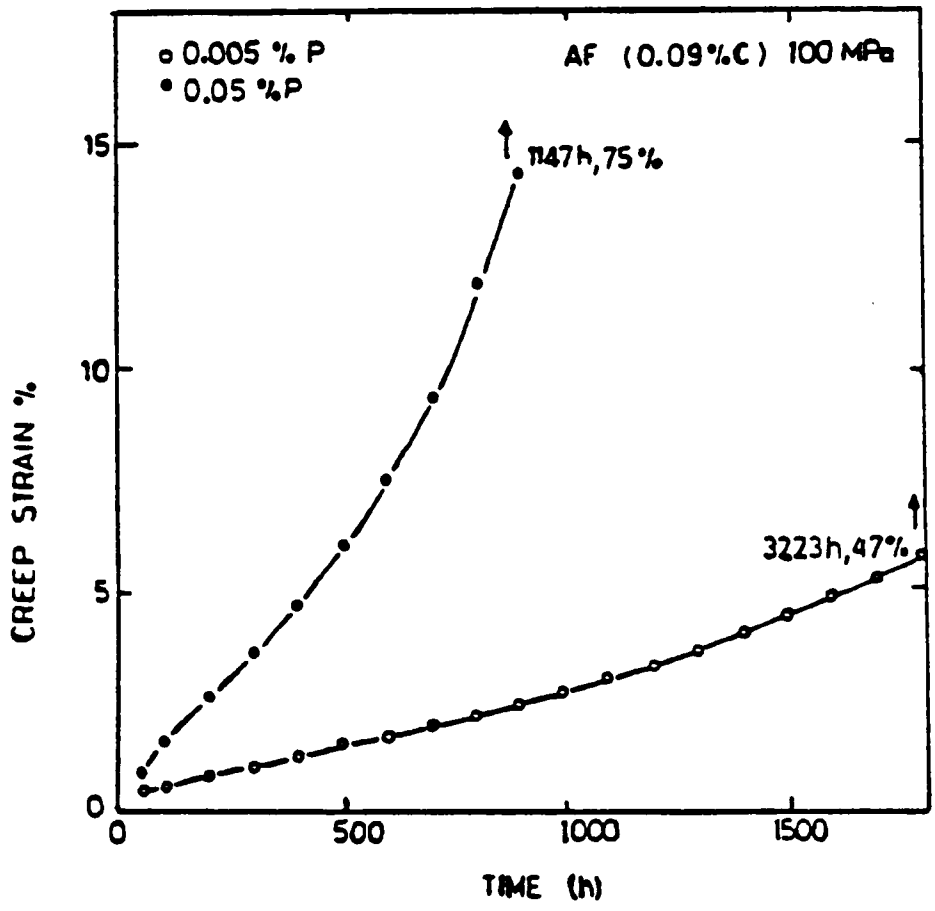


Figure 22. Comparison of creep curves for 2¼Cr-1Mo with and without a phosphorus addition (0.05% vs. 0.005% P).

Source: Pilling, J., Ridley, N., and Gooch, D. J., "The Effect of Phosphorus on Creep in 2.25%Cr-1%Mo Steels," Acta. Met., 30(8), 1587-1595 (1982).

compares the creep behavior of 0.09 carbon 2-1/4Cr-1Mo steel in the phosphorus-doped and phosphorus-free condition. The creep rate of the doped steel is significantly higher. Metallographic examination reveals that the phosphorus seems to accelerate M_2C dissolution in the high carbon steel but not in the low carbon metal. It is theorized that phosphorus and molybdenum cosegregate to the grain boundaries with the molybdenum diffusing along the dislocation network formed by creep. In the low carbon steel, a significant amount of molybdenum is already in solution to feed the segregation and the M_2C precipitates are unaffected. However, in the high carbon steel, virtually all of the molybdenum is contained by the carbides. Thus the affinity of the diffusing phosphorus atoms for molybdenum results in the induced dissolution of the M_2C. The loss of M_2C in the 0.09 percent carbon material weakens the matrix and results in higher creep rates and rupture ductility. The 0.021 percent carbon steel, having lost no M_2C, is relatively unaffected.

In combination, the elements, tin, phosphorus, and antimony can influence the action of other strengthening additions. Viswanathan (78) has indicated that the combined addition of large amounts of these three elements to 1-1/4Cr-1/2Mo steel does not affect the short time creep strength or ductility of the material measured at 538°C (1000°F). However, the relative amounts of these impurities can determine whether the addition of boron has a beneficial or detrimental effect on creep properties. In another paper, Viswanathan (59) states that similar interactions between impurity

and strengthening alloying elements occur for titanium and titanium plus boron.

Manganese and Nickel

Manganese and nickel are added to low alloy ferritic steels for a number of reasons. One function of manganese is to tie up the sulfur in steel in the form of MnS inclusions (65). This prevents the formation of FeS which can lead to hot tearing. Both manganese and nickel increase hardenability by retarding the formation of ferrite and pearlite on cooling from austenitizing temperatures (67). Chung et al. (83) have experimented with 2-1/4Cr-1Mo steel, investigating the effect of varying manganese and nickel additions. They report that adding 1.0 percent manganese results in a 30 percent reduction in short time rupture strength (maximum rupture time, 1000 hours) at 600°C and a 15 percent decrease at 500°C. An alloy with 0.5 percent manganese and 0.5 percent nickel suffers a strength reduction only half that of the 1.0 percent manganese formulation. Doubling the nickel level to 1.0 percent while holding the manganese constant does nothing to decrease the strength any further. Sachs et al. (67) have seen similar trends in 2-1/4Cr-1Mo steel tested at 621°C. High levels of manganese and nickel (manganese up to 1.7 percent, nickel up to 2.2 percent) reduce rupture life considerably relative to conventional 2-1/4Cr-1Mo steel. This negative effect decreases as the manganese and nickel contents are decreased.

4. STRESS RUPTURE DATA ANALYSIS

The objective of stress rupture testing is to gather data on rupture time as a function of applied stress and test temperature for a particular material with the goal of characterizing its behavior sufficiently so as to permit establishment of allowable stress levels for design purposes. Structures or components to be used at elevated temperatures are generally expected to operate for a minimum of 100,000+ hours. Since it is impractical to test material for such long periods to determine the design stresses associated with that life, data are collected for shorter rupture times and analyzed to determine the relationship between stress and rupture time. Then extrapolations to 100,000 hours are made and the stresses thus obtained used to develop design criteria.

Log Stress/Log Rupture Time

Many methods have been evolved as suitable for data analysis and extrapolation. By far, the simplest technique involves plotting log stress vs. log rupture time. This method takes advantage of the fact that data plotted in this manner, in general, fall on a straight line. Linear regression techniques are applied and the coefficients which define the equation of the best fit straight line derived. It is then a simple matter to extrapolate to rupture times of 100,000 hours and determine the associated stress. However, implicit in this method is the assumption that the behavior is linear to 100,000+ hours. Unfortunately, at elevated temperatures, many metallurgical systems are not microstructurally stable. Significant

microstructural change in the rupture specimen during the test will alter the slope of the log stress/log rupture time line. Relatively rapid changes, such as recrystallization, produce an abrupt change in slope, replacing the expected straight line with two straight line segments, joined at a point and having differing slopes. Gradual changes such as oxidation, grain growth, or precipitate growth/evolution produce a gradual slope change, causing the line to become curved. Instabilities are more prevalent at high stresses or temperatures. Wilson (57) has indicated that, for 2-1/4Cr-1Mo steel, the straight line log stress/log rupture time approach is not dependable for test temperatures above about 1000^{o}F.

Time-Temperature Parameters

Another data analysis technique involves the use of time/temperature parameters. These parameters are based on an Arrhenius type equation. Invoking the Arrhenius relation implies that creep to rupture is a thermally activated process governed by a single mechanism. However, as stated by Goldhoff (86), studies have shown that there can be many deformation mechanisms at work during creep rupture. Thus the basis for the parameter approach is not theoretically rigorous. Despite this fact, parameters are widely used in the analysis of rupture data and can be quite useful. The technique has the advantage that all of the data for a given heat of material taken at various temperatures can be depicted on a single master curve. Four of the more common parameters in use are

Orn-Sherby-Dorn, Larson-Miller, Manson-Haferd, and Manson-Succop (86).

The latest data analysis techniques make extensive use of computers and are not as rigid in assigning an a priori relationship between stress, rupture time, and temperature. Among others, Booker (87,88) and Manson (89,90,91) are currently active in this field. Booker's approach utilizes a computer program which requires an input consisting of a list of the possible terms to be used to construct a parametric relation and the stress rupture data. The program then combines the terms to generate a multiplicity of parametric equations, fits the data to each, then outputs a ranked list of the models which give the best fit. It is then up to the analyst to choose the fit which not only describes the data well but also predicts reasonable behavior for the material upon extrapolation.

Minimum Commitment Method

Although originally designed to allow the rupture data to determine the exact form of the parametric relation used to describe a material's stress rupture behavior, Manson's minimum commitment method (MCM) (89,90,91) has evolved into a form which uses a fixed analytical expression. In its most general form, the MCM relation is given by

$$\log(t_r)(1+AQ)+Q=G \qquad (2)$$

where "t_r" is the rupture time in hours, "Q" is a function of temperature, "G" is a function of stress, and "A" is a structural

stability factor characteristic of the material. The value of "A" is usually small and is often set to zero. The temperature function, "Q", has been defined as

$$(3) \qquad Q=R_1(T-T_m)+R_2([1/T]-[1/T_m])$$

where "T" is the absolute test temperature, "T_m" is an absolute temperature at the mid-range of the data, and "R_1" and "R_2" are regression constants. The minimum commitment method has been applied to the analysis of multiple heats of data. For this application, the stress function, "G", is given by

$$(4) \qquad G=B+C\log(s)+Ds+Es^2$$

In this equation, "B", "C", "D", and "E" are constants determined by regression and "s" is stress. In the multi-heat case, the terms "B" and "Clog(s)" are heat centering terms and, as such, the values of "B" and "C" change for each heat of material.

Manson has published a computer program (91) suited for running on a desk-top personal computer which performs the MCM analysis on multi-heats of data. All data are input into the program in a single file. The program does the analysis and then prints out the values of the constants which, when inserted in the MCM relation, describe the rupture behavior of each heat of material as well as the average behavior of all of the data considered as a single population.

5. SUMMARY

The preceding literature review has discussed, in detail, the microstructure of 2-1/4Cr-1Mo steel (base metal and weld metal) and its effect on stress rupture properties. In addition, the effects of

elevated temperature exposure (PWHT, tempering, in service exposure) and chemical composition have also been addressed. Finally, a brief discussion of some of the analytical techniques currently being used to characterize the stress rupture behavior of materials based on data collected during rupture testing has been presented.

The important points concerning the microstructure of 2-1/4Cr-1Mo steel are summarized as follows:

a. Depending on the cooling rate from temperatures above the A_3 during welding or heat treatment, the microstructure obtained is typically bainitic or ferritic/bainitic. Cooling rate is controlled by the cooling method employed, the weld energy input, the preheat/interpass temperature, and the member size and thickness. The amount of ferrite formed can also be influenced by the carbon content of the material. Under extremely rapid cooling conditions, martensite may also form.

b. The alloy carbides in the microstructure precipitate and evolve according to a complex scheme determined by Baker and Nutting (17). The details of the scheme are similar for martensitic and bainitic microstructures but differ significantly for ferrite.

c. The evolution of the carbides in 2-1/4Cr-1Mo weld metal appears to be slowed by increases in carbon content.

The influence of microstructure on stress rupture strength may be summarized as follows:

a. The primary strengthening alloy carbide in 2-1/4Cr-1Mo steel is M_2C. This precipitate can form in any of the microconstituents found in 2-1/4Cr-1Mo steel (martensite, bainite, ferrite) but persists during tempering for a much longer time in the ferrite.

b. Prolonged exposure to elevated temperatures results in a continuous decrease in stress rupture strength as a result of carbide evolution, coarsening, spheroidization, and agglomeration.

c. The loss of strength described in "b" above may be significantly slowed by the addition of strong carbide formers such as titanium or niobium which precipitate as MC carbides. These precipitates are effective creep strengtheners and are more stable than M_2C.

d. Significant increases in stress rupture strength may be realized by mild tempering or PWHT treatments to produce a material with high room temperature tensile strength. However, the strength advantage thus obtained decreases with increasing service temperature and is insignificant above about $900^{0}F$.

e. The strength of all 2-1/4Cr-1Mo steel, however heat treated, approaches a common value given sufficient time at temperature as the microstructure evolves to one of overaged equilibrium carbides in a carbon-saturated ferrite matrix.

f. The influence on rupture strength of introducing polygonal ferrite into an otherwise bainitic material is not clear.

g. Solid solution strengthening plays a minor role in conferring stress rupture strength to 2-1/4Cr-1Mo steel. Interactions between substitutional (chromium, molybdenum) and interstitial (carbon, nitrogen) atoms are described.

h. Some evidence exists that the stress rupture strength of fully bainitic 2-1/4Cr-1Mo steel increases with decreasing prior austenite grain size.

The effects of individual alloying elements may be summarized as follows:

a. Decreased rupture strength has been associated with increases in levels of chromium, silicon, aluminum, and manganese.

b. Improved rupture strength is obtained by increasing the levels of molybdenum, vanadium, titanium, and niobium.

c. Stress rupture strength increases as the carbon content is increased. However, the effect is only significant for carbon levels below about 0.04 percent. Furthermore, as the temperature increases, the strengthening effect decreases until at 1000^{o}F, the strength advantage becomes insignificant.

d. The influence of boron additions on rupture strength is not clear and appears to depend on the levels of other elements present including titanium, phosphorus, tin, and antimony.

e. Tin and phosphorus appear to increase the creep rate with the latter also increasing the rupture ductility. The influence of phosphorus is further bolstered by increases in the carbon content.

f. At levels up to 1.0 percent, increases in the nickel content do not affect rupture strength.

The discussion of the analysis of stress rupture data may be summarized as follows:

a. The objective of stress rupture testing is to gather data on rupture time as a function of applied stress and test temperature for a particular material with the goal of characterizing its behavior sufficiently so as to permit establishment of allowable stress levels for design purposes.

b. Some of the analytical techniques currently employed in rupture data analysis include the log stress/log rupture time method, various time/temperature parameter methods, and the Manson minimum commitment method.

CHAPTER 3

MATERIALS AND EXPERIMENTAL PROCEDURE

The goal of this program was to investigate the effect of carbon content and PWHT on the stress rupture strength of 2-1/4Cr-1Mo filler metals. In order to establish the correlation between carbon level and rupture strength, rupture testing of weld metals with carbon contents in the range of 0.02 to 0.13 weight percent was conducted. For this phase of the study, the PWHT selected was 1300°F/25 hrs. Secondly, the effect of PWHT on the rupture strength of 0.08-0.09 carbon weld metal was evaluated using a PWHT of 1175°F/25.5 hrs.

In support of the rupture testing effort, extensive microstructural examination of the above weld metals in the as-welded, PWHT, and rupture tested condition was performed using the SEM and STEM. This microstructural work was aimed at characterizing the microstructure as a function of carbon content and PWHT with the ultimate goal of correlating the microstructure with the stress rupture properties. SEM examination of the weld metals revealed the dependence of microconstituent morphology on prior material history. Furthermore, to obtain information on the type, size, morphology, distribution, and composition of the alloy carbides present, STEM examination of carbide extraction replicas taken from weld metal specimens was also conducted.

Weld metal specimens were thermally cycled on the Gleeble using a variety of thermal cycles designed to simulate the thermal history occurring in the coarse-grained region of the HAZ during welding.

Cooling conditions were chosen to span the normal range of weld energy inputs characteristic of welds in heavy-section Cr-Mo materials. A dilatometric technique was employed to detect the weld metal transformation during cycling and the data obtained used to construct CCT diagrams. SEM examination of the resulting microstructures were then performed to determine the microconstituents produced as a consequence of the thermal history.

1. MATERIALS

Four 2-1/4Cr-1Mo weld metals were used in this program with carbon contents of 0.02-0.03, 0.04-0.05, 0.08-0.09, and 0.12-0.13 weight percent. The carbon range is given instead of a fixed value reflecting the variability observed in the carbon level from analysis to analysis. This variation most probably results from the inhomogeneity of weld metal deposits as well as from statistical variation in the analysis results. The chemical compositions of the four weld metals studied are shown in Table 3.

The weld metal specimens were made from material extracted from shielded metal arc weldments. These weldments were fabricated in 2-1/4 to 2-1/2 inch thick SA 387 Grade 22 plate using a single-V groove preparation employing a backing bar. The chemical composition of the base plate is given in Table 3. The electrodes used were all of the E9018-B3 type, except for those utilized to make the 0.02-0.03 carbon weldment which were E9015-B3L electrodes. Welding was conducted using good low hydrogen practice, a preheat temperature of 300^{o}F, and an interpass temperature of 500^{o}F. Subsequent to the

Table 3. Chemical composition of base metals and weld metals employed in the study.

	Base Metal		Weld Metal			
Element	BP-1	BP-2	0.02-0.03C	0.04-0.05C	0.08-0.09C	0.12-0.13C
C	0.11	0.11	0.024	0.045	0.091	0.13
Mn	0.39	0.38	0.96	0.66	0.59	0.52
P	0.010	0.011	0.019	0.013	0.010	0.010
S	0.018	0.022	0.024	0.018	0.014	0.013
Si	0.18	0.29	0.75	0.31	0.39	0.37
Cu	0.17	0.15	0.11	0.08	0.024	0.027
Ni	0.23	0.15	0.09	0.08	0.033	0.036
Cr	2.29	2.07	2.39	2.31	2.48	2.52
Mo	1.15	0.88	1.20	1.11	1.17	1.18
V	0.003	0.004	0.006	0.014	0.015	0.008
As	0.016	0.007	0.026	0.017	0.003	0.003
Sb	0.003	0.009	0.002	0.002	0.004	0.004
Sn	0.012	0.012	0.008	0.003	0.002	0.002
Al	ND*	0.008	ND	ND	0.014	0.013
B	ND	0.0003	ND	ND	0.0004	0.0004

*ND - Not Determined

completion of welding, each weldment was post-heated at 400°F for 4 hours and then cooled in still air. Details of the groove geometry, electrode type and size, as well as welding parameters are summarized in Table 4.

2. STRESS RUPTURE TESTING

To determine the effects of carbon content and PWHT on stress rupture strength, rupture testing of the 2-1/4Cr-1Mo weld metal was conducted in two phases. In the first phase, specimens of weld metal PWHT 1300°F/25 hrs. and having carbon contents of 0.02-0.03, 0.04-0.05, 0.08-0.09, and 0.12-0.13 weight percent were rupture tested at 850, 950, and 1050°F, temperatures selected as being representative of the current and anticipated operating range of 2-1/4Cr-1Mo pressure vessels. The PWHT employed produced Class 2 properties (as defined for SA 387 Grade 22 steel) in the weld metal. The tensile strength range for this class of material is 75 to 100 KSI.

In phase 2, only the 0.08-0.09 carbon weld metal was studied. This material, PWHT 1175°F/25.5 hrs., was rupture tested at 950 and 1050°F. The phase 2 PWHT produced weld metal properties in agreement with those proposed by the Metal Properties Council (93) for a new class of SA 387 Grade 22 steel, i.e. Class 3. This proposed class of SA 387 has an allowable tensile strength range of 90 to 110 KSI.

Stress rupture specimens tested in this program consisted of 100 percent weld metal and were fabricated with their longitudinal axis parallel to the welding direction. As shown in Figure 23, the

Table 4. Welding procedure and parameters employed in fabrication of the 2-1/4Cr-1Mo SMA weldments.

Weldment I.D.	Base Plate I.D.	Thickness	Type	Angle	Root	Electrode Type	Dia.	Arc Voltage	Current
0.02-0.03C	BP-1	2 1/4"	Single V	25°	3/4"	E9015-B3L	1/8"	24-28 V	145 A
							5/32"	24-28 V	195 A
0.04-0.05C	BP-1	2 1/4"	Single V	18°	1/2"	E9018-B3	1/8"	24-28 V	135 A
							5/32"	24-28 V	180 A
0.08-0.09C	BP-2	2 1/2"	Single V	30°	3/4"	E9018-B3	5/32"	24-28 V	160-210 A
							3/16"	24-28 V	220-290 A
0.12-0.13C	BP-2	2 1/2"	Single V	30°	3/4"	E9018-B3	5/32"	24-28 V	160-210 A
							3/16"	24-28 V	220-290 A

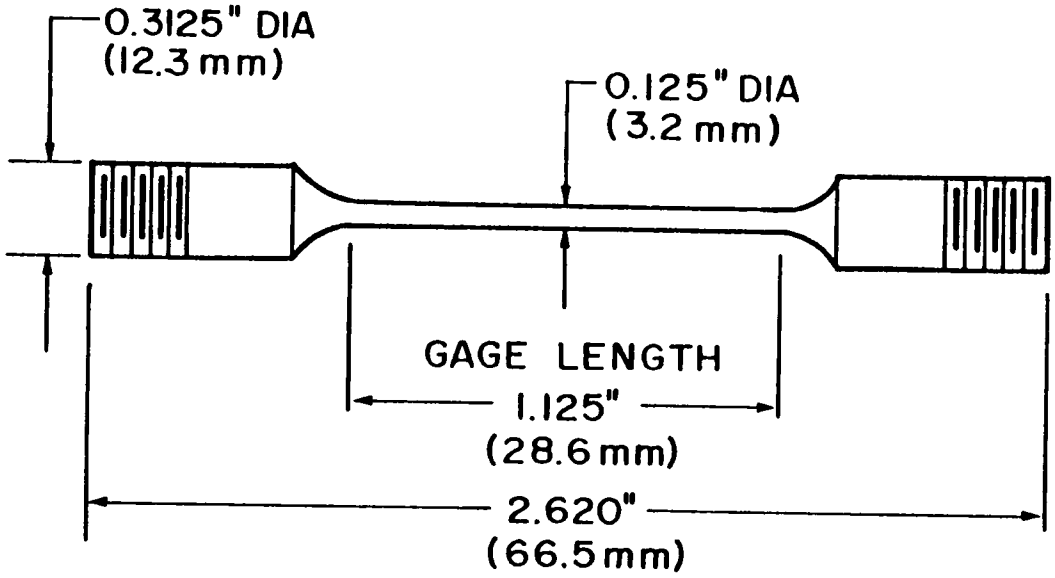


Figure 23. Stress-rupture test specimen.

Source: Pendley, M. R., "High Temperature Properties of 2-1/4Cr-1Mo Steel Weld Metals," M. S. Thesis, University of Tennessee, Knoxville, TN (1980).

specimen gage length was 1.125 inches with a gage diameter of 0.125 inches. The small size of the rupture specimen not only increased the number of specimens which could be fabricated from a given length of weldment, but also kept the load requirements necessary to obtain rupture times in the range of ten to several thousand hours within the capabilities of the testing apparatus.

Rupture testing was conducted on eight constant load, dead-weight creep frames. Each frame contains a three-zone furnace with the power level for each zone being independently adjustable. Each furnace is controlled by a Leeds and Northrup Electromax III controller which utilizes a chromel-alumel thermocouple to monitor the temperature at the center of the middle zone. All furnaces were profiled and the zone controls used to obtain a constant temperature profile over the specimen gage length ($\pm 1^{o}F$).

Each specimen was mounted in a testing frame and suspended within the creep frame furnace. See Figure 24 for a schematic view of the test geometry. A chromel-alumel thermocouple wired to the center of the specimen gage length was connected to a digital temperature meter which, in turn, was used to monitor the temperature of the specimen during testing. To minimize the convection of air through the furnace, both the top and bottom orifices of the furnace were packed with ceramic wool. At the beginning of each test, the specimens were heated to the desired temperature and stabilized there before any load was applied. Loading was in uniaxial tension with the load a constant throughout the test. In addition to temperature,

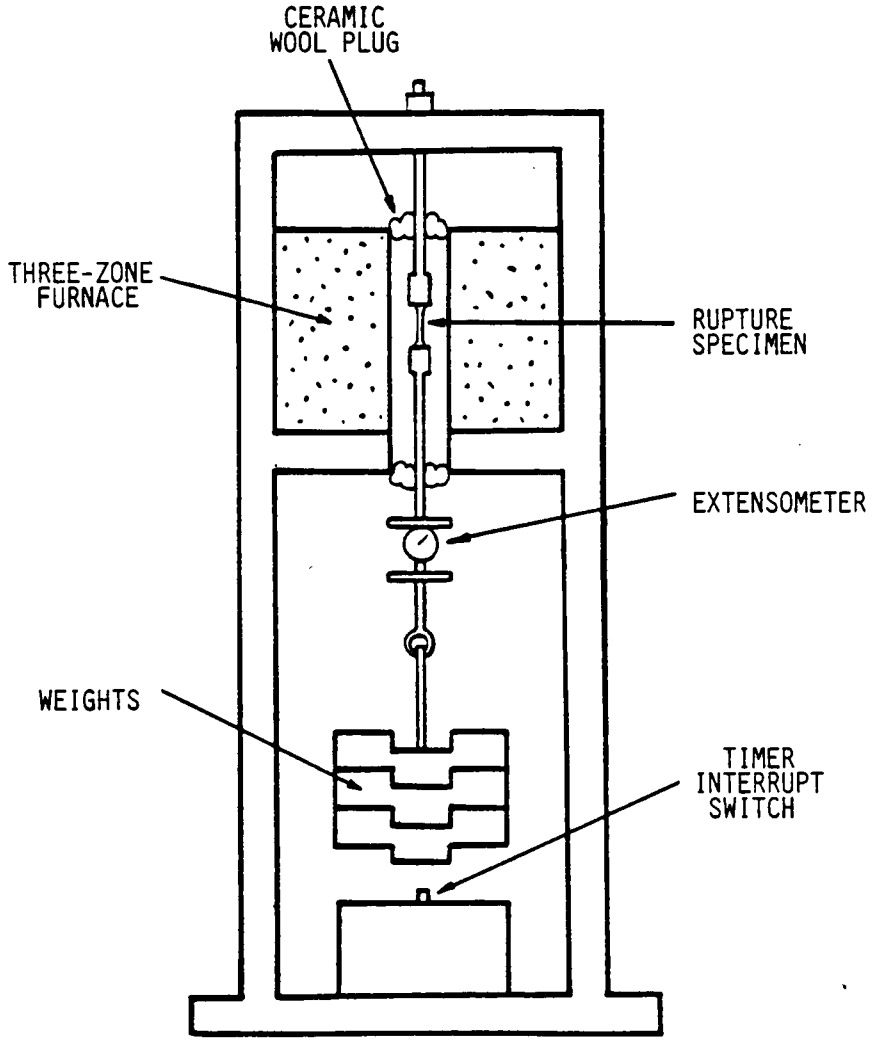


Figure 24. Schematic of creep frame with specimen in place.

Source: Pendley, M. R., "High Temperature Properties of 2-1/4Cr-1Mo Steel Weld Metals," M. S. Thesis, University of Tennessee, Knoxville, TN (1980).

specimen extension, measured by a dial gauge attached to the testing frame, was also recorded as a function of time.

The obtained SMA weld metal rupture data were analyzed using three techniques; (a) the log stress/log rupture time method, (b) the Larson-Miller parameter method, and (c) the Manson minimum commitment method. The results were examined to determine the effect of carbon content and PWHT on stress rupture strength. Comparisons of the 100,000 hour stress predictions derived using each method were also made.

In an attempt to gain further insight into the dependence of the rupture strength of weld metal on carbon content and PWHT, additional rupture data were collected from the literature with the restriction that only data from tests of 100 percent weld metal specimens in the PWHT condition be considered. During the compilation, data from all welding processes were considered. However, because the thesis research dealt primarily with SMA weld metal, a second abbreviated set of data consisting of only SMA material was created.

In order to facilitate determination of the correlation between stress rupture strength and both carbon content and PWHT, the augmented data were partitioned using two criteria. First the data were separated by temper parameter (P), the value of which is directly related to the degree of PWHT. Based on the work done by Baker and Nutting (17) to describe the carbides in 2-1/4Cr-1Mo steel as a function of tempering time and temperature (see Figure 4, p.24), average temper parameter values characteristic of the regime boundaries in the figure were calculated and used to define the

dividing points for the data base. The resulting temper parameter ranges employed were P<32.0, 32.0<P<36.2, 36.2<P<37.5, and P>37.5. The second partitioning criterion was based on weld metal carbon content. Keeping in mind the dependence of rupture strength on carbon level reported by Copeland and Licina (9), the carbon ranges established were C<0.02, 0.02<C<0.04, 0.04<C<0.08, 0.08<C<0.12, and C>0.12. Partitioning by carbon level was performed within each temper parameter range so that observed variations in strength were minimally affected by PWHT variation.

For analysis of rupture data using the log stress/log rupture time approach, a model for stress as a function of rupture given by

$$\log(s)=A+B\log(t_r) \tag{5}$$

was assumed where "s" is stress in KSI, "t_r" is rupture time in hours and "A" and "B" are regression constants. Using linear regression analysis, a best fit straight line was calculated. Stress for 100,000 hour rupture was also obtained by extrapolation. Because this model does not include a temperature term, the above analysis had to be performed for each test temperature at which data were available.

Analysis of rupture data using the Larson-Miller parameter was also conducted. A parameter value for each data point was calculated using the equation,

$$LMP=(T+460)(C+\log[t_r])\times 10^{-3} \tag{6}$$

where "T" is the test temperature in degrees Fahrenheit, "C" is a constant, and "t_r" is the rupture time in hours. A value of 20 was used for "C" for all analyses and is generally accepted as an average

value applicable in most cases. After plotting the data on a log stress vs. Larson-Miller parameter graph, curves were fitted to the data using regression analysis techniques. In a majority of cases, a quadratic equation of the form

$$\log(s)=A+B(LMP)+D(LMP)^2 \quad (7)$$

was used in the analysis where "s" is stress in KSI, "LMP" is the Larson-Miller parameter, and "A", "B", and "D" are regression constants. The resulting curves provided a reasonable data fit except where only few data points were available. In such cases, application of a quadratic fit sometimes resulted in a curve which was concave upward. As an alternative, in such cases, regression was performed using a linear fit of the form,

$$\log(s)=A+B(LMP) \quad (8)$$

The curve fits were used to calculate stress for 100,000 hour rupture.

Stress rupture data analysis using the Manson minimum commitment method was performed on an IBM PC using a computer program designed by Manson (91) and modified by Pepe (98). The details of the Manson method have already been discussed in the literature review. From files stored on magnetic disc, data listed by heat were read and processed using regression analysis. The constants determined were used to construct isotherms which defined the average behavior of the material having data in the input file. Heat constants were also calculated which made it possible to draw isotherms for each individual heat of material. Determination of the 100,000 hour stresses associated with each isotherm as well as the statistical

parameters describing the scatter of the data about the fitted curves was accomplished using additional computer programs developed by Pepe (98).

3. TENSILE TESTING

Room temperature and elevated temperature tensile tests of weld metal in the as-welded, Class 2, Class 3, and aged Class 3 condition were performed per ASTM E8-81. Room temperature test results of the PWHT weld metals were used to determine whether the materials conformed with the requirements of Class 2 or Class 3. Tensile specimens were all weld metal with their longitudinal axis parallel to the welding direction. A standard 0.250 gage diameter specimen per ASTM E8-81 was employed. Values determined from the tensile test included 0.2 percent yield strength, ultimate tensile strength, percent elongation, and percent reduction in area.

4. METALLOGRAPHIC PREPARATION

The bulk of the microstructural analysis of these weld metals was performed using the SEM or STEM. Because of the exceptionally fine microstructure of the materials, optical microscopy was of minimal value. SEM examination at magnifications up to 10,000X was employed to characterize the morphology of the major micro-constituents. The alloy carbides in the microstructure proved to be too small to analyze using the SEM. As an alternative means of studying the precipitates, carbides were extracted from the surface of polished and etched specimens using carbon film replication

techniques. With the aid of a STEM, the resulting extraction replicas were examined at magnifications up to 200,000X with selected carbides identified by their X-ray spectra and, in some cases, electron diffraction patterns.

Weld metal samples to be examined microstructurally in the SEM were cut, mounted, and ground on successively finer emory papers starting with 180 grit and ending with 3/0. Polishing was accomplished using 9 micron and 1 micron diamond. Just prior to etching, the specimens were given a light polish using 0.06 micron alumina suspended in distilled water. The etchant found to give optimum results consisted of 73 percent reagent grade methanol, 2 percent concentrated nitric acid, and 25 percent saturated picral. Swab etching was used.

In preparation for viewing in the SEM, the epoxy on the metallographic mount was coated with carbon paint to provide a conductive path for the electrons from the sample to the microscope stage. To improve resolution at high magnifications, the surface of the specimen was then sputtered with gold to produce a layer approximately 250 angstroms thick.

An AMR 900 Scanning Electron Microscope was used to examine the microstructures. Experience revealed that the best micrographs were obtained when the polished surface of the metallographic specimen was given a relatively heavy etch and viewed with the specimen tilted about 30 degrees toward the detector.

In work performed at the University of California at Santa Barbara, specimens for STEM analysis were prepared in a manner

similar to that used for SEM samples. The polished surface was then etched using 2 percent nital. After etching, a thin film of carbon was vapor-deposited on the specimen surface. Using an electrolyte consisting of 50 ml. perchloric acid, 750 ml. ethanol, and 140 ml. distilled water, the carbon coated specimen was electropolished using a current density of 1.2 amperes per square centimeter of exposed sample surface. As a result of the electropolishing action, the matrix around the carbides dissolved, freeing the carbon film from the specimen surface. The film, with the extracted carbides, floated to the surface of the electrolyte and was caught on a fine mesh grid. This "extraction replica" was then examined on a JEM 200CX scanning transmission electron microscope.

5. TRANSFORMATION STUDIES

The transformation behavior of 0.08-0.09 and 0.12-0.13 carbon weld metal was determined with the aid of a 510 Gleeble. Developed at Rensselaer Polytechnic Institute (RPI), the Gleeble is a "high speed time/temperature control device" (99) which can impose a pre-programmed thermal cycle on a metallic sample. The specimen is clamped at each end in water-cooled copper jaws which also serve as points of electrical contact. The sample is resistance heated. A small wire thermocouple percussion welded to the sample is used to monitor the specimen temperature both for recording and control purposes. The pre-programmed thermal cycle is achieved by continuously altering the balance between the resistance heating and

the cooling resulting from heat flow down the length of the sample to the water-cooled jaws.

For conducting transformation studies, the Gleeble is also fitted with a high speed dilatometer which senses variation in the specimen diameter due to thermal expansion/contraction as well as volumetric changes which result from phase transformations. The dilatometer signal is fed to a multi-channel light beam oscillograph where a resulting trace of specimen dilation and temperature as a function of time is recorded. Determination of transformation start and finish temperatures is accomplished by plotting relative dilation as a function of temperature. Start and finish temperatures are indicated by the points at which the plot deviates from linear expansion/contraction behavior.

Weld metal transformation specimens 0.250 inches in diameter and 4 inches long were thermally cycled in the Gleeble. Seven thermal cycles were used to determine transformation behavior, each with a peak temperature of 2400^{o}F. Six of the cycles corresponded to the thermal histories of material immediately adjacent to the fusion line in two inch thick steel plate preheated to 400^{o}F and welded with energy inputs of 35, 60, 80, 100, 127, and 150 KJ/IN respectively. These inputs are in the range characteristic of SMAW and SAW, two welding processes commonly used in the fabrication of 2-1/4Cr-1Mo pressure vessels. The seventh thermal cycle was obtained by heating the specimen to 2400^{o}F at the same rate as employed in the other cycles. However, on reaching the peak temperature, the Gleeble was shut off, allowing the specimen to cool at the maximum rate

determined by the geometry of the sample/cooling jaw assembly. Analysis of the cooling profile indicated that it was roughly equivalent to that resulting from an 18 KJ/IN weld in 2 inch plate at room temperature. Figure 25 is a graphical representation of the thermal cycles employed in the transformation study.

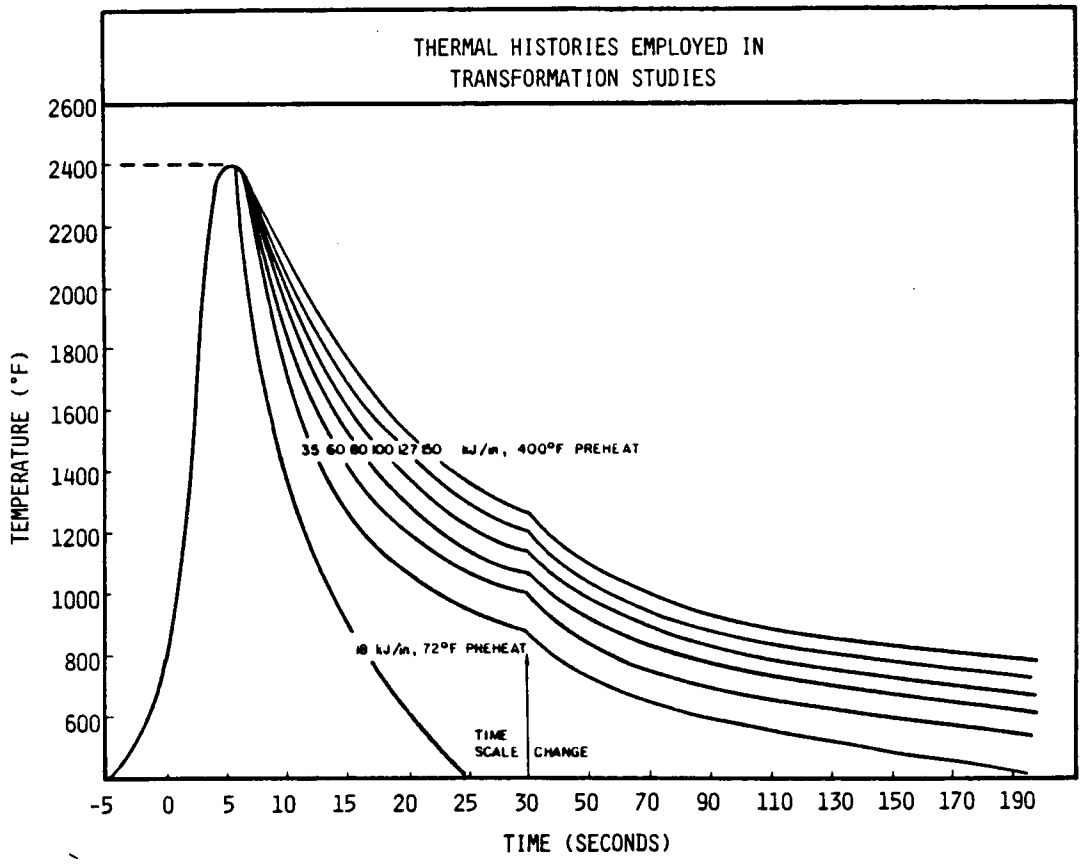


Figure 25. Gleeble thermal cycles employed in transformation determinations.

CHAPTER 4

RESULTS AND DISCUSSION

1. STRESS RUPTURE DATA ANALYSIS

Despite the volume of stress rupture data that has been collected for 2-1/4Cr-1Mo weld metal, only limited analysis has been done to determine the effects of PWHT and carbon content on stress rupture strength of these materials. Wagner and Seth (84) have analyzed rupture data to ascertain the correlation between room temperature tensile strength (related to PWHT) and rupture properties. Their data base consisted of data from tests of weld metal in the as-welded, quenched and tempered, and PWHT condition. By partitioning their data by room temperature tensile strength alone, they ignored the microstructural differences which result from these varying treatments, differences which, although not affecting room temperature strength, can influence rupture behavior. Klueh and Canonico (71), Campbell (70), and Pendley (85) have all investigated the correlation between carbon content and stress rupture strength. The experimental work of Klueh and Canonico (71) and Campbell (70) yielded conflicting results and therefore did not clarify the relationship between carbon and rupture strength. Pendley (85) reviewed the literature for stress rupture data of PWHT weld metal which he analyzed after partitioning it by carbon content. However, his partitioning scheme did not take into account variations in PWHT (and therefore temper parameter) associated with the data. As a

consequence, the results of his analysis reflected not only the effect of carbon on rupture behavior but the effect of PWHT as well.

The analysis of rupture data obtained from weld metal testing in this program as well as from the literature has been conducted in a way so as to avoid these pitfalls. As described previously, the data were partitioned by tempering parameter as well as carbon content in an attempt to minimize the variables which might affect the analysis. Three analytical techniques were employed independently to determine the relationship between stress rupture strength and both carbon level and PWHT.

Analysis Techniques

Of the three methods employed in the analysis, the Larson-Miller technique proved to be the easiest to use. The Larson-Miller approach allows all of the rupture data for a given material to be plotted on a single curve, regardless of test temperature. The stress for 100,000 hour rupture at any temperature of interest is then obtained by inserting the Larson-Miller value which describes that time/temperature combination into the log stress vs. Larson-Miller parameter equation determined by regression and solving for stress. If one stays within the parameter range described by the data, the 100,000 hour stress thus obtained is an interpolated value and lacks the degree of uncertainty characteristic of values which necessarily are determined by curve extrapolations using the other two analysis methods. A benefit of this interpolation technique is that 100,000 hour rupture stresses may be obtained for temperatures

at which no data are available, i.e., as long as the Larson-Miller parameter value characteristic of 100,000 hours at that temperature falls within the parameter range described by the data.

In contrast to the Larson-Miller technique where rupture data for all test temperatures are collapsed onto a master curve, the log stress/log rupture time method requires a curve to be determined at each test temperature. As a result, the data must be partitioned by test temperature, greatly reducing the number of data points available for derivation of each curve. Without a sufficient number of data points available to "average out" the scatter characteristic of rupture data, the curves obtained by regression analysis become descriptive of the few data available rather than of the material in general. As a result, the 100,000 hour stresses derived from extrapolations of the curves are affected as well. Thus, efforts to observe the influence of such factors as PWHT or carbon content on 100,000 hour stress are significantly hampered.

The limitation on the calculable 100,000 hour stresses to temperatures at which data are known also hampers efforts to compare materials (as in comparison of weld metal by temper parameter or carbon content). The rupture strength of two materials may only be compared if they share a common test temperature.

The minimum commitment method developed by Manson (91) shares some of the advantages and disadvantages of the two techniques previously discussed. Like the Larson-Miller method, once a curve fitting equation is obtained from the data, 100,000 hour stresses can be determined for any test temperature, even if data at that

temperature is not available. However, caution needs to be exercised in using the technique to describe rupture behavior beyond the range of temperatures at which data are known. Such stresses may prove to be unrealistic. In comparison with the log stress/log rupture time technique, extrapolated 100,000 hour stress values obtained using Manson's method are also detrimentally affected when the data available are limited. Infrequently, the isotherms defining the relation between log stress and log rupture time fit the data well in the rupture time interval spanned by the data but predict unrealistic behavior at shorter or longer rupture times. In the latter case, the curves usually fail to reach the 100,000 hour level, curving back toward shorter rupture times and making prediction of 100,000 hour stresses impossible.

A possible explanation for the occurrence of erratic curve behavior is based on mathematical analysis of the Manson equation. This equation, for A=0, becomes

$$(9) \qquad \log(t_r)=B+C\log(s)+Ds+Es^2-R_1(T-T_m)-R_2[(1/T)-(1/T_m)]$$

In the isothermal case, "T" is a constant and the last two terms can be absorbed by "B" to make a new constant, "B_1". Equation 9 thus becomes

$$(10) \qquad \log(t_r)=B_1+C\log(s)+Ds+Es^2$$

Furthermore, the "log(s)" term can be converted to "ln(s)" by dividing by ln(10), another constant which can, in turn, be absorbed

by "C" to make "C_1". The equation obtained is

$$\log(t_r)=B_1+C_1\ln(s)+Ds+Es^2 \qquad (11)$$

Equation 11 can be differentiated with respect to "s" and set equal to zero to determine the maxima and minima of the curve described by the equation. Upon simplification, the result is

$$2Es^2+Ds+C_1=0 \qquad (12)$$

Using the quadratic formula, one obtains

$$s=[-D+(D^2-8EC_1)^{1/2}][1/4E]. \qquad (13)$$

Assuming that both solutions to equation 13 are real, this equation indicates that the curve can have both a maximum and a minimum. Stated another way, the curve can reverse its direction twice, much in the same way as a curve described by a cubic equation in "s". Therefore, the data for a particular data set must be best represented by the portion of the Manson curve which is well away from a maximum or minimum, i.e., the maximum or minimum does not occur in the rupture time interval of interest, in order for an acceptable curve fit to be obtained. Unfortunately, this requirement is not always met and problems therefore do arise. Elimination of this difficulty would require modification of the Manson model to remove either the "log(s)" or the "s^2" term. Such an action, however, would sacrifice some of the ability of the obtained curves to conform to the data.

The following is a presentation of the results of the various rupture data analyses. Because many of the curves in the figures fall close to one another, they are shown without data points to avoid confusion which would arise due to data overlap. Graphs with

data points included are located in Appendix A. Appendix B contains a list of the stress rupture data examined during the analysis.

Larson-Miller Parameter Analysis

Literature Data Analysis (Larson-Miller Parameter). Figures 26 through 33 are plots of log stress vs. Larson-Miller parameter for the stress rupture data collected from the literature for PWHT 2-1/4Cr-1Mo weld metal. Figures 26, 28, 30, and 32 are derived from all of the data considered as a single population regardless of welding process while Figures 27, 29, 31, and 33 have been prepared for SMA data only. Table 5 presents the stress for 100,000 hour rupture as a function of test temperature and temper parameter calculated from regression analyses of log stress vs. Larson-Miller parameter plots. Values are given for both the entire stress rupture data base and for the SMA data only. Table 6 contains the 100,000 hour stresses similarly obtained as a function of test temperature and carbon content for each temper parameter range in the complete set of data. Table 7 presents the stresses derived from the SMA data only.

Figures 26 and 27 depict the best fit curves for log stress vs. Larson-Miller parameter for each temper parameter range. Figure 26 represents the entire data base while Figure 27 is derived from the SMA data only. Examination of the figures and the corresponding stresses in Table 5 reveals the following trends. First, the stress for 100,000 hour rupture generally decreases as the temper parameter increases. This holds true at least for service temperatures in the

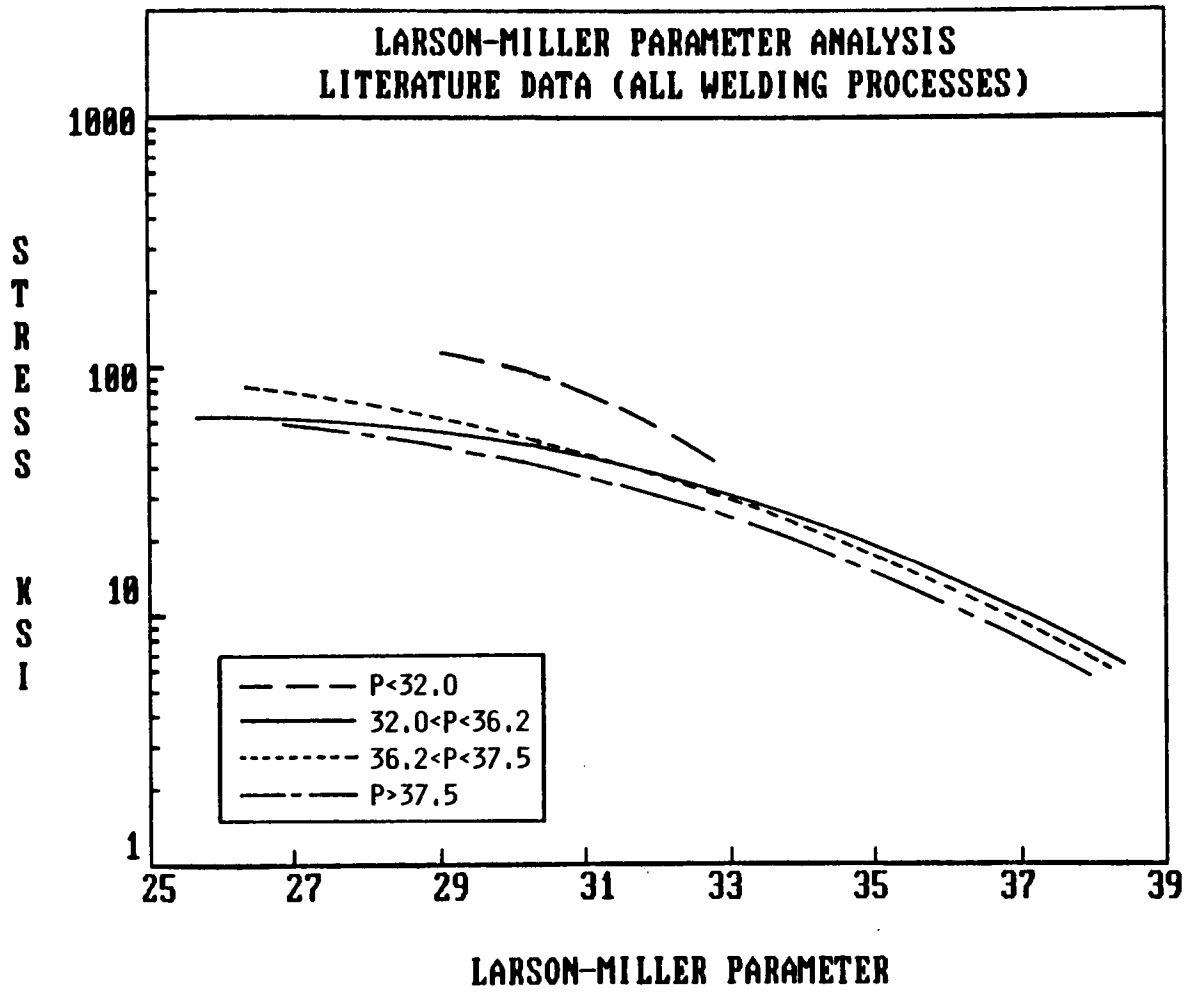


Figure 26. Stress rupture behavior of 2-1/4Cr-1Mo weld metal as a function of temper parameter determined by analysis of literature data for weld metal deposited by a variety of welding processes.

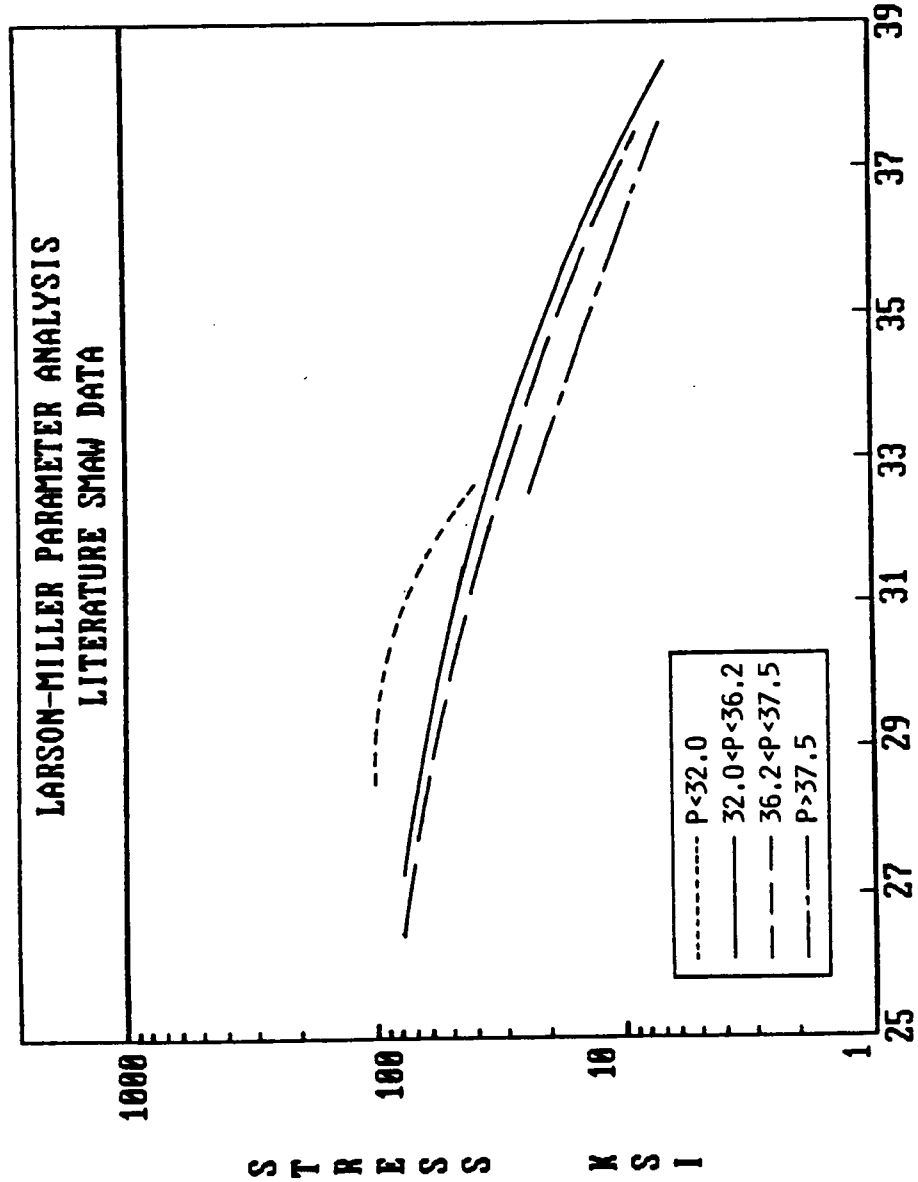


Figure 27. Stress rupture behavior of 2-1/4Cr-1Mo SMA weld metal as a function of temper parameter determined by analysis of literature data.

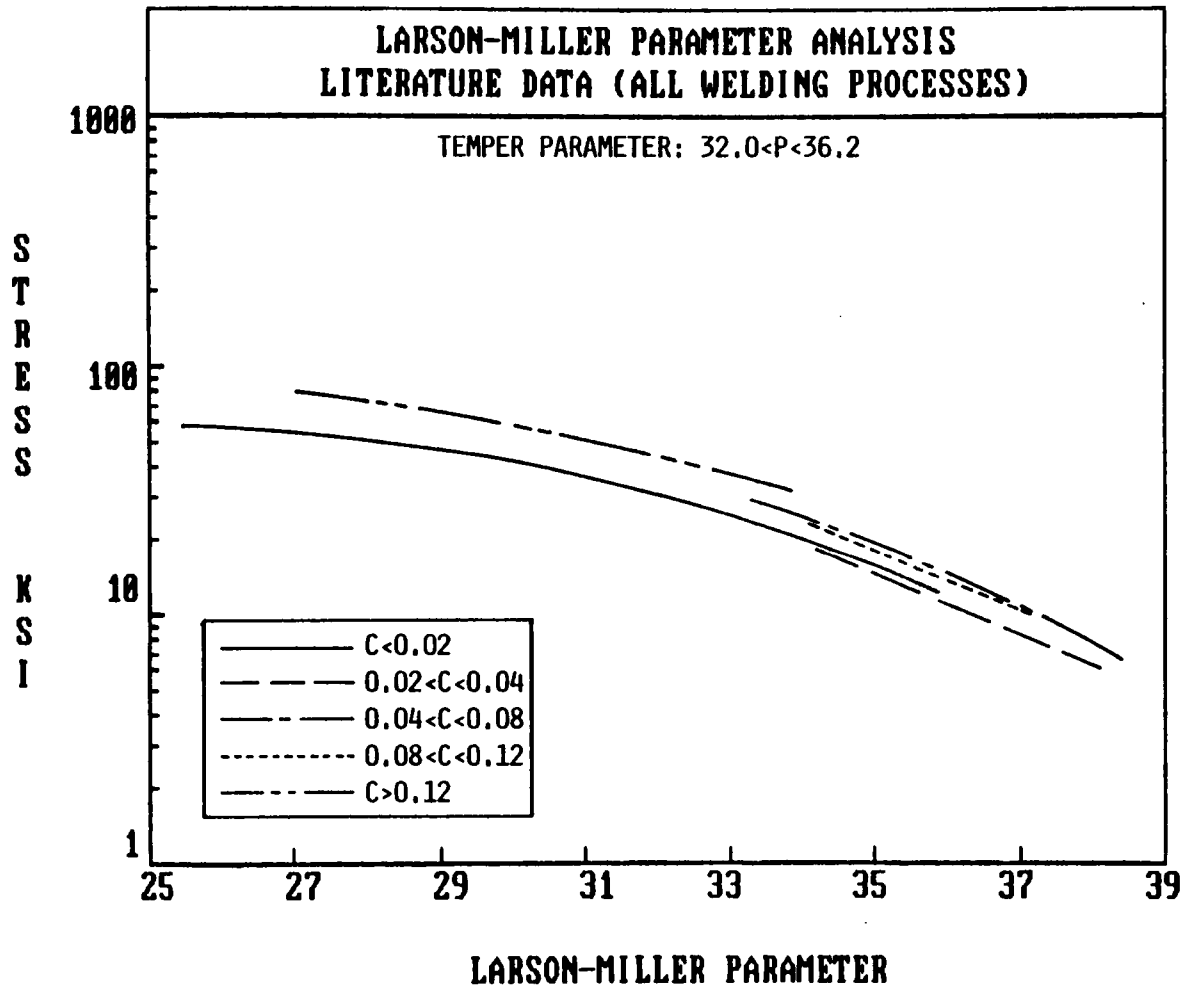


Figure 28. Stress rupture behavior of PWHT 2-1/4Cr-1Mo weld metal (32.0<P<36.2) as a function of carbon content determined by analysis of literature data for weld metal deposited by a variety of welding processes.

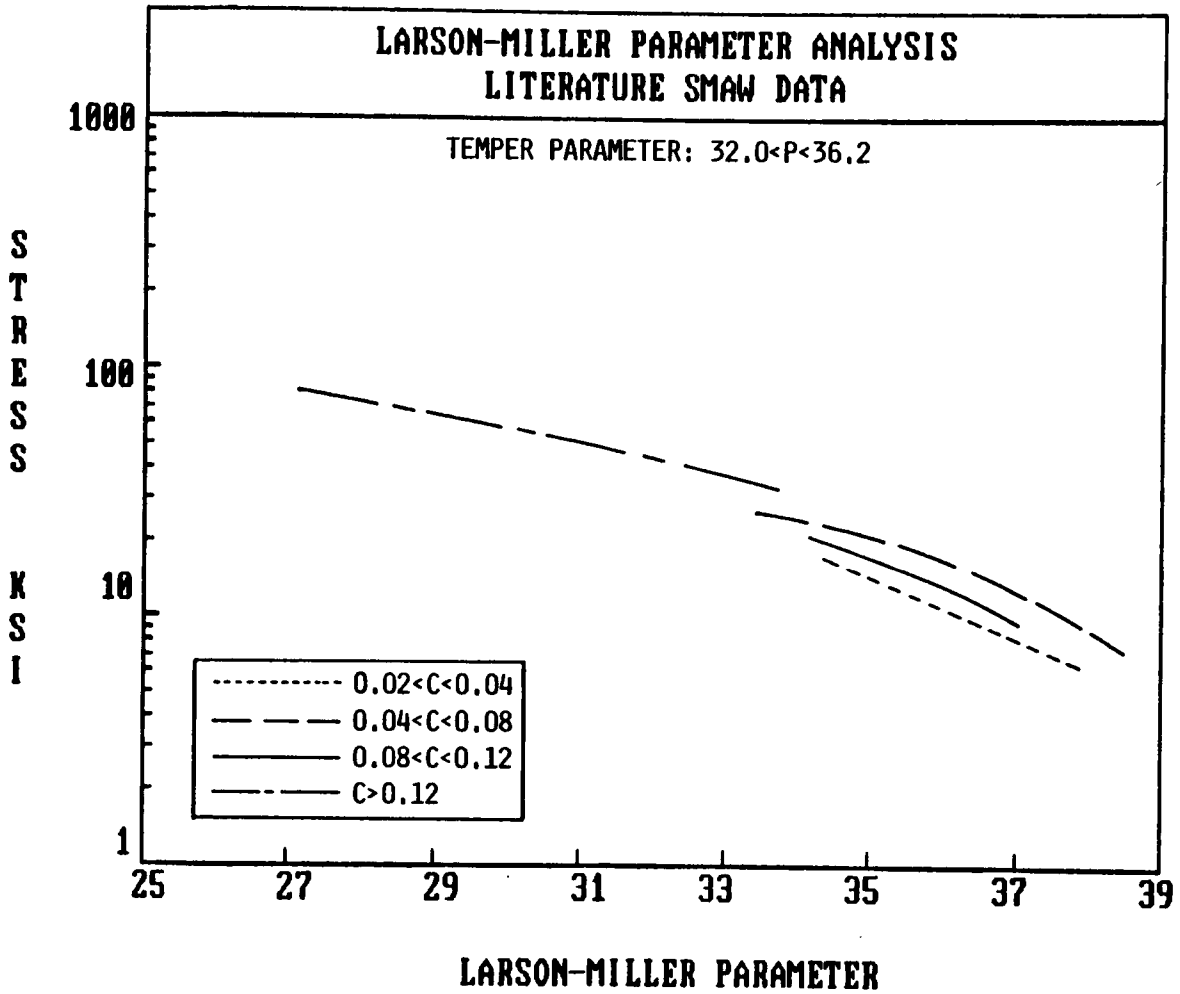


Figure 29. Stress rupture behavior of PWHT 2-1/4Cr-1Mo SMA weld metal (32.0<P<36.2) as a function of carbon content determined by analysis of literature data.

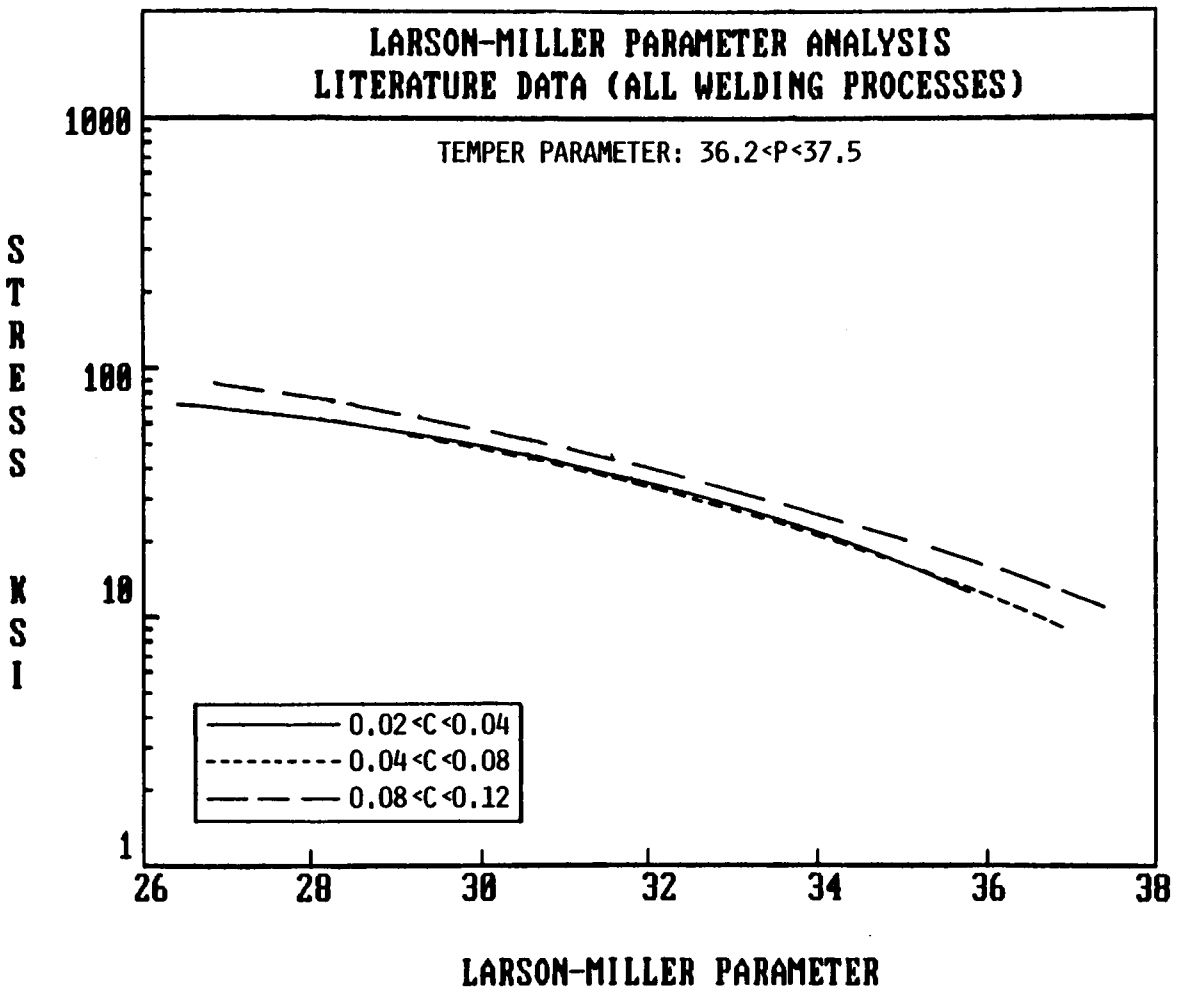


Figure 30. Stress rupture behavior of PWHT 2-1/4Cr-1Mo weld metal (36.2<P<37.5) as a function of carbon content determined by analysis of literature data for weld metal deposited by a variety of welding processes.

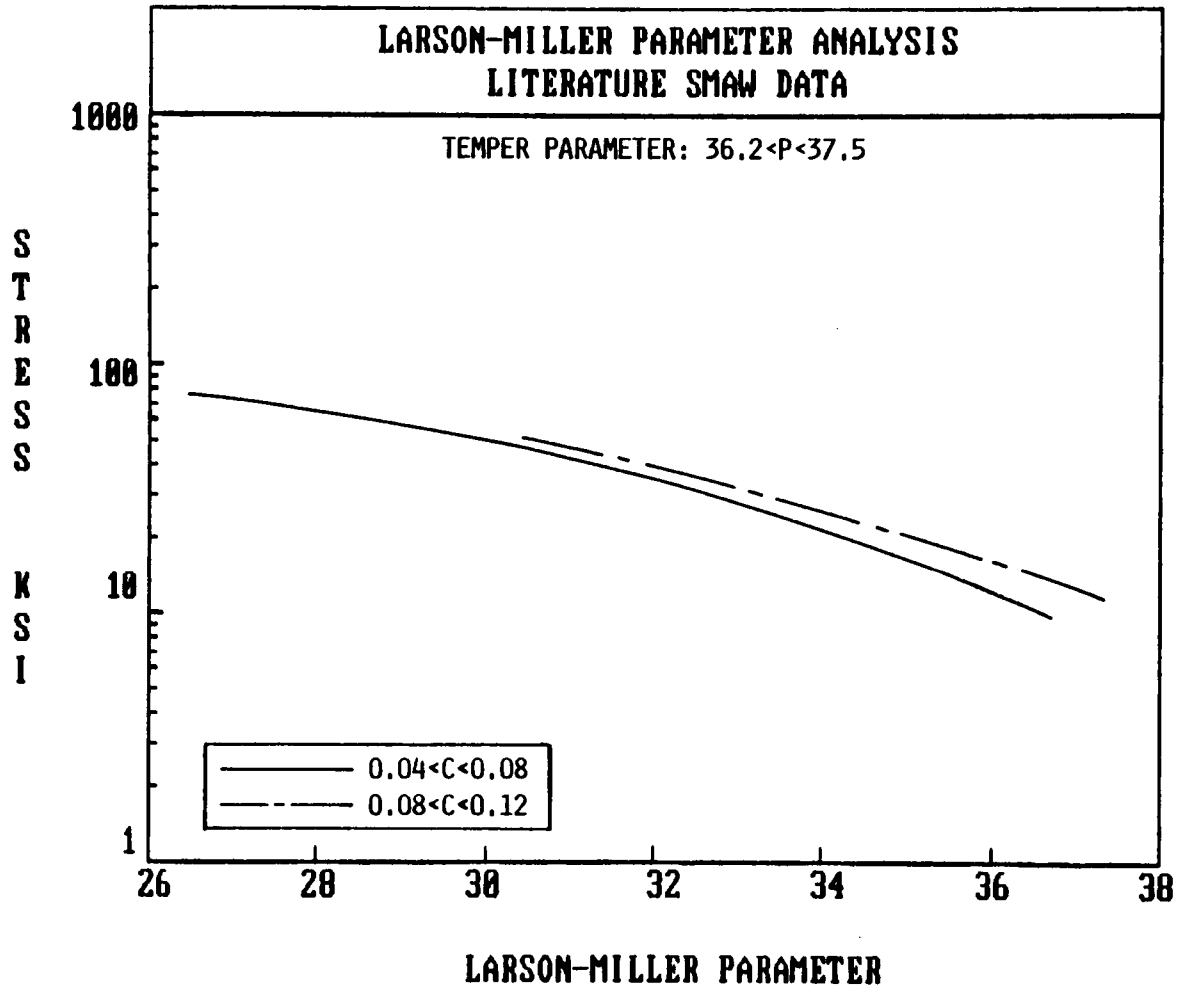


Figure 31. Stress rupture behavior of PWHT 2-1/4Cr-1Mo SMA weld metal (36.2<P<37.5) as a function of carbon content determined by analysis of literature data.

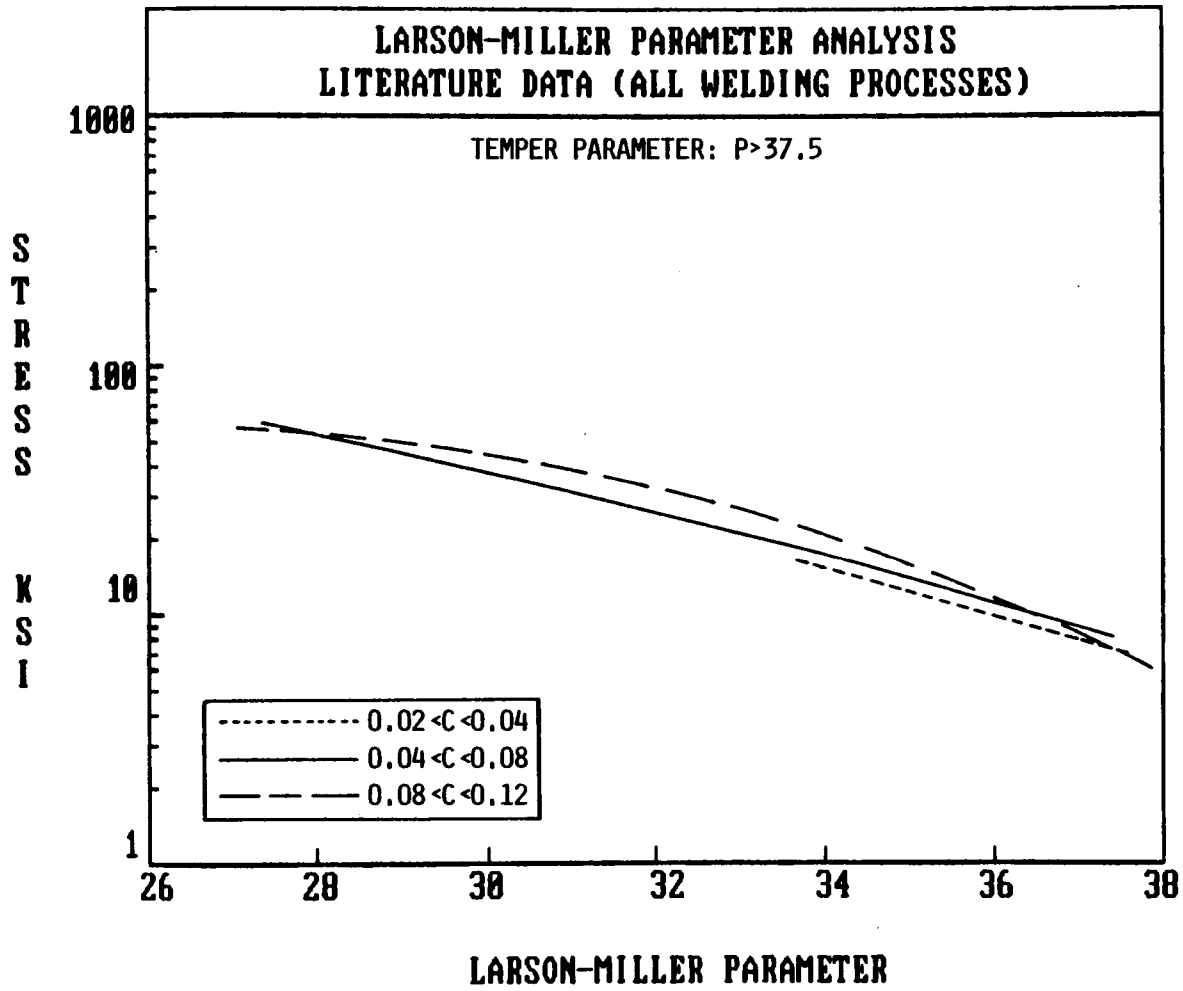


Figure 32. Stress rupture behavior of PWHT 2-1/4Cr-1Mo weld metal (P>37.5) as a function of carbon content determined by analysis of literature data for weld metal deposited by a variety of welding processes.

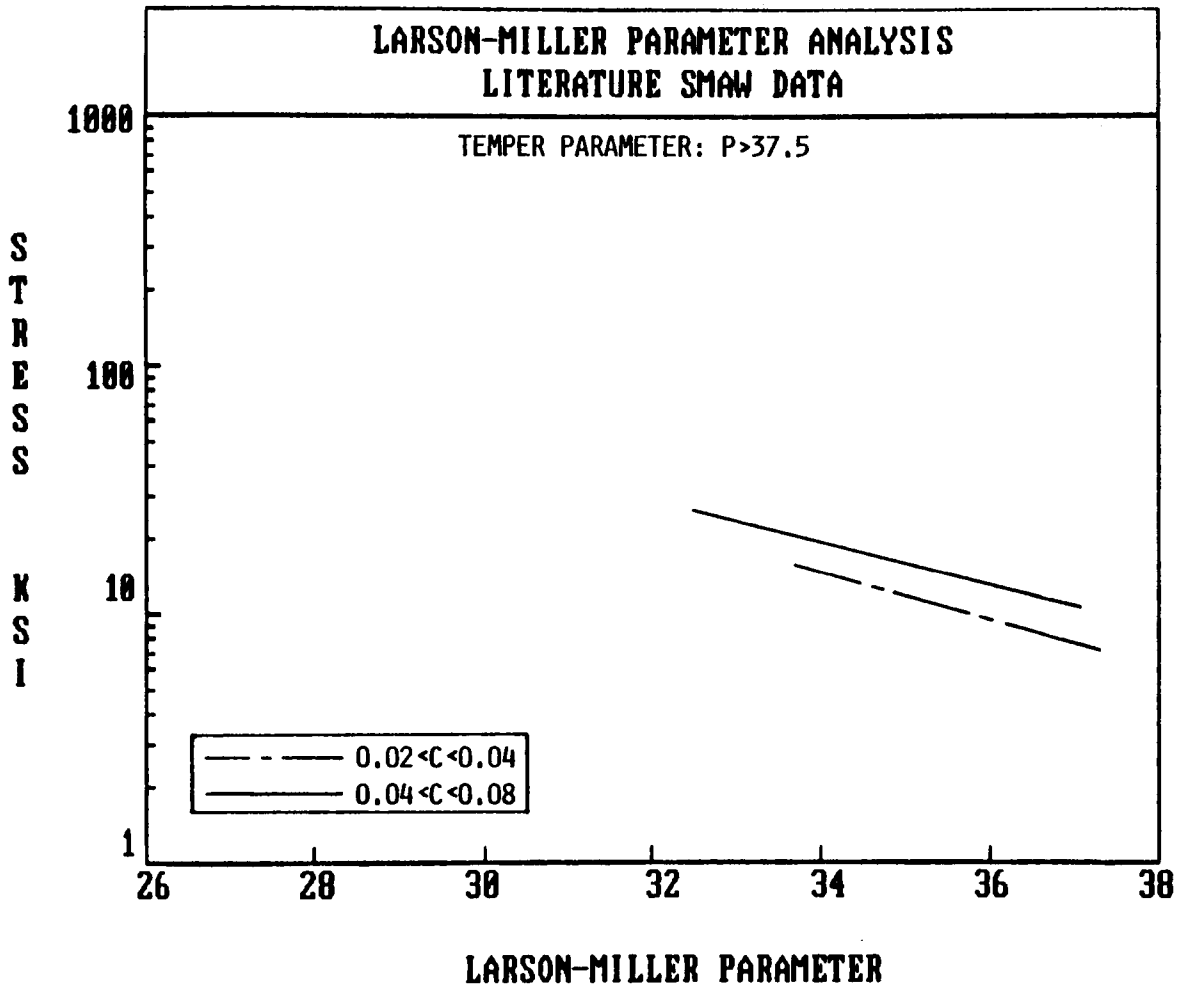


Figure 33. Stress rupture behavior of PWHT 2-1/4Cr-1Mo SMA weld metal (P>37.5) as a function of carbon content determined by analysis of literature data.

Table 5. Stress for 100,000 hour rupture as a function of test temperature and temper parameter determined by Larson-Miller analysis of 2-1/4Cr-1Mo weld metal literature data.

Data	Temper Parameter Range	Stress for 100,000 Hour Rupture (KSI)						
		750°F	800°F	850°F	900°F	950°F	1000°F	1050°F
All	P<32.0	92.7	67.7	41.6	-	-	-	-
	32.0<P<36.2	47.3	39.5	31.1	23.8	17.1	13.0	7.9
	36.2<P<37.5	49.3	39.6	30.0	22.5	15.8	11.0	-
	P>37.5	40.4	32.9	25.3	19.0	13.4	9.3	6.0
SMA Only	P<32.0	90.6	66.4	37.8	-	-	-	-
	32.0<P<36.2	53.9	44.1	34.0	25.7	18.2	12.8	8.3
	36.2<P<37.5	47.4	38.5	29.9	23.0	16.8	12.2	-
	P>37.5	-	-	24.5	17.0	12.2	9.4	-

Table 6. Stress for 100,000 hour rupture as a function of test temperature, carbon content, and temper parameter determined by Larson-Miller analysis of 2-1/4Cr-1Mo weld metal literature data considered independent of deposition process.

Temper Parameter	Carbon Content	Stress for 100,000 Hour Rupture (KSI)						
		750°F	800°F	850°F	900°F	950°F	1000°F	1050°F
32.0<P<36.2	C<0.02	38.9	32.5	25.7	19.9	14.5	-	-
	0.02<C<0.04	-	-	-	-	13.2	9.4	6.5
	0.04<C<0.08	-	-	-	24.6	18.0	12.7	8.2
	0.08<C<0.12	-	-	-	-	16.9	12.2	-
	C>0.12	53.7	45.7	37.8	31.3	-	-	-
36.2<P<37.5	0.02<C<0.04	47.0	37.9	28.7	21.3	14.7	-	-
	0.04<C<0.08	46.9	38.0	29.0	21.6	15.1	10.4	-
	0.08<C<0.12	54.0	43.8	34.0	26.2	19.3	14.2	-
P>37.5	0.02<C<0.04	-	-	-	14.9	11.1	8.5	-
	0.04<C<0.08	35.7	28.6	22.3	17.5	13.4	10.3	-
	0.08<C<0.12	43.5	36.3	28.3	21.3	14.8	10.1	6.3

Table 7. Stress for 100,000 hour rupture as a function of test temperature, carbon content, and temper parameter determined by Larson-Miller analysis of 2-1/4Cr-1Mo SMA weld metal literature data.

Temper Parameter	Carbon Content	Stress for 100,000 Hour Rupture (KSI)						
		750°F	800°F	850°F	900°F	950°F	1000°F	1050°F
32.0<P<36.2	0.02<C<0.04	-	-	-	-	13.2	9.4	6.5
	0.04<C<0.08	-	-	-	24.5	19.8	14.7	9.5
	0.08<C<0.12	-	-	-	22.1	17.2	12.2	-
	C>0.12	53.7	45.7	37.8	31.3	-	-	-
36.2<P<37.5	0.04<C<0.08	46.9	38.0	29.1	22.0	15.6	11.0	-
	0.08<C<0.12	50.9	41.5	32.6	25.5	19.1	14.3	-
P>37.5	0.02<C<0.04	-	-	-	14.9	11.1	8.5	-
	0.04<C<0.08	-	-	23.9	18.9	14.7	11.6	-

range of 750 to 1050°F. However, the strength advantage gained by lightly tempering 2-1/4Cr-1Mo weld metal (P<32.0) decreases as the temperature increases from 750°F until, at about 875°F, it is not significant. Second, the 100,000 hour rupture stresses for the various temper parameter ranges approach a common value as the service temperature increases. At 750°F, the spread in stresses is 40 to 50 KSI but decreases to 4 KSI as the temperature approaches 1000°F.

Figures 28 and 29 show the best fit curves for 2-1/4Cr-1Mo weld metal PWHT with 32.0<P<36.2 for each carbon content range. Considering these figures along with Tables 6 and 7, it is apparent that the 100,000 hour rupture stress increases with carbon content. However, this increase does not appear to be uniformly continuous. The lowest 100,000 hour stresses are indicated by the C<0.02 and 0.02<C<0.04 curves which fall together. At a higher stress level, the curves for the 0.04C<C0.08 and 0.08<C<0.12 data fall together. This behavior is best illustrated by Figure 28. Finally, the 100,000 hour stresses for C>0.12 are consistently above those for all the lower carbon materials. Unfortunately, the data in the high carbon range are such that the curve does not extend to LMP values above approximately 34. As a result, the 100,000 hour rupture stresses can not be determined for temperatures above 900°F without extrapolating.

Figures 30 and 31 show the best fit curves for 2-1/4Cr-1Mo weld metal PWHT with 36.2<P<37.5 as a function of carbon content. When examined along with Tables 6 and 7, a trend of increasing 100,000 hour rupture strength with increasing carbon content is once again

observed. Curves from the entire data base show the strength of $0.02<C<0.04$ weld metal and $0.04<C<0.08$ weld metal to be comparable with that for $0.08<C<0.12$ material falling significantly higher. In comparison, curves for the SMA data alone indicate a strength increase when the carbon level increases from $0.04<C<0.08$ to $0.08<C<0.12$ percent.

Figures 32 and 33 show the best fit curves for weld metal PWHT with $P>37.5$ (see also Tables 6 and 7). The rupture strength appears to be directly related to carbon content. The curve for $0.02<C<0.04$ falls consistently below that for the higher carbon material. Further examination reveals that the $0.08<C<0.12$ weld metal has a higher 100,000 hour rupture strength than the $0.04<C<0.08$ material. However, the strength advantage diminishes continuously as the temperature increases from $750^{o}F$ (strength difference 9 KSI) to $1000^{o}F$ (difference only 0.2 KSI).

The dependence of the stress-rupture strength of 2-1/4Cr-1Mo weld metal on welding process has not been specifically addressed in this program. However, using Tables 6 and 7, the strengths predicted from the analysis of the total literature data base (data from a variety of welding processes) can be compared to those derived from the analysis of the SMA data alone. In some temper parameter or carbon content ranges, the predictions based on the SMA data are a few KSI higher than those for the total data base, while in others the reverse is true. Thus, based on this analysis of the data available, it appears that the stress-rupture strength of 2-1/4Cr-1Mo

SMA weld metal is comparable in magnitude with that determined for weld metal deposited by a variety of welding processes.

UTK Data Analysis (Larson-Miller Parameter). Figures 34 through 36 are log stress vs. Larson-Miller parameter plots derived from analysis of UTK data. Figures are presented showing the effect of PWHT and carbon content on stress rupture strength. Tables 8 and 9 list the calculated 100,000 hour rupture stresses derived from the fits in the figures.

Figure 34 depicts the effect of PWHT on the rupture behavior of the weld metals independent of carbon content. Inspection of the figure along with the values in Table 8 indicates that the 100,000 hour rupture strength of the Class 3 material is significantly higher than that for Class 2 weld metals. As expected, the strength advantage diminishes with increasing temperature, decreasing from 14 KSI at 750^{o}F to 3 KSI at 1050^{o}F.

Figure 35 shows the effect of carbon content on the stress rupture strength of the Class 2 weld metal. Examination of the figure reveals that the strength of the 0.02-0.03C material is noticeably below that of the 0.04-0.05, 0.08-0.09, and 0.12-0.13 carbon weld metals which are comparable in strength. This observation is confirmed by inspection of Table 9. Even at lower service temperatures, the spread in strengths of the higher carbon materials is only 1.5 KSI.

Considering the results obtained above, the Class 2 data were reanalyzed, combining the 0.04-0.05, 0.08-0.09, and 0.12-0.13 carbon

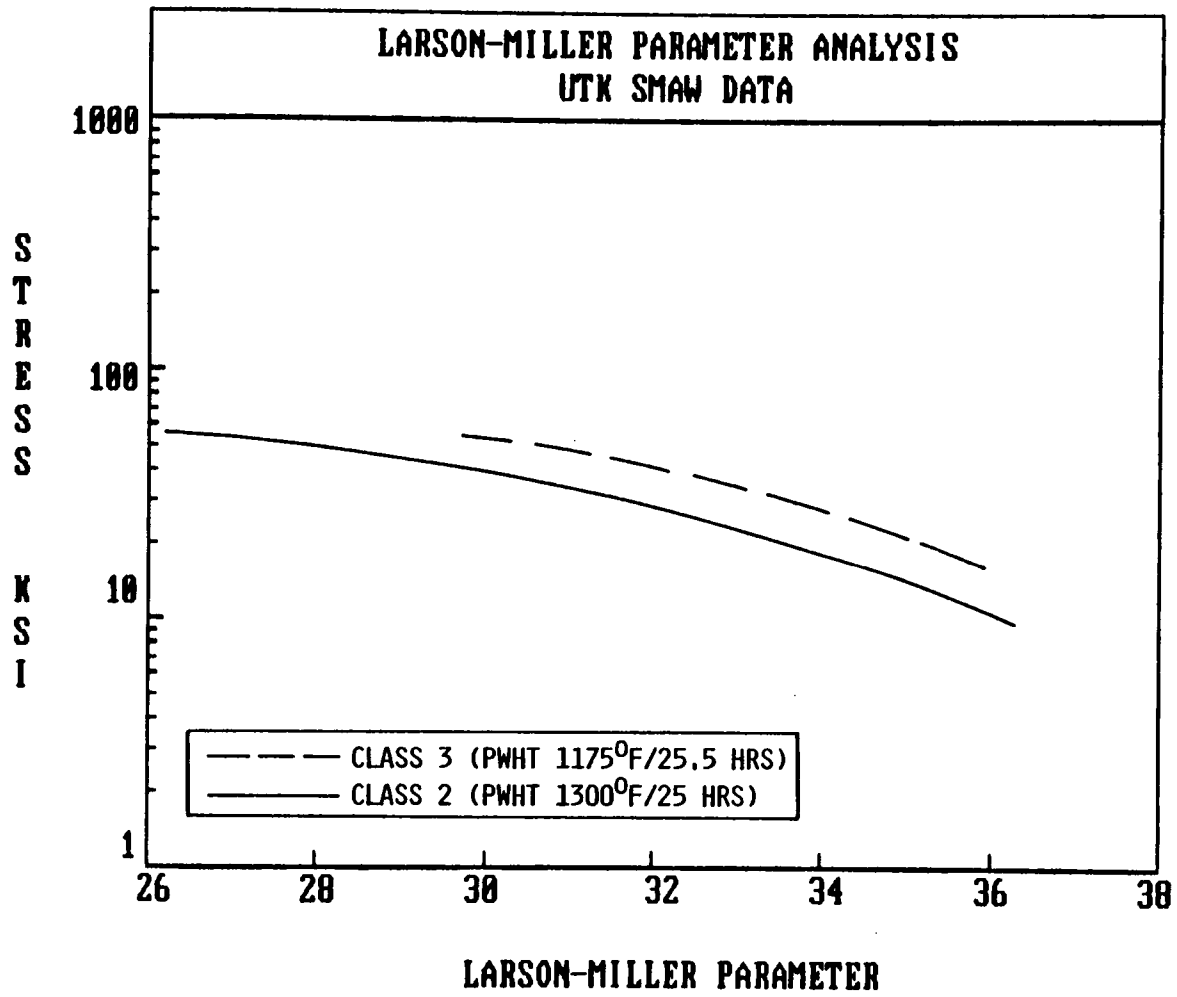


Figure 34. Stress rupture behavior of 2-1/4Cr-1Mo SMA weld metal as a function of temper parameter determined by analysis of UTK data.

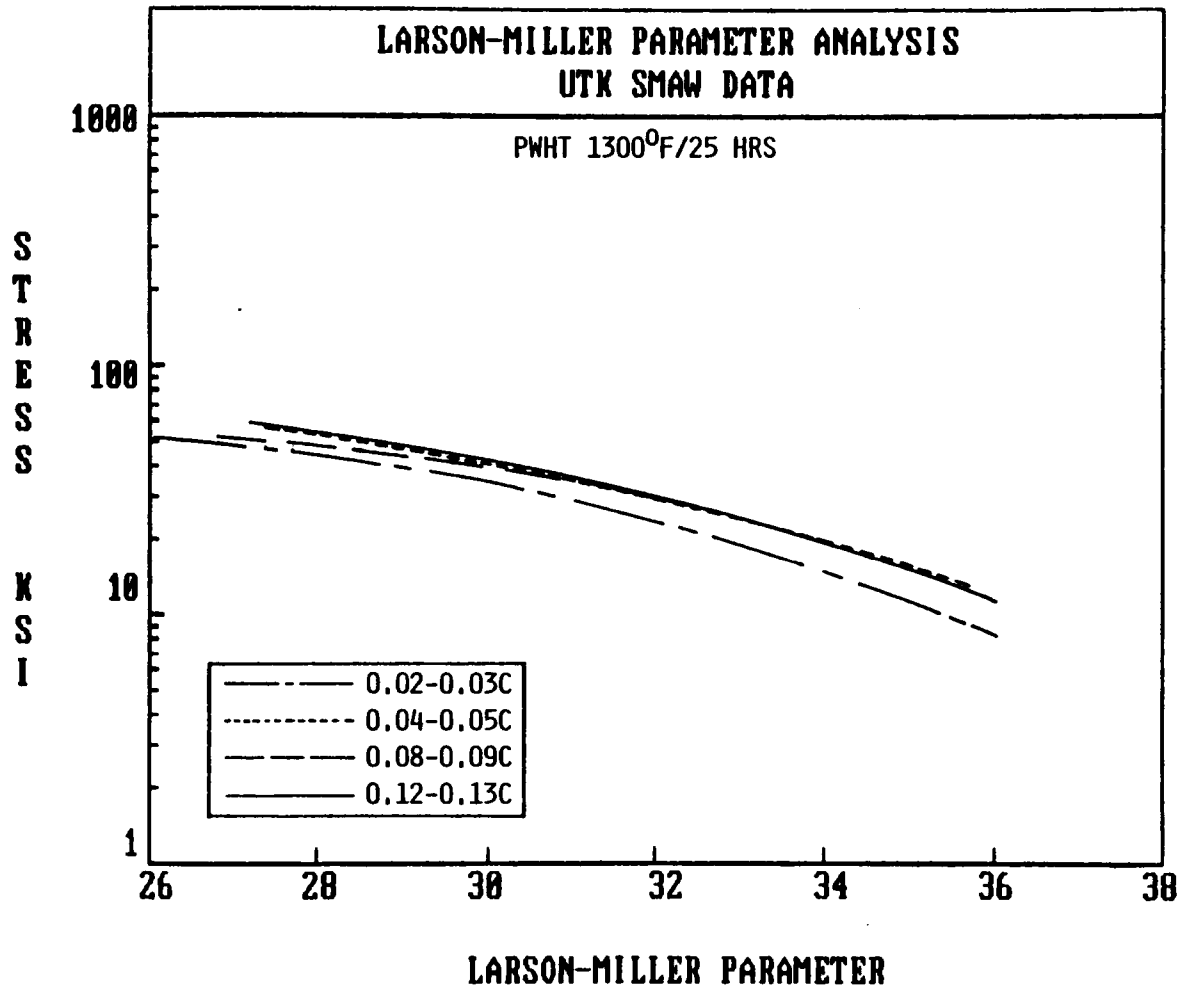


Figure 35. Stress rupture behavior of 2-1/4Cr-1Mo SMA weld metal PWHT 1300°F/25 hrs. as a function of carbon content determined by analysis of UTK data.

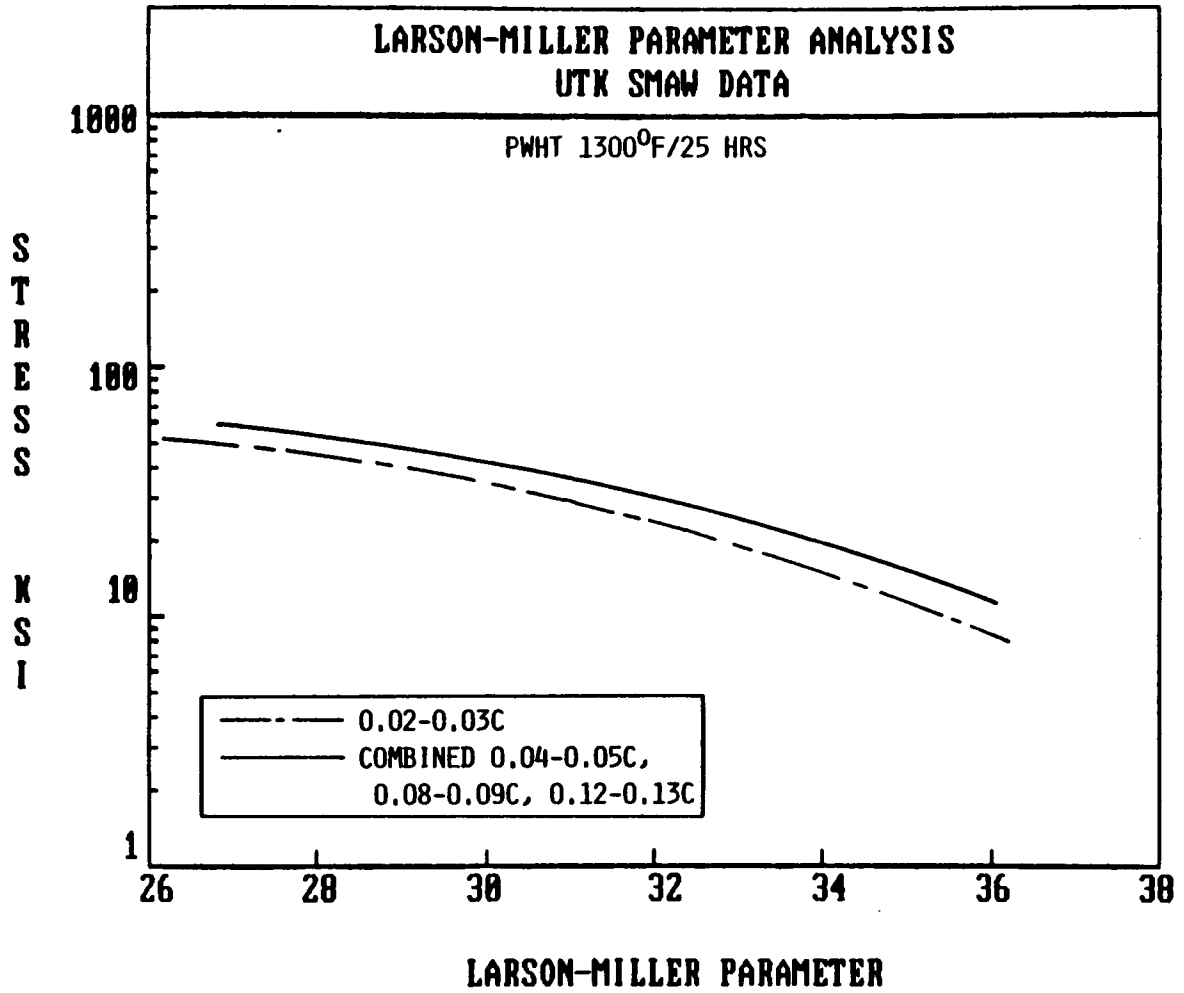


Figure 36. Stress rupture behavior of 0.02-0.03 and 0.04-0.13 carbon 2-1/4Cr-1Mo SMA weld metal PWHT 1300°F/25 hrs. as a function of carbon content determined by analysis of UTK data.

Table 8. Stress for 100,000 hour rupture as a function of test temperature and PWHT determined by Larson-Miller analysis of UTK 2-1/4Cr-1Mo SMA weld metal data.

	Stress for 100,000 Hour Rupture (KSI)	
Temperature (^{o}F)	Class 3 (P=35.0)	Class 2 (P=37.7)
750	51.1	36.9
800	44.0	30.5
850	35.5	23.8
900	27.7	18.3
950	20.1	13.2
1000	14.2	9.5
1050	9.2	6.3

Table 9. Stress for 100,000 hour rupture as a function of test temperature and carbon content for 2-1/4Cr-1Mo SMA weld metal PWHT 1300°F/25 hrs. determined by Larson-Miller analysis of UTK data.

Carbon Content	Stress for 100,000 Hour Rupture (KSI)						
	750°F	800°F	850°F	900°F	950°F	1000°F	1050°F
0.02-0.03	32.0	25.8	19.6	14.7	10.3	7.1	4.6
0.04-0.05	38.6	31.7	24.9	19.5	14.6	10.8	7.7
0.08-0.09	38.2	31.8	25.1	19.4	14.1	10.2	6.8
0.12-0.13	39.8	32.5	25.2	19.3	13.9	10.0	6.7
Combined (0.04-0.13)	38.9	32.0	25.1	19.4	14.2	10.3	7.0

data into a single population. Figure 36 shows the curves obtained and more clearly illustrates the difference in strength between the 0.02-0.03 carbon weld metal and that of the higher carbon materials. Table 9 lists the stresses calculated for the combined data population.

Analyses to determine the effect of carbon content on the rupture strength of the Class 3 weld metal were not performed. Testing of the Class 3 material was limited to only one lot of filler metal with a carbon level of 0.08-0.09 percent.

Combined Analysis of Literature and UTK Data (Larson-Miller Parameter). The effect of expanding the SMA data base with the addition of the UTK data is shown in Figures 37 through 39 and Tables 10 and 11. These figures are summary plots constructed to compare the curves for various temper parameter ranges and carbon contents. Only those curves which were altered by the addition/combination of the data are shown. For the curves not affected, the reader is referred to the previous figures for SMA literature data. Tables 10 and 11 contain the calculated 100,000 hour rupture stresses for each temper parameter range and carbon content range respectively.

Figure 37 is a plot of log stress vs. Larson-Miller parameter as a function of temper parameter for combined SMA literature data and UTK data. Extrapolated 100,000 hour stresses for the curves in the figure are given in Table 10. Comparing Tables 5 (p. 108) and 10 shows that the addition of UTK data to the SMA literature data base has a negligible effect on the predicted 100,000 hour stress values.

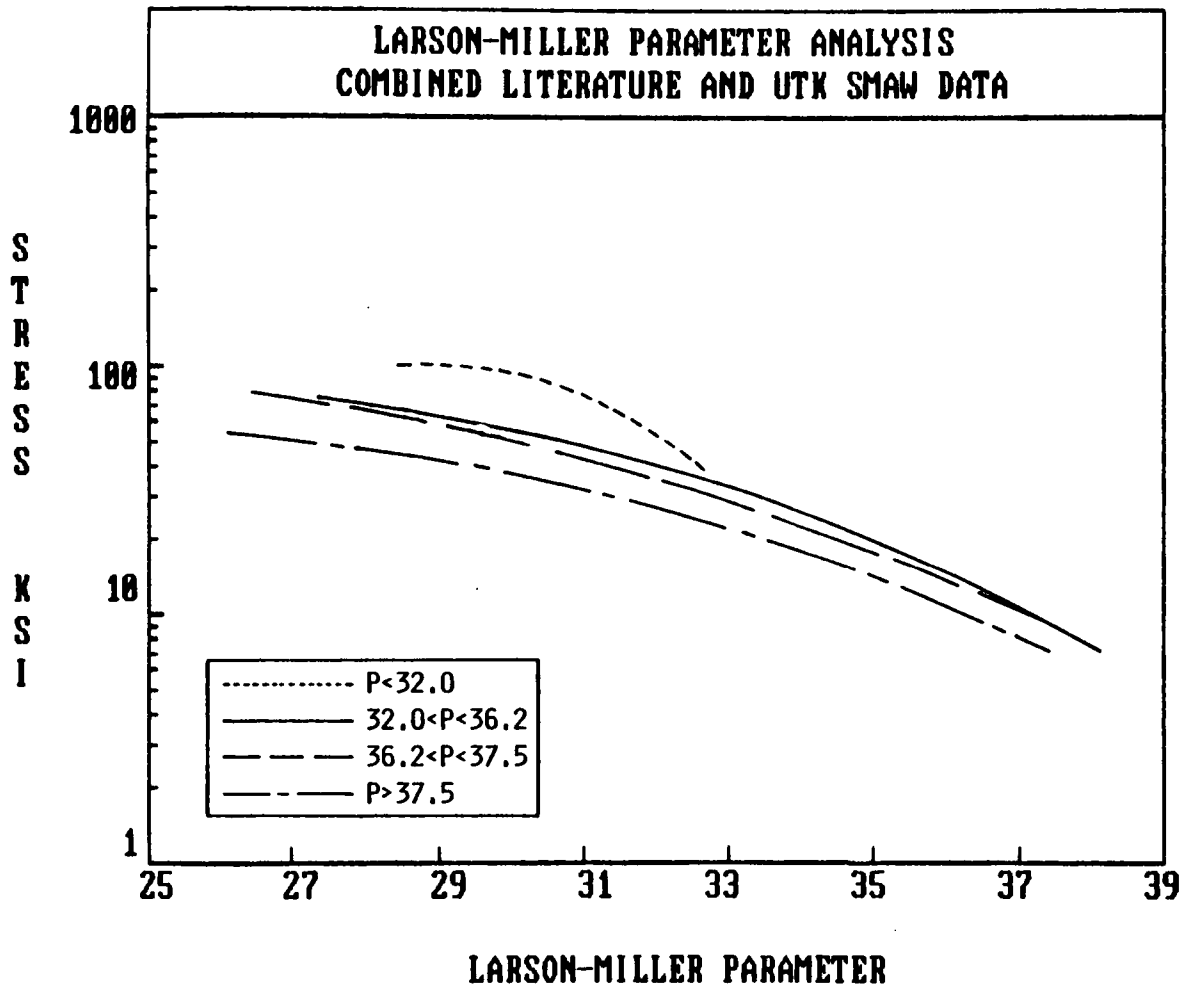


Figure 37. Stress rupture behavior of 2-1/4Cr-1Mo SMA weld metal as a function of temper parameter determined by analysis of combined literature and UTK data.

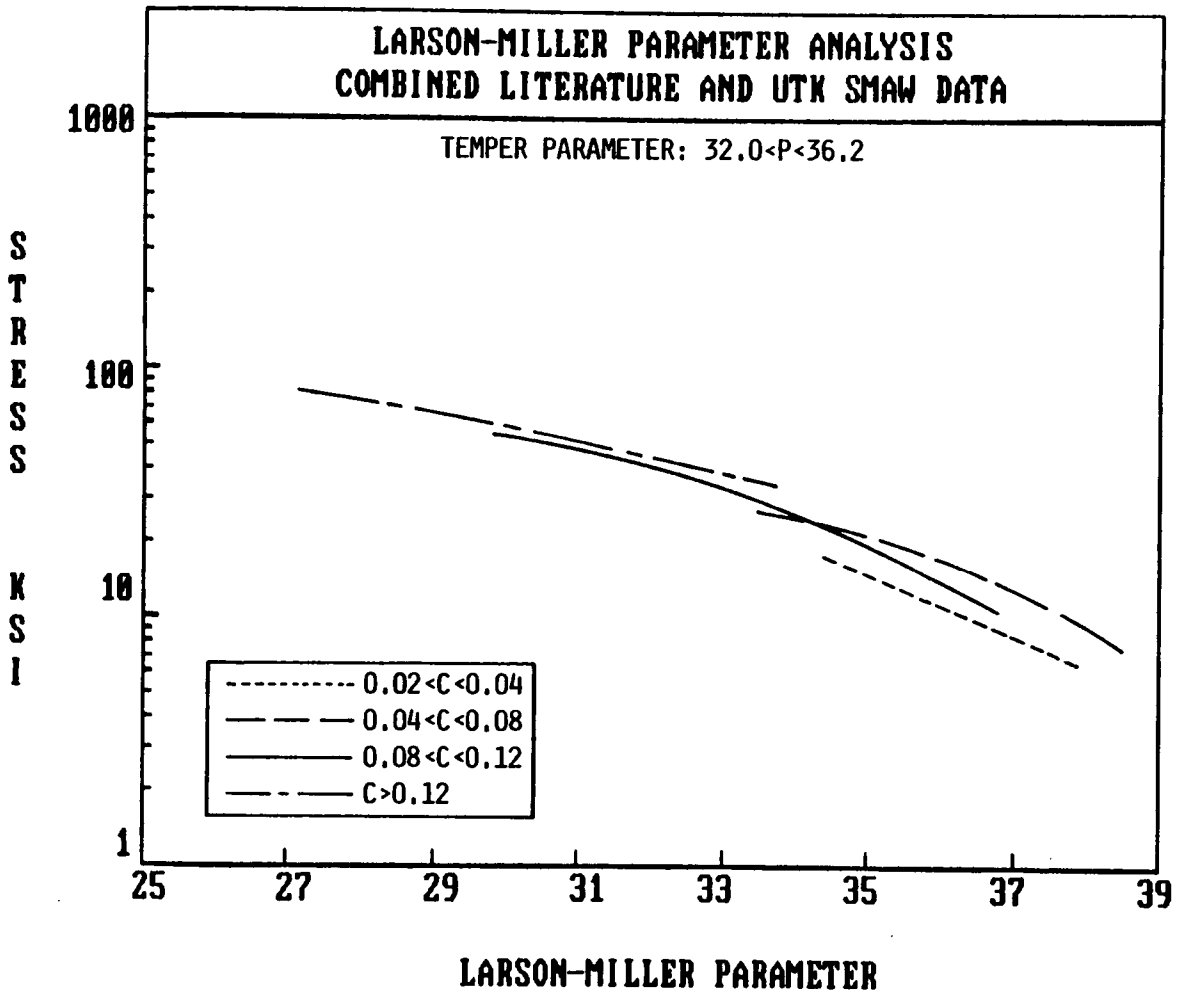


Figure 38. Stress rupture behavior of PWHT 2-1/4Cr-1Mo SMA weld metal (32.0<P<36.2) as a function of carbon content determined by analysis of combined literature and UTK data.

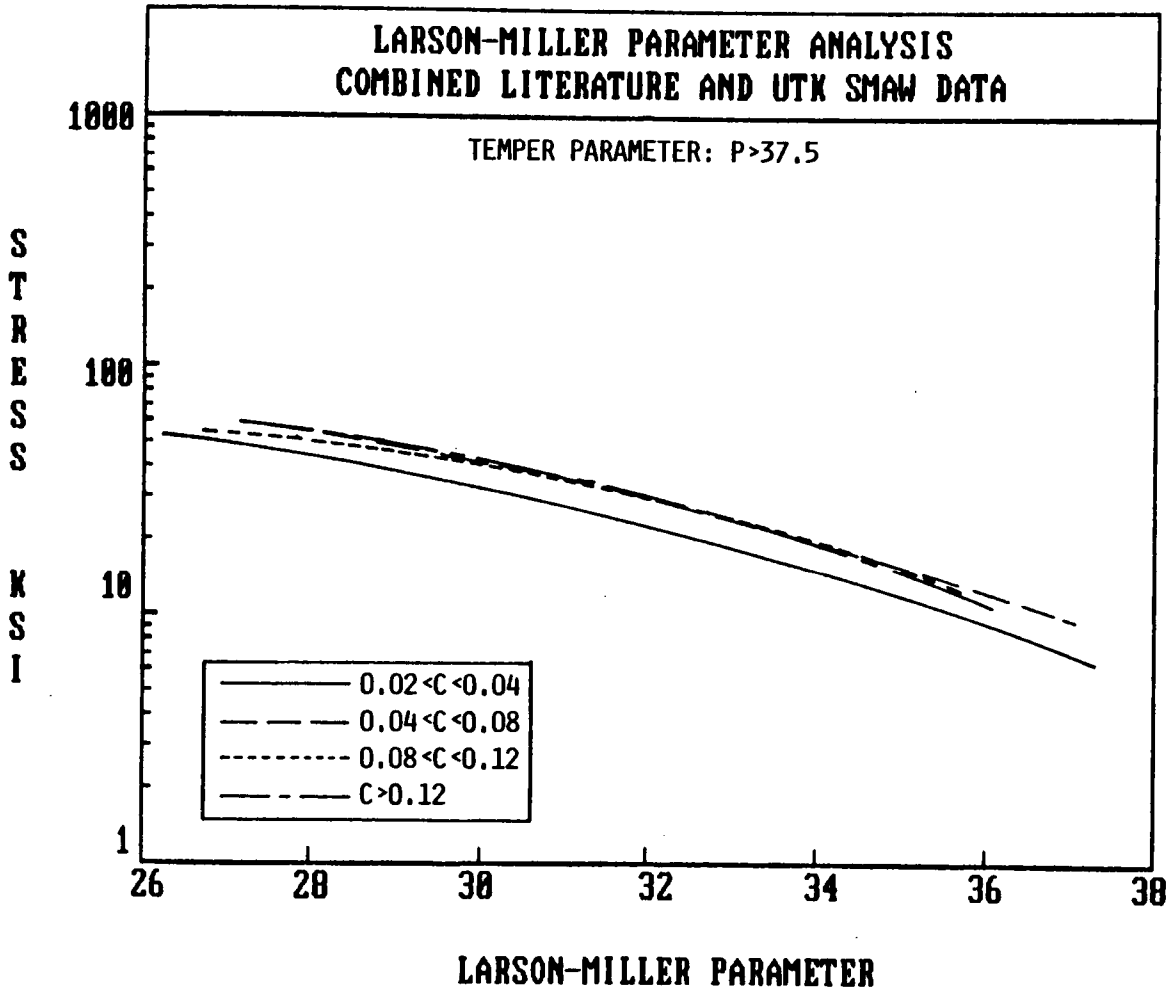


Figure 39. Stress rupture behavior of PWHT 2-1/4Cr-1Mo SMA weld metal (P>37.5) as a function of carbon content determined by analysis of combined literature and UTK data.

Table 10. Stress for 100,000 hour rupture of 2-1/4Cr-1Mo SMA weld metal as a function of test temperature and temper parameter determined by Larson-Miller analysis of combined literature and UTK data.

Temper Parameter Range	Stress for 100,000 Hour Rupture (KSI)						
	750°F	800°F	850°F	900°F	950°F	1000°F	1050°F
P<32.0	90.6	66.4	37.8	-	-	-	-
32.0<P<36.2	54.0	44.4	34.4	26.0	18.4	12.8	8.3
36.2<P<37.5	47.4	38.5	29.9	23.0	16.8	12.2	-
P>37.5	36.8	30.3	23.7	18.2	13.2	9.4	-

Table 11. Stress for 100,000 hour rupture of 2-1/4Cr-1Mo SMA weld metal as a function of test temperature and temper parameter determined by Larson-Miller analysis of combined literature and UTK data.

Temper Parameter	Carbon Content	Stress for 100,000 Hour Rupture (KSI)						
		750°F	800°F	850°F	900°F	950°F	1000°F	1050°F
32.0<P<36.2	0.02<C<0.04	-	-	-	-	13.2	9.4	6.5
	0.04<C<0.08	-	-	-	24.5	19.8	14.7	9.5
	0.08<C<0.12	51.0	44.3	35.3	26.6	18.2	12.0	-
	C>0.12	53.7	45.7	37.8	31.3	-	-	-
36.2<P<37.5	0.04<C<0.08	46.9	38.0	29.1	22.0	15.6	11.0	-
	0.08<C<0.12	50.9	41.5	32.6	25.5	19.1	14.3	-
P>37.5	0.02<C<0.04	31.3	25.5	19.7	15.2	11.1	8.1	-
	0.04<C<0.08	38.3	31.3	24.6	19.5	14.8	11.3	-
	0.08<C<0.12	38.2	31.8	25.1	19.4	14.1	-	-
	C>0.12	39.8	32.5	25.2	19.3	13.9	-	-

Comparison of Figures 37 and 27 (p. 101) bears this out as the curves are essentially unchanged, the only exception being that the curve for weld metal PWHT with P>37.5 is extended to lower Larson-Miller parameter values.

Figure 38 shows the effect of carbon content on rupture behavior of PWHT weld metal (32.0<P<36.2) as indicated by combined SMA literature and UTK data. The only curve to be altered by the addition of the new data is that for 0.08<C<0.12. Comparison with Figure 29 (p. 103) indicates that that curve has been extended to lower values of the Larson-Miller parameter, crossing the curve for 0.04<C<0.08 and approaching that for C>0.12. This marks a reversal in the strength ranking of the 0.04<C<0.08 and the 0.08<C<0.12 weld metals for values of LMP<34. Comparison of Tables 11 and 7 (p. 110) reveals how the predicted stress for 100,000 hour rupture has been affected by the data addition. Except for temperatures greater than 900^{o}F (where the 0.04<C<0.08 weld metal has a greater strength than the higher carbon 0.08<C<0.12 material), the 100,000 hour rupture strength increases with carbon content.

Figure 39 is a plot for weld metal PWHT with P>37.5 and is constructed using SMA literature data and UTK data. It is in this parameter range that the addition of the new data has had the greatest effect on the curves describing rupture behavior as a function of carbon content. This is probably because the literature data for this parameter range is limited (11 data points, C<0.07, test temperatures 1000-1100^{o}F) and is insufficient to adequately characterize the weld metal behavior. The introduction of the

Class 2 UTK data increases the data base by a factor of 10 to 109 data points and doubles the range of both the Larson-Miller parameter and the carbon content. Comparing Figures 39 and 33 (p.107), both the rupture curves for the $0.02<C<0.04$ weld metal fall consistently below those for the higher carbon materials. Figure 39 indicates that the rupture behavior of weld metals with carbon contents greater than 0.04 percent is independent of carbon level. This fact is verified by inspection of Table 11. The stress for 100,000 hour rupture of the $0.04<C<0.08$, $0.08<C<0.12$, and $C>0.12$ are of nearly identical magnitude over the entire temperature range.

In summary, rupture data analysis using the Larson-Miller parameter indicates that the rupture strength of 2-1/4Cr-1Mo weld metal is improved by decreasing the time and/or temperature of PWHT (decreasing temper parameter) with the greatest improvement obtained for PWHT's characterized by temper parameter values below 32.0. However, the strength advantage thus obtained is only realized for applications at temperatures less than about $900^{o}F$. At higher temperatures, sufficient additional tempering occurs during service to lower the rupture strength to a value more comparable with that of weld metals given a more extensive PWHT. The addition of carbon to 2-1/4Cr-1Mo weld metal, in general, increases rupture strength for materials PWHT with $P<37.5$. However, for weld metals given a more extensive PWHT ($P>37.5$), the beneficial effects of increasing the carbon content is limited to carbon levels below 0.04 weight percent. At higher carbon levels, little additional strengthening is realized.

Log Stress/Log Rupture Time Analysis

Literature Data Analysis (Log Stress/Log Rupture Time). Figures 40 through 45 are plots of log stress vs. log rupture time derived from the SMA literature data partitioned by temper parameter. Figures 40, 41, 42, and 43 have been determined for the data in the parameter ranges $P<32.0$, $32.0<P<36.2$, $36.2<P<37.5$, and $P>37.5$ respectively. Each figure depicts individual curves for each test temperature of interest.

Table 12 presents the extrapolated 100,000 hour rupture stress values as a function of temper parameter and test temperature for the SMA literature data. In general (at least at temperatures below $1000^{o}F$), the 100,000 hour weld metal rupture strength decreases as the temper parameter increases. In particular, at $850^{o}F$, weld metal PWHT with $P<32.0$ has a significantly higher strength than material given a more extensive PWHT. However, as the temperature increases, this strength advantage diminishes until, at $900^{o}F$, it is insignificant. These trends are in general agreement with conclusions drawn from the Larson-Miller analysis. Little can be said about the 100,000 hour stresses at temperatures greater than $1000^{o}F$ since the scatter in the stress values is sufficient to mask any trends.

No clear cut dependence of rupture strength on carbon content is apparent from the results of the log stress/log rupture time analysis of the SMA literature data. Due to data availability, comparisons by carbon content are limited to one temper parameter range

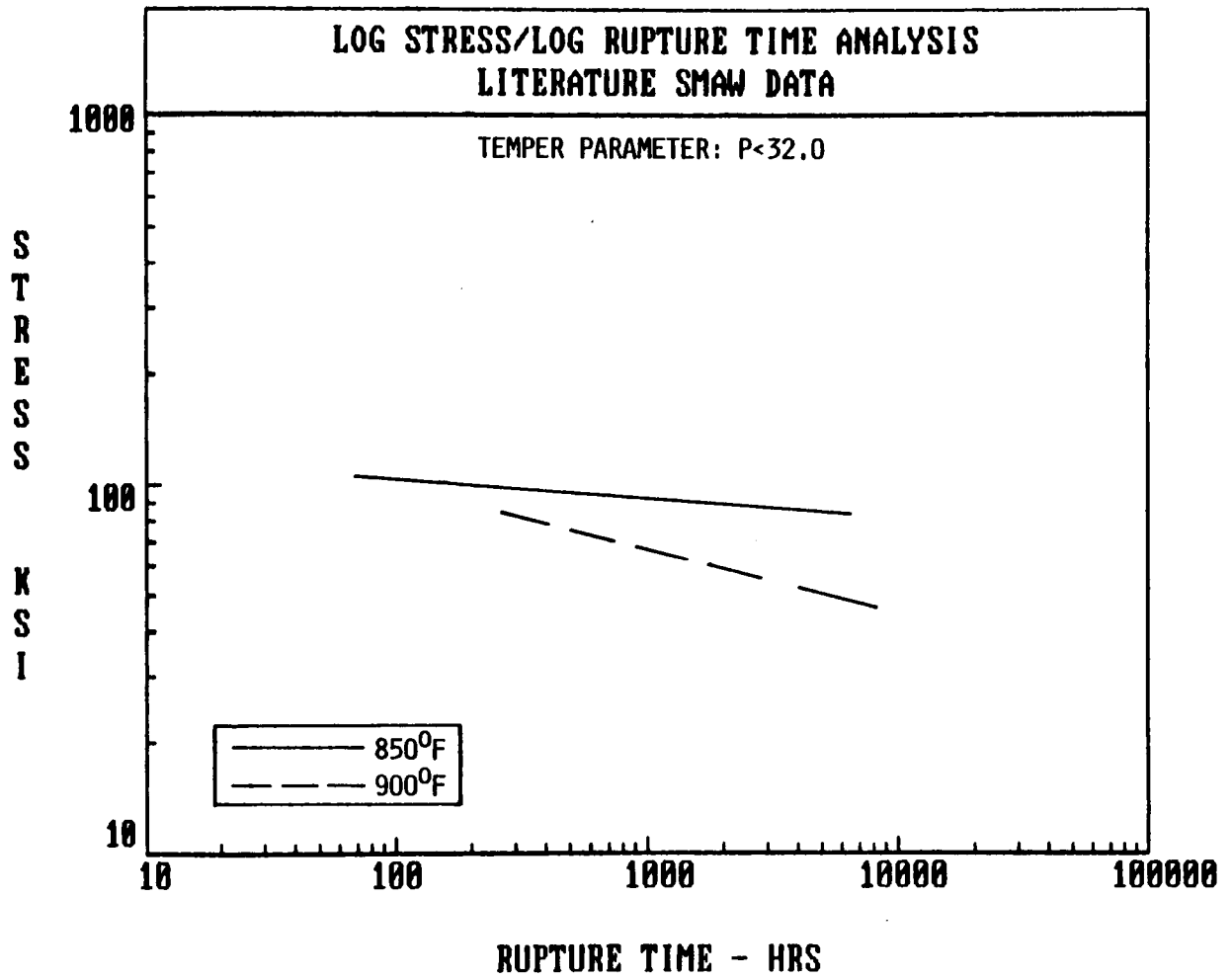


Figure 40. Stress rupture behavior of PWHT 2-1/4Cr-1Mo SMA weld metal (P<32.0) as a function of test temperature determined by analysis of literature data.

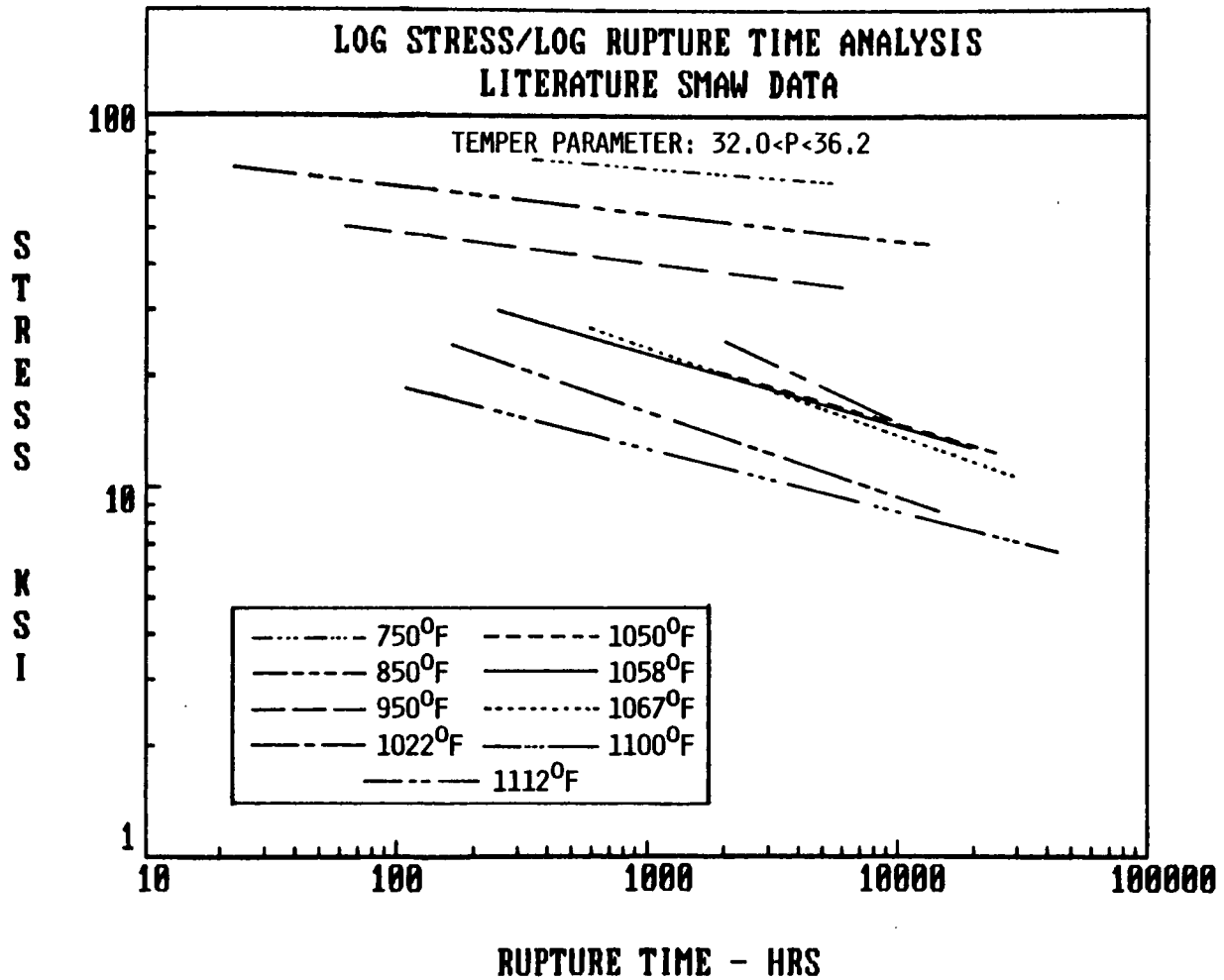


Figure 41. Stress rupture behavior of PWHT 2-1/4Cr-1Mo SMA weld metal (32.0<P<36.2) as a function of test temperature determined by analysis of literature data.

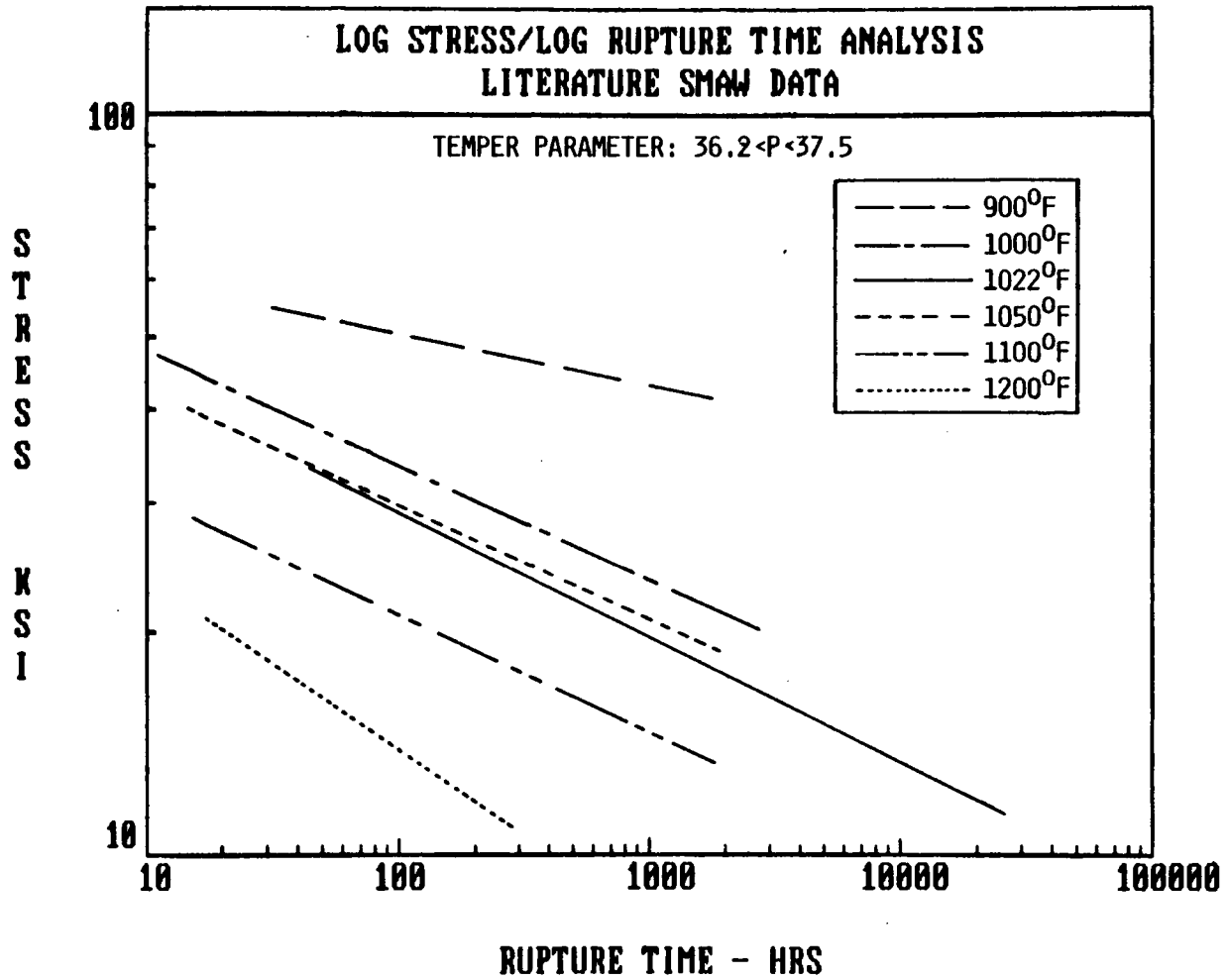


Figure 42. Stress rupture behavior of PWHT 2-1/4Cr-1Mo SMA weld metal (36.2<P<37.5) as a function of test temperature determined by analysis of literature data.

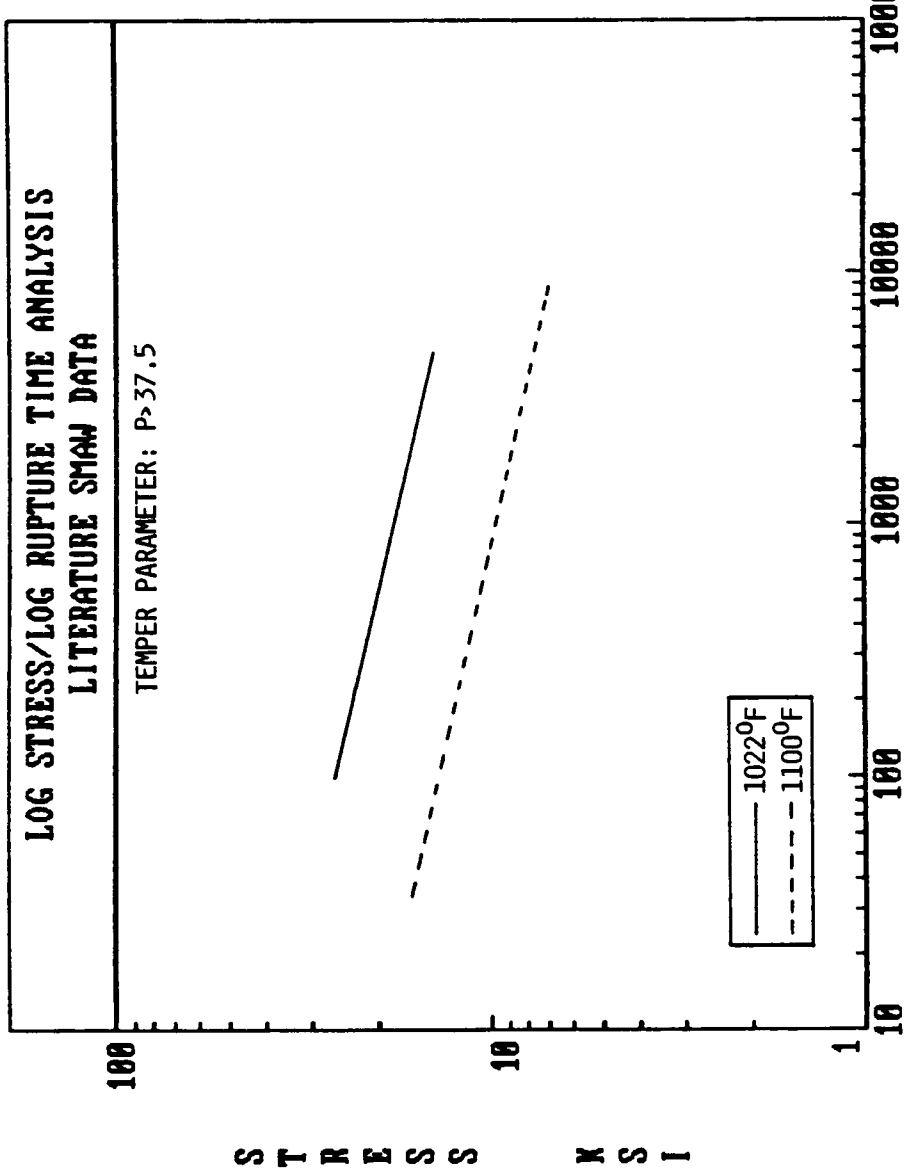


Figure 43. Stress rupture behavior of PWHT 2-1/4Cr-1Mo SMA weld metal (P>37.5) as a function of test temperature determined by analysis of literature data.

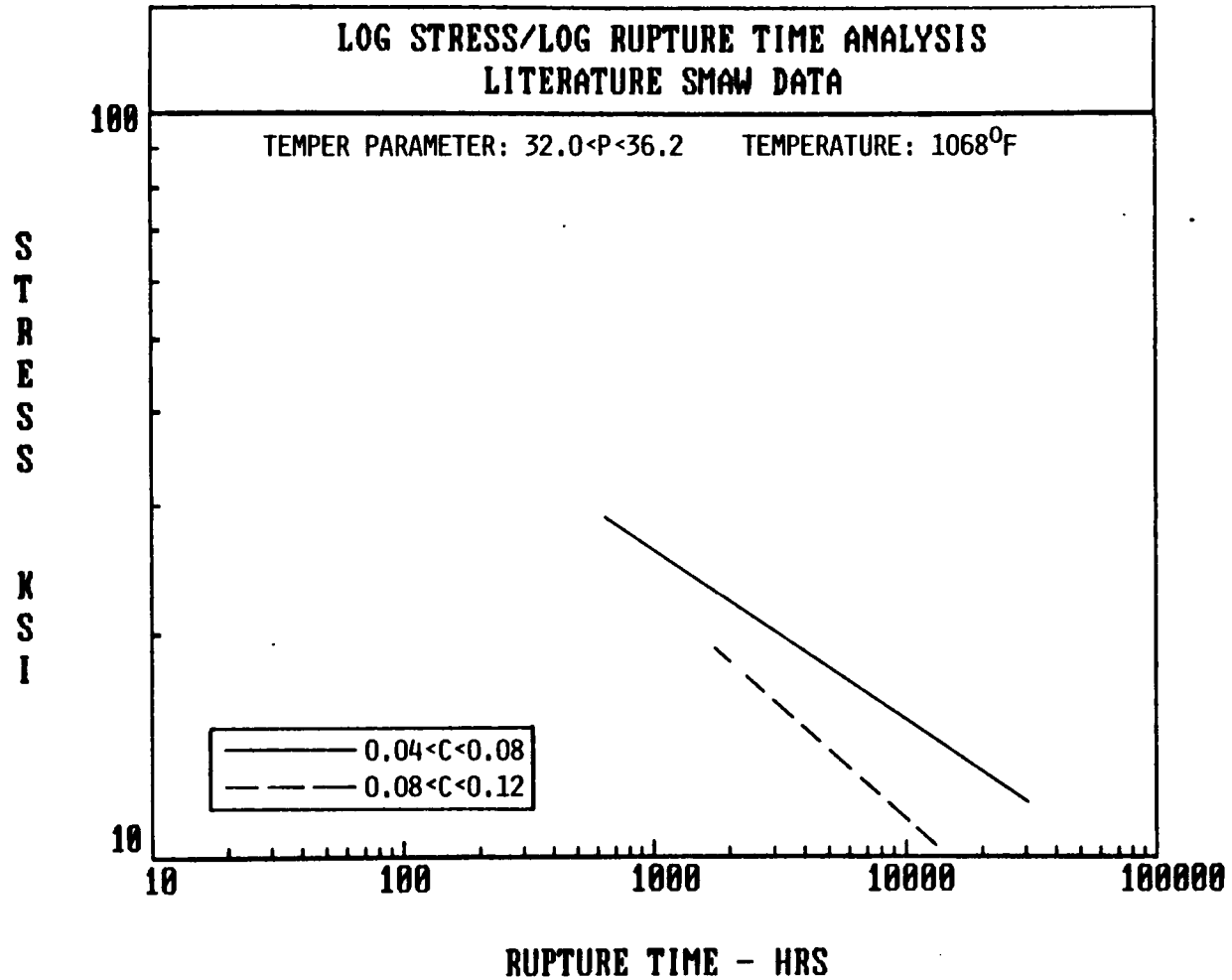


Figure 44. Stress rupture behavior of PWHT 2-1/4Cr-1Mo weld metal ($32.0 < P < 36.2$) at $1068^{\circ}F$ as a function of carbon content determined by analysis of literature data.

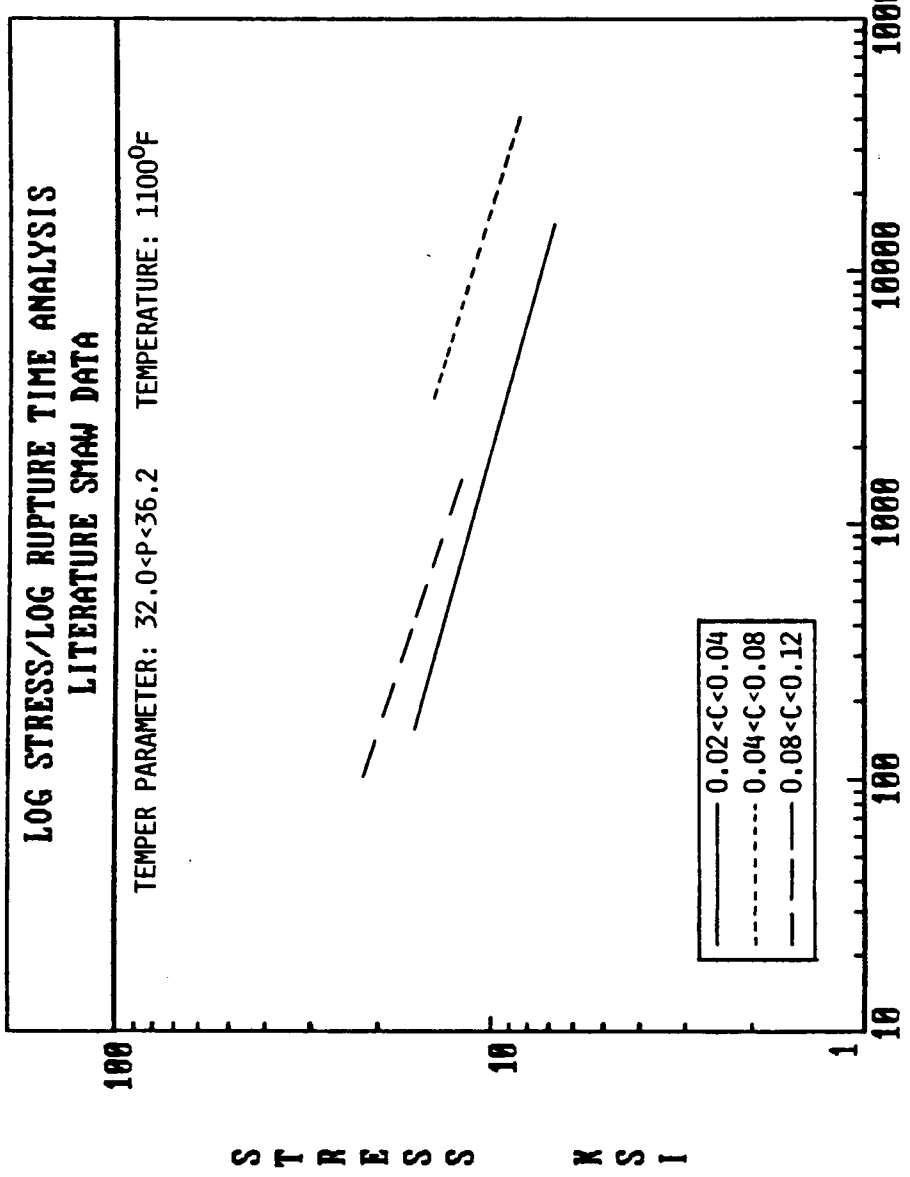


Figure 45. Stress rupture behavior of PWHT 2-1/4Cr-1Mo SMA weld metal ($32.0<P<36.2$) at $1100^{o}F$ as a function of carbon content determined by analysis of literature data.

Table 12. Stress for 100,000 hour rupture as a function of test temperature and temper parameter determined by log stress/log rupture time analysis of 2-1/4Cr-1Mo SMA weld metal literature data.

Temperature (^{o}F)	Stress for 100,000 Hour Rupture (KSI)			
	P<32.0	32.0<P<36.2	36.2<P<37.5	P>37.5
750	-	53.8	-	-
850	71.8	39.9	-	-
900	29.9	-	31.8	-
950	-	27.1	-	-
1000	-	-	12.4	-
1022	-	7.0	9.4	8.8
1050	-	9.4	10.3	-
1058	-	9.5	-	-
1067	-	7.9	-	-
1100	-	5.8	7.2	4.8
1112	-	5.5	-	-
1200	-	-	3.0	-

(32.0<P<36.2) and two temperatures (1068 and 1100°F) (see Figures 44 and 45). The relationship between carbon level and rupture strength indicated by these figures as well as by Table 13 is inconsistent. Figure 44 would seem to indicate that strength falls with an increase in carbon content. Figure 45 shows the strength of the highest and lowest carbon weld metals to be similar while that for the intermediate carbon material is superior. No clear cut trend is therefore discernible.

UTK Data Analysis (Log Stress/Log Rupture Time). Figures 46 through 55 are log stress vs. log rupture time plots obtained for the UTK data. Values of 100,000 hour rupture stress determined by extrapolation of the curves in the figures may be found in Tables 14 and 15.

Figures 46 through 48 illustrate the effect of carbon content on rupture behavior for four carbon content weld metals tested in the Class 2 condition at 850, 950, and 1050°F. It is apparent from these figures that, at all three temperatures, the rupture curve for the low carbon weld metal (0.02-0.03C) is consistently below those for the higher carbon materials with the latter curves falling together. The extrapolated stress values given in Table 14 confirm this trend. Thus, for these Class 2 materials, rupture strength is relatively insensitive to carbon content variations except for levels below 0.04 percent where it appears to increase with increasing carbon levels.

Table 13. Stress for 100,000 hour rupture as a function of test temperature, carbon content, and temper parameter determined by log stress/log rupture time analysis of 2-1/4Cr-1Mo SMA weld metal literature data.

Condition	Stress for 100,000 Hour Rupture (KSI)										
	750°F	850°F	900°F	950°F	1000°F	1022°F	1050°F	1058°F	1067°F	1100°F	1112°F
32.0<P<36.2											
0.02<C<0.04	-	-	-	-	-	-	-	-	-	4.7	-
0.04<C<0.08	-	-	-	-	-	7.0	9.4	9.5	8.9	7.0	5.5
0.08<C<0.12	-	-	-	-	-	-	-	-	5.6	4.6	-
C>0.12	53.8	39.9	-	27.1	-	-	-	-	-	-	-
36.2<P<37.5											
0.04<C<0.08	-	-	31.8	-	15.6	9.4	-	-	-	10.1	-
0.08<C<0.12	-	-	-	-	-	-	6.0	-	-	-	-
P>37.5											
0.02<C<0.04	-	-	-	-	-	-	-	-	-	4.8	-
0.04<C<0.08	-	-	-	-	-	8.8	-	-	-	-	-

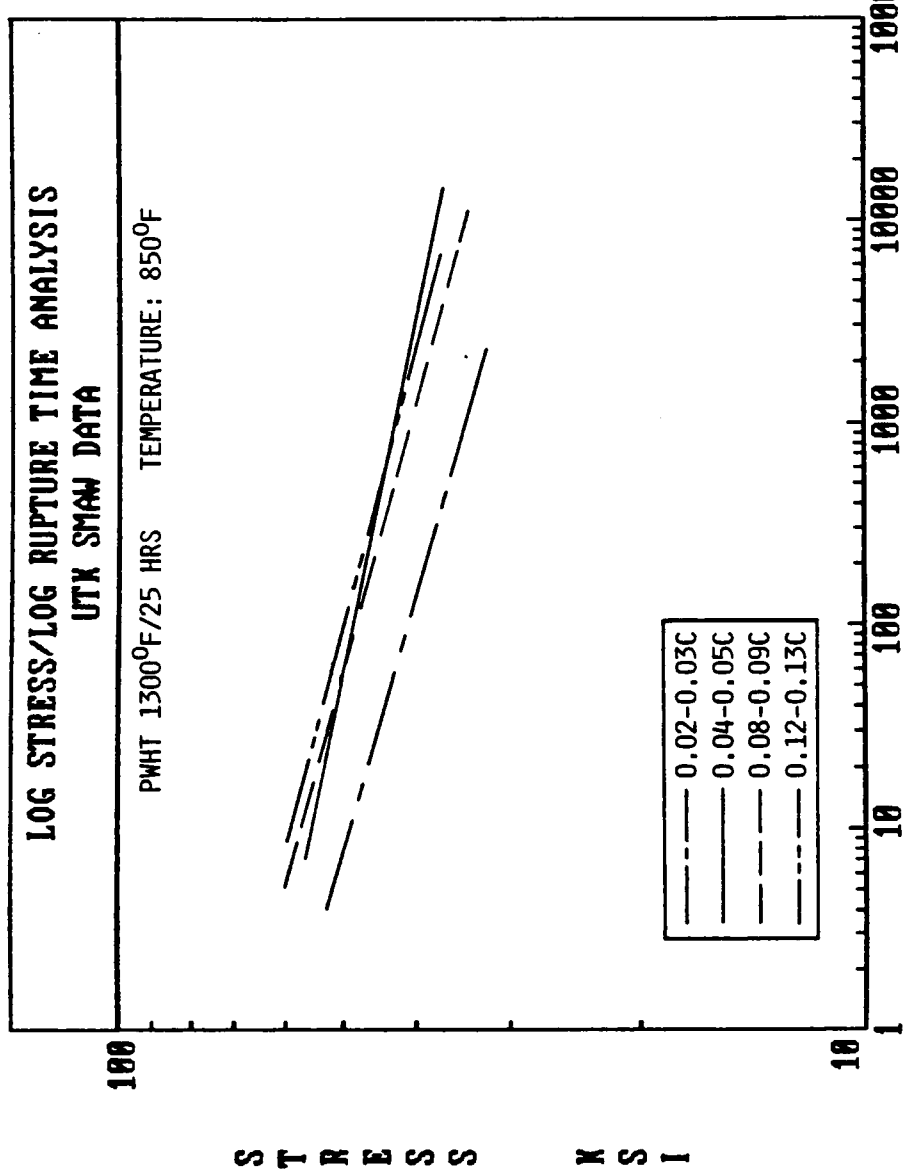


Figure 46. Stress rupture behavior of 2-1/4Cr-1Mo SMA weld metal (PWHT 1300°F/25 hrs.) at 850°F as a function of carbon content determined by analysis of UTK data.

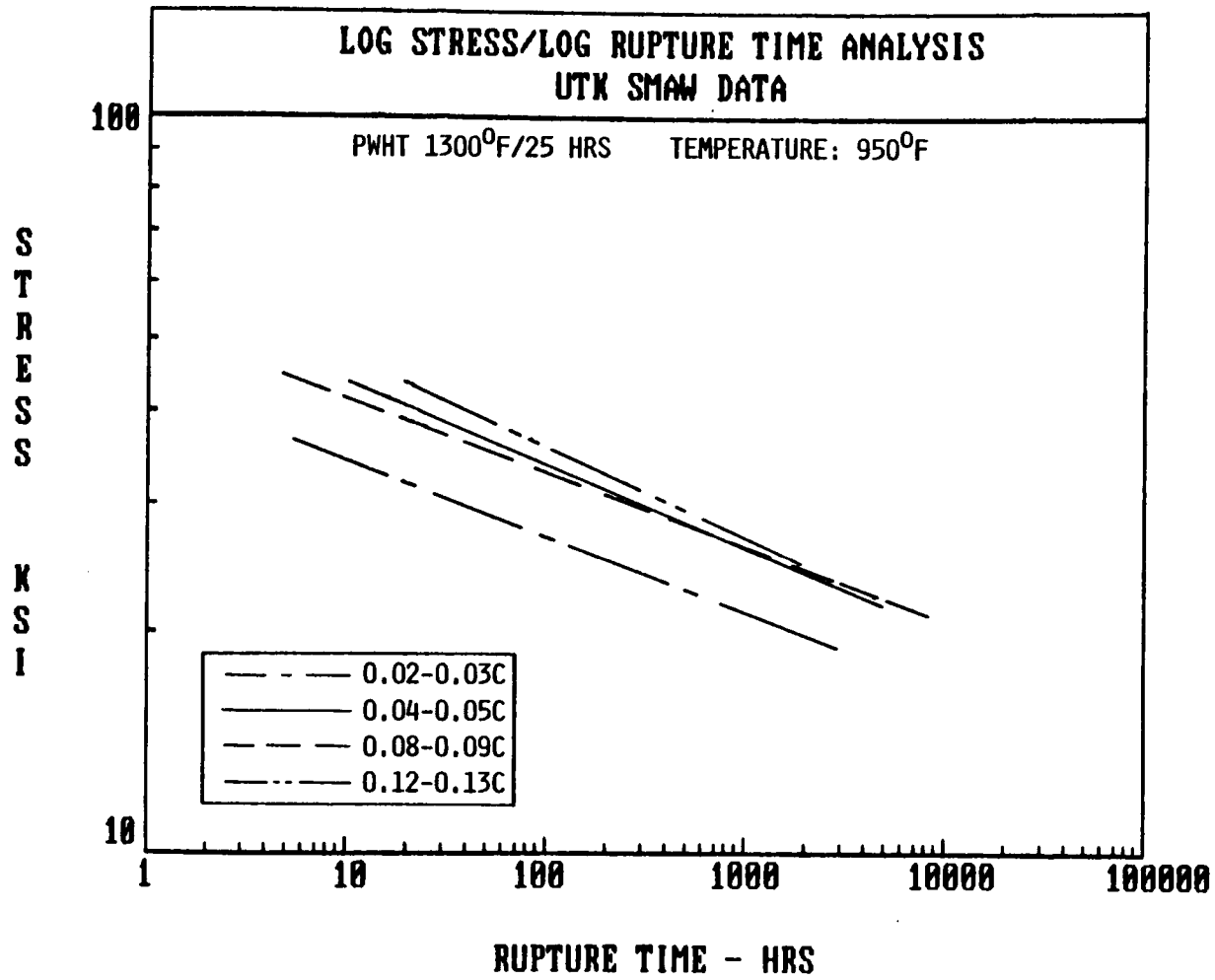


Figure 47. Stress rupture behavior of 2-1/4Cr-1Mo SMA weld metal (PWHT 1300°F/25 hrs.) at 950°F as a function of carbon content determined by analysis of UTK data.

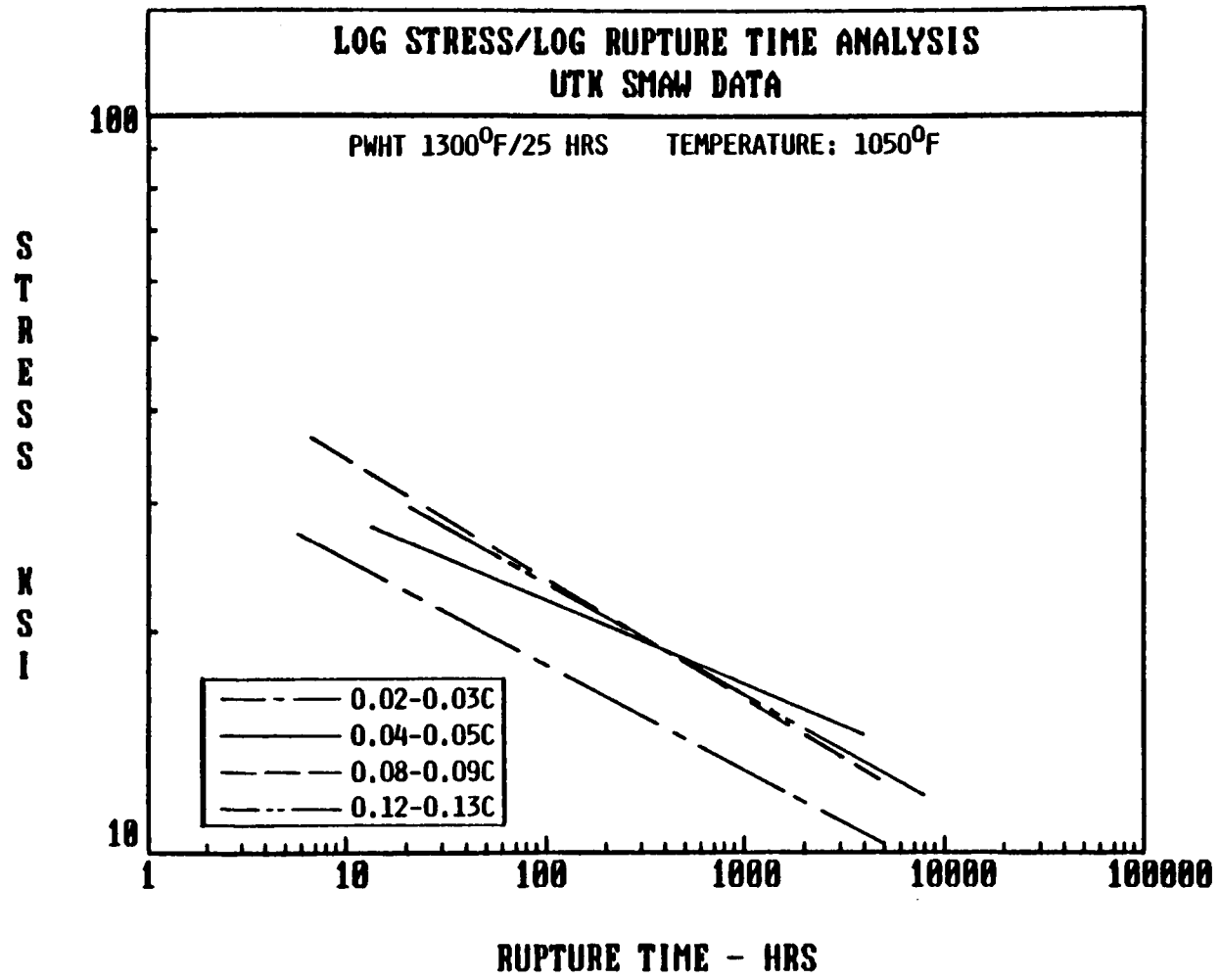


Figure 48. Stress-rupture behavior of 2-1/4Cr-1Mo SMA weld metal (PWHT 1300°F/25 hrs.) at 1050°F as a function of carbon content determined by analysis of UTK data.

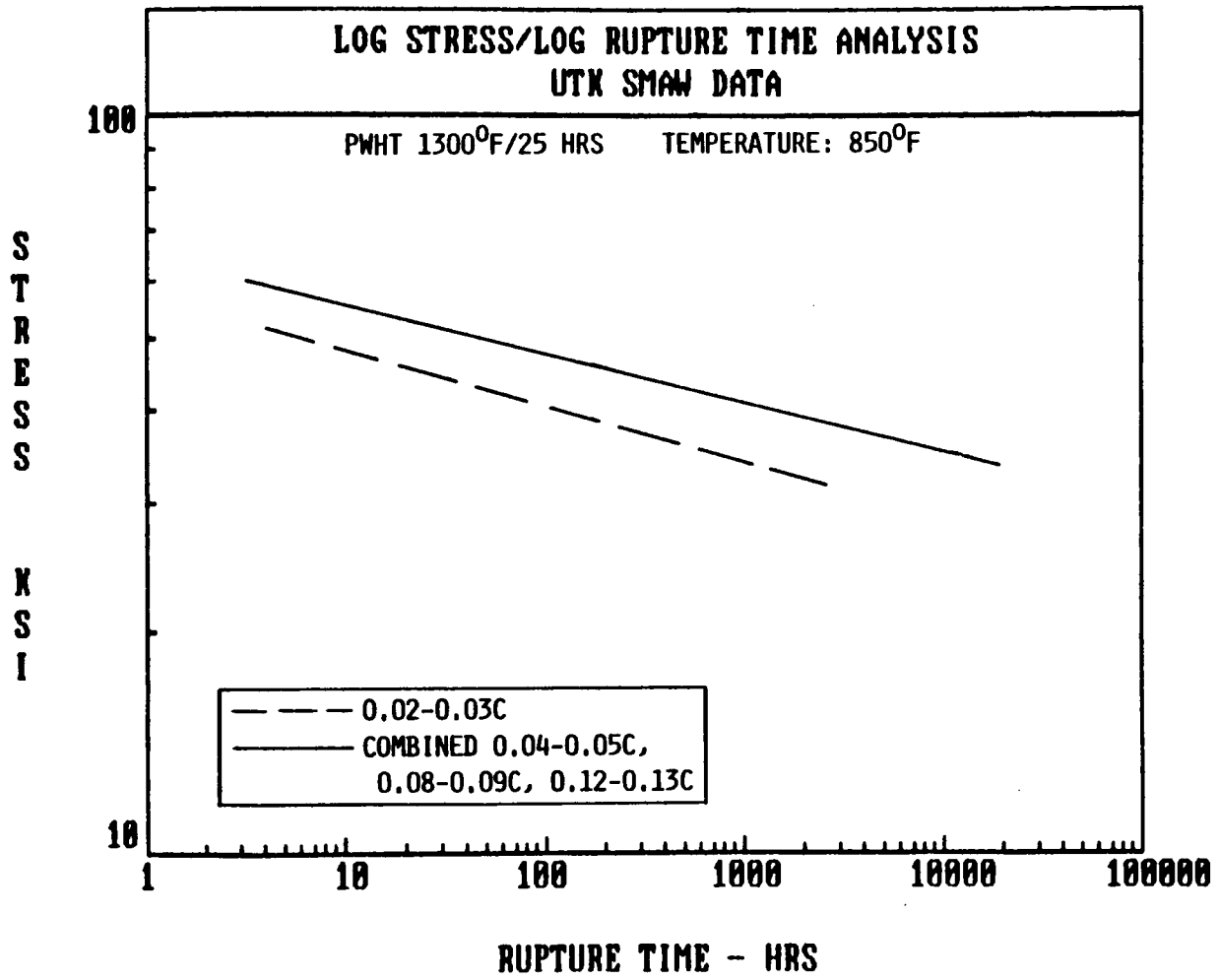


Figure 49. Stress rupture behavior of 0.02-0.03 and 0.04-0.13 carbon 2-1/4Cr-1Mo SMA weld metal (PWHT 1300°F/25 hrs.) at 850°F as a function of carbon content determined by analysis of UTK data.

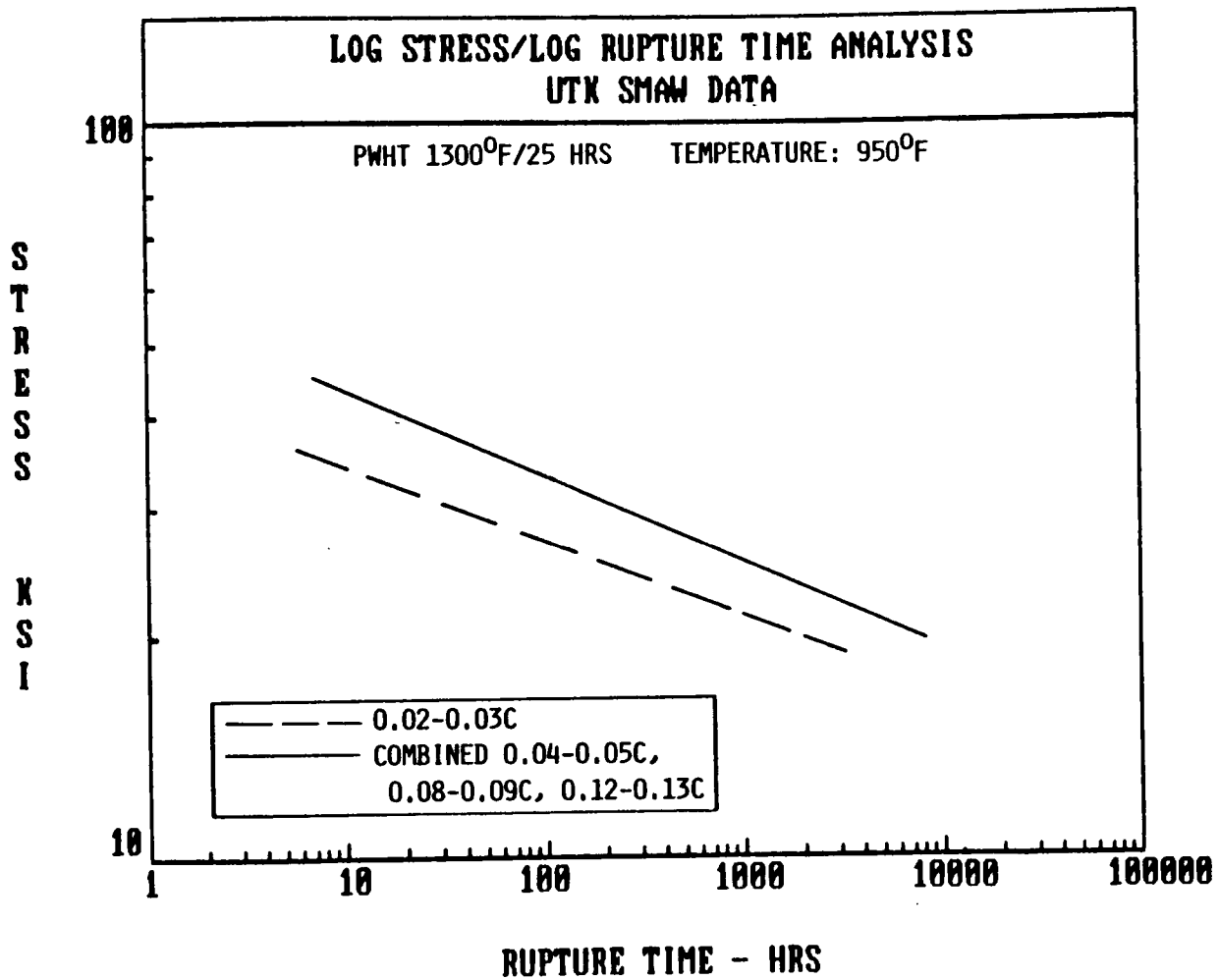


Figure 50. Stress rupture behavior of 0.02-0.03 and 0.04-0.13 carbon 2-1/4Cr-1Mo SMA weld metal (PWHT 1300°F/25 hrs.) at 950°F as a function of carbon content determined by analysis of UTK data.

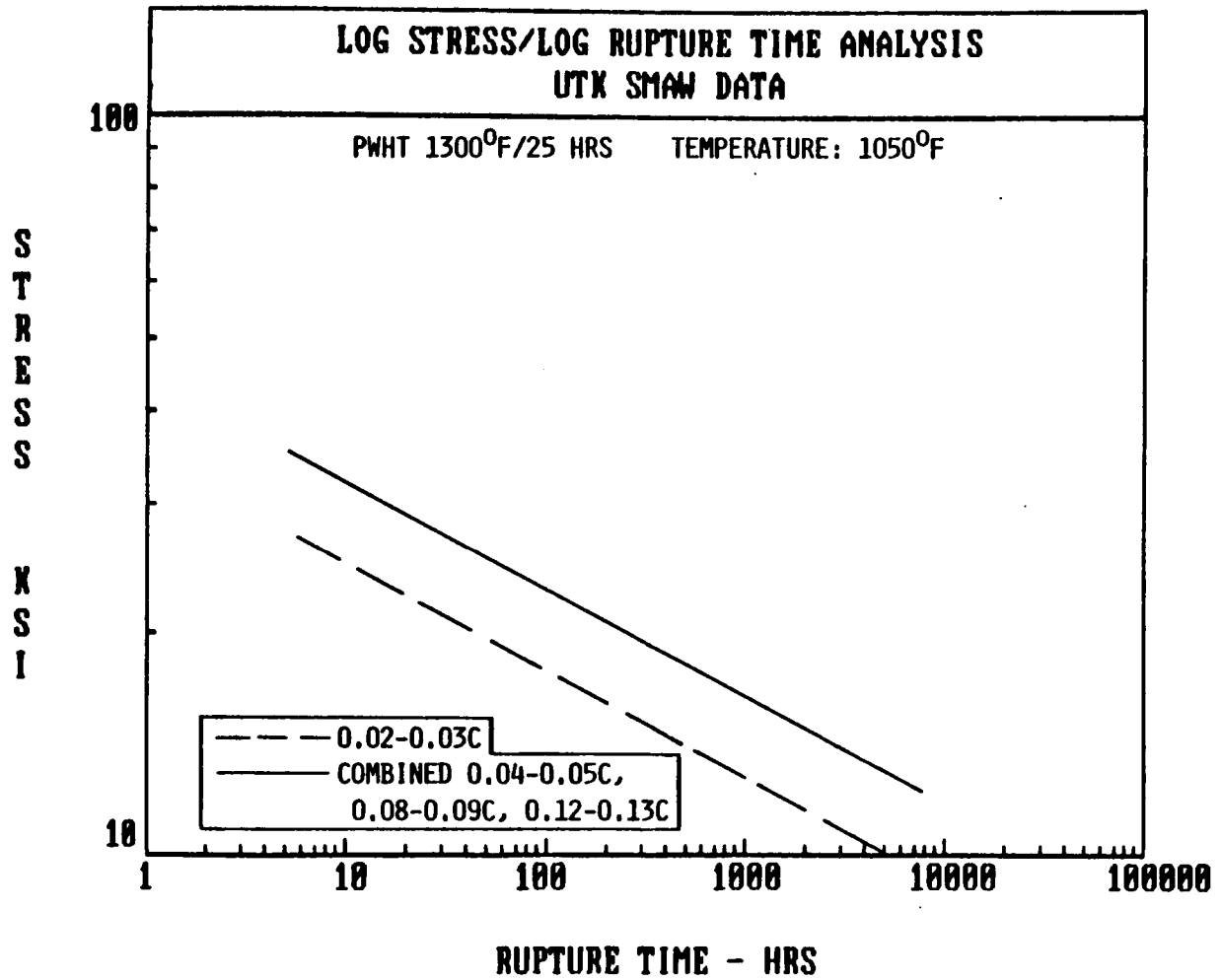


Figure 51. Stress rupture behavior of 0.02-0.03 and 0.04-0.13 carbon 2-1/4Cr-1Mo SMA weld metal (PWHT 1300°F/25 hrs.) at 1050°F as a function of carbon content determined by analysis of UTK data.

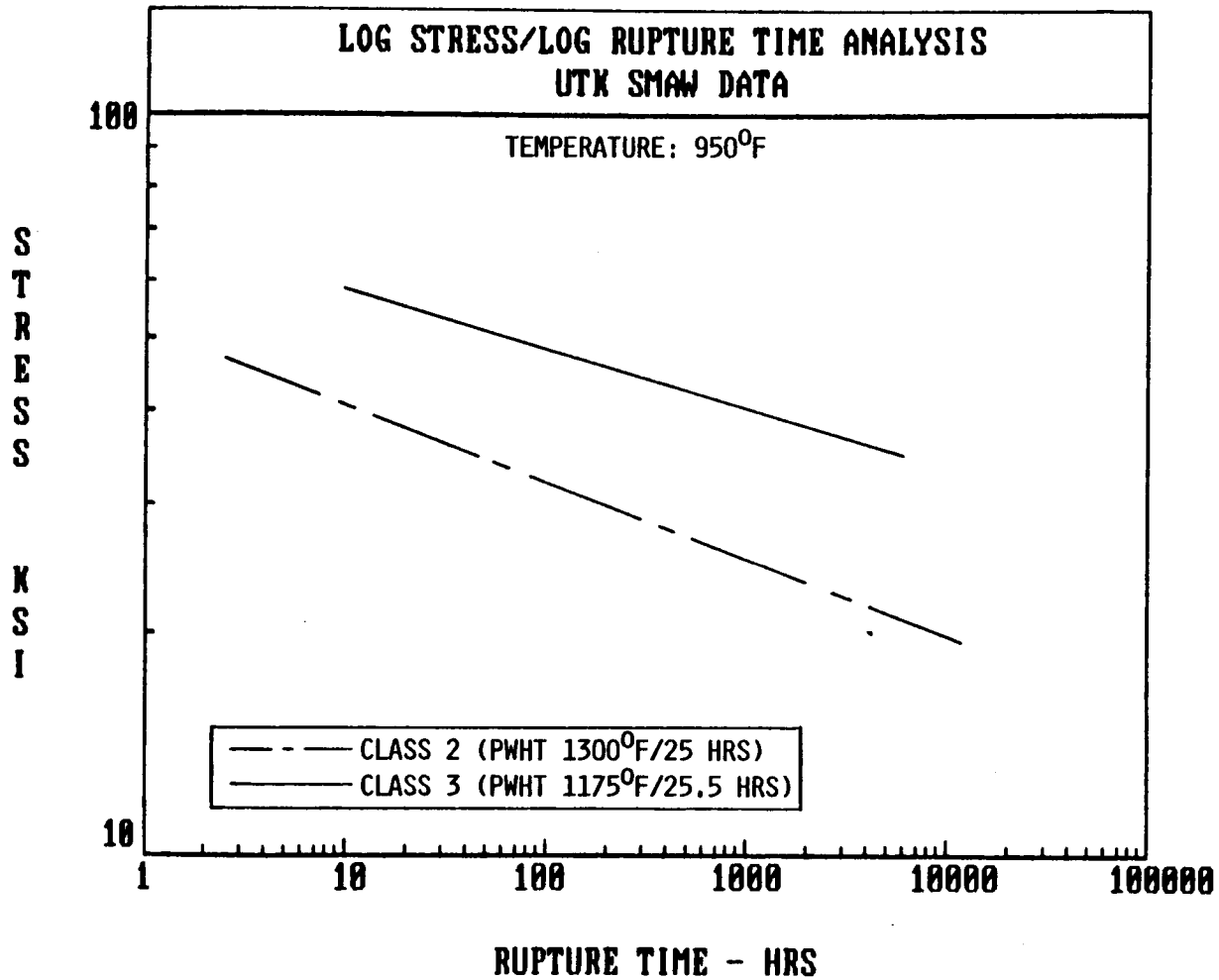


Figure 52. Stress rupture behavior of 2-1/4Cr-1Mo SMA weld metal at 950°F as a function PWHT determined by analysis of UTK data.

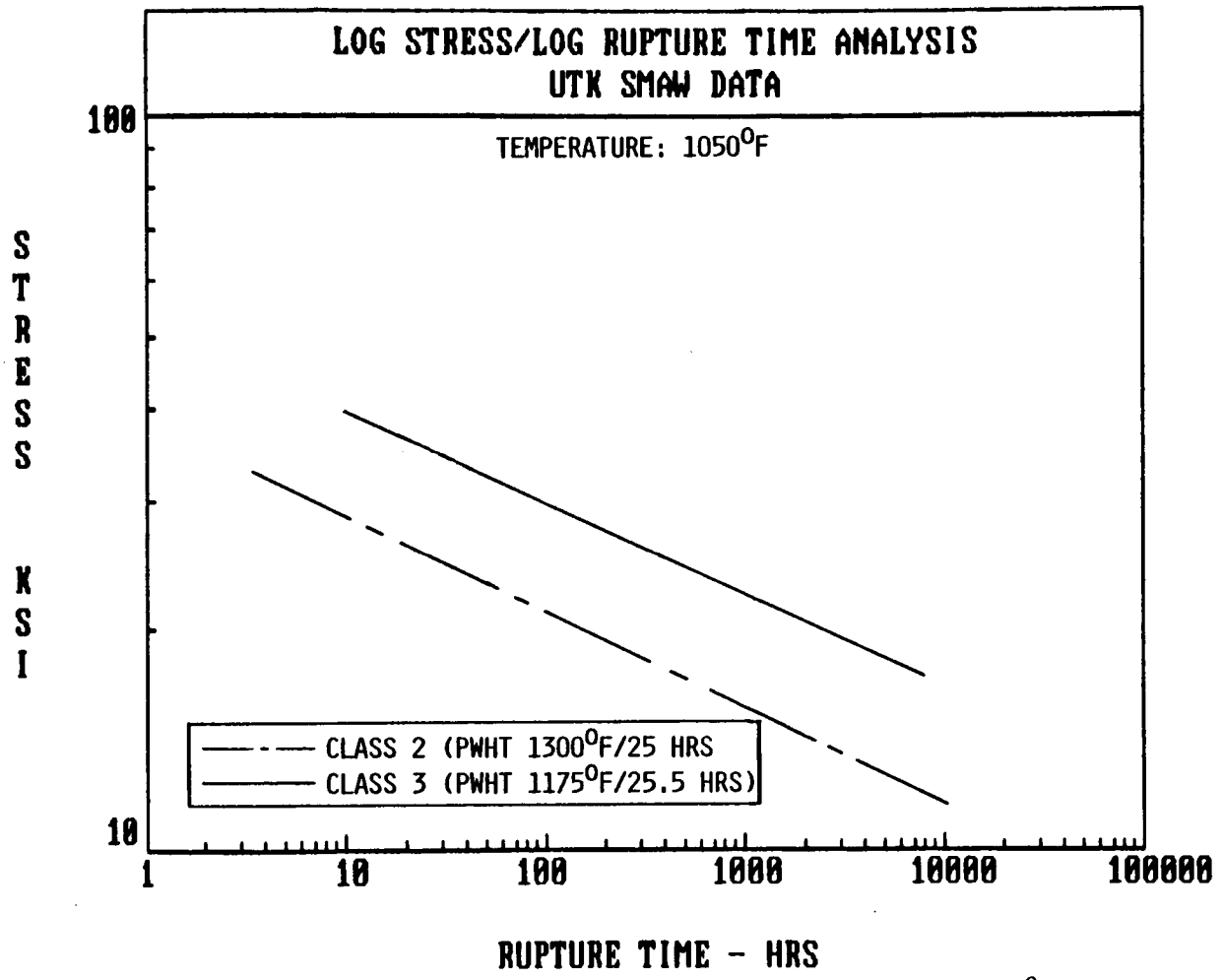


Figure 53. Stress rupture behavior of 2-1/4Cr-1Mo SMA weld metal at 1050°F as a function of PWHT determined by analysis of UTK data.

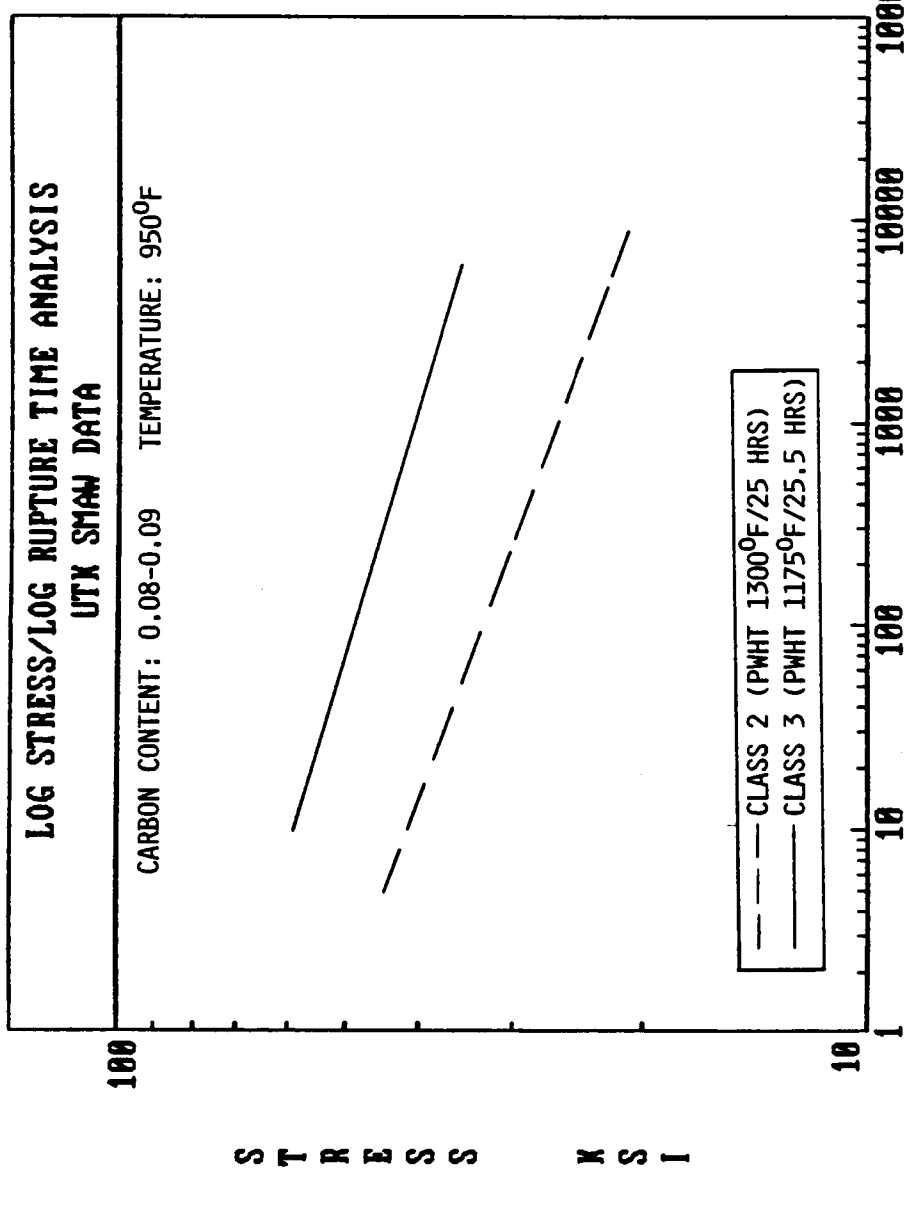


Figure 54. Stress rupture behavior of 0.08-0.09 carbon 2-1/4Cr-1Mo SMA weld metal at 950°F as a function of PWHT determined by analysis of UTK data.

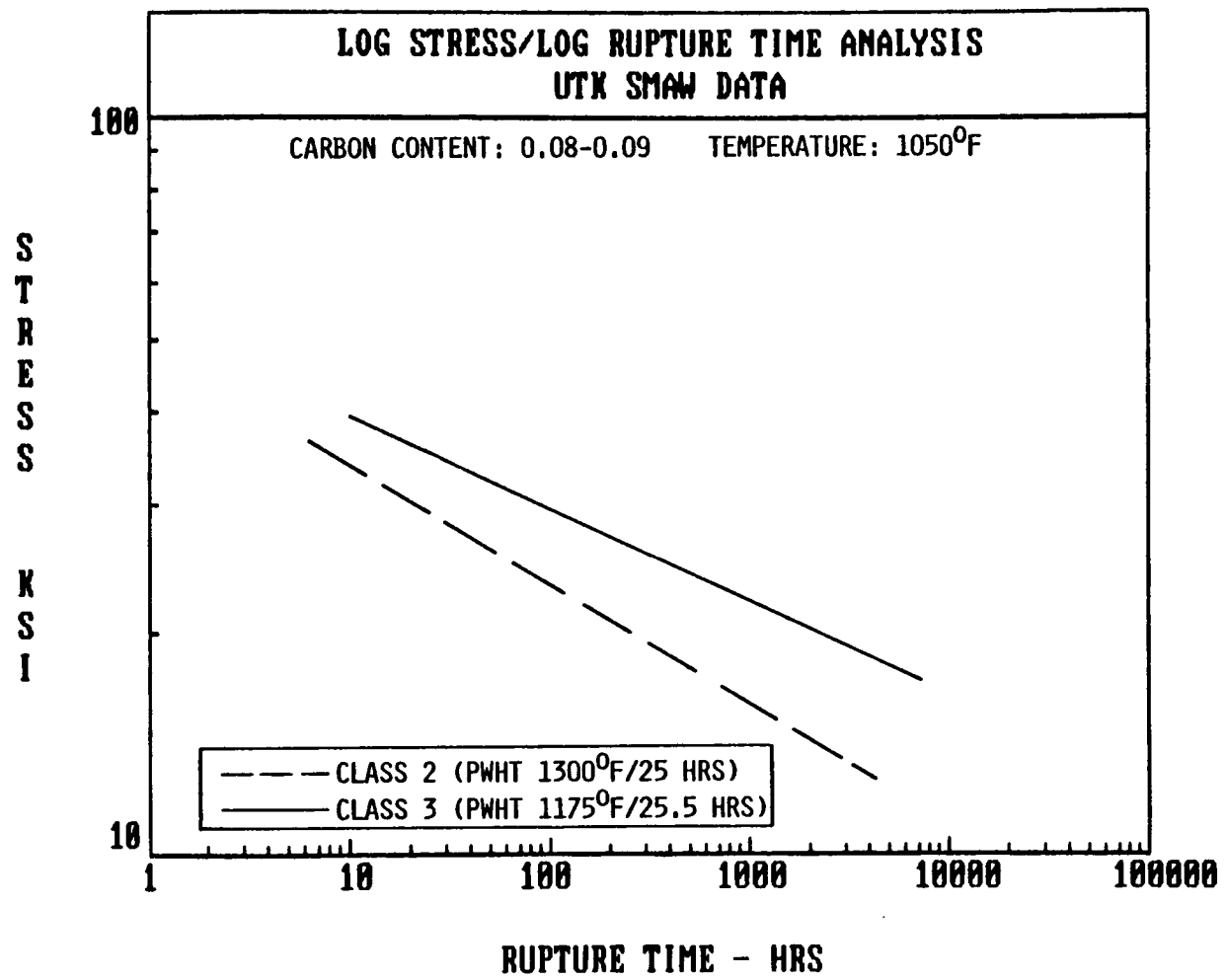


Figure 55. Stress rupture behavior of 0.08-0.09 carbon 2-1/4Cr-1Mo SMA weld metal at 1050°F as a function of PWHT determined by analysis of UTK data.

Table 14. Stress for 100,000 hour rupture as a function of test temperature and carbon content determined by log stress/log rupture time analysis of C1. 2 UTK data.

Carbon Content	Stress for 100,000 Hour Rupture (KSI)		
	850°F	950°F	1050°F
0.02-0.03	24.4	13.2	6.6
0.04-0.05	32.6	15.5	9.8
0.08-0.09	28.4	16.7	7.7
0.12-0.13	29.9	15.2	8.1
0.04-0.05, 0.08-0.09, 0.12-0.13 Combined	30.3	15.7	8.4

Table 15. Stress for 100,000 hour rupture of 2-1/4Cr-1Mo SMA weld metal as a function of temperature and PWHT determined by log stress/log rupture time analysis of UTK data.

Data	Temper Parameter	Stress for 100,000 Hour Rupture (KSI)		
		850°F	950°F	1050°F
Class 3	35.0	-	28.5	13.2
Class 2	37.7	29.9	15.6	8.6
Class 2 w/o 0.02-0.03C	37.7	30.3	15.7	8.4

In light of the observed strength dependence on carbon content, experimental data for the 0.04-0.05, 0.08-0.09, and 0.12-0.13 carbon weld metal have been combined and analyzed as a single population. The resulting curves, shown in Figures 49, 50, and 51, summarize the rupture behavior of the Class 2 weld metal as a function of test temperature and carbon content.

Figures 52 and 53 compare the rupture behavior of the Class 2 and Class 3 weld metal at 950 and 1050°F independent of carbon content. Examination of these plots reveals the superior rupture strength of the Class 3 weld metal. Corresponding values of 100,000 hour stress given in Table 15 indicate that the Class 3 weld metal 100,000 hour rupture stress is roughly 1 1/2 times that for Class 2 material at both temperatures.

The stress rupture behavior of the Class 2 and Class 3 weld metals illustrated in Figures 52 and 53 is somewhat affected by the fact that the Class 2 data employed in the analysis is from testing of four carbon content weld metals. A more accurate comparison of Class 2 and Class 3 rupture behavior is shown in Figures 54 and 55 in which the curves are derived form the analysis of 0.08-0.09 carbon weld metal. Examination of the figures indicates that the superior strength of the Class 3 weld metal remains evident.

Combined Analysis of Literature and UTK Data (Log Stress/Log Rupture Time). Figures 56 through 62 are plots of log stress vs. log rupture time derived from regression analyses of SMA literature and UTK data combined. Figures 56 and 57 present the curves for

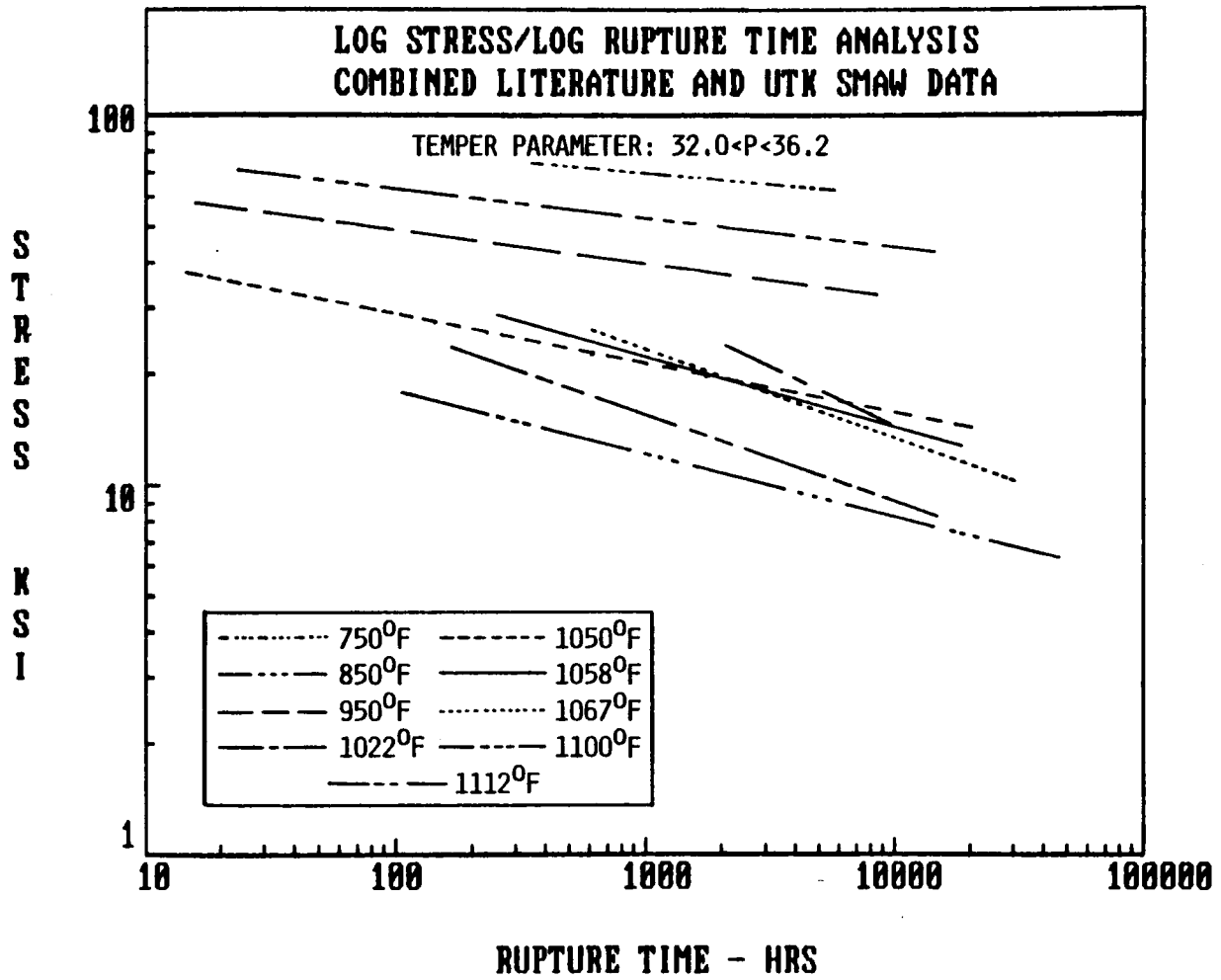


Figure 56. Stress rupture behavior of PWHT 2-1/4Cr-1Mo SMA weld metal (32.0<P<36.2) as a function of test temperature determined by analysis of combined literature and UTK data.

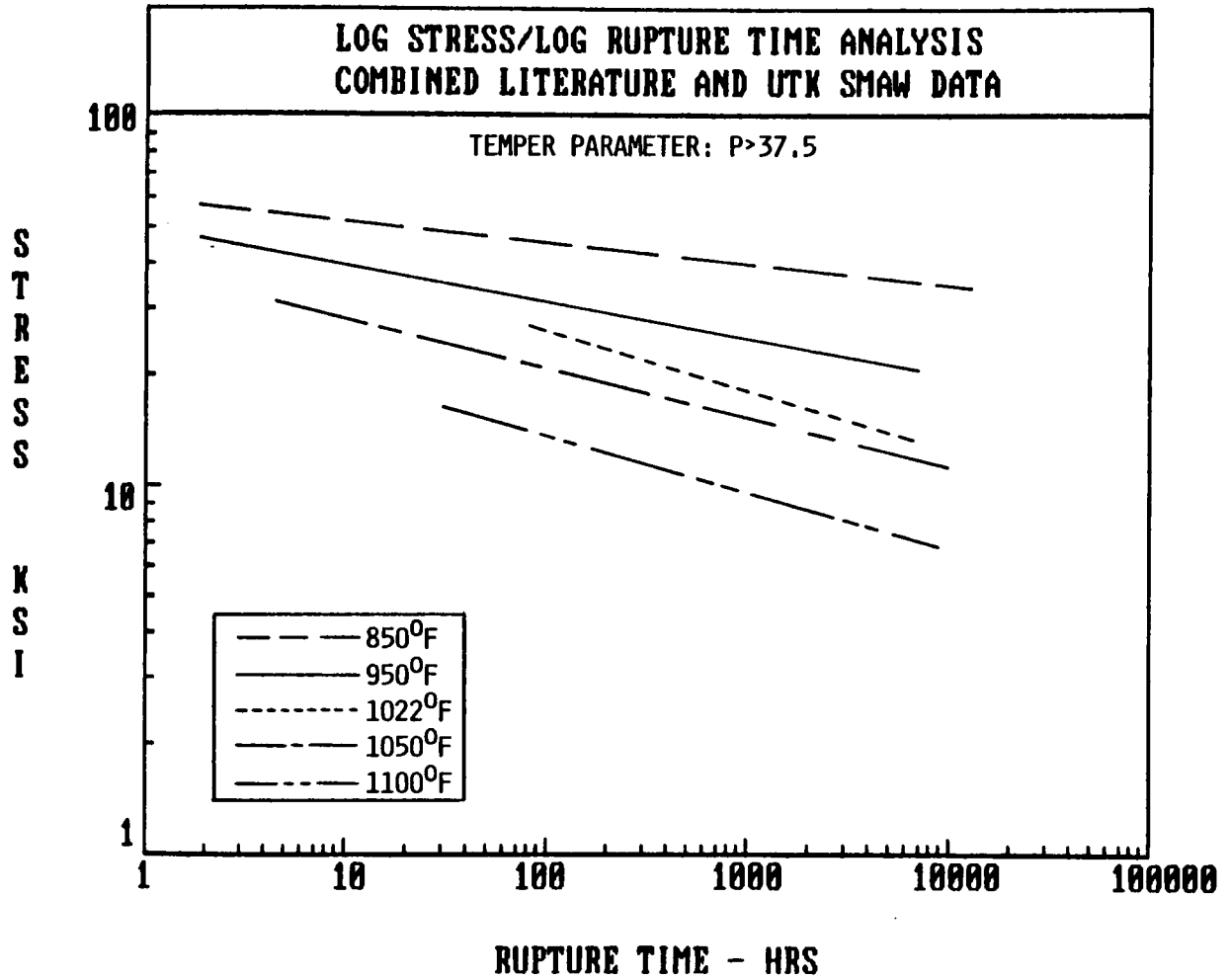


Figure 57. Stress rupture behavior of PWHT 2-1/4Cr-1Mo SMA weld metal (P>37.5) as a function of test temperature determined by analysis of combined literature and UTK data.

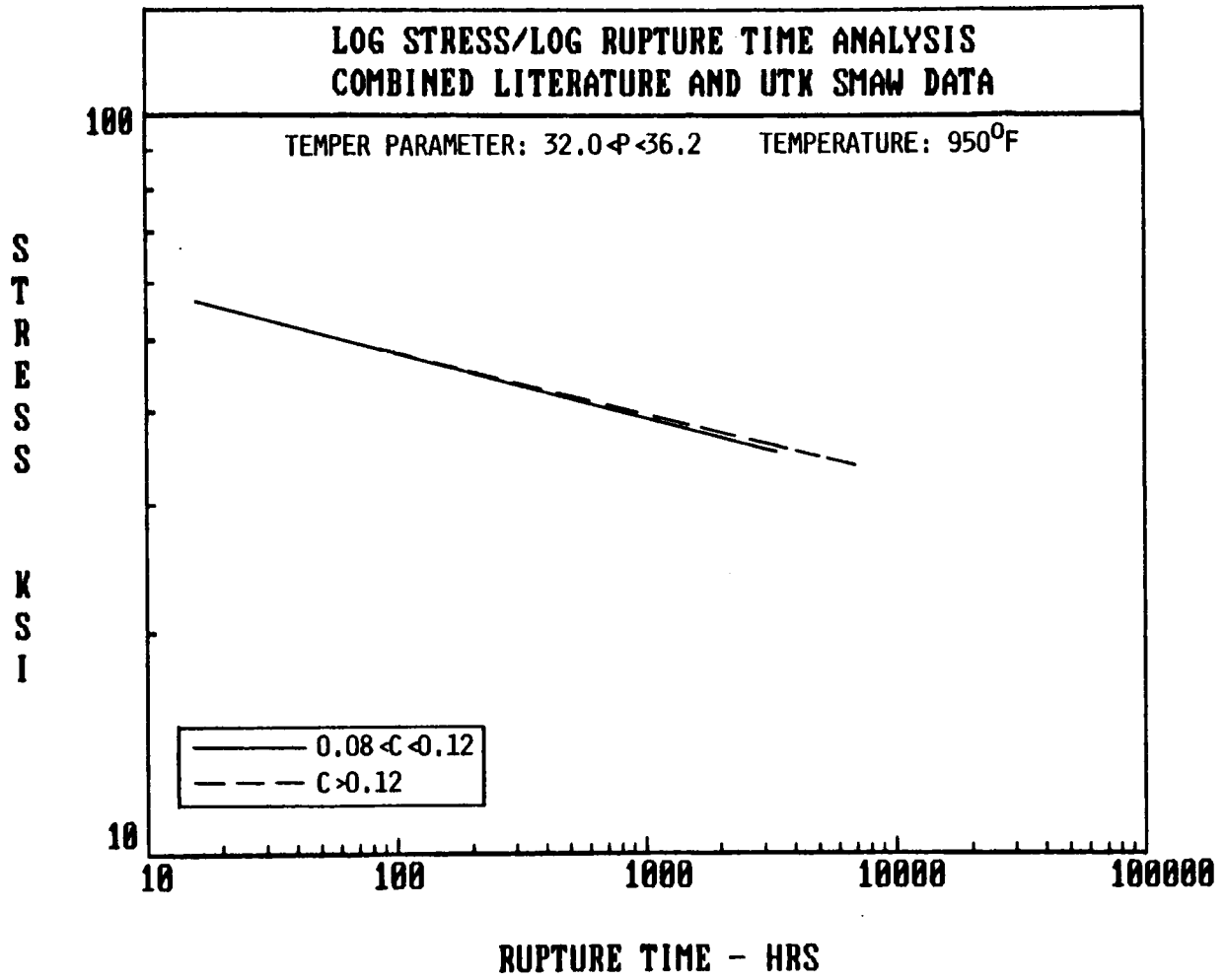


Figure 58. Stress rupture behavior of PWHT 2-1/4Cr-1Mo SMA weld metal (32.0<P<36.2) at 950°F as a function of carbon content determined by analysis of combined literature and UTK data.

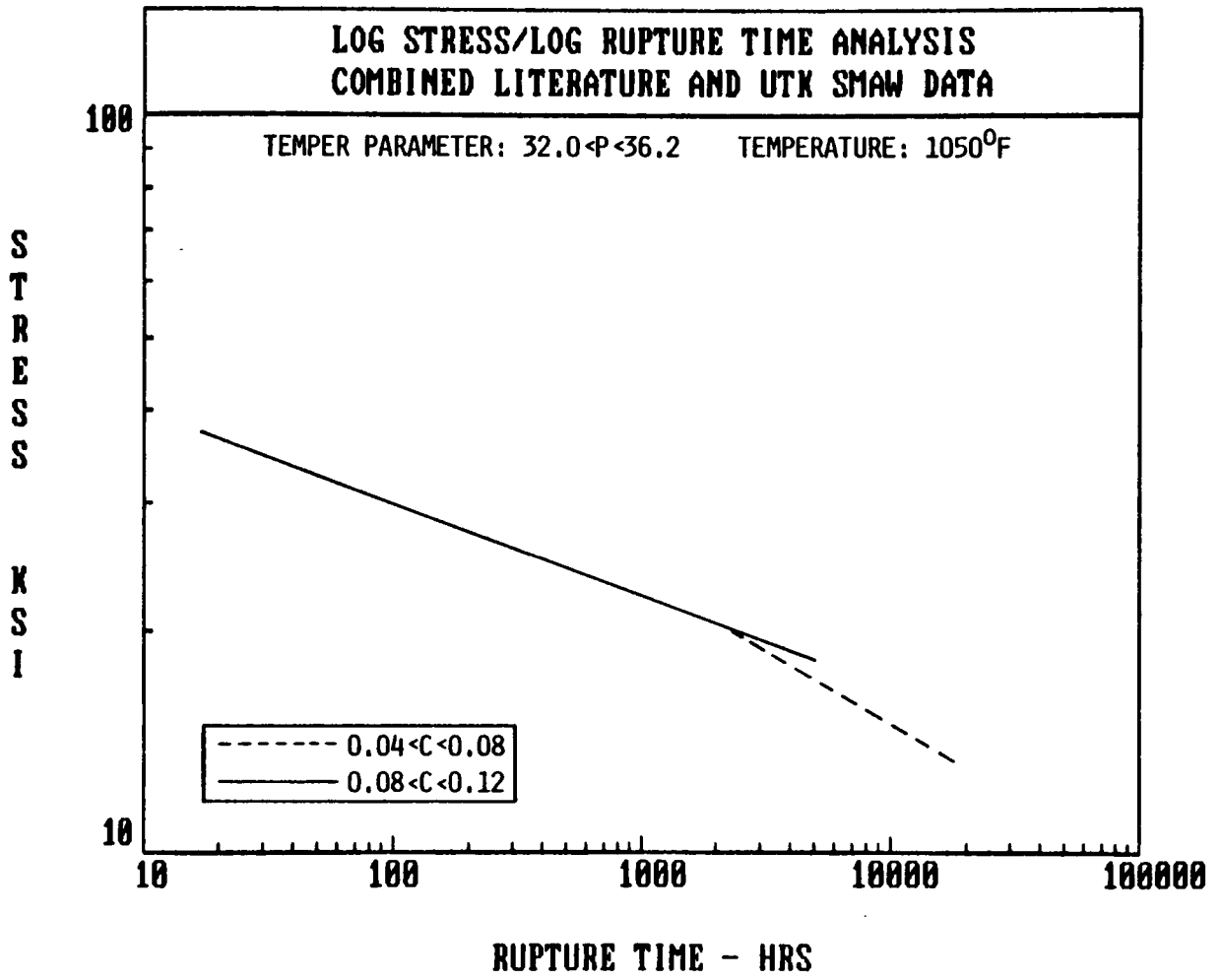


Figure 59. Stress rupture behavior of PWHT 2-1/4Cr-1Mo SMA weld metal (32.0<P<36.2) at 1050°F as a function of carbon content determined by analysis of combined literature and UTK data.

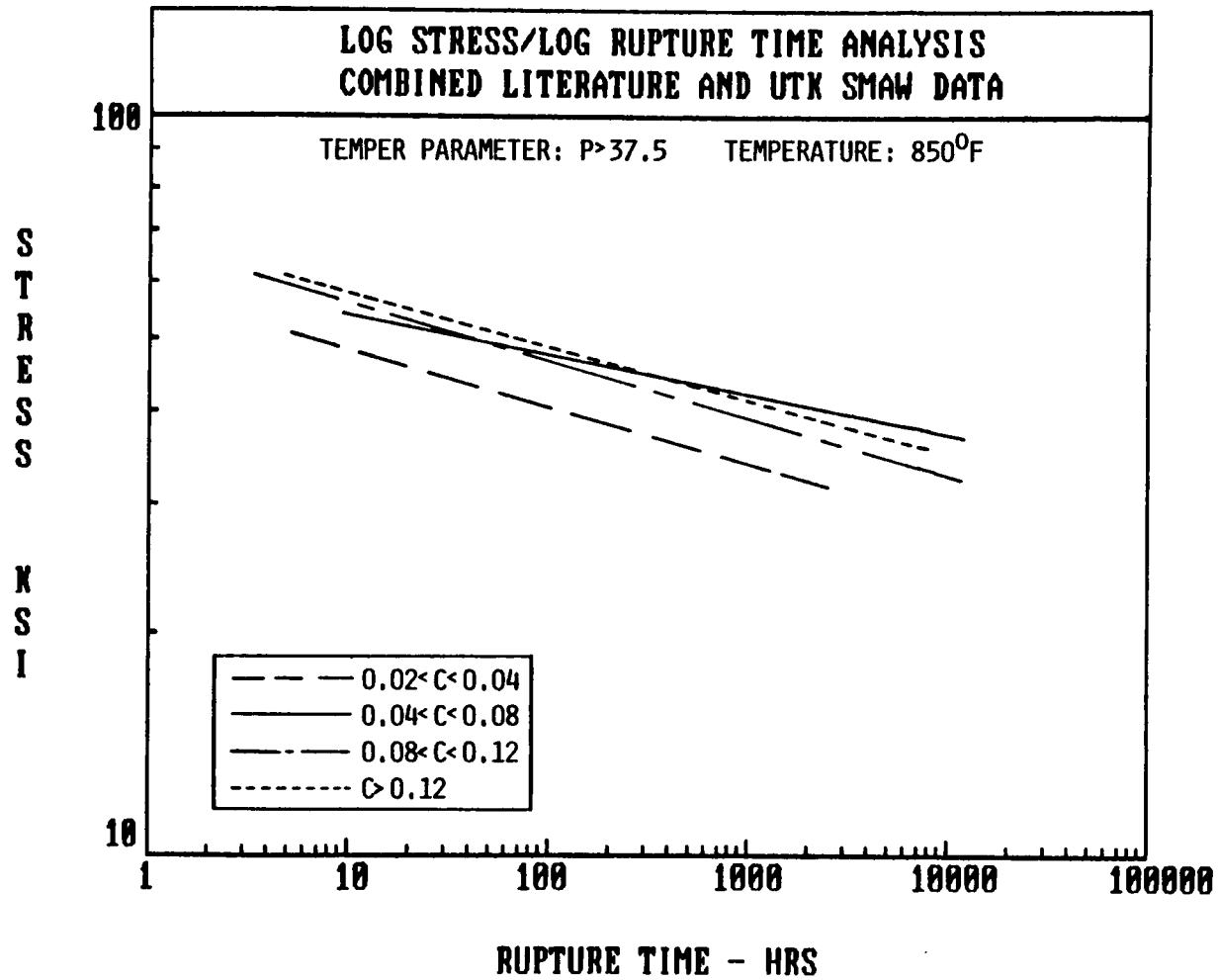


Figure 60. Stress rupture behavior of PWHT 2-1/4Cr-1Mo SMA weld metal (P>37.5) at 850°F as a function of carbon content determined by analysis of combined literature and UTK data.

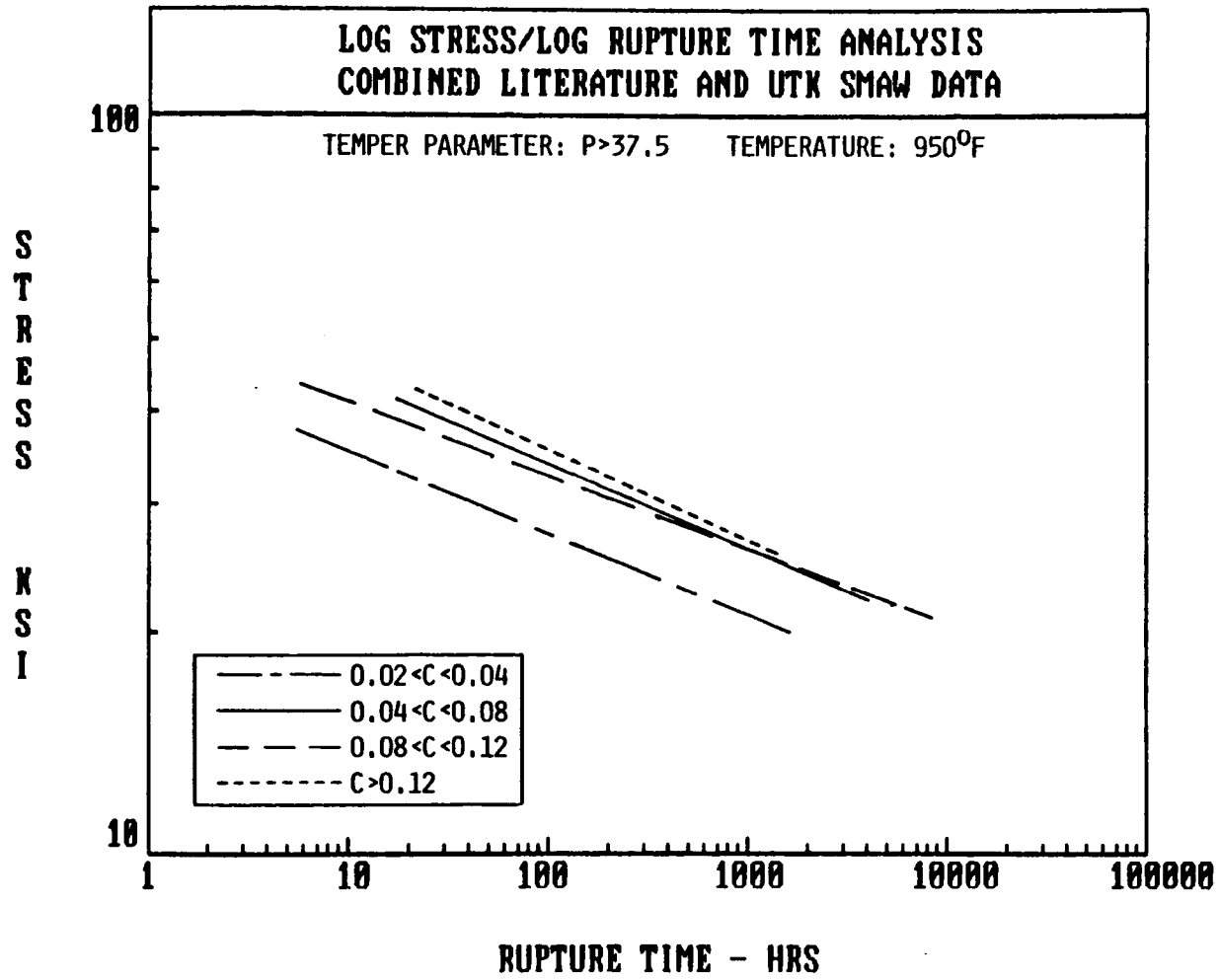


Figure 61. Stress rupture behavior of PWHT 2-1/4Cr-1Mo SMA weld metal (P>37.5) at 950°F as a function of carbon content determined by analysis of combined literature and UTK data.

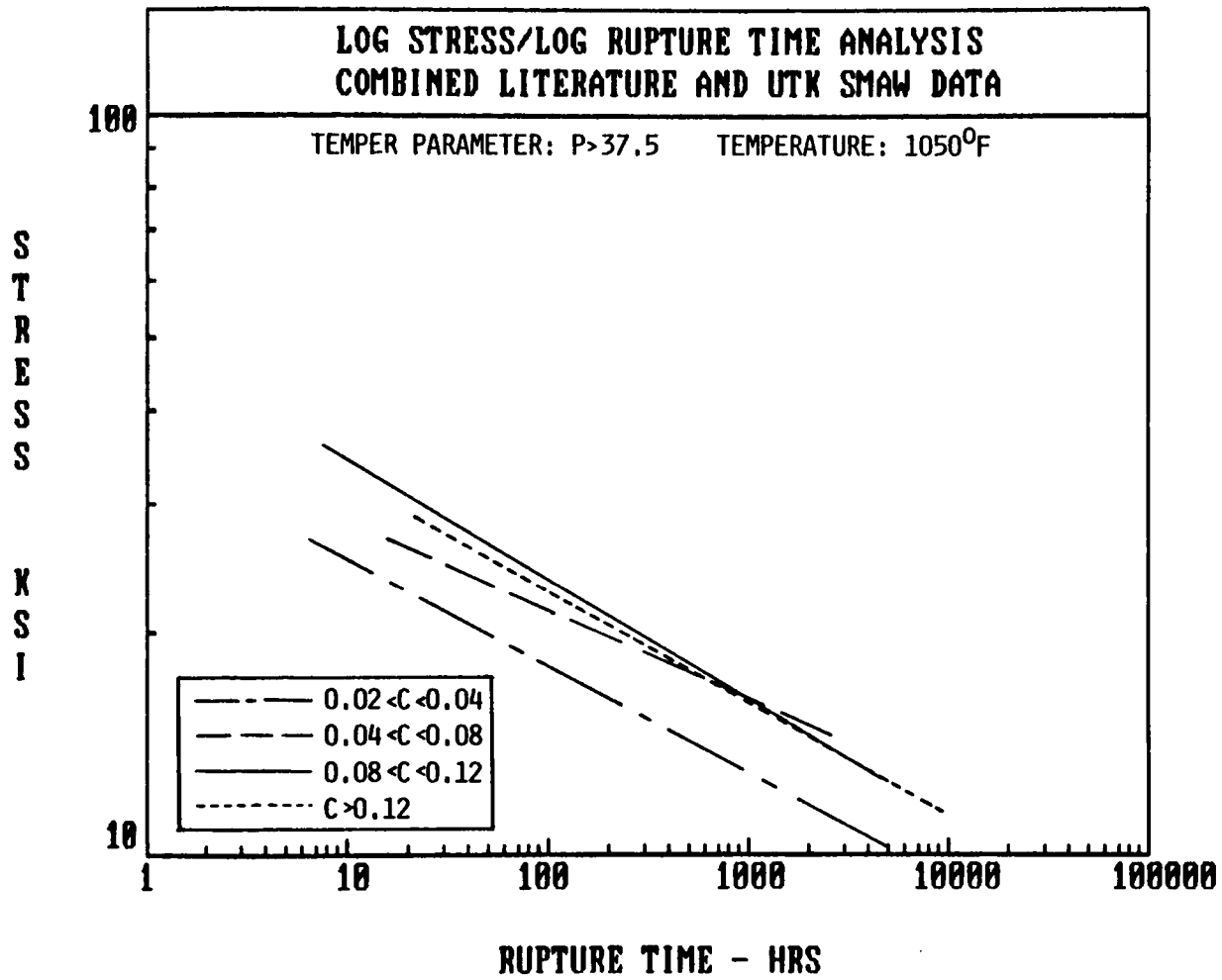


Figure 62. Stress rupture behavior of PWHT 2-1/4Cr-1Mo SMA weld metal (P>37.5) at 1050°F as a function of carbon content determined by analysis of combined literature and UTK data.

$32.0<P<36.2$ and $P>37.5$ respectively as modified by the addition of UTK data. Figures 58 and 59 show the effect of carbon level on the rupture behavior of weld metal PWHT with $32.0<P<36.2$ at 950 and $1050^{o}F$ respectively. Similarly, Figures 60, 61, and 62 illustrate the carbon effect for PWHT material ($P>37.5$) at 850, 950, and $1050^{o}F$. In general, only those curves which have been altered by the data addition have been included.

Tables 16 and 17 list the 100,000 hour stresses for various test temperatures extrapolated from the figures above. Table 16 lists the stresses as a function of temper parameter. Table 17 illustrates the effect of carbon content on the 100,000 hour rupture stress within each temper parameter range. Comparing Tables 12 (p. 134) and 16, it is evident that, in the temper parameter range $32.0<P<36.2$, the 100,000 hour stress at $950^{o}F$ remains essentially unchanged. However, the $1050^{o}F$ stress increases by a third. Comparison of Figures 56 and 41 (p.129) indicates that the increase is due to a decrease in slope of the curve in response to the data addition. For the temper parameter range, $P>37.5$, the addition of the UTK data only increases the number of test temperatures studied as the two data bases in this range possess no common temperatures.

Because of the variation in the 100,000 hour stresses obtained using the log stress/log rupture time analysis, the effects of PWHT and carbon content on rupture strength are difficult to observe. At temperatures below $1050^{o}F$, Table 16 shows some evidence of decreasing rupture strength with increasing temper parameter. In Table 17, the only consistent relationship between carbon level and rupture

Table 16. Stress for 100,000 hour rupture of 2-1/4Cr-1Mo weld metal as a function of test temperature and temper parameter determined by log stress/log rupture time analysis of combined literature and UTK data.

	Stress for 100,000 Hour Rupture (KSI)			
Temperature (^{o}F)	P<32.0	32.0<P<36.2	36.2<P<37.5	P>37.5
750	-	53.8	-	-
850	71.8	39.9	-	31.3
900	29.9	-	31.8	-
950	-	26.9	-	16.4
1000	-	-	12.4	-
1022	-	7.0	9.4	8.8
1050	-	12.1	10.3	8.4
1058	-	9.5	-	-
1067	-	7.9	-	-
1100	-	5.8	7.2	4.8
1112	-	5.5	-	-
1200	-	-	3.0	-

Table 17. Stress for 100,000 hour rupture of 2-1/4Cr-1Mo SMA weld metal as a function of test temperature, carbon content, and temper parameter determined by log stress/log rupture time analysis of combined literature and UTK data.

Condition	Stress for 100,000 Hour Rupture (KSI)										
	750°F	850°F	900°F	950°F	1000°F	1022°F	1050°F	1058°F	1067°F	1100°F	1112°F
32.0<P<36.2											
0.02<C<0.04	-	-	-	-	-	-	-	-	-	4.7	-
0.04<C<0.08	-	-	-	-	-	7.0	9.4	9.5	8.9	7.0	5.5
0.08<C<0.12	-	-	-	26.7	-	-	14.1	-	5.6	4.6	-
C>0.12	53.8	39.9	-	27.1	-	-	-	-	-	-	-
36.2<P<37.5											
0.04<C<0.08	-	-	31.8	-	15.6	9.4	-	-	-	10.1	-
0.08<C<0.12	-	-	-	-	-	-	6.0	-	-	-	-
P>37.5											
0.02<C<0.04	-	24.4	-	13.2	-	-	6.6	-	-	4.8	-
0.04<C<0.08	-	32.6	-	15.4	-	8.8	9.8	-	-	-	-
0.08<C<0.12	-	28.4	-	16.7	-	-	7.7	-	-	-	-
C>0.12	-	29.9	-	15.2	-	-	8.1	-	-	-	-

strength is observed for the weld metal PWHT with P>37.5 and tested at 850, 950, and 1050°F. However, these 100,000 hour rupture stresses are entirely a result of the addition of the UTK data to the literature data base. Consequently, the same dependence of strength on carbon content is observed as that seen for the UTK data alone.

In summary, the results of the log stress/log rupture time data analysis are in general agreement with those obtained using the Larson-Miller parameter technique. For temperatures below 1000°F, the weld metal rupture strength decreases with increasing temper parameter. The influence of PWHT on the 100,000 hour rupture stress at temperatures above 1000°F is masked by data scatter effects. Determination of the relationship between carbon content and rupture strength using log stress/log rupture time analysis is limited to weld metal PWHT P>37.5 due to the limited data availability. In this temper parameter range, rupture strength increases with carbon content up to 0.04-0.05 weight percent. The rupture strength of higher carbon weld metals appears insensitive to carbon level.

Manson Minimum Commitment Method

Literature Data Analysis (Manson MCM). Figures 63 through 66 are stress rupture curves for the SMA literature data as determined using the Manson MCM technique. These four figures present isothermal rupture curves for each temper parameter range including P<32.0, 32.0<P<36.2, 36.2<P<37.5, and P>37.5 respectively. The isotherms are projected to 100,000 hours except in those instances where the fit calculated by the Manson method predicts long term

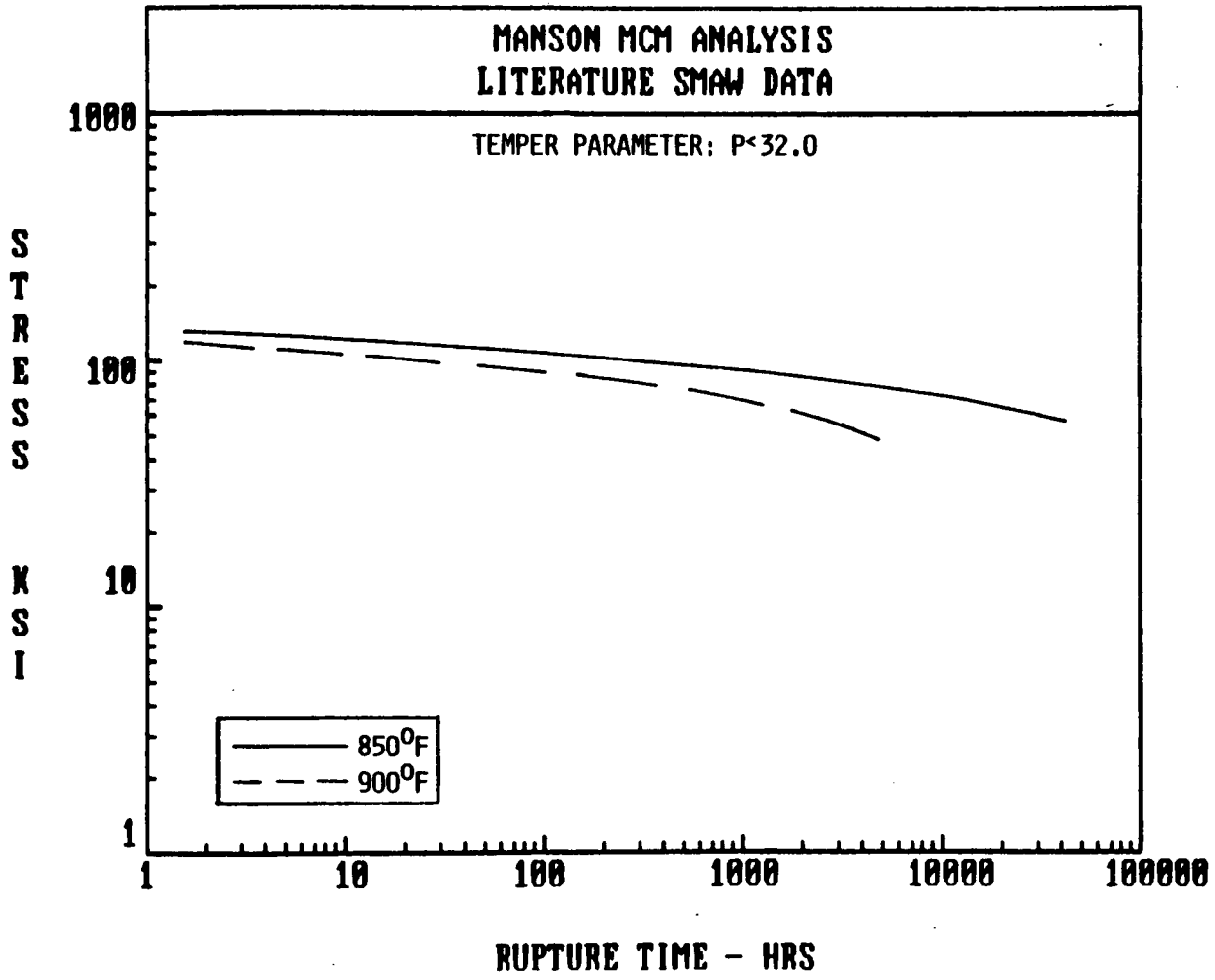


Figure 63. Stress rupture behavior of PWHT 2-1/4Cr-1Mo SMA weld metal (P<32.0) as a function of test temperature determined by Manson MCM analysis of literature data.

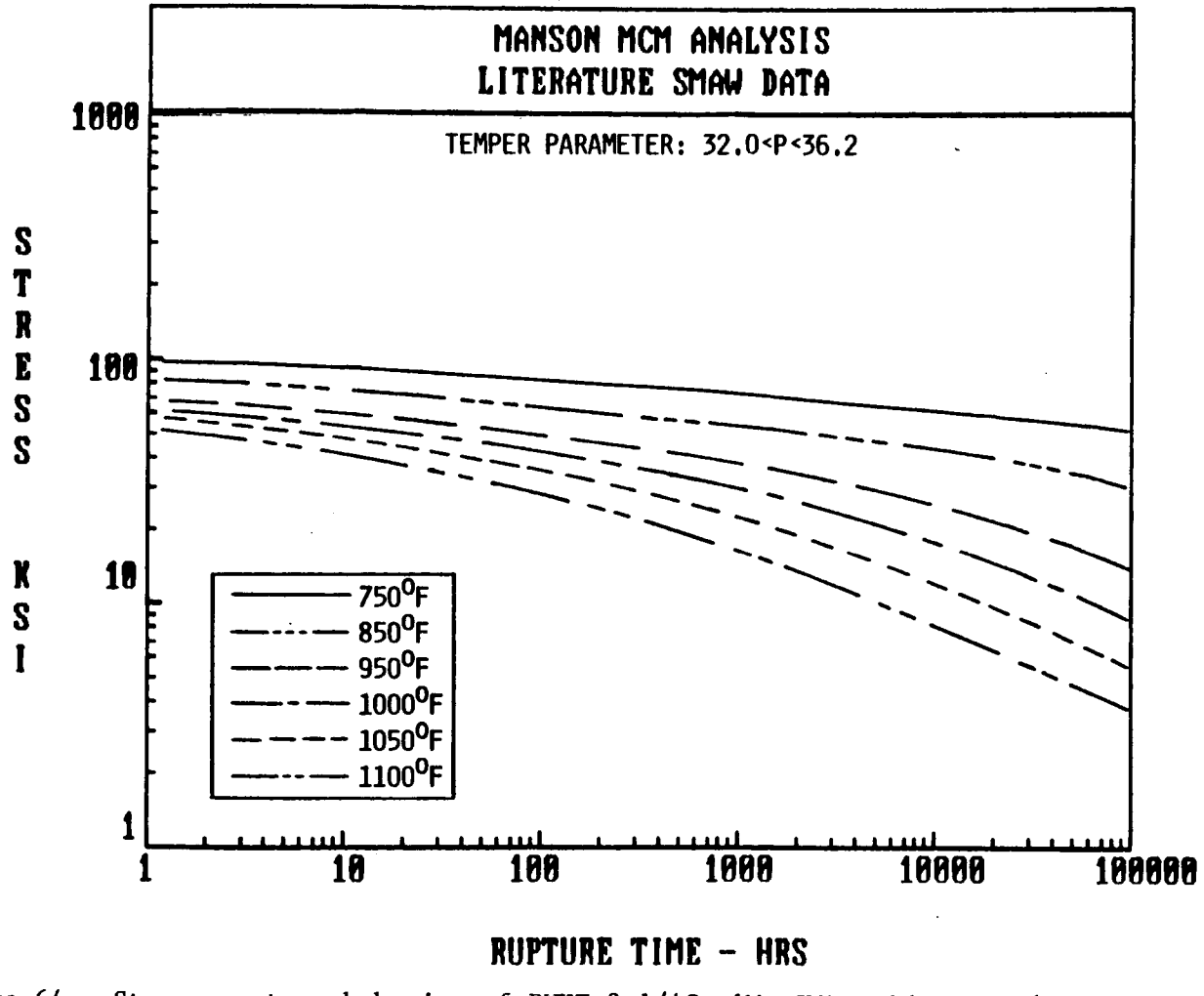


Figure 64. Stress rupture behavior of PWHT 2-1/4Cr-1Mo SMA weld metal (32.0<P<36.2) as a function of test temperature determined by Manson MCM analysis of literature data.

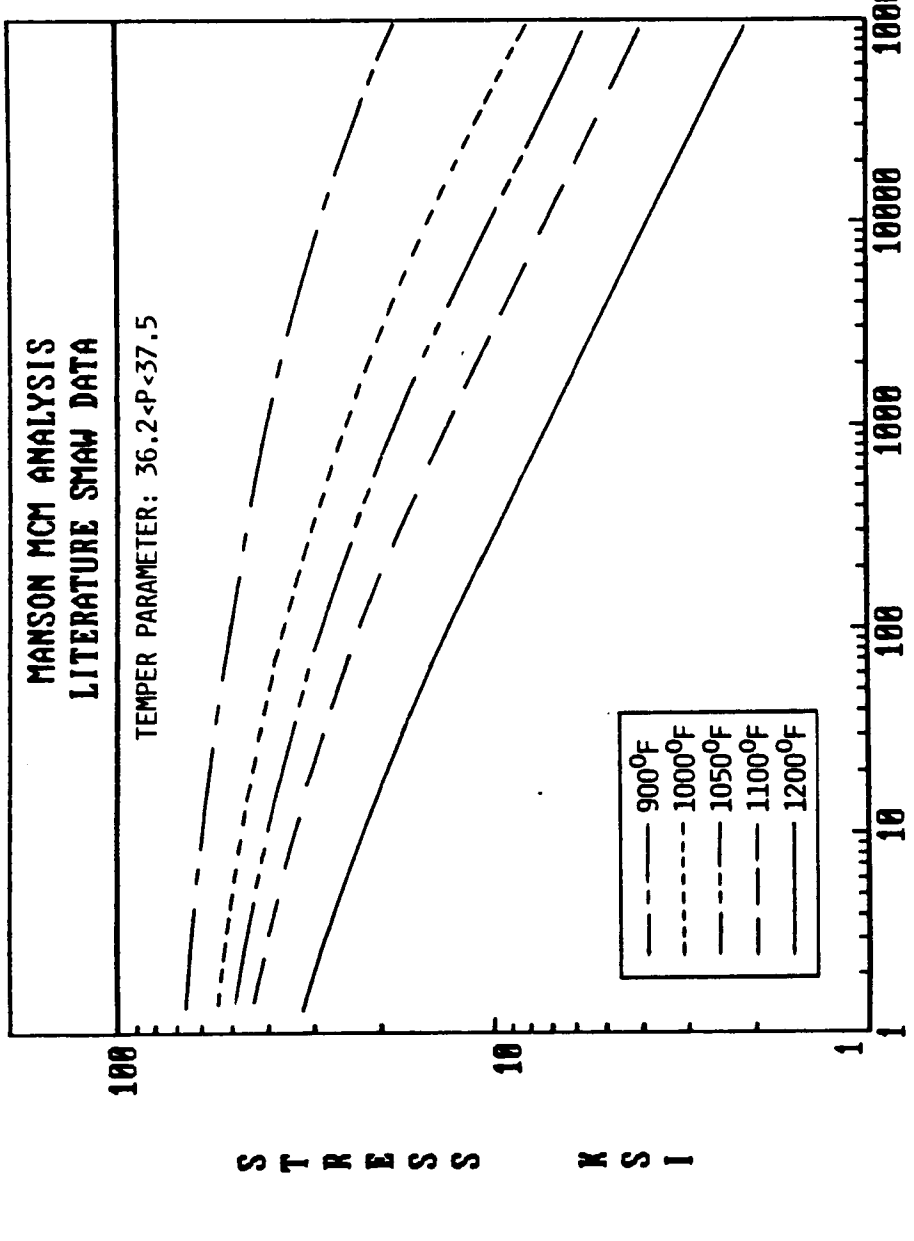


Figure 65. Stress rupture behavior of PWHT 2-1/4Cr-1Mo SMA weld metal (36.2<P<37.5) as a function of test temperature determined by Manson MCM analysis of literature data.

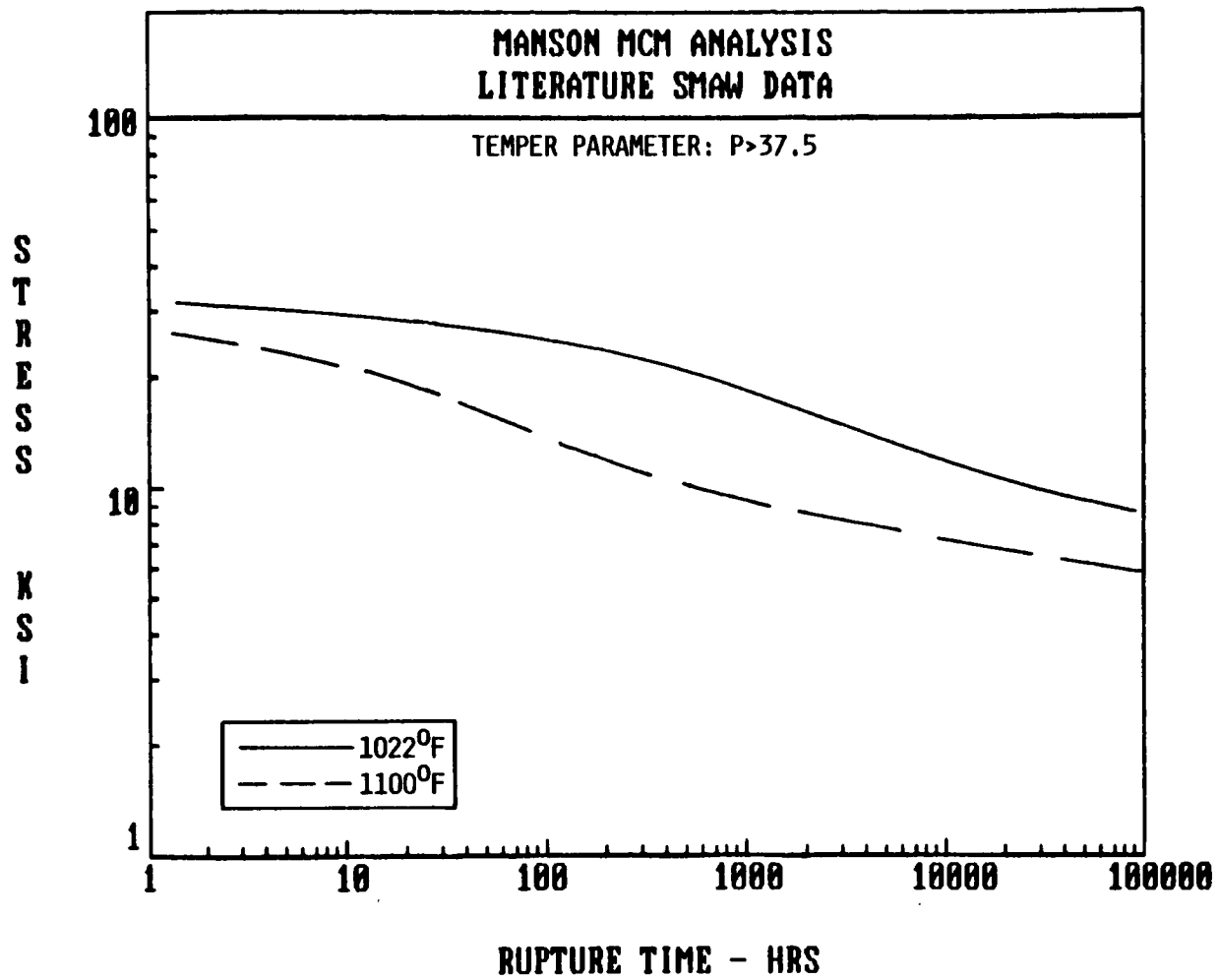


Figure 66. Stress rupture behavior of PWHT 2-1/4Cr-1Mo SMA weld metal (P>37.5) as a function of test temperature determined by Manson MCM analysis of literature data.

behavior which is in gross contradiction with reality. In those cases, the curves have been truncated at the approximate point where the prediction becomes unreasonable.

Table 18 lists the extrapolated 100,000 hour rupture stresses associated with Figures 63 through 66. The rupture strengths listed for weld metal PWHT with P<32.0 have been obtained using the iterative program previously described and are for test temperatures at which there is no data available. Although the isotherms for 850 and 900°F (for which some data exist) are not well behaved, the point at which the individual curves become unreasonable moves to longer rupture times as the test temperature decreases. Based on this trend, the stress for 100,000 hour rupture at 750 and 800°F have been determined and have been used to give some idea of the magnitude of those stresses. The values are enclosed in parentheses to indicate that they are extrapolations.

Some correlation between temper parameter and the 100,000 hour rupture strength of PWHT SMA weld metal can be discerned by examining Table 18. In general, the rupture strength decreases with increasing temper parameter. This is especially evident at temperatures below about 950°F where the magnitude of the stresses is large compared to the uncertainty introduced by data scatter effects. In the case of weld metal PWHT with P<32.0, the 750 and 800°F stress values indicate that, in this low temperature regime, the rupture strength of mildly PWHT weld metal is significantly higher than that of material given a more extensive PWHT. This same trend has been observed in the

Table 18. Stress for 100,000 hour rupture of 2-1/4Cr-1Mo SMA weld metal as a function of test temperature and temper parameter determined by Manson MCM analysis of literature data.

	Stress for 100,000 Hour Rupture (KSI)			
Temperature (^{o}F)	P<32.0	32.0<P<36.2	36.2<P<37.5	P>37.5
750	(98.0)	52.7	---	---
800	(77.1)	42.2	---	---
850	---	31.7	---	---
900	---	22.0	17.8	---
950	---	14.2	11.7	---
1000	---	8.9	7.8	---
1022	---	7.3	6.6	8.4
1050	---	5.6	5.4	6.8
1058	---	5.3	5.1	6.5
1067	---	4.9	4.8	6.3
1100	---	3.7	3.8	5.8
1112	---	3.3	3.5	---
1200	---	---	2.1	---

results of both the Larson-Miller parametric analysis and the log stress-log rupture time analysis.

Comparison of the stresses for weld metal PWHT with $32.0<P<36.2$ and $36.2<P<37.5$ indicates that the former has a higher strength but that the strength difference decreases with increasing temperature until at about 1050°F, it becomes insignificant. The analysis indicates that the rupture stresses for extensively PWHT weld metal ($P>37.5$) are higher than the corresponding stresses for the weld metals given a less severe PWHT. However, these values are based on the analysis of only ten data points taken at only two temperatures. Examination of Figure 66 shows that the curves derived from the analysis decrease in slope with increasing rupture time, behavior which results in elevation of the 100,000 hour stresses relative to those which would be obtained if the curves had the more typical concave down shape. With the amount of data available, it is impossible to say whether the curve shape observed in Figure 66 is an accurate representation of the rupture behavior of severely tempered weld metal or is just an artifact of the data analysis technique. Based on the results of previous analyses using different methods, the latter is suspected.

Figures 67 through 71 are stress rupture curves for SMA literature rupture data partitioned by temper parameter and carbon content. Figures 67, 68, and 69 are for weld metal PWHT with $32.0<P<36.2$ and with carbon contents in the range of $0.04<C<0.08$, $0.08<C<0.12$, and $C>0.12$ respectively. Figures 70 and 71 have been constructed for weld metal PWHT with $36.2<P<37.5$ and carbon contents

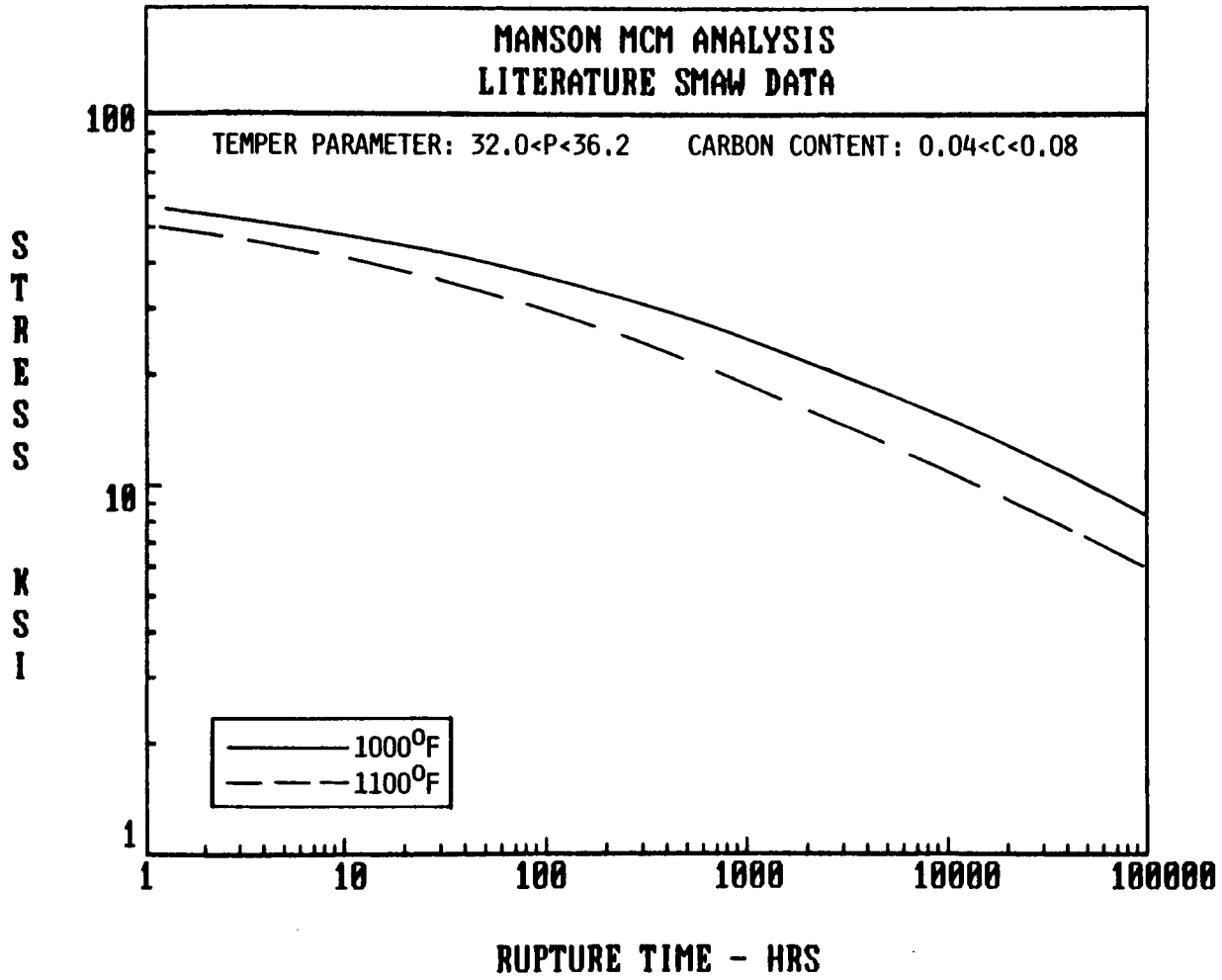


Figure 67. Stress rupture behavior of PWHT 2-1/4Cr-1Mo SMA weld metal (32.0<P<36.2) with carbon content in the range of 0.04<C<0.08 determined by analysis of literature data.

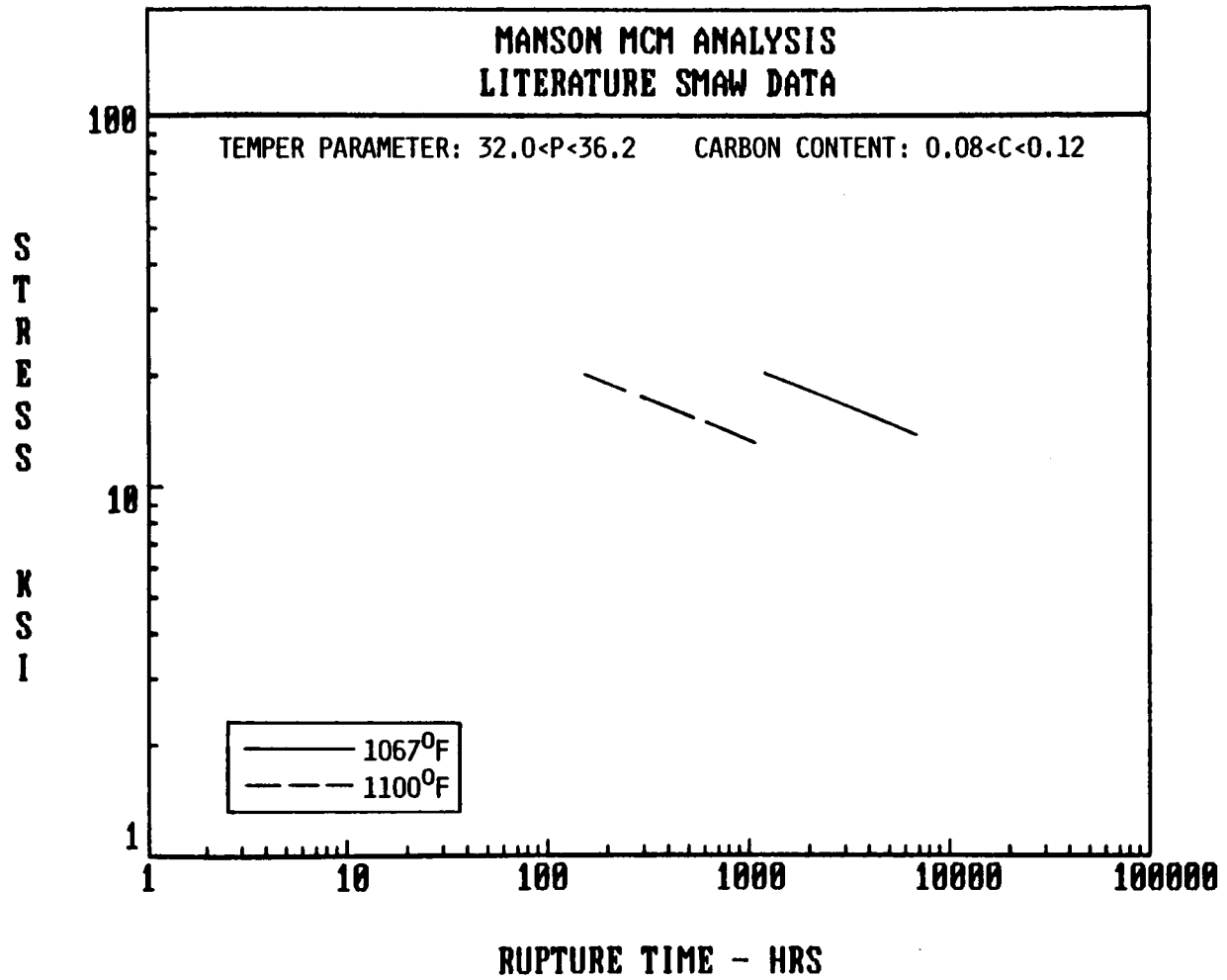


Figure 68. Stress rupture behavior of PWHT 2-1/4Cr-1Mo SMA weld metal (32.0<P<36.2) with carbon content in the range of 0.08<C<0.12 determined by analysis of literature data.

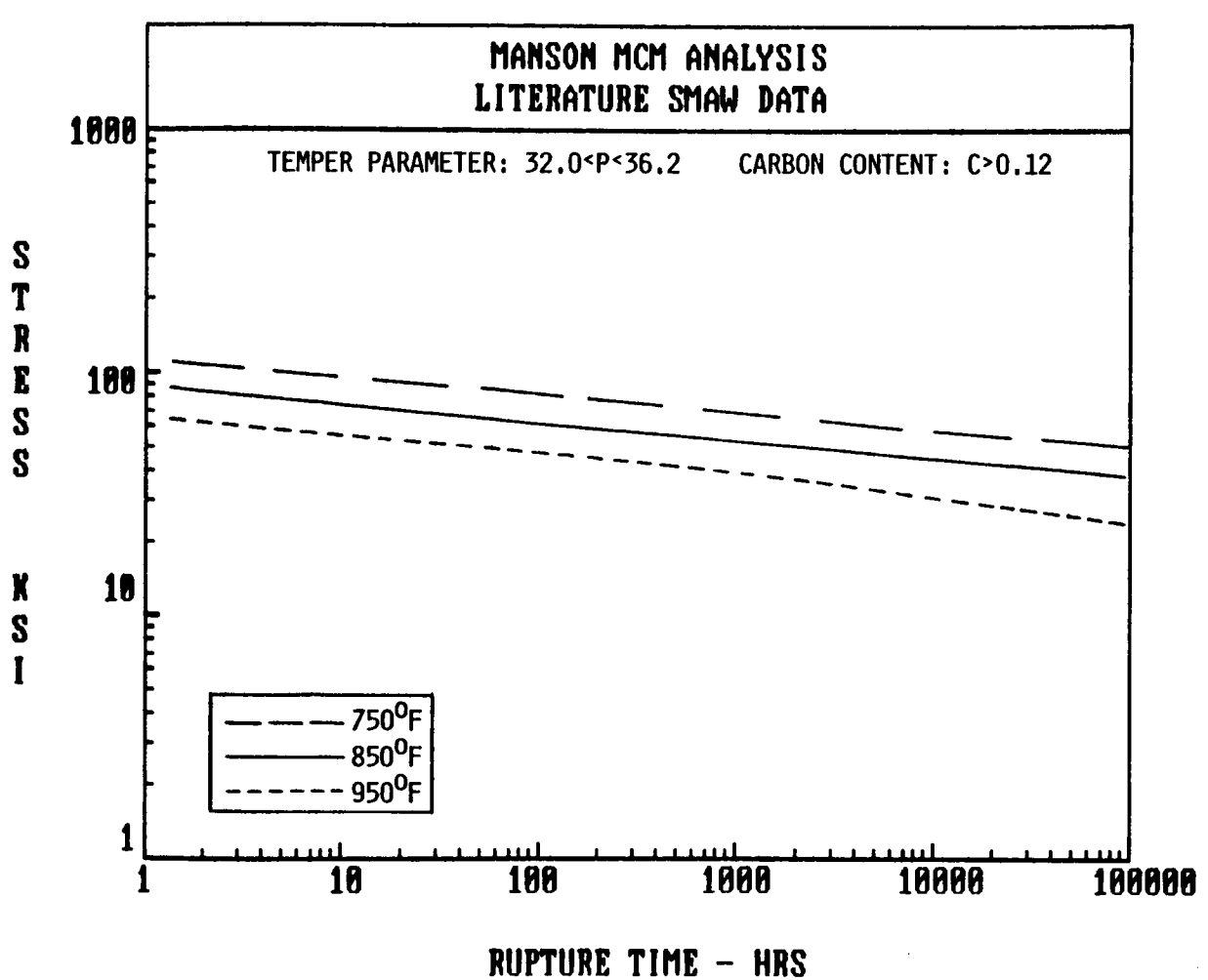


Figure 69. Stress rupture behavior of PWHT 2-1/4Cr-1Mo SMA weld metal (32.0<P<36.2) with carbon content in the range of C>0.12 determined by analysis of literature data.

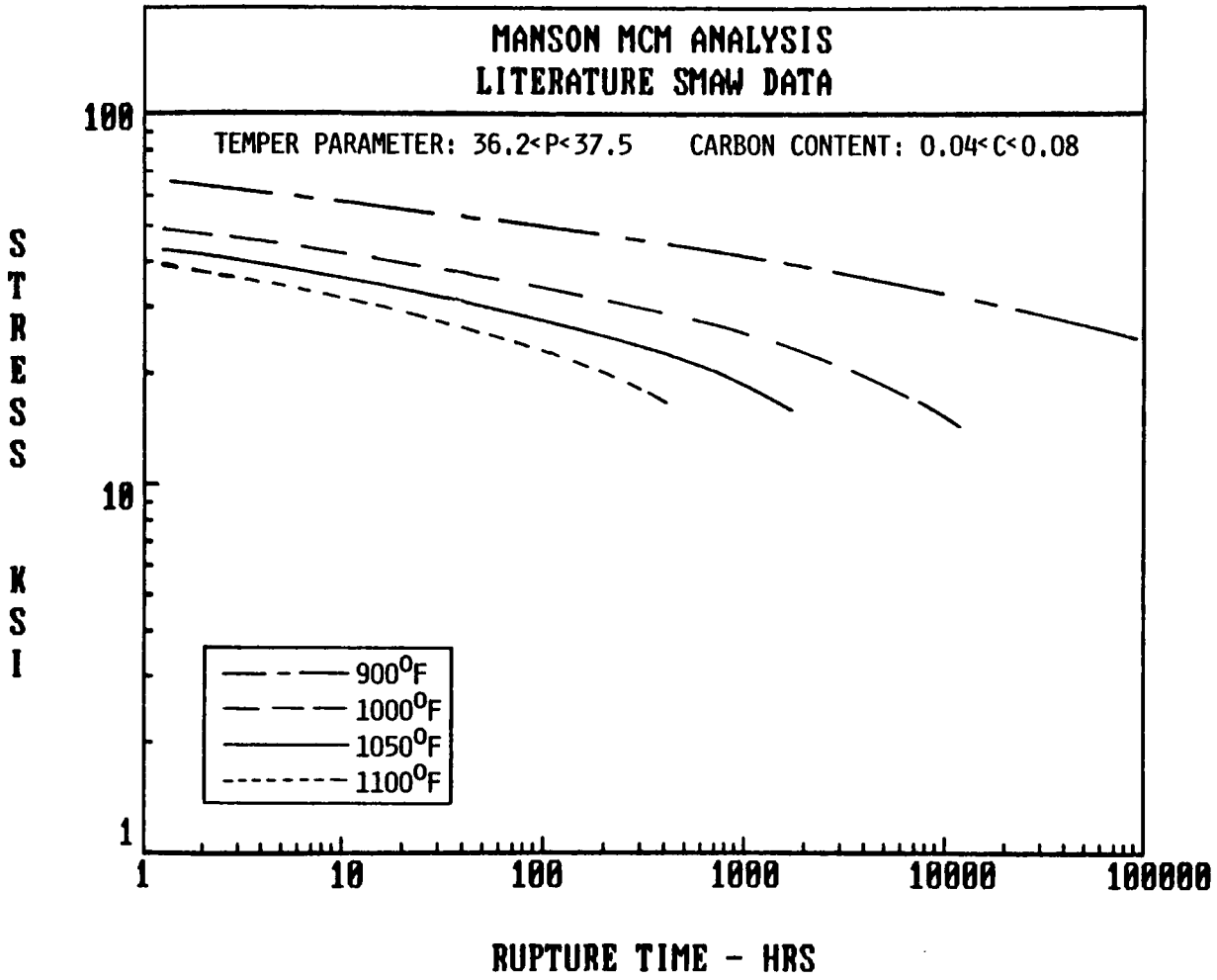


Figure 70. Stress rupture behavior of PWHT 2-1/4Cr-1Mo SMA weld metal (36.2<P<37.5) with carbon content in the range of 0.04<C<0.08 determined by analysis of literature data.

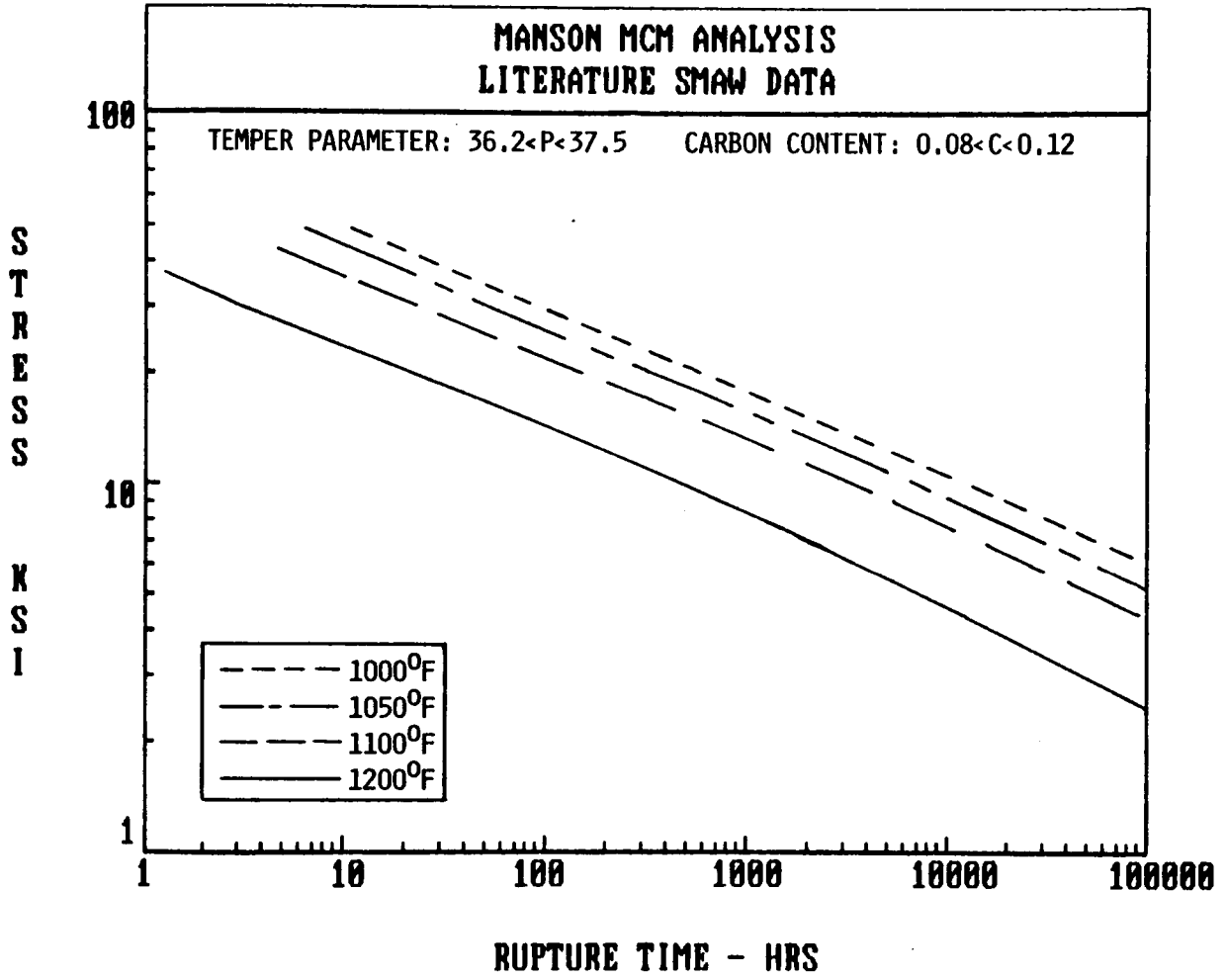


Figure 71. Stress rupture behavior of PWHT 2-1/4Cr-1Mo SMA weld metal (36.2<P<37.5) with carbon content in the range of 0.08<C<0.12 determined by analysis of literature data.

in the range of 0.04<C<0.08 and 0.08<C<0.12 respectively. Some of the curves in Figures 68, 70, and 71 have been edited to remove those portions which are not considered accurate.

Table 19 lists the 100,000 hour rupture stresses obtained for SMA literature data partitioned by temper parameter and carbon content. However, because of the paucity of valid 100,000 hour stresses resulting from such factors as unrealistic curve fits and limited rupture data, the table is of little use in determining the effect of carbon content on rupture strength. Within each temper parameter range, the 100,000 hour stresses at any one temperature are not known for more than one of the carbon content ranges thus limiting comparison.

UTK Data Analysis (Manson MCM). Figures 72, 73, and 74 are stress rupture curves derived from the Manson analysis of UTK data obtained during this program. Figure 72 shows the rupture behavior of 2-1/4Cr-1Mo SMA weld metal PWHT 1175^{o}F/25.5 hours to Class 3 properties. Similarly, Figures 73 and 74 have been constructed for weld metal PWHT 1300^{o}F/25 hours to Class 2 strength. Figure 73 is based on the analysis of the four lots of weld metal with carbon in the range of 0.02 to 0.13 weight percent. Previous analysis has indicated that the rupture strength of the lowest carbon material (0.02-0.03C) is of significantly lower magnitude than that of the three higher carbon content weld metals. As a result, an additional analysis of the Class 2 weld metals has been performed excluding the 0.02-0.03C data. The resulting curves are depicted in Figure 74.

Table 19. Stress for 100,000 hour rupture of 2-1/4Cr-1Mo SMA weld metal as a function of test temperature, carbon content, and temper parameter determined by Manson MCM analysis of literature data.

Temperature (°F)	Stress for 100,000 Hour Rupture (KSI)			
	32.0<P<36.2		36.2<P<37.5	
	0.04<C<0.08	C>0.12	0.04<C<0.08	0.08<C<0.12
750	---	51.7	---	---
800	---	45.0	---	---
850	---	38.1	---	---
900	---	31.1	24.3	---
950	---	23.8	13.1	---
1000	---	---	---	6.0
1022	8.7	---	---	5.6
1050	8.2	---	---	5.2
1058	8.0	---	---	5.0
1067	7.6	---	---	4.9
1100	6.1	---	---	4.2
1112	5.5	---	---	4.0
1200	---	---	---	2.5

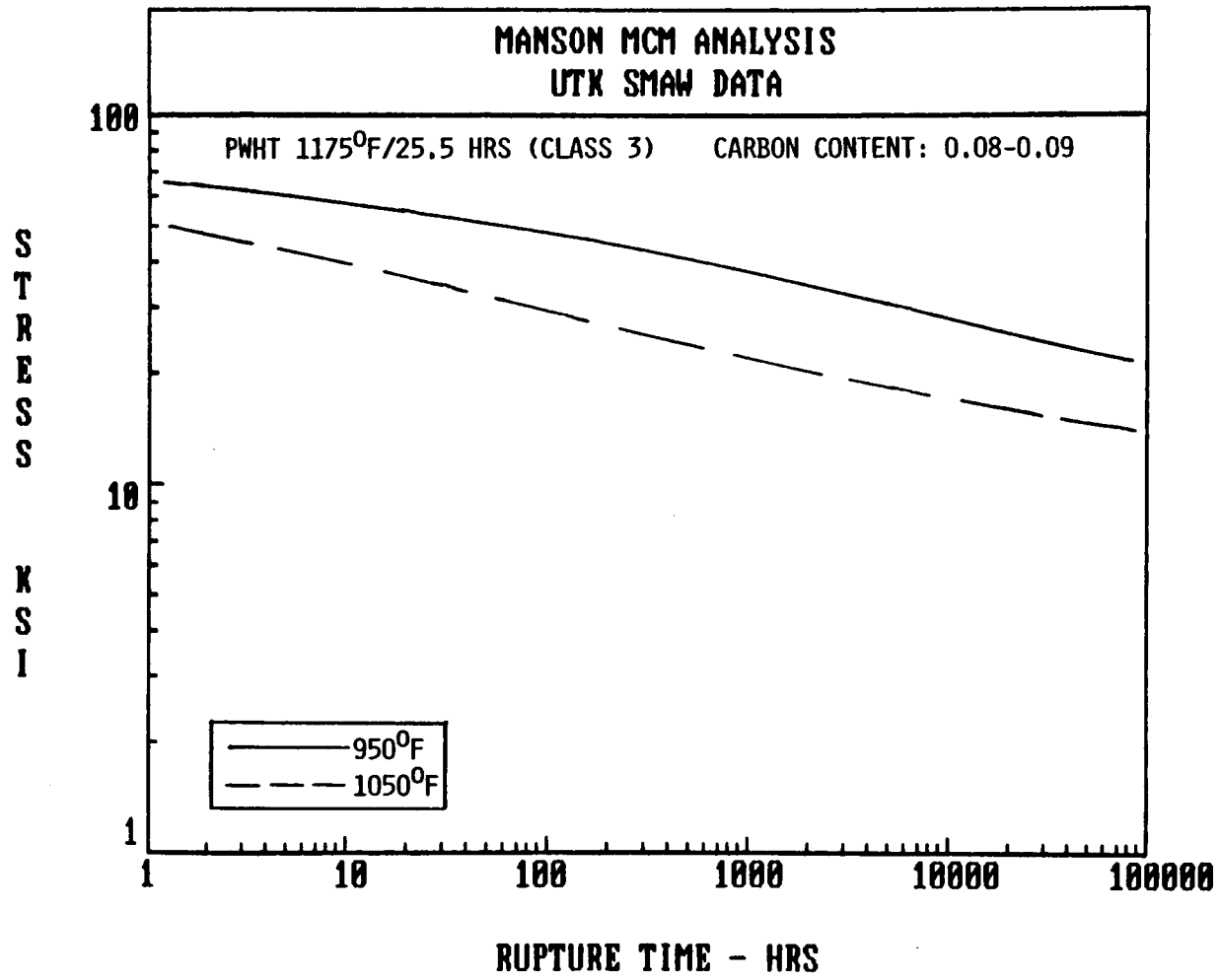


Figure 72. Stress rupture behavior of 0.08-0.09 carbon 2-1/4Cr-1Mo Class 3 SMA weld metal as a function of test temperature determined by analysis of UTK data.

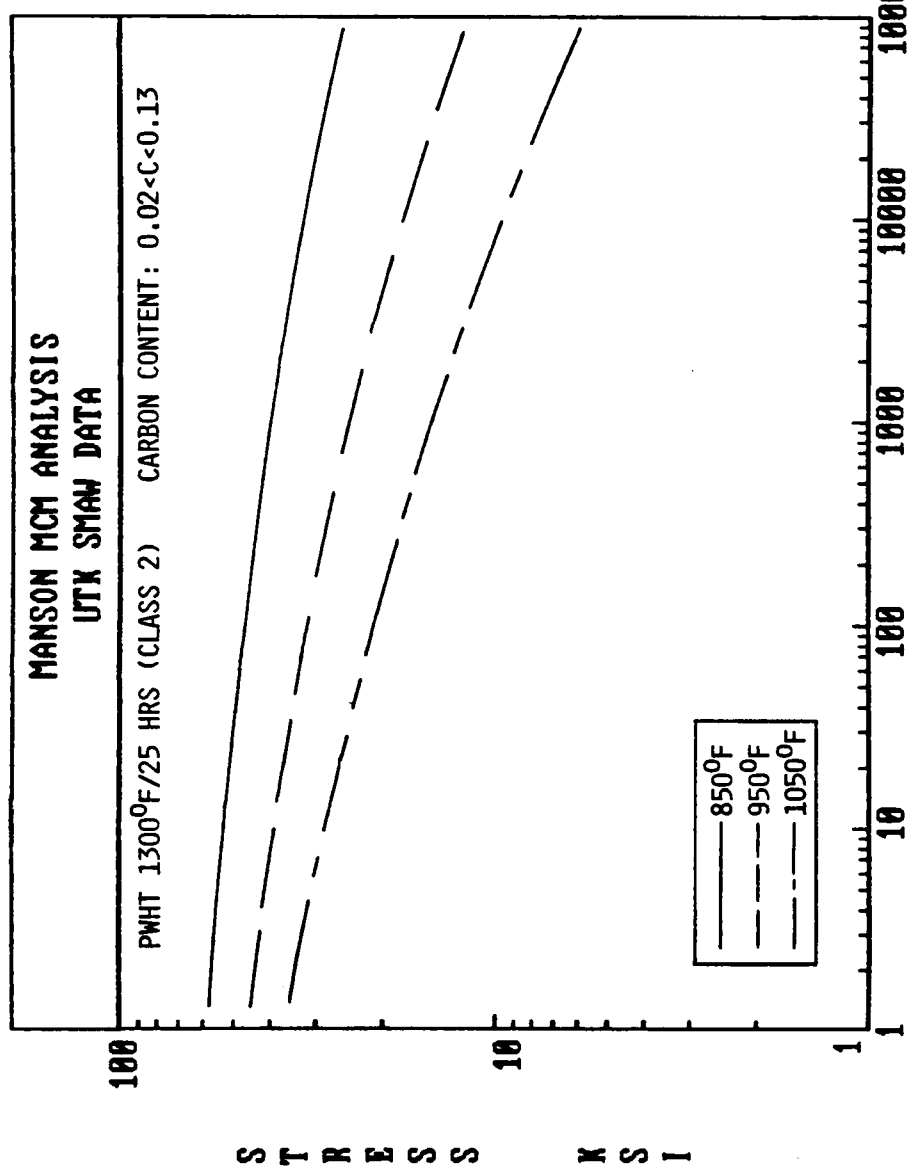


Figure 73. Stress rupture behavior of 2-1/4Cr-1Mo Class 2 SMA weld metal as a function of test temperature determined by analysis of UTK data.

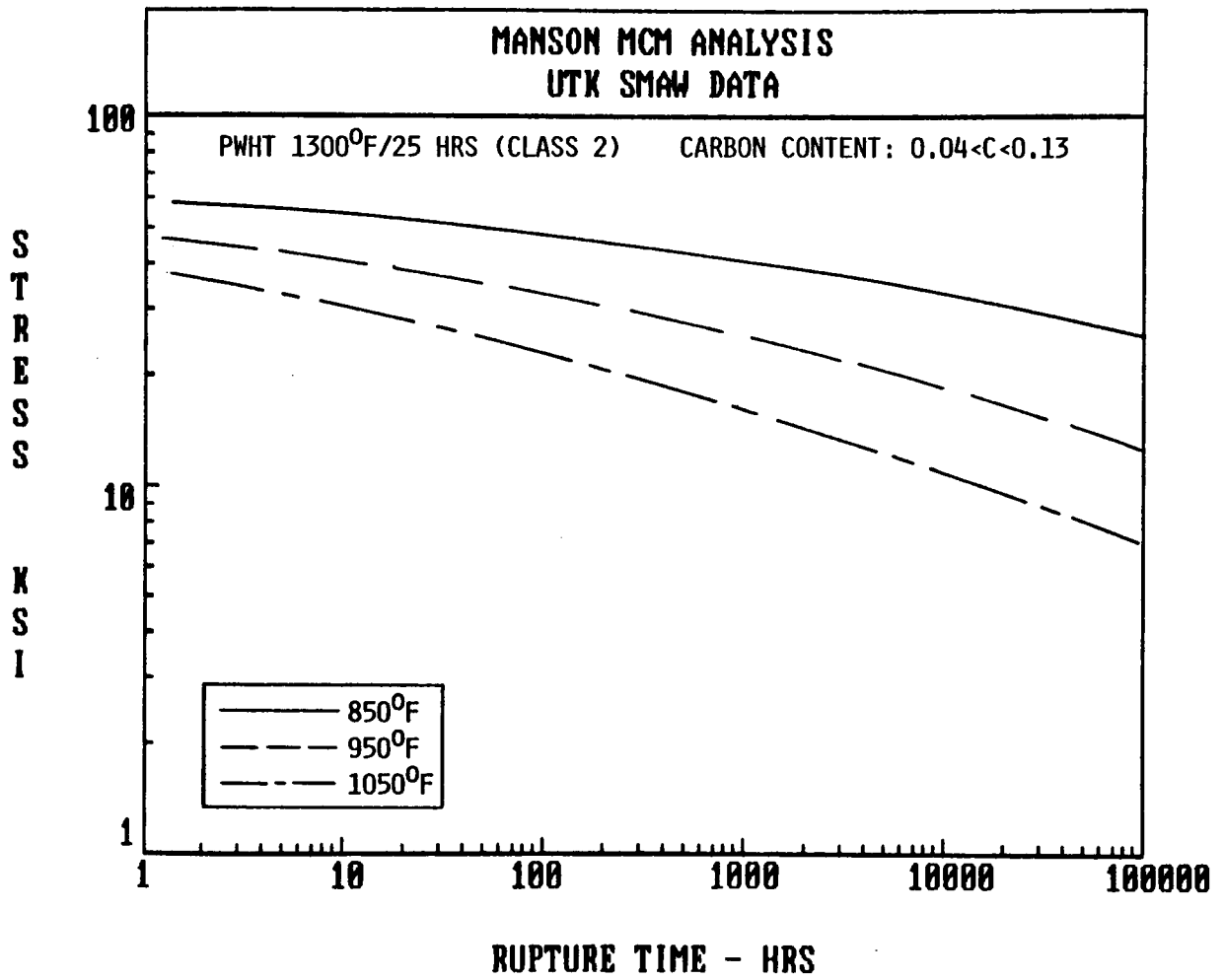


Figure 74. Stress rupture behavior of all 2-1/4Cr-1Mo Class 2 SMA weld metal except the 0.02-0.03 carbon material as a function of test temperature determined by analysis of UTK data.

Table 20 lists the 100,000 hour stresses calculated for the Class 2 and Class 3 weld metals. Comparison of the stresses in the first two columns reveals that, in the temperature range of 850 to 1050°F, the 100,000 hour rupture strength of the Class 3 material is 1 1/2 to 2 1/2 times greater than that determined for the Class 2 weld metal based on all of the Class 2 data (0.02-0.13 carbon range). In addition, when the 0.02-0.03C weld metal data are not included in the Class 2 characterization (column 3), the strength determined for the Class 2 weld metal is noticeably greater.

Figures 75 through 78 are stress rupture curves for Class 2 SMA weld metal having carbon contents of 0.02-0.03, 0.04-0.05, 0.08-0.09, and 0.12-0.13 weight percent. Table 21 lists the associated 100,000 hour rupture stresses for each weld metal as a function of test temperature. Inspection of the table reveals that the rupture strength of the 0.02-0.03C weld metal is lower than that of the three higher carbon content weld metals which are comparable in magnitude. However, Manson's method predicts that the strength difference between the low carbon material and the remaining three weld metals decreases with increasing temperature, becoming insignificant at 1050°F.

Combined Literature and UTK Data Analysis (Manson MCM). The Class 2 and Class 3 PWHT weld metals used in the UTK program are characterized by temper parameter values of 37.7 and 35.0 respectively. As a result, only the data analysis results for the

Table 20. Stress for 100,000 hour rupture of 2-1/4Cr-1Mo weld metal as a function of test temperature and PWHT determined by Manson MCM analysis of UTK data.

Temperature (^{o}F)	Stress for 100,000 Hour Rupture (KSI)		
	Class 3	Class 2	
		0.02-0.13C	0.04-0.13C
850	37.3	25.0	26.0
900	28.2	17.3	18.2
950	21.7	11.7	12.8
1000	17.3	8.1	9.4
1022	15.8	7.0	8.3
1050	14.1	5.8	7.3

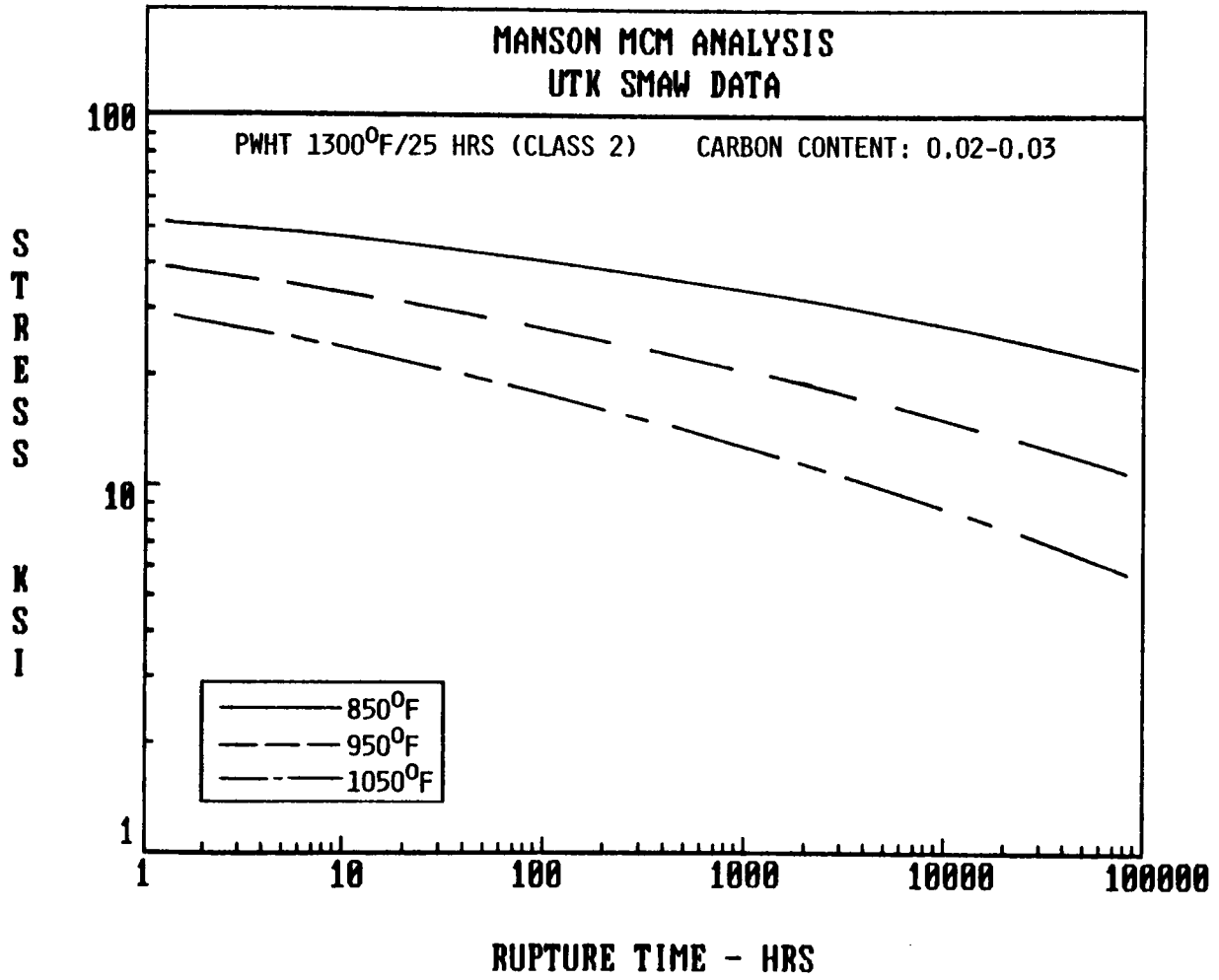


Figure 75. Stress rupture behavior of 0.02-0.03 carbon 2-1/4Cr-1Mo Class 2 SMA weld metal as a function of test temperature determined by analysis of UTK data.

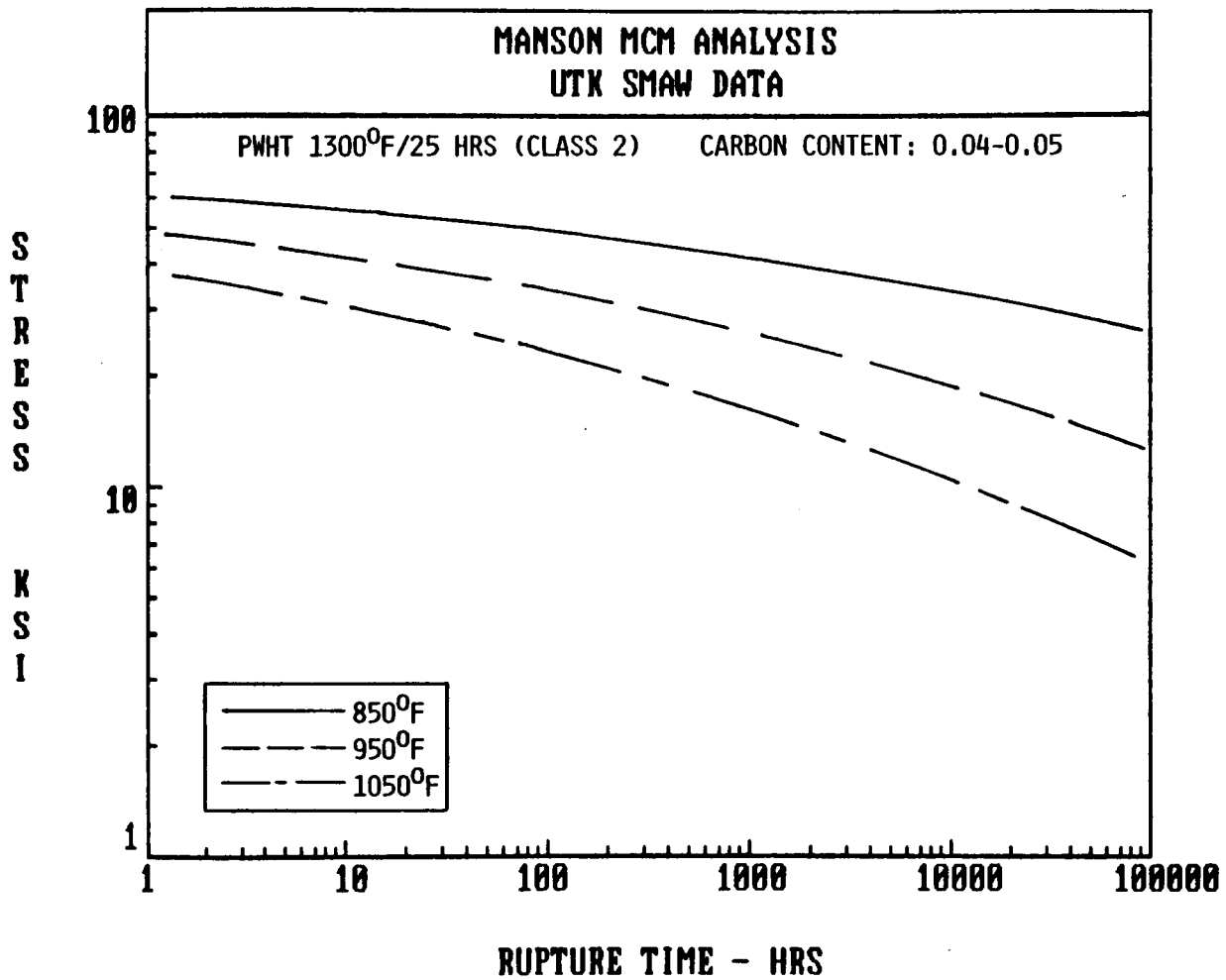


Figure 76. Stress rupture behavior of 0.04-0.05 carbon 2-1/4Cr-1Mo Class 2 SMA weld metal as a function of test temperature determined by analysis of UTK data.

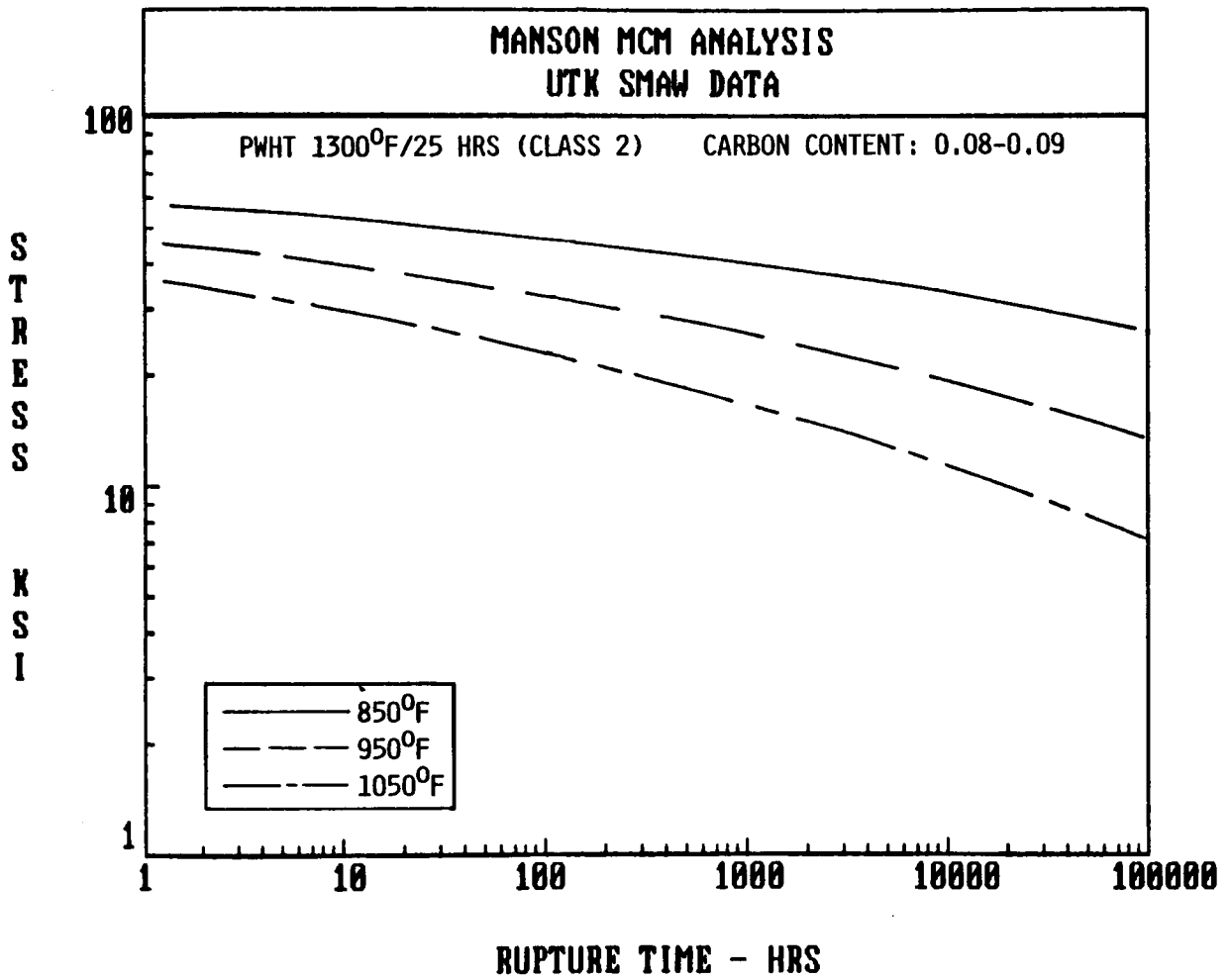


Figure 77. Stress rupture behavior of 0.08-0.09 carbon 2-1/4Cr-1Mo Class 2 SMA weld metal as a function of test temperature determined by analysis of UTK data.

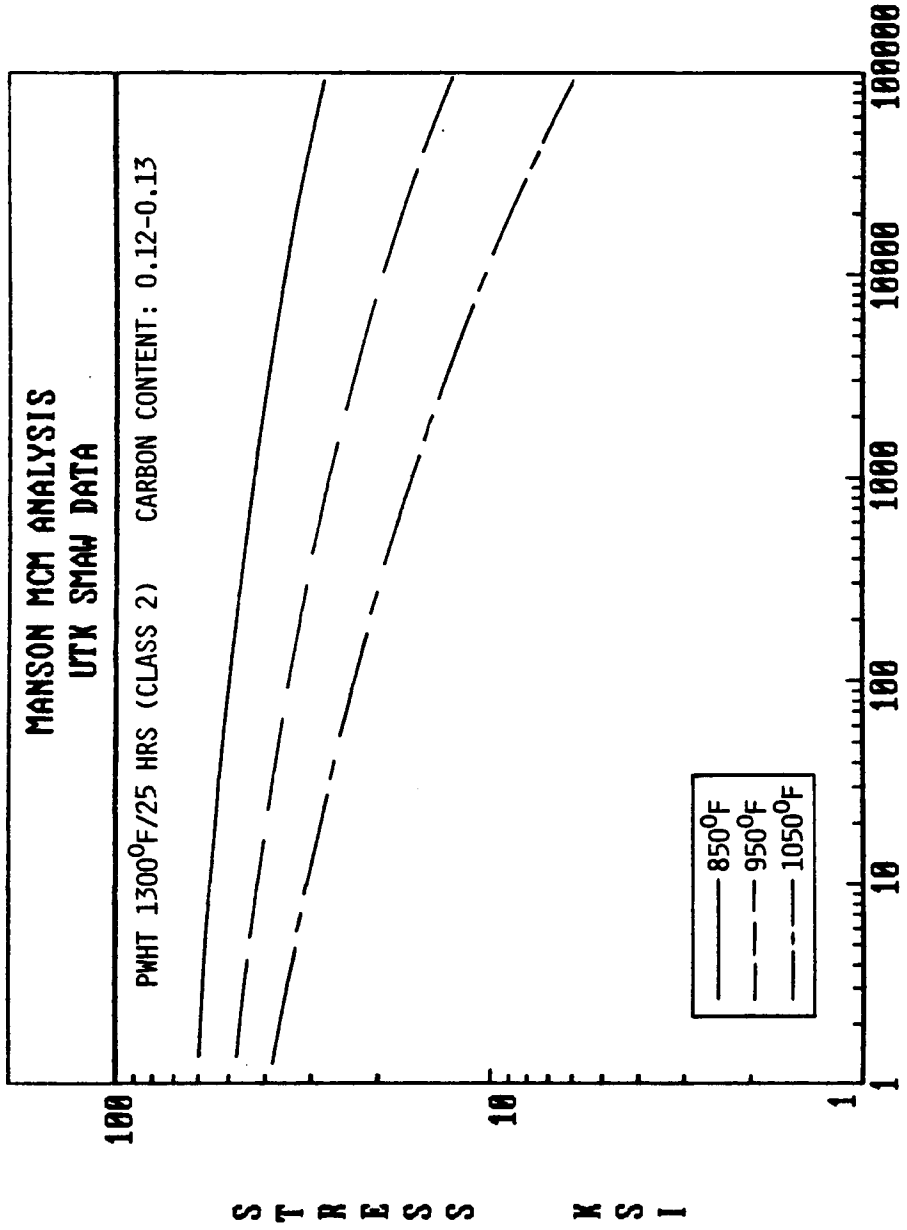


Figure 78. Stress rupture behavior of 0.12-0.13 carbon 2-1/4Cr-1Mo Class 2 SMA weld metal as a function of test temperature determined by analysis of UTK data.

Table 21. Stress for 100,000 hour rupture of 2-1/4Cr-1Mo Class 2 SMA weld metal as a function of test temperature and carbon content determined by Manson MCM analysis of UTK data.

Carbon Content	Stress for 100,000 Hour Rupture (KSI)					
	850°F	900°F	950°F	1000°F	1022°F	1050°F
0.02-0.03C	20.9	14.7	10.4	7.6	6.7	5.8
0.04-0.05C	26.9	18.7	12.7	8.7	7.5	6.2
0.08-0.09C	26.5	19.0	13.5	9.8	8.6	7.4
0.12-0.13C	27.4	19.0	12.7	8.6	7.3	6.0
Combined (0.04-0.13C)	26.0	18.2	12.8	9.4	8.3	7.3

temper parameter ranges $32.0<P<36.2$ and $P>37.5$ are affected by the experimental data addition.

Figures 79 and 80 are stress rupture curves for the above temper parameter ranges as derived for the combined SMA data. All isotherms are typical in shape, allowing iteration of the 100,000 hour rupture stresses over the entire temperature range covered by the data. Comparison of Figures 66 (p. 164) and 80 shows that the addition of the Class 2 UTK data to the SMA literature data base for $P>37.5$ has had a beneficial effect on the curve shape of the 1022 and 1100°F isotherms, eliminating the decrease in curve slope at rupture times greater than 100 hours and lowering the predicted 100,000 hour rupture stresses to more conservative values. Table 22 lists the rupture stresses as a function of temperature and temper parameter range.

Comparing Tables 22 and 18 (p. 166) reveals that the addition of the UTK data to the SMA literature data base has widened the temperature range over which the 100,000 hour rupture stress can be predicted for weld metal PWHT with $P>37.5$. This has made it possible to obtain a clearer determination of the correlation between temper parameter and rupture strength. For temperatures below 1000°F, the rupture strength clearly decreases with increasing temper parameter. At temperatures above 1000°F, the 100,000 hour stresses of weld metal PWHT with $32.0<P<36.2$, $36.2<P<37.5$, and $P>37.5$ are all of similar magnitude with the strength of the $32.0<P<36.2$ weld metal slightly higher than that of the more extensively PWHT materials. This

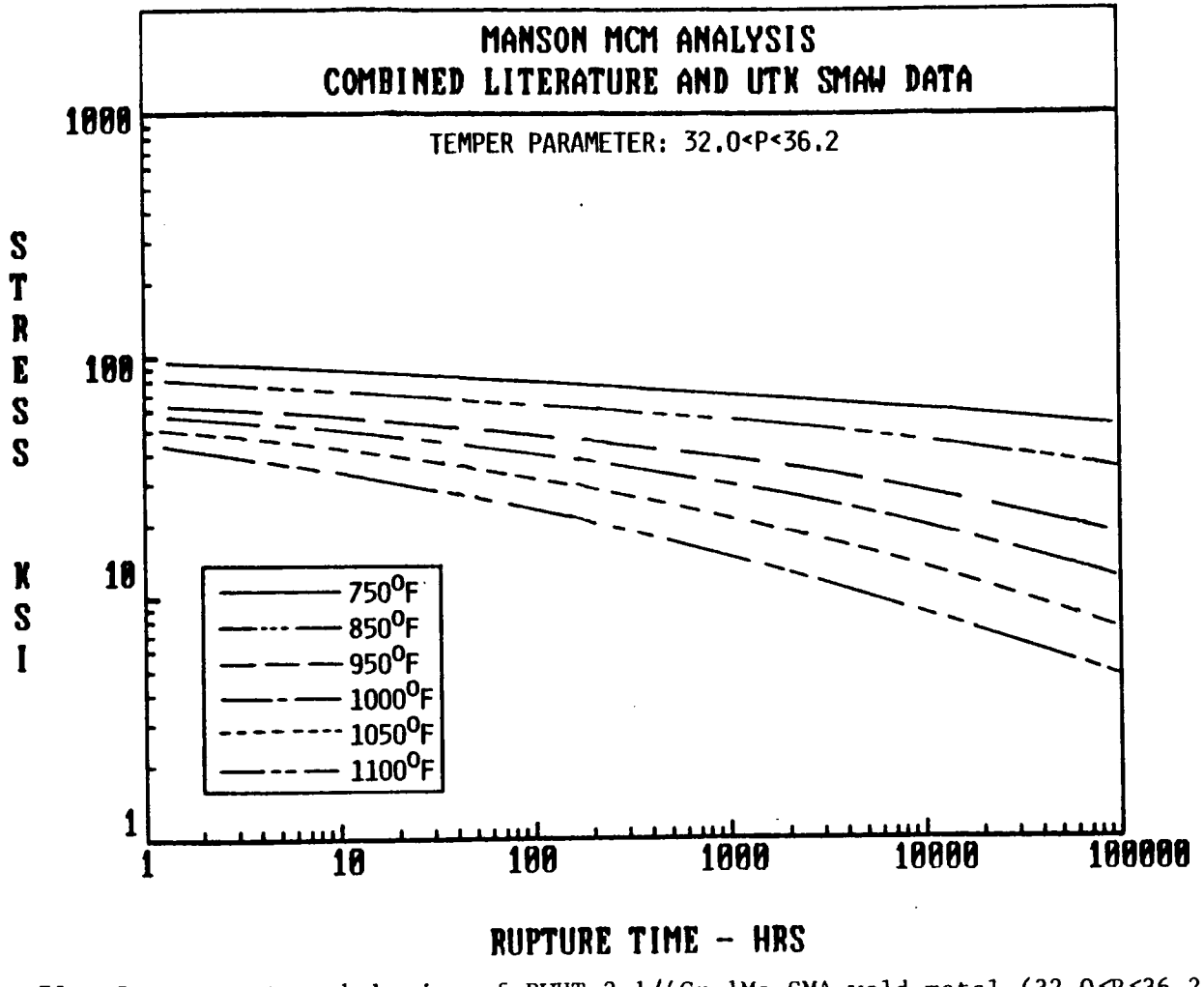


Figure 79. Stress rupture behavior of PWHT 2-1/4Cr-1Mo SMA weld metal (32.0<P<36.2) as a function of test temperature determined by Manson MCM analysis of combined literature and UTK data.

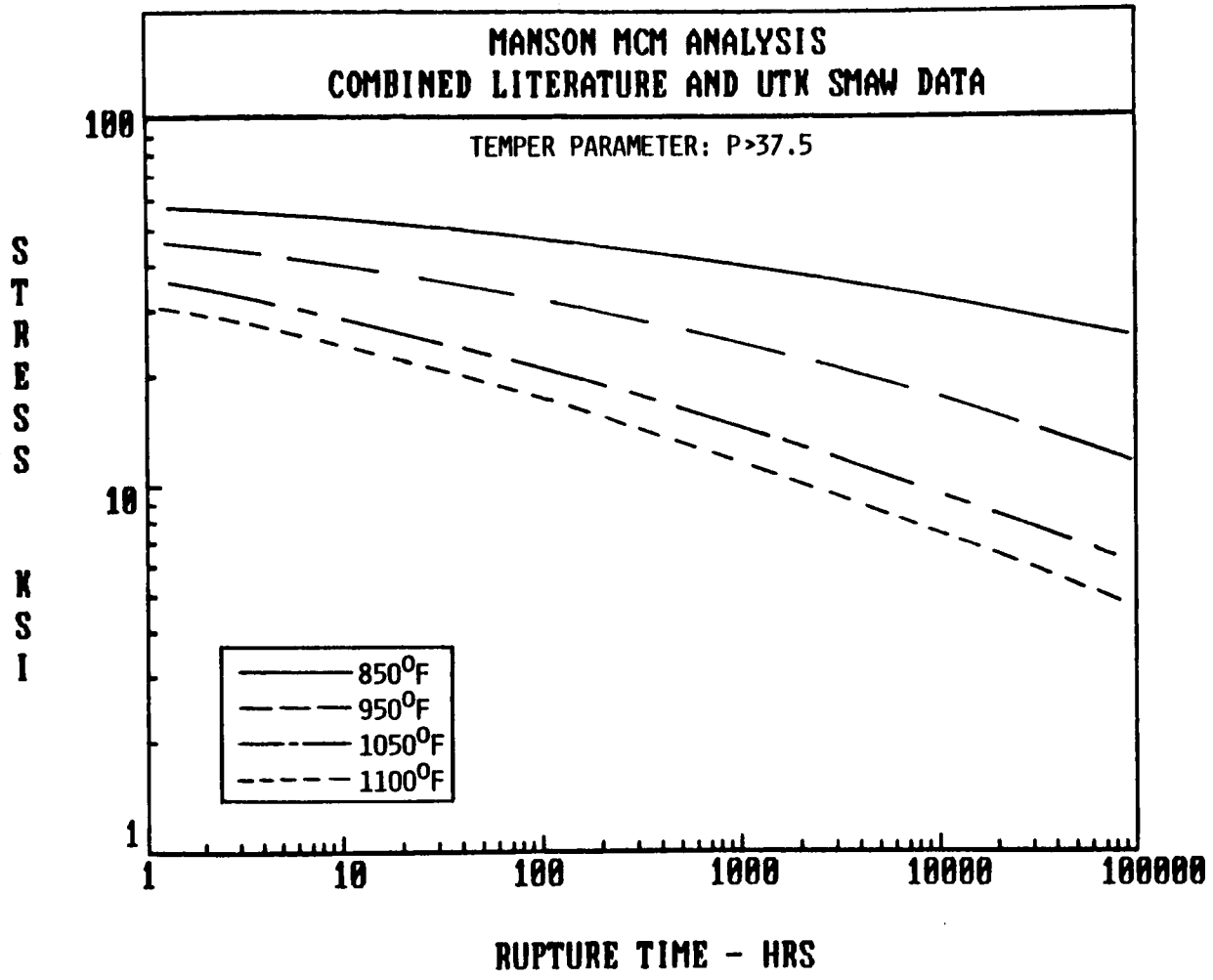


Figure 80. Stress rupture behavior of PWHT 2-1/4Cr-1Mo SMA weld metal (P>37.5) as a function of test temperature determined by Manson MCM analysis of combined literature and UTK data.

Table 22. Stress for 100,000 hour rupture of 2-1/4Cr-1Mo SMA weld metal as a function of test temperature and temper parameter determined by Manson MCM analysis of combined literature and UTK data.

	Stress for 100,000 Hour Rupture (KSI)			
Temperature (^{o}F)	P<32.0	32.0<P<36.2	36.2<P<37.5	P>37.5
750	(98.0)	53.2	---	---
800	(42.2)	44.3	---	---
850	---	35.2	---	24.7
900	---	26.3	17.8	16.8
950	---	18.3	11.7	11.4
1000	---	12.0	7.8	8.1
1022	---	9.9	6.6	7.0
1050	---	7.6	5.4	6.0
1058	---	7.1	5.1	5.8
1067	---	6.5	4.8	5.5
1100	---	4.8	3.8	4.7
1112	---	4.3	3.5	---
1200	---	---	2.1	---

difference decreases as the temperature increases. At 1100°F, the stresses all fall within a one KSI band.

Figures 81 through 85 are stress rupture curves for the combined SMA rupture data partitioned by temper parameter and carbon content. Figure 81 has been constructed using the results of the analysis of data for weld metal PWHT with $32.0<P<36.2$ and having a carbon content of $0.08<C<0.12$. Figures 82, 83, 84, and 85 are for weld metal PWHT with $P>37.5$ and having carbon levels in the range of $0.02<C<0.04$, $0.04<C<0.08$, $0.08<C<0.12$, and $C>0.12$ respectively. Table 23 lists the 100,000 hour rupture stresses derived from the curves.

Comparing Tables 19 (p. 174) and 23, one finds that the addition of the UTK data to the SMA literature data base makes it possible to predict the 100,000 hour rupture stresses over a much wider range of tempering conditions and carbon levels. However, even with the added stress values, little can be said about the dependence of rupture strength on carbon content for weld metal PWHT with $32.0<P<36.2$ and $36.2<P<37.5$. It is for the most severely tempered material ($P>37.5$) that the effect of carbon can be seen. Inspection of the table reveals that the rupture strength of the lowest carbon content weld metal is noticeably below that of the three higher carbon materials which have comparable strengths. The stresses for the $0.08<C<0.12$ weld metal differ slightly from those for the $0.04<C<0.08$ and $C>0.12$ weld metals. However, this may be the result of using the Manson model and not a real effect. Examination of Figure 84 shows that the curves obtained for this particular set of data are not "well behaved".

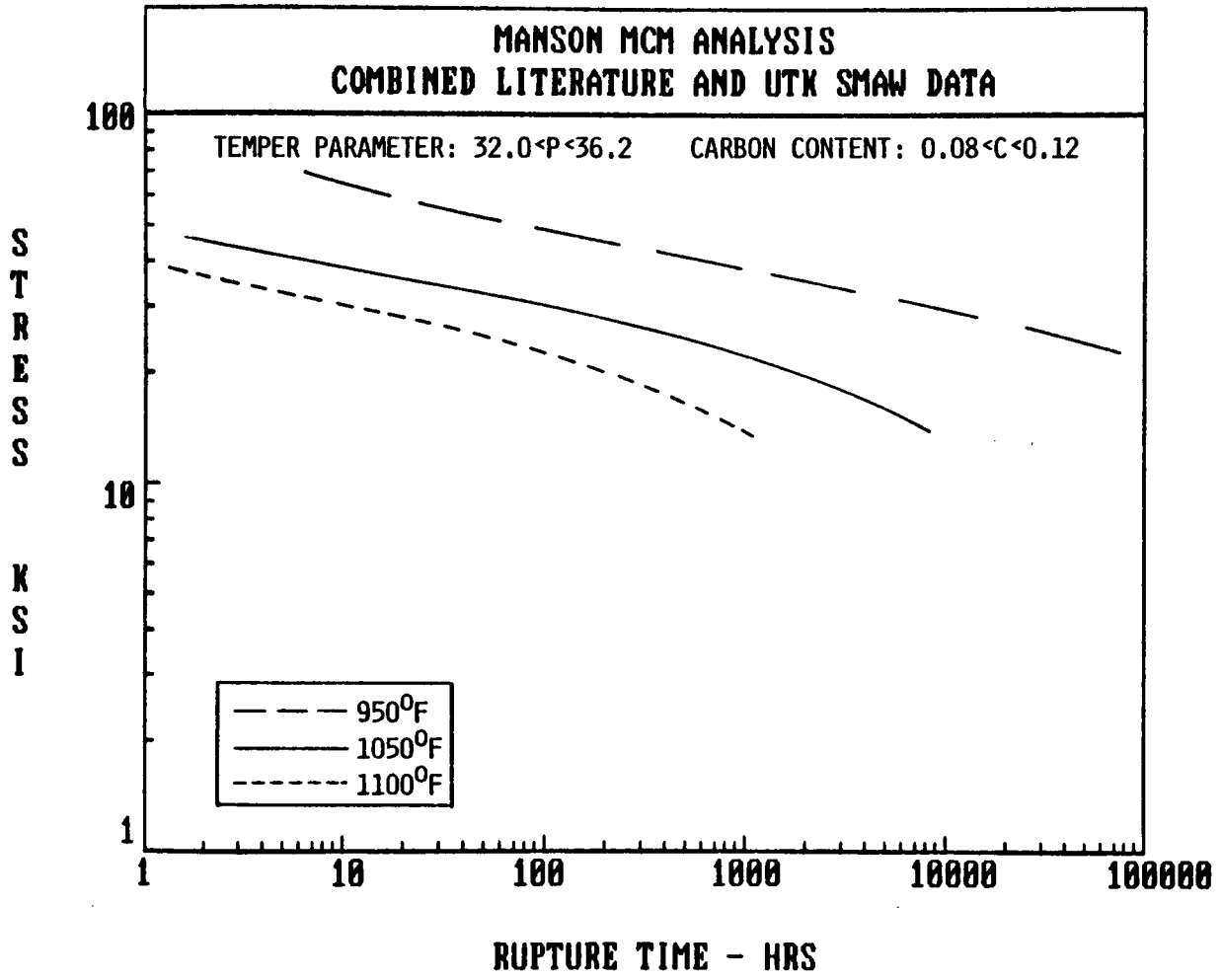


Figure 81. Stress rupture behavior of PWHT 2-1/4Cr-1Mo SMA weld metal (32.0<P<36.2) with carbon content in the range of 0.08<C<0.12 determined by analysis of combined literature and UTK data.

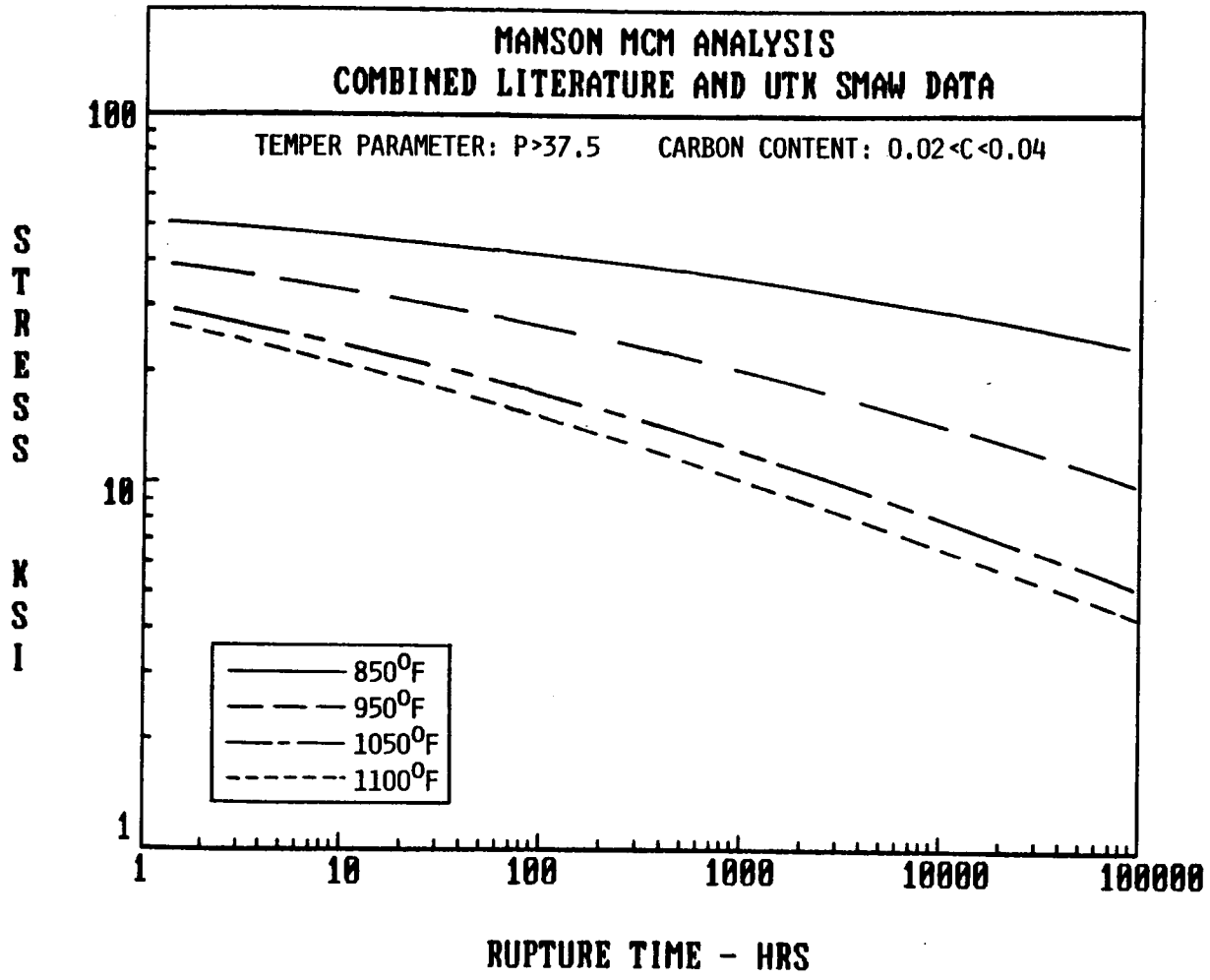


Figure 82. Stress rupture behavior of PWHT 2-1/4Cr-1Mo SMA weld metal (P>37.5) with carbon content in the range of 0.02<C<0.04 determined by analysis of combined literature and UTK data.

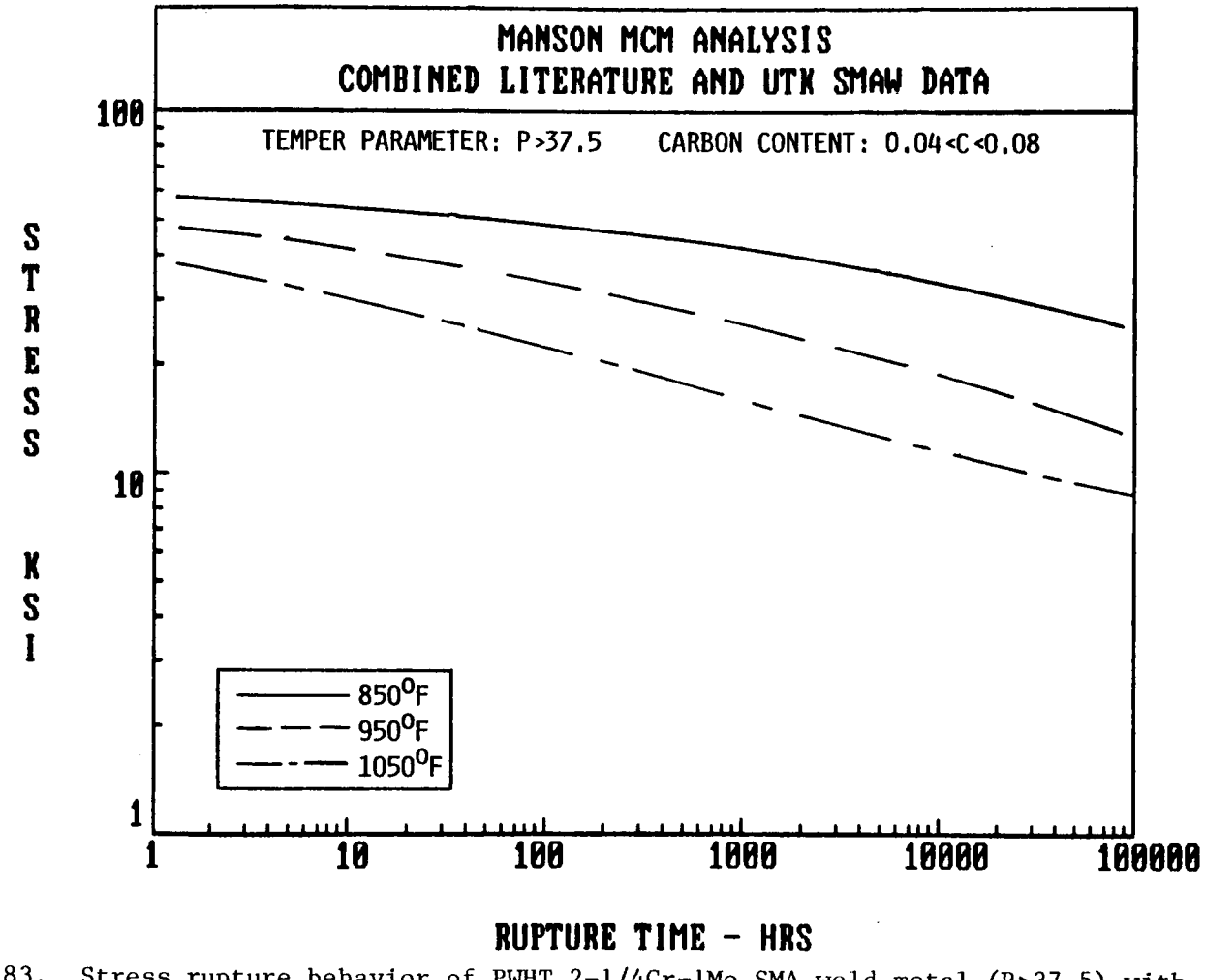


Figure 83. Stress rupture behavior of PWHT 2-1/4Cr-1Mo SMA weld metal (P>37.5) with carbon content in the range of 0.04<C<0.08 determined by analysis of combined literature and UTK data.

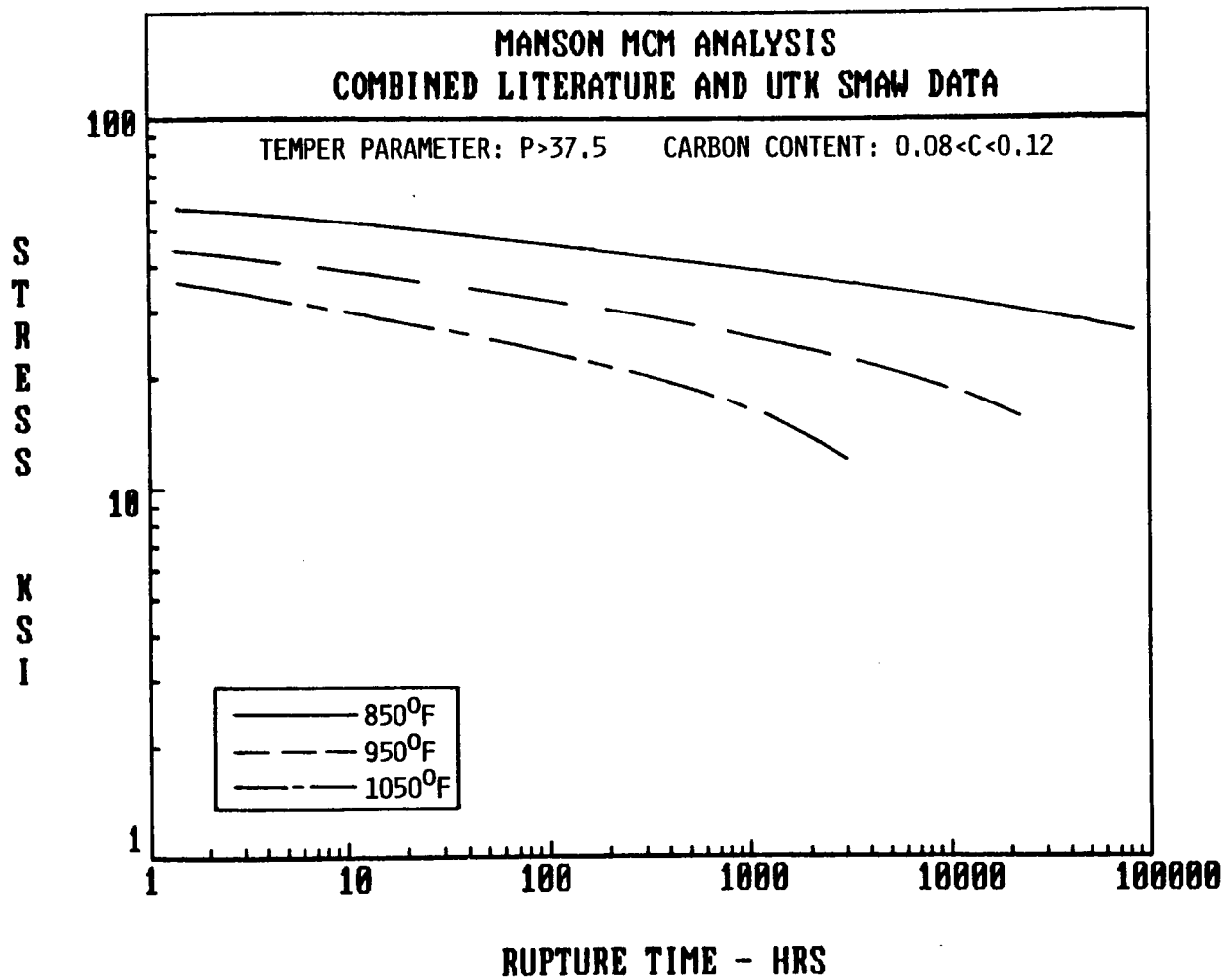


Figure 84. Stress rupture behavior of PWHT 2-1/4Cr-1Mo SMA weld metal (P>37.5) with carbon content in the range of 0.08<C<0.12 determined by analysis of combined literature and UTK data.

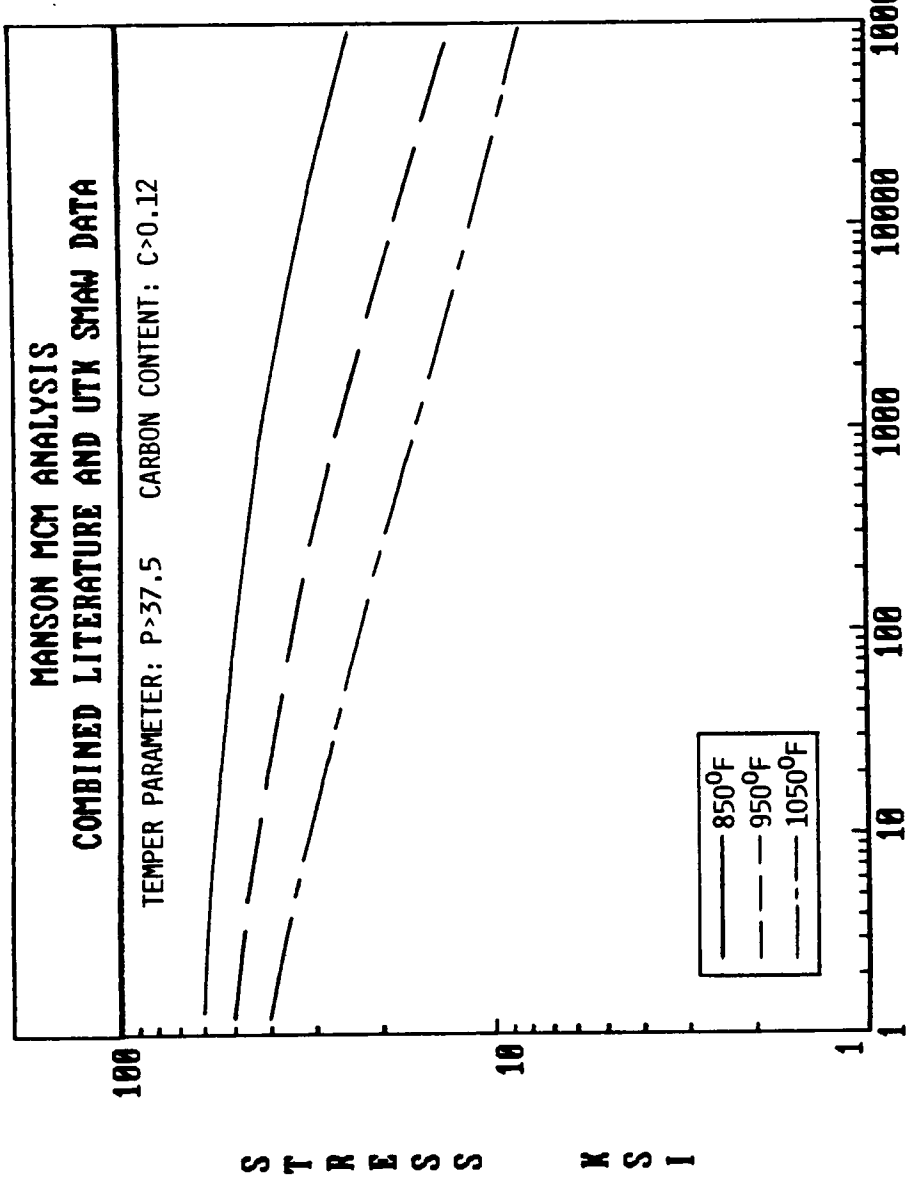


Figure 85. Stress rupture behavior of PWHT 2-1/4Cr-1Mo SMA weld metal (P>37.5) with carbon content in the range of C>0.12 determined by analysis of combined literature and UTK data.

Table 23. Stress for 100,000 hour rupture of 2-1/4Cr-1Mo SMA weld metal as a function of test temperature, carbon content, and temper parameter determined by Manson MCM analysis of combined literature and UTK data.

	Stress for 100,000 Hour Rupture (KSI)										
Condition	750°F	800°F	850°F	900°F	950°F	1000°F	1022°F	1050°F	1067°F	1100°F	1200°F
32.0<P<36.2											
0.04<C<0.08	---	---	---	---	---	---	8.7	8.2	7.6	6.1	---
0.08<C<0.12	---	---	---	---	22.4	13.2	---	---	---	---	---
C>0.12	51.7	45.0	38.1	31.1	23.8	---	---	---	---	---	---
36.2<P<37.5											
0.04<C<0.08	---	---	---	24.3	13.1	---	---	---	---	---	---
0.08<C<0.12	---	---	---	---	---	6.0	5.6	5.2	4.9	4.2	2.5
P>37.5											
0.02<C<0.04	---	---	22.8	14.8	9.7	6.9	6.1	5.3	4.9	4.2	---
0.04<C<0.08	---	---	25.6	17.9	13.3	10.6	9.7	8.8	---	---	---
0.08<C<0.12	---	---	27.1	18.7	10.0	---	---	---	---	---	---
C>0.12	---	---	24.3	17.3	13.1	10.4	9.5	8.6	---	---	---

Conclusions Obtained from the Data Analysis

The analysis of stress rupture data for PWHT 2-1/4Cr-1Mo weld metal using the Larson-Miller parameter technique, the log stress/log rupture time technique, and the Manson minimum commitment method indicates the following:

a. The 100,000 hour rupture strength decreases as the temper parameter increases. However, the strength difference arising from variations in PWHT diminishes with increasing test temperature. This effect is particularly pronounced for weld metal PWHT with P<32.0 which, at 750°F, has a 100,000 hour rupture strength 40 tO 45 KSI higher than that for weld metal PWHT with 32.0<P<36.2. This strength advantage falls rapidly with increasing test temperature and disappears at approximately 900°F.

b. For weld metal PWHT with P<37.5, the 100,000 hour rupture strength appears to increase with increasing carbon content. However, the strengthening effect of carbon diminishes as the test temperature is increased.

c. For weld metal PWHT with P>37.5, the 100,000 hour rupture strength appears to increase with carbon content for levels up to about 0.04-0.05 weight percent. Weld metals having higher carbon contents have similar rupture strengths.

d. The stress rupture strength of PWHT 2-1/4Cr-1Mo SMA weld metal compares well with that determined from data for weld metal deposited by a variety of welding processes.

e. With respect to the data obtained from testing in this program, the following conclusions may be drawn:

   1. 0.08-0.09 carbon weld metal PWHT to proposed Class 3 condition exhibits significantly higher rupture strength at 950 and 1050°F than does the same material PWHT to Class 2.

   2. Rupture test results for weld metal PWHT 1300°F/25 hrs. (Class 2) indicate that the rupture strength of 0.02-0.03 carbon material is significantly lower than that exhibited by the higher carbon weld metals. Furthermore, the strengths of the latter are of similar magnitude.

f. Rupture testing of 2-1/4Cr-1Mo SMA weld metals conducted during this program has contributed significantly to the understanding of the rupture behavior of these materials.

   1. The effect of carbon content on the rupture strength of Class 2 SMA weld metal has been determined and may be employed to define proper industrial practice in the use of higher carbon filler metals to achieve improved strength.

   2. The rupture behavior of 2-1/4Cr-1Mo SMA weld metal PWHT to proposed Class 3 strength has been characterized, contributing to the data base to be used to evaluate the feasibility of using 2-1/4Cr-1Mo steel in the Class 3 condition.

3. The rupture data acquired for the Class 2 weld metal increases by a factor of ten the amount of data available for 2-1/4Cr-1Mo SMA weld metal PWHT with P>37.5.

2. COMPARISON OF DATA ANALYSIS TECHNIQUES

The same stress rupture data were analyzed using three different techniques. The 100,000 hour stresses obtained from each of the methods have been compared and the methods ranked based on the degree of conservatism exhibited by the stress values. Furthermore, using the "r^2" values determined during regression as a guide, the analytical techniques were also compared to discover which method best described the rupture behavior of the weld metal. The value of "r^2" varies between zero and one and can be used to characterize the quality of the curve fit to the data. As "r^2" approaches one, the quality of the fit increases.

Table 24 lists the 100,000 hour rupture stresses obtained from the analysis of combined literature data and UTK data for PWHT 2-1/4Cr-1Mo SMA weld metal. Stresses are given as a function of temper parameter and test temperature. The table presents the stresses determined using the Larson-Miller parameter, log stress-log rupture time, and Manson minimum commitment techniques and is constructed in such a way as to facilitate comparison of the values.

The most conservative 100,000 hour stress values are given by the Manson method while the log stress-log rupture time stresses are the least conservative. The stresses obtained using the

Table 24. Stress for 100,000 hour rupture of 2-1/4Cr-1Mo SMA weld metal as a function of test temperature and temper parameter determined by analysis of combined literature and UTK data.

Temper Parameter	Stress for 100,000 Hour Rupture (KSI)											r^2
	750°F	800°F	850°F	900°F	950°F	1000°F	1022°F	1050°F	1067°F	1100°F	1200°F	
P<32.0												
LM	90.6	66.4	37.8	---	---	---	---	---	---	---	---	0.96
LSLRT	---	---	71.8	29.9	---	---	---	---	---	---	---	**
MCM	(98.0)	(42.2)	---	---	---	---	---	---	---	---	---	0.82
32.0<P<36.2												
LM	54.0	44.4	34.4	26.0	18.4	12.8	---	8.3	---	---	---	0.94
LSLRT	53.8	---	39.9	---	26.9	---	7.0	12.1	7.9	5.8	---	**
MCM	53.2	44.3	35.2	26.3	18.3	12.0	9.9	7.6	6.5	4.8	---	0.73
36.2<P<37.5												
LM	47.4	38.5	29.9	23.0	16.8	12.2	---	---	---	---	---	0.92
LSLRT	---	---	---	31.8	---	12.4	9.4	10.3	---	7.2	3.0	**
MCM	---	---	---	17.8	11.7	7.8	6.6	5.4	4.8	3.8	2.1	0.84
P>37.5												
LM	36.8	30.3	23.7	18.2	13.2	9.4	---	---	---	---	---	0.94
LSLRT	---	---	31.3	---	16.4	---	8.8	8.4	---	4.8	---	**
MCM	---	---	24.7	16.8	11.4	8.1	7.0	6.0	5.5	4.7	---	0.70

** r^2 values unique to each temperature

Larson-Miller technique fall between except at temperatures less than about 850°F where they are comparable to those determined using the Manson method. The greater magnitude of the log stress-log rupture time values is probably a result of the use of a model which assumes a linear relationship between log stress and log rupture time. Modification of the model to include a "$(\log[t_r])^2$" term would likely bring the 100,000 hour stresses more in line with those obtained using the other two analytical techniques.

Inspection of Table 24 reveals that the best curve fits to the data are obtained using the Larson-Miller approach. This is based on the observation that the "r^2" values for the Larson-Miller technique are consistently greater than those for the more conservative Manson method. Larson-Miller "r^2" values are, in general, greater than 0.90 while those for the Manson technique fall in the 0.70 to 0.90 range.

Of the three techniques employed to analyze the stress rupture data in this program, the Larson-Miller parameter method appears to be the most favored. The economy of time and effort involved in plotting all of the rupture data for a material on one curve coupled with the fact that the 100,000 hour stresses thus obtained are interpolated and are not extrapolations based on anticipated future behavior make it an inviting method to use. As indicated above, the "r^2" values which characterize the Larson-Miller curves derived by regression are consistently higher than those obtained for the other techniques. It is true that the 100,000 hour rupture stresses obtained using the Larson-Miller approach are not as conservative as those derived using the minimum commitment method. However, the

Manson curves do not fit the data as well, casting doubt on the accuracy of the associated 100,000 hour rupture stress predictions. Thus, of the three analytical techniques employed in this study, the Larson-Miller parameter method appears to the best technique for the analysis of stress rupture data.

3. TENSILE TESTING

Tensile tests of the 2-1/4Cr-1Mo weld metals were performed at room temperature and at 850, 950, and 1050°F. The tensile properties were observed to be a function of carbon content and PWHT.

The room temperature and elevated temperature tensile properties of the 0.02-0.03, 0.04-0.05, 0.08-0.09, and 0.12-0.13 carbon weld metals PWHT 1300°F/25 hrs. are compared in Table 25. This table shows that the strength (UTS and 0.2% YS) of the 0.02-0.03 carbon weld metal consistently falls below those of the three higher carbon content materials. The strengths of the latter three weld metals are comparable in magnitude although there is, in general, a relatively small increase in strength in response to increasing carbon content. No correlation between ductility and carbon content was observed.

The stress allowables specified by Divisions 1 and 2 of Section VIII of the ASME Boiler and Pressure Vessel Code (100) and the tensile strengths determined for the individual weld metal/PWHT combinations are compared in Table 26. As indicated, the values for Division 1 and Division 2 stress allowables have been derived by multiplying the tabulated values in the code by four and three respectively. This is in accordance with Appendix P of Division 1

Table 25. Tensile test results for 2-1/4Cr-1Mo weld metal PWHT 1300°F/25 hrs.

Temperature (°F)	Weld Metal	UTS (KSI)	0.2% YS (KSI)	Percent Elongation	% Reduction in Area
80	0.02-0.03C	70.3	41.8	33.5	51.3
	0.04-0.05C	78.3	66.9	24.7	71.3
	0.08-0.09C	80.9	63.4	25.0	71.9
	0.12-0.13C	84.5	62.8	33.0	72.0
850	0.02-0.03C	53.1	35.8	28.5	75.0
	0.04-0.05C	60.1	52.1	23.9	71.7
	0.08-0.09C	61.4	51.8	26.0	75.3
	0.12-0.13C	63.0	52.9	27.0	62.5
950	0.02-0.03C	41.1	29.2	35.9	81.5
	0.04-0.05C	51.2	45.4	32.7	80.1
	0.08-0.09C	52.8	47.9	29.0	81.8
	0.12-0.13C	51.8	46.4	44.0	84.5
1050	0.02-0.03C	32.7	26.5	53.1	88.7
	0.04-0.05C	40.4	37.9	36.6	84.4
	0.08-0.09C	43.0	38.9	42.0	88.8
	0.12-0.13C	43.5	39.5	55.0	90.9

Table 26. Comparison of stress allowables from ASME Boiler and Pressure Vessel Code and tensile test results for 2-1/4Cr-1Mo weld metal PWHT 1300°F/25 hrs.

Code/Material	Stress Allowable/UTS (KSI)			
	RT	850°F	950°F	1050°F
Sec. VIII, Div. 1, Class 1[a]	60.0	57.6	44.0	23.2
Sec. VIII, Div. 1, Class 2[a]	75.0	65.2	44.0	23.2
Sec. VIII, Div. 2, Class 1[b]	60.0	43.5	--	--
Sec. VIII, Div. 2, Class 2[b]	75.0	65.4	--	--
0.02-0.03C	70.3	53.1	41.1	32.7
0.04-0.05C	78.3	60.1	51.2	40.4
0.08-0.09C	80.9	61.4	52.8	43.0
0.12-0.13C	84.5	63.0	51.8	43.5

[a]From UCS 23. Values for 850, 950, and 1050°F are 4 times the allowable given in the chart.

[b]From ACS 1. Value at 850 is 3 times the allowable given in the chart.

and Appendix 1 of Division 2 which describe the basis for establishing the stress allowables (100). Inspection of Table 26 indicates that the 0.02-0.03 carbon weld metal does not comply with Class 2 allowables under either division of the code except at 1050°F. However, it does meet Class 1 in most cases with the exception of a lower strength at 850 and 950°F. Examination of Table 26 also reveals that the 0.04-0.05, 0.08-0.09, and 0.12-0.13 carbon weld metals PWHT 1300°F/25 hrs. meet the Class 2 strength requirements of both divisions of Section VIII (100) except at 850°F. At this temperature, these materials satisfy the Class 1 but not the the Class 2 requirements.

Table 27 presents the tensile test data obtained for the 0.08-0.09 carbon weld metal as a function of PWHT. Test results are also included for as-welded material to serve as a baseline to which the PWHT values may be compared. Three PWHT's are represented in the table; Class 2 (1300°F/25 hrs.), Class 3 (1175°F/25.5 hrs.), and aged Class 3 (1175°F/25.5 hrs. plus 1193°F/21.5 hrs.). Examination of the table confirms that the 0.08-0.09 carbon weld metal PWHT 1175°F/25.5 hrs. meets the proposed room temperature tensile strength requirements of 90 to 110 KSI for Class 3 SA 387 Grade 22 steel (93). Furthermore, in comparing the Class 2 and Class 3 tensile properties, it is evident that the strength of the Class 3 weld metal is significantly greater than that exhibited by the Class 2 material. At room temperature, the Class 3 tensile strength is 20 percent greater, a strength advantage which increases with temperature to 50 percent at 1050°F. The ductilities of the two materials are

Table 27. Tensile test results for 0.08-0.09 carbon 2-1/4Cr-1Mo weld metal as a function of condition.

Temperature (°F)	Weld Metal	Condition	Temper Parameter	UTS (KSI)	0.2% YS (KSI)	Percent Elongation	% Reduction in Area
80	0.08-0.09C	As-Welded	--	134.0	125.0	18.0	38.9
		Class 3[a]	35.0	97.7	85.6	23.0	68.8
		Aged Class 3[b]	35.6	101.5	88.4	21.5	68.9
		Class 2[c]	37.7	80.9	63.4	25.0	71.9
950	0.08-0.09C	Class 3	35.0	70.3	64.3	14.9	72.8
		Aged Class 3	35.6	72.8	63.0	19.6	69.9
		Class 2	37.7	52.8	47.9	29.0	81.8
1050	0.08-0.09C	Class 3	35.0	62.8	60.0	17.9	77.3
		Aged Class 3	35.6	65.1	60.6	24.6	77.0
		Class 2	37.7	43.0	38.9	42.0	88.8

[a]Class 3 - PWHT 1175°F/25.5 hrs.

[b]Aged Class 3 - PWHT 1175°F/25.5 hrs. , Aged 1193°F/21.5 hrs.

[c]Class 2 - PWHT 1300°F/25 hrs.

similar at room temperature but diverge considerably as the temperature is increased with the ductility of the Class 3 weld metal falling well below that of the Class 2 material. Table 27 may also be employed to illustrate the changes in the Class 3 weld metal tensile properties as a result of an aging treatment designed to simulate 100,000 hour service at 950°F. Comparison of the Class 3 and the aged Class 3 weld metal properties indicates that the aging treatment has little effect on the strength and ductility of the Class 3 material.

Comparison of the room temperature and elevated temperature tensile strengths of the four carbon content weld metals PWHT 1300°F/25 hrs. with the observed rupture behavior of those materials reveals a similar dependence on carbon content. In both instances, the strength of the 0.02-0.03 carbon weld metal is significantly below that of the other three carbon content materials. This indicates that tensile test results may possibly be useful in predicting relative stress rupture behavior.

It is apparent from Table 26 that the use of low carbon 2-1/4Cr-1Mo filler metals with carbon levels below about 0.04 weight percent in the construction of Class 2 vessels will not permit the allowable strengths to be obtained. The 0.02-0.03 carbon material tested in this study failed to meet Class 2 requirements at all temperatures below 1050°F. It is recognized that the 1300°F/25 hrs. PWHT employed is more severe than that recommended by Section VIII of the ASME code (100) and that under less stringent conditions, the 0.02-0.03 carbon weld metal might possibly conform to the Class 2

requirements. However, welds in vessels often experience multiple PWHT's during fabrication/weld repair, the effects of which could add up to produce an effect similar to that observed for the 1300°F/25 hrs PWHT.

The use of lower temperature PWHT's to achieve enhanced tensile properties has been demonstrated using the 1175°F/25.5 hrs. PWHT. However, this strength advantage is gained at the expense of lost ductility. Using the Class 2 weld metal tensile properties for comparison, the ductility of the Class 3 weld metal is comparable to the Class 2 material at room temperature. However, as the temperature increases, the difference in ductility between the Class 2 and Class 3 weld metals grows in magnitude with the Class 3 material exhibiting lower ductility.

The tensile properties of the Class 3 weld metal appear to be relatively stable at 950°F. Comparison of the properties of the Class 3 and the aged Class 3 weld metals determined at room temperature, 950, and 1050°F indicate that strength and ductility of 0.08-0.09 carbon Class 3 weld metal are relatively unaffected by an aging treatment designed to simulate 100,000 hour service at 950°F.

4. MICROSTRUCTURAL ANALYSIS

Microstructural characterization of the 2-1/4Cr-1Mo weld metals was performed in order to provide enhanced understanding of the elevated temperature behavior. The examination of the 0.08-0.09 and 0.12-0.13 carbon weld metals thermally cycled on the Gleeble was accomplished to verify the conclusions arrived at during dilatometric

studies. Using the SEM, the as-transformed microstructures were described as a function of carbon content and weld energy input. Furthermore, the observed trends were explained in terms of the mechanisms operable during the on-cooling transformations. In the studies related to the stress rupture testing effort, the 0.02-0.03, 0.04-0.05, 0.08-0.09, and 0.12-0.13 carbon weld metals were examined in the as-welded, PWHT, and rupture tested condition. Using the SEM and STEM, the microstructures were characterized as a function of carbon content. Microstructural changes resulting from elevated temperature exposure during PWHT and rupture testing were also examined. Finally, to gain an understanding of the structural changes which occur during prolonged service, 2-1/4Cr-1Mo weld metal with 15 years of service at 1050^{o}F was examined.

Transformation Studies

Transformation studies of the 0.08-0.09 and 0.12-0.13 carbon weld metals using a dilatometric method were conducted on the Gleeble. Specimens were subjected to a thermal cycle designed to simulate the thermal history experienced by previously deposited weld metal during the placement of subsequent weld beads. Cooling conditions were chosen to span the normal range of weld energy inputs characteristic of welds in heavy-section Cr-Mo materials. A peak temperature of 2400^{o}F was employed in order to simulate the coarse-grained region of the HAZ. The coarse-grained region was singled out for investigation because of its propensity to form microconstituents associated with weldability problems.

The results of the transformation effort have shown that the as-transformed microstructure of the 0.08-0.09 and 0.12-0.13 carbon weld metals is primarily bainite. Continuous cooling transformation (CCT) diagrams obtained for the two materials are shown in Figures 86 and 87. Cooling curves characteristic of the seven thermal cycles used in the study are shown with the transformation start and finish temperatures indicated on each curve. Included in the figures are the A_{c1} and A_{c3} temperatures determined during the rapid heating portion of the weld thermal cycle. Examination of the figures reveals that the transformation start and finish temperatures decrease with increasing cooling rate. Furthermore, at corresponding cooling rates, the transformation temperatures for the 0.12-0.13 carbon weld metal are 50 to 100F^{o} lower than those observed for the 0.08-0.09 carbon material.

Metallographic examination of the transformation specimens for both the 0.08-0.09 and 0.12-0.13 carbon weld metals has confirmed the Gleeble dilatometric studies, i.e., that the as-transformed microstructure is primarily bainitic. This is true over the entire range of energy inputs employed. The bulk of the microstructure has a morphology characteristic of upper bainite, identifiable by its lath-like arrangement of ferrite with elongated constituents (composed of a combination of carbide and retained austenite) (4,45,95) located at the lath boundaries and aligned parallel to the longitudinal lath axis.

The predominantly bainitic microstructure of the 0.08-0.09 and 0.12-0.13 carbon weld metals is as expected. Figure 2 (p. 19), a

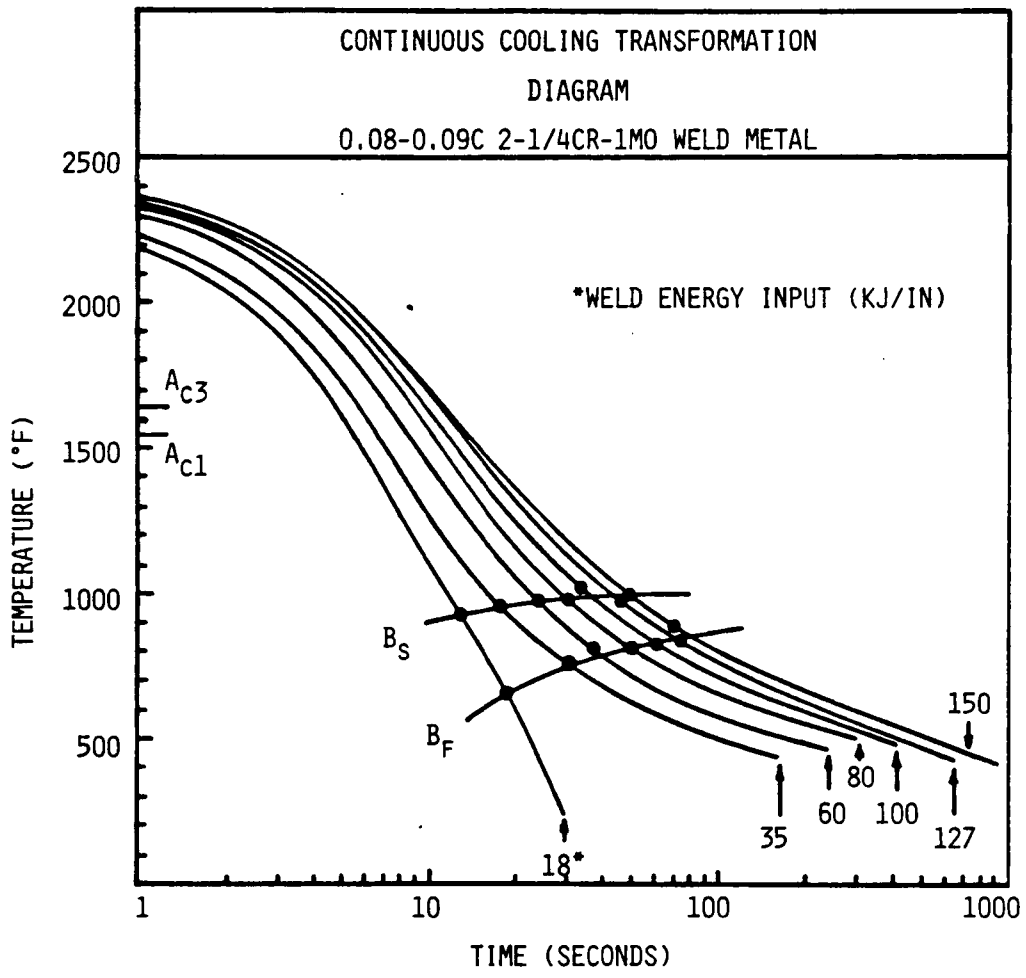


Figure 86. Continuous cooling transformation diagram for 0.08-0.09 carbon 2-1/4Cr-1Mo weld metal.

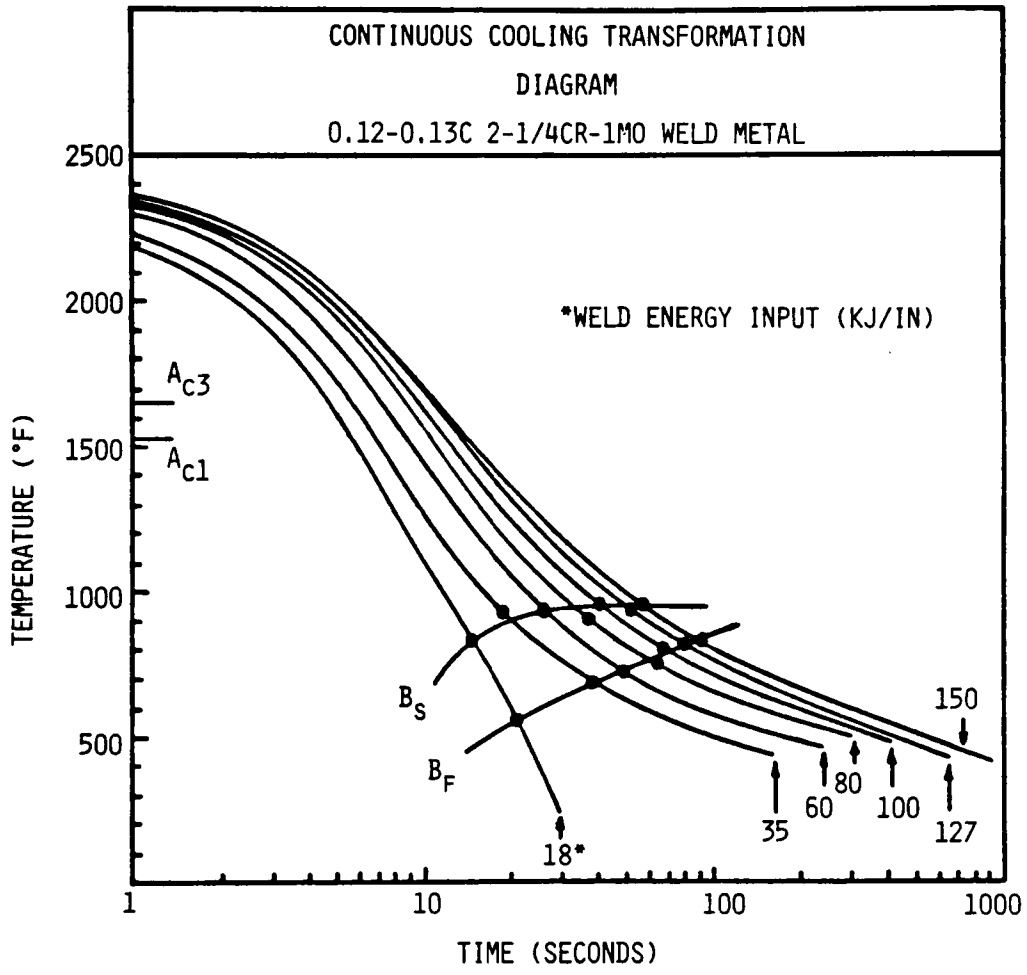


Figure 87. Continuous cooling transformation diagram for 0.12-0.13 carbon 2-1/4Cr-1Mo weld metal.

CCT diagram for 0.1 percent carbon 2-1/4Cr-1Mo steel (4), shows a wide bainite shelf which projects out beyond the ferrite/pearlite nose, indicating that a fully bainitic structure results over a wide range of cooling rates. The absence of martensite in the weld metal structure is understood when one notes that for martensite to form, a cooling rate of approximately 5000C^{o} per minute must be achieved.

The 50 to 100F^{o} difference between the bainite start temperatures of the 0.08-0.09 and 0.12-0.13 carbon weld metals is attributable to the higher carbon content of the latter material. Inspection of the compositions as given in Table 3 (p. 79) for the two weld metals reveals that the levels of the other elements in each are almost identical. There is a factor of two difference in the vanadium contents with the 0.12-0.13 carbon weld metal having half the vanadium of the lower carbon material. However, the levels present are well below that expected to significantly affect behavior.

Microstructure of the 0.08-0.09 carbon weld metal. Three bainite morphologies have been observed in the 0.08-0.09 carbon weld metal microstructures; lath-like, granular, and massive. An example of the lath-like morphology which predominates at low energy inputs is shown in Figure 88. As the cooling rate decreases (energy input increases), not only does the fraction of the microstructure that is lath-like decrease, but the laths grow wider, making the structure coarser. Furthermore, the stringers of carbide/austenite present at the lath boundaries at low energy inputs are gradually replaced with

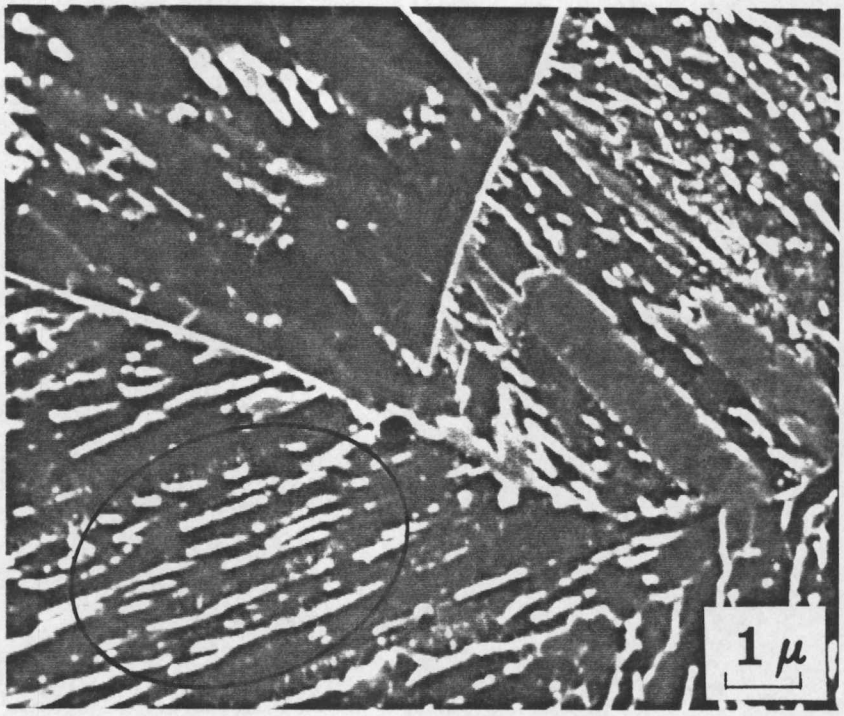


Figure 88. Lath bainite in 0.08-0.09 carbon 2-1/4Cr-1Mo weld metal thermally cycled 18 KJ/IN, 10000X, SEM.

constituents which are less elongated and more widely spaced. Eventually at high energy inputs, these constituents become less rod-like and more equiaxed.

Observed variations in bainite morphology as a function of energy input and carbon content may be explained on the basis of the austenite to upper bainite transformation. The formation of upper bainite is initiated by the nucleation and growth of a lath of ferrite from the austenite (94,95). The driving force for the transformation is the free energy difference between the austenite and the bainitic ferrite (95). Because the first ferrite formed is low in carbon, extensive carbon migration occurs to the ferrite/austenite interface and then into the austenite. As the ferrite lath grows, carbon is continuously rejected into the austenite ahead of the advancing interface.

There is significant evidence that the austenite transforms to bainitic ferrite by a shear process (95). As a result, transformation strains arise which lead to deformation in both the ferrite and the austenite. The deformation strains, in turn, play a significant role in determining the upper bainite morphology. Researchers (94,95) have observed rapid side-by-side nucleation of ferrite laths to form a bundle of parallel laths. Evidence appears to indicate that this sympathetic nucleation phenomenon arises as a result of the transformation strains. As these laths grow together, the austenite trapped between becomes increasingly enriched in carbon. In low carbon alloy steels like 2-1/4Cr-1Mo, this austenite may be retained at the lath boundaries or partially transform to

ferrite and carbide (45). Any ferrite that forms does so epitaxially on the edge of the adjacent lath. The final structure is therefore one of parallel ferrite laths with austenite or an austenite/carbide aggregate at the lath boundaries. Furthermore, since the austenite to bainite transformation can initiate at more than one location within a grain, the fully transformed prior austenite grain may contain numerous lath bundles, each with its own orientation.

Closer inspection reveals that the ferrite laths in upper bainite do not continuously grow by a diffusional mechanism after nucleation. Instead, each lath consists of substructural units, 10 to 15 microns in length, which are aligned end to end with their longitudinal axis parallel to the longitudinal axis of the lath (94). It is thought that the limited length of these subunits is dictated by the strains which accumulate in the austenite as the subunit grows. Apparently a strain level is finally achieved which terminates subunit growth and leads to the nucleation of a new unit. The length of the laths themselves is apparently only constrained by how far the lath can grow before encountering either a prior austenite grain boundary or already transformed material (95).

Considering the above discussion, morphological changes observed in lath bainite in response to changes in cooling rate (weld energy input) may be explained. It has been noted that the austenite to bainite transformation temperature decreases as the cooling rate increases (see Figures 86 and 87, pp. 210, 211). As the temperature of the transformation is diminished, the diffusivity of carbon required for the ferrite laths to grow decreases. As a result, the

lateral growth of the laths is inhibited and the laths become narrower (95). Furthermore, since the lath boundaries are the sites of the carbide/austenite stringers, these constituents become closer together as well. These mechanisms therefore explain the finer lath structure observed at low energy inputs.

The tendency for the stringers of carbide/austenite at the lath boundaries to become more continuous at higher cooling rates (lower energy inputs) has been addressed by Pickering (95). He has indicated that the amount of carbon enrichment in the austenite (at the lath boundaries) required to initiate the transformation of the austenite to ferrite plus carbide is reduced with a decrease in transformation temperature. Because the maximum availability of carbon is limited by the carbon content of the weld metal, decreasing the amount of carbon necessary to enrich a given amount of austenite implies that a greater amount of enriched austenite may be produced. The resulting increased availability of carbide/austenite leads to more continuous stringers of that constituent at the lath boundaries.

As the lath-like microconstituent decreases in response to slower cooling rate (increasing weld energy input), it is replaced by a more granular constituent as illustrated in Figure 89. The granular microstructures consist of a bainitic-ferritic matrix that contains small islands of irregular outline which show no evidence of internal structure at magnifications to 10,000X. The islands appear to be elevated above the surrounding ferrite matrix, indicating that they are etchant resistant. They also seem to be randomly

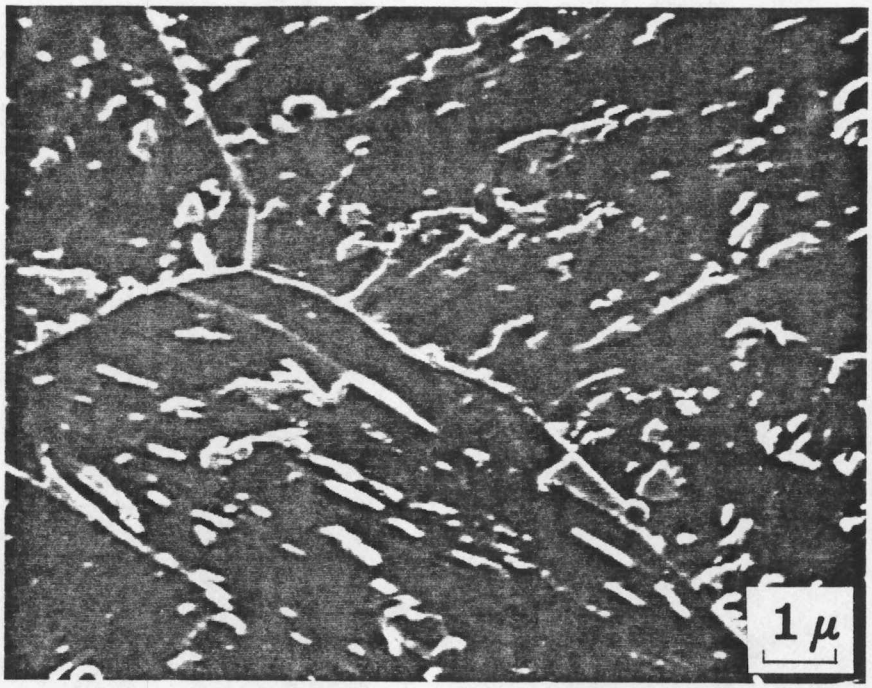


Figure 89. Granular bainite in 0.08-0.09 carbon 2-1/4Cr-1Mo weld metal thermally cycled 80 KJ/IN, 10000X, SEM.

distributed throughout the non-lath regions of the prior austenite grains.

Massive constituents significantly larger than the islands in the granular bainite have been observed in all transformation specimens to varying degrees, apparently independent of cooling rate (weld energy input). These constituents, indicated by arrows in Figure 90, are irregular in shape and resistant to etchant attack. Some of the massive regions are elongated in one direction and are aligned with their longitudinal axis parallel to the surrounding lath bainite. In some cases, particles may be discerned within the massive constituents.

Granular and massive bainites are known upper bainite morphologies. Granular bainite, as observed in the weld metals in this study, has been described by Klueh (8) as islands of a second constituent dispersed in a bainitic-ferritic matrix. Habraken and Economopoulos (45) have determined that these islands are composed of a combination of martensite and residual austenite. Massive bainite occurs as coarse plates of irregular outline with little internal structure discernible without the aid of transmission electron microscopy. Sometimes, faint evidence of particles may be detected which appear to be embedded within the plates (see Figure 90). X-ray analysis indicates that these particles are two-phase, austenite-martensite (45). Shackleton and Kelly (96) have reported similar massive constituents which they have identified as plates of massive bainitic ferrite embedded with carbides.

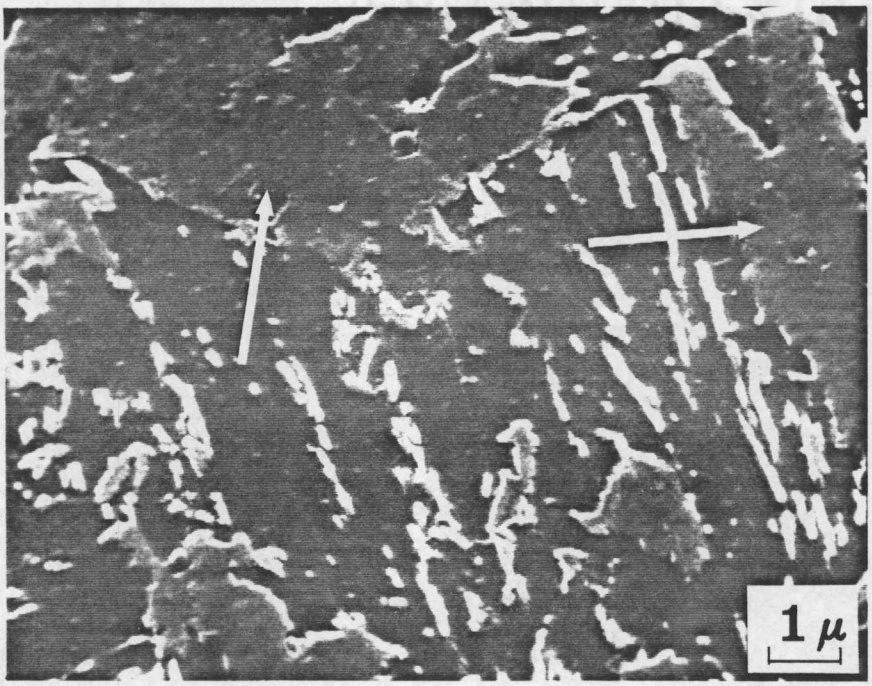


Figure 90. Massive bainite in 0.08-0.09 carbon 2-1/4Cr-1Mo weld metal thermally cycled 60 KJ/IN, 10000X, SEM.

The precise mechanism of formation of these granular and massive constituents is not well understood and will not be discussed in great detail. However, Habraken and Economopoulos (45) have noted that they appear to occur only as a result of continuous cooling. Furthermore, they have found that such structures only occur over a particular range of cooling rates. To illustrate the concept, they have presented a general CCT diagram in which the cooling time range over which bainite occurs has been divided up into three vertical bands (see Figure 91). They have found that in many of the steels studied, granular/massive constituents only occur in region II of the figure. This observation is only in partial agreement with the occurrence of granular and massive constituents in the weld metal transformation specimens. Although the portion of the microstructure with a granular aspect increases as the cooling rate decreases (energy input increases), the massive constituents observed in the weld metals are present over the full range of weld cooling rates.

The only deviation from a fully bainitic structure occurs in weld metal subjected to a thermal cycle corresponding to 150 KJ/IN. Traces of polygonal ferrite may be found at the prior austenite grain boundaries in the microstructure which otherwise consists of granular bainite (see Figure 92). However, the polygonal ferrite is not uniformly distributed throughout the weld, occuring only in the weld metal at the interpass boundaries.

The formation of polygonal ferrite in the weld metal subjected to a 150 KJ/IN thermal cycle is a result of the relatively slow cooling rate characteristic of that thermal history. The restriction

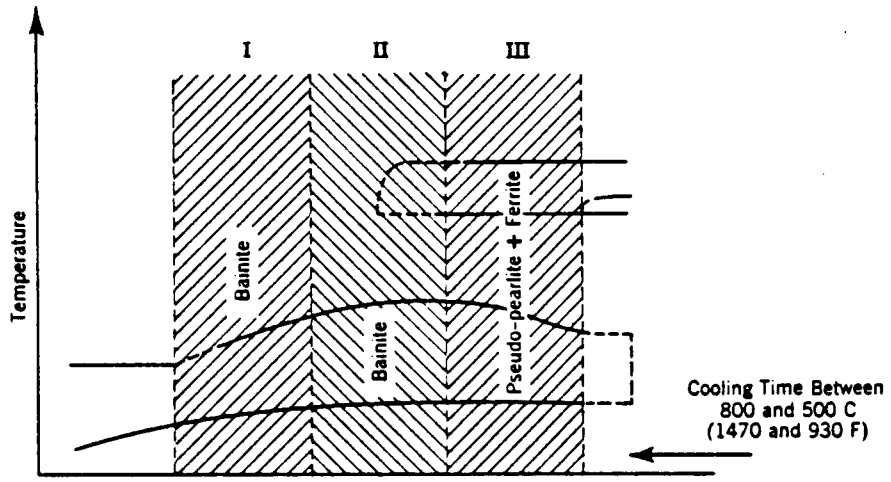


Figure 91. Three zones in the intermediate transformation range defined in terms of temperature and cooling time between 800 and 500°C.

Source: Habraken, L. T. and Economopoulos, M., "Bainitic Microstructures in Low-Carbon Alloy Steels and Their Mechanical Properties," Symposium on Transformation and Hardenability in Steels, Climax Molybdenum Co. (1967).

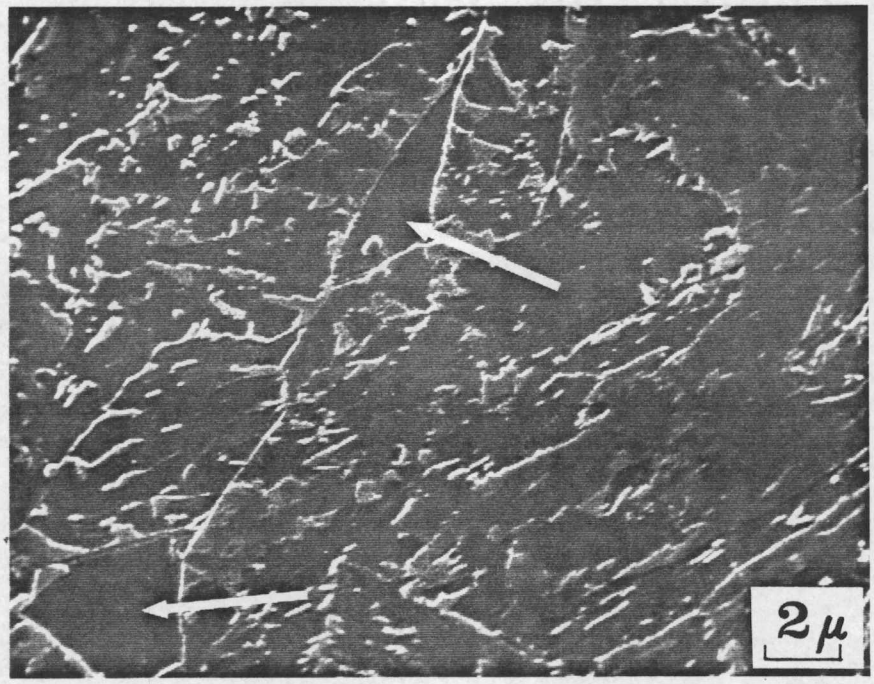


Figure 92. Polygonal ferrite at the prior austenite grain boundaries of a granular bainite matrix. Material is 0.08-0.09 carbon 2-1/4Cr-1Mo weld metal thermally cycled 150 KJ/IN, 5000X, SEM.

of the ferrite to the weld metal in the interpass boundary region is due to the reduced hardenability of that region as a result of the grain refining action of the original weld thermal cycle. The formation of polygonal ferrite was not detected by dilatometric means because the volumetric change accompanying the formation of trace amounts of ferrite was of insufficient magnitude to be resolved by the dilatometer.

Microstructure of the 0.12-0.13 carbon weld metal. The observations made concerning the 0.08-0.09 carbon weld metal microstructures and their dependence on cooling rate (weld energy input) are, in general, the same for the 0.12-0.13 carbon material. The lath bainite predominates at low energy inputs and is gradually replaced by granular bainite as the energy input increases. Massive structures are also in evidence, although occurring to a lesser degree. As in the lower carbon material, the 0.12-0.13 carbon weld metal cycled with an energy input of 150 KJ/IN contains traces of polygonal ferrite in the regions adjacent to the fusion line of each individual weld bead.

Despite these similarities, the higher carbon content of the 0.12-0.13 carbon weld metal does have a noticeable effect on the as-transformed microstructures. The most significant is the occurrence of a previously absent constituent in the rapidly cooled material (18 KJ/IN). Shown in Figure 93, the constituent occurs as elongated regions whose internal structure consists of a fine dispersion of particles. At the limits of the resolution of the SEM

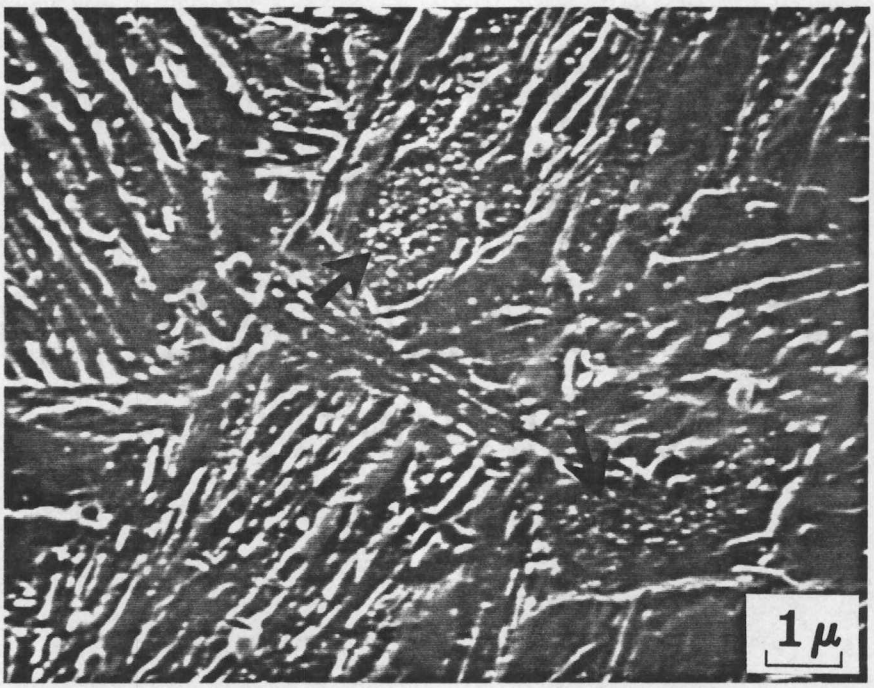
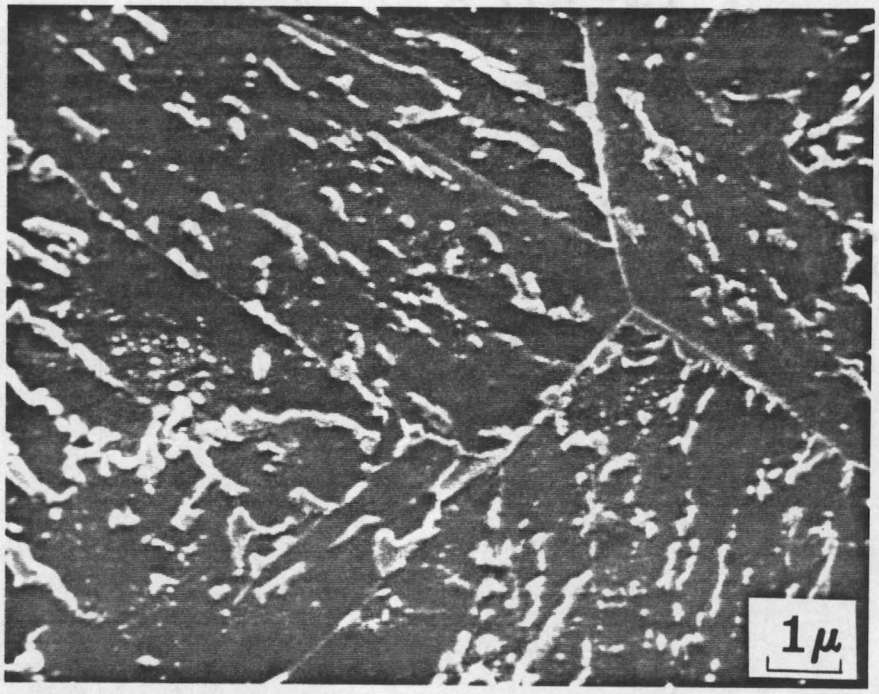


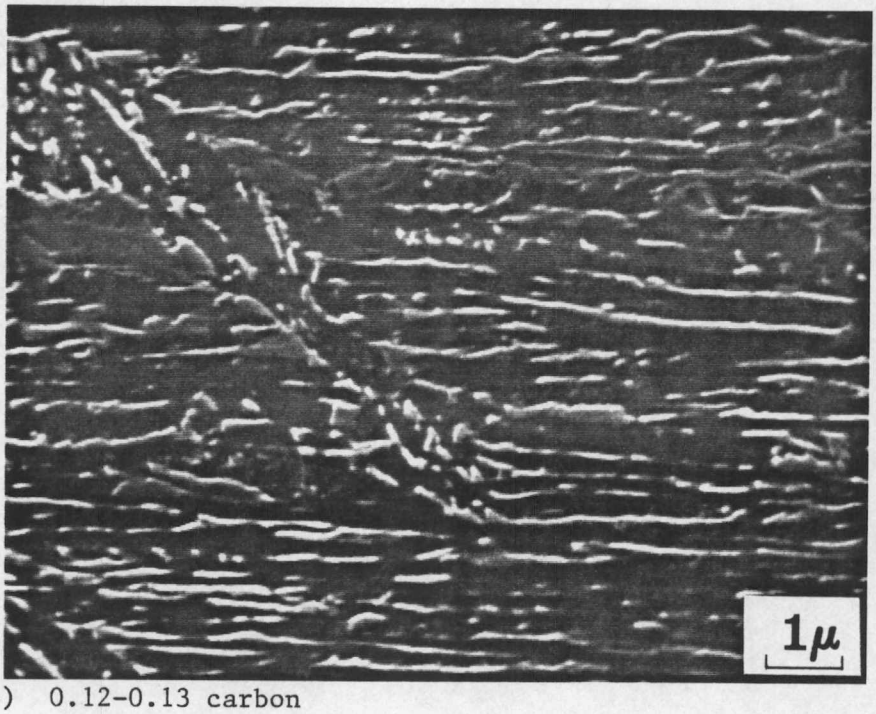
Figure 93. Upper bainite matrix containing a second constituent, possibly lower bainite or auto-tempered martensite. Material is 0.12-0.13 carbon 2-1/4Cr-1Mo weld metal thermally cycled 18 KJ/IN, 10000X, SEM.

(300 angstroms), the particles appear to be randomly distributed and have a spheroidal morphology. Habraken and DeBrouwer (97) have identified similar constituents in tool steel as auto-tempered martensite. However, Habraken and Economopoulos (45) have indicated that in low carbon, low alloy steels, it is difficult to distinguish between auto-tempered martensite and lower bainite. The identity of this constituent is therefore uncertain.

All other microstructural differences between the 0.08-0.09 and the 0.12-0.13 carbon weld metal are matters of degree. With respect to the lath-like upper bainite, the structure of the higher carbon weld metal appears to be finer, i.e., the laths are narrower than those observed in the corresponding 0.08-0.09 carbon material having experienced the same thermal history. Furthermore, the amount of carbide/austenite constituent present at the lath boundaries of the 0.12-0.13 carbon weld metal appears to be greater than that observed in the lower carbon content weld metal. In particular, at energy inputs equal to or less than 80 KJ/IN, the carbide/austenite stringers appear to be more continuous, occupying a greater percentage of the lath boundaries. This dependence of morphology on carbon content is apparent in Figure 94 which compares the two weld metals cycled at identical energy inputs. Considering the granular bainite, the islands in the higher carbon weld metal appear more numerous. Finally, the massive structures so obvious at all energy inputs in the 0.08-0.09 carbon weld metal appear to occur far less frequently in the 0.12-0.13 carbon material. Those observed in the



(a) 0.08-0.09 carbon



(b) 0.12-0.13 carbon

Figure 94. Comparison of 0.08-0.09 and 0.12-0.13 carbon 2-1/4Cr-1Mo weld metal thermally cycled 60 KJ/IN, 10000X, SEM.

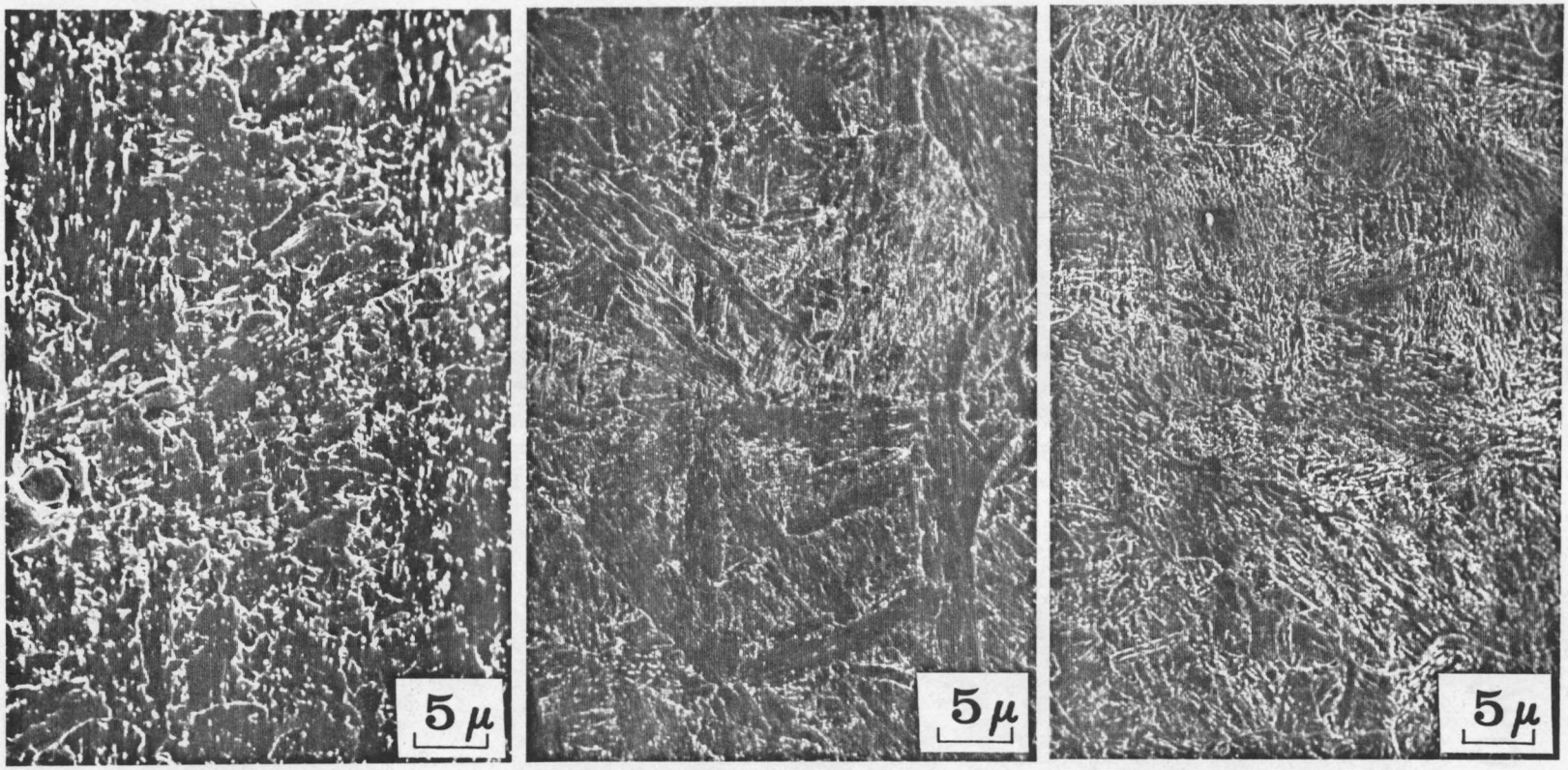
higher carbon weld metal at 150 KJ/IN appear to be less resistant to etchant attack, revealing more evidence of internal structure.

The finer structure of the lath bainite in the 0.12-0.13 carbon weld metal is a consequence of the higher carbon content. During the transformation of austenite to lath bainite, ferrite laths nucleate and grow into the austenite. Growth of the ferrite is accomplished by the rejection of carbon into the austenite ahead of the moving ferrite/austenite interface. When the carbon content of the weld metal is increased, the rate of carbon diffusion is reduced because of the decreased carbon gradient between the ferrite and the surrounding austenite. This, in turn, inhibits lateral growth of the ferrite laths and produces a finer structure (95).

The increase in the amount of carbide/austenite constituent at the lath boundaries may also be explained in terms of the increased carbon level of the weld metal. More carbon is available to produce carbide/austenite which, in turn, results in greater amounts of this constituent at the lath boundaries (95).

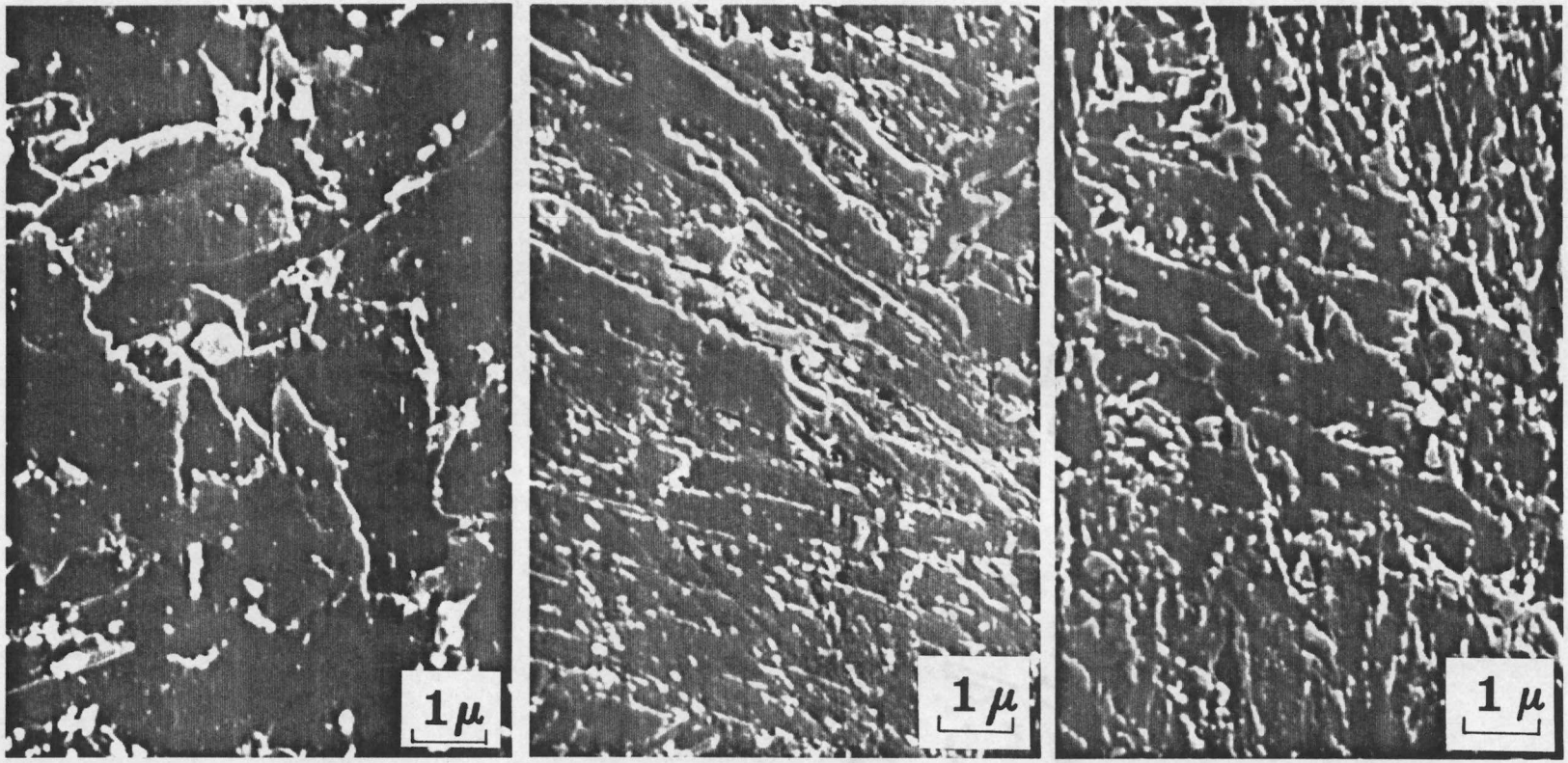
As-Welded Weld Metal Microstructure

SEM examination of the four carbon content SMA weld metals in the as-welded condition has revealed that their microstructures are fully bainitic (Figures 95 and 96) with the exception of the 0.02-0.03 carbon weld metal which contains traces of polygonal ferrite (Figure 97). The bainite morphologies observed are all typical of upper bainite with the predominant morphology being lath-like or granular.



(a) 0.04-0.05 carbon (b) 0.08-0.09 carbon (c) 0.12-0.13 carbon

Figure 95. Comparison of the as-welded microstructure of 0.04-0.05, 0.08-0.09, and 0.12-0.13 carbon 2-1/4Cr-1Mo weld metal, 2000X, SEM.



(a) 0.04-0.05 carbon (b) 0.08-0.09 carbon (c) 0.12-0.13 carbon

Figure 96. Comparison of the as-welded microstructure of 0.04-0.05, 0.08-0.09, and 0.12-0.13 carbon weld metal, 10000X, SEM.

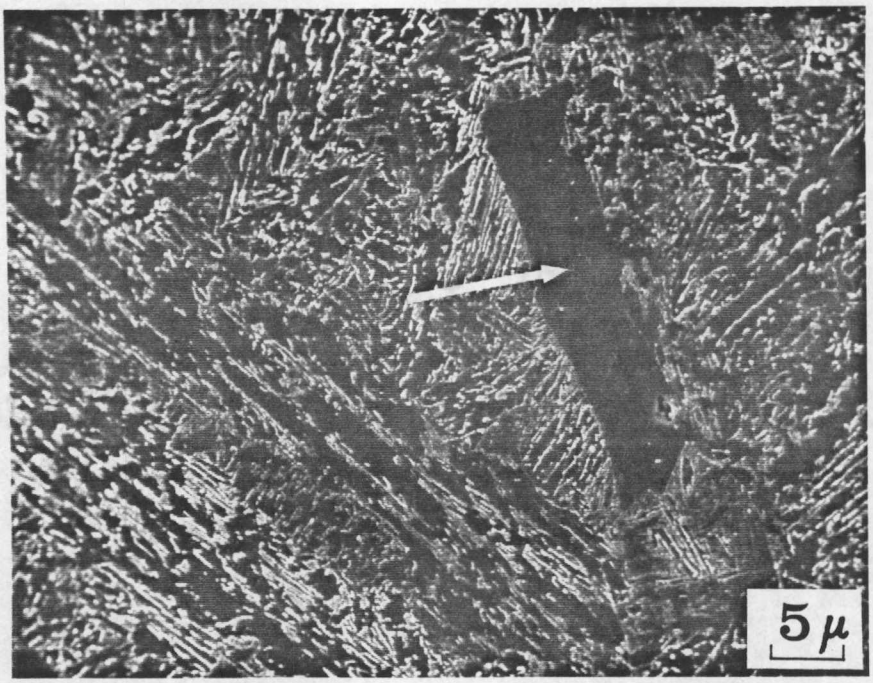
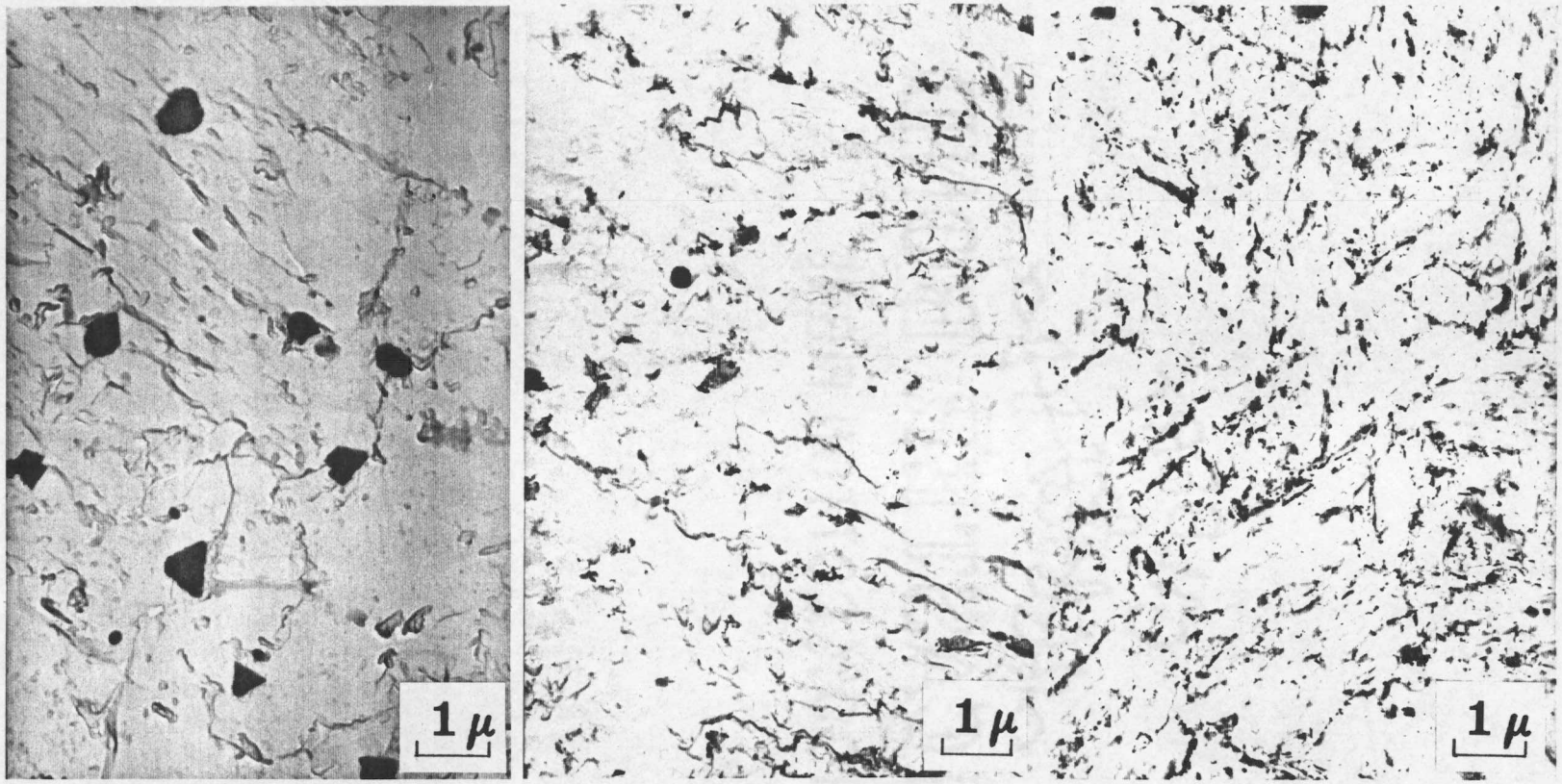


Figure 97. Polygonal ferrite in lath bainite matrix of as-welded 0.02-0.03 carbon 2-1/4Cr-1Mo weld metal, 2000X, SEM.

Some microstructural variation from sample to sample may be attributed to differences in carbon content. Considering the 0.04-0.05, 0.08-0.09, and 0.12-0.13 carbon weld metals shown in Figure 96, the amount of carbide increases as the carbon content increases. Furthermore, the bainite becomes finer with increasing levels of carbon. The former trend is a result of an increased availability of carbon to produce carbide/retained austenite coupled with the decreased levels of carbon enrichment required to retain austenite in a higher carbon material. The latter occurs because the increased bulk carbon level decreases the carbon gradient in the austenite adjacent to the ferrite/austenite interface during the bainite formation, slowing carbon diffusion and inhibiting the lateral growth of the ferrite.

Carbide extraction replicas of as-welded 0.04-0.05, 0.08-0.09, and 0.12-0.13 carbon weld metals have been examined using the STEM (see Figure 98). The microstructures observed in the replicas are somewhat different from those seen in polished and etched specimens on the SEM. Although the surface relief of the samples from which the replicas were taken is preserved, only the carbides are present for identification and examination. The shrouding effect of possible retained austenite in the microstructures has been eliminated.

Table 28 summarizes the occurrence of alloy carbides in the various weld metals as determined by STEM analysis. The information is presented as a function of carbon content and weld metal condition. Location codes used to indicate the preferential sites for each carbide type are defined at the bottom of the table.



(a) 0.04-0.05 carbon (b) 0.08-0.09 carbon (c) 0.12-0.13 carbon

Figure 98. Carbide morphology and distribution of as-welded 0.04-0.05, 0.08-0.09, and 0.12-0.13 carbon 2-1/4Cr-1Mo weld metal as shown by carbide extraction replica, 9000X, STEM.

Table 28. The occurrence of various alloy carbides in 2-1/4Cr-1Mo weld metal as a function of carbon content and PWHT.

	Weld Metal						
	PWHT 1300°F/25 hrs.				PWHT 1175°F/ 25.5 hrs.	As-Welded	
Carbide	0.02-0.03C	0.04-0.05C	0.08-0.09C	0.12-0.13C	0.08-0.09C	0.08-0.09C	0.12-0.13C
M_3C	NF[a]	NF	NF	NF	NF	B,m	B,m
M_2C	M[b]	NF	NF	NF	M	M	M
M_7C_3	M,b[c]	M,b	M,b	M,b	M,b	NF	NF
$M_{23}C_6$	B[c],m[b]	B,m	B,m	B,m	B,m	NF	NF
$M_{23}C_6$+M_6C[d]	NF	NF	NF	B,m	NF	NF	NF
M_6C	NF	M	M	M	M	NF	NF
M_6C+M_2C	M	NF	NF	NF	NF	NF	NF

[a]Carbide not found.

[b]Carbide found in the matrix. Capital letter indicates predominant location.

[c]Carbide found at constituent boundaries. Capital letter indicates predominant location.

[d]Plus sign (+) indicates two carbides bound together.

As indicated by the table, the only carbides observed in the as-welded materials are M_3C and M_2C, with the M_2C being present only in small amounts. M_3C is an iron-rich precipitate (37) which has the structure of cementite but may contain significant amounts of chromium and some molybdenum. The M_3C carbides occur primarily at grain/lath boundaries and become more prevalent as the weld metal carbon content increases. The M_3C found has no consistent morphology, occurring as rod-like precipitates, irregular particles, and sometimes as triangular-shaped plates (See Figure 98a). In isolated locations, clusters of rod-like M_3C precipitates have been observed, presumably having precipitated during the decomposition of an island of retained austenite. The other alloy carbide found in the as-welded microstructures, M_2C, is a molybdenum-rich carbide (37) which occurs as a fine dispersion of acicular precipitates within the bainitic/ferritic matrix.

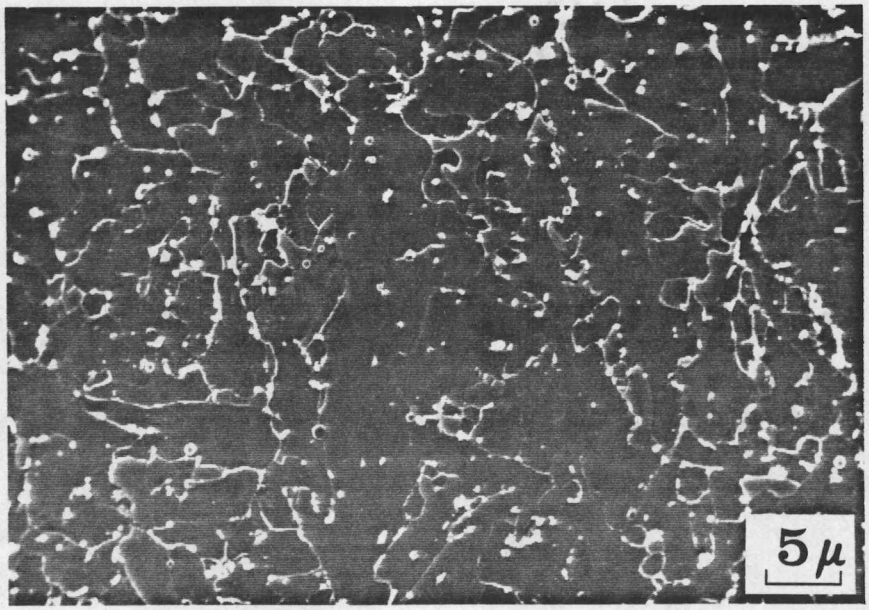
The occurrence of only M_3C and M_2C in the as-welded microstructures appears consistent with the Baker and Nutting (17) carbide evolutionary sequence for 2-1/4Cr-1Mo steel. Thermal cycling of the weld metal by subsequent weld passes reheats the microstructure, transforming any epsilon carbide to M_3C and initiating the precipitation of some M_2C. However, time at temperature is insufficient to form M_7C_3, $M_{23}C_6$, or M_6C carbides which appear later in the evolutionary sequence.

Post-Weld Heat Treated Weld Metal Microstructure

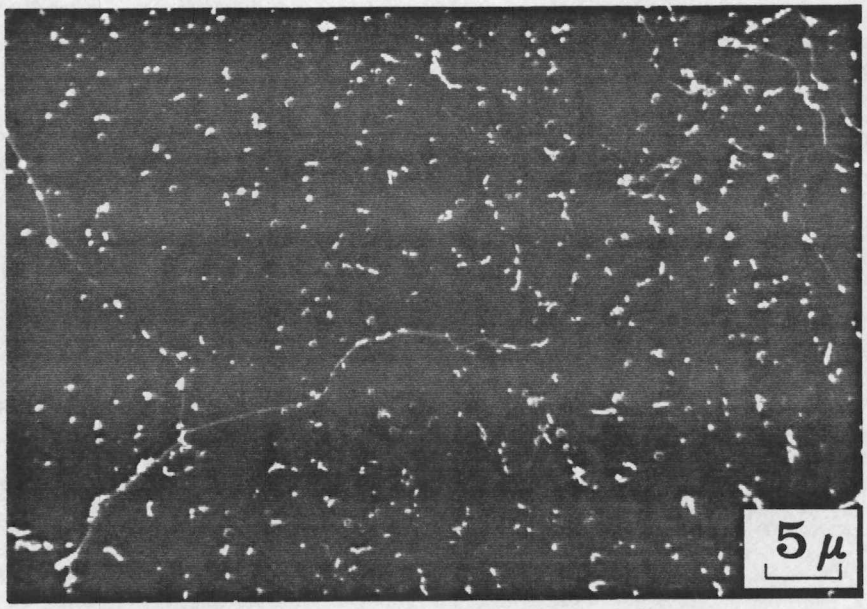
For discussion purposes, the four carbon content weld metals PWHT 1300°F/25 hrs. (Class 2) may be divided into two categories. In the first is the 0.02-0.03 carbon weld metal whose microstructure has been so altered by PWHT that no trace remains of the bainitic structure in existence prior to heat treatment. The second category contains the 0.04-0.05, 0.08-0.09, and 0.12-0.13 carbon weld metals. Their microstructures have only been modified by PWHT and may be characterized as tempered bainite.

SEM examination of the PWHT 0.02-0.03 carbon weld metal reveals a microstructure which consists of equiaxed ferrite grains with alloy carbides present within the grains as well as at the grain boundaries. No traces remain of the retained austenite stringers evident in the as-welded material, those stringers having transformed during tempering to carbides and ferrite.

Inspection of the weld metal located near the interpass boundaries (see Figure 99a) reveals a microstructure consisting of an irregular distribution of small equiaxed ferrite grains in a coarser ferrite matrix. Carbides occur predominantly at the grain boundaries of the smaller grains with only a few visible within the coarser ferrite matrix. The structure is reminiscent of that seen in a cold worked material heated long enough to cause recrystallization but for an insufficient period to allow significant grain growth. The prevalence of carbides at the grain boundaries may indicate that grain growth has been inhibited by the precipitates.



(a) Structure near interpass boundary.



(b) Structure away from interpass boundary.

Figure 99. Variation in microstructure of 0.02-0.03 carbon 2-1/4Cr-1Mo weld metal PWHT 1300°F/25 hrs. (Class 2) as a function of location, 2000X, SEM.

In contrast, the material at some distance from the interpass boundaries, shown in Figure 99b, has carbides both within the grains as well as at the grain boundaries. Furthermore, the ferrite grains are much larger than those in the fine-grained weld metal. There is some evidence of grain growth in the microstructure. Figure 100 shows a grain boundary in the coarse-grained region whose curvature may be indicative of grain boundary migration.

The recrystallization of bainitic 2-1/4Cr-1Mo steel during tempering has been observed by Baker and Nutting (17) as well as Woodhead and Quarrel (37). Recrystallization has been associated with a decrease in the number of carbides present within the matrix. Furthermore, Baker and Nutting (17) have noted that $M_{23}C_6$ carbides often appear at the boundaries of the recrystallized ferrite grains.

Unlike that seen in the PWHT 0.02-0.03 carbon material, the microstructures of the 0.04-0.05, 0.08-0.09, and 0.12-0.13 carbon weld metals PWHT 1300^{o}F/25 hrs. still retain some of the features characteristic of upper bainite. This is particularly evident in those regions possessing a lath-like structure prior to post-weld heat treatment. In those locations, the directionality of the lath structure has been preserved although the morphology of the ferrite has been altered somewhat. The ferrite exists as elongated islands aligned parallel to one another with carbides at the island boundaries as well as within the ferrite matrix. These islands are significantly wider than the laths from which they formed, giving the effect of a coarsened microstructure. Such a structure is illustrated in Figure 101.

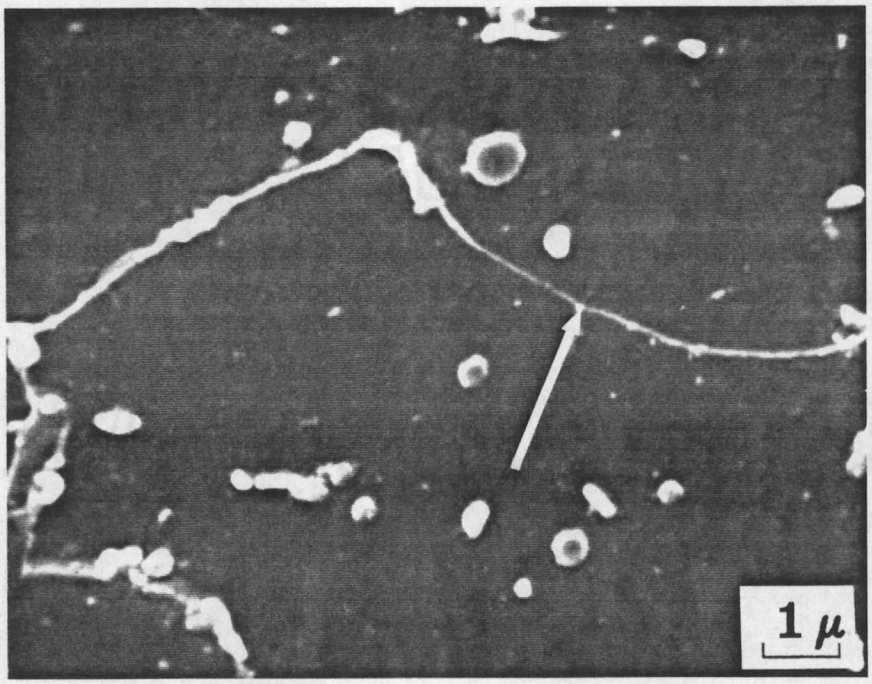
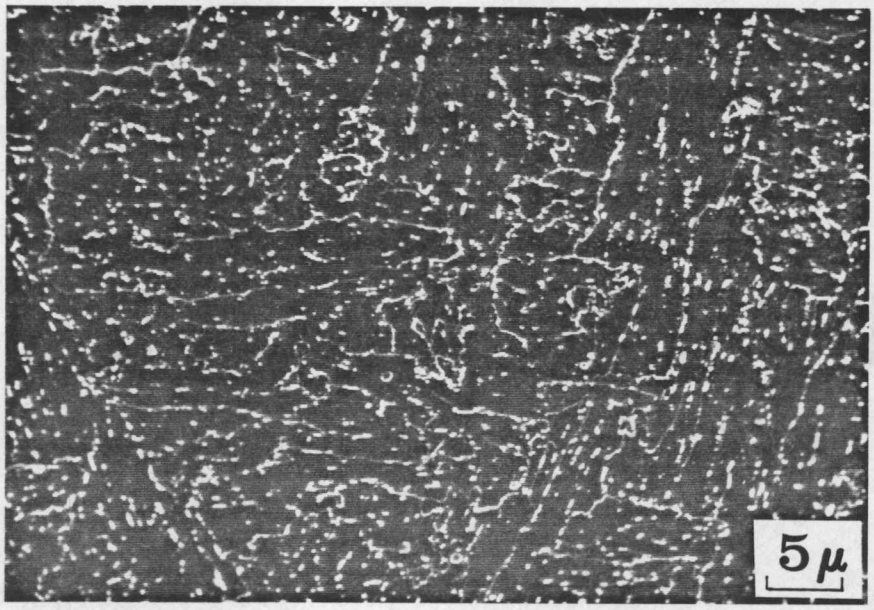
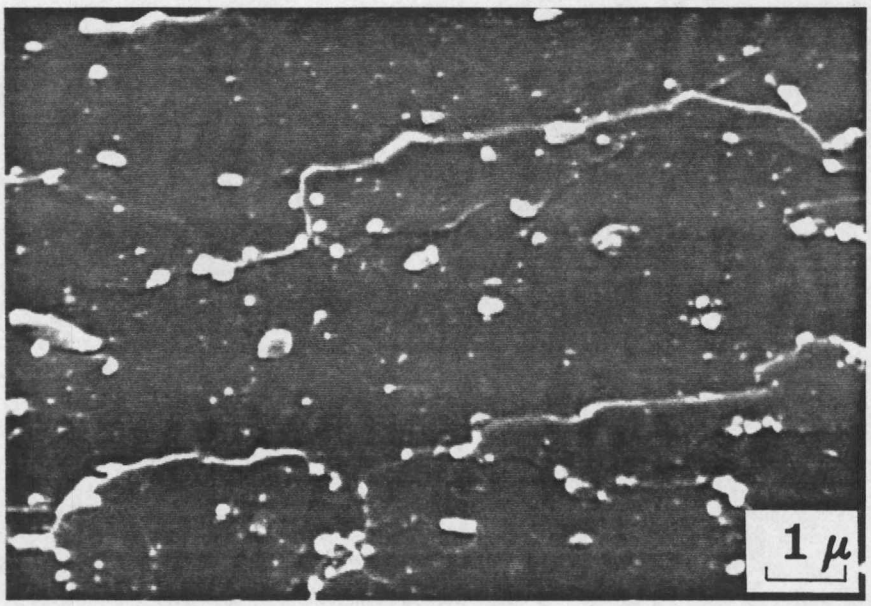


Figure 100. Region of 0.02-0.03 carbon 2-1/4Cr-1Mo weld metal PWHT 1300°F/25 hrs. (Class 2) showing grain boundary curvature indicative of grain boundary migration, 10000X, SEM.



(a) 2000X, SEM



(b) 10000X, SEM

Figure 101. Tempered bainite structure of 0.08-0.09 carbon 2-1/4Cr-1Mo weld metal PWHT 1300°F/25 hrs (Class 2).

The coarsening of lath-like constituents during tempering has been addressed by Krauss (47). He has indicated that the coarsening mechanism is based on the elimination of the low angle boundaries between laths having a similar orientation. According to Pickering (95), the orientation difference between neighboring bainite laths is often quite small, perhaps as low as 6 degrees. The elimination of low angle boundaries effectively merges neighboring laths to produce wider elongated structures similar to those observed in the PWHT weld metal microstructures.

Other than the gross microstructural differences between the PWHT 0.02-0.03 carbon weld metal and the other three higher carbon PWHT materials (0.04-0.05, 0.08-0.09, 0.12-0.13) discussed above, no dependence of microstructure on changes in carbon content have been detected in the SEM micrographs. The microstructures of the latter look very similar. The carbides visible during SEM examination all appear to be somewhat spheroidized, having no consistent shape. This may be attributed to the extensive thermal treatment required to attain Class 2 properties (1300^{o}F/25 hrs., temper parameter P=37.7).

A more detailed analysis of the carbides present in these weld metal microstructures as a function of carbon content has been obtained by STEM examination of carbide extraction replicas. The types of carbides found in the PWHT microstructure are given in Table 28 (p. 233). Inspection of the table shows that M_7C_3, $M_{23}C_6$, and M_6C occur in all four of the weld metals with an additional carbide, M_2C, present in the 0.02-0.03 carbon material. Again, this is in agreement with the carbide sequence of Baker and Nutting (17).

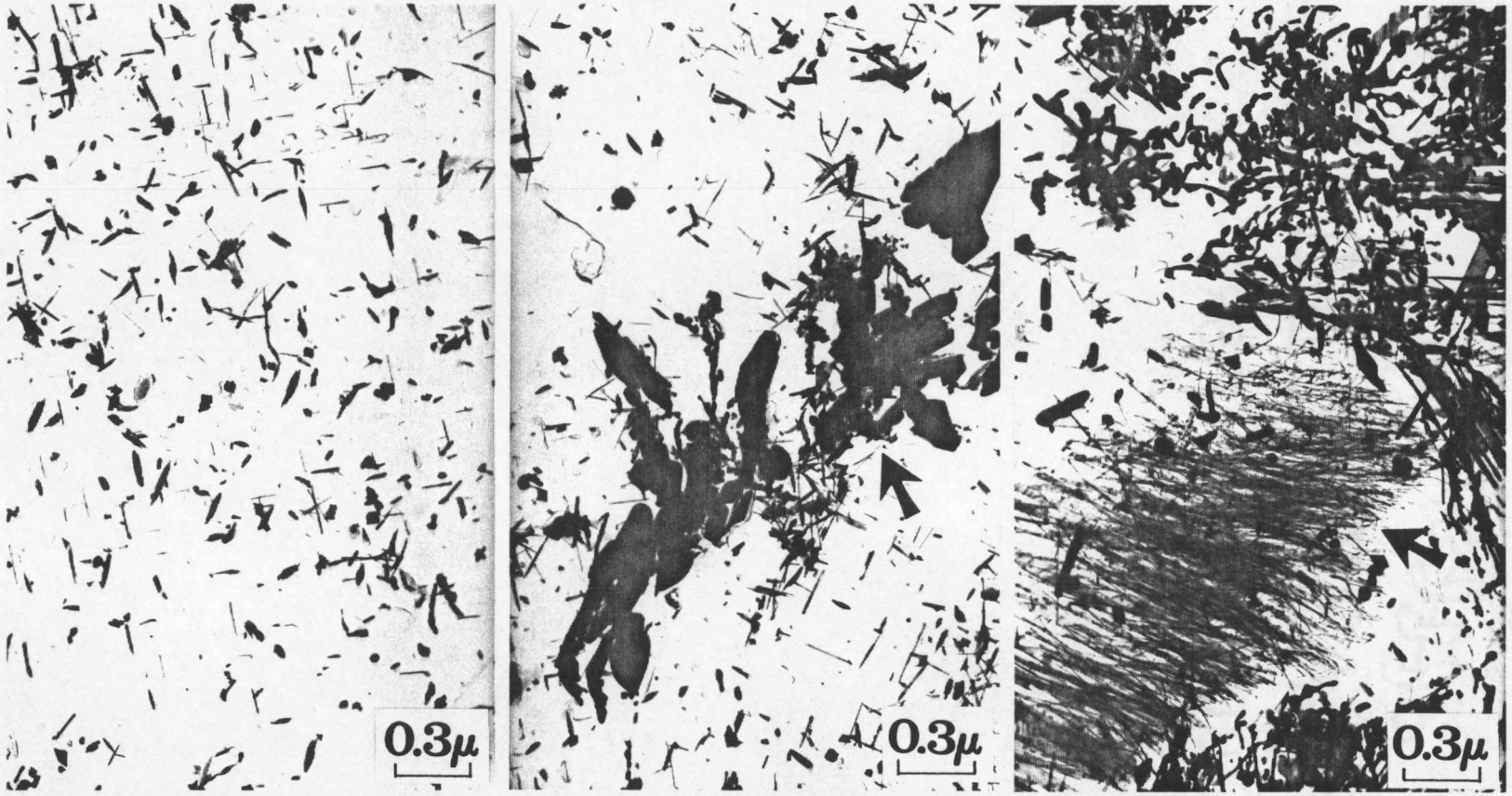
In the three higher carbon content weld metals, tempering has eliminated all traces of M_3C and M_2C and has resulted in the formation of the more stable precipitates, $M_{23}C_6$, M_7C_3, and M_6C. The persistence of M_2C in the 0.02-0.03 carbon microstructure may be a result of the presence of polygonal ferrite in the as-welded microstructure. As indicated by Baker and Nutting (17), the M_2C that forms in ferrite during tempering appears early in the tempering process and persists until ultimately being replaced by M_6C. This is in contrast to the occurrence of carbides in bainite where the M_2C is soon replaced by M_7C_3 and $M_{23}C_6$.

In two instances, the table contains references to carbides which are "bound together". For the 0.02-0.03 carbon weld metal, M_6C and M_2C have been found together whereas in the 0.12-0.13 carbon weld metal, $M_{23}C_6$ and M_6C occur together. Baker and Nutting (17) have indicated that M_6C is believed to nucleate at existing carbide particles. It is therefore possible that what is observed as two carbides bound together is actually M_6C nucleating at the interface of a precursor precipitate. In the case of the 0.02-0.03 carbon material, M_6C is known to follow M_2C in the carbide sequence for polygonal ferrite. Furthermore, in bainite, M_6C forms from M_7C_3 and $M_{23}C_6$.

STEM analysis has also provided an enhanced understanding of the carbide morphologies found in the PWHT weld metals. Considering the gross microstructural difference between the 0.02-0.03 carbon weld metal and the three higher carbon materials, the carbide morphologies observed in the lowest carbon weld metal are quite different from

those seen in the other three. Three distinct precipitate morphologies may be found in the 0.02-0.03 carbon material; acicular needles, massive precipitates, and fringes. These may be seen in Figure 102. The acicular needles are believed to be M_2C carbides which have precipitated within the polygonal ferrite. M_2C would not be expected to persist in bainite based on the Baker and Nutting (17) sequence. The massive precipitates are M_7C_3, $M_{23}C_6$, or M_6C, depending on their location. M_7C_3 and $M_{23}C_6$ do not form within polygonal ferrite, appearing only in the bainite. However, M_6C can appear in either constituent. The fringes are M_2C. Many researchers (17,37) have reported the occurrence of such structures within ferritic/bainitic 2-1/4Cr-1Mo steels.

The mode of formation of fringed M_2C at ferrite/austenite interfaces during cooling has been discussed by Baker and Nutting (17). Because of the relative solubilities of ferrite and austenite for carbon and molybdenum, on cooling from the A_{r3}, the newly formed polygonal ferrite is enriched in molybdenum while the remaining, yet-to-be transformed, austenite becomes enriched in carbon. At the ferrite/austenite interface, the concentration of molybdenum and carbon is relatively high, making the nucleation of M_2C possible. Once precipitated, the M_2C carbides can grow, obtaining molybdenum and carbon from the surrounding matrix. The growth direction most favored is that in which the greatest supply of carbon and molybdenum can be maintained at the carbide/matrix interface. Because of the higher diffusivity of the carbon atoms relative to the molybdenum atoms, it is easier for the carbides to



(a) Needles (b) Massive precipitates (c) Fringes

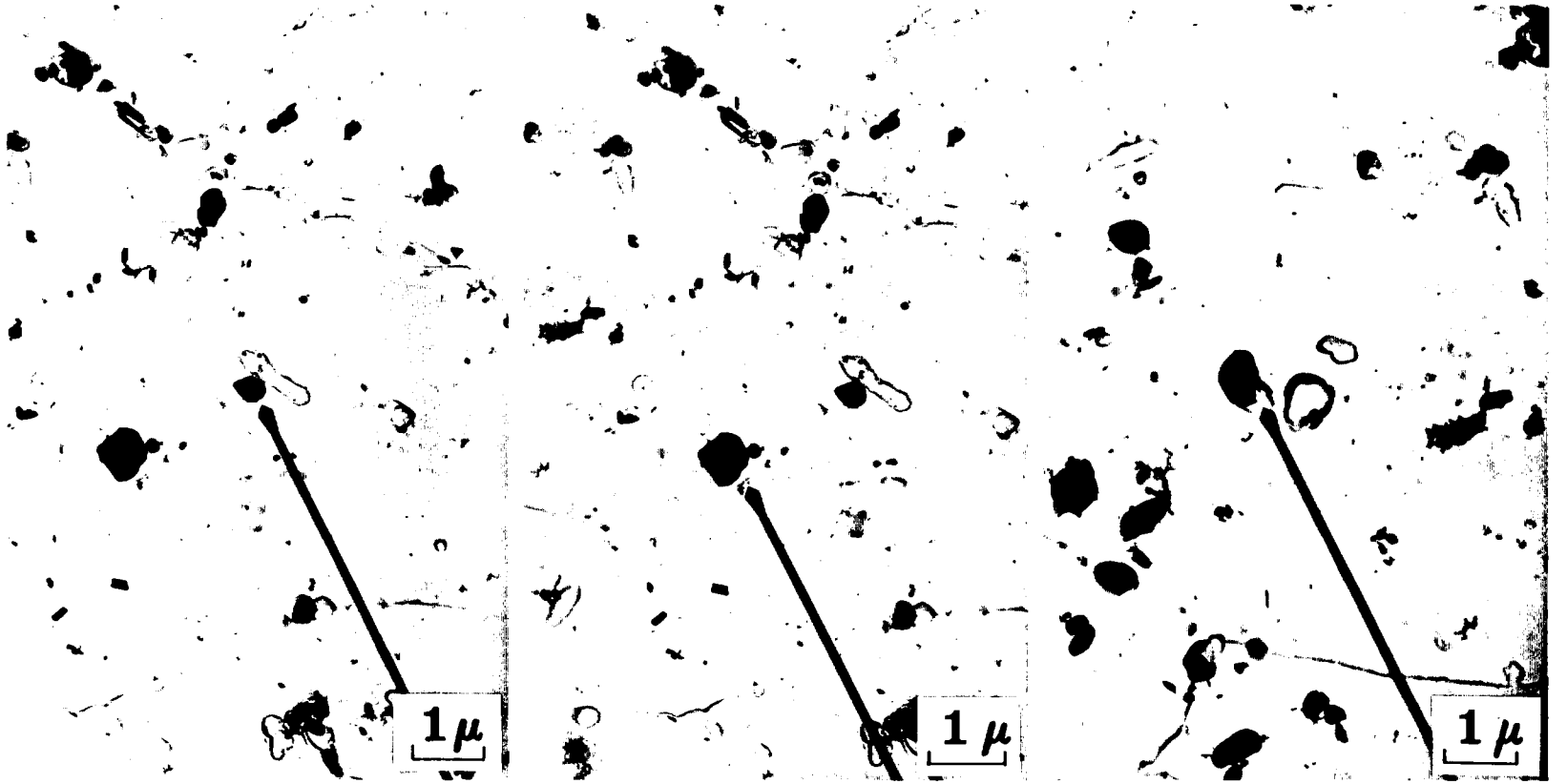
Figure 102. Carbide morphologies in 0.02-0.03 carbon 2-1/4Cr-1Mo weld metal PWHT 1300°F/25 hrs. as shown by carbide extraction replica, 37000X, STEM.

grow into the molybdenum-rich phase, minimizing the distance which the slowly diffusing molybdenum atoms must travel to reach the carbide/matrix interface. Thus the carbides grow into the ferrite.

The formation of M_2C fringes can be inhibited if the cooling rate is sufficiently high (17). However, if some austenite is retained in the microstructure on cooling, as in the case of the as-welded 0.02-0.03 carbon weld metal, then, during tempering, fringes of M_2C may nucleate and grow at the retained austenite/ferrite interface, drawing carbon from the enriched austenite.

The carbide distribution and morphologies apparent in the extraction replicas for the 0.04-0.05, 0.08-0.09, and 0.12-0.13 carbon weld metals are essentially the same. As indicated in Table 28 (p. 233), the carbides present include M_7C_3, $M_{23}C_6$, and M_6C with the M_7C_3 and M_6C precipitates occurring predominantly in the matrix and the $M_{23}C_6$ at grain/lath boundaries. Independent of location, the majority of the carbides are spheroidal although a few rod-like precipitates may be seen within the matrix. Woodhead and Quarrel (37) have warned of the pitfalls of identifying carbides by their morphology and distribution and have given many examples where such a practice leads to erroneous conclusions. The uselessness of this approach is well illustrated by Figure 103 which shows the similar morphologies exhibited by M_7C_3, $M_{23}C_6$, and M_6C precipitates in 0.04-0.05 carbon weld metal.

Carbide morphologies and distributions characteristic of the 0.04-0.05, 0.08-0.09, and 0.12-0.13 carbon weld metals PWHT



(a) M_7C_3 (b) $M_{23}C_6$ (c) M_6C

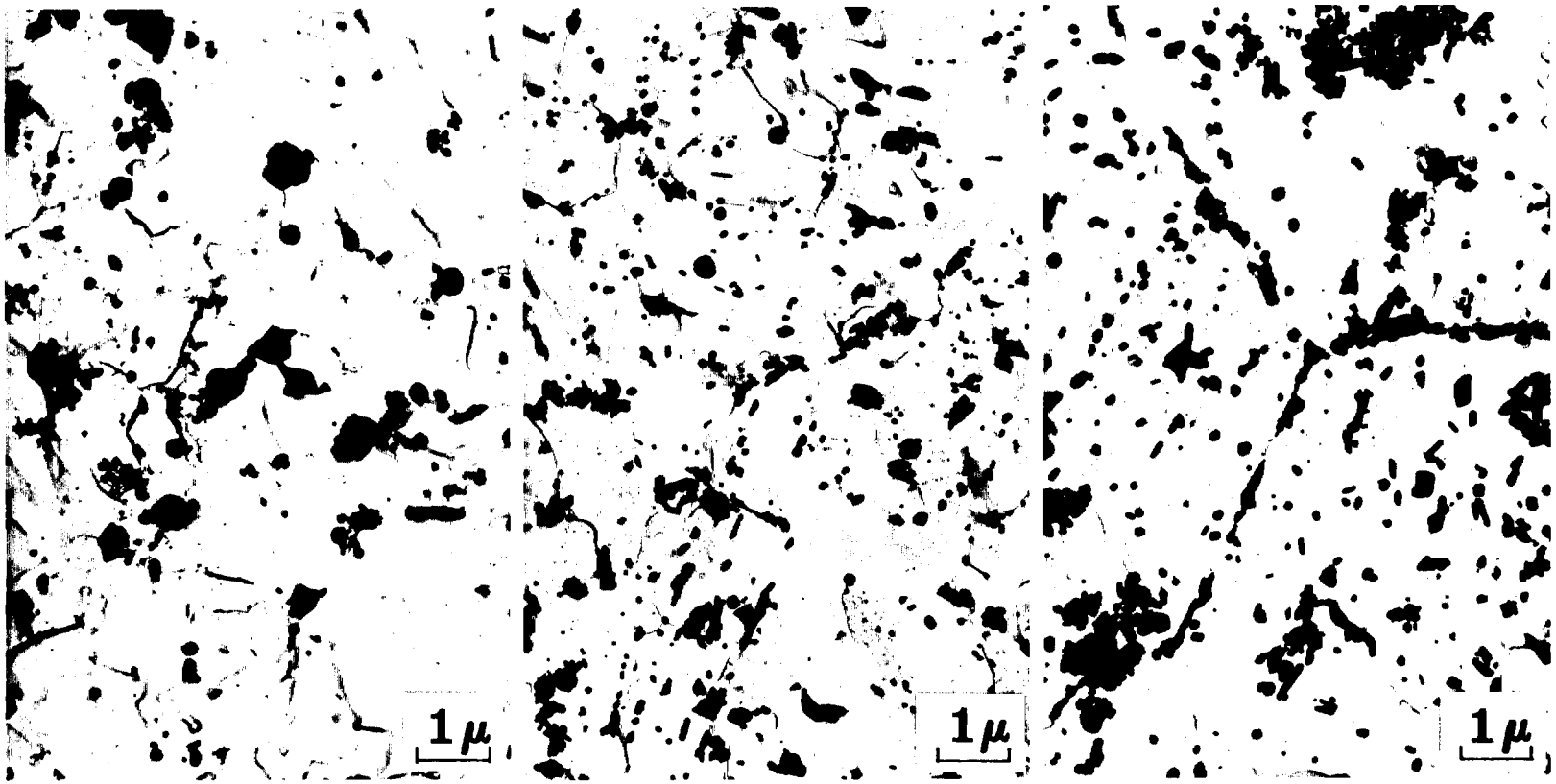
Figure 103. Similar morphologies of M_7C_3, $M_{23}C_6$, and M_6C carbides in 0.04-0.05 carbon 2-1/4Cr-1Mo weld metal PWHT 1300°F/25 hrs. (Class 2) as shown by carbide extraction replica. Pointers indicate the precipitate identified, 10000X, STEM.

1300°F/25 hrs. are shown in Figure 104. Comparison of the micrographs in the figure indicates that the number of carbides in a given area generally increases with carbon content.

The general microstructure of 0.08-0.09 carbon weld metal PWHT 1175°F/25.5 hrs. (Class 3), as revealed by SEM examination, retains many of the features characteristic of the as-welded microstructure. No coarsening of the ferrite constituents is apparent. The substructure within the prior austenite grains, whether lath-like or granular, remains quite evident, perhaps even more so as a result of carbide precipitation at prior austenite grain boundaries and substructure boundaries. A fine dispersion of carbides, barely resolvable at 10,000X, has also precipitated within the ferrite matrix (see Figure 105).

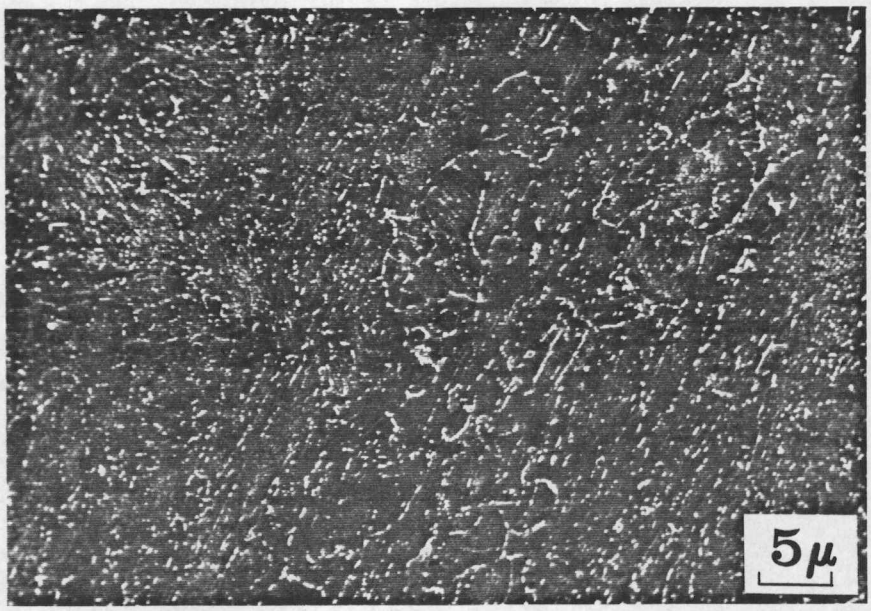
Upon examination of Class 3 weld metal carbide extraction replicas (see Figure 106), a fine distribution of acicular precipitates within the ferrite matrix is evident. These carbides, identified as M_2C, are generally recognized as the primary creep strengthening agent in 2-1/4Cr-1Mo steel (17,37,45,48,50). Also visible in the replicas are much larger carbides at the lath and prior austenite grain boundaries which are predominantly $M_{23}C_6$. Some larger precipitates can also be found in the matrix, although not in significant quantities. The analysis has shown them to be mostly M_7C_3 and M_6C.

The occurrence of M_2C in the Class 3 weld metal microstructure is in agreement with the carbide evolutionary sequence (17). Using the temper parameter as a guide ($P_{cl.2}$=37.7, $P_{cl.3}$=35.0), it is

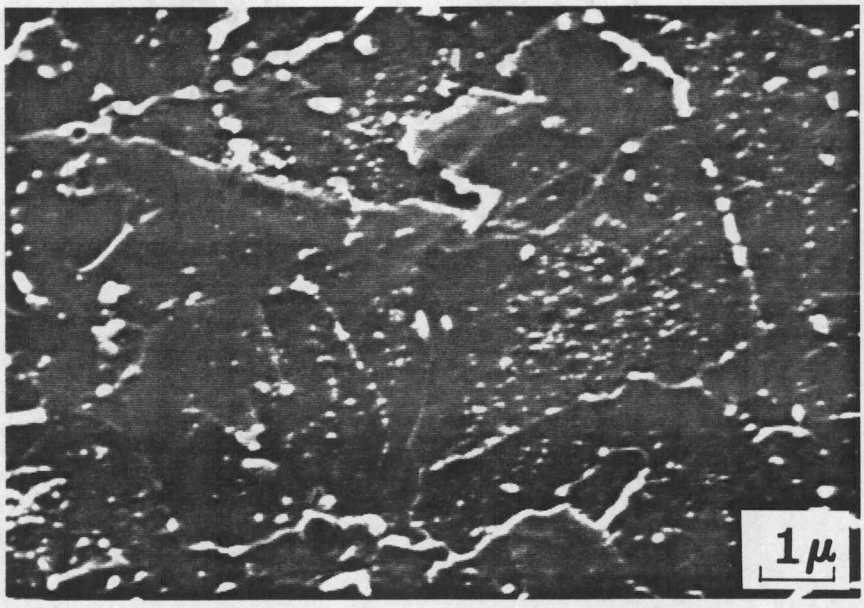


(a) 0.04-0.05 carbon (b) 0.08-0.09 carbon (c) 0.12-0.13 carbon

Figure 104. Carbide morphology and distribution in 0.04-0.05, 0.08-0.09, and 0.12-0.13 carbon 2-1/4Cr-1Mo weld metal PWHT 1300°F/25 hrs. (Class 2) as shown by carbide extraction replica, 9000X, SEM.



(a) 2000X, SEM



(b) 10000X, SEM

Figure 105. Microstructure of 0.08-0.09 carbon 2-1/4Cr-1Mo weld metal PWHT 1175°F/25.5 hrs. (Class 3).

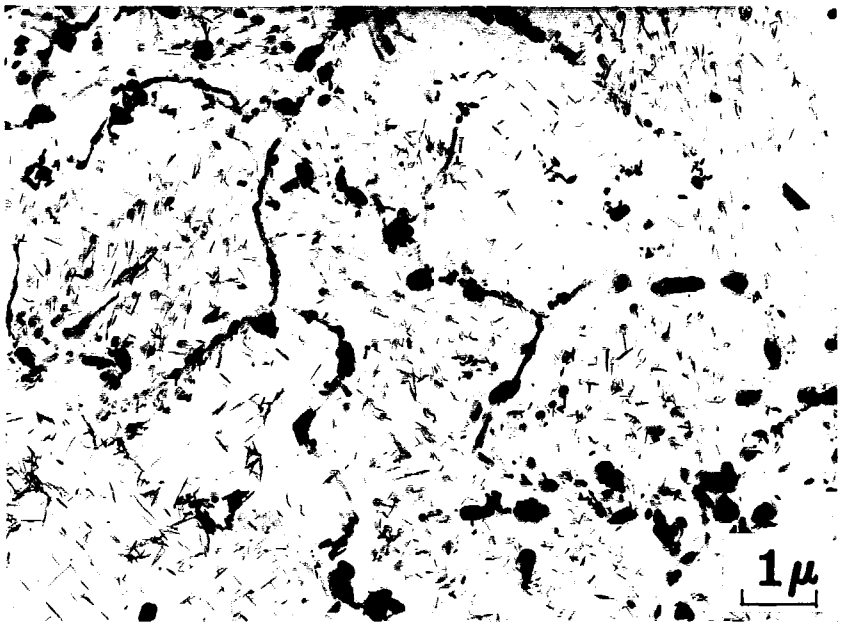


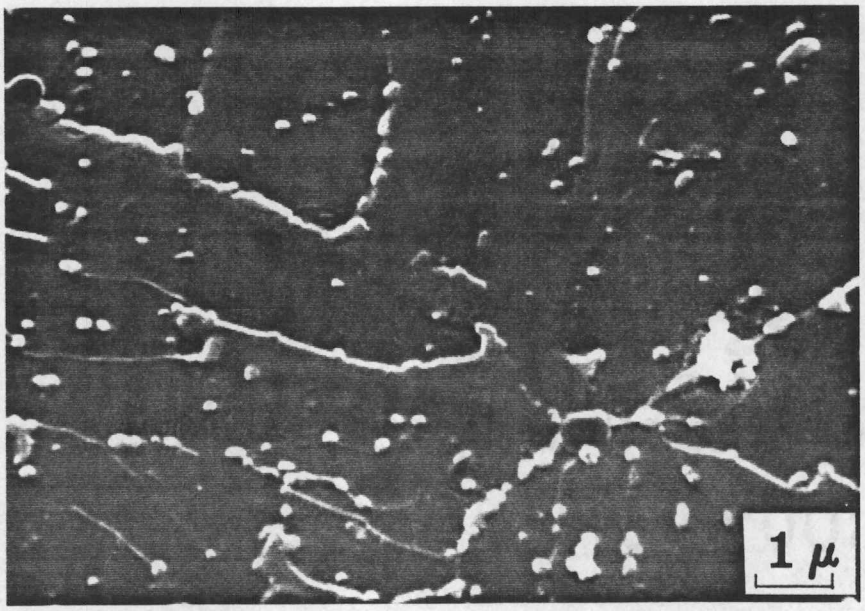
Figure 106. Carbide morphology and distribution in 0.08-0.09 carbon 2-1/4Cr-1Mo weld metal PWHT 1175°F/25.5 hrs. (Class 3) as shown by carbide extraction replica, 10000X, SEM.

expected that the evolution of carbides toward the equilibrium precipitate (M_6C) during the Class 3 PWHT occurs to a lesser degree than during the Class 2 treatment. As previously indicated, the Class 2 microstructure contains only M_7C_3, $M_{23}C_6$, and M_6C, the last three carbides in the evolutionary chain. In the Class 2 material, the M_2C forms and then dissolves prior to the completion of PWHT. In contrast, the time and temperature of the Class 3 PWHT is sufficient to precipitate M_2C but insufficient to dissolve it. M_7C_3, $M_{23}C_6$, and M_6C are also present. The M_7C_3 and $M_{23}C_6$ carbides are associated with the disappearance of M_3C in the microstructure while M_6C is the last precipitate to appear, growing at the expense of all other carbides.

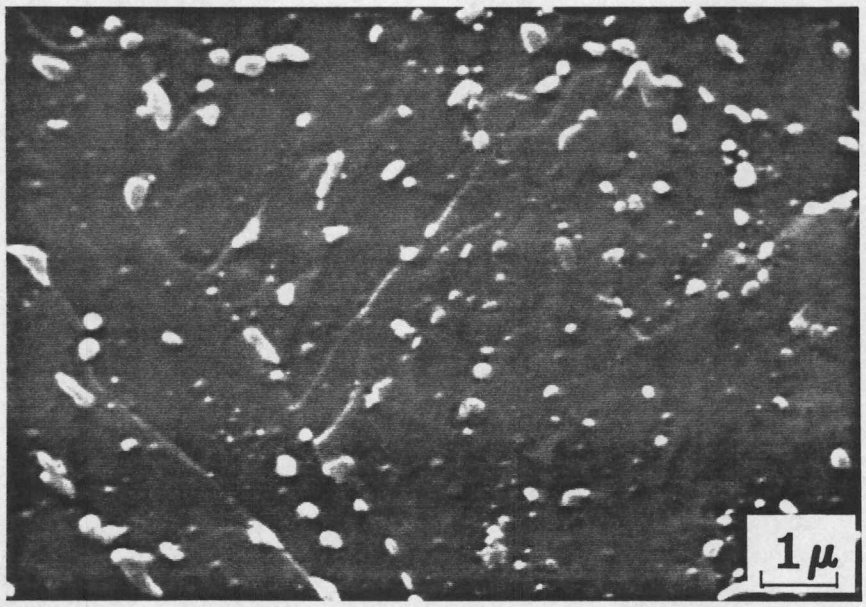
Stress-Rupture Specimen Microstructure

SEM examination of Class 2 weld metal removed from tested stress-rupture specimens indicates that, even after 5000 hours at 1050°F, the microstructure is essentially the same as that observed in the PWHT material (see Figure 107). This appears to be true for all Class 2 rupture tested weld metal independent of carbon content.

This observation may be explained with the aid of Table 29. Based on a temper parameter approach, the table lists the times at 1300°F which correspond to 5000 hours at 850, 950, and 1050°F. Similarly, times at 1175°F which are equivalent to 3000 hours at 950 and 1050°F are also shown. Inspection of the table indicates that at 850 and 950°F, the equivalent 1300°F exposure is much less than one hour. Thus, the probability of significant microstructural change in



(a) PWHT 1300°F/25 hrs. (Class 2).



(b) PWHT + rupture tested 1050°F/5200 hrs.

Figure 107. Comparison of 0.12-0.13 carbon 2-1/4Cr-1Mo weld metal PWHT 1300°F/25 hrs. (Class 2) before and after rupture testing, 10000X, SEM.

Table 29. Time/temperature equivalence between rupture test condition and PWHT.

Rupture Test Condition		Equivalent PWHT Condition	
Temperature (°F)	Time (Hrs.)	Temperature (°F)	Time
850	5000	1300	16 Secs.
950	5000	1300	6 Mins.
1050	5000	1300	2 Hrs.
950	3000	1175	2 Hrs.
1050	3000	1175	48 Hrs.

addition to that resulting from PWHT at 1300°F for 25 hours is small. By comparison, 5000 hours at 1050°F is equivalent to about 2 hours at 1300°F. This is less than 10 percent of the total PWHT time. Considering the extent of PWHT given the weld metal prior to rupture testing, it is evident that any microsturctural changes resulting from the time at temperature during the rupture test would be slight.

In 0.08-0.09 carbon weld metal PWHT 1175°F/25.5 hrs. (Class 3) and stress rupture tested at 950 and 1050°F for times up to about 3000 hours, no gross morphological changes in the bainitic ferrite constituent have been noted which may be attributed to the elevated temperature exposure during the rupture tests. Furthermore, examination of SEM micrographs has revealed no evidence of coarsening of the lath or granular bainite structure.

Microstructural changes detected with the use of the SEM have been limited to the carbides visible in the weld metal. Even after 3000 hours at 950°F, the fine precipitates previously observed within the matrix of the PWHT material (identified as M_2C during STEM analysis of extraction replicas) persist. However, as shown in Figure 108, weld metal rupture tested for 3000 hours at 1050°F exhibits very little evidence of M_2C carbides, perhaps indicating a general dissolution of the acicular precipitate during the test. Those which can be seen appear to occur only in the regions of bainitic ferrite well separated from the grain/lath boundary carbides. The boundary precipitates have been identified as $M_{23}C_6$. Baker and Nutting (17) have noted that the nucleation and growth of $M_{23}C_6$ is accompanied by the dissolution of adjacent M_2C precipitates

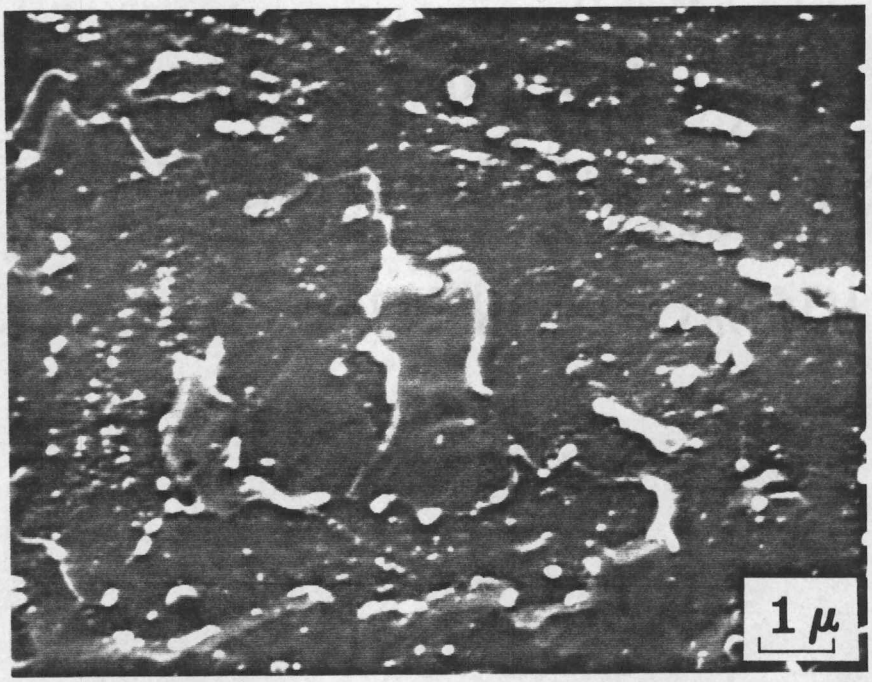


Figure 108. Microstructure of 0.08-0.09 carbon 2-1/4Cr-1Mo weld metal PWHT 1175°F/25.5 hrs (Class 3) after rupture testing at 1050°F for 3100 hours, 10000X, SEM.

and probably indicates the incorporation of the liberated molybdenum atoms into the $M_{23}C_6$ structure.

Other than the fine M_2C precipitates visible within the bainitic ferrite matrix, the only other carbides readily discernible in the SEM micrographs are the boundary carbides. These are present in the PWHT weld metal as well as in material rupture tested at 950 and 1050°F. No gross changes in the size or amount of boundary carbides have been detected between the as-PWHT weld metal and that which has been rupture tested.

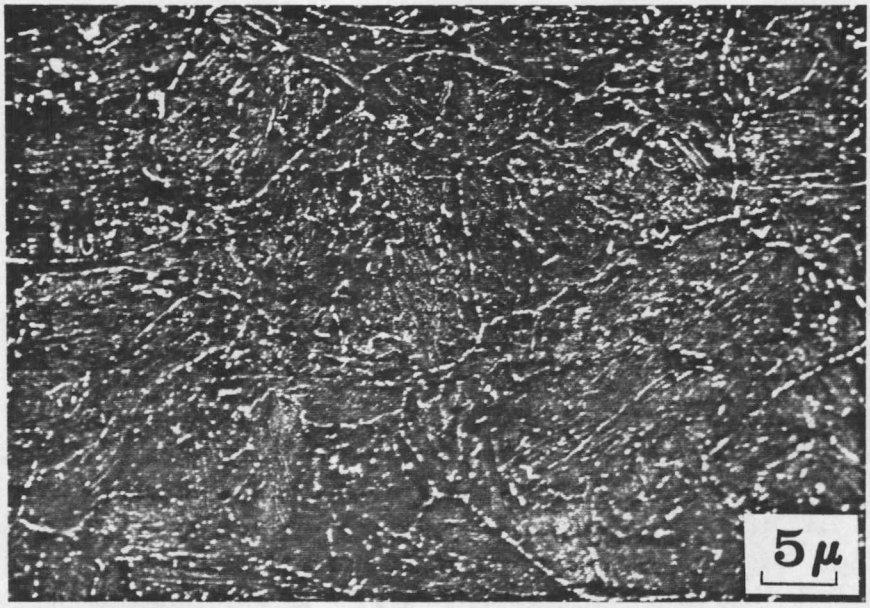
Table 29 (p. 252) shows that 3000 hours at 950°F is equivalent to 2 hours at 1175°F while the same exposure at 1050°F corresponds to 48 hours at 1175°F. In the case of the 950°F rupture tested material, 2 hours at 1175°F is short compared to the PWHT time (25.5 hours) at the same temperature, indicating that any microstructural changes resulting from the 950°F rupture test are likely to be small compared to those induced by PWHT. However, the equivalent time at 1175°F corresponding to the 1050°F rupture test (48 hours) is almost twice the PWHT time at the same temperature. Therefore, significant modification of the microstructure is anticipated. These predictions, based on the temper parameter, agree with experimental observations. The 950°F rupture tested weld metal microstructure is basically the same as that of the as-PWHT material while the 1050°F rupture tested material exhibits substantial dissolution of M_2C.

The observations of carbide changes during rupture tests of Class 3 weld metal have raised questions about the microstructural stability of this class of material during service. Because the

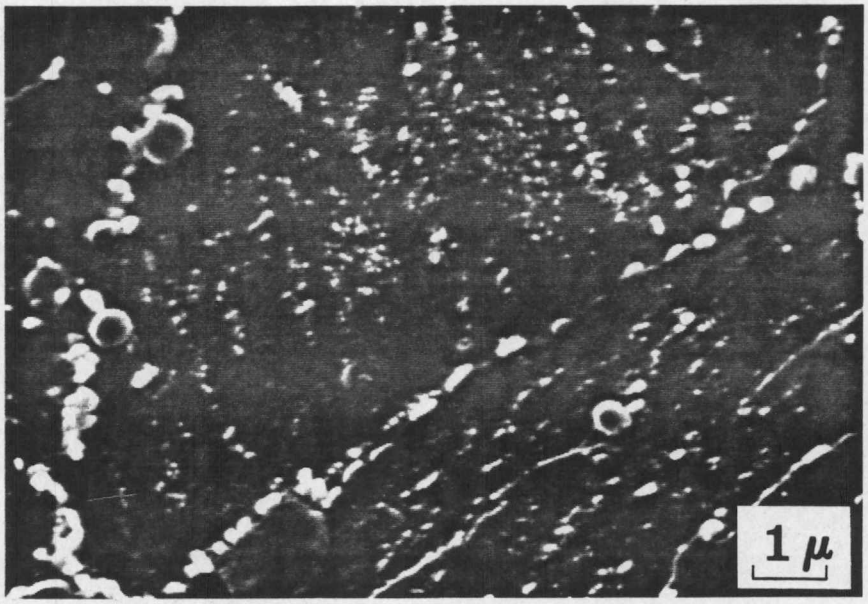
service life of welded 2-1/4Cr-1Mo pressure vessels is significantly longer (a minimum of 100,000 hours) than the longest rupture test interval used in this study, even greater changes may occur in the carbides during service than those observed here, detrimentally affecting the rupture strength. To address this problem, weld metal PWHT 1175°F/25 hrs. (Class 3) has been given an additional "aging" treatment to simulate 100,000 hours at 950°F. Such a treatment is equivalent to 36 hours at 1175°F.

The microstructure of the aged weld metal is shown in Figure 109. There is still a significant amount of M_2C present in the matrix, not as much as in the material rupture tested at 950°F for 3000 hours but certainly more than in the same weld metal rupture tested at 1050°F for an identical period. In some places, the boundary carbides appear to be larger and more prevalent than in the rupture tested specimens. The matrix adjacent to these boundary precipitates is devoid of any M_2C.

As indicated, the carbide condition in the aged weld metal falls somewhere between that observed in the 950°F rupture tested material and that seen in the 1050°F rupture tested weld metal. Using the temper parameter, the time at 1175°F which corresponds to the various post-PWHT treatments of each of these materials can be calculated. The values for the rupture tested samples are 2 hours and 48 hours for the 950 and 1050°F rupture tested materials respectively. In comparison, the aging treatment is equivalent to 36 hours at 1175°F. Ranking these values in the order of increasing time, one finds that the order is the same as that obtained by ranking the specimens in



(a) 2000X, SEM



(b) 10000X, SEM

Figure 109. Microstructure of 0.08-0.09 carbon 2-1/4Cr-1Mo weld metal PWHT 1175°F/25.5 hrs. after aging 1193°F/21.5 hrs. to simulate 100,000 hours at 950°F.

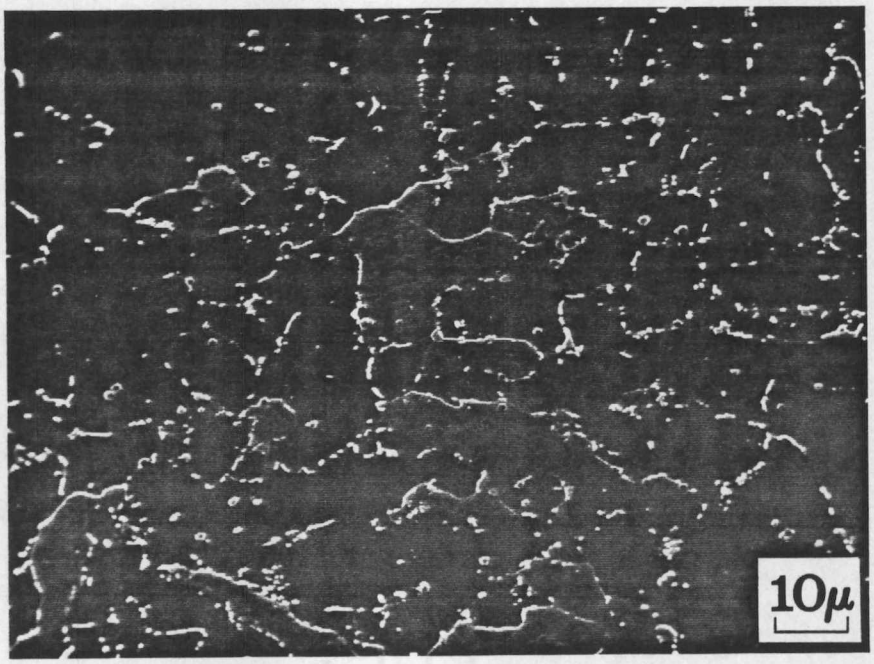
the order of decreasing presence of M_2C. Thus, the observed trends are in agreement with the predictions based on the temper parameter.

Microstructure of Pipe Weld Metal Having Seen Extensive Service

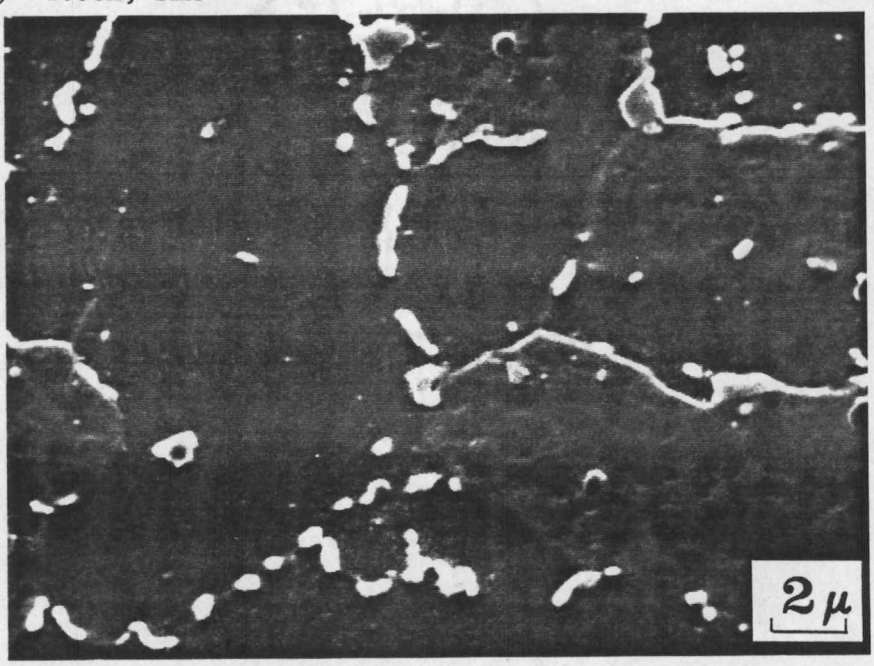
Microstructural evaluation of 2-1/4Cr-1Mo pipe weld metal subjected to 15 years of service at 1050°F was performed using the SEM. As seen in Figure 110, the microstructure consists of a ferrite matrix with islands of a second microconstituent scattered throughout. Other than having a rough surface texture, the islands exhibit no internal structure. Their shape and size vary considerably from place to place within the microstructure.

Spheroidized carbides are also apparent within the microstructure. These precipitates are located within the ferrite matrix and at the boundaries of the island constituent. Closer inspection indicates that the carbides are not randomly scattered throughout the ferrite matrix but define a network within the ferrite. These precipitates are probably located on the boundaries of individual ferrite grains. Using the carbides to mark the position of the ferrite grain boundaries, it is apparent that, in most of the microstructure, the ferrite grains are generally equiaxed.

In light of the extensive tempering experienced by this weld metal (equivalent to 35.5 hours at 1300°F), the equiaxed grain structure of the ferrite is likely a result of recrystallization made possible by a combination of elevated temperature and carbide growth and dissolution. Furthermore, the occurrence of carbides at the boundaries of newly recrystallized grains is typical of the process.



(a) 1000X, SEM



(b) 5000X, SEM

Figure 110. Microstructure of 2-1/4Cr-1Mo pipe weld metal subjected to 1050°F for 15 years.

The island-like microconstituent scattered within the ferrite matrix is considered to be a significantly overtempered form of the granular structures found in granular bainite. These structures consist of martensite and/or retained austenite in the as-welded microstructure. Sufficient tempering not only causes transformation of these constituents to ferrite and carbides but can, through carbide evolution, induce dissolution of the carbides within the structures in favor of nucleation and growth of M_6C at the boundaries.

Correlation of the Results of the Microsturctural Analysis with Observed Stress Rupture Behavior

The findings of the microstructural analysis has cast some light on the reasons behind the observed stress rupture behavior of the 2-1/4Cr-1Mo weld metal tested during this program.

The superior rupture strength of the 0.08-0.09 carbon weld metal PWHT 1175^{o}F/25.5 hrs. (Class 3) is primarily a result of the strengthening effect of the acicular M_2C carbides present in the matrix. A secondary factor may be the fineness of the bainitic structure. In contrast to that observed in the 0.08-0.09 carbon weld metal PWHT 1300^{o}F/25 hrs. (Class 2), the Class 3 microstructure retains most of the features characteristic of the as-welded (as-transformed) material, with little or no evidence of any coarsening of the ferritic constituents. The fine bainitic substructure also contributes to the overall strength due to the

increased presence of numerous boundaries between the bainitic ferrite structures which serve as barriers to dislocation movement.

The observed dependence of 2-1/4Cr-1Mo Class 2 weld metal rupture strength on carbon content is apparently a result of the major microconstituents present in the microstructure. SEM examination of the weld metals indicates that the lowest carbon content material (0.02-0.03 percent carbon) consists of non-bainitic ferrite while the higher carbon weld metals possess a tempered bainite structure. This correlates with the results of rupture tests which indicate that the 0.02-0.03 carbon weld metal rupture strength is significantly lower than the strengths of the other three higher carbon materials. The 0.02-0.03 carbon weld metal which appears bainitic in the as-welded condition may recrystallize during PWHT to form the non-bainitic ferrite structure, lowering the rupture strength. In contrast, the higher carbon weld metals remain bainitic during PWHT. Some coarsening of the bainitic structure does occur accompanied by the growth and evolution of the alloy carbides. STEM analysis shows that the carbides present in these materials consist of the last three precipitates in the evolutionary chain ($M_{23}C_6$, M_7C_3, M_6C) existing in a spheroidized condition. These precipitates probably do not confer as much rupture strength to the weld metal as do the finer carbides existing in the Class 3 weld metal, making the overall strength a strong function of the bainitic morphology of the microstructure.

Because of the extensive PWHT given the Class 2 weld metal ($1300^{o}F$/25 hrs.), the microstructural stability of the Class 2

material is high for service use. The carbides present in the matrix, as has already been indicated, are the last three in the evolutionary sequence. Any microstructural change caused by extended service at elevated temperature would likely consist of further spheroidization of the carbides with the amount of M_6C increasing at the expense of the M_7C_3 and $M_{23}C_6$ precipitates. This should have little effect on the rupture strength.

CHAPTER 5

CONCLUSIONS

The goal of this program has been to investigate the effect of carbon content and PWHT on the stress rupture behavior of 2-1/4Cr-1Mo weld metal. The following is a summary of the conclusions obtained during the course of the study.

The analysis of stress rupture data for PWHT 2-1/4Cr-1Mo weld metal using the Larson-Miller parameter technique, the log stress/log rupture time technique, and the Manson minimum commitment method indicates the following:

a. The 100,000 hour rupture strength decreases as the temper parameter increases. However, the strength difference arising from variations in PWHT diminishes with increasing test temperature. This effect is particularly pronounced for weld metal PWHT with $P<32.0$ which, at $750^{o}F$, has a 100,000 hour rupture strength 40 to 45 KSI higher than that for weld metal PWHT with $32.0<P<36.2$. This strength advantage falls rapidly with increasing test temperature and disappears at approximately $900^{o}F$.

b. For weld metal PWHT with $P<37.5$, the 100,000 hour rupture strength appears to increase with increasing carbon content. However, the strengthening effect of carbon diminishes as the test temperature is increased.

c. For weld metal PWHT with $P>37.5$, the 100,000 hour rupture strength appears to increase with carbon content for levels

up to about 0.04-0.05 weight percent. Weld metals having higher carbon contents have similar rupture strengths.

d. The stress rupture strength of PWHT 2-1/4Cr-1Mo SMA weld metal compares well with that determined from data for weld metal deposited by a variety of welding processes.

e. With respect to the data obtained from testing in this program, the following conclusions may be drawn:

   1. 0.08-0.09 carbon weld metal PWHT to proposed Class 3 condition exhibits significantly higher rupture strength at 950 and 1050°F than does the same material PWHT to Class 2.

   2. Rupture test results for weld metal PWHT 1300°F/25 hrs. (Class 2) indicate that the rupture strength of 0.02-0.03 carbon material is significantly lower than that exhibited by the higher carbon weld metals. Furthermore, the strengths of the latter are of similar magnitude.

f. Rupture testing of 2-1/4Cr-1Mo SMA weld metals conducted during this program has contributed significantly to the understanding of the rupture behavior of these materials.

   1. The effect of carbon content on the rupture strength of Class 2 SMA weld metal has been determined and may be employed to define proper industrial practice in the use of higher carbon filler metals to achieve improved strength.

2. The rupture behavior of 2-1/4Cr-1Mo SMA weld metal PWHT to proposed Class 3 strength has been characterized, contributing to the data base to be used to evaluate the feasibility of using 2-1/4Cr-1Mo steel in the Class 3 condition.
3. The rupture data acquired for the Class 2 weld metal increases by a factor of ten the amount of data available for 2-1/4Cr-1Mo SMA weld metal PWHT with P>37.5.

Comparison of the three rupture data analysis techniques employed in this study indicates the following:

a. The most conservative 100,000 hour stress values are given by the Manson method while the log stress-log rupture time stresses are the least conservative.
b. The best curve fits to the data are obtained using the Larson-Miller technique with the associated "r^2" values being consistently greater than those for the more conservative Manson method.
c. The Larson-Miller parameter method appears to be the best technique for the analysis of rupture data.

Room temperature and elevated temperature tensile tests of 2-1/4Cr-1Mo weld metal indicate the following:

a. For weld metal PWHT 1300^{o}F/25 hrs., the tensile strength and yield strength of the 0.02-0.03 carbon weld metal falls consistently below those of the higher carbon content materials which are comparable in magnitude. Moreover, the

0.02-0.03 carbon weld metal given this PWHT fails to meet the Class 2 requirements of Section VIII of the ASME Boiler and Pressure Vessel Code.

b. Comparison of the room temperature and elevated temperature tensile strengths of the four carbon content weld metals PWHT 1300°F/25 hrs. with their rupture behavior indicates that tensile test results may be useful in predicting relative stress rupture behavior.

c. The tensile strength of 0.08-0.09 carbon weld metal PWHT 1175°F/25.5 hrs (Class 3) is significantly greater than that exhibited by the same weld metal PWHT to the Class 2 condition. However, the enhanced strength is gained at the expense of elevated temperature ductility.

d. The strength and ductility of 0.08-0.09 carbon Class 3 weld metal are relatively unaffected by an aging treatment designed to simulate 100,000 hour service at 950°F.

The following conclusions have been drawn concerning the transformation studies of 0.08-0.09 and 0.12-0.13 carbon 2-1/4Cr-1Mo weld metal using thermal cycles designed to simulate the thermal history occurring in the coarse-grained region of the weld metal HAZ.

a. The microstructure of the as-transformed weld metal is fully bainitic except in the material thermally cycled 150 KJ/IN (2400°F peak temperature, 2 inch plate, 400°F preheat) where traces of polygonal ferrite occur at the prior austenite grain boundaries.

b. The bainite start and finish temperatures decrease with increasing cooling rate as well as increasing carbon content.

c. The bainite morphologies observed in the as-transformed weld metal are lath-like, granular, and massive. The lath bainite predominates at faster cooling rates and is gradually replaced by granular bainite as the cooling rate decreases. Some massive bainite is present at all cooling rates.

d. Increasing the cooling rate and/or weld metal carbon content increases the fineness of the bainitic microstructure.

Examination of the as-welded 2-1/4Cr-1Mo weld metals reveals the following:

a. The microstructure of the four carbon content weld metals are fully bainitic with the exception of the 0.02-0.03 carbon material which contains traces of polygonal ferrite.

b. The as-welded microstructure becomes finer as the weld metal carbon content increases.

c. Carbides found in the as-welded weld metal include M_3C and M_2C in agreement with the Baker and Nutting (17) carbide evolutionary sequence for 2-1/4Cr-1Mo steel.

Microstructural examination of the weld metals in the PWHT condition indicates the following:

a. The structure of the 0.02-0.03 carbon weld metal PWHT 1300^{o}F/25 hrs. consists of an equiaxed ferrite matrix

containing carbides. The carbides are M_2C, M_7C_3, $M_{23}C_6$, and M_6C and exist in the microstructure as needles, large spheroidized particles, or fringes.

b. Post-weld heat treating the 0.04-0.05, 0.08-0.09, and 0.12-0.13 carbon weld metals 1300°F/25 hrs. coarsens the microstructure but does not erase evidence of the as-welded bainitic structure. The carbides occuring in this PWHT material are M_7C_3, $M_{23}C_6$, and M_6C in agreement with the Baker and Nutting (17) carbide evolutionary sequence. The amount of carbide increases with carbon content. The carbide morphologies are predominantly spheroidal.

c. The microstructure of the 0.08-0.09 carbon weld metal PWHT 1175°F/25.5 hrs. (Class 3) is similar to the as-welded structure, exhibiting little or no coarsening of the bainitic constituent. A fine dispersion of acicular M_2C precipitates occurs within the prior austenite grains in addition to M_7C_3, $M_{23}C_6$, and M_6C.

Examination of the PWHT weld metal microstructure after rupture testing to determine structural changes resulting from the rupture test conditions reveals the following:

a. No microstructural change relative to the PWHT structure is observed in the Class 2 weld metal rupture tested at 1050°F for 5000 hours.

b. Changes in the 0.08-0.09 carbon Class 3 weld metal as a consequence of rupture testing are limited to the carbides. Rupture testing at 950°F for times up to 3000 hours has

little apparent effect on the carbides. However, testing at 1050°F for the same interval results in significant dissolution of the M_2C in the matrix accompanied by growth of the $M_{23}C_6$ carbides at the constituent boundaries.

c. An aging treatment (1193°F/21.5 hrs.) applied to the 0.08-0.09 carbon Class 3 weld metal to simulate 100,000 hours of service at 950°F results in minimal dissolution of the M_2C carbides in the matrix.

The following correlations between the weld metal microstructure and stress rupture behavior have been noted:

a. The superior rupture strength of the 0.08-0.09 carbon Class 3 weld metal is primarily a result of the strengthening effect of the acicular M_2C carbides present in the matrix. This strength persists during service at 950°F but is significantly reduced at 1050°F as a consequence of dissolution of the M_2C carbides.

b. The carbon content controls the rupture strength of weld metal PWHT 1300°F/25 hrs. (Class 2) by determining the major microconstituents in the PWHT microstructure. The 0.02-0.03 carbon weld metal, which has the lowest rupture strength, consists of non-bainitic ferrite. In contrast, the microstructure of the higher carbon content weld metals is tempered bainite, resulting in rupture strengths which are similar in magnitude despite variations in carbon content.

c. Because of the extensive PWHT given the Class 2 weld metal, the microstructural stability of this material is high for service use. The carbides present in the microstructure are the last three in the carbide sequence and have a morphology and distribution poorly suited to confer any rupture strength to the material. As a result, the rupture strength of the Class 2 weld metal is strong function of the bainitic nature of the microstructure. Any microstructural changes resulting from service at elevated temperatures would consist of further spheroidization of the carbides and would have little effect on the rupture strength of the weld metal.

LIST OF REFERENCES

LIST OF REFERENCES

1. Swift, R. A., "Effects of Composition and Heat Treatment on the Mechanical Properties of 300-mm-Gage 2-1/4Cr-1Mo Steel Plate," Application of 2-1/4Cr-1Mo Steel for Thick-Wall Pressure Vessels, ASTM STP 755, ASTM, 166-188 (1982).

2. Lautzenheiser, C. R., Use of Quenched and Tempered 2-1/4Cr-1Mo Steel, SWRI Project No. 07-1579, Southwest Research Institute (1965).

3. Properties of Carbon and Alloy Stainless Steel Tubing for High-Temperature and High-Pressure Service, Technical Bulletin No. 6G, Babcock and Wilcox Co. (1955).

4. Wada, T. and Eldis, G. T., "Transformation Characteristics of 2-1/4Cr-1Mo Steel," Application of 2-1/4Cr-1Mo Steel for Thick-Wall Pressure Vessels, ASTM STP 755, ASTM, 343-362 (1982).

5. Bland, J., "The Arc-Welding of 2.25%Cr-1%Mo Alloy Steel Pipe," Weld J., 35(4) Res. Suppl., 181-s to 194-s (1956).

6. Mandich, L. S., Fogelmen, E. L., and Gulya, J. A., "Elevated Temperature Properties of Heavy Gauge Cr-Mo Steel Plates," Symposium on Heat Treated Steels for Elevated Temperature Service, ASME, New Orleans, LA (1966).

7. Zeisloft, R. H., Leyda, W. E., and Domain, H. A., "Low Carbon 2-1/4Cr-1Mo Steels," Low Carbon and Stabilized 2-1/4% Chromium 1% Molybdenum Steels, ASM (1970).

8. Klueh, R. L., "The Effect of Carbon on 2.25Cr-1Mo Steel (I). Microstructural and Tensile Properties," J. Nuclear Materials, 54, 55-63 (1974).

9. Copeland, J. F. and Licina, G. J., "A Review of 2-1/4Cr-1Mo Steel for LMFBR Steam Generator Applications," Symposium on Structural Materials for Service at Elevated Temperatures in Nuclear Power Generation, ASME, Houston, TX (1975).

10. Scott, T. E., "Pressure Vessels for Coal Liquifaction - An Overview," Application of 2-1/4Cr-1Mo Steel for Thick-Wall Pressure Vessels, ASTM STP 755, ASTM, 7-25 (1982).

11. "ASTM A 387-79b, Standard Specification for Pressure Vessel Plates, Alloy Steel, Chromium Molybdenum," 1982 Annual Book of ASTM Standards, Part 4, ASTM, 360-362 (1982).

12. Bynum, J. E., Ellis, F. V., and Roberts, B. W., "Creep, Tensile Properties, and Constitutive Equations for 2-1/4Cr-1Mo Steel,"

Symposium on Structural Materials for Service at Elevated Temperatures in Nuclear Power Generation, ASME, Houston, TX (1975).

13. Emmanuel, G. , Leyda, W. E., and Rozic, E. J., "Versatility of 2-1/4Cr-1Mo as a Pressure Vessel Material," Symposium on 2-1/4 Chrome 1 Molybdenum Steel In Pressure Vessels and Piping, ASME-MPC, Denver, CO (1970).

14. Smith, G. V., "The Strength of 2-1/4Cr-1Mo Steel at Elevated Temperatures," Symposium on 2-1/4 Chrome 1 Molybdenum Steel in Pressure Vessels and Piping, ASME-MPC, Denver, CO (1970).

15. Carpenter, O. R. and Emmanuel, G. N., "The Use of Quenched and Tempered 2.25Cr-1Mo Steel for the Fabrication of Advanced Design Pressure Vessels," Symposium on Heat Treated Steels for Elevated Temperature Service, ASME, New Orleans, LA (1966).

16. Stone, D., Ruoff, S., Wanagel, J. and Li, C. Y., "Hydrogen Attack in Cr-Mo Steels at Elevated Temperatures," Fossil Energy Materials Program Quarterly Report, ORNL/FMP-84/1, 153-172 (1984).

17. Baker, R. G. and Nutting, J., "The Tempering of 2-1/4Cr-1Mo Steel after Quenching and Normalizing," JISI, 192, 257-268 (1959).

18. "ASTM A 542-79, Standard Specification for Pressure Vessel Plates, Alloy Steel, Quench and Tempered Chromium Molybdenum," 1982 Annual Book of ASTM Standards, Part 4, ASTM, 498-500 (1982).

19. Sims, J. E. and Fuchs, R., "Influence of Welding Processes on the Mechanical Properties of 2-1/4Cr-1Mo Weld Metals," ASM for Metals Congress, St. Louis, MO (1982).

20. Bonta, J. E. and Sikora, O. G., "Fabrication of Heavy-Wall Pressure Vessels," Application of 2-1/4Cr-1Mo Steel for Thick-Wall Pressure Vessels, ASTM STP 755, ASTM, 255-274 (1982).

21. Thomas, R. D., "Welding Technology Assessment for Pressure Vessels and Components for Coal Conversion Processes," Proceedings of the Symposium on the Behavior of Joints in High Temperature Materials, Pettin, Netherlands, 63-85 (1981).

22. "Electroslag and Electrogas Welding," Welding Handbook, Volume 2, 7th Ed., AWS, 226-248 (1978).

23. "Electroslag Welding," Metals Handbook, Vol. 6, 9th Ed., ASM, 225-237 (1983).

24. "Shielded Metal Arc Welding," Metals Handbook, Vol. 6, 9th Ed., ASM, 75-95 (1983).

25. "Shielded Metal Arc Welding," Welding Handbook, Vol. 2, 7th Ed., AWS, 43-76 (1978).

26. Farrell, W. J., "A Portable 100-kW Electron Beam Welding System for Pressure Vessel Fabrication," Application of 2-1/4Cr-1Mo Steel for Thick-Wall Pressure Vessels, ASTM STP 755, ASTM, 297-325 (1982).

27. "Electron Beam Welding," Metals Handbook, Vol. 6, 9th Ed., ASM, 609-646 (1983).

28. "Electron Beam Welding," Welding Handbook, Vol. 3, 7th Ed., AWS, 169-215 (1980).

29. "Gas Metal Arc Welding," Metals Handbook, Vol. 6, 9th Ed., ASM, 153-181 (1983).

30. "Gas Metal Arc Welding," Welding Handbook, Vol. 2, 7th Ed., AWS, 113-152 (1978).

31. Nutting, J. and Arrowsmith, J. M., "The Metallography of Creep-Resistant Steels," ISI Special Report No. 70, 147-165 (1961).

32. Verhoeven, John D., "Precipitation from Solid Solutions," Fundamentals of Physical Metallurgy, John Wiley and Sons, 363-420 (1975).

33. Guard, Ray W., "Alloying for Creep Resistance," Mechanical Behavior of Materials at Elevated Temperatures, McGraw-Hill, 270-287 (1961).

34. Shoeck, Gunther, "Theories of Creep," Mechanical Behavior of Materials at Elevated Temperatures, McGraw-Hill, 79-107 (1961).

35. Reed-Hill, Robert E., "Precipitation Hardening," Physical Metallurgy Principles, 2nd Ed., D. Van Nostrand Co., 358-377 (1973).

36. Dieter, George E., "Creep and Stress Rupture," Mechanical Metallurgy, 2nd Ed., McGraw-Hill, 451-489 (1976).

37. Woodhead, J. H. and Quarrel, A. G., "Role of Carbides in Low Alloy Creep-Resisting Steels," JISI, 203, 605-620 (1965).

38. Reed-Hill, Robert E., "Diffusion in Substitutional Solid Solutions," Physical Metallurgy Principles, 2nd Ed., D. Van Nostrand Co., 378-430 (1973).

39. Verhoeven, John D., "Diffusion," Fundamentals of Physical Metallurgy, John Wiley and Sons, 137-167 (1975).

40. Klueh, R. L., "Heat Treatment Effects on Creep and Rupture Behavior of Annealed 2.25Cr-1Mo Steel," Met. Trans. A, 9A(11), 1619-1623 (1978).

41. Jones, W. B. and Van Den Avyle, "Substructure and Strengthening Mechanisms in 2.25Cr-1Mo Steel at Elevated Temperatures," Met. Trans. A, 11A(8), 1275-1286 (1980).

42. Reed-Hill, Robert E., "Solid Solutions," Physical Metallurgy Principles, 2nd Ed., D. Van Nostrand Co., 326-357 (1973).

43. Brown, R. M., Rege, R. H., and Spaeder, C. E., Jr., "The Properties of Normalized and Tempered and of Quenched and Tempered 6-1/4 Inch Thick Plates of 2-1/4Cr-1Mo Steel," Symposium on Heat Treated Steels for Elevated Temperature Service, ASME, New Orleans, LA (1966).

44. Richey, M. W., "The Weldability of Cr-Mo Steels for Fossil Energy Applications," M. S. Thesis, University of Tennessee, Knoxville, TN (1984).

45. Habraken, L. T. and Economopoulos, M., "Bainitic Microstructures in Low-Carbon Alloy Steels and Their Mechanical Properties," Symposium on Transformation and Hardenability in Steels, Climax Molybdenum Co., (1967).

46. Kar, R. J. and Todd, J. A., "Discussion on Transformation Characteristics", Application of 2-1/4Cr-1Mo Steel for Thick-Wall Pressure Vessels, ASTM STP 755, ASTM, 361-362 (1982).

47. Krauss, G., "Tempering of Steel," Principles of Heat Treatment of Steel, ASM, 187-227 (1980).

48. Murphy, M. C. and Branch, G. D., "Metallurgical Changes in 2.25Cr-1Mo Steels During Creep-Rupture Test," JISI, 209, 554-561 (1971).

49. Pilling, J. and Ridley, N., "Tempering of 2.25%Cr-1%Mo Low Carbon Steels," Met. Trans. A, 13A(4), 557-563 (1982).

50. Pilling, J., Ridley, N., and Gooch, D. J.,"The Effect of Titanium on Creep Strength in 2.25PctCr-1PctMo Steels," Met. Trans. A, 14A(7), 1443-1449 (1983).

51. Miller, R. F., Benz, W. G., and Unverzagt, W. E., "The Creep Strength of 17 Low Alloy Steels at 1000oF," ASTM Proc., 40, 771-781 (1940).

52. Smith G. V., "Supplemental Report on the Elevated-Temperature Properties of Chromium-Molybdenum Steels," ASTM Data Series, ASTM, DS 6S2.

53. Argent, B. B., Van Niekerk, M. N., and Redfern, G. A., "Creep of Ferritic Steels," JISI, 208, 830-843 (1970).

54. Emmanuel, G. N. and Leyda, W., "Long-Time High Temperature Properties of Cr-Mo Weld Metal," Symposium on Properties of Weldments at Elevated Temperatures, AWS, Chicago, IL (1968).

55. Sangdahl, G. S. and Vorhees, H. R., "Quenched and Tempered 2-1/4Cr-1Mo Steel at Elevated Temperatures - Tests and Evaluation," Current Evaluation of 2-1/4 Chrome 1 Molybdenum Steel in Pressure Vessels and Piping, ASME-MPC, New Orleans, LA (1972).

56. Smith, G. V., "Elevated Temperature Strength and Ductility of Quenched and Tempered 2-1/4Cr-1Mo Steel," Current Evaluation of 2-1/4 Chrome 1 Molybdenum Steel in Pressure Vessels and Piping, ASME-MPC, New Orleans, LA (1972).

57. Wilson, D. J., "The Influence of Simulated Service Exposure on the Rupture Strengths of Grade 11, Grade 22, and Type 204 Steels," Journal of Engineering Materials and Technology, Transactions of the ASME, 96(1), 10-21 (1974).

58. Klueh, R. L., "The Effect of Carbon on 2.25Cr-1Mo Steel (II). Creep-Rupture Properties," J. Nucl. Mat., 54, 53-63 (1974).

59. Viswanathan, V., "Effect of Ti and Ti+B Additions on the Creep Properties of 1.25Cr-0.5Mo Steels," Met. Trans. A, 57-61 (1977).

60. Klueh, R. L., "Creep and Rupture Behavior of a Bainitic (Normalized and Tempered) 2-1/4Cr-1Mo Steel," ORNL-5273, Oak Ridge National Laboratory (1977).

61. Cane, B. J. and Fidler, R. S., "The Effect of Microstructure and Grain Size on the Creep and Rupture Properties of 2-1/4Cr1Mo and 9Cr1Mo Steels," International Conference on Ferritic Steels for Fast Reactor Steam Generators, British Nuclear Energy Society, London, UK (1977).

62. Gooch, D. J., "Effects of Trace Elements on Creep Strength and Ductility of Low Carbon 2.25Cr-1Mo Steels," Met. Sci., 15(2), 45-54 (1981).

63. "Mechanical and Metallurgical Properties of a 3Cr-1Mo-1/4V-Ti-B Pressure Vessel Steel for Coal Liquefaction Reactor," NEDO/JSW Data Sheet, Series No. CLR-C, New Energy Development Organization, The Japan Steel Works Ltd. (1981).

64. Rawlins, Carl E., Prescott, G. R., Braun, C. F., McGuire, W. J., and Lorentz, R. E., Report to the American Petroleum Institute on a Program to Study Materials for Pressure Vessel Service with Hydrogen at High Temperatures and Pressures, MPC (1982).

65. Finnie, Lain and Heller, William R., "Creep Behavior of Specific Metals," Creep of Engineering Materials, McGraw-Hill, 90-113 (1959).

66. Wada, T. and Biss, V. A., "Restoration of Elevated Temperature Tensile Strength in 2.25Cr-1Mo Steel," Met. Trans. A, 14A(5), 845-855 (1983).

67. Sachs, K., Baldock, A. J., and Evans, D. G., "The Creep Strength of Welds in Thick Steampipes," Proceedings of the Conference on Welding Creep-Resistant Steels, Cambridge, UK (1970).

68. Prescott, G. R. and Braun, C. F., "Update on Modified 2-1/4Cr-1Mo and 3Cr-Mo Alloys," MPC, HPV-7 (1983).

69. Kotecki, D. J., Private Communication, Teledyne McKay, November 6, 1984.

70. Campbell, H. C., "Influence of Carbon on Stress-Rupture Properties of Cr-Mo Weld Metal," Weld J., 42(6) Res. Suppl., 64-s to 70-s (1965).

71. Klueh, R. L. and Canonico, D. A., "Creep Rupture Properties of 2-1/4Cr-1Mo Steel Weldments with Varying Carbon Contents," Weld J., 55(12) Res. Suppl., 381-s to 388-s (1976).

72. Ishiguro, T., Murakami, Y., Ohnishi, K., and Watanabe, J., "A 2-1/4Cr-1Mo Pressure Vessel Steel with Improved Creep Rupture Strength," Application of 2.25Cr-1Mo Steel for Thick Wall Pressure Vessels, Denver, CO (1980).

73. Batte, A. D., and Murphy, M. C., "Creep-Rupture Properties of 2-1/4Cr-1Mo Weld Deposits, " Weld J., 52(6) Res. Suppl., 261-s to 267-s (1973).

74. Rogers, P., Phelps, B., and Murphy, M. C., "The Creep-Rupture Properties of 2-1/4%Cr-1%Mo Submerged Arc Weld Metal," Proceedings of the Conference on Welding Creep-Resistant Steels, Cambridge, UK (1970).

75. Miller, R. F., Benz, W. G., and Day, M. J., "The Creep Strength, Stability of Microstructure, and Oxidation Resistance of Cr-Mo and 18Cr-8Ni Steels," Trans. ASM, 32, 381-400 (1944).

76. Egnell, L., "Mechanical Properties and Weldability of a Columbium Stabilized Steel with 2-1/4% Chrome and 1% Molybdenum

for Sodium-Cooled Fast Reactor Systems," Low Carbon and Stabilized 2-1/4% Chromium 1% Molybdenum Steels, ASM (1970).

77. Husslage, W. and Cortland, W., "Creep Behavior of 2-1/4Cr1MoNiNb Steel," International Conference on Ferritic Steels for Fast Reactor Steam Generators, British Nuclear Energy Society, London, UK (1977).

78. Viswanathan, R., "Effect of Sb, P, Sn, and B on the Microstructure and Creep Properties of Normalized and Tempered 1.25Cr-0.5Mo Steels," Met. Trans. A, 1135-1141 (1975).

79. Improvement in High Temperature Properties of Heavy Section 2-1/4Cr-1Mo Steel, Kawasaki Steel Corporation, (1982).

80. Miller, R. F. and Kearny, N. J., "Effect of Deoxidation Practice on Creep Strength of Carbon-Molybdenum Steels at 850 and 1000°F," ASME Trans., 65, 309-314 (1943).

81. Hopkin, L. M. T. and Jenkinson, E. A., "Creep Resistance and Metallographic Structure of 2-1/4Cr-1Mo Steel with and without a Tin Addition," JISI, 200(5), 356-359 (1962).

82. Pilling, J., Ridley, N., and Gooch, D. J., "The Effect of Phosphorus on Creep in 2.25%Cr-1%Mo Steels," Acta. Met., 30(8), 1587-1595 (1982).

83. Chung, D. W., Todd, J. A., and Parker, E. R., "Design of Low Alloy Steels for Thick Walled Pressure Vessels," Fossil Energy Materials Program Quarterly Report, ORNL/FMP-81/4, 53-66 (1982).

84. Wagner, L. E. and Seth, B. B., "Creep Rupture Behavior of 2 1/4%Cr-1%Mo Weld Metal," Properties of Steel Weldments for Elevated Temperature Pressure Containment Applications, MPC-9, ASME, 103-138 (1978).

85. Pendley, M. R., "High Temperature Properties of 2-1/4Cr-1Mo Steel Weld Metals," M. S. Thesis, University of Tennessee, Knoxville, TN (1980).

86. Goldhoff, R. M., "The Evaluation of Elevated Temperature Creep and Rupture Strength Data: An Historical Perspective," Characterization of Materials for Service at Elevated Temperatures, MPC-7, ASME, 247-265 (1978).

87. Booker, M. K. and Booker, B. L. P., "New Methods for Analysis of Materials Strength Data for the Asme Boiler and Pressure Vessel Code," Use of Computers in Managing Material Property Data, MPC-14, ASME.

88. Booker, M. K., "Use of Generalized Regression Models for the Analysis of Stress Rupture Data," Characterization of Materials for Service at Elevated Temperatures, MPC-7, ASME, 459-499 (1978).

89. Manson, S. S. and Ensign, C. R., "Interpolation and Extrapolation of Creep Rupture Data by the Minimum Commitment Method - Part I. Focal Point Convergence," Characterization of Materials for Service at Elevated Temperatures, MPC-7, ASME, 299-397 (1978).

90. Manson, S. S. and Ensign, C. R., "Interpolation and Extrapolation of Creep Rupture Data by the Minimum Commitment Method - Part II. Oblique Translation," Characterization of Materials for Service at Elevated Temperatures, MPC-7, ASME, 399-425 (1978).

91. Manson, S. S. and Muralidharan, V., "Analysis of Creep Rupture Data for Five Multiheat Alloys by the Minimum Commitment Method Using Double Heat Term Centering Technique," Progress in Analysis of Fatigue and Stress Rupture, MPC-23, ASME,1-45 (1984).

92. Lundin, C. D. and Kelley, S. C., "Elevated Temperature Properties of 2-1/4Cr-1Mo Weld Metal," Unpublished Quarterly Report, Welding Research and Engineering Group, Chemical, Metallurgical, and Polymer Engineering, University of Tennessee, Knoxville, TN (Jan. 1984).

93. "Materials for Pressure Vessels for Hydrogen Service," Frontiers-News of the Metal Properties Council, 12(1) (Feb. 1983).

94. Oblak, J. M. and Hehemann, R. F., "Structure and Growth of Widmanstatten Ferrite and Bainite," Symposium on Transformation and Hardenability in Steels, Climax Molybdenum Co. (1967).

95. Pickering, F. B., "The Structure and Properties of Bainite in Steels," Symposium on Transformation and Hardenability in Steels, Climax Molybdenum Co. (1967).

96. Shackleton, D. N. and Kelly, P. M., "Morphology of Bainite," Physical Properties of Martensite and Bainite, Special Report 93, Iron and Steel Institute, London, UK (1965).

97. Habraken, L. and DeBrouwer, J., De Ferri Metallographia - Metallographic Atlas of Iron, Steels and Cast Irons, Vol. 1, Presses Academiques Europeennes, Bruxelles, Belgium (1966).

98. Pepe, J. J., Private Communication, Turbine Technology Laboratory, General Electric Co., Dec. 10, 1984.

99. Savage, W. F., "Apparatus for Studying the Effects of Rapid Thermal Cycles and High Strain Rates on the Elevated Temperature Behavior of Materials," Journal of Applied Polymer Science, VI(21), 303-315 (1962).

100. ASME Boiler and Pressure Vessel Code, Section VIII: Rules for Construction of Pressure Vessels, ASME, New York, NY (1984).

101. Lundin, C. D., Kruse, B. J., and Pendley, M. R., "High Temperature Properties of 2 1/4Cr-1Mo Weld Metal," WRC Bulletin 277, Welding Research Council (May 1982).

102. "Elevated Temperature Properties of Weld-Deposited Metals and Weldments," ASTM STP 226, ASTM, 45-58 (1966).

103. Bruscato, R., "Temper Embrittlement and Creep Embrittlement of 2 1/4Cr-1Mo Shielded Metal Arc Weld Deposits," Weld J., 49(4) Res. Suppl., 148-s to 156-s (1970).

104. Leyda, W. E., Katz, L., Gold, M., and Snyder, R. L., "Stress Rupture Properties of C-Mo, Cr-Mo, Stainless Steel, and Ni-Cr-Fe Welds," Properties of Steel Weldments for Elevated Temperature Pressure Containment Applications, MPC and ASME, San Francisco, CA (1978).

105. Williamson, J. and Branch, G. D., "Internal Pressure Creep-Rupture Testing of Butt-Welded 1/2%Cr-1/2%Mo-1/4%V Tubes," Proceedings of the Conference on Welding Creep-Resistant Steels, Cambridge, UK (1970).

106. Hopkin, L. M. T., Murray, D., and Duval, D., "Creep Properties of Some Butt Welds in Steampipes," JISI, 203, 819-825 (1965).

107. Kaufman, W. J., "Results of Long-Time Creep Tests on Steel with 1%Cr-0.5%Mo, with 2 1/4%Cr-1%Mo, and with 1/2%Mo-1/4%V," Proceedings of the International Conference on High Temperature Steels, ERA Translation J/E/T215, Dusseldorf, FRG (1960).

108. Simmons, W. F., and Cross, H. D., "The Elevated Temperature Properties of Chromium Molybdenum Steels," ASTM STP 151, ASTM (1953).

109. Lundin, C. D. and Kruse, B. J., "High Temperature Properties of 2 1/4Cr-1Mo GTA-HW Weld Metal," Unpublished Report, Chemical, Metallurgical, and Polymer Engineering, University of Tennessee, Knoxville TN (Aug. 1981).

110. Lundin, C. D. and Kruse, B. J., "Stress-Rupture Evaluation of Electron Beam Weldments," Unpublished Report, Welding Research and Engineering Group, Chemical, Metallurgical, and Polymer

APPENDICES

APPENDIX A

COMPREHENSIVE DATA ANALYSIS PRESENTATIONS

This appendix presents the rupture data and associated curve fits in graphical form. Designated as A1 through A96, these figures depict the results of the Larson-Miller parameter analysis, the log stress/log rupture time analysis, and the Manson minimum commitment method respectively. For each analysis technique, the data are presented in the following order; literature data, UTK data, and combined literature and UTK data. A detailed account of the contents of this appendix is given in the List of Figures.

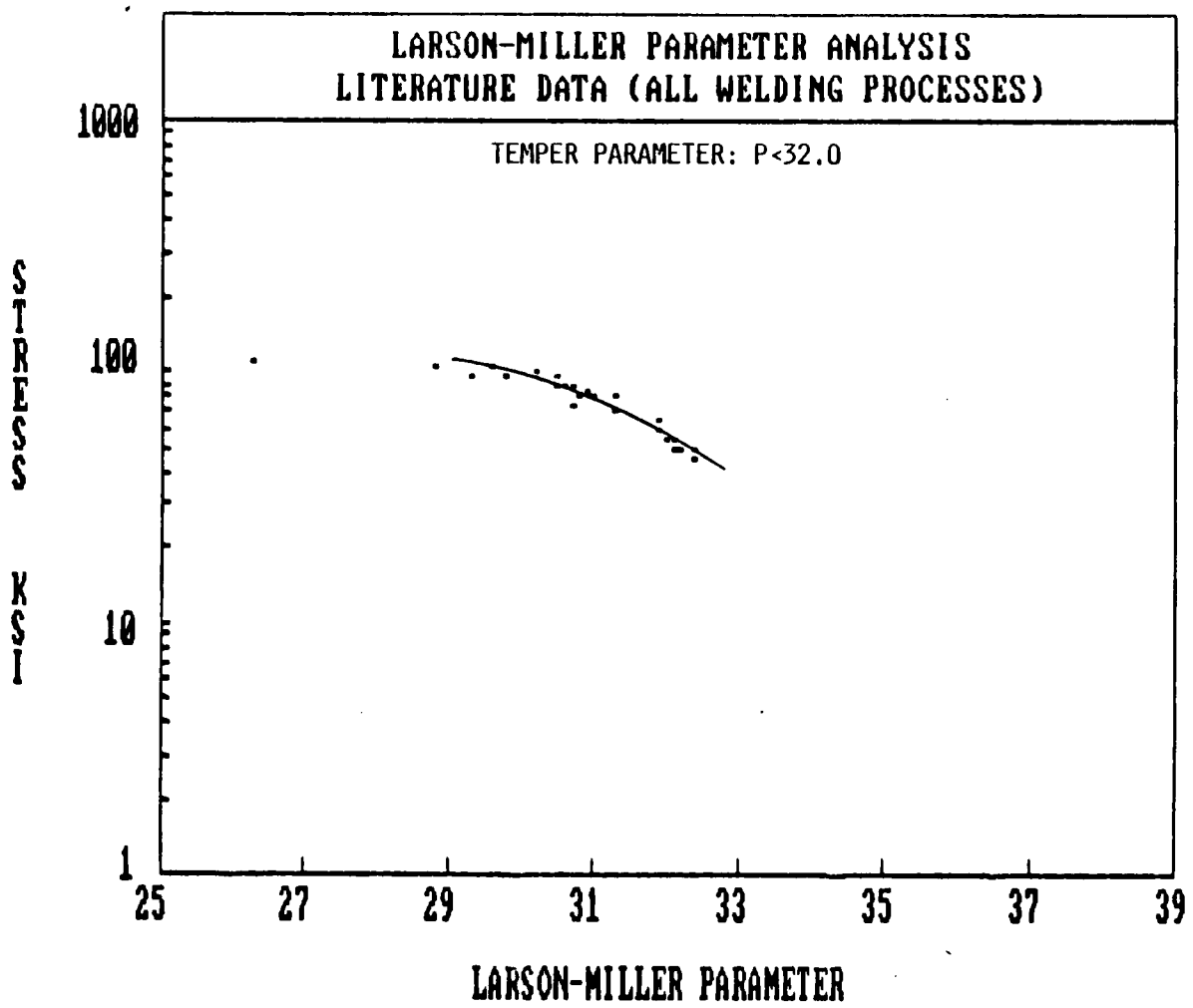


Figure A1. Larson-Miller parameter analysis of PWHT 2-1/4Cr-1Mo weld metal (P<32.0) determined from literature data for weld metal deposited by a variety of welding processes.

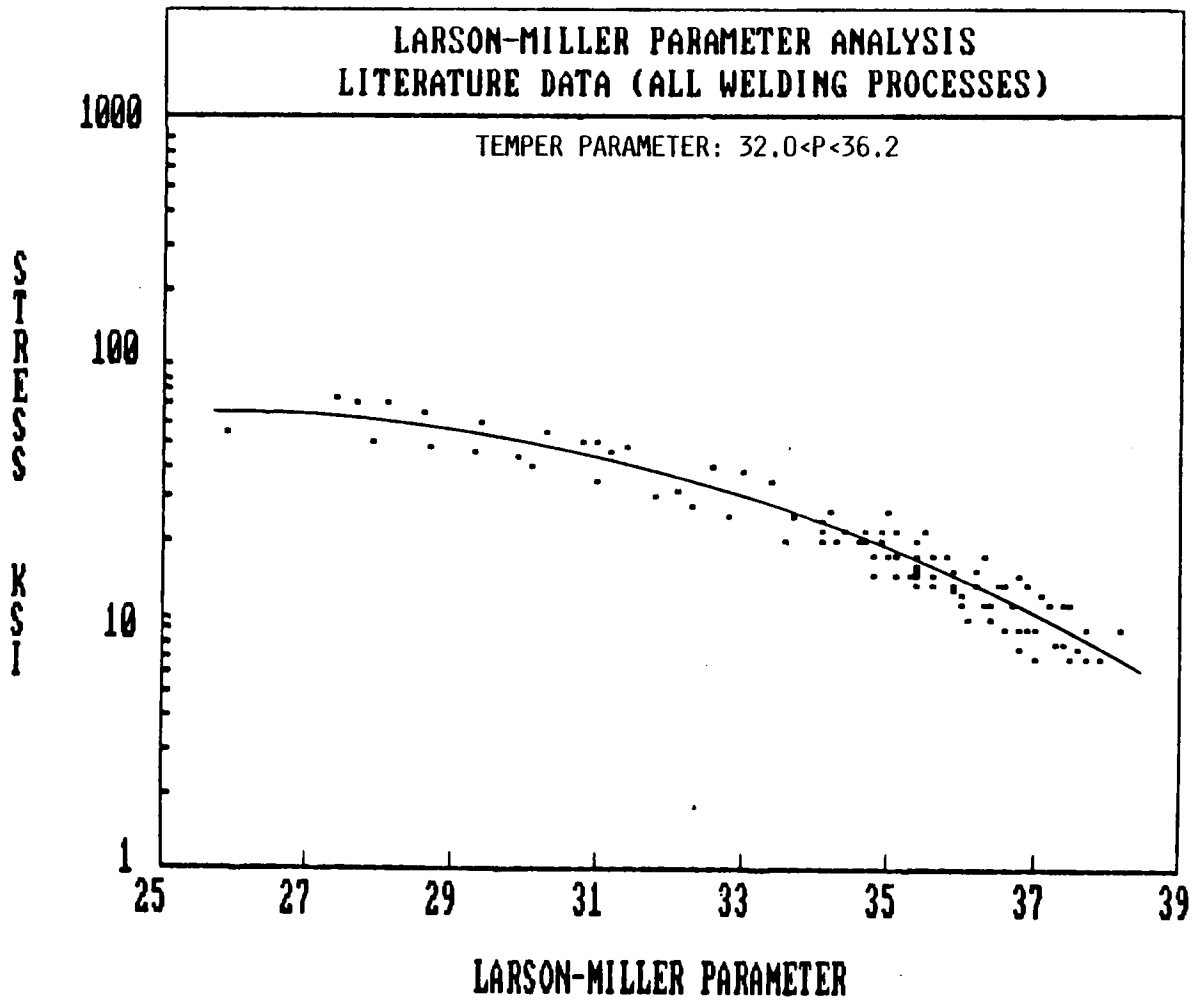


Figure A2. Larson-Miller parameter analysis of PWHT 2-1/4Cr-1Mo weld metal (32.0<P<36.2) determined from literature data for weld metal deposited by a variety of welding processes.

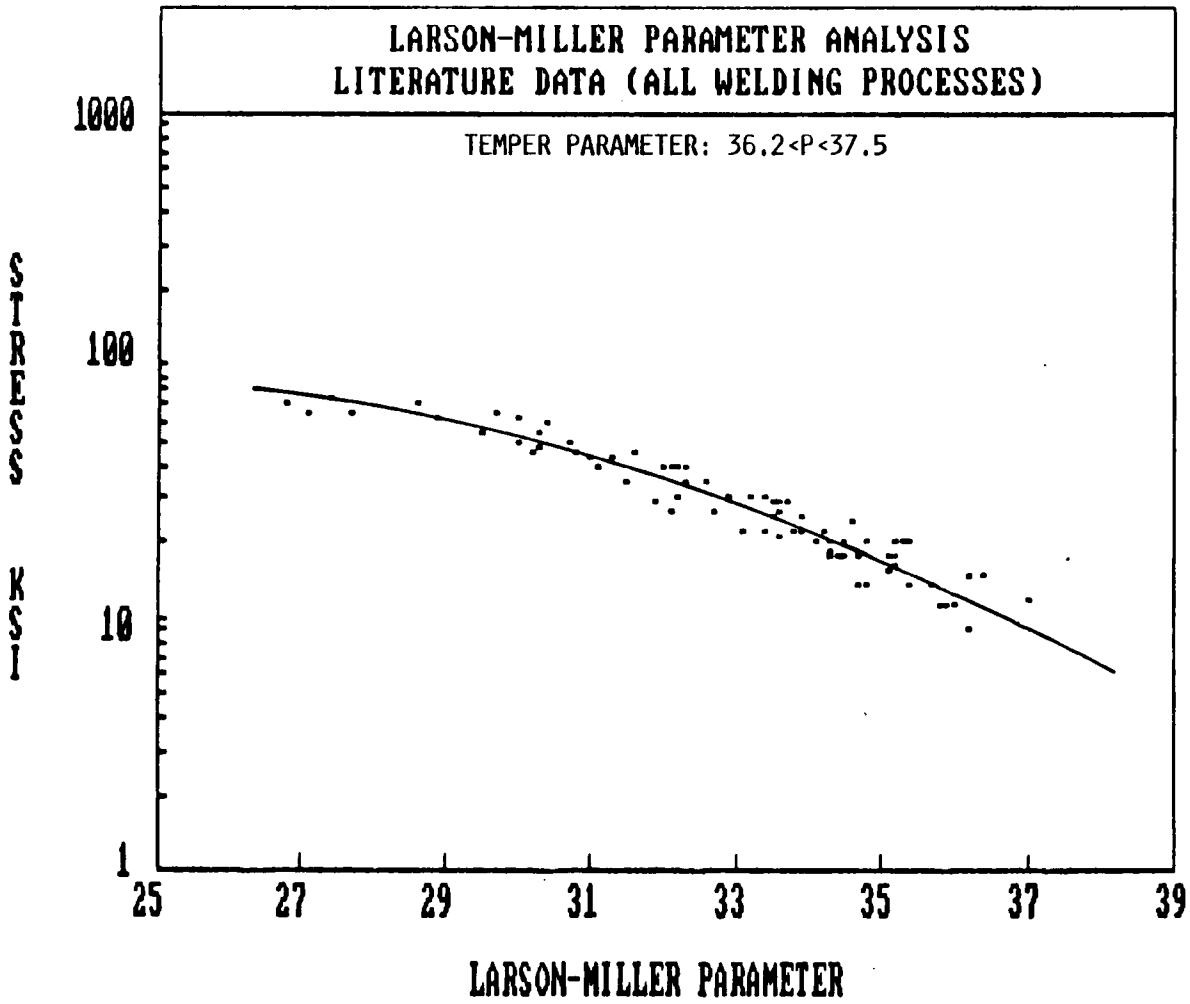


Figure A3. Larson-Miller parameter analysis of PWHT 2-1/4Cr-1Mo weld metal (36.2<P<37.5) determined from literature data for weld metal deposited by a variety of welding processes.

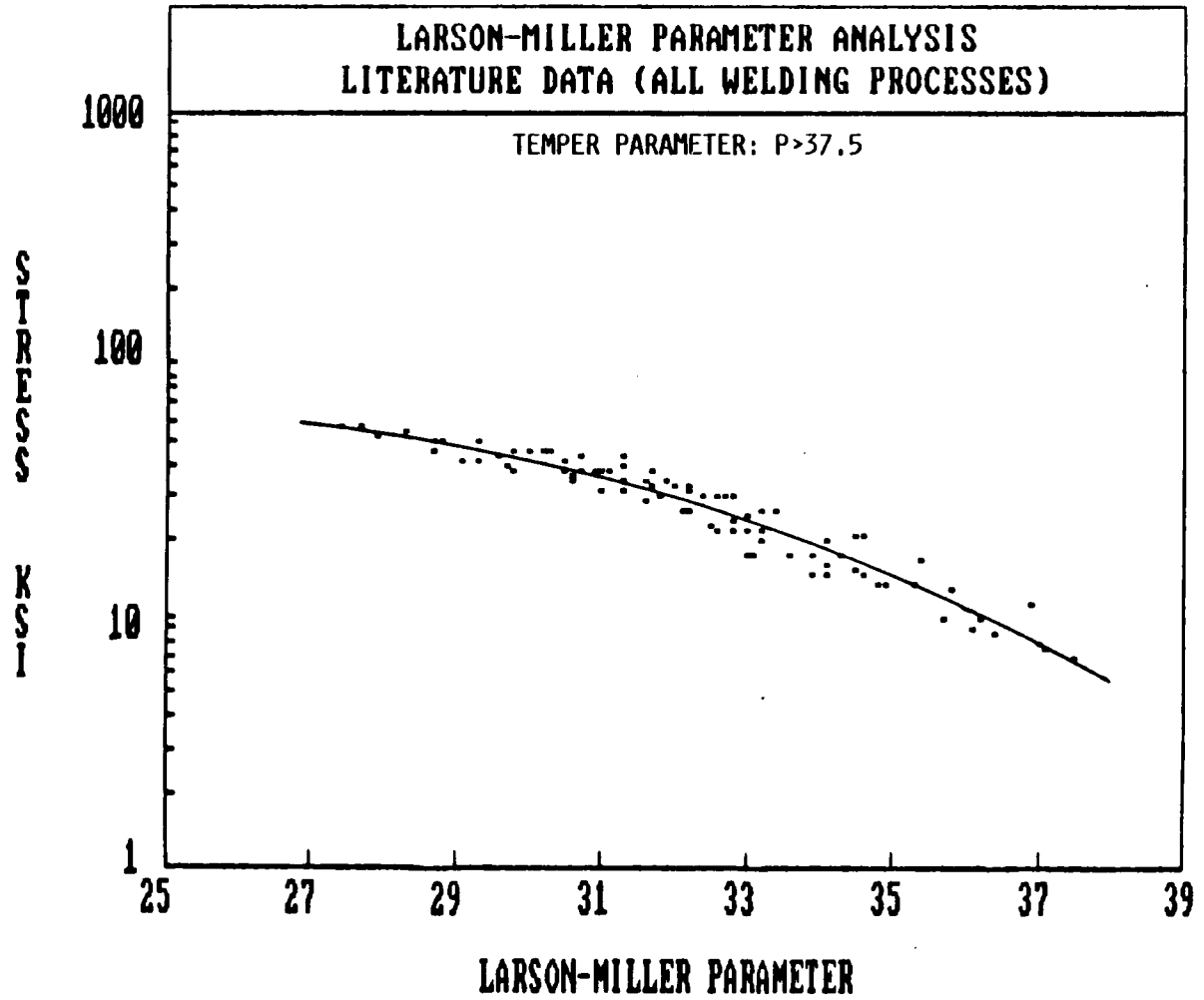


Figure A4. Larson-Miller parameter analysis of PWHT 2-1/4Cr-1Mo weld metal (P>37.5) determined from literature data for weld metal deposited by a variety of welding processes.

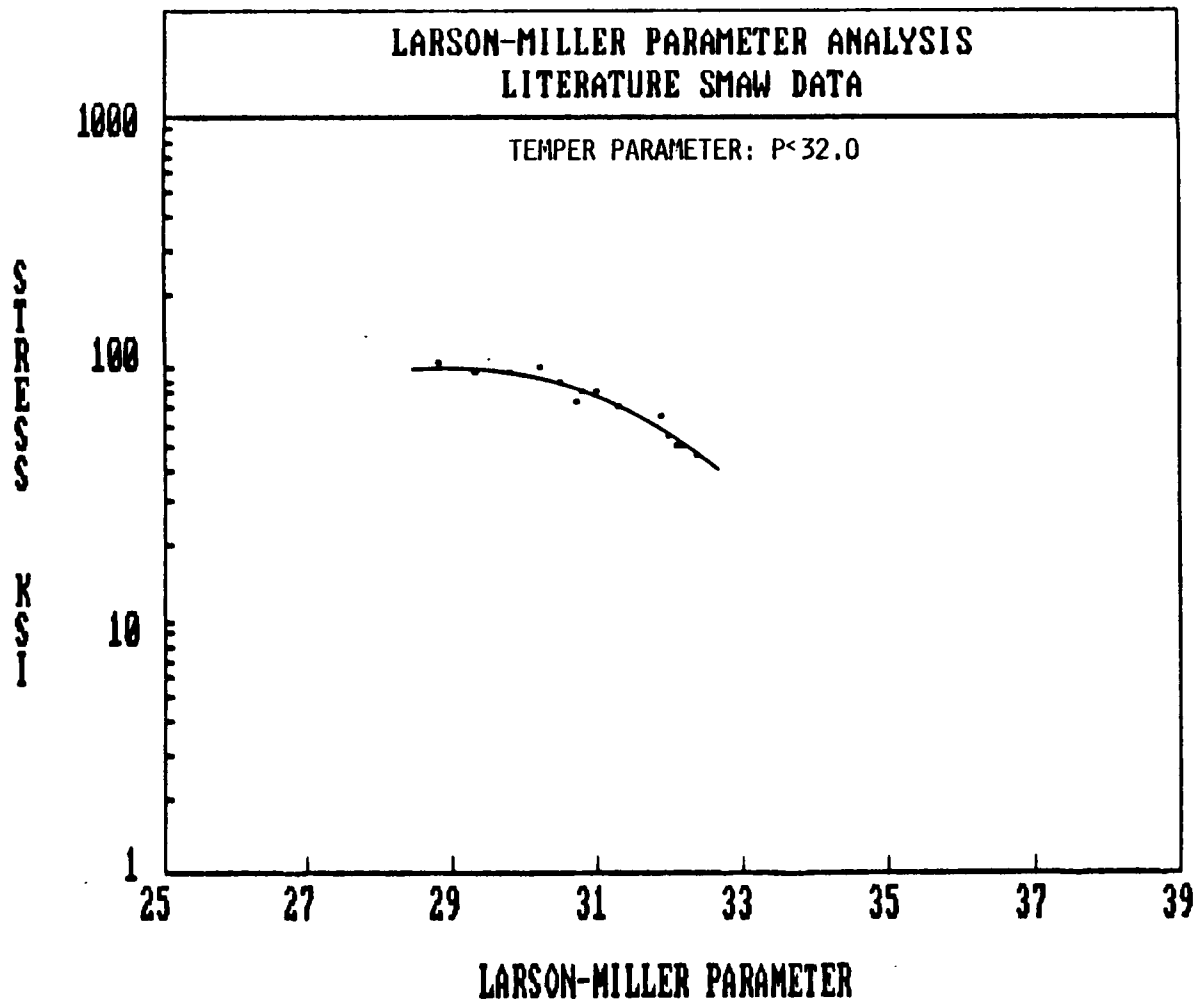


Figure A5. Larson-Miller parameter analysis of PWHT 2-1/4Cr-1Mo weld metal (P<32.0) determined from literature data for SMA weld metal.

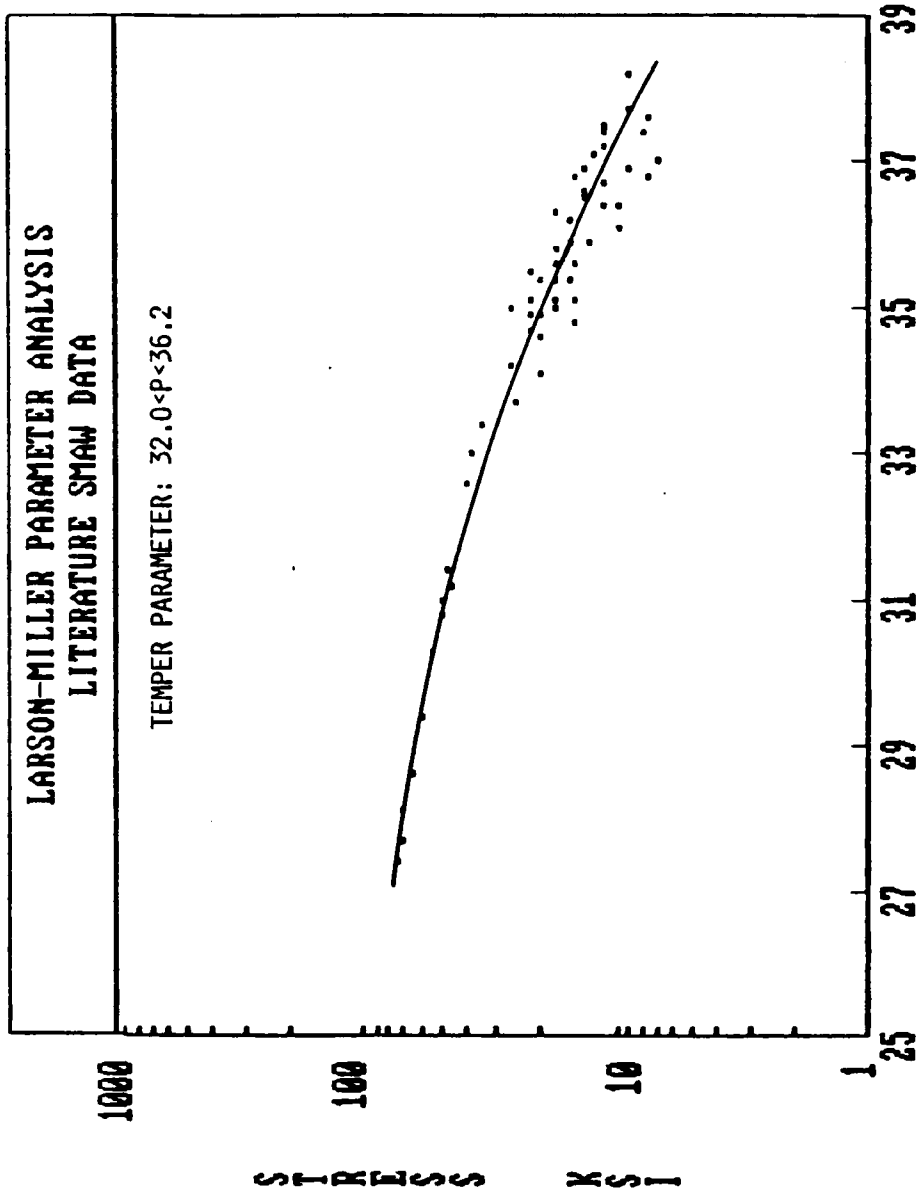


Figure A6. Larson-Miller parameter analysis of PWHT 2-1/4Cr-1Mo SMA weld metal (32.0<P<36.2) determined from literature data.

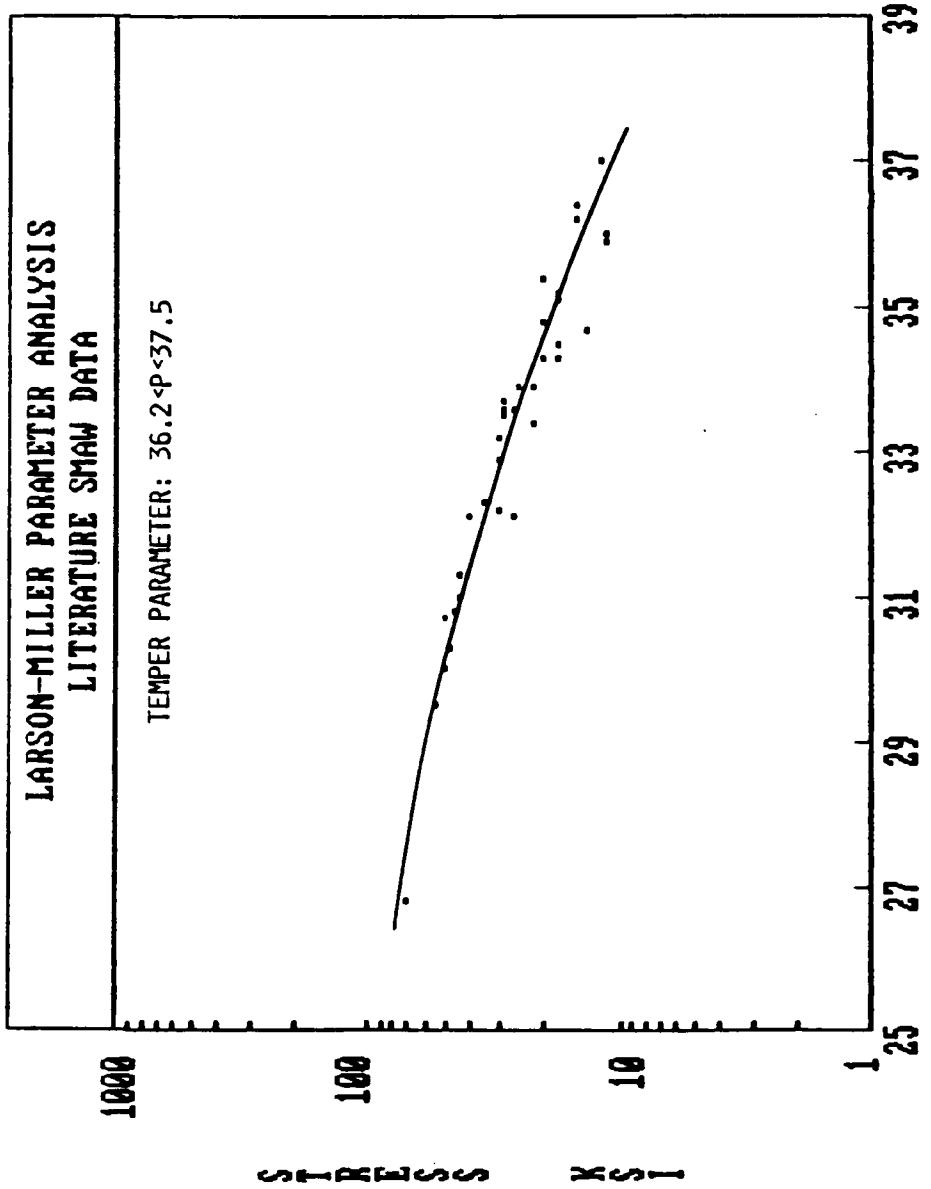


Figure A7. Larson-Miller parameter analysis of PWHT 2-1/4Cr-1Mo SMA weld metal (36.2<P<37.5) determined from literature data.

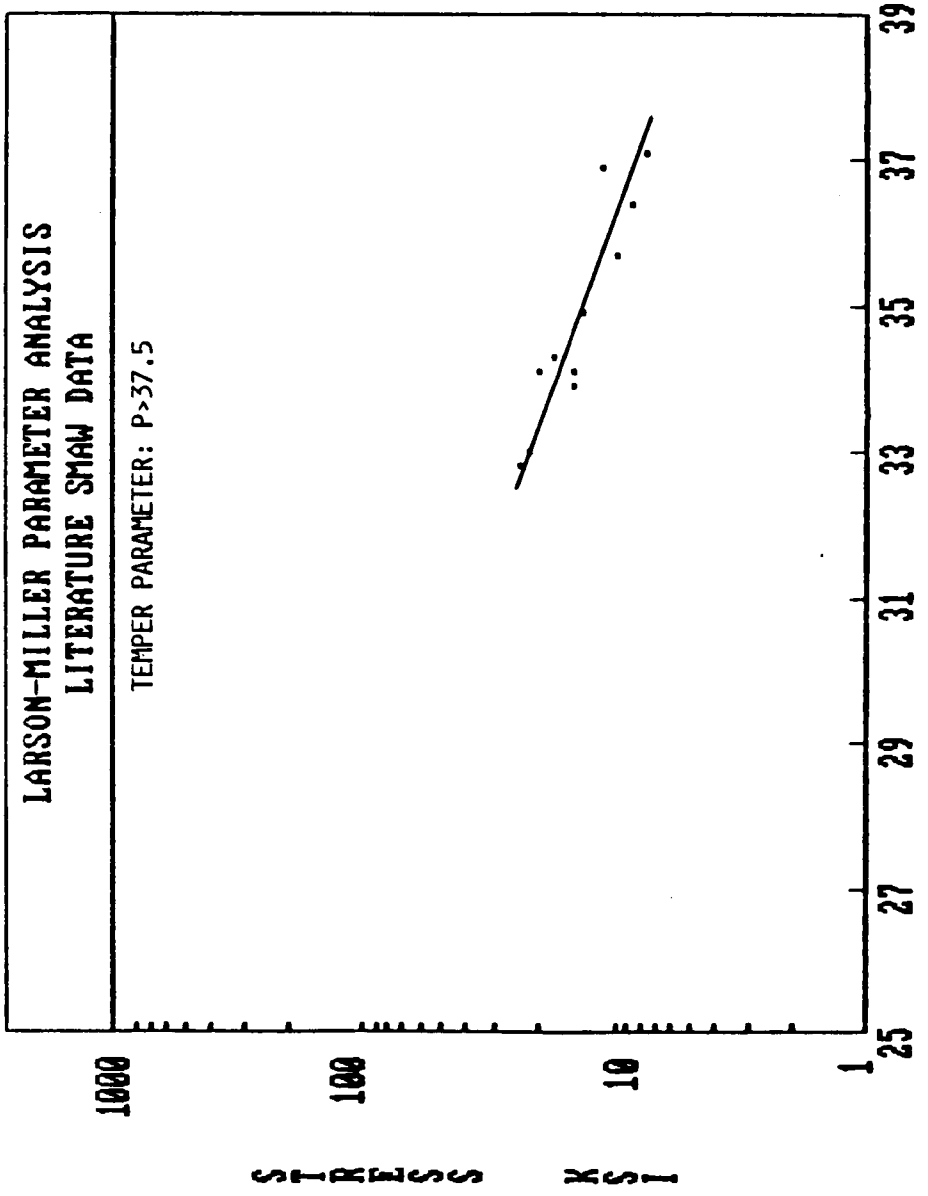


Figure A8. Larson-Miller parameter analysis of PWHT 2-1/4Cr-1Mo SMA weld metal (P>37.5) determined from literature data.

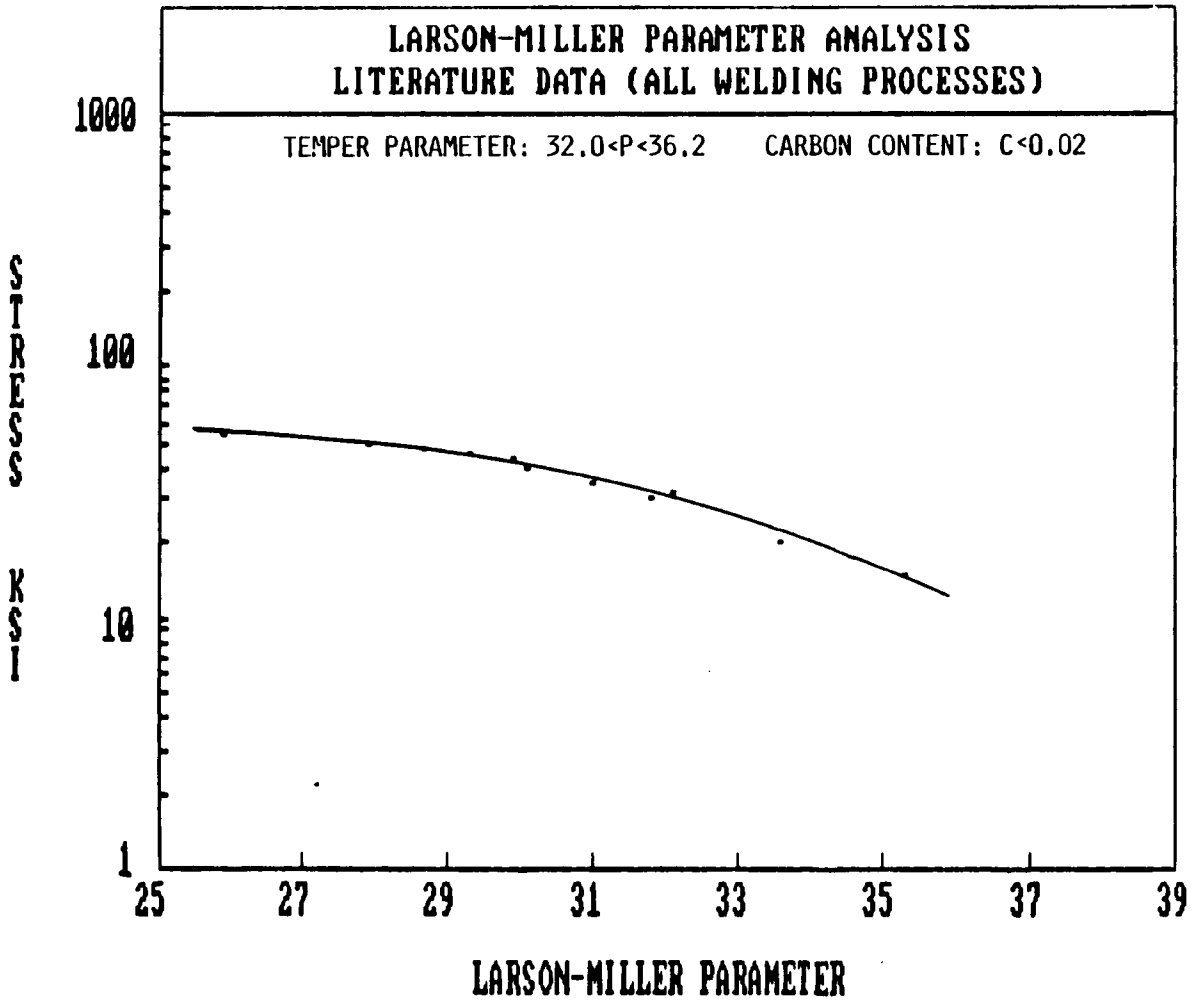


Figure A9. Larson-Miller parameter analysis of PWHT 2-1/4Cr-1Mo weld metal (32.0<P<36.2, C<0.02) determined from literature data for weld metal deposited by a variety of welding processes.

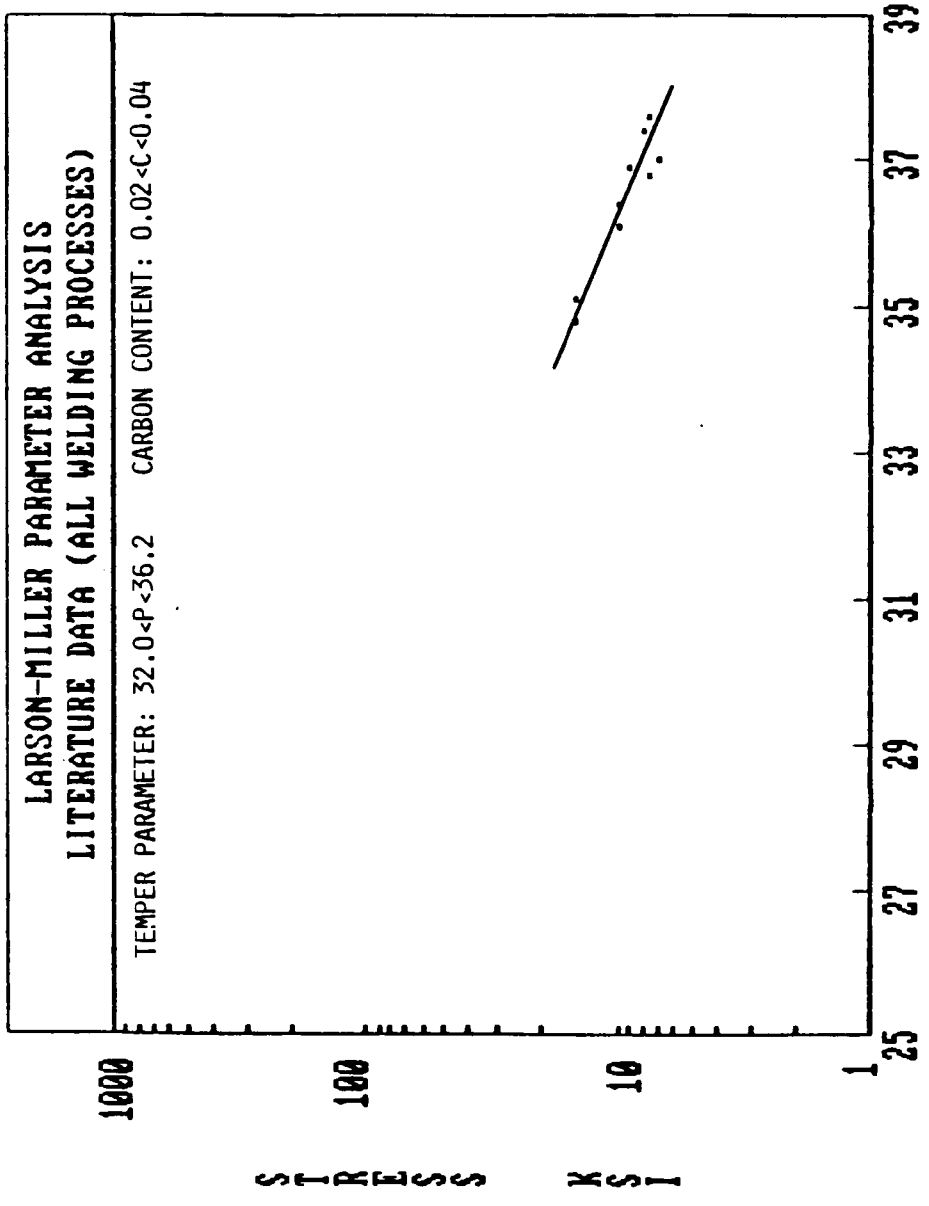


Figure A10. Larson-Miller parameter analysis of PWHT 2-1/4Cr-1Mo weld metal (32.0<P<36.2, 0.02<C<0.04) determined from literature data for weld metal deposited by a variety of welding processes.

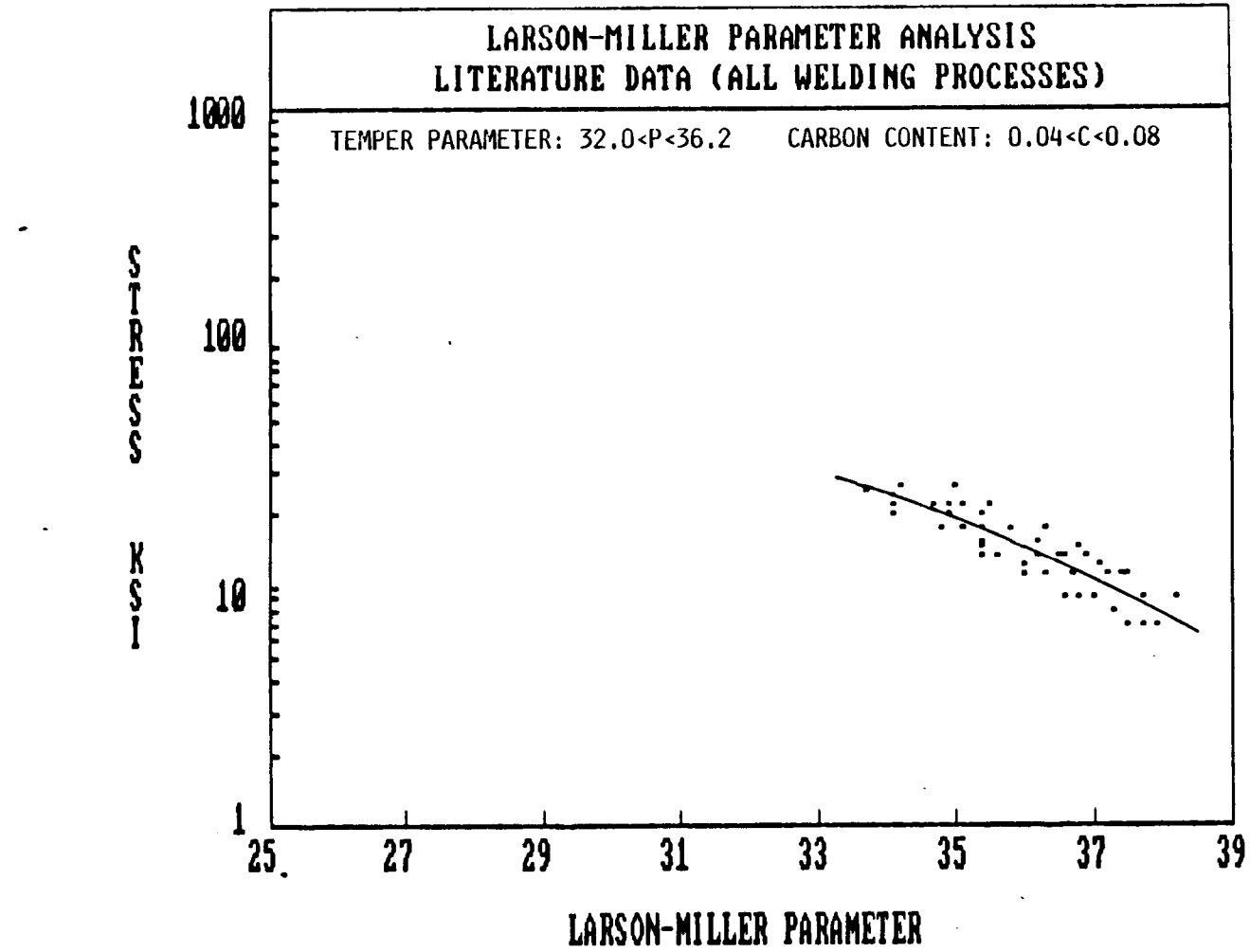


Figure All. Larson-Miller parameter analysis of PWHT 2-1/4Cr-1Mo weld metal (32.0<P<36.2, 0.04<C<0.08) determined from literature data for weld metal deposited by a variety of welding processes.

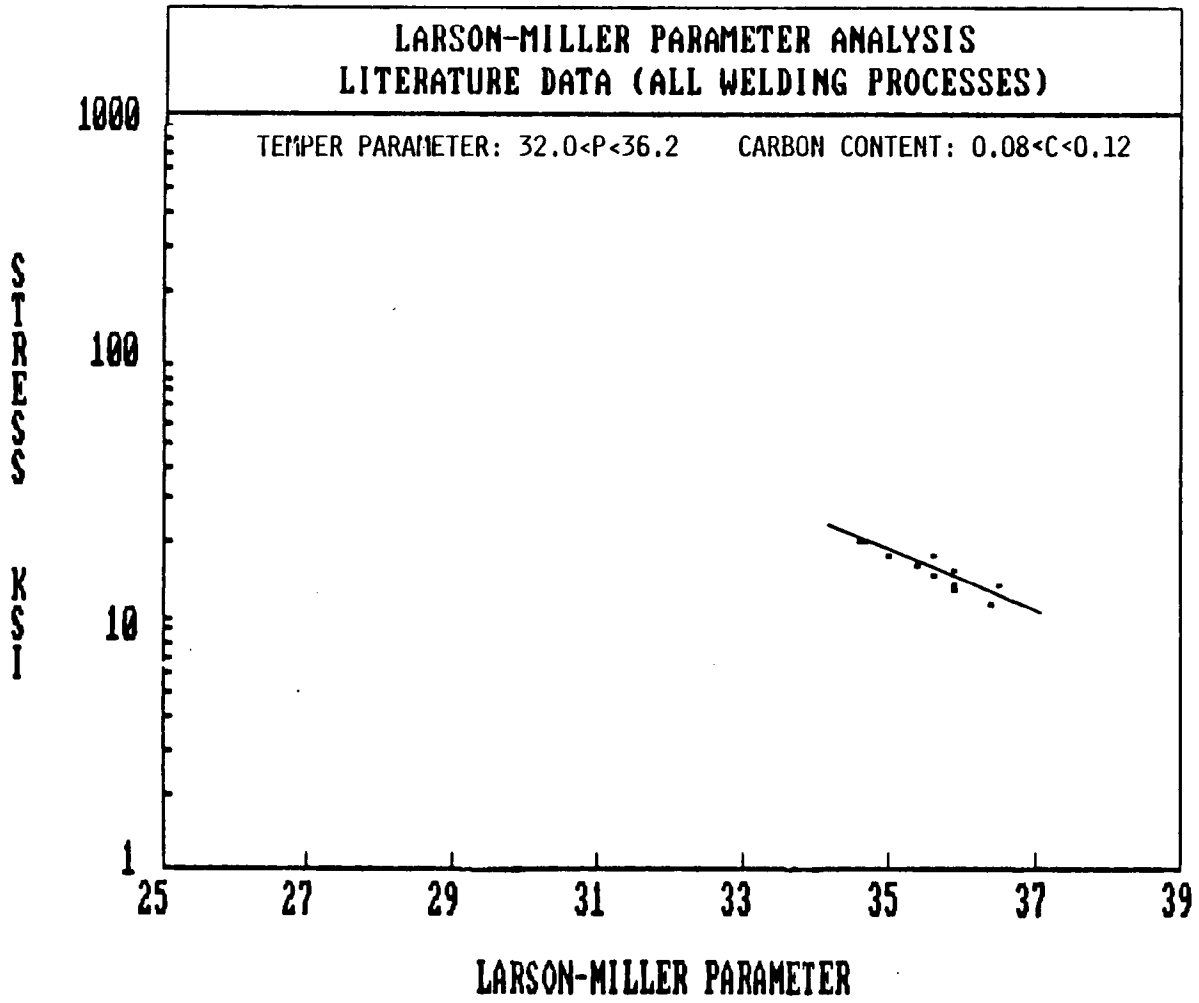


Figure A12. Larson-Miller parameter analysis of PWHT 2-1/4Cr-1Mo weld metal (32.0<P<36.2, 0.08<C<0.12) determined from literature data for weld metal deposited by a variety of welding processes.

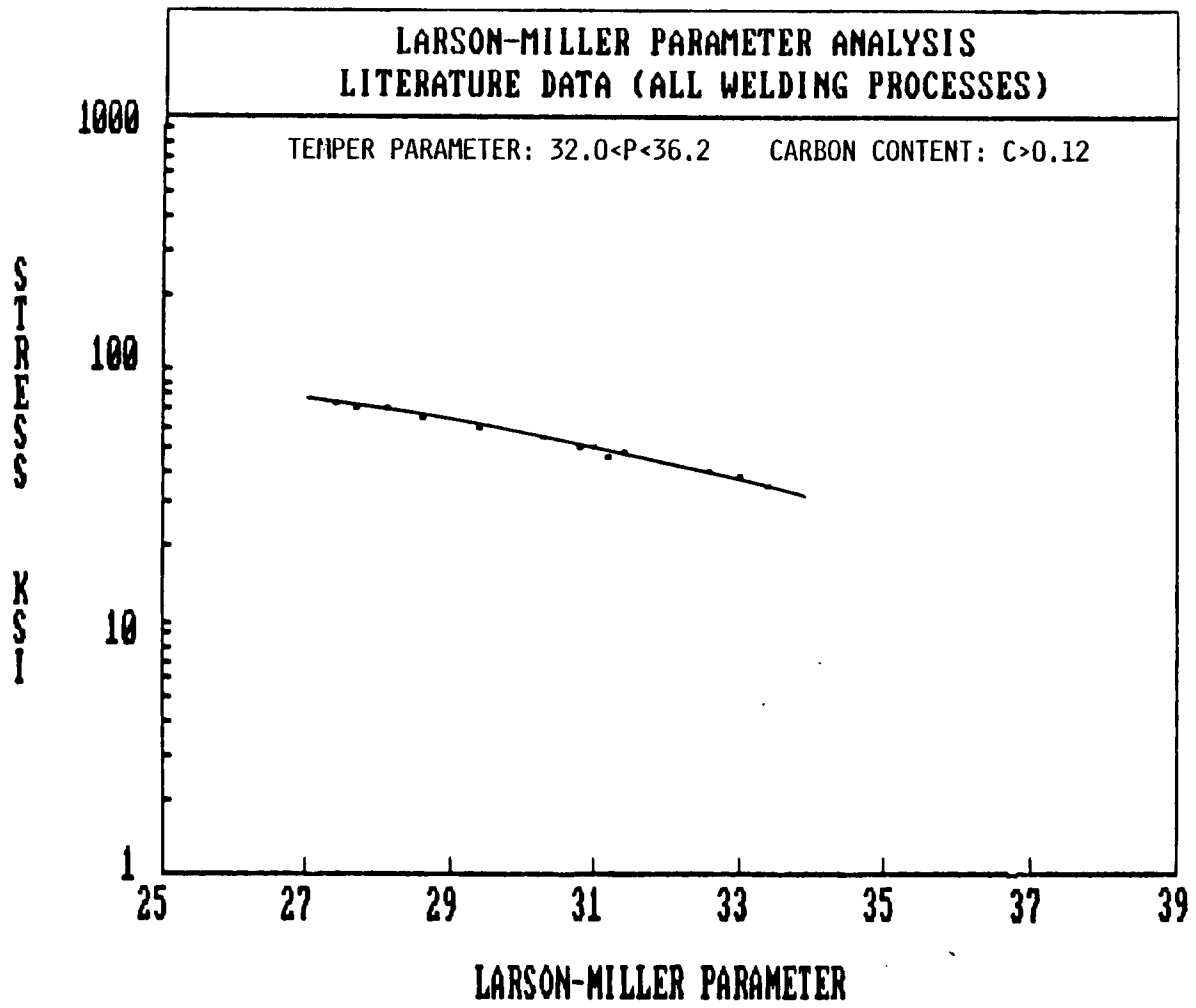


Figure A13. Larson-Miller parameter analysis of PWHT 2-1/4Cr-1Mo weld metal (32.0<P<36.2, C>0.12) determined from literature data for weld metal deposited by a variety of welding processes.

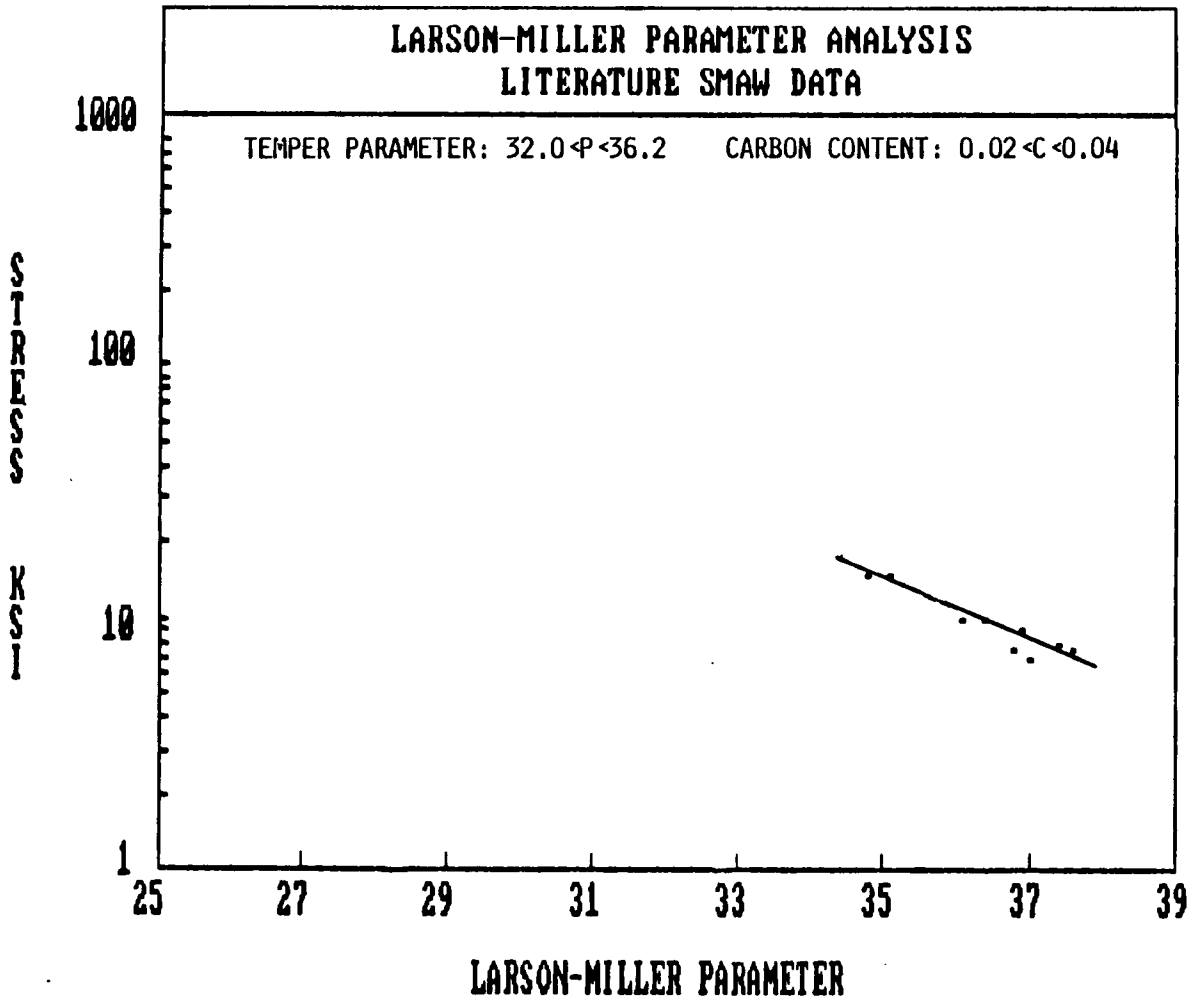


Figure A14. Larson-Miller parameter analysis of PWHT 2-1/4Cr-1Mo SMA weld metal (32.0<P<36.2, 0.02<C<0.04) determined from literature data.

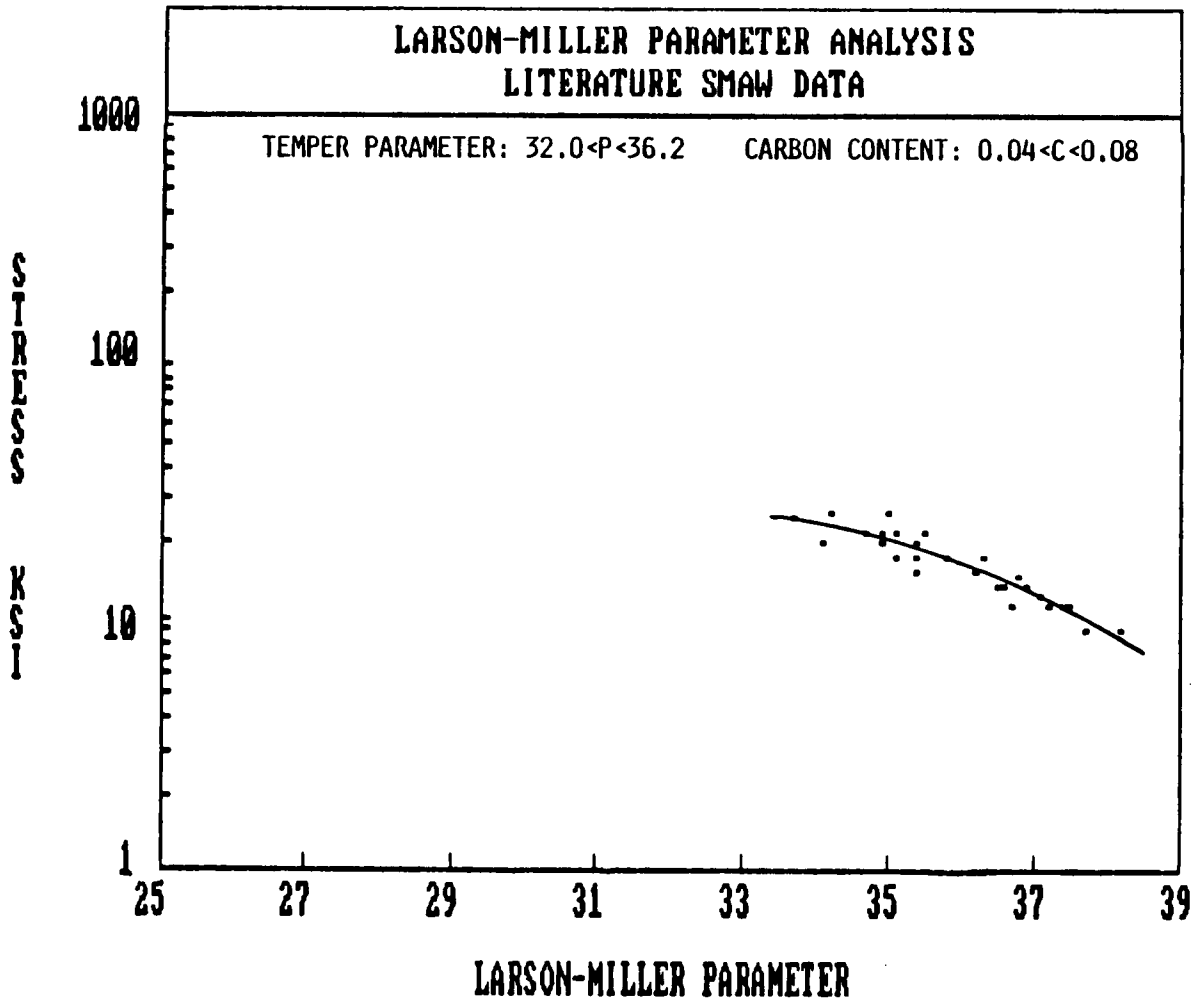


Figure A15. Larson-Miller parameter analysis of PWHT 2-1/4Cr-1Mo SMA weld metal (32.0<P<36.2, 0.04<C<0.08) determined from literature data.

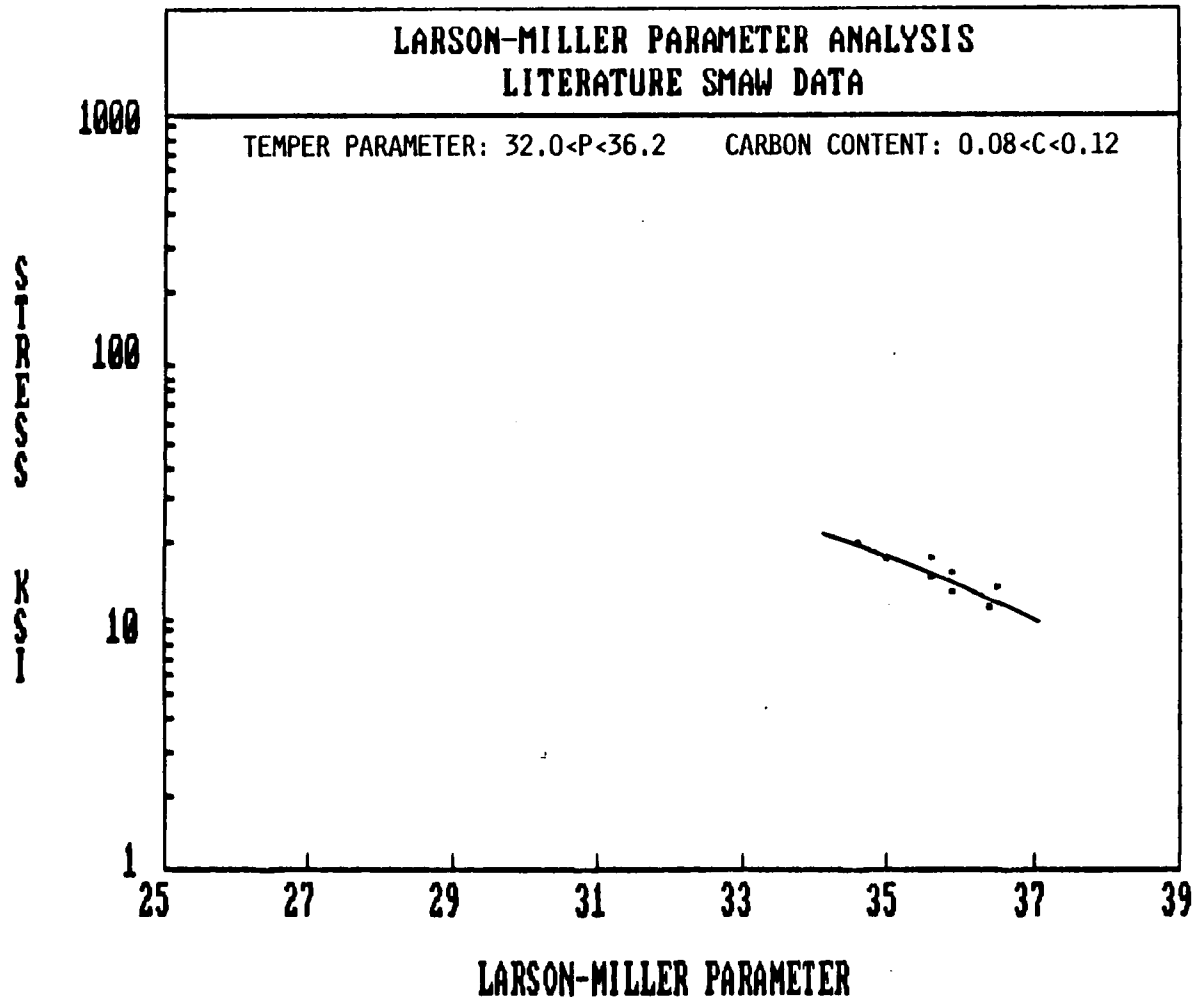


Figure A16. Larson-Miller parameter analysis of PWHT 2-1/4Cr-1Mo SMA weld metal (32.0<P<36.2, 0.08<C<0.12) determined from literature data.

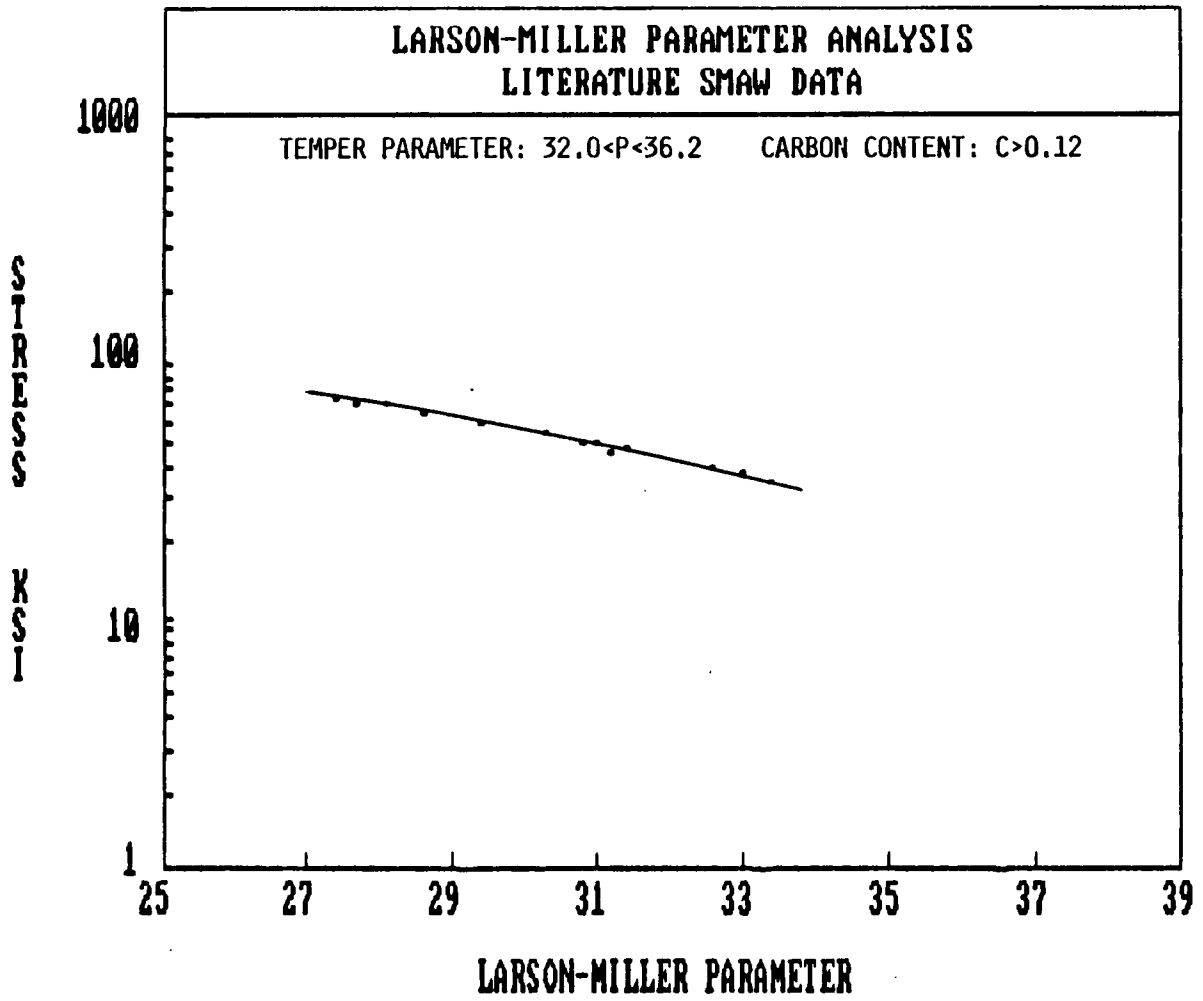


Figure A17. Larson-Miller parameter analysis of PWHT 2-1/4Cr-1Mo SMA weld metal (32.0<P<36.2, C>0.12) determined from literature data.

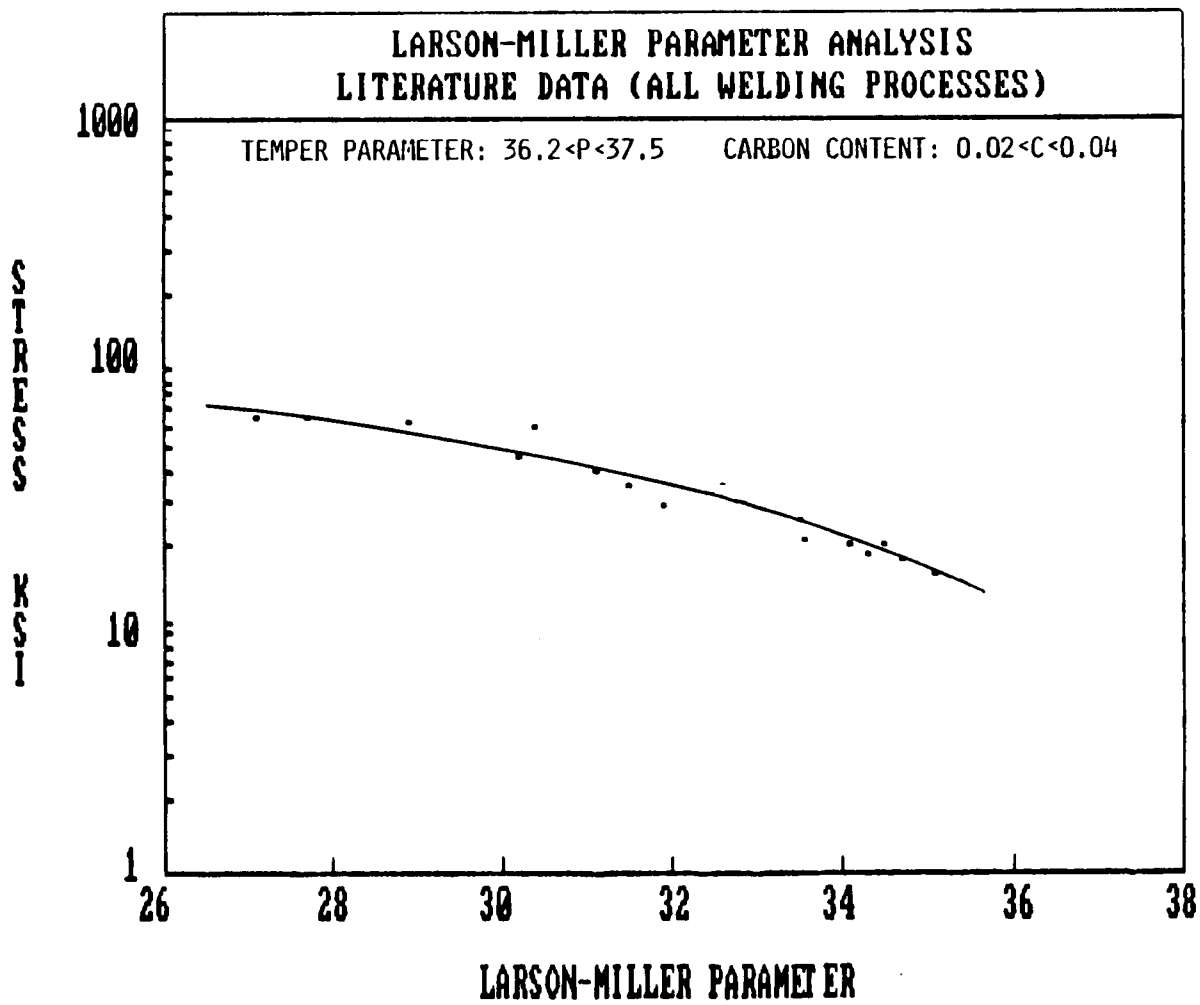


Figure A18. Larson-Miller parameter analysis of PWHT 2-1/4Cr-1Mo weld metal (36.2<P<37.5, 0.02<C<0.04) determined from literature data for weld metal deposited by a variety of welding processes.

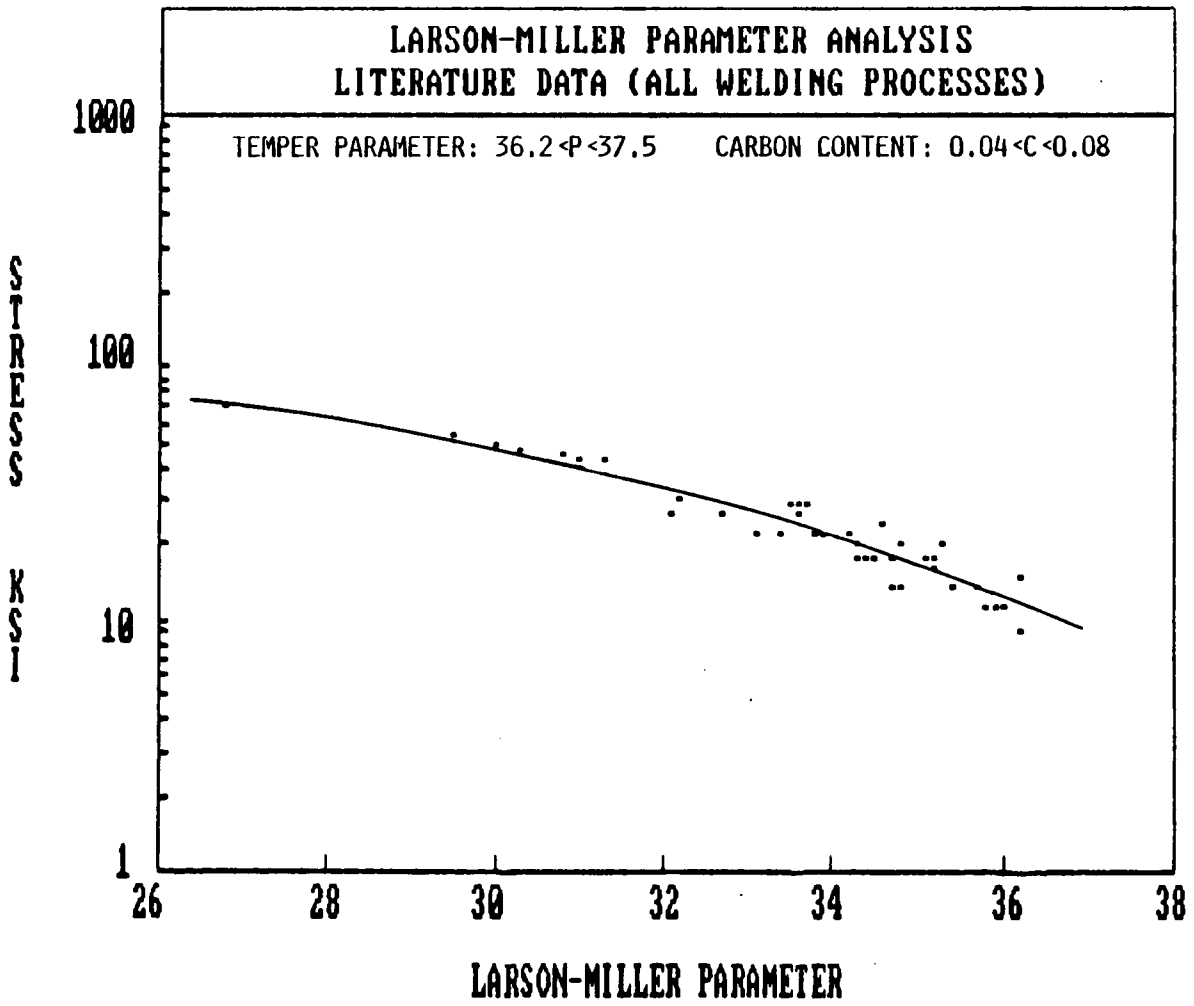


Figure A19. Larson-Miller parameter analysis of PWHT 2-1/4Cr-1Mo weld metal (36.2<P<37.5, 0.04<C<0.08) determined from literature data for weld metal deposited by a variety of welding processes.

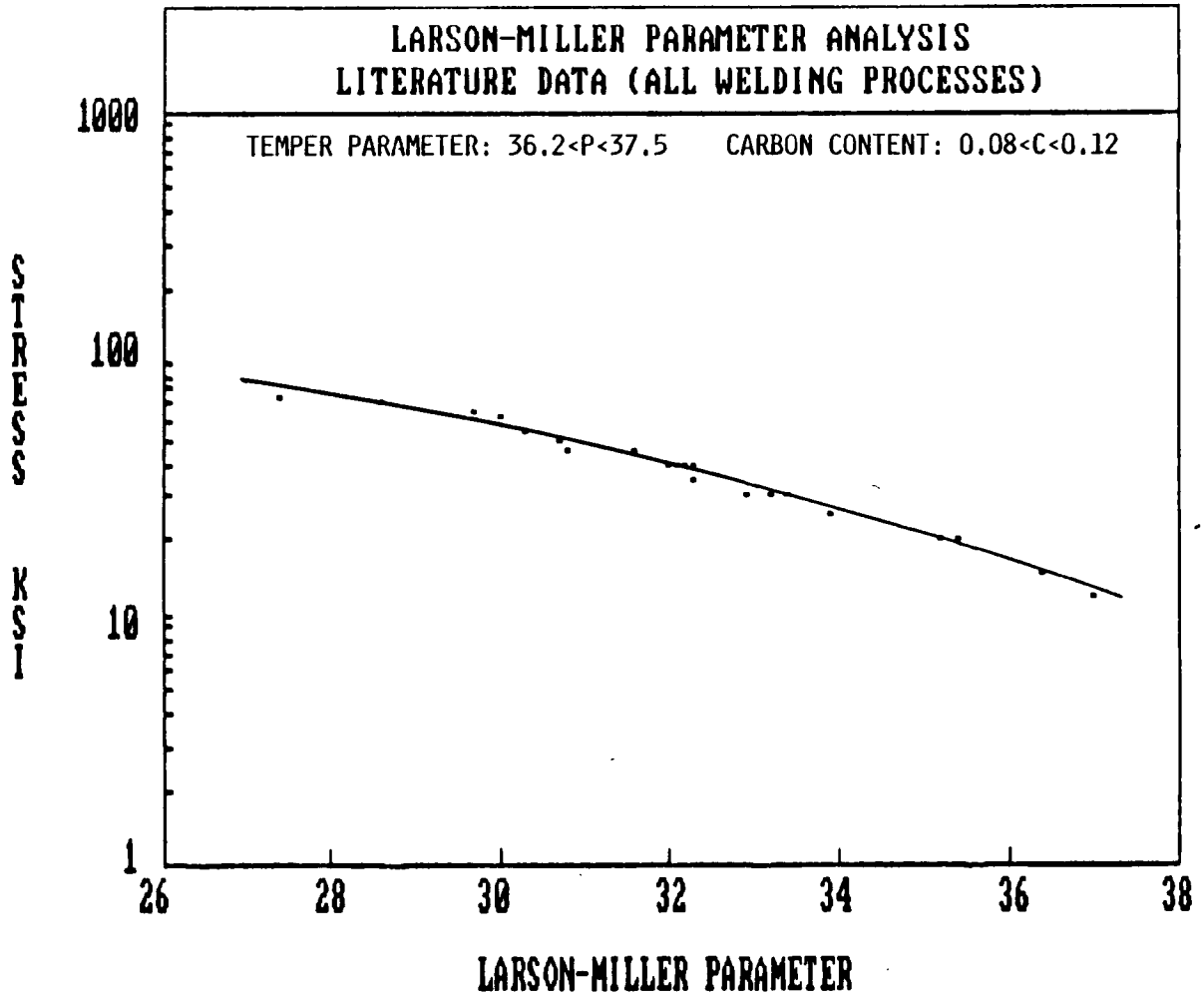


Figure A20. Larson-Miller parameter analysis of PWHT 2-1/4Cr-1Mo weld metal (36.2<P<37.5, 0.08<C<0.12) determined from literature data for weld metal deposited by a variety of welding processes.

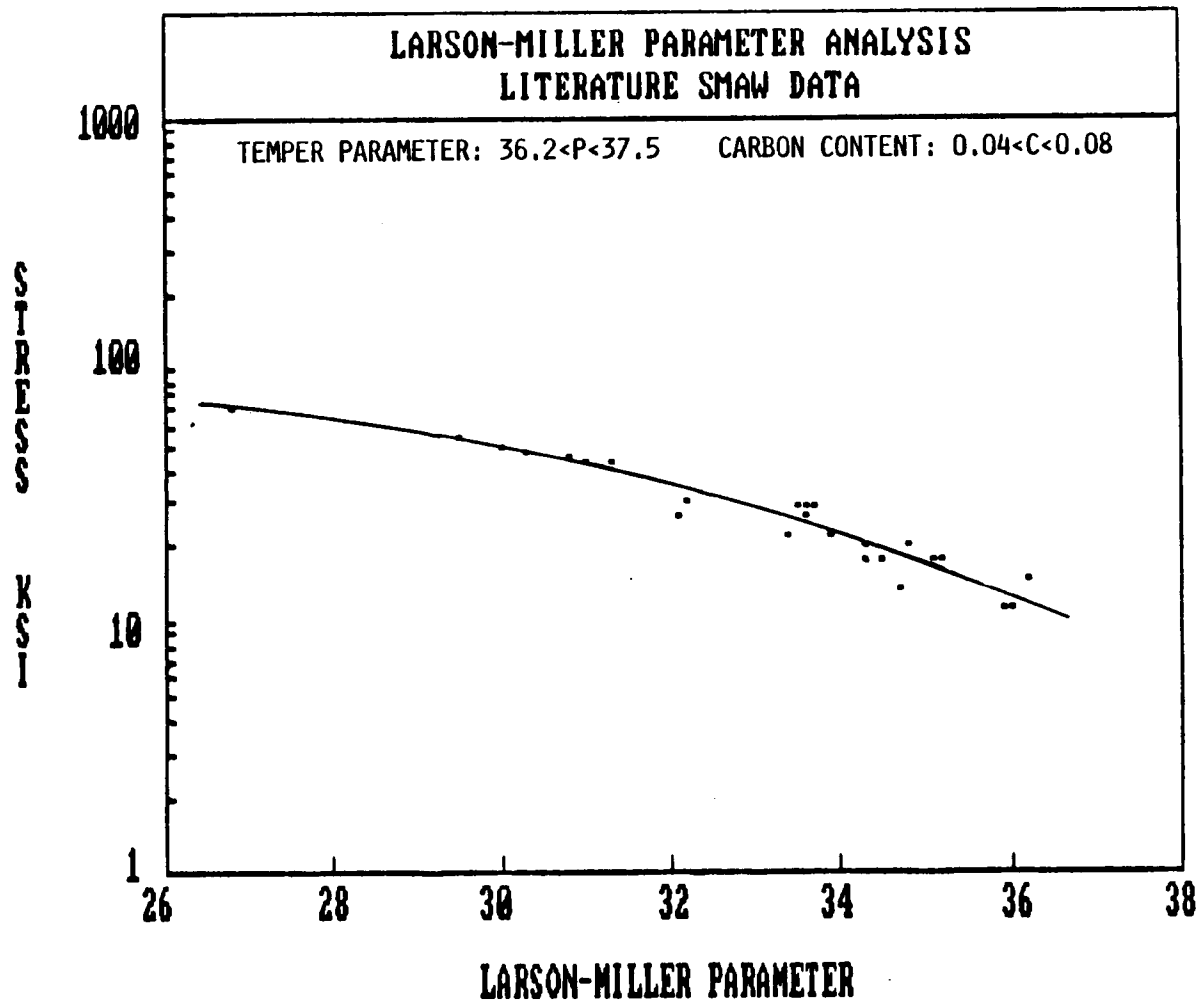


Figure A21. Larson-Miller parameter analysis of PWHT 2-1/4Cr-1Mo SMA weld metal (36.2<P<37.5, 0.04<C<0.08) determined from literature data.

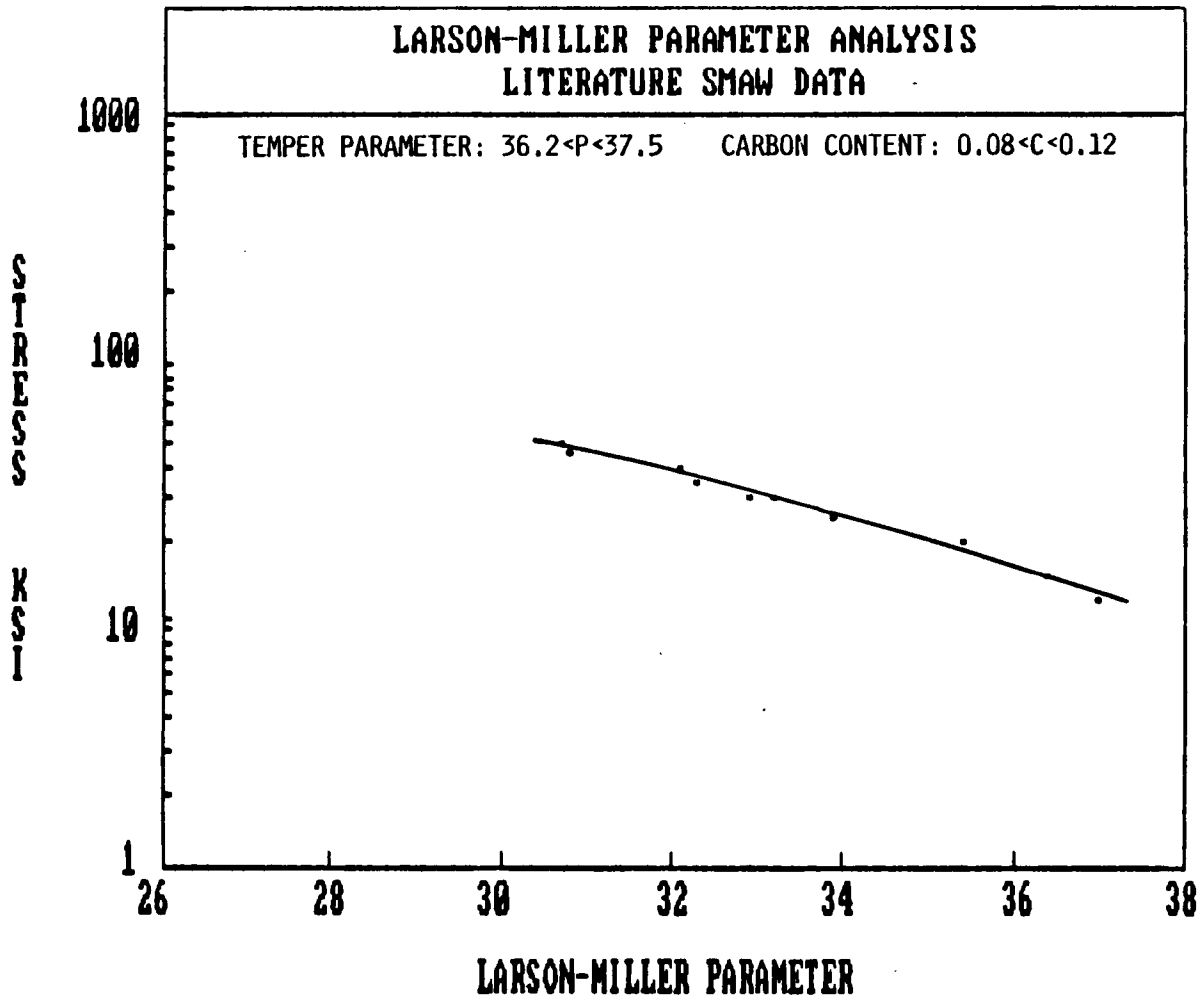


Figure A22. Larson-Miller parameter analysis of PWHT 2-1/4Cr-1Mo SMA weld metal (36.2<P<37.5, 0.08<C<0.12) determined from literature data.

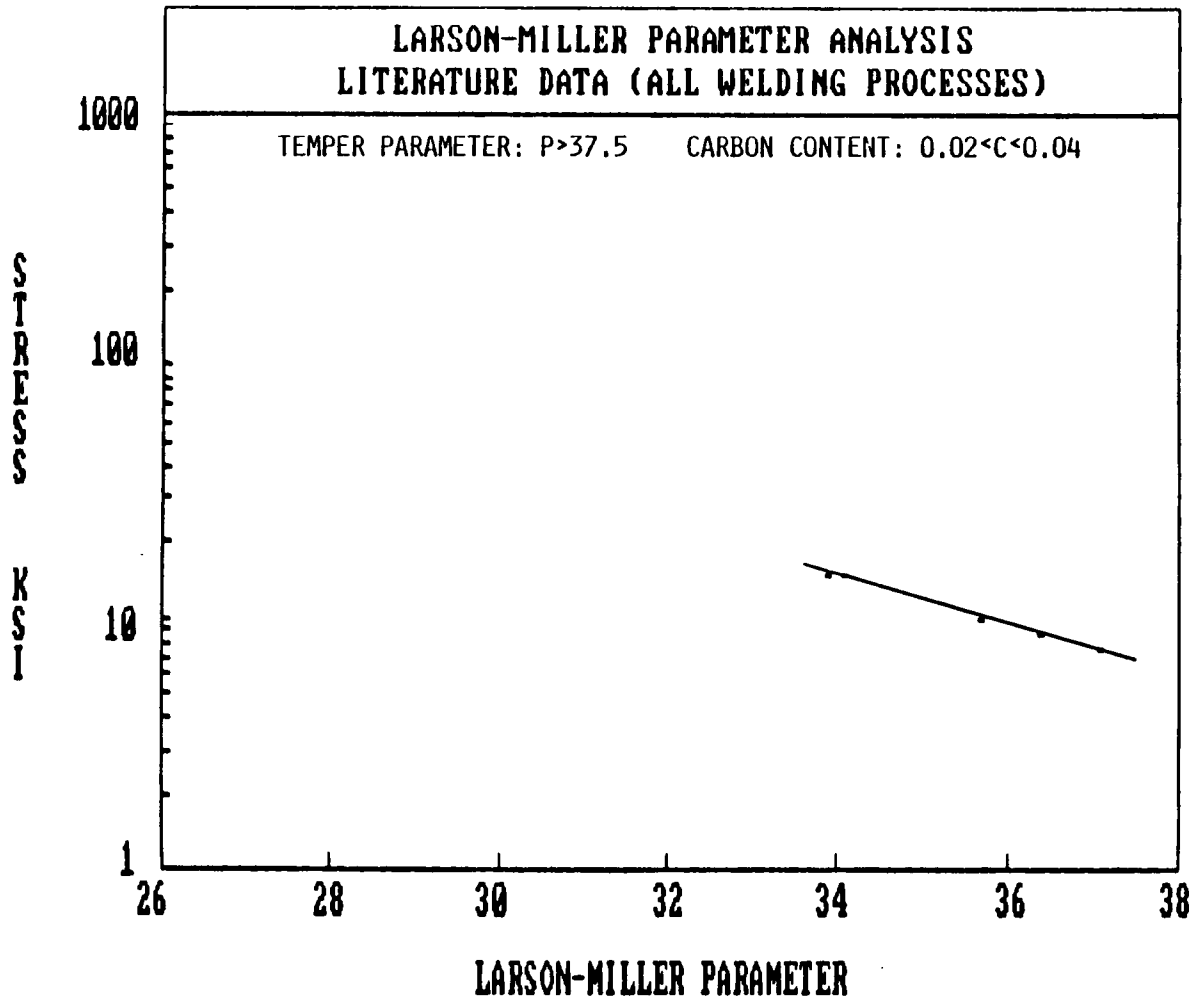


Figure A23. Larson-Miller parameter analysis of PWHT 2-1/4Cr-1Mo weld metal (P>37.5, 0.02<C<0.04) determined from literature data for weld metal deposited by a variety of welding processes.

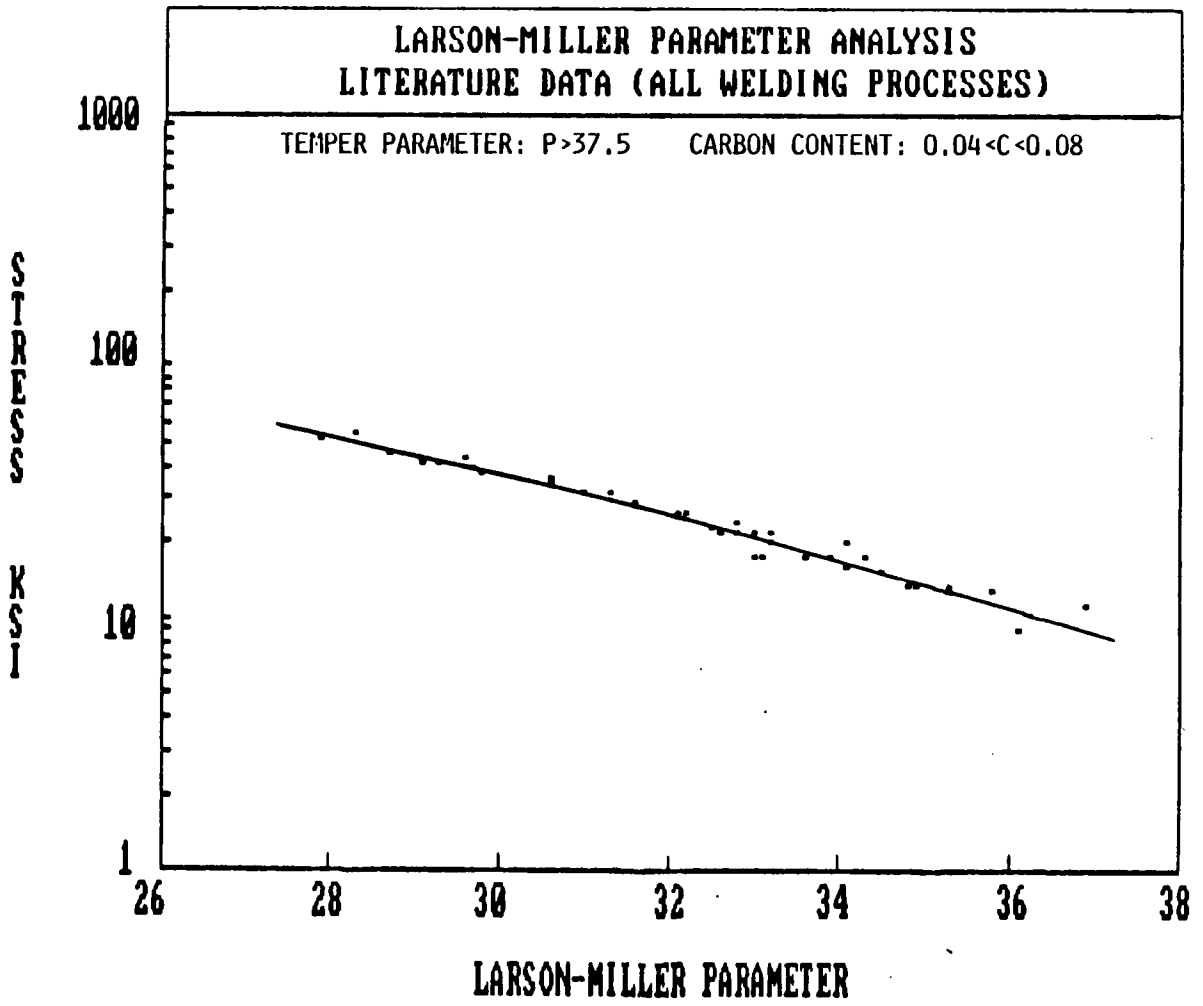


Figure A24. Larson-Miller parameter analysis of PWHT 2-1/4Cr-1Mo weld metal (P>37.5, 0.04<C<0.08) determined from literature data for weld metal deposited by a variety of welding processes.

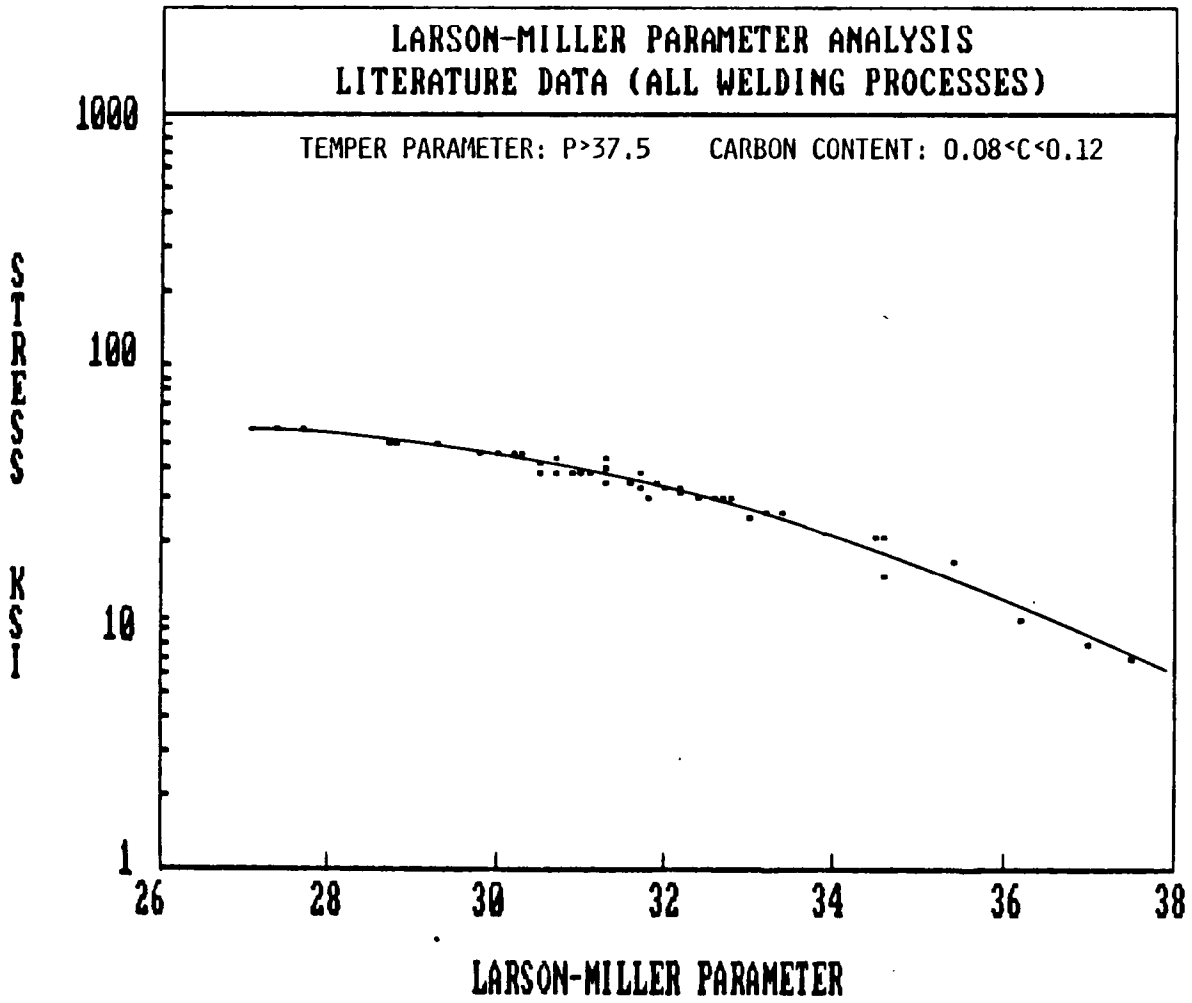


Figure A25. Larson-Miller parameter analysis of PWHT 2-1/4Cr-1Mo weld metal (P>37.5, 0.08<C<0.12) determined from literature data for weld metal deposited by a variety of welding processes.

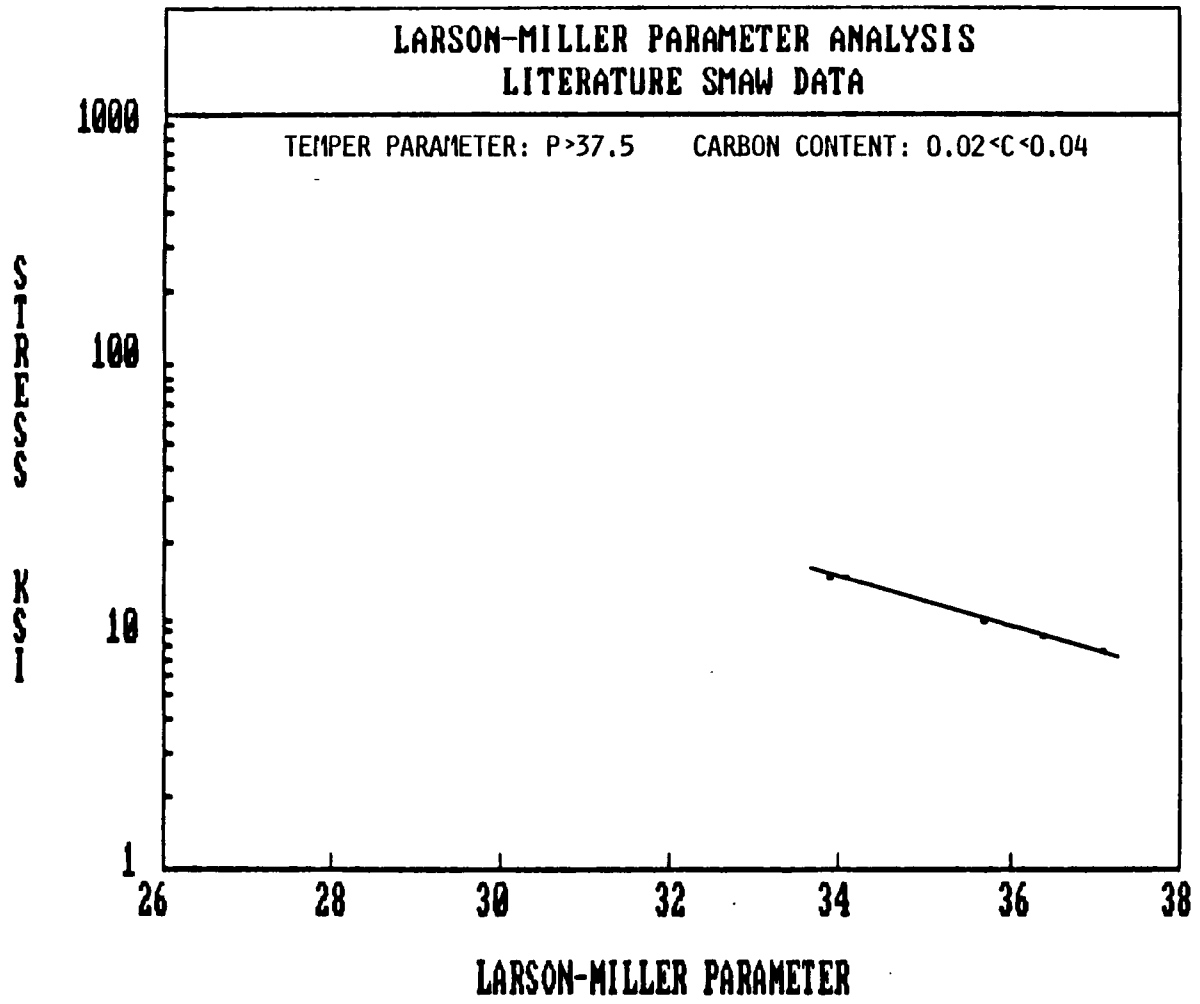


Figure A26. Larson-Miller parameter analysis of PWHT 2-1/4Cr-1Mo SMA weld metal (P>37.5, 0.02<C<0.04) determined from literature data.

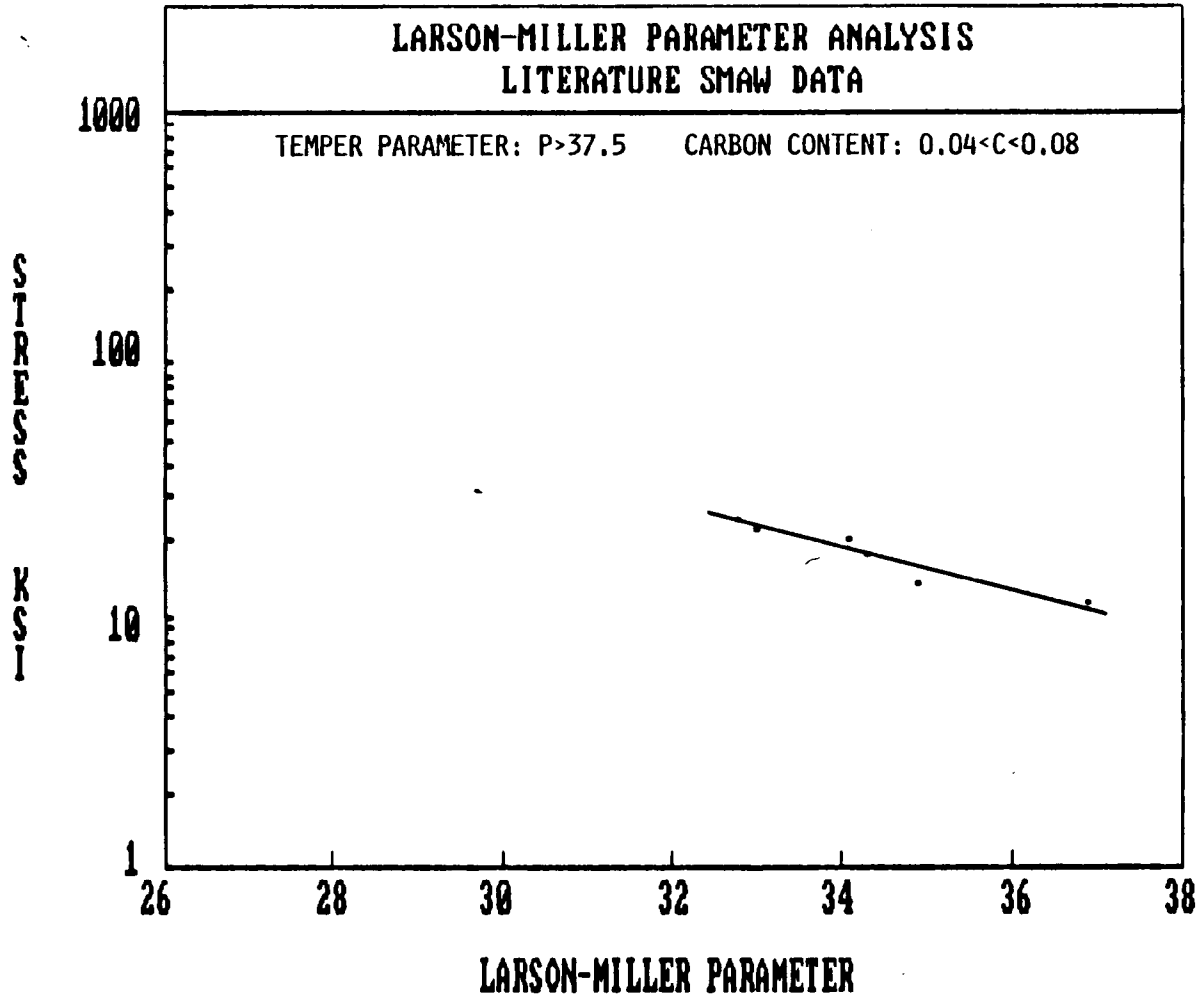


Figure A27. Larson-Miller parameter analysis of PWHT 2-1/4Cr-1Mo SMA weld metal (P>37.5, 0.04<C<0.08) determined from literature data.

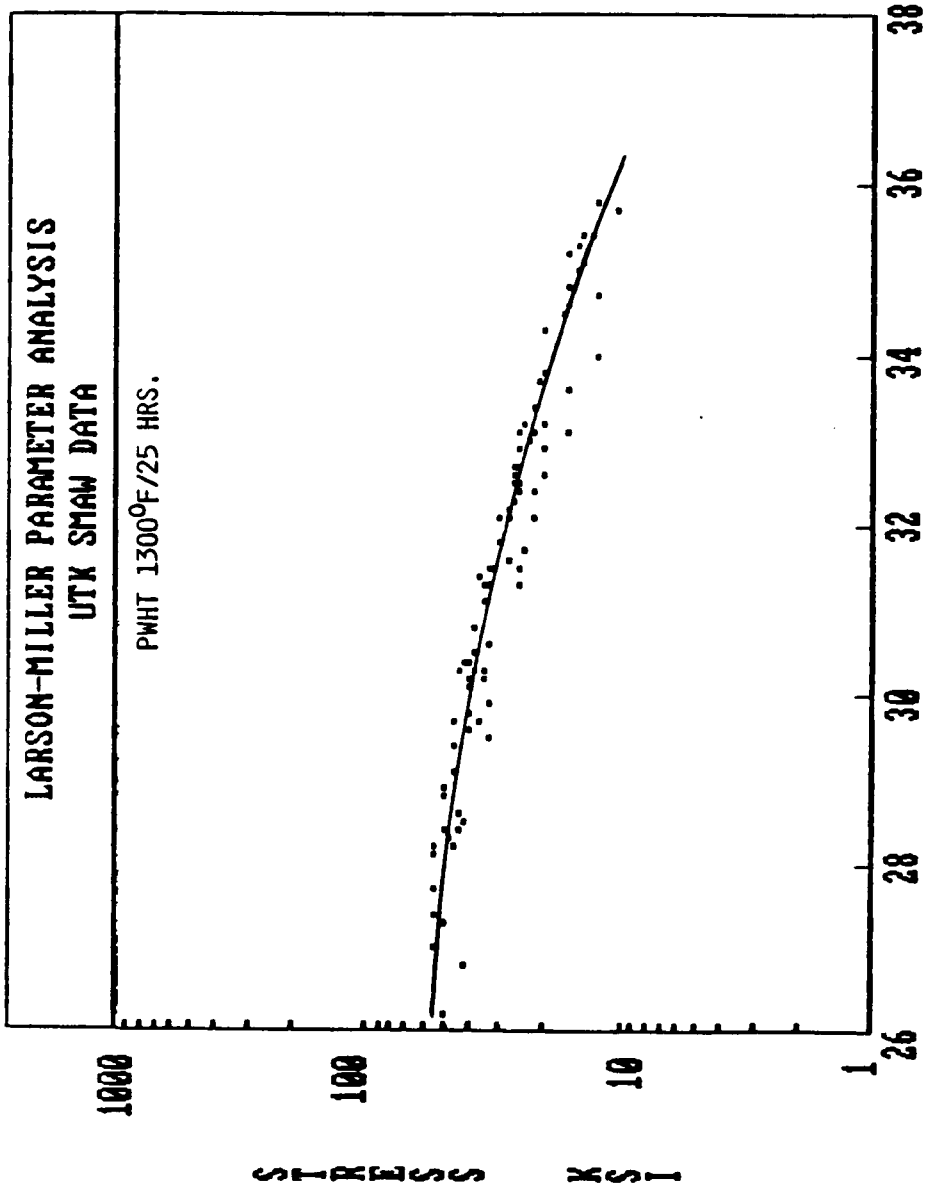


Figure A28. Larson-Miller parameter analysis of 2-1/4Cr-1Mo SMA weld metal PWHT 1300°F/25 hrs. (Class 2) determined from UTK data.

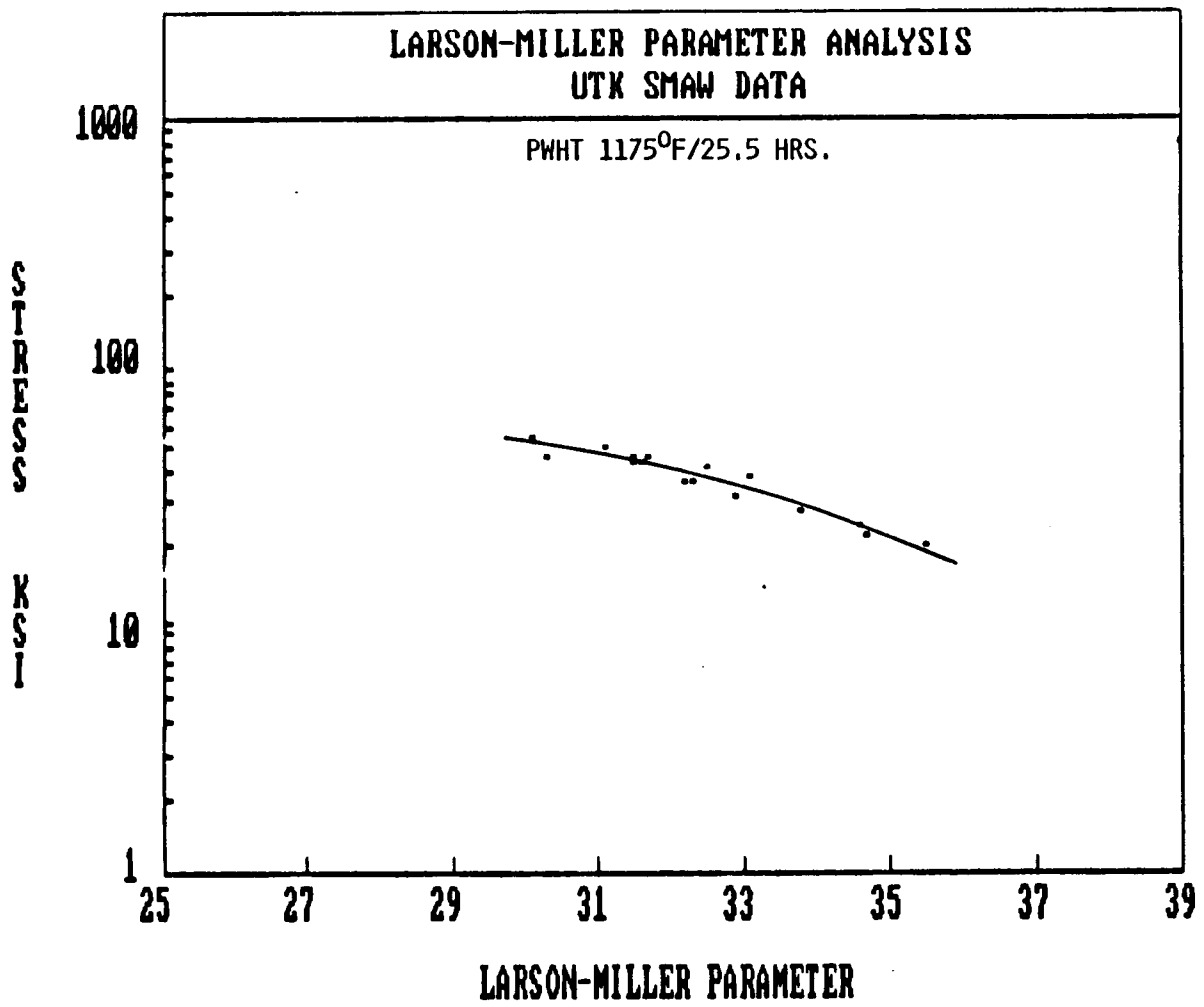


Figure A29. Larson-Miller parameter analysis of 2-1/4Cr-1Mo SMA weld metal PWHT 1175°F/25.5 hrs. (Class 3) determined from UTK data.

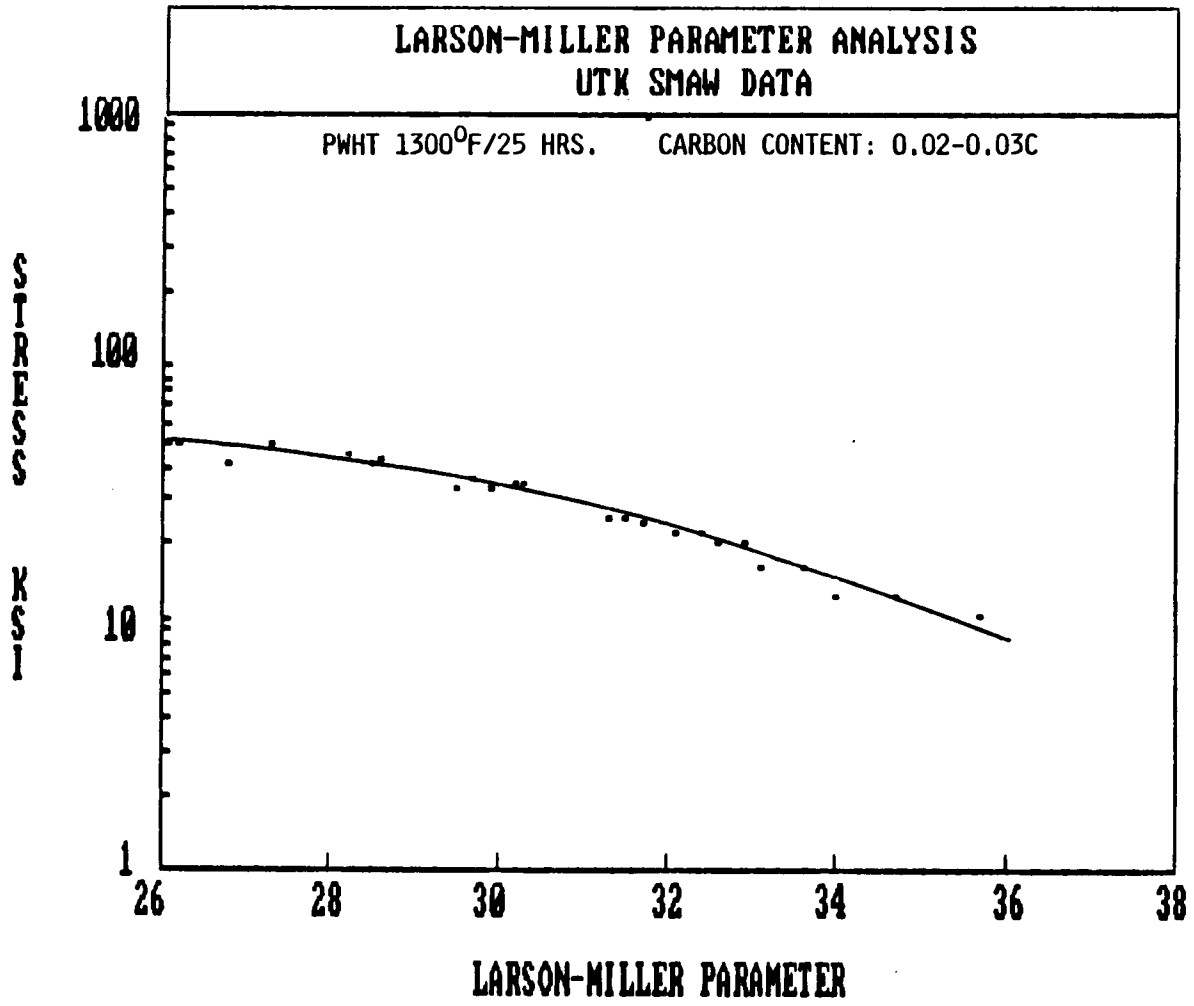


Figure A30. Larson-Miller parameter analysis of 2-1/4Cr-1Mo SMA weld metal PWHT 1300°F/25 hrs. (Class 2, 0.02-0.03C) determined from UTK data.

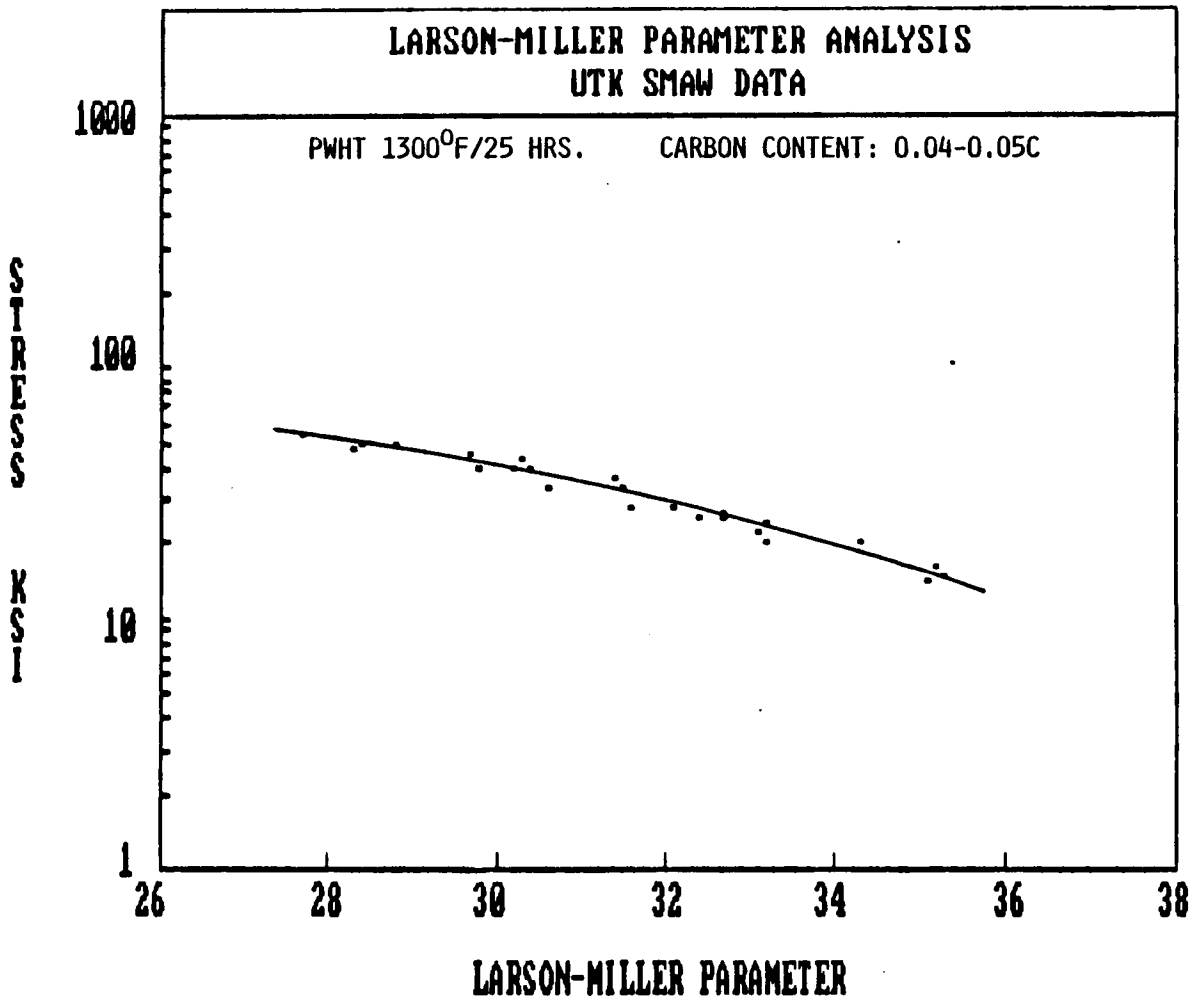


Figure A31. Larson-Miller parameter analysis of 2-1/4Cr-1Mo SMA weld metal PWHT 1300°F/25 hrs. (Class 2, 0.04-0.05C) determined from UTK data.

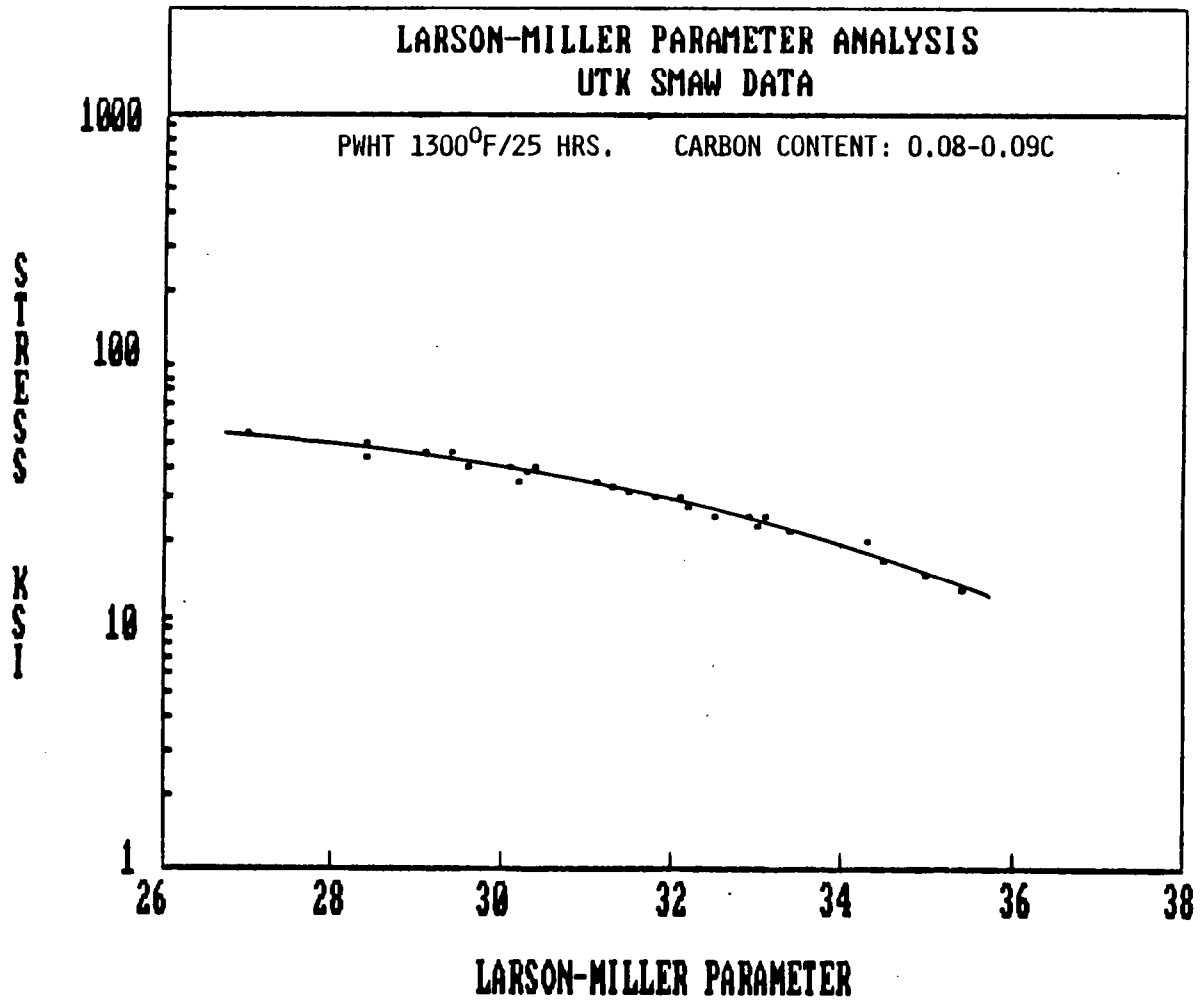


Figure A32. Larson-Miller parameter analysis of 2-1/4Cr-1Mo SMA weld metal PWHT 1300°F/25 hrs. (Class 2, 0.08-0.09C) determined from UTK data.

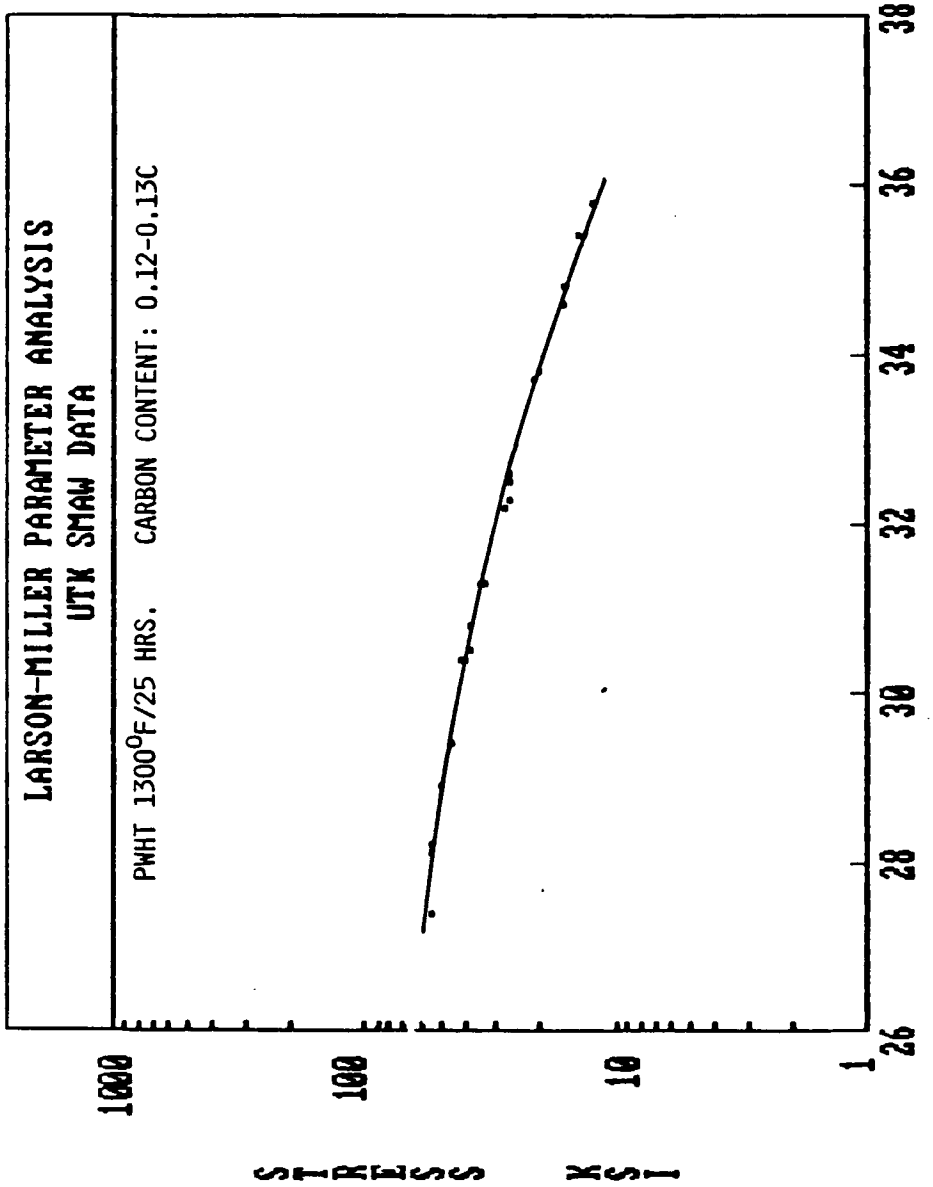


Figure A33. Larson-Miller parameter analysis of 2-1/4Cr-1Mo SMA weld metal PWHT 1300°F/25 hrs. (Class 2, 0.12-0.13C) determined from UTK data.

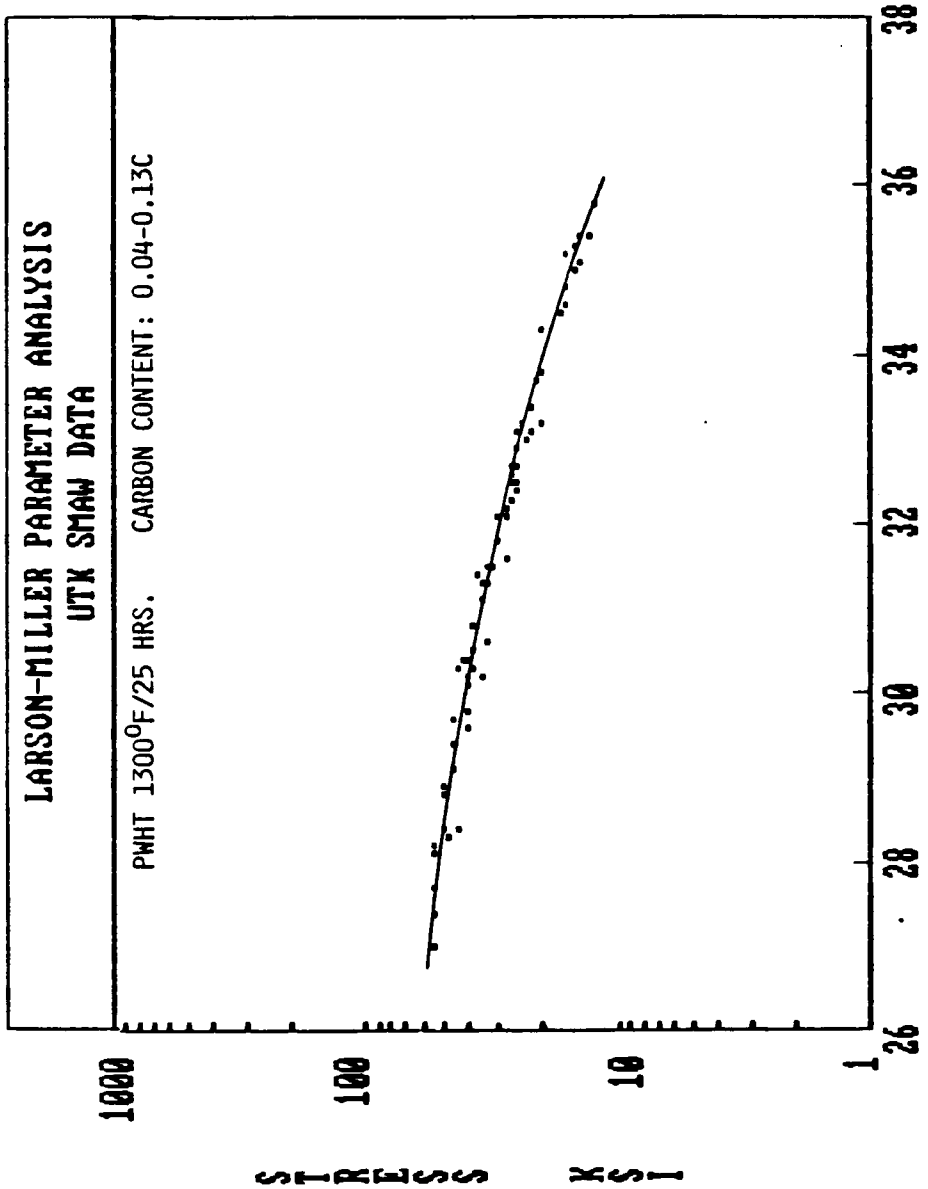


Figure A34. Larson-Miller parameter analysis of 2-1/4Cr-1Mo SMA weld metal PWHT 1300°F/25 hrs. (Class 2, 0.04-0.13C) determined from UTK data.

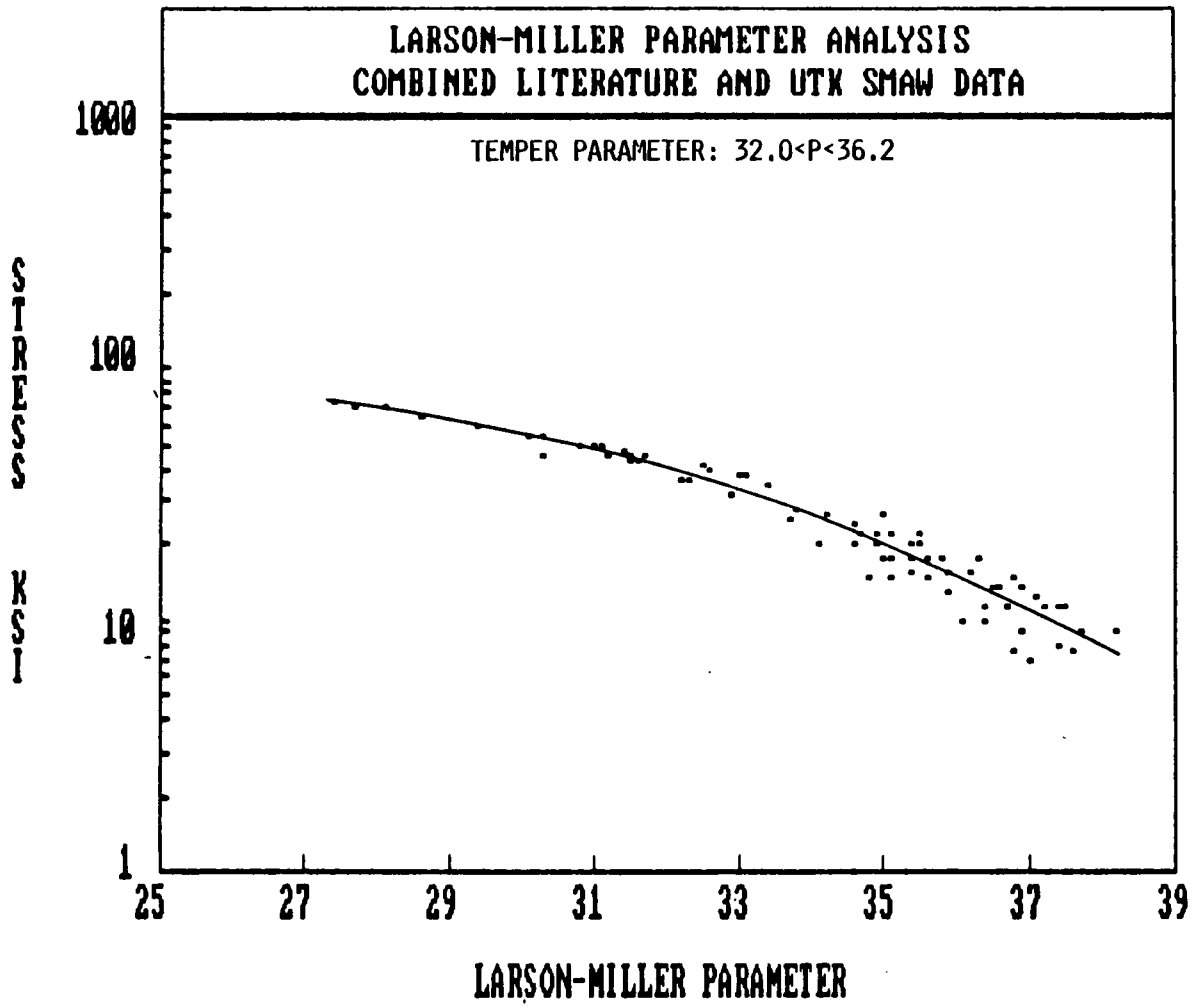


Figure A35. Larson-Miller parameter analysis of PWHT 2-1/4Cr-1Mo SMA weld metal (32.0<P<36.2) determined from combined literature and UTK data.

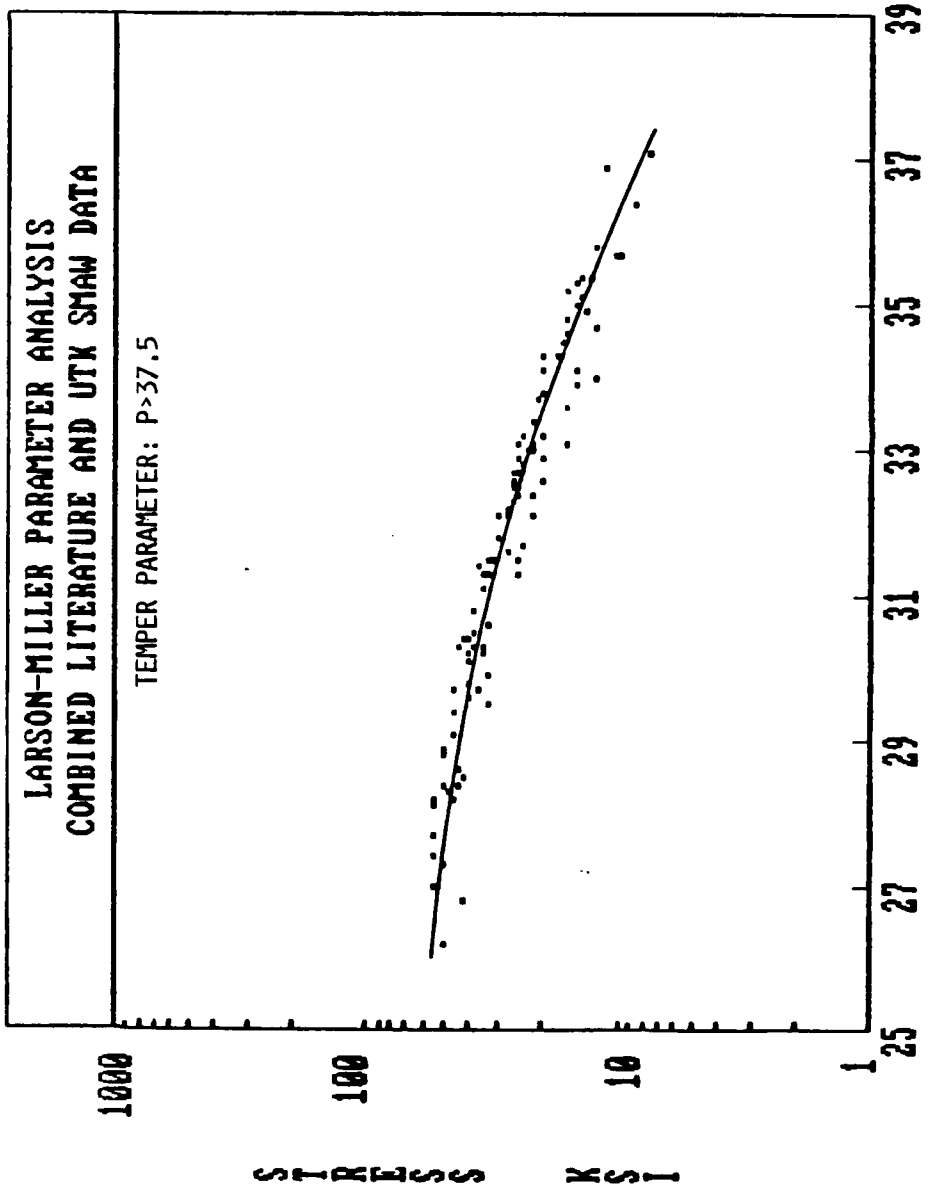


Figure A36. Larson-Miller parameter analysis of PWHT 2-1/4Cr-1Mo SMA weld metal (P>37.5) determined from combined literature and UTK data.

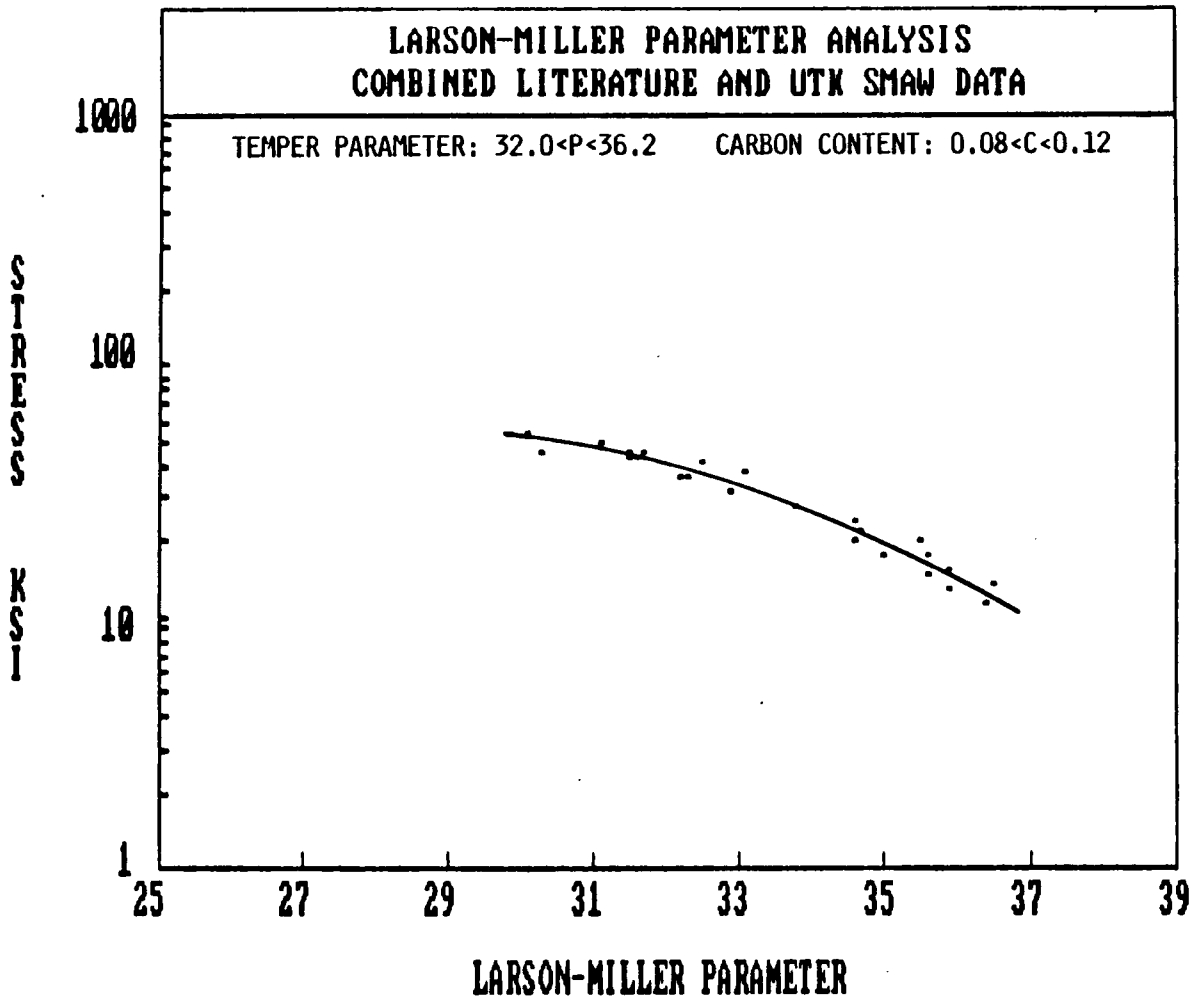


Figure A37. Larson-Miller parameter analysis of PWHT 2-1/4Cr-1Mo SMA weld metal (32.0<P<36.2, 0.08<C<0.12) determined from combined literature and UTK data.

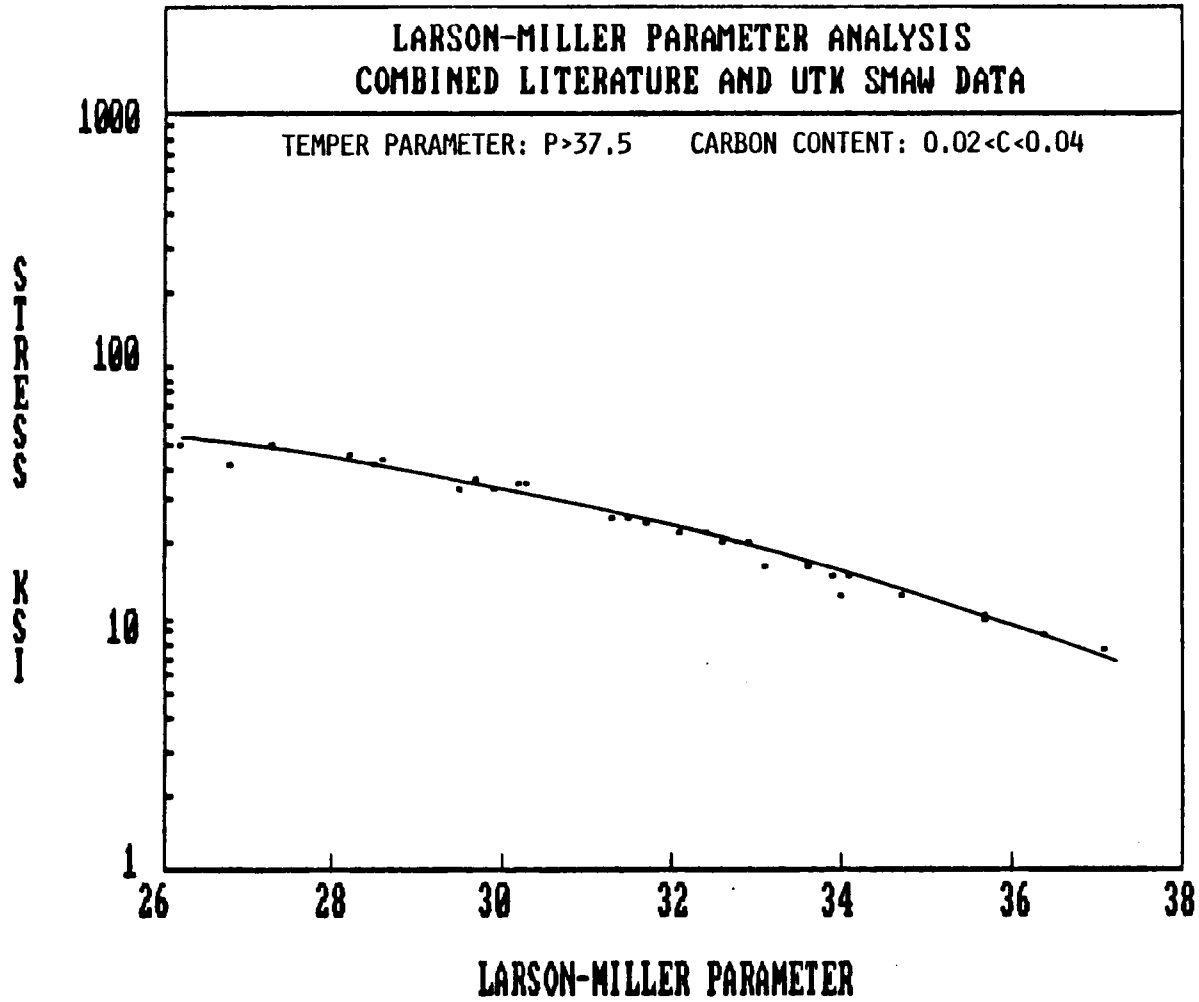


Figure A38. Larson-Miller parameter analysis of PWHT 2-1/4Cr-1Mo SMA weld metal (P>37.5, 0.02<C<0.04) determined from combined literature and UTK data.

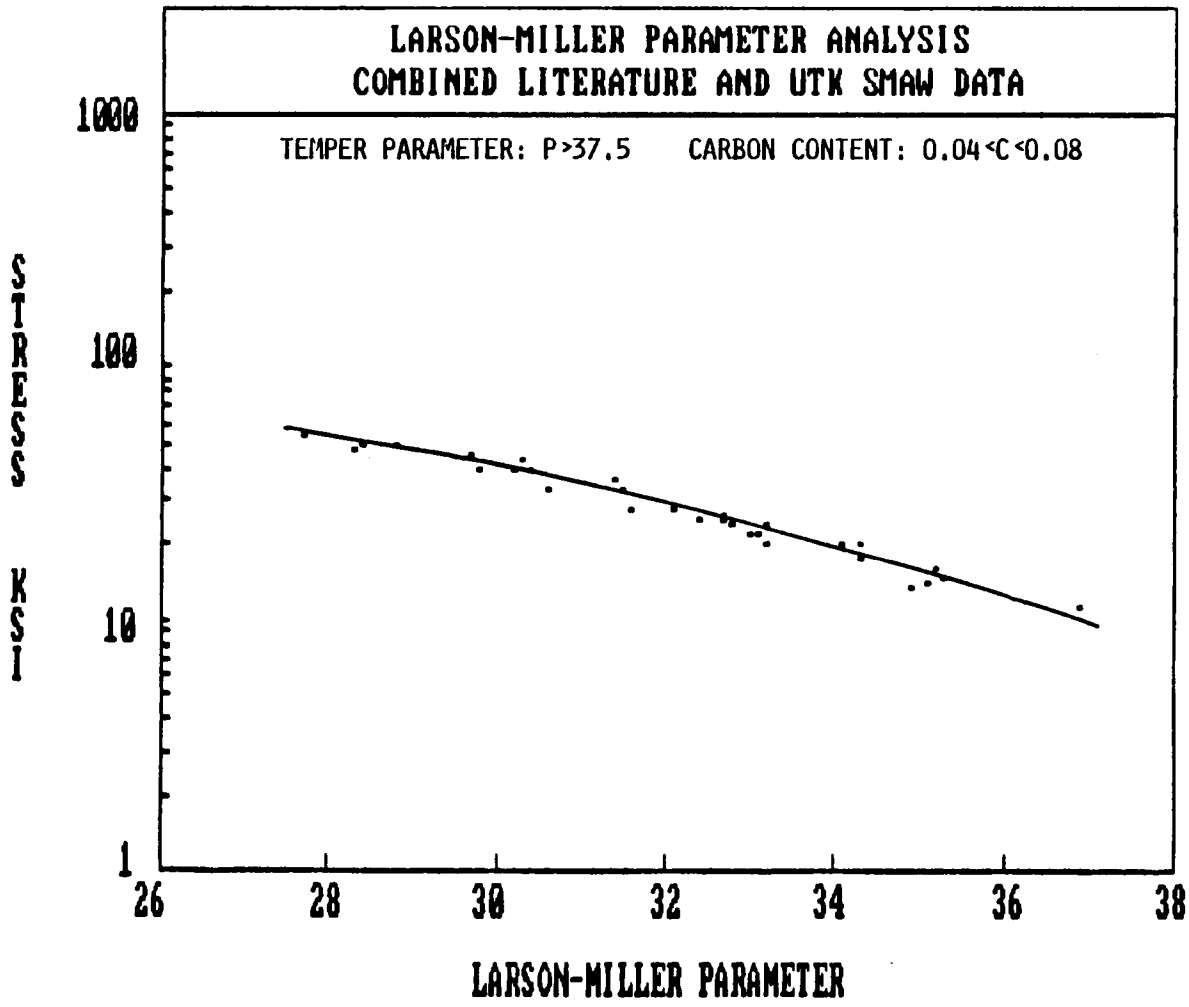


Figure A39. Larson-Miller parameter analysis of PWHT 2-1/4Cr-1Mo SMA weld metal (P>37.5, 0.04<C<0.08) determined from combined literature and UTK data.

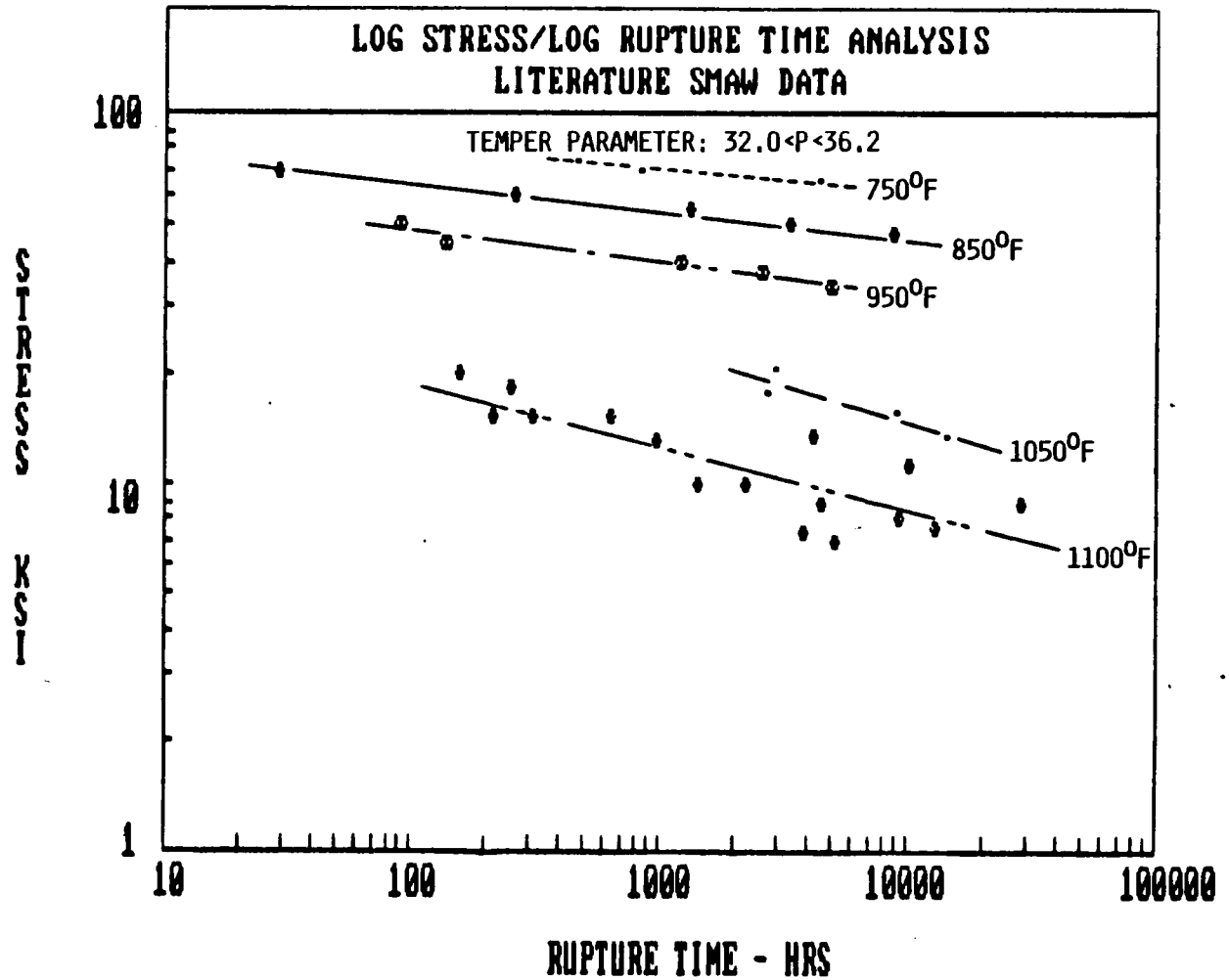


Figure A40. Log stress/log rupture time analysis of PWHT 2-1/4Cr-1Mo SMA weld metal (32.0<P<36.2) at 750, 850, 950, 1050, and 1100°F as determined from literature data.

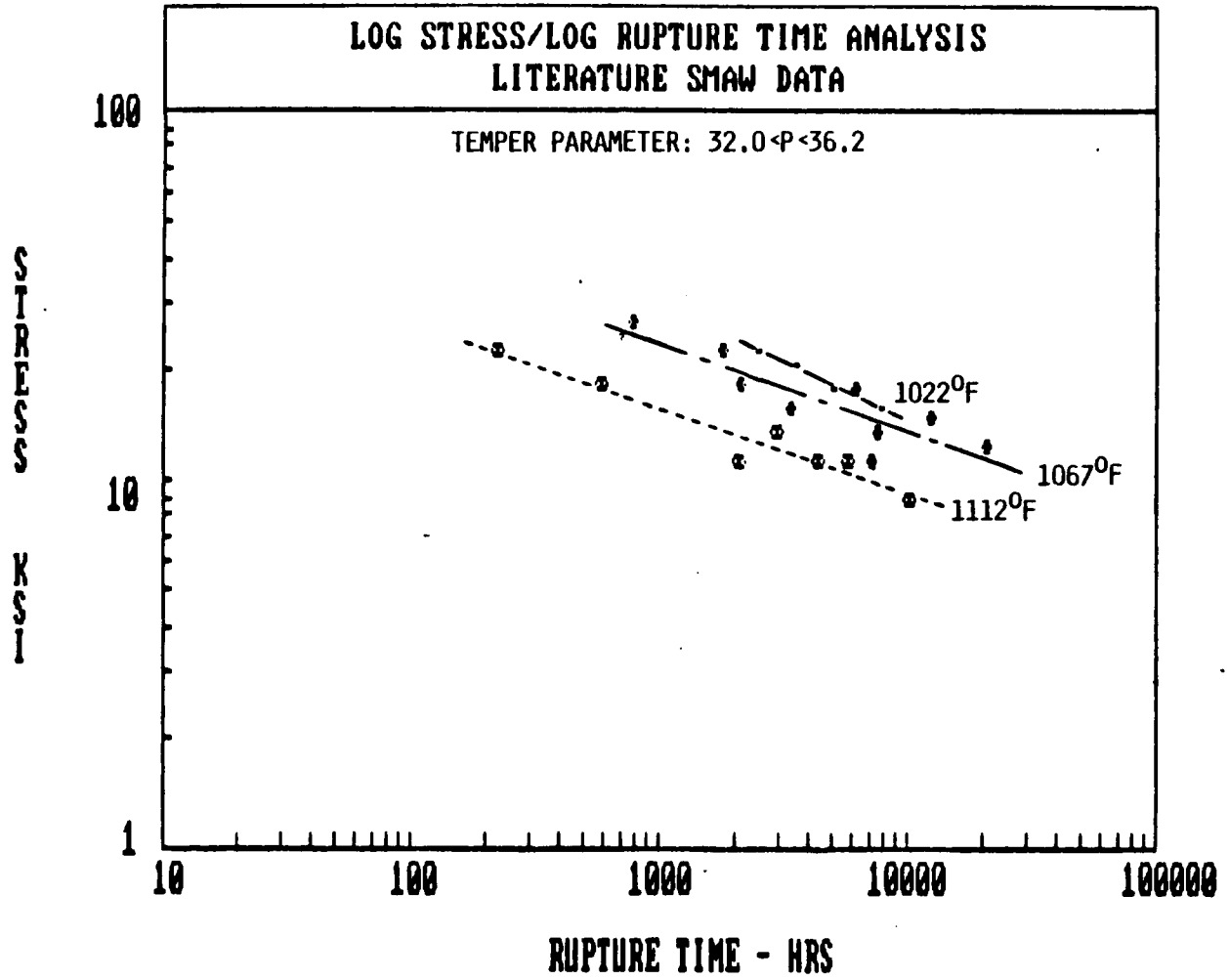


Figure A41. Log stress/log rupture time analysis of PWHT 2-1/4Cr-1Mo SMA weld metal (32.0<P<36.2) at 1022, 1067, and 1112°F as determined from literature data.

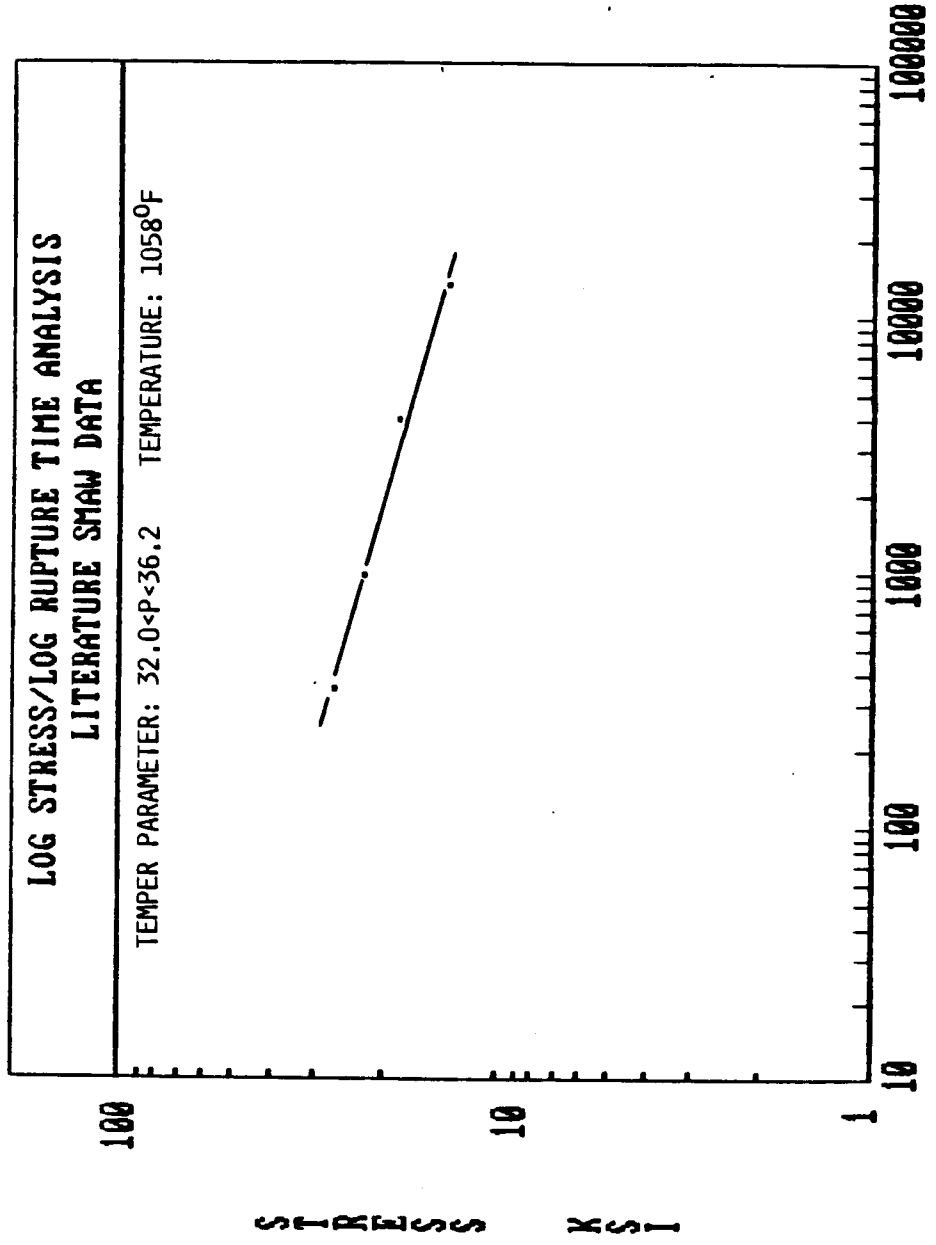


Figure A42. Log stress/log rupture time analysis of PWHT 2-1/4Cr-1Mo SMA weld metal (32.0<P<36.2) at 1058°F as determined from literature data.

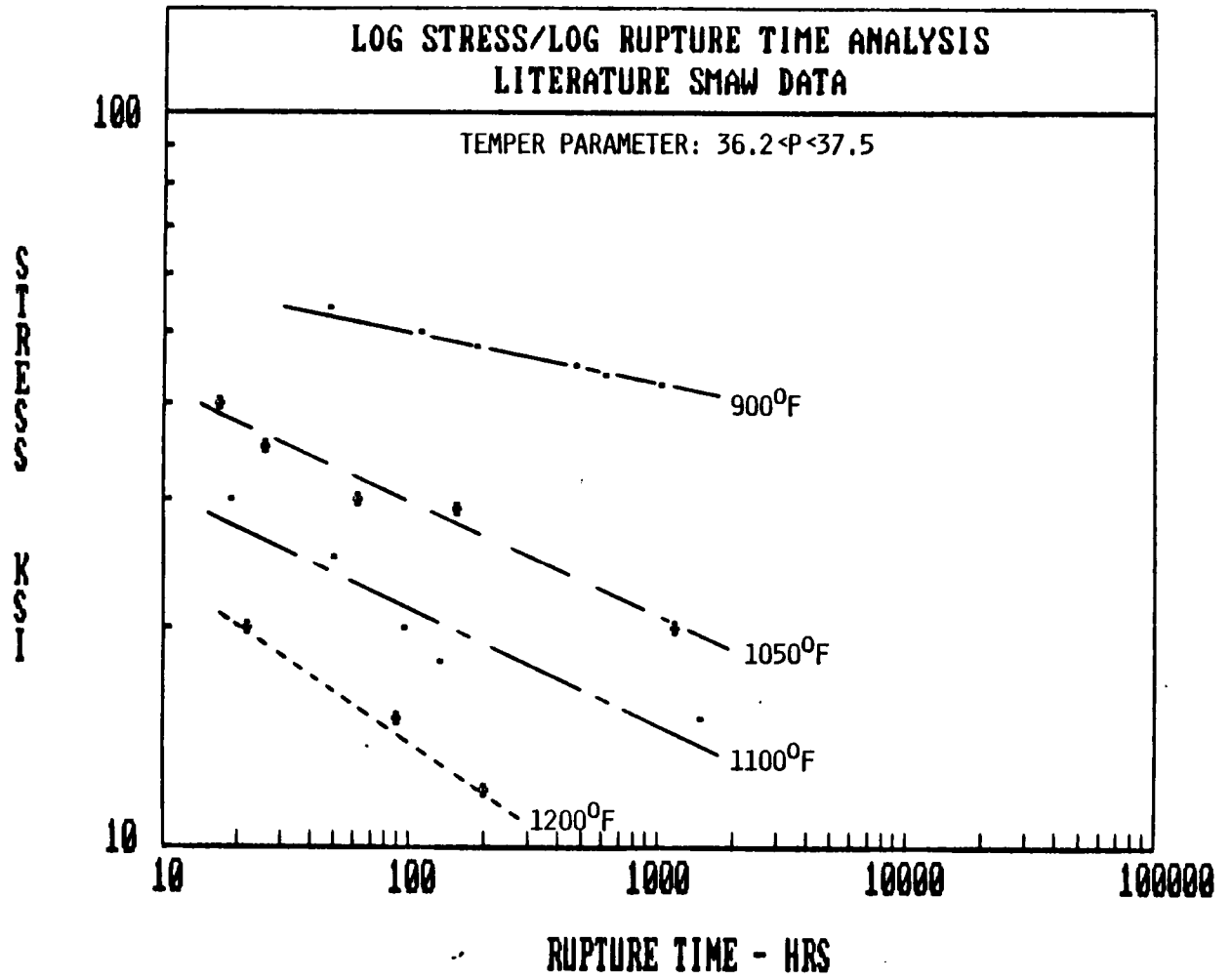


Figure A43. Log stress/log rupture time analysis of PWHT 2-1/4Cr-1Mo SMA weld metal (36.2<P<37.5) at 900, 1050, 1100, and 1200°F as determined from literature data.

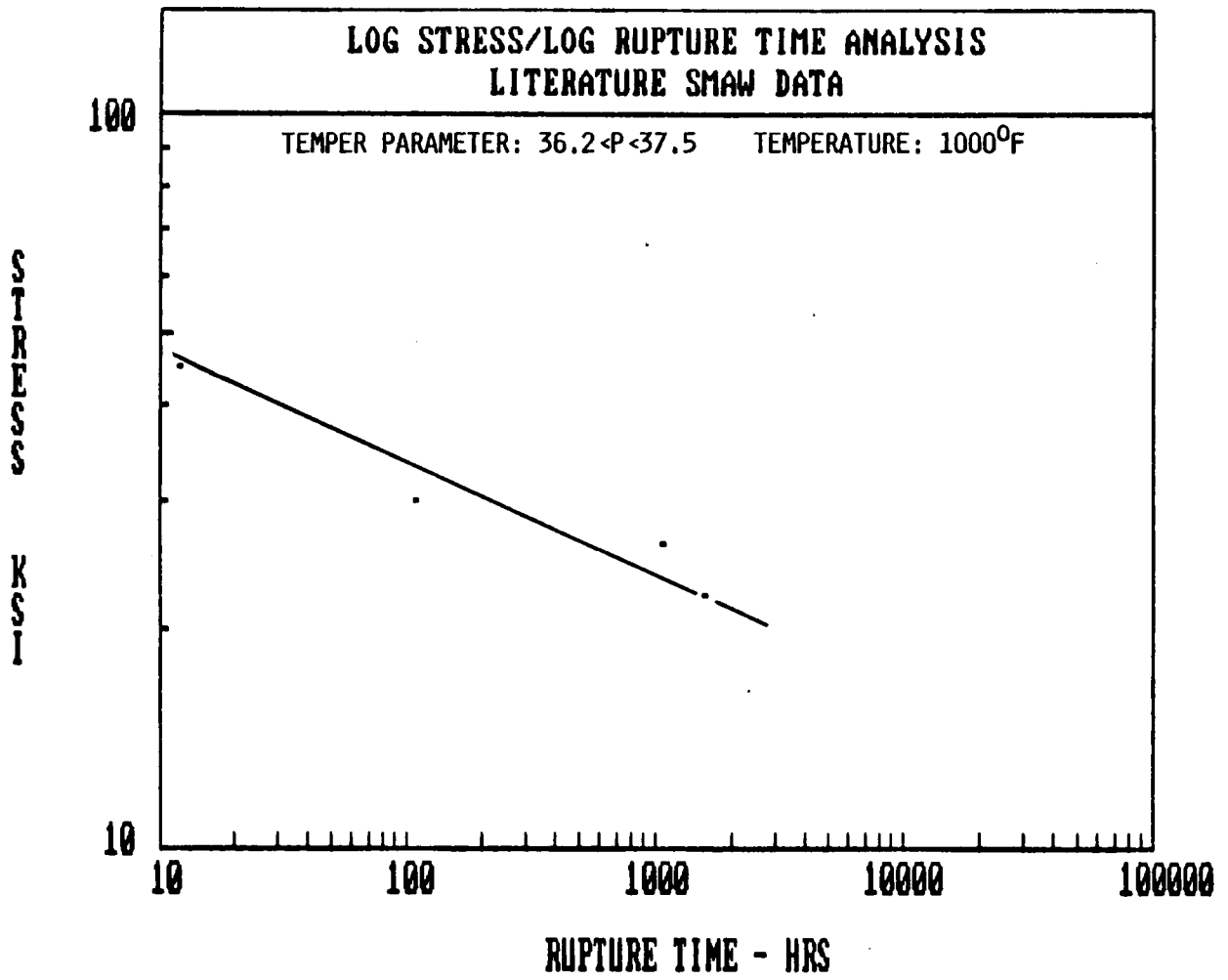


Figure A44. Log stress/log rupture time analysis of PWHT 2-1/4Cr-1Mo SMA weld metal (36.2<P<37.5) at 1000°F as determined from literature data.

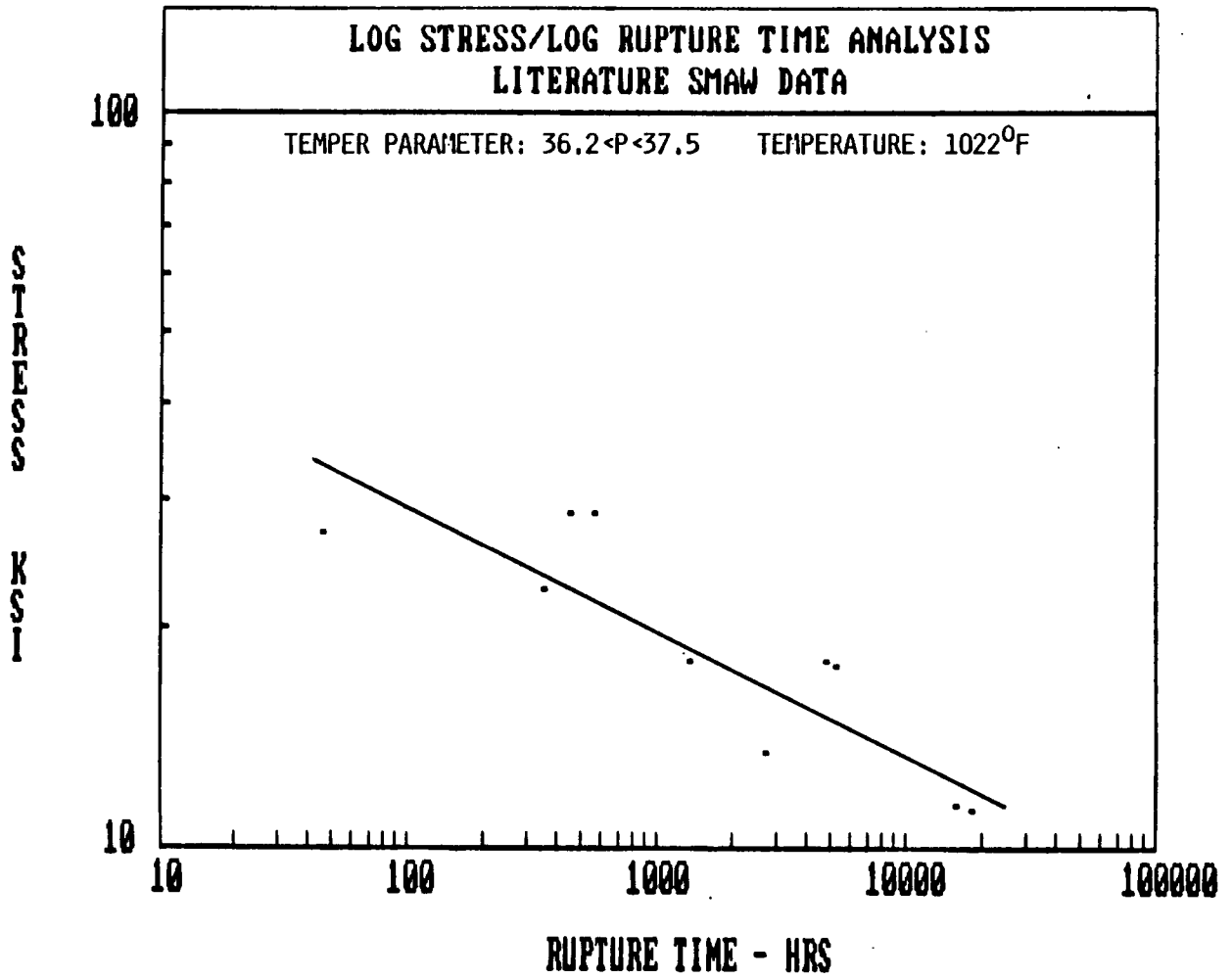


Figure A45. Log stress/log rupture time analysis of PWHT 2-1/4Cr-1Mo SMA weld metal (36.2<P<37.5) at 1022°F as determined from literature data.

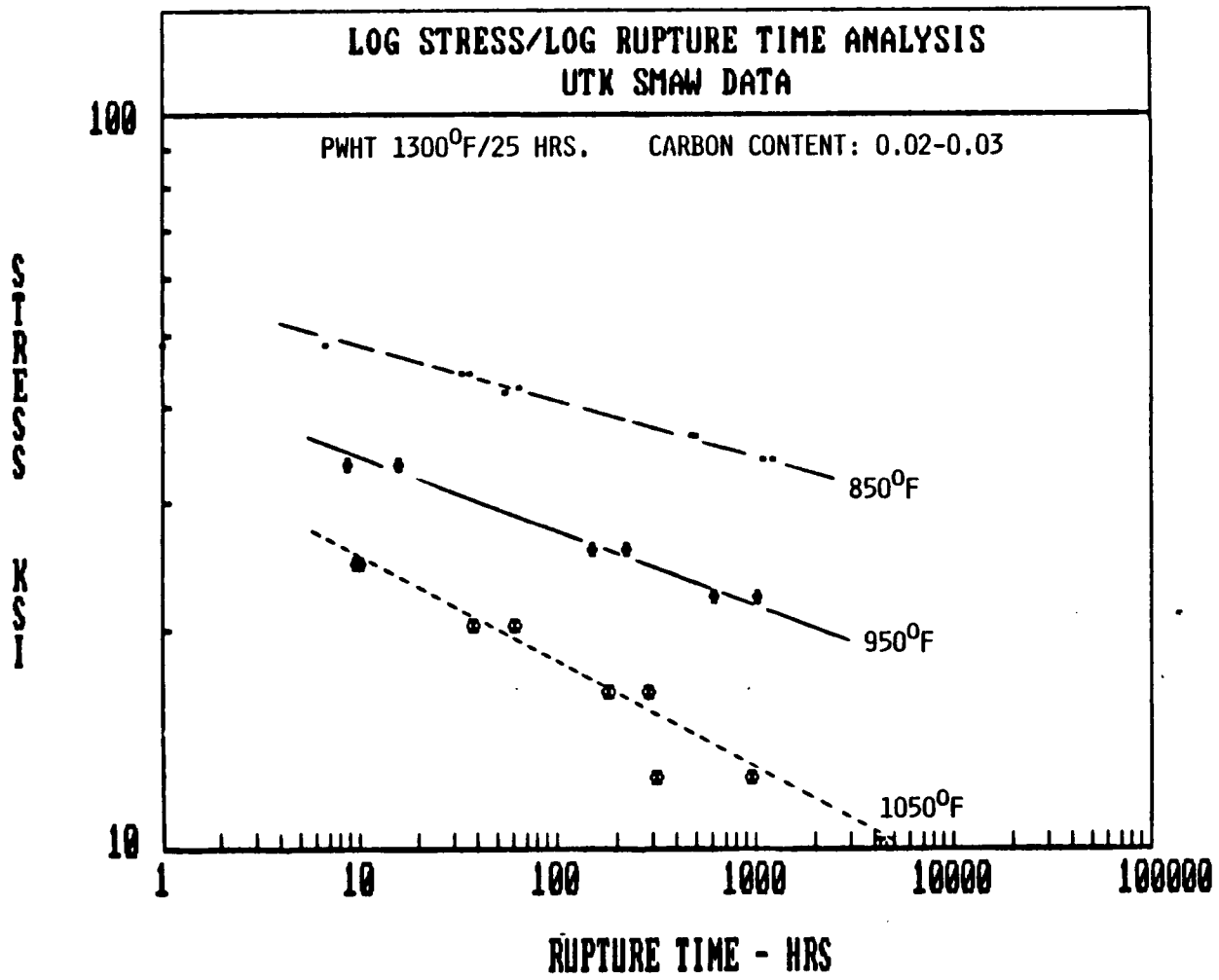


Figure A46. Log stress/log rupture time analysis of 2-1/4Cr-1Mo SMA weld metal PWHT 1300°F/25 hrs. (Class 2, 0.02-0.03C) at 850, 950, and 1050°F as determined from UTK data.

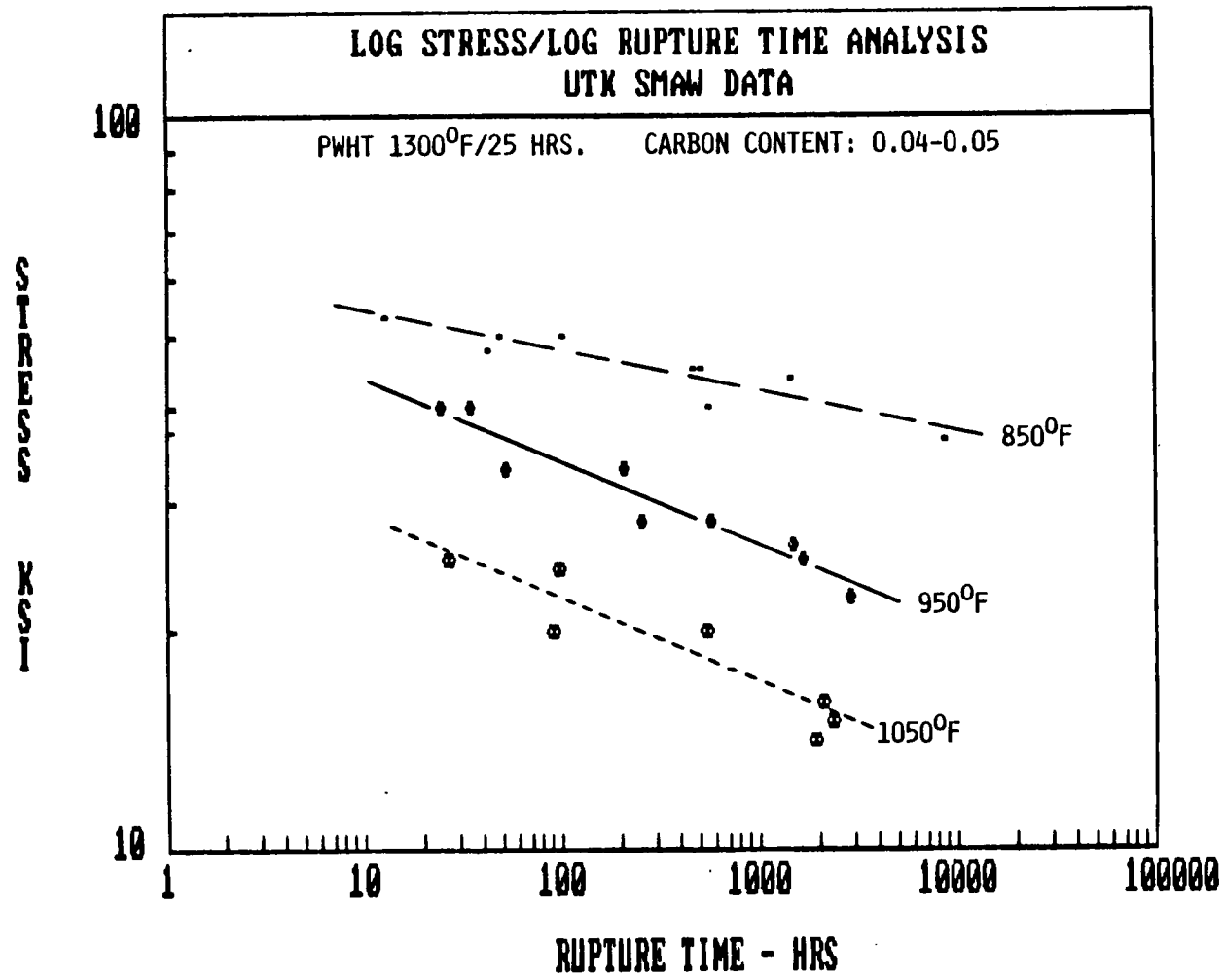


Figure A47. Log stress/log rupture time analysis of 2-1/4Cr-1Mo SMA weld metal PWHT 1300°F/25 hrs. (Class 2, 0.04-0.05C) at 850, 950, and 1050°F as determined from UTK data.

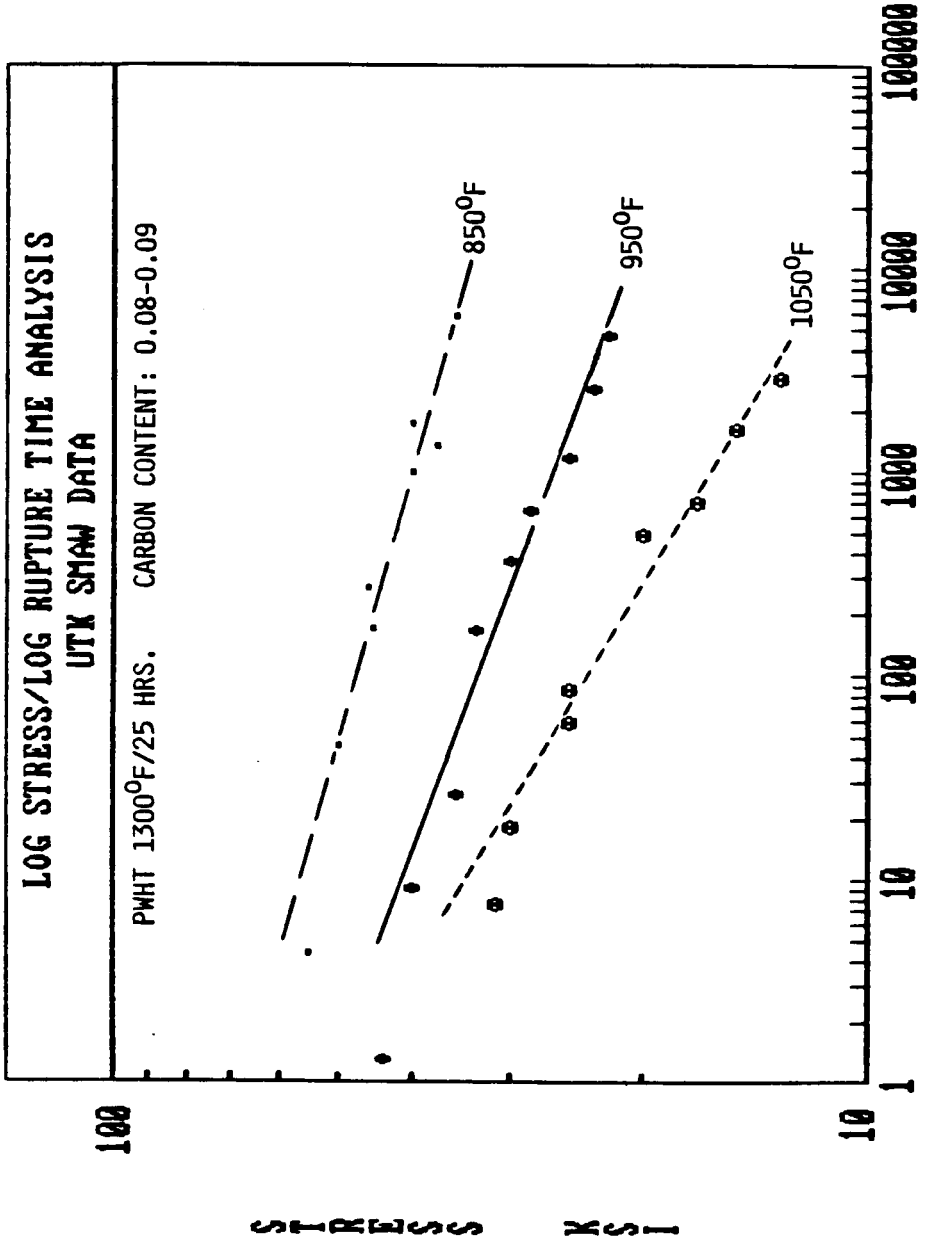


Figure A48. Log stress/log rupture time analysis of 2-1/4Cr-1Mo SMA weld metal PWHT 1300°F/25 hrs. (Class 2, 0.08-0.09C) at 850, 950, and 1050°F as determined from UTK data.

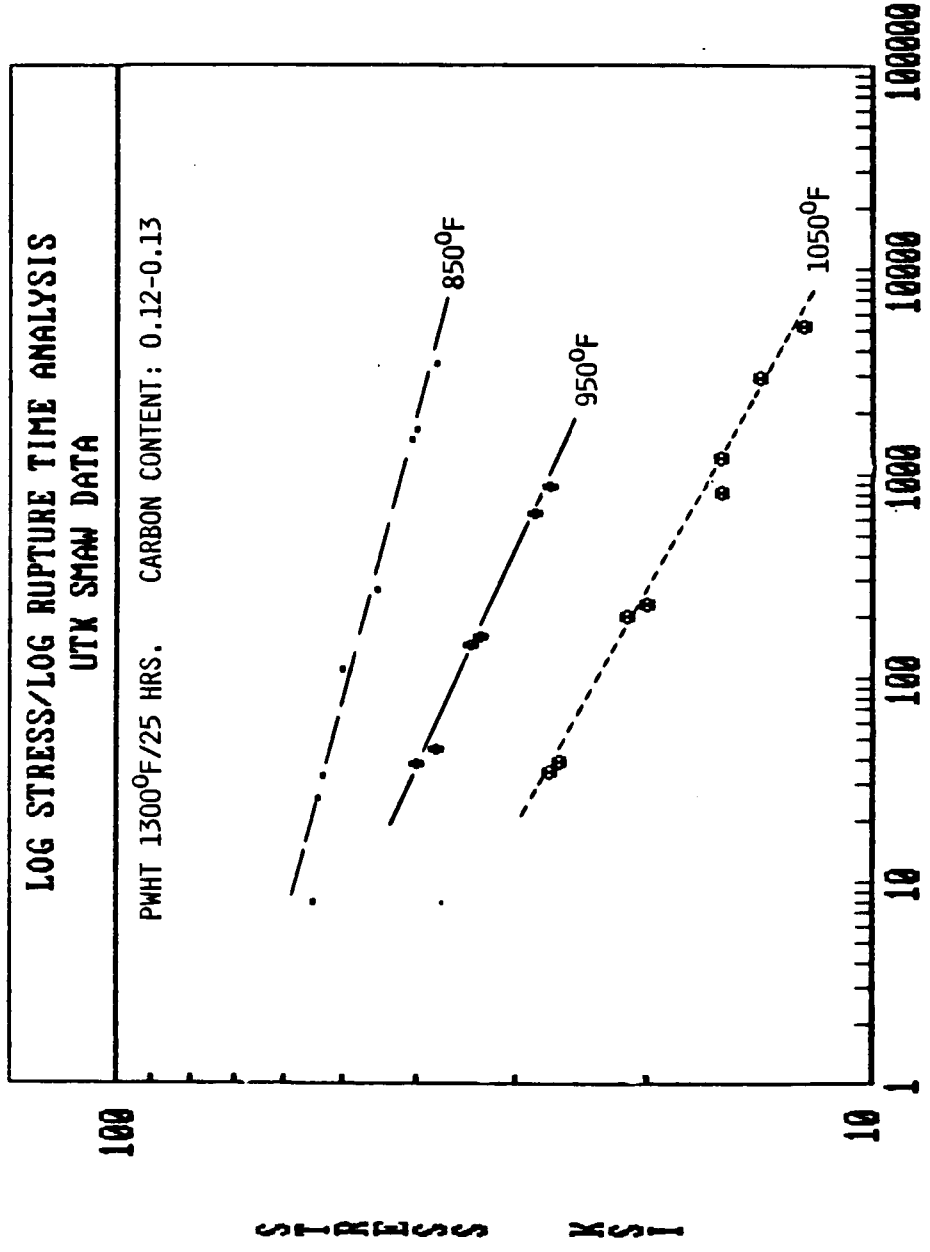


Figure A49. Log stress/log rupture time analysis of 2-1/4Cr-1Mo SMA weld metal PWHT 1300°F/25 hrs. (Class 2, 0.12-0.13C) at 850, 950, and 1050°F as determined from UTK data.

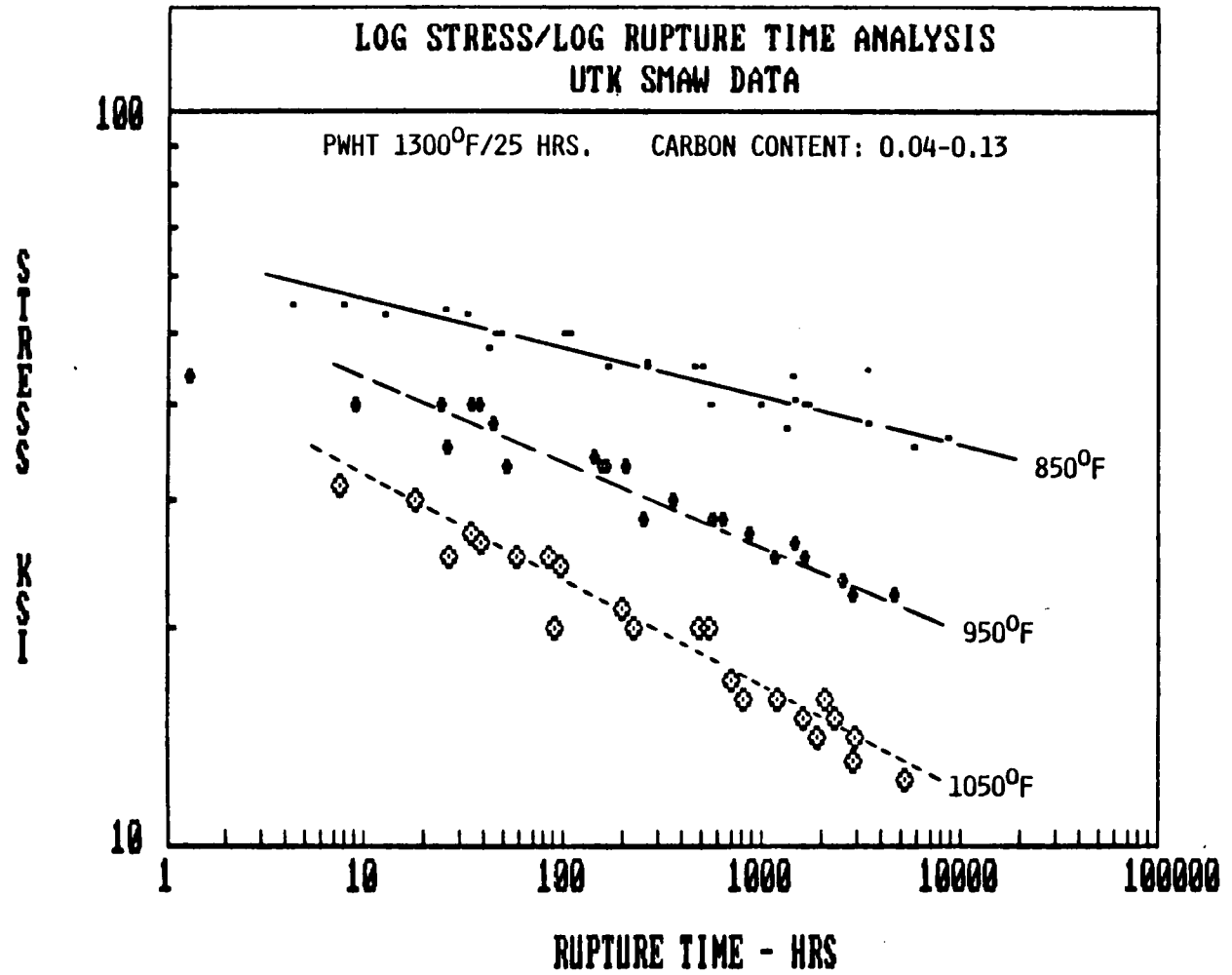


Figure A50. Log stress/log rupture time analysis of 2-1/4Cr-1Mo SMA weld metal PWHT 1300°F/25 hrs. (Class 2, 0.04-0.13C) at 850, 950, and 1050°F as determined from UTK data.

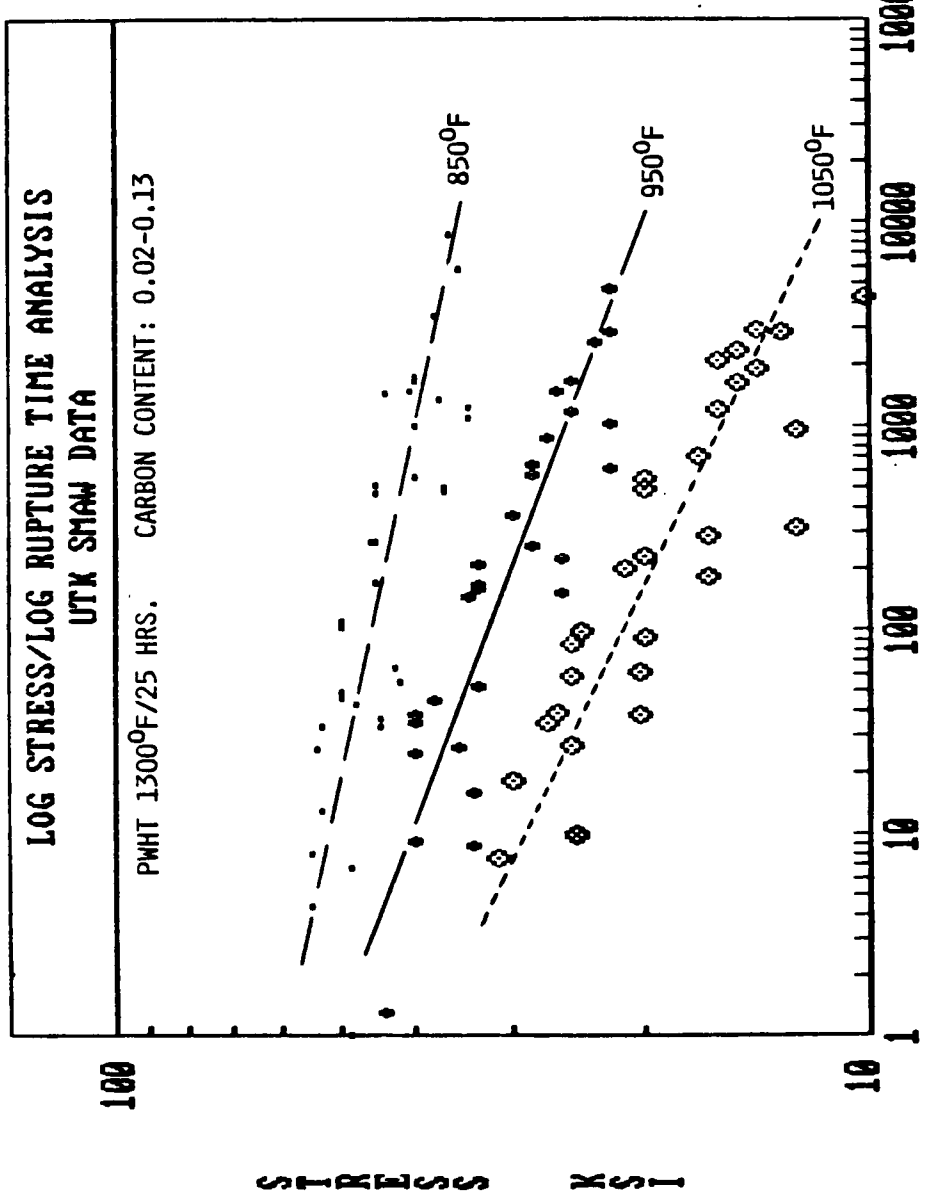


Figure A51. Log stress/log rupture time analysis of 2-1/4Cr-1Mo SMA weld metal PWHT 1300°F/25 hrs. (Class 2, 0.02-0.13C) at 850, 950, and 1050°F as determined from UTK data.

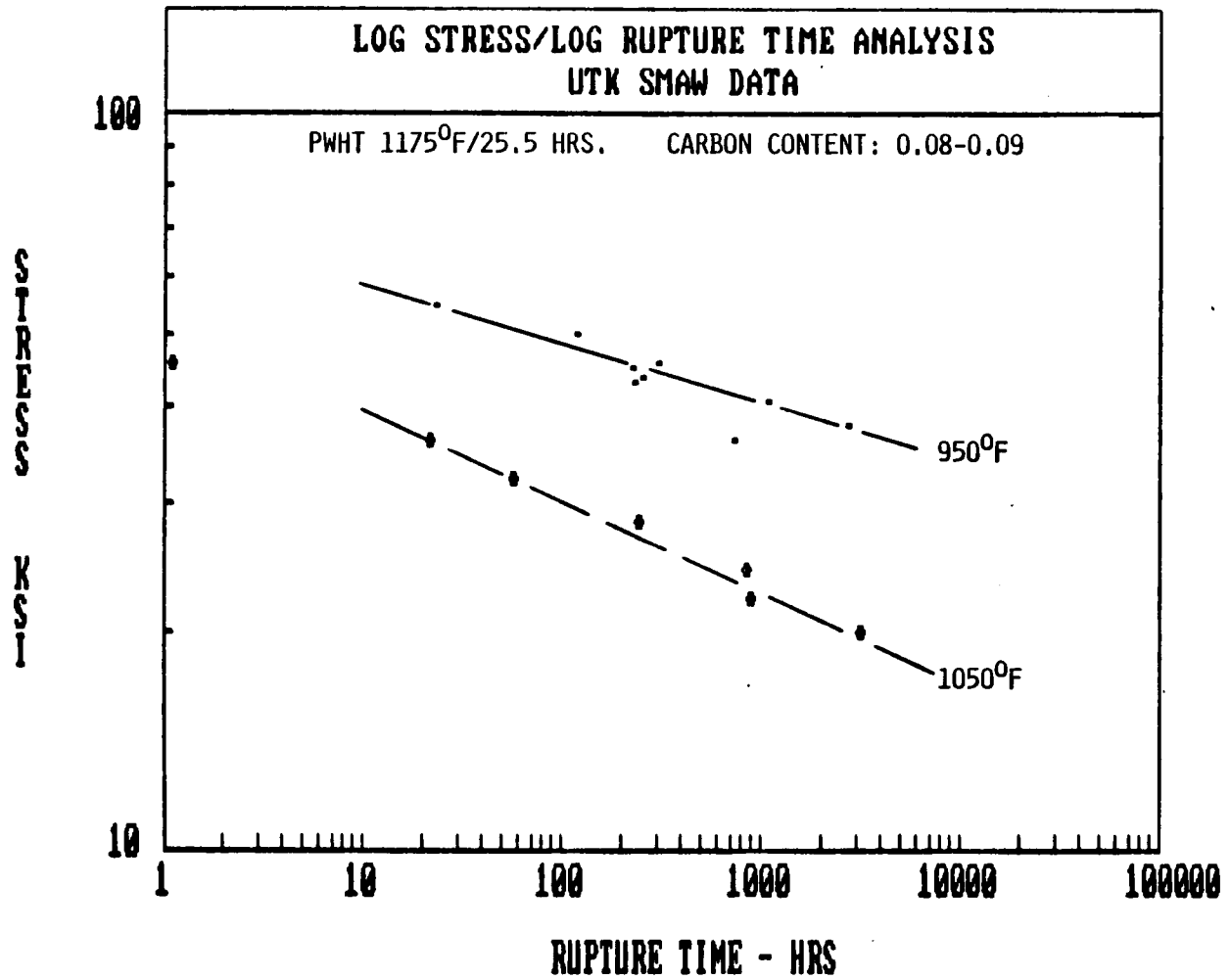


Figure A52. Log stress/log rupture time analysis of 2-1/4Cr-1Mo SMA weld metal PWHT 1175°F/25.5 hrs. (Class 3, 0.08-0.09C) at 950 and 1050°F as determined from UTK data.

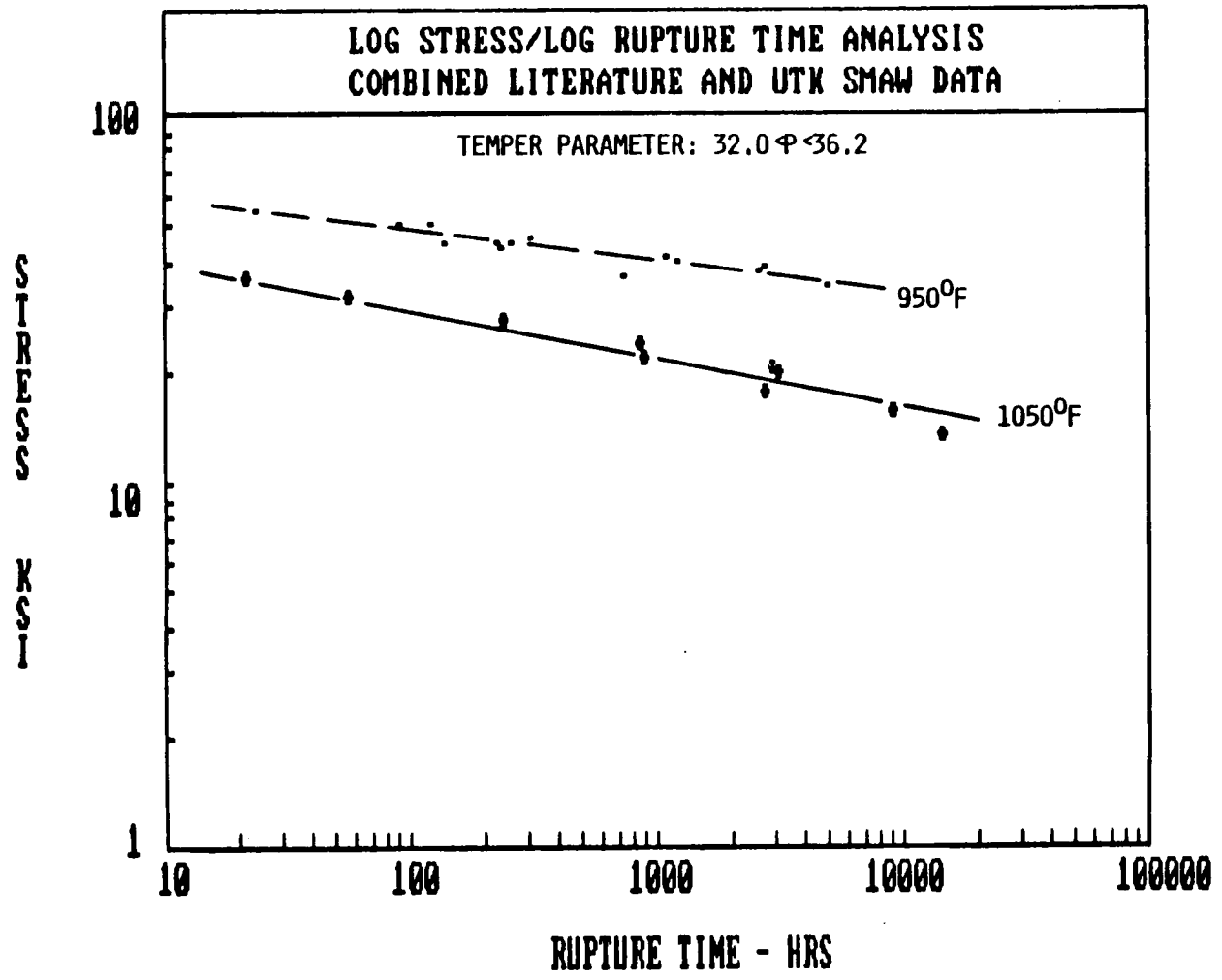


Figure A53. Log stress/log rupture time analysis of PWHT 2-1/4Cr-1Mo SMA weld metal (32.0<P<36.2) at 950 and 1050°F as determined from combined literature and UTK data.

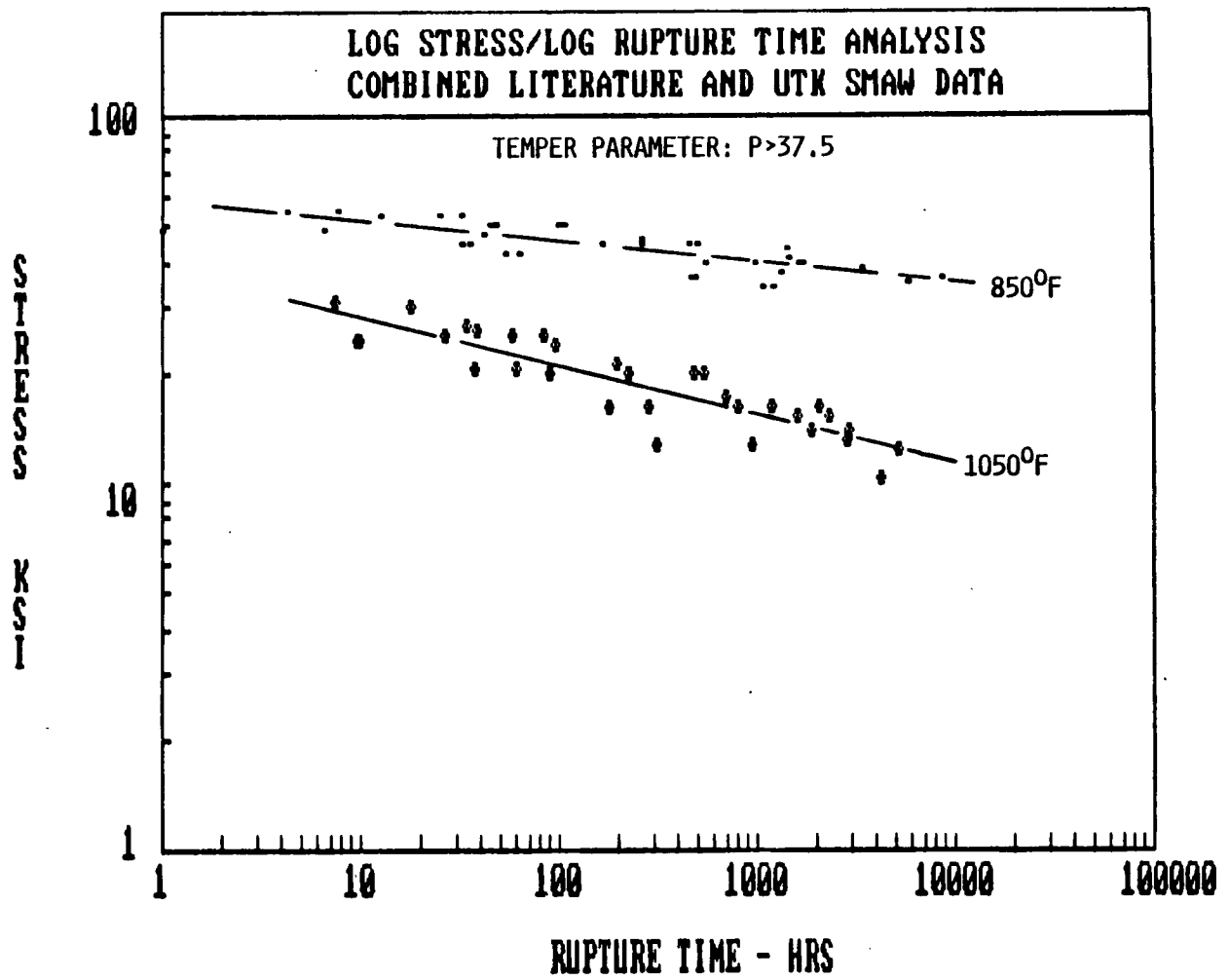


Figure A54. Log stress/log rupture time analysis of PWHT 2-1/4Cr-1Mo SMA weld metal (P>37.5) at 850 and 1050°F as determined from combined literature and UTK data.

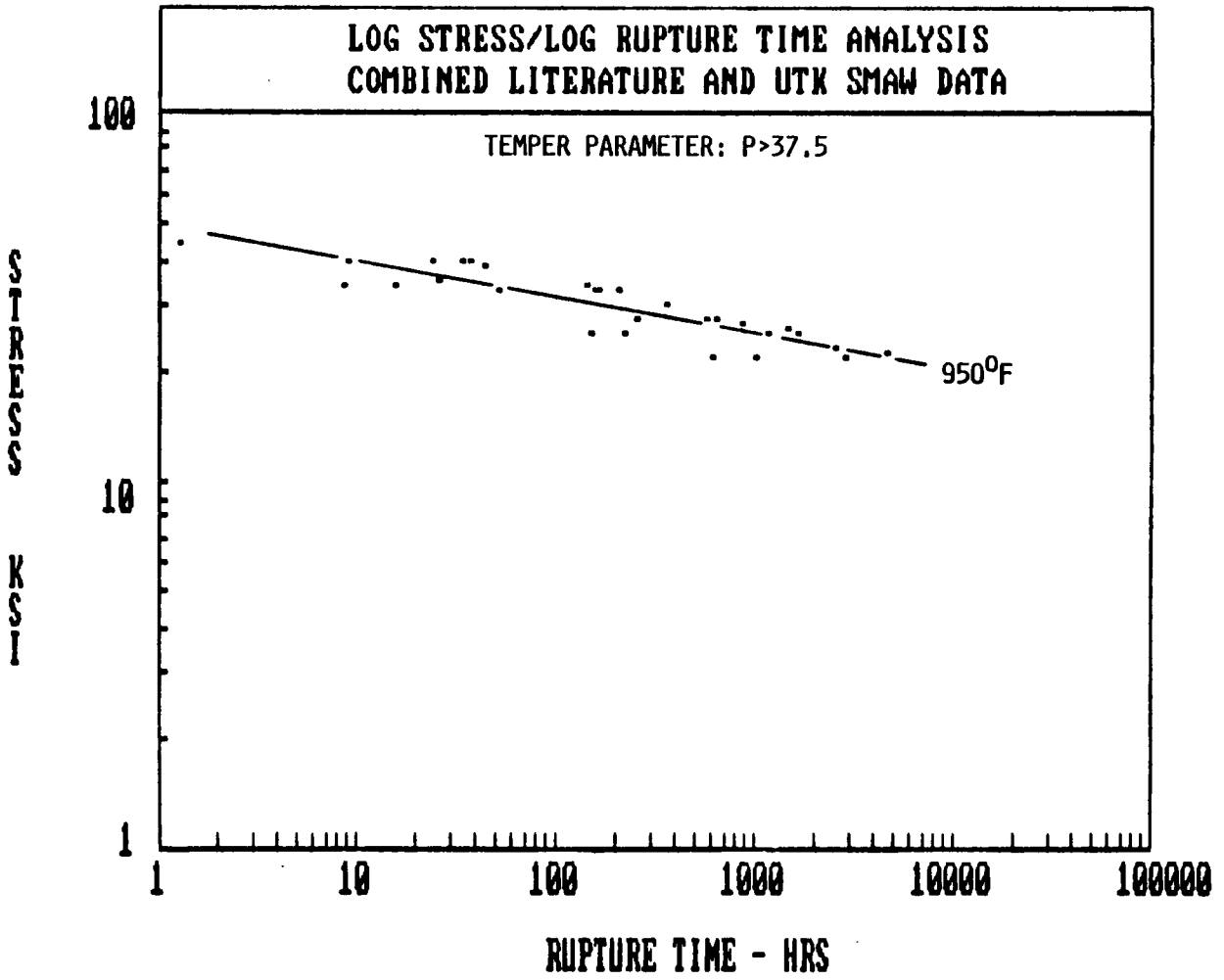


Figure A55. Log stress/log rupture time analysis of PWHT 2-1/4Cr-1Mo SMA weld metal (P>37.5) at 950°F as determined from combined literature and UTK data.

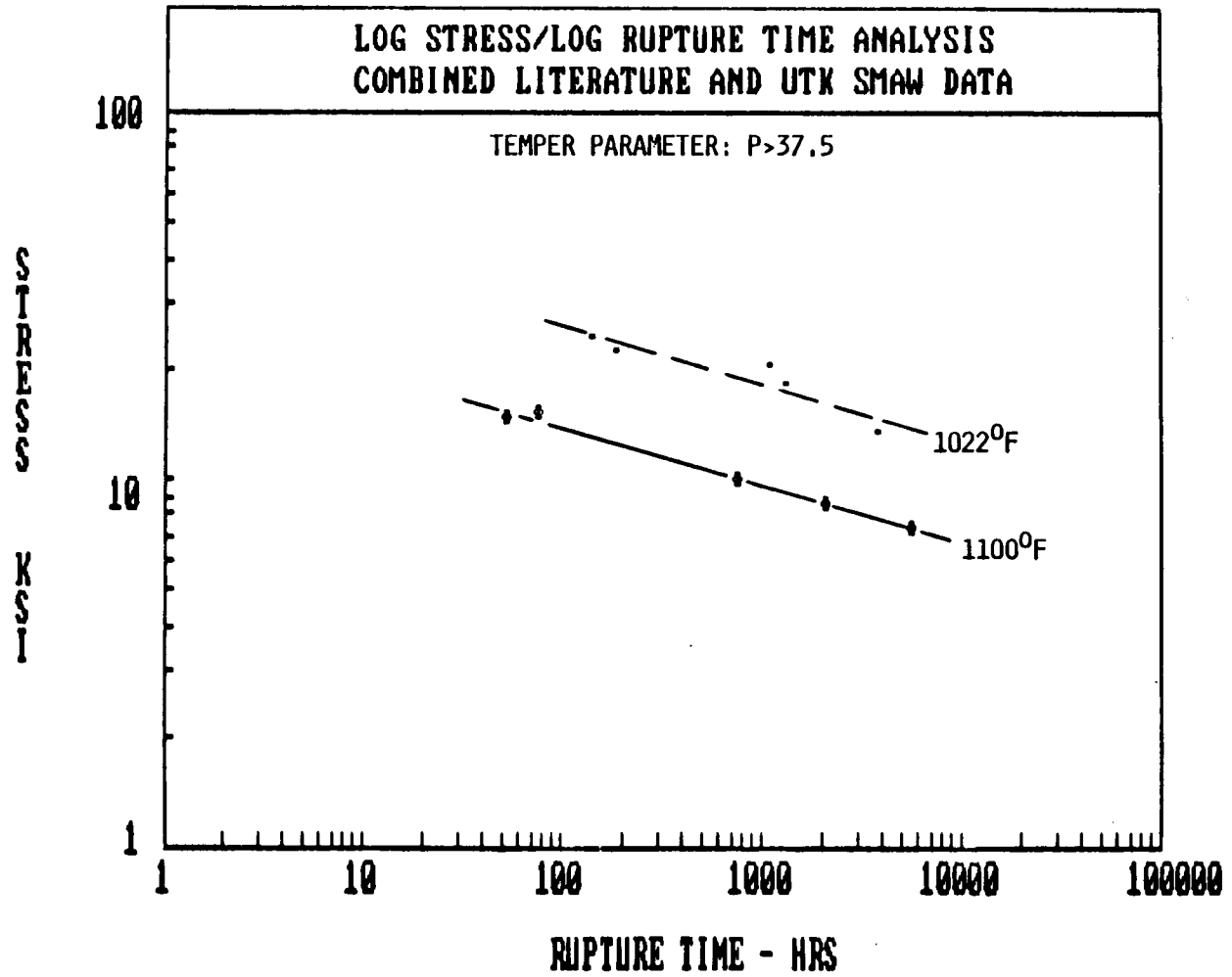


Figure A56. Log stress/log rupture time analysis of PWHT 2-1/4Cr-1Mo SMA weld metal (P>37.5) at 1022 and 1100°F as determined from combined literature and UTK data.

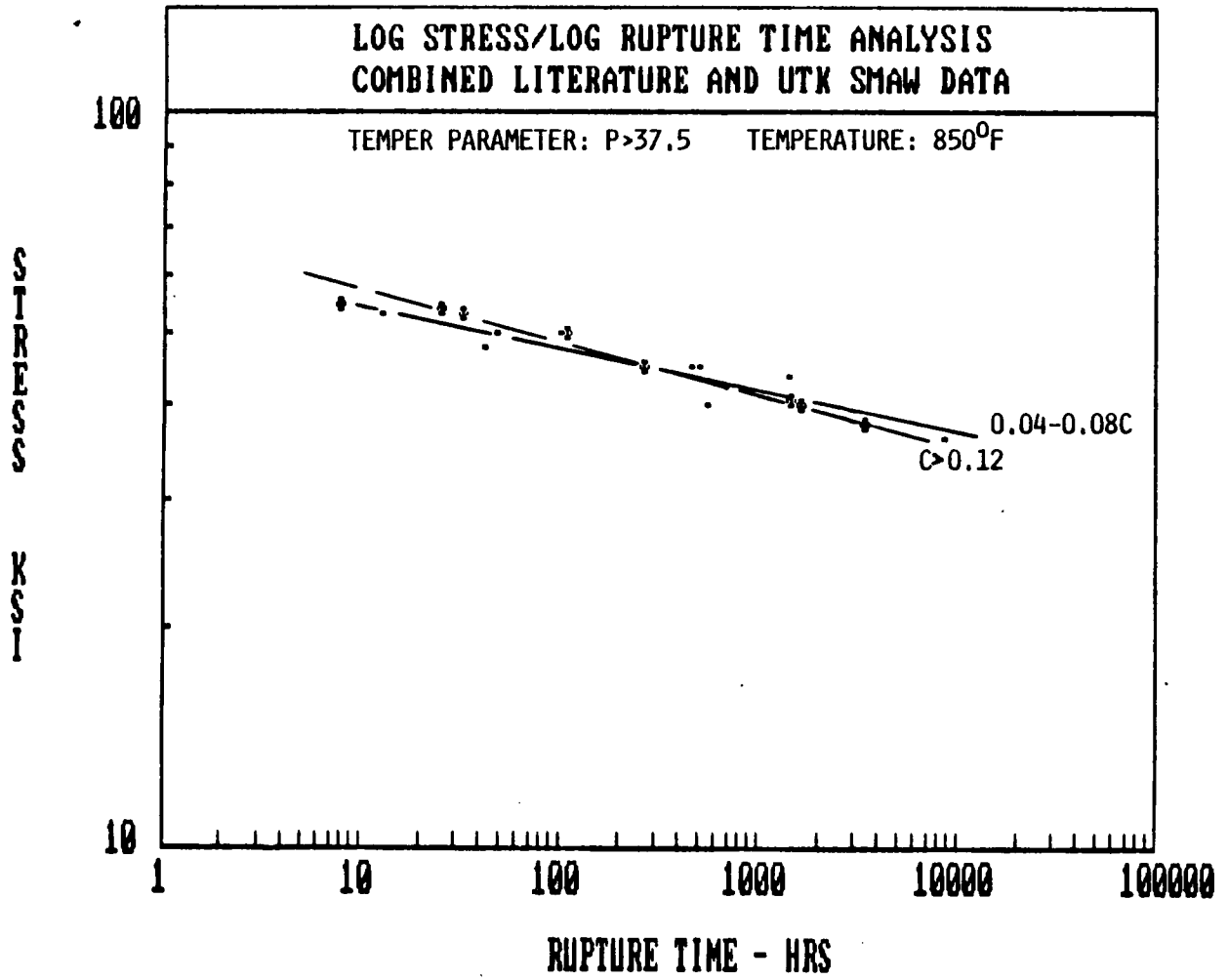


Figure A57. Log stress/log rupture time analysis of PWHT 2-1/4Cr-1Mo SMA weld metal (P>37.5, 850°F) with carbon contents of 0.04-0.08 and C>0.12 as determined from combined literature and UTK data.

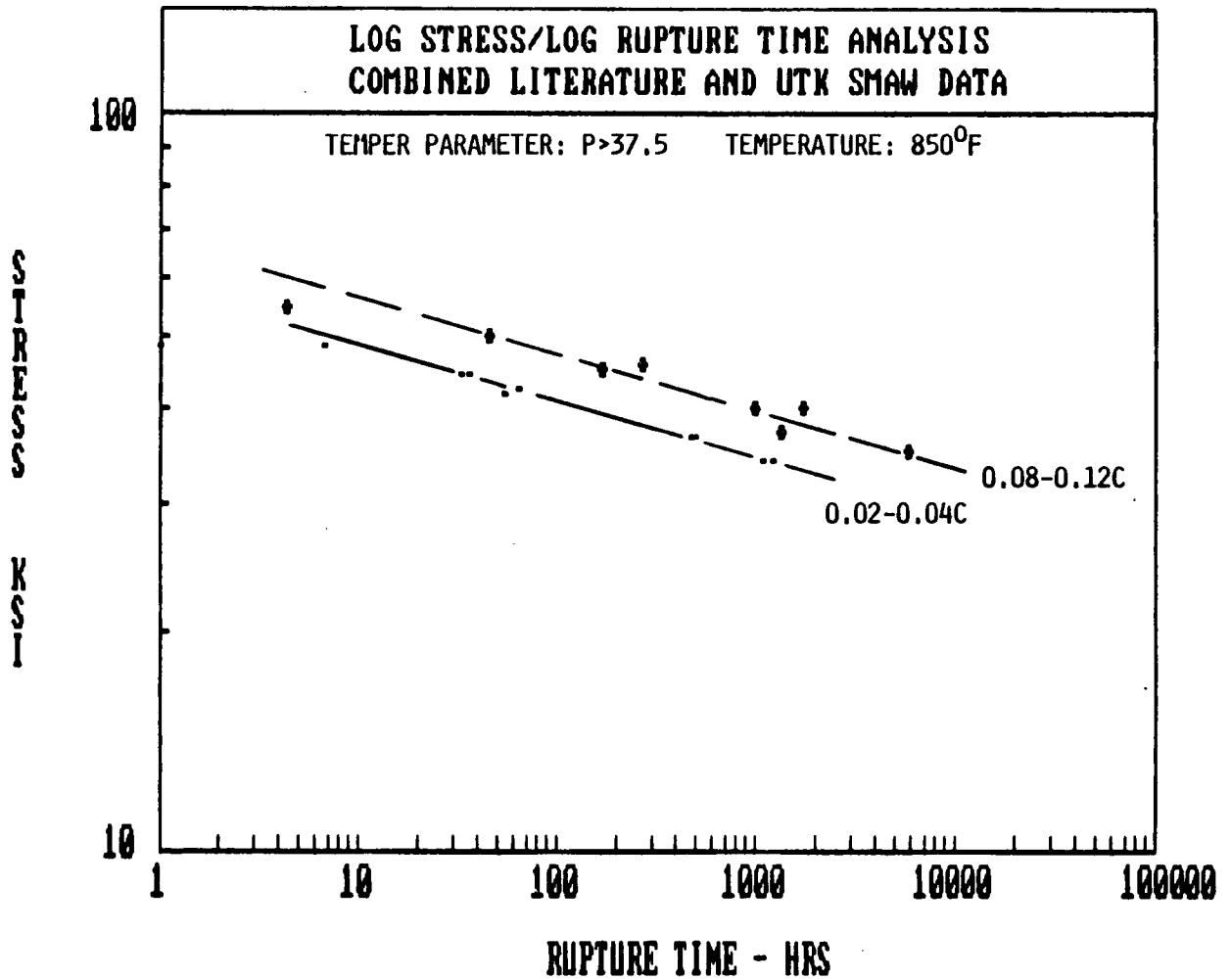


Figure A58. Log stress/log rupture time analysis of PWHT 2-1/4Cr-1Mo SMA weld metal (P>37.5, 950°F) with carbon contents of 0.02-0.04 and 0.08-0.12 as determined from combined literature and UTK data.

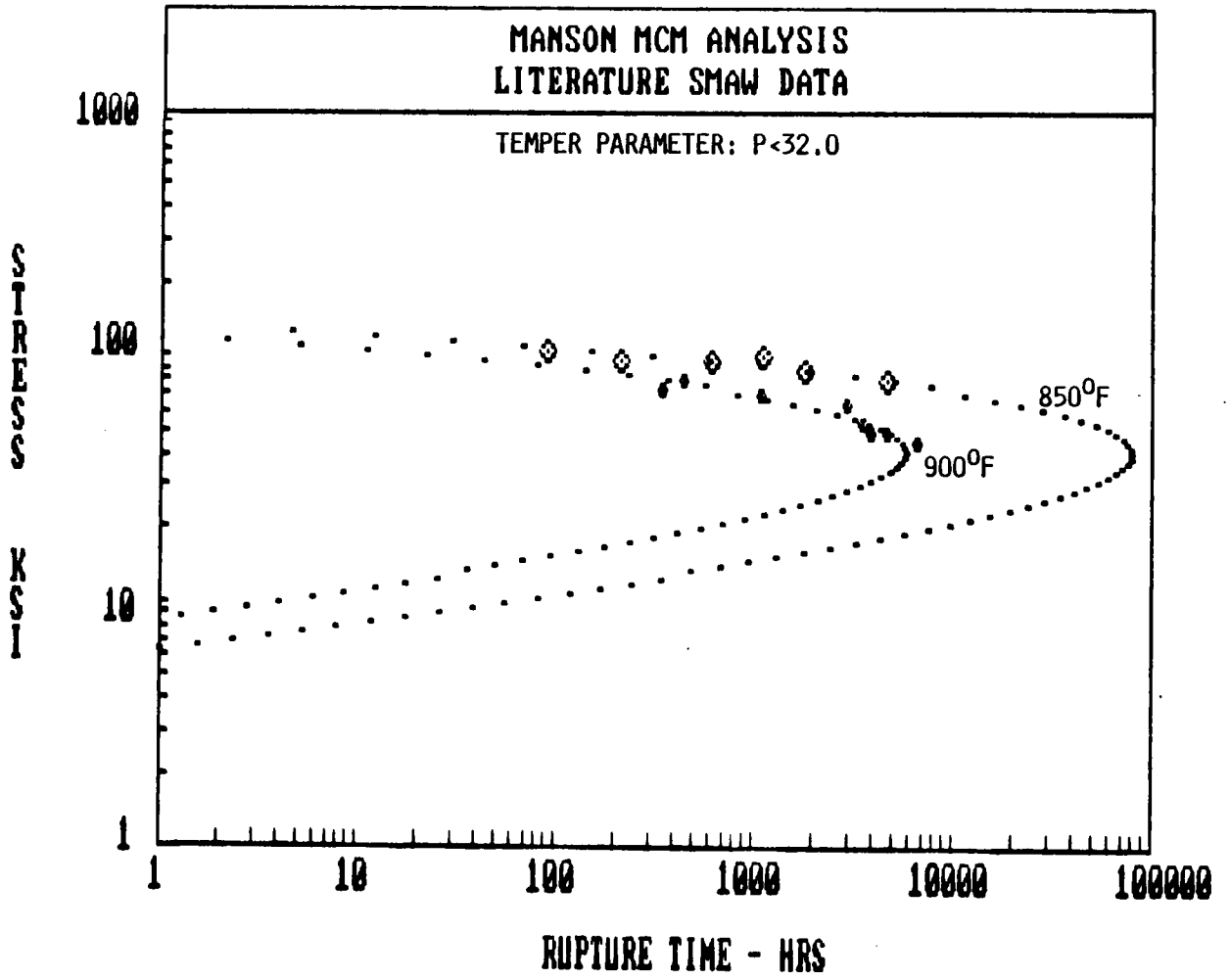


Figure A59. Manson MCM analysis of PWHT 2-1/4Cr-1Mo SMA weld metal (P<32.0) at 850 and 900°F as determined from literature data.

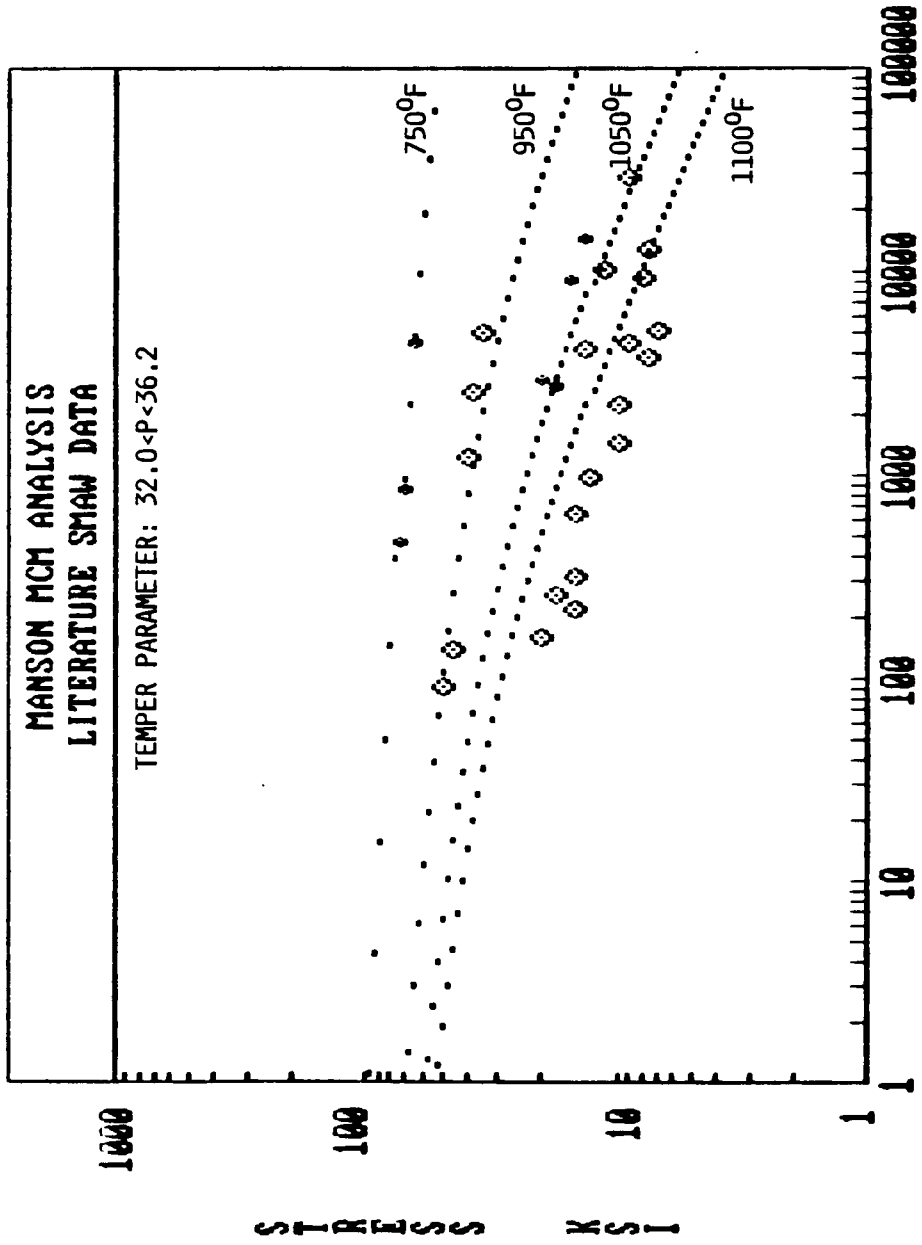


Figure A60. Manson MCM analysis of PWHT 2-1/4Cr-1Mo SMA weld metal (32.0<P<36.2) at 750, 950, 1050, and 1100°F as determined from literature data.

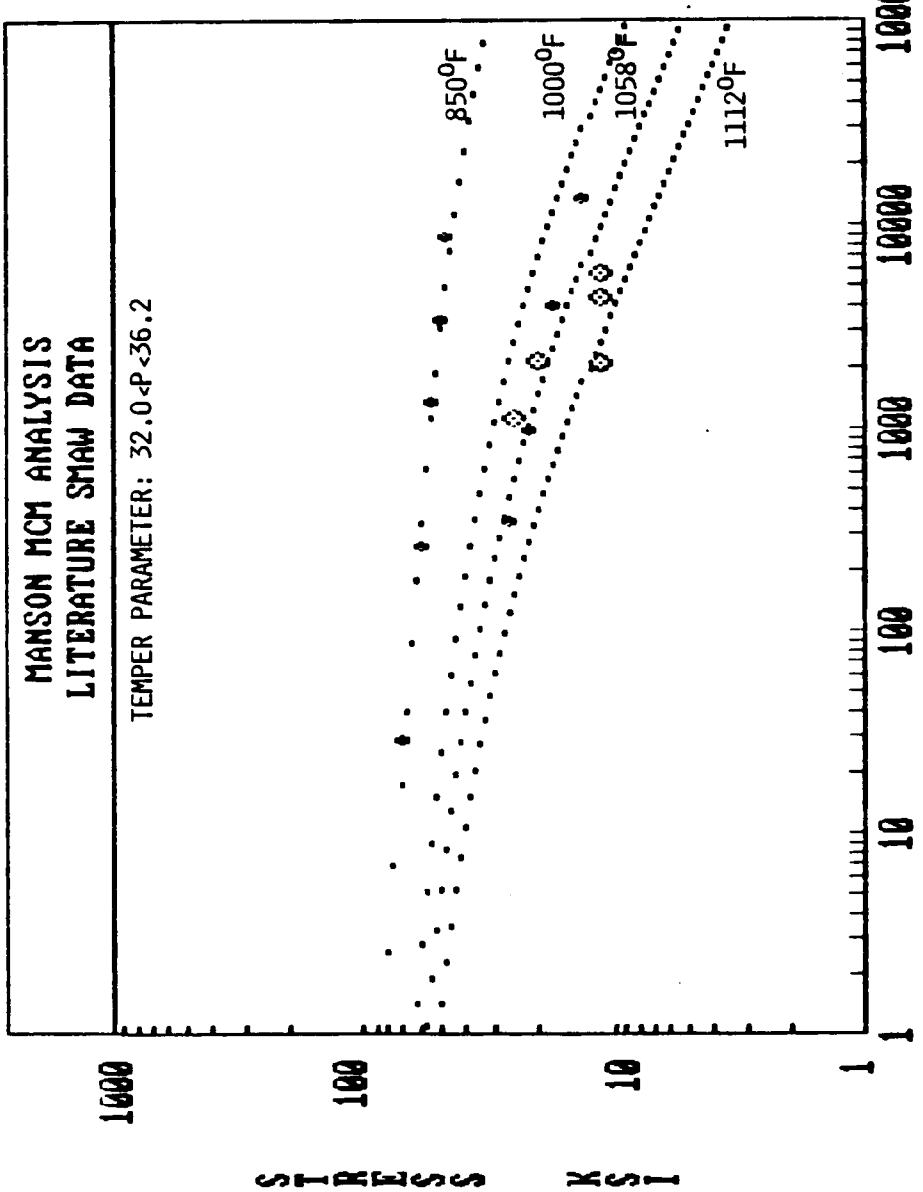


Figure A61. Manson MCM analysis of PWHT 2-1/4Cr-1Mo SMA weld metal (32.0<P<36.2) at 850, 1000, 1058, and 1112°F as determined from literature data.

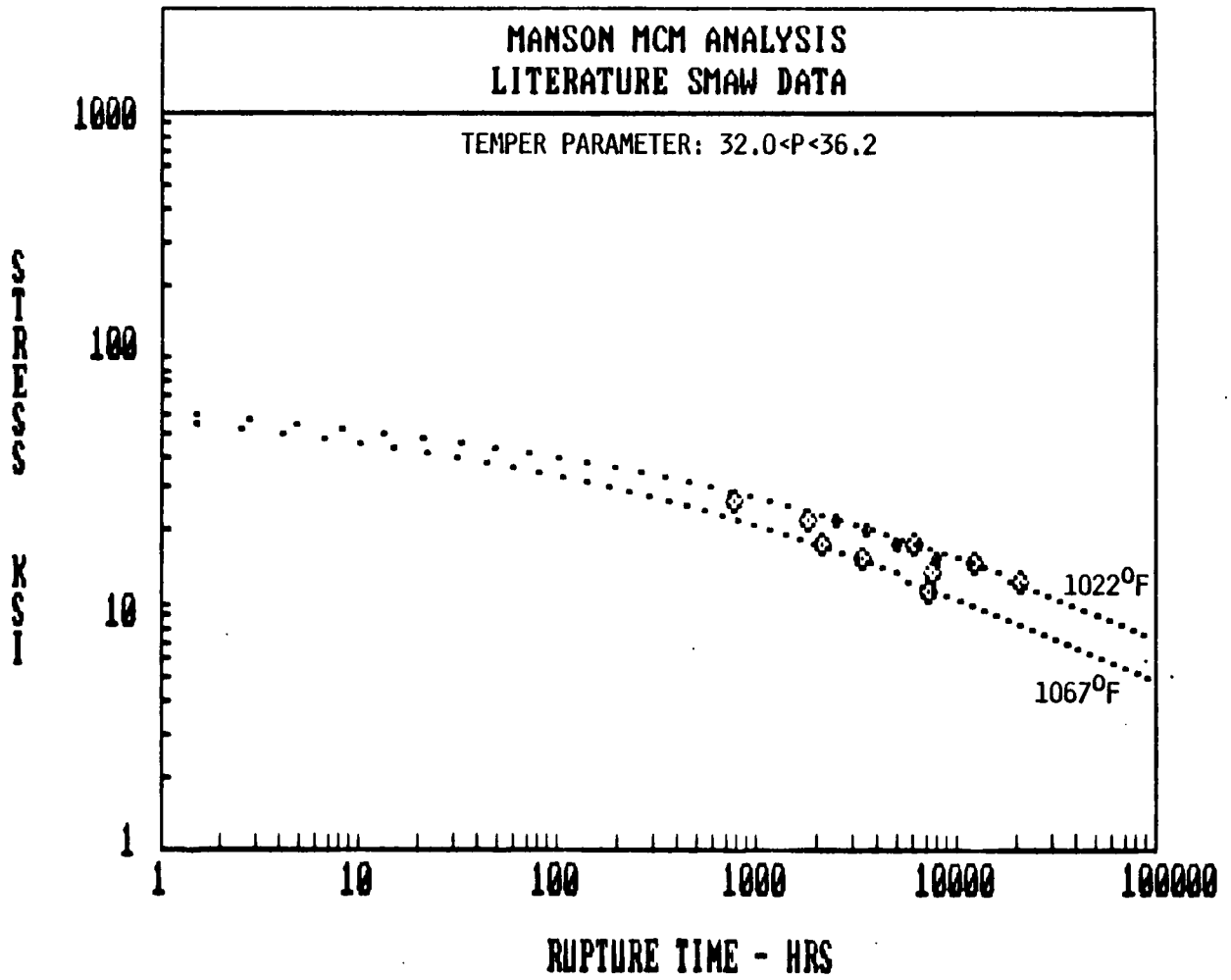


Figure A62. Manson MCM analysis of PWHT 2-1/4Cr-1Mo SMA weld metal (32.0<P<36.2) at 1022 and 1067°F as determined from literature data.

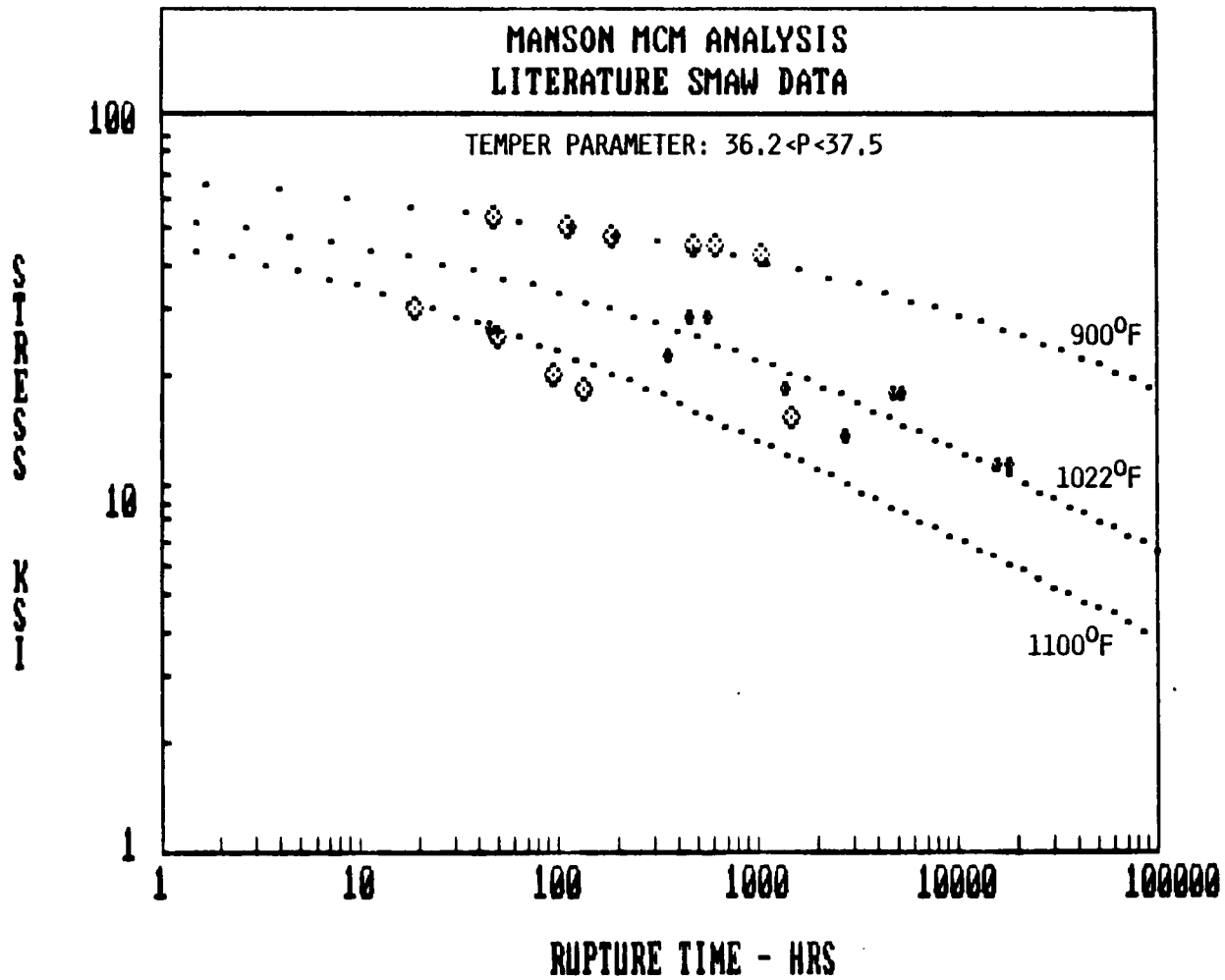


Figure A63. Manson MCM analysis of PWHT 2-1/4Cr-1Mo SMA weld metal (36.2<P<37.5) at 900, 1022, and 1100°F as determined from literature data.

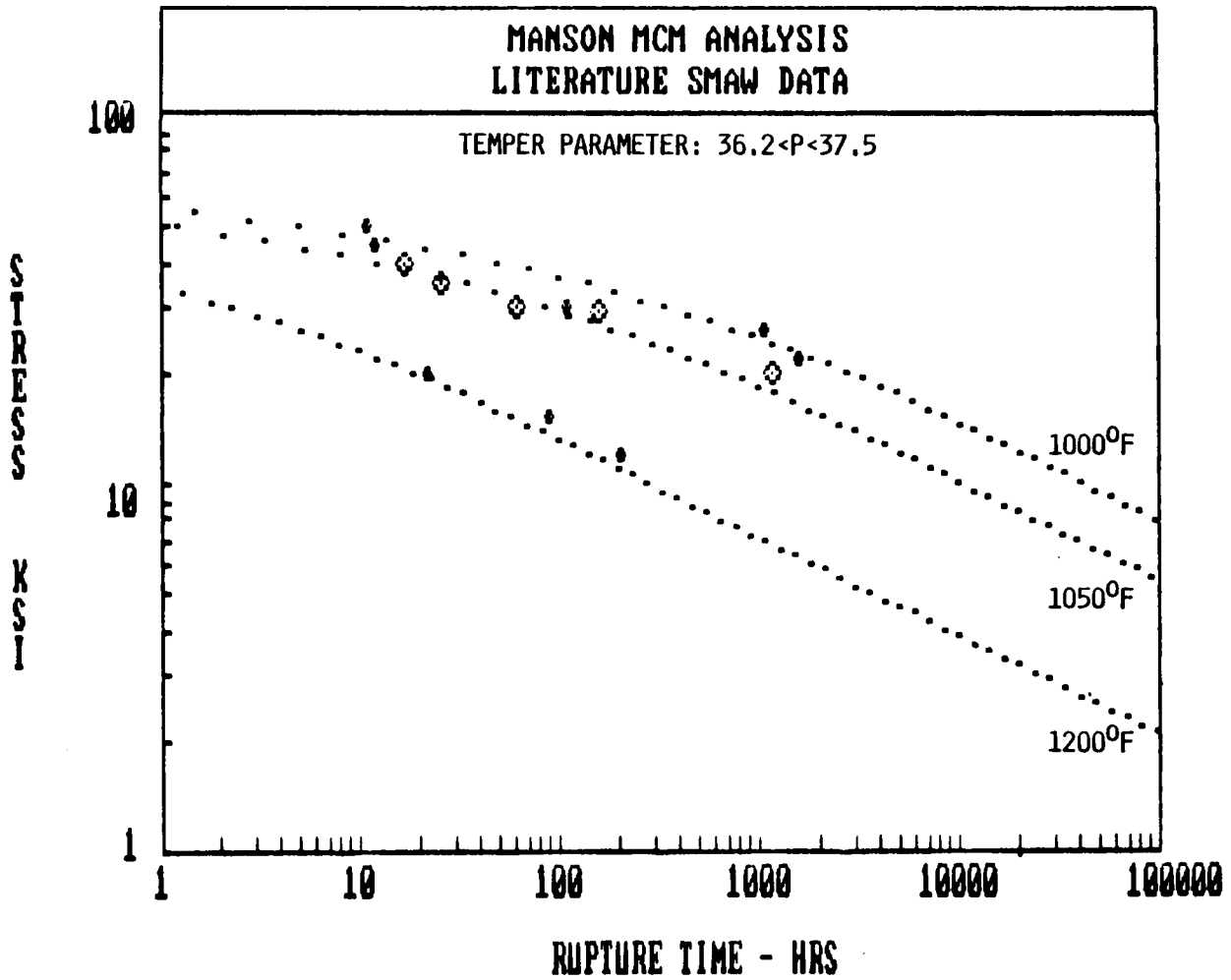


Figure A64. Manson MCM analysis of PWHT 2-1/4Cr-1Mo SMA weld metal (36.2<P<37.5) at 1000, 1050, and 1200°F as determined from literature data.

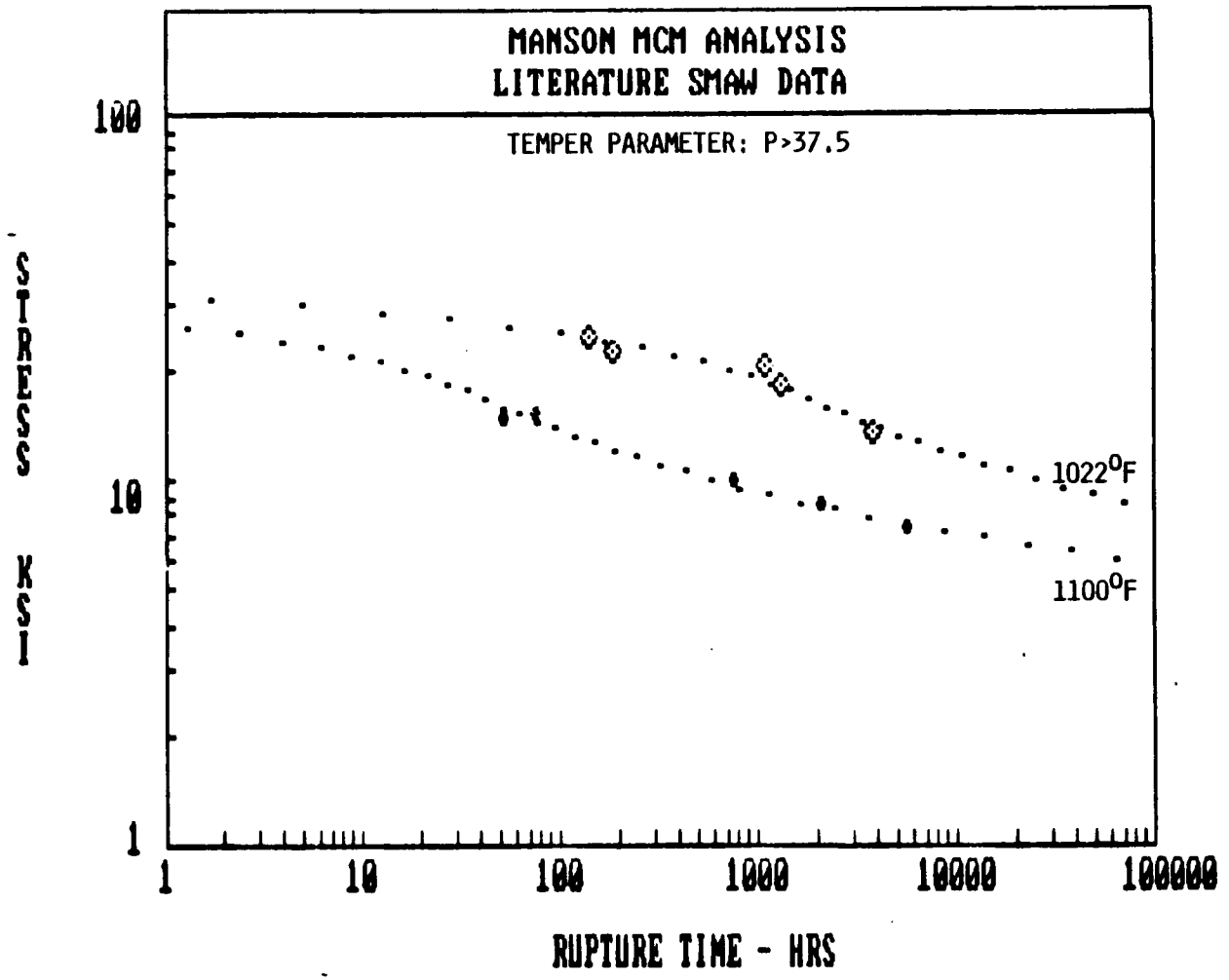


Figure A65. Manson MCM analysis of PWHT 2-1/4Cr-1Mo SMA weld metal (P>37.5) at 1022 and 1100°F as determined from literature data.

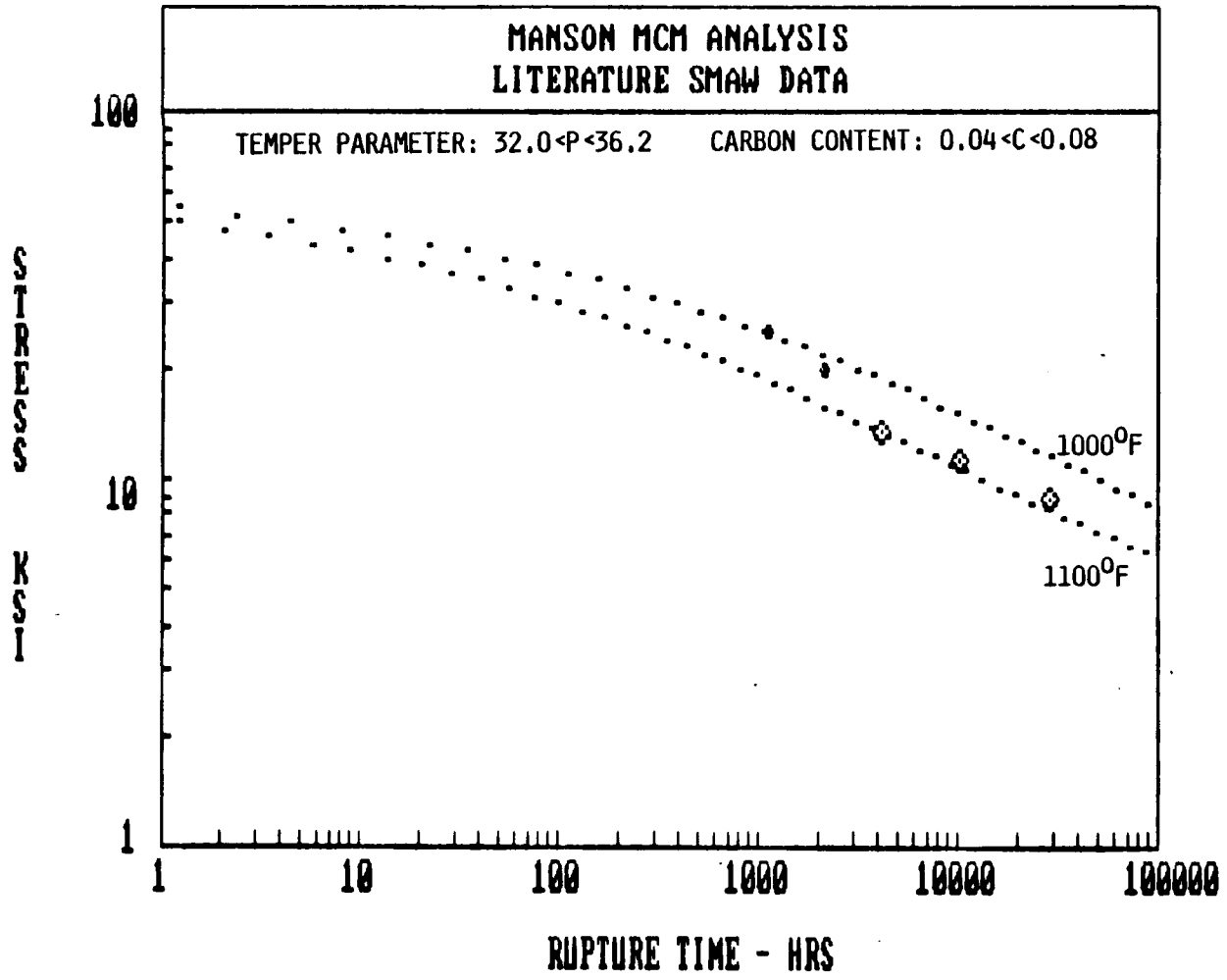


Figure A66. Manson MCM analysis of PWHT 2-1/4Cr-1Mo SMA weld metal (32.0<P<36.2, 0.04<C<0.08) at 1000 and 1100°F as determined from literature data.

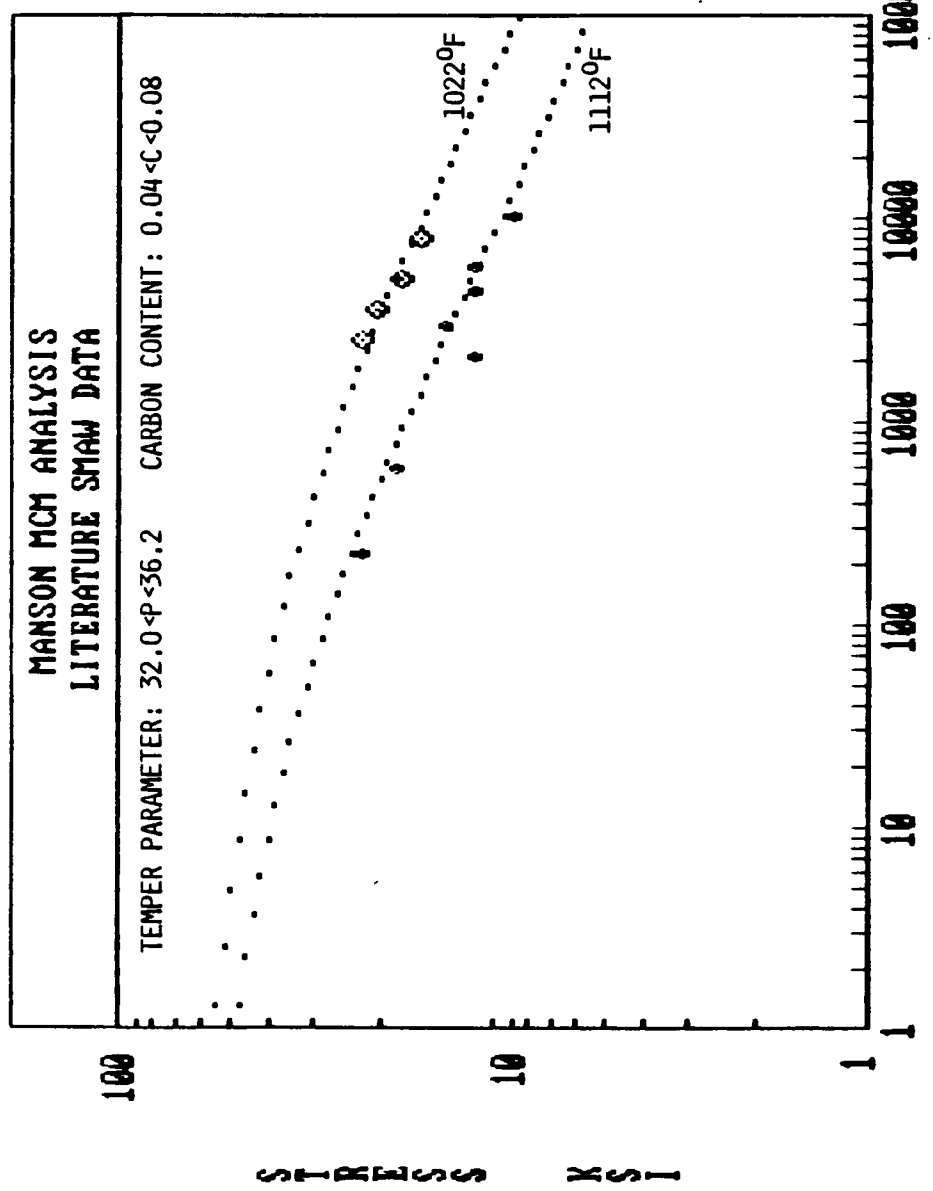


Figure A67. Manson MCM analysis of PWHT 2-1/4Cr-1Mo SMA weld metal (32.0<P<36.2, 0.04<C<0.08) at 1022 and 1112°F as determined from literature data.

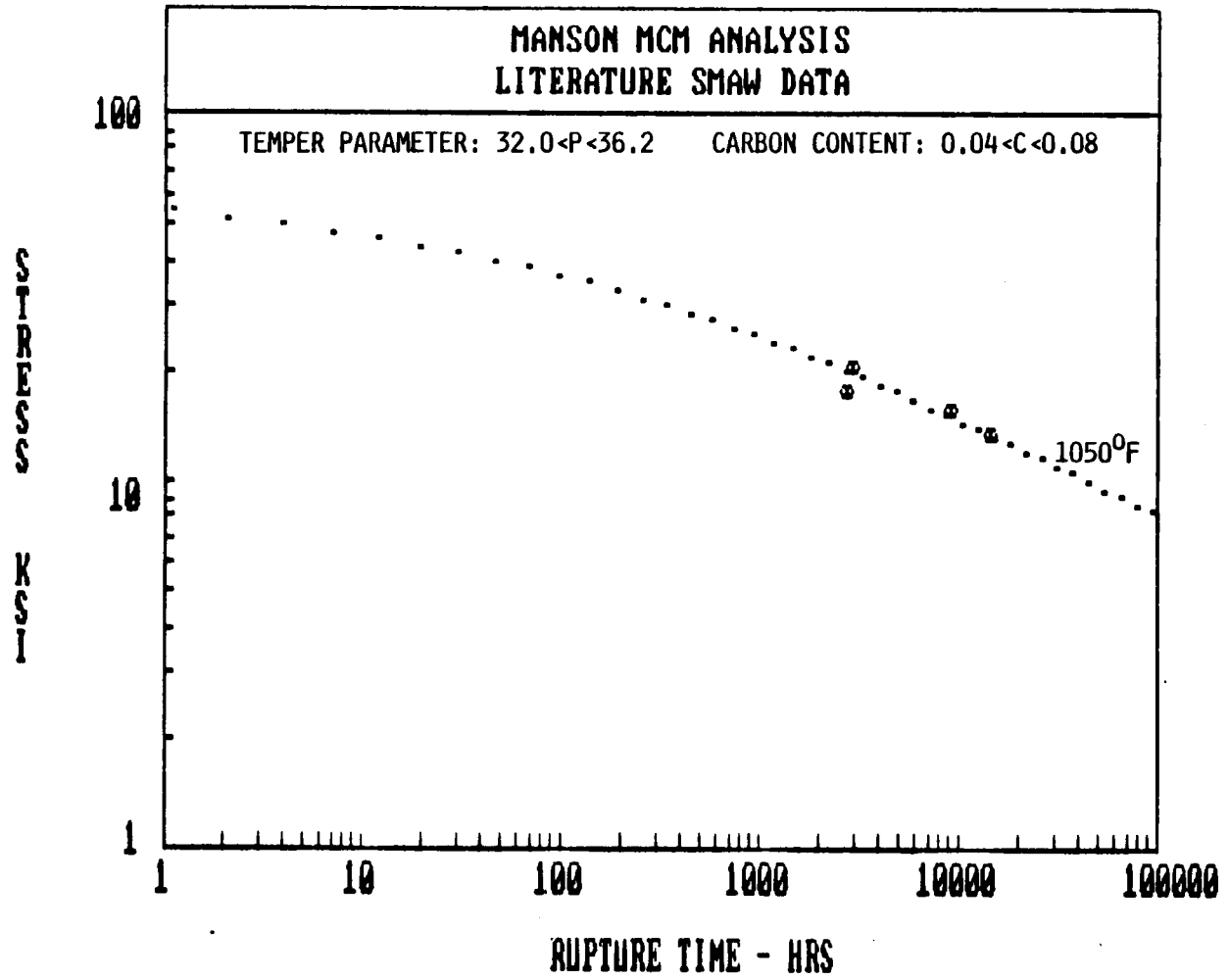


Figure A68. Manson MCM analysis of PWHT 2-1/4Cr-1Mo SMA weld metal (32.0<P<36.2, 0.04<C<0.08) at 1050°F as determined from literature data.

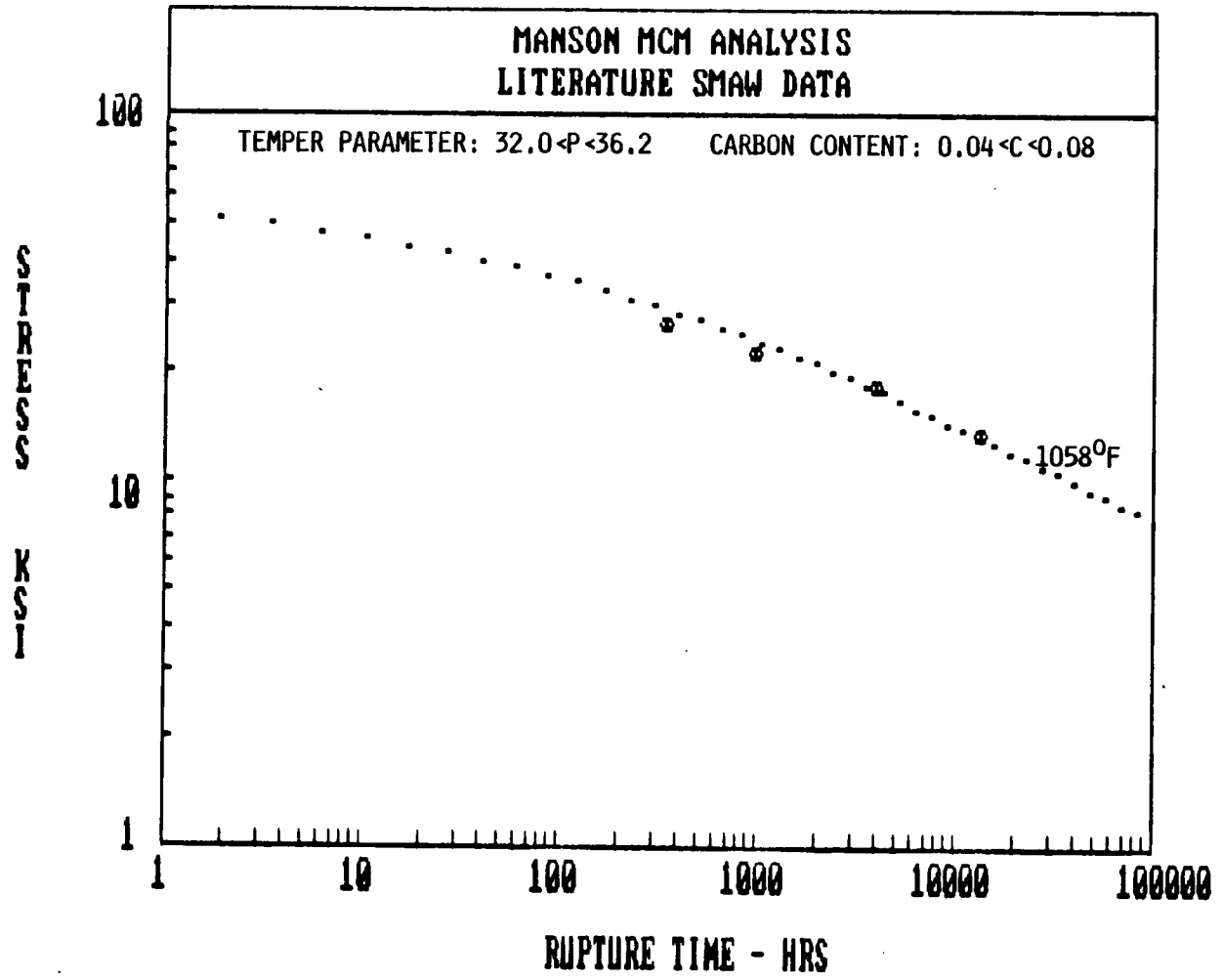


Figure A69. Manson MCM analysis of PWHT 2-1/4Cr-1Mo SMA weld metal (32.0<P<36.2, 0.04<C<0.08) at 1058°F as determined from literature data.

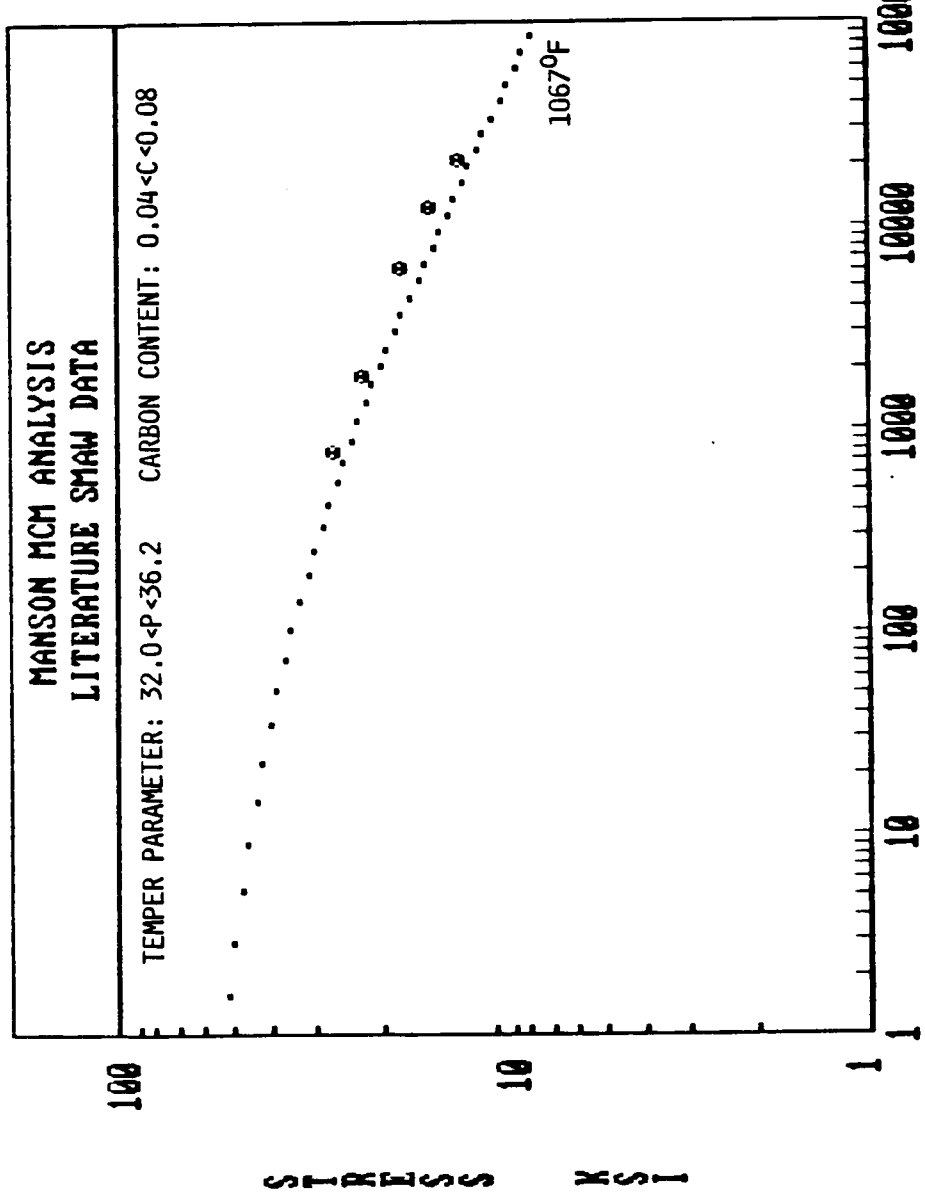


Figure A70. Manson MCM analysis of PWHT 2-1/4Cr-1Mo SMA weld metal (32.0<P<36.2, 0.04<C<0.08) at 1067°F as determined from literature data.

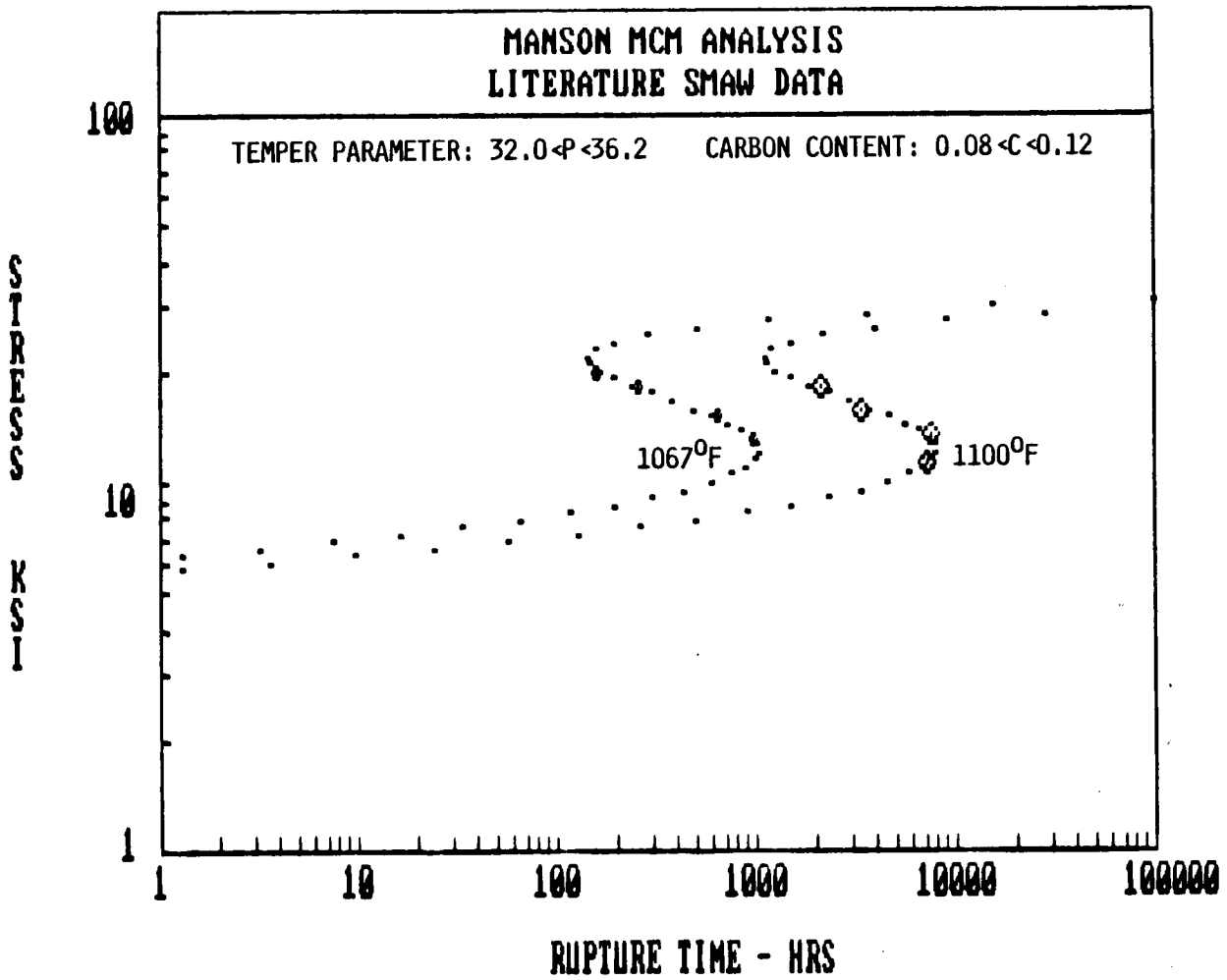


Figure A71. Manson MCM analysis of PWHT 2-1/4Cr-1Mo SMA weld metal (32.0<P<36.2, 0.08<C<0.12) at 1067 and 1100°F as determined from literature data.

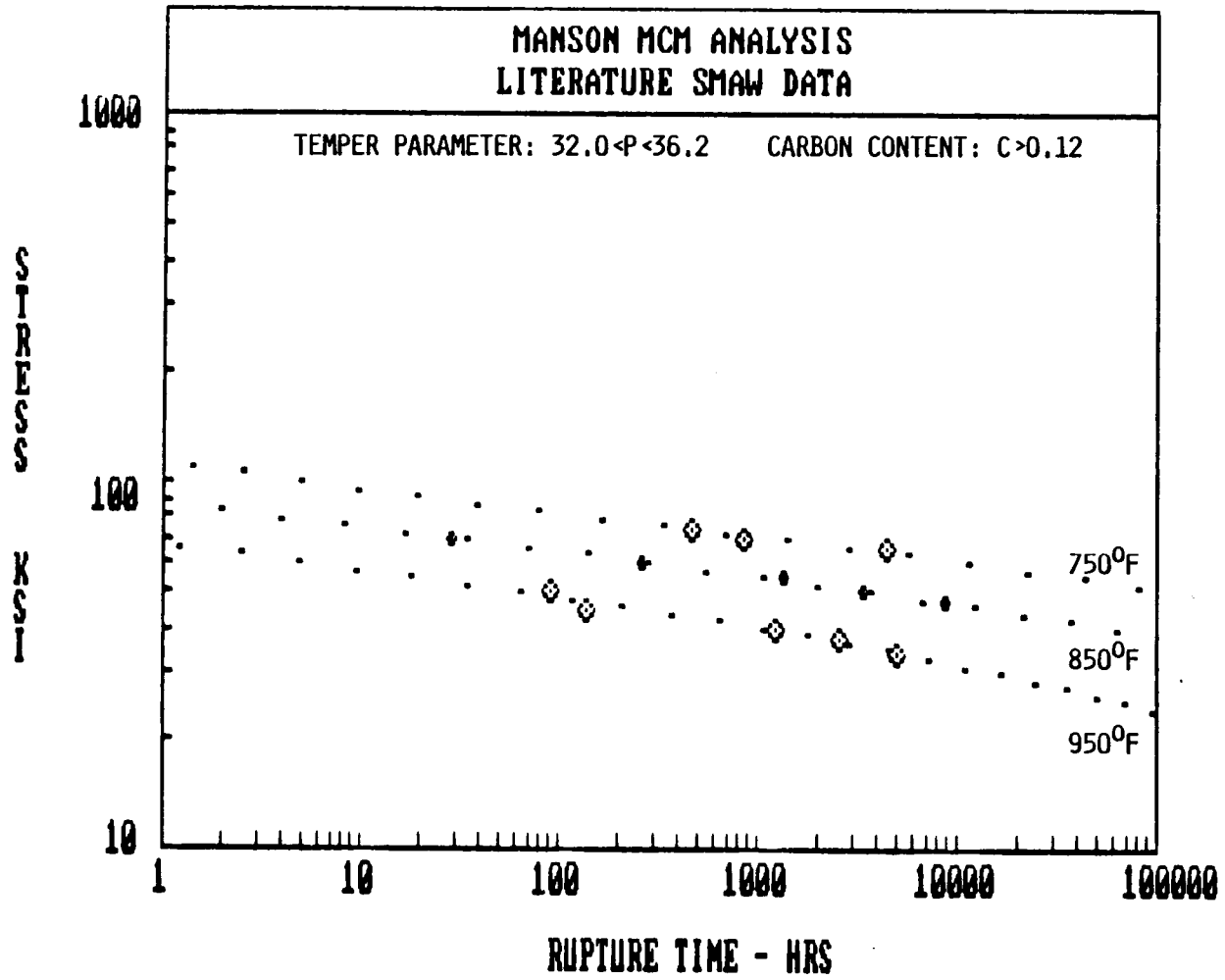


Figure A72. Manson MCM analysis of PWHT 2-1/4Cr-1Mo SMA weld metal (32.0<P<36.2, C>0.12) at 750, 850, and 950°F as determined from literature data.

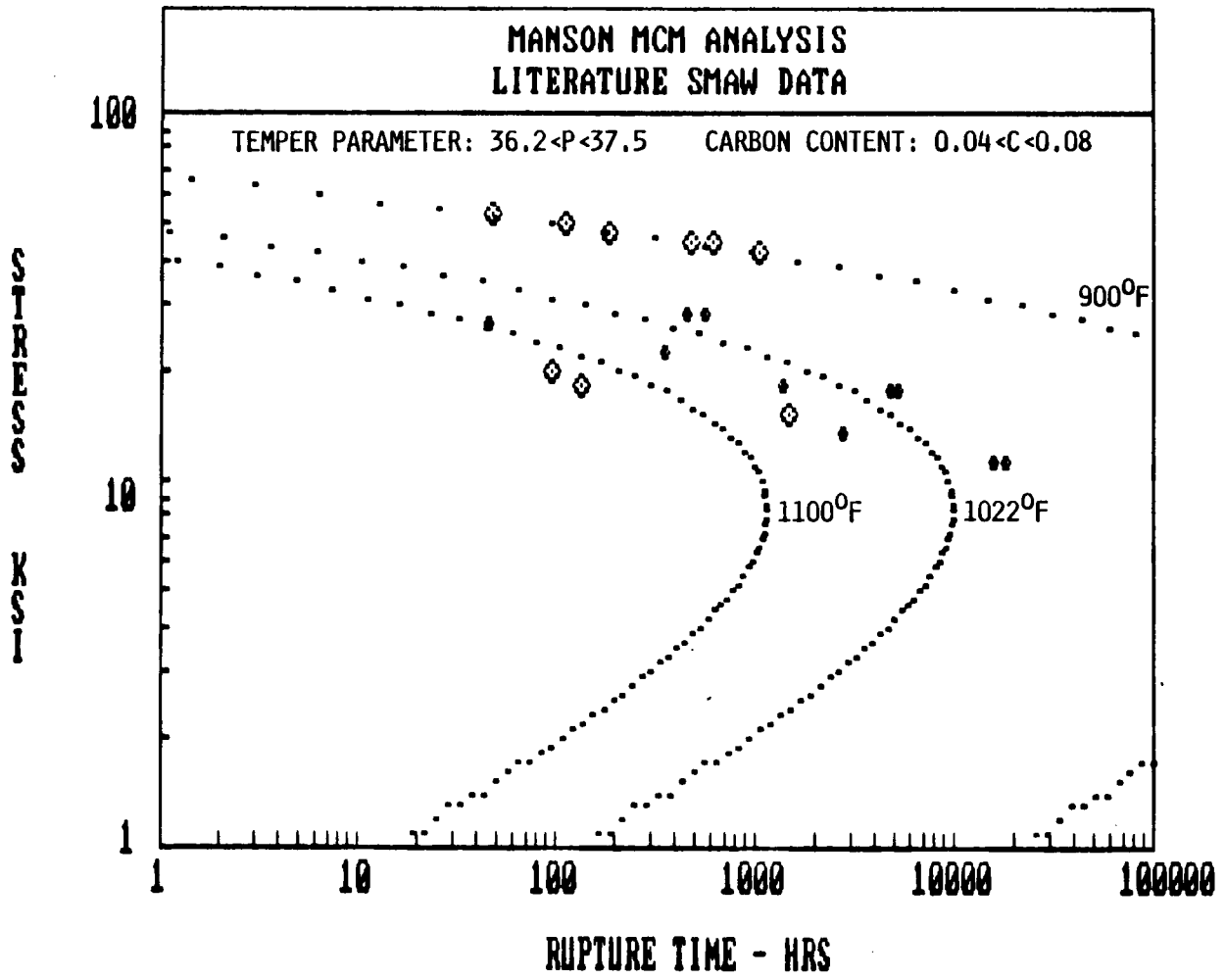


Figure A73. Manson MCM analysis of PWHT 2-1/4Cr-1Mo SMA weld metal (36.2<P<37.5, 0.04<C<0.08) at 900, 1022, and 1100°F as determined from literature data.

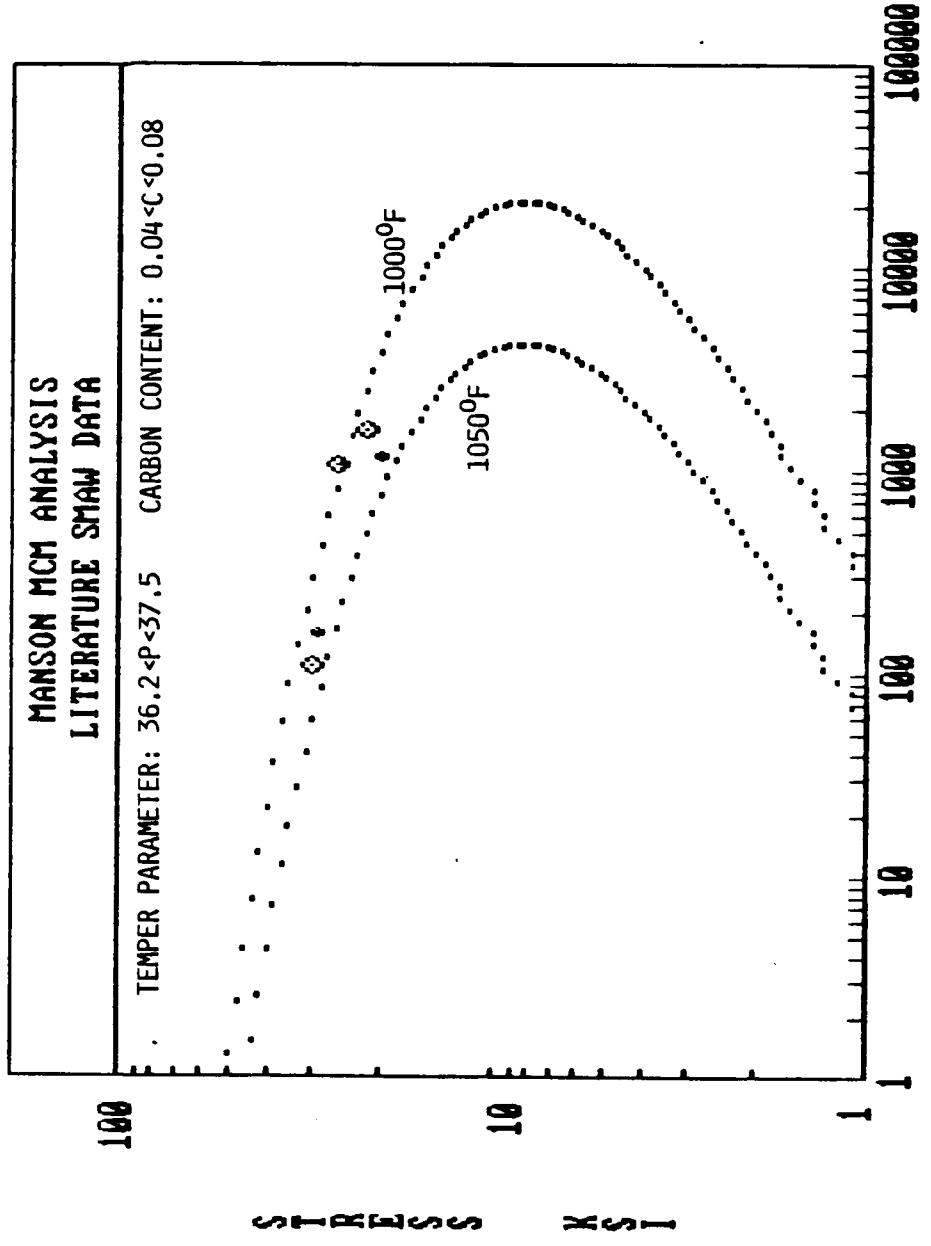


Figure A74. Manson MCM analysis of PWHT 2-1/4Cr-1Mo SMA weld metal (36.2<P<37.5, 0.04<C<0.08) at 1000 and 1050°F as determined from literature data.

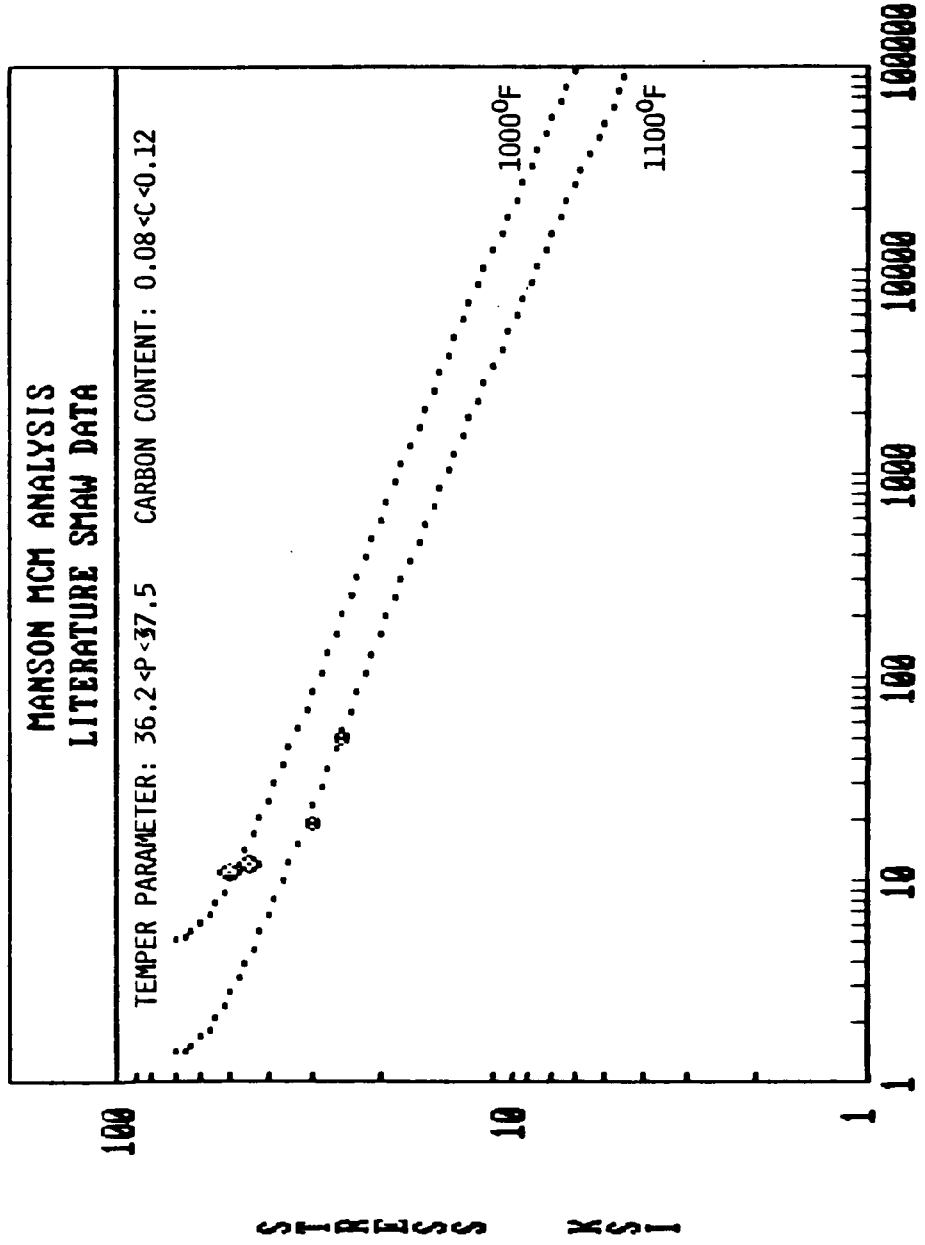


Figure A75. Manson MCM analysis of PWHT 2-1/4Cr-1Mo SMA weld metal (36.2<P<37.5, 0.08<C<0.12) at 1000 and 1100°F as determined from literature data.

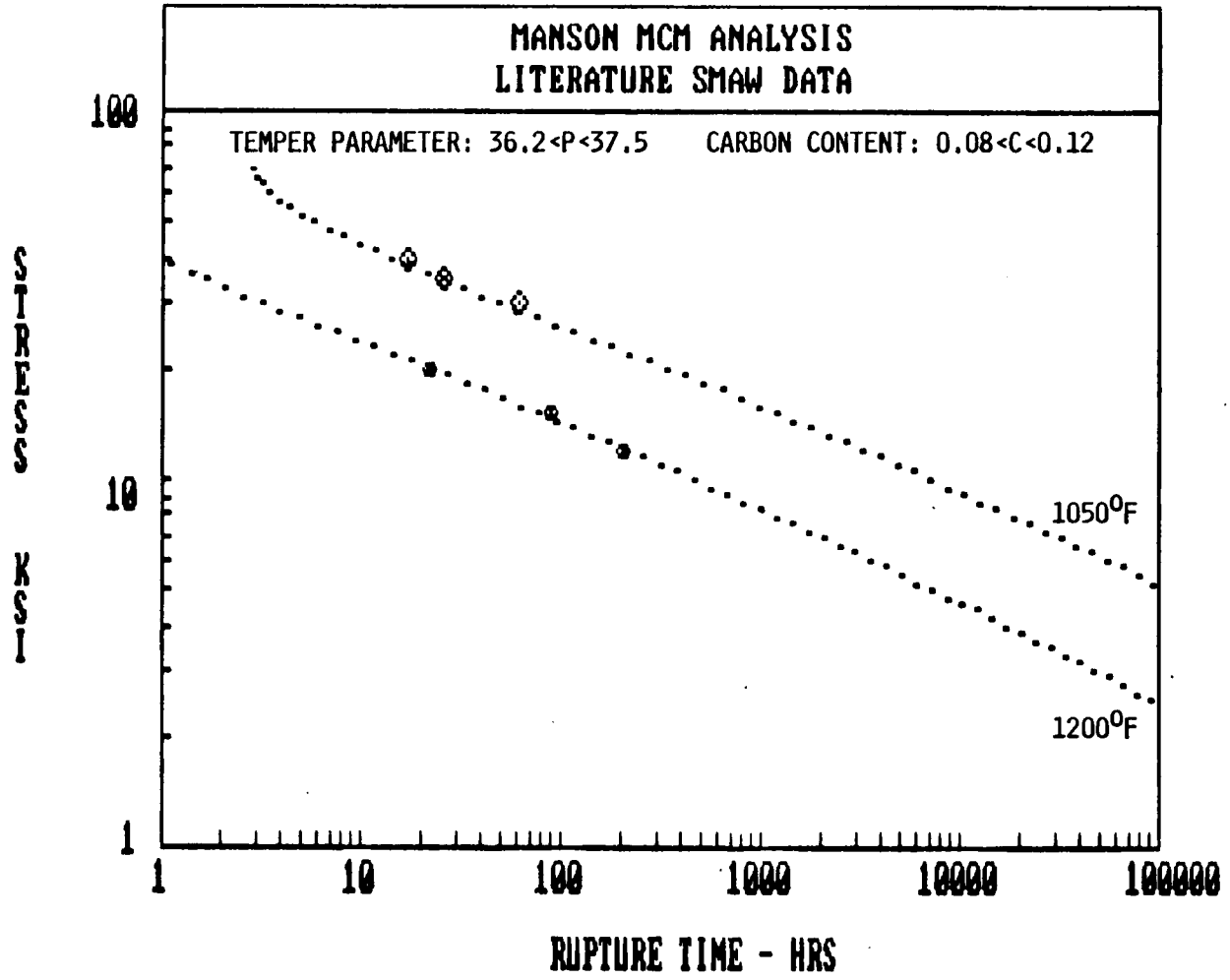


Figure A76. Manson MCM analysis of PWHT 2-1/4Cr-1Mo SMA weld metal (36.2<P<37.5, 0.08<C<0.12) at 1050 and 1200°F as determined from literature data.

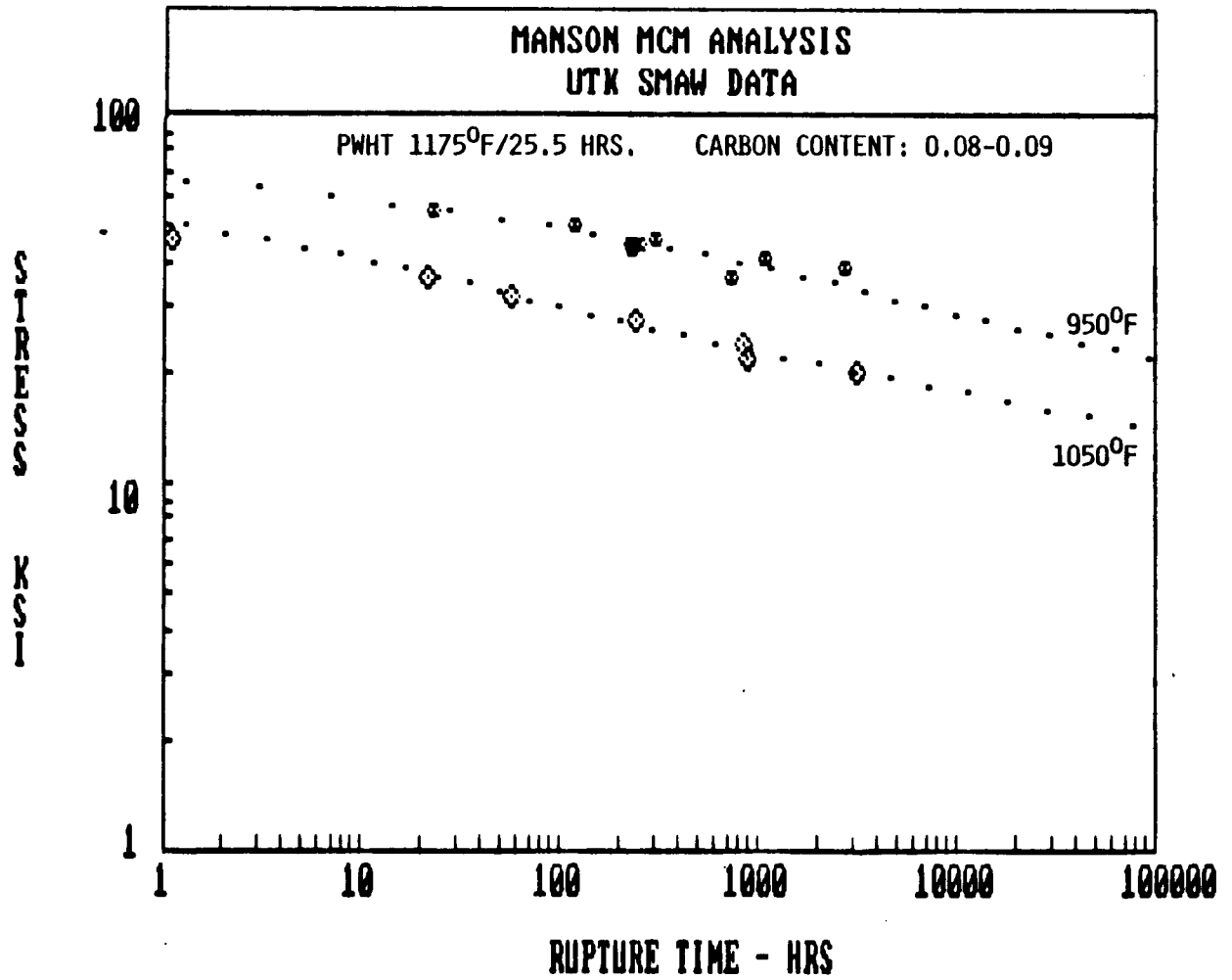


Figure A77. Manson MCM analysis of 2-1/4Cr-1Mo SMA weld metal PWHT 1175°F/25.5 hrs. (Class 3, 0.08-0.09C) at 950 and 1050°F as determined from UTK data.

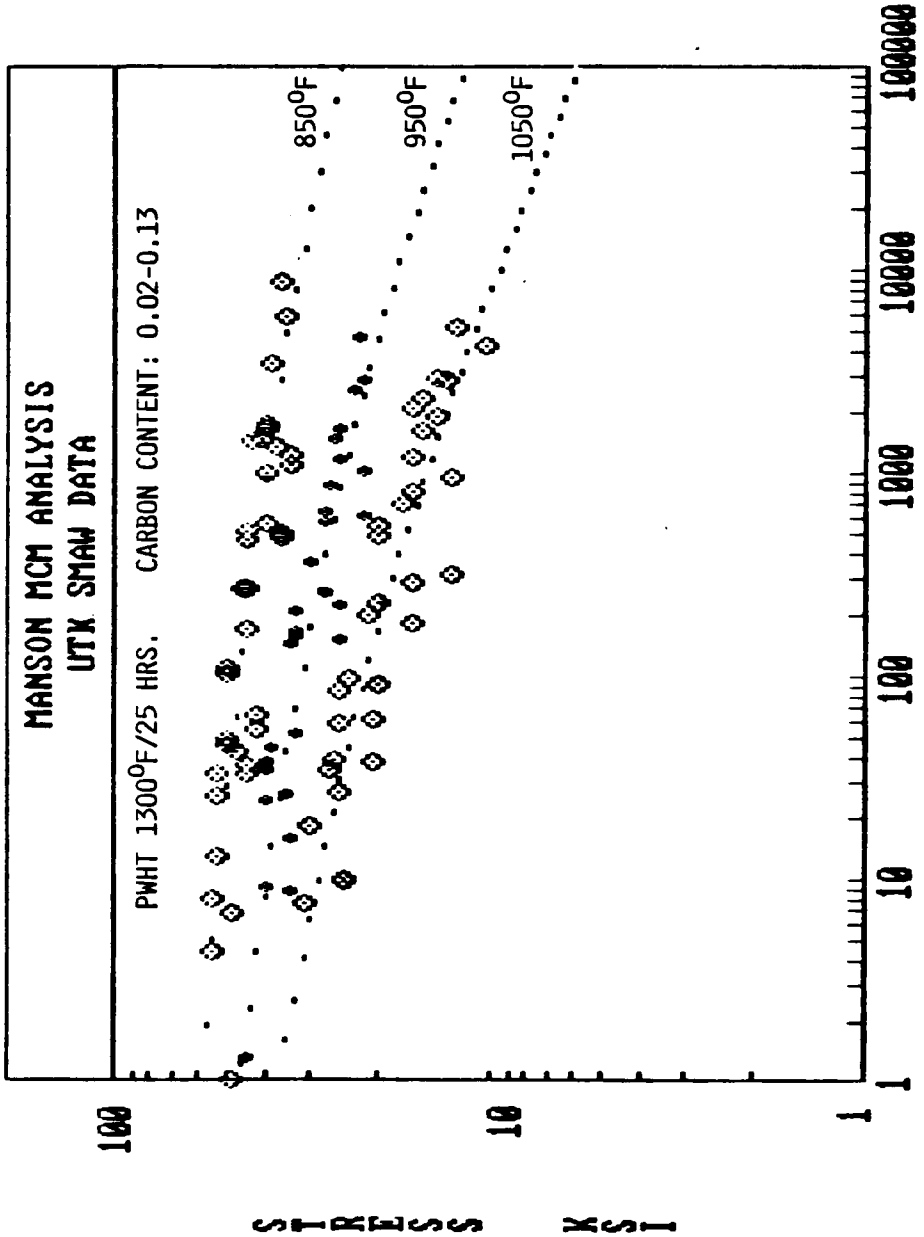


Figure A78. Manson MCM analysis of 2-1/4Cr-1Mo SMA weld metal PWHT 1300°F/25 hrs. (Class 2, 0.02-0.13C) at 850, 950, and 1050°F as determined from UTK data.

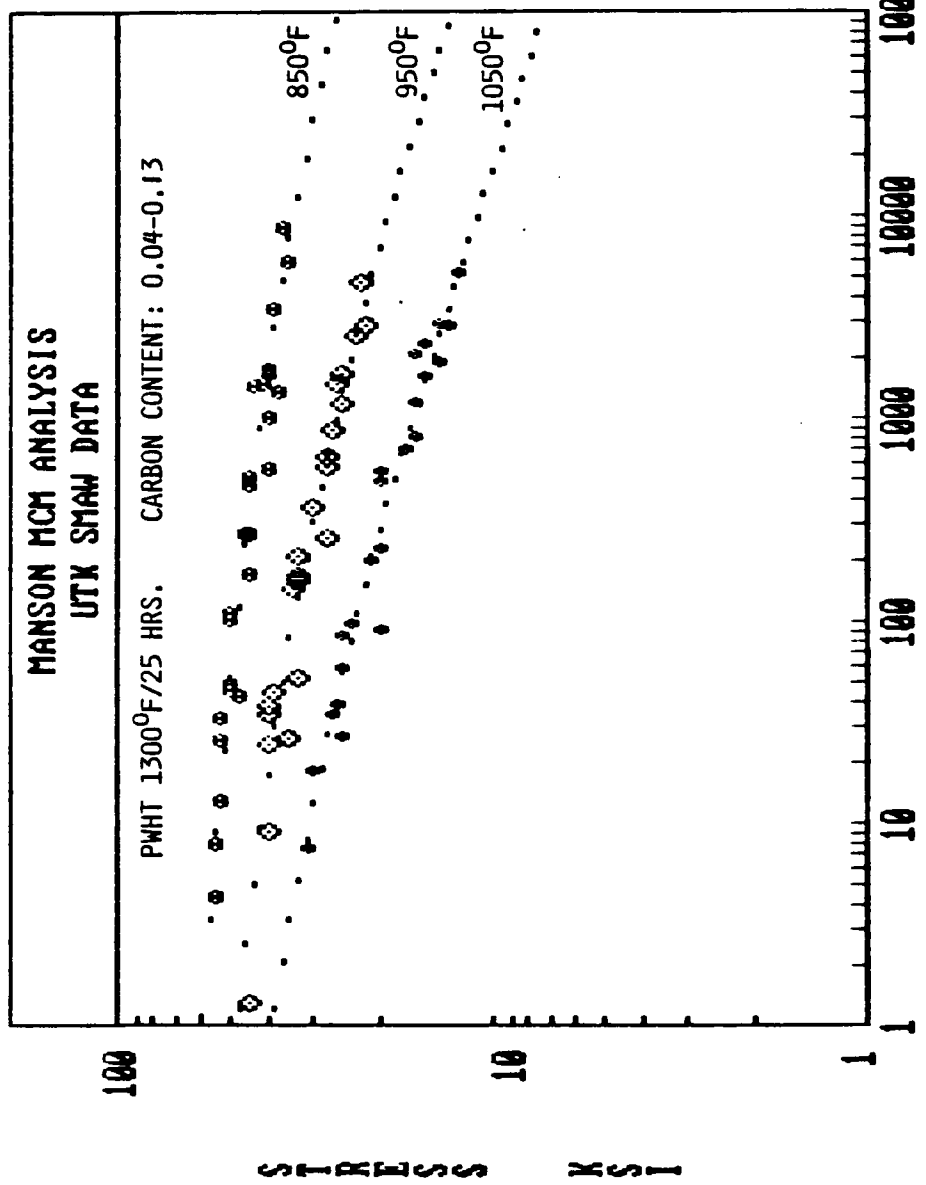


Figure A79. Manson MCM analysis of 2-1/4Cr-1Mo SMA weld metal PWHT 1300°F/25 hrs. (Class 2, 0.04-0.13C) at 850, 950, and 1050°F as determined from UTK data.

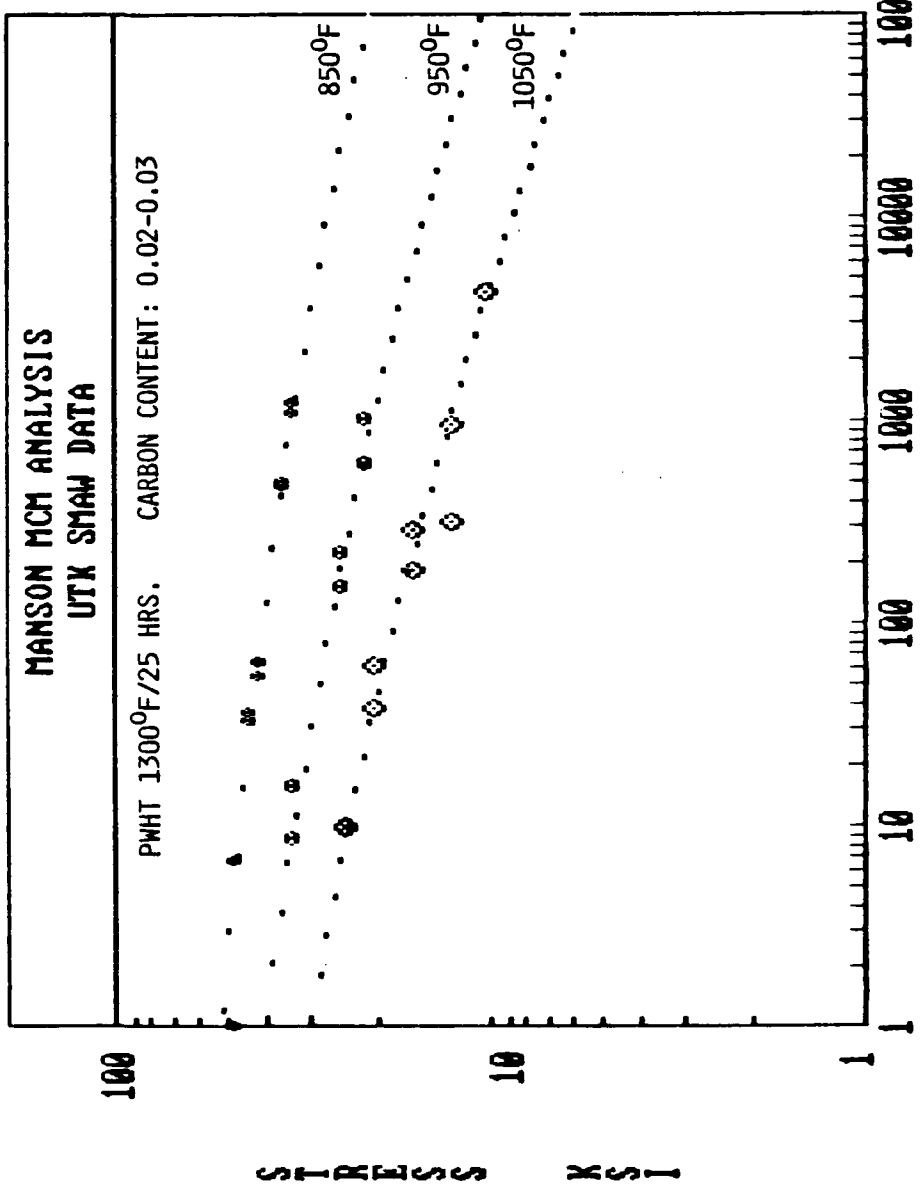


Figure A80. Manson MCM analysis of 2-1/4Cr-1Mo SMA weld PWHT 1300°F/25 hrs. Class 2, 0.02-0.03C) at 850, 950, and 1050°F as determined from UTK data.

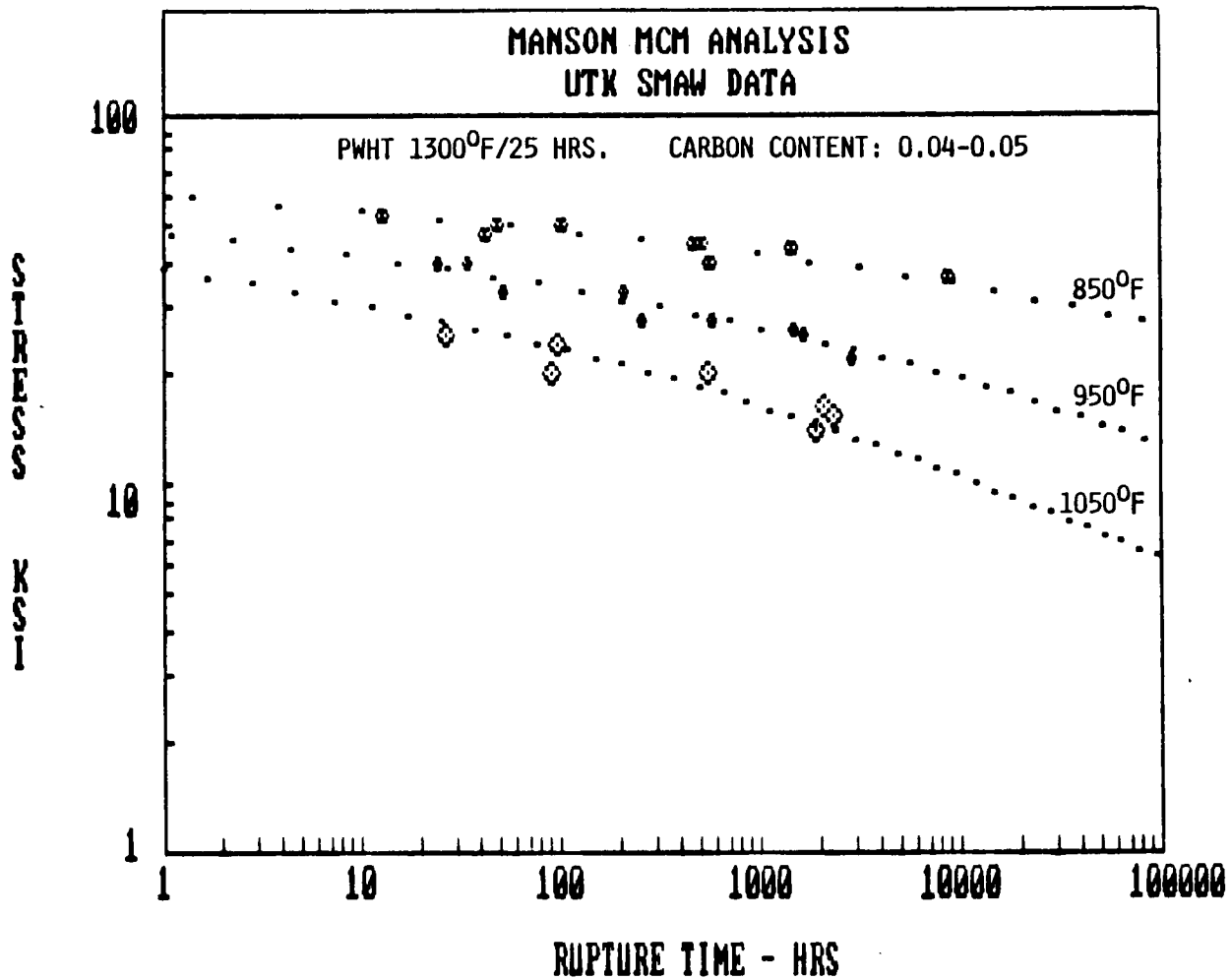


Figure A81. Manson MCM analysis of 2-1/4Cr-1Mo SMA weld metal PWHT 1300°F/25 hrs. (Class 2, 0.04-0.05C) at 850, 950, and 1050°F as determined from UTK data.

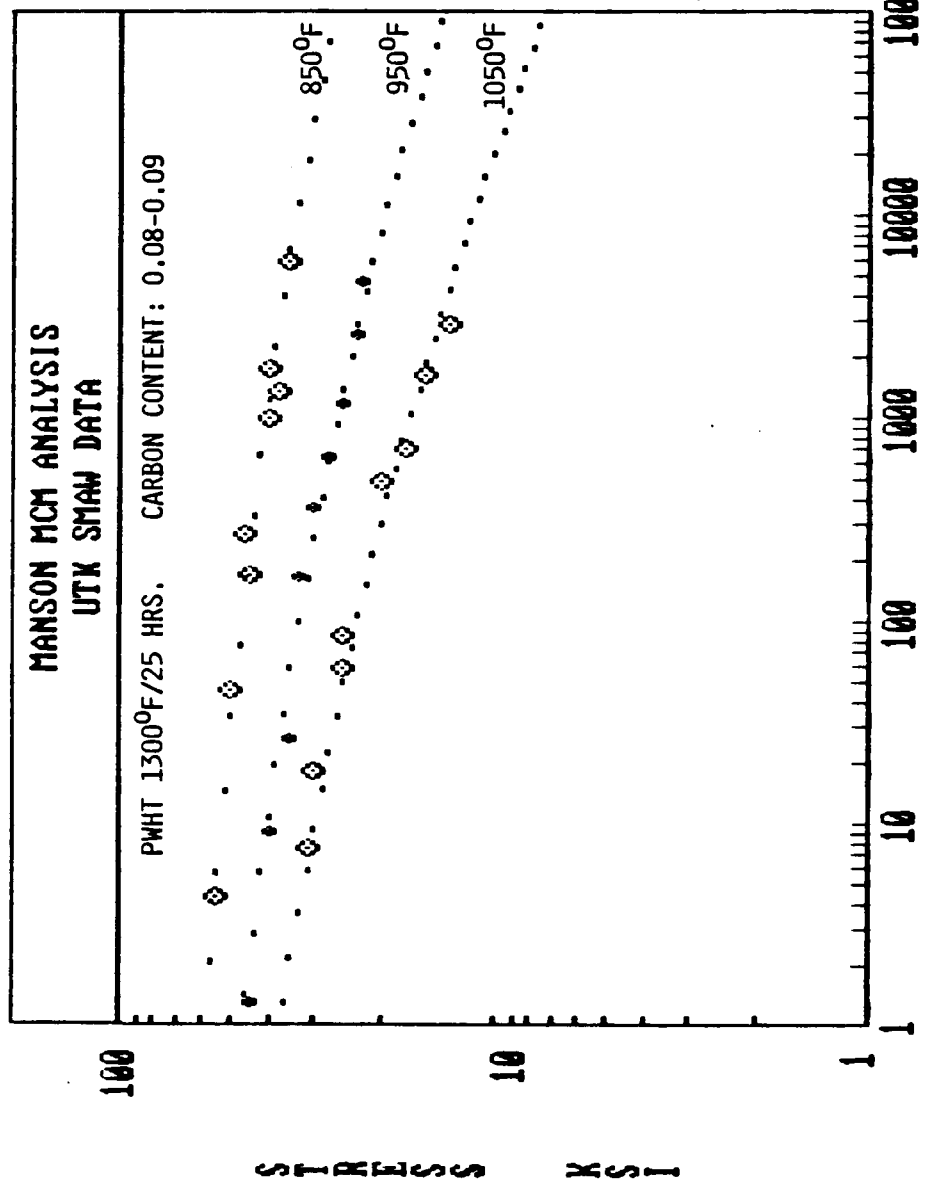


Figure A82. Manson MCM analysis of 2-1/4Cr-1Mo SMA weld metal PWHT 1300°F/25 hrs. (Class 2, 0.08-0.09C) at 850, 950, and 1050°F as determined from UTK data.

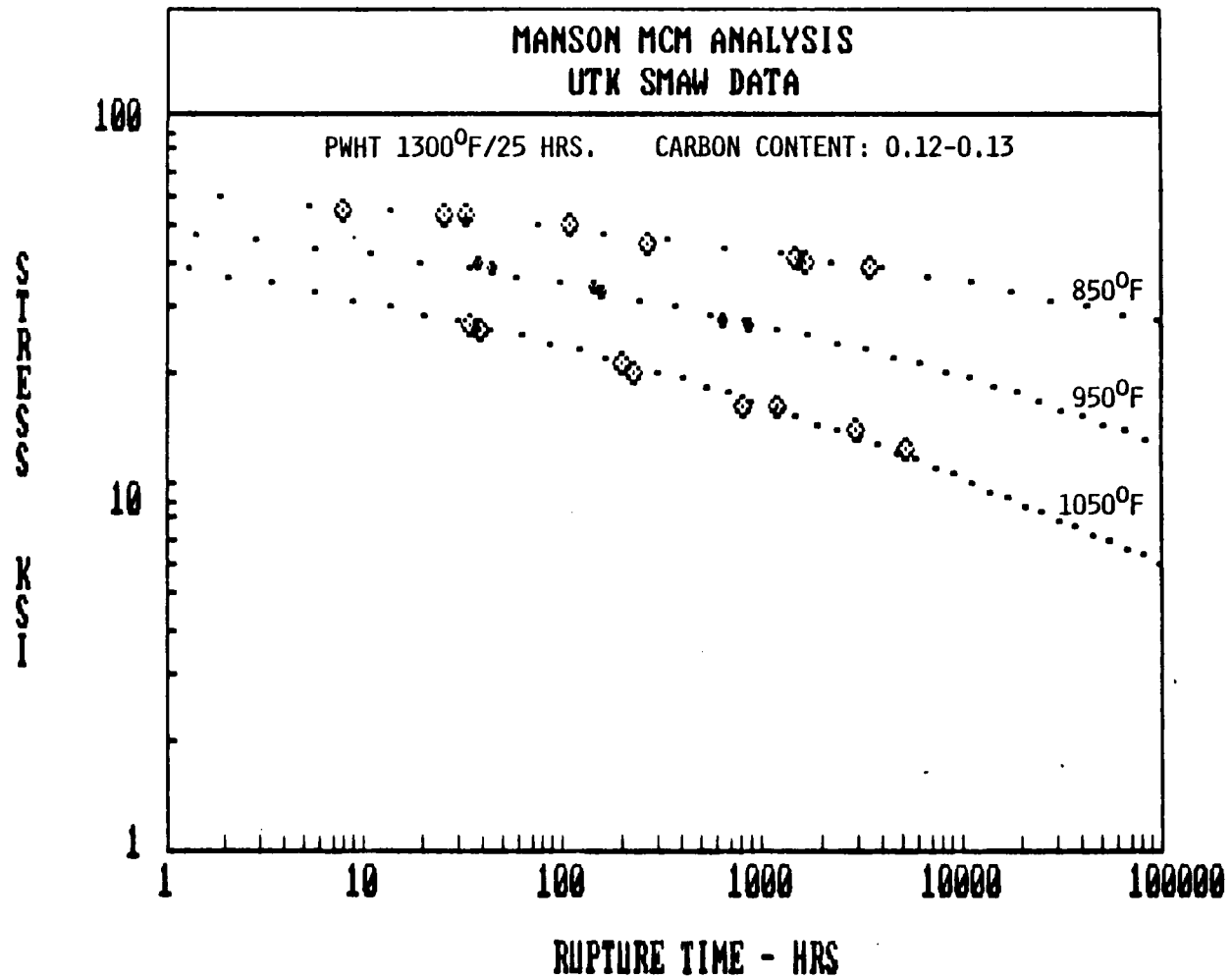


Figure A83. Manson MCM analysis of 2-1/4Cr-1Mo SMA weld metal PWHT 1300°F/25 hrs. (Class 2, 0.12-0.13C) at 850, 950, and 1050°F as determined from UTK data.

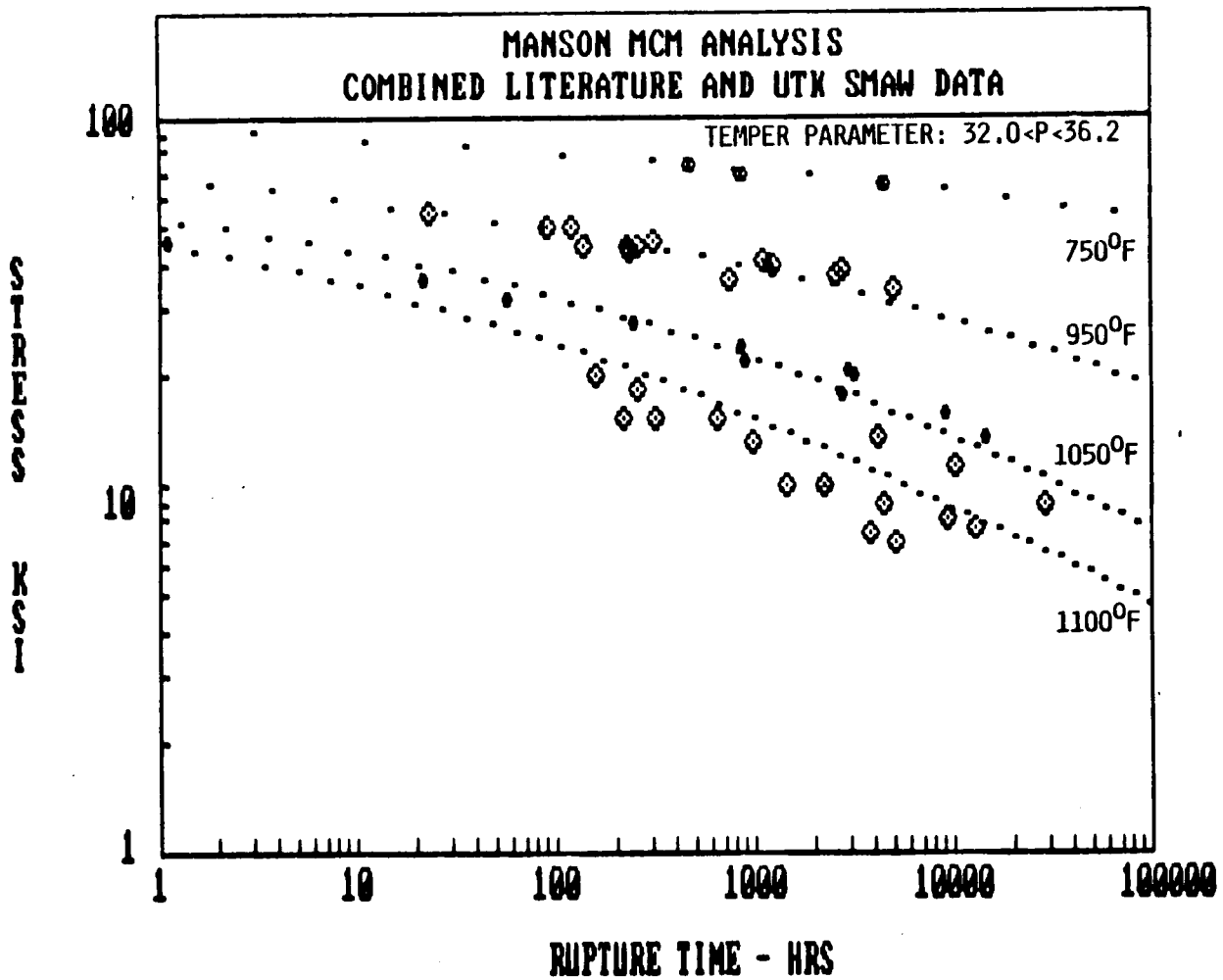


Figure A84. Manson MCM analysis of PWHT 2-1/4Cr-1Mo SMA weld metal (32.0<P<36.2) at 750, 950, 1050, and 1100°F as determined from combined literature and UTK data.

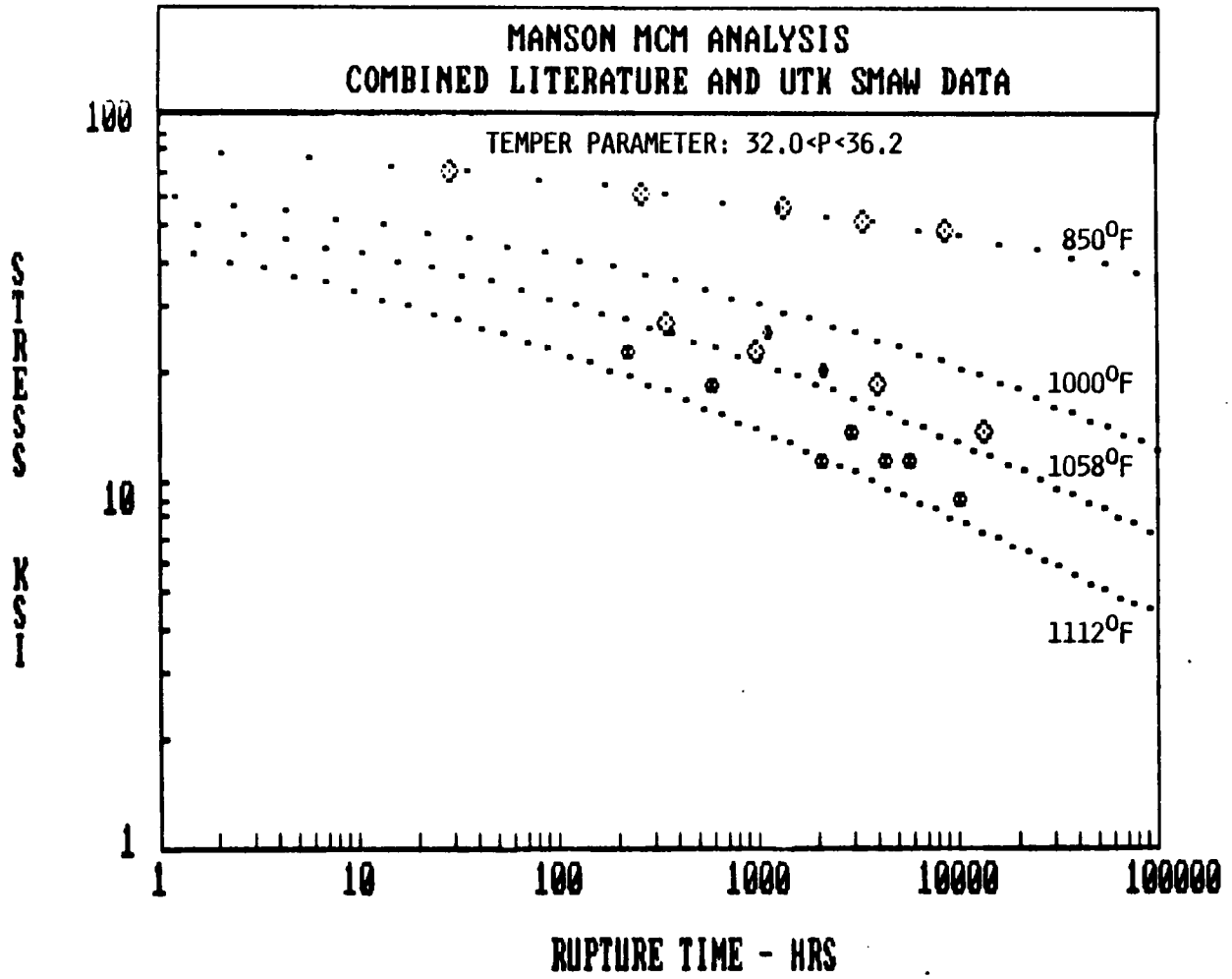


Figure A85. Manson MCM analysis of PWHT 2-1/4Cr-1Mo SMA weld metal (32.0<P<36.2) at 850, 1000, 1058, 1112 °F as determined from combined literature and UTK data.

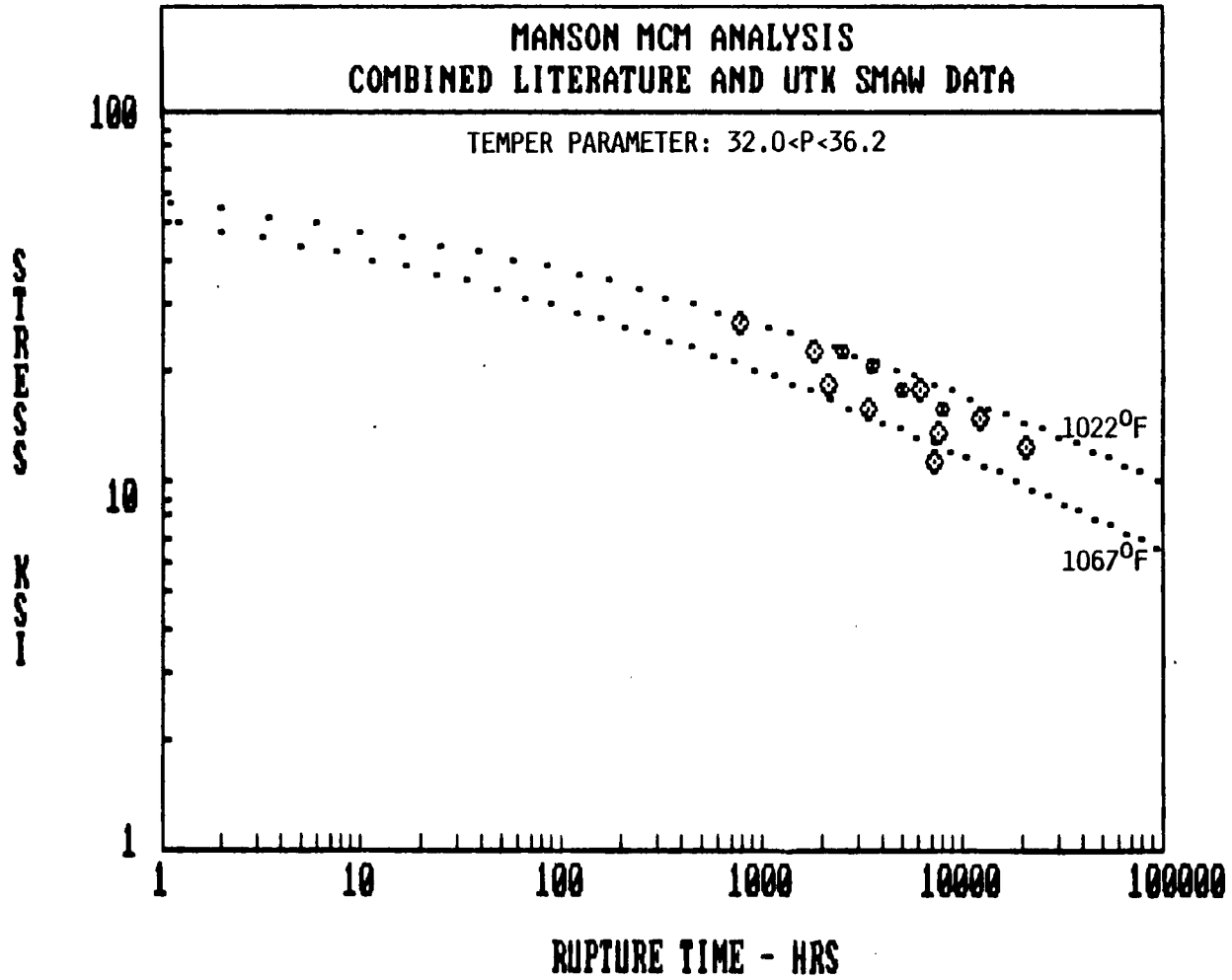


Figure A86. Manson MCM analysis of PWHT 2-1/4Cr-1Mo SMA weld metal (32.0<P<36.2) at 1022 and 1067°F as determined from combined literature and UTK data.

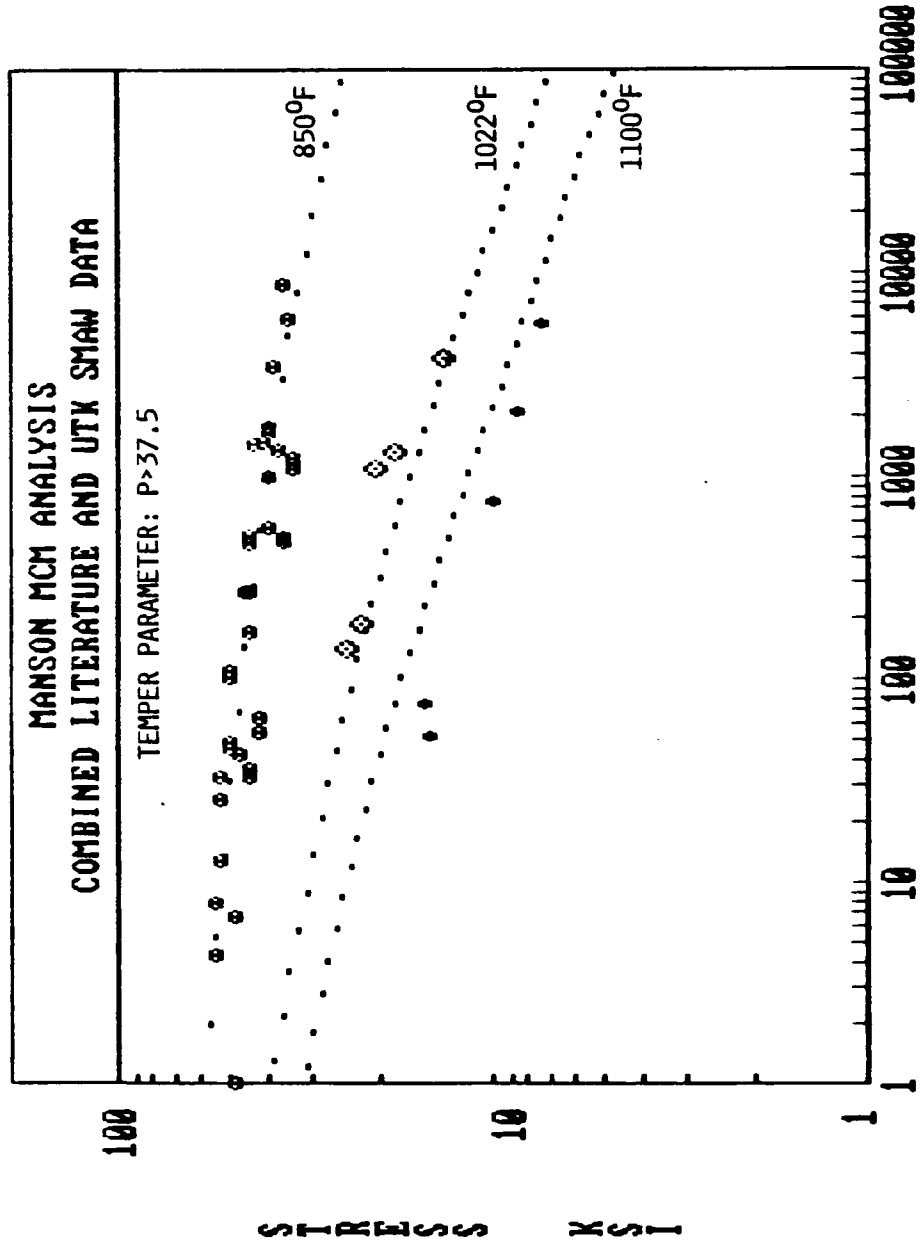


Figure A87. Manson MCM analysis of PWHT 2-1/4Cr-1Mo SMA weld metal (P>37.5) at 850, 1022, 1100°F as determined from combined literature and UTK data.

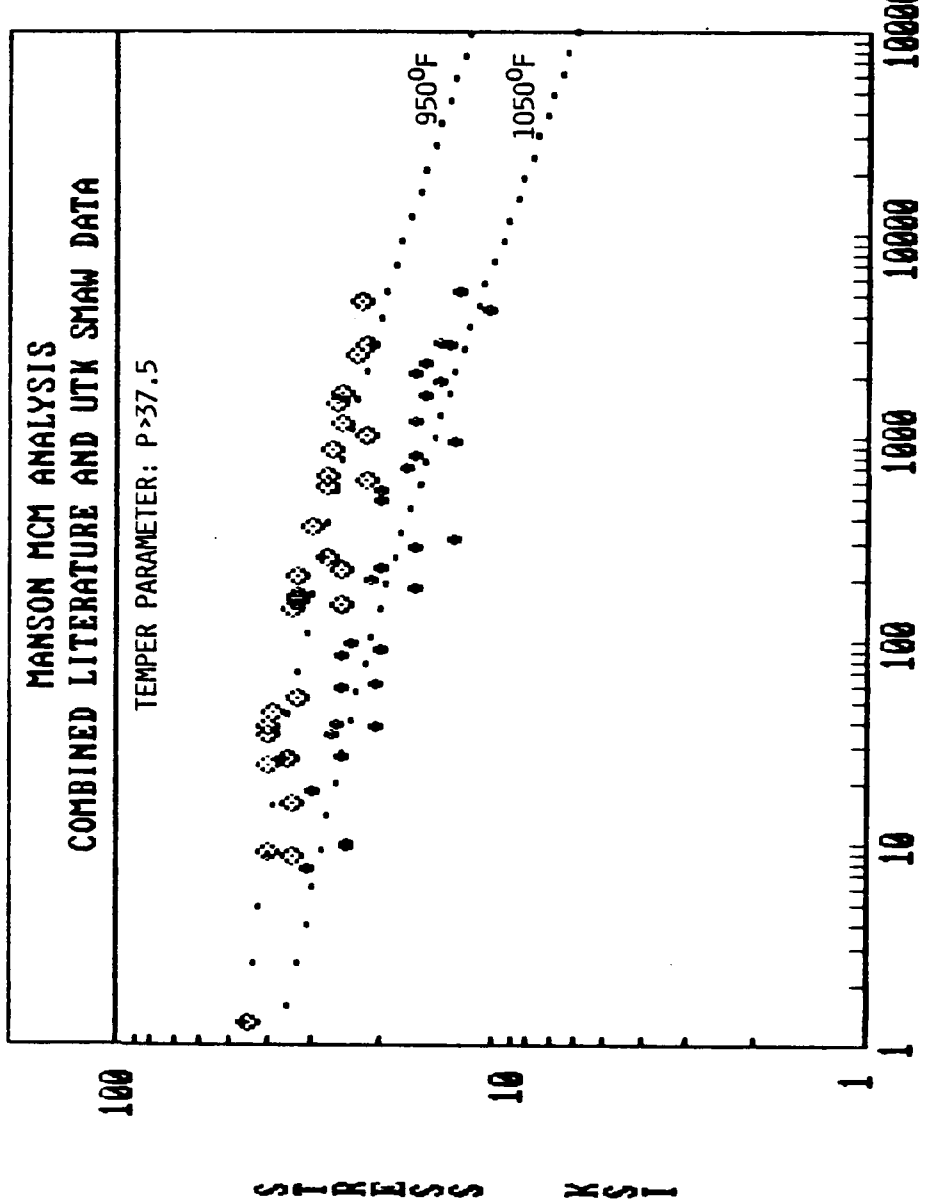


Figure A88. Manson MCM analysis of PWHT 2-1/4Cr-1Mo SMA weld metal (P>37.5) at 950 and 1050°F as determined from combined literature and UTK data.

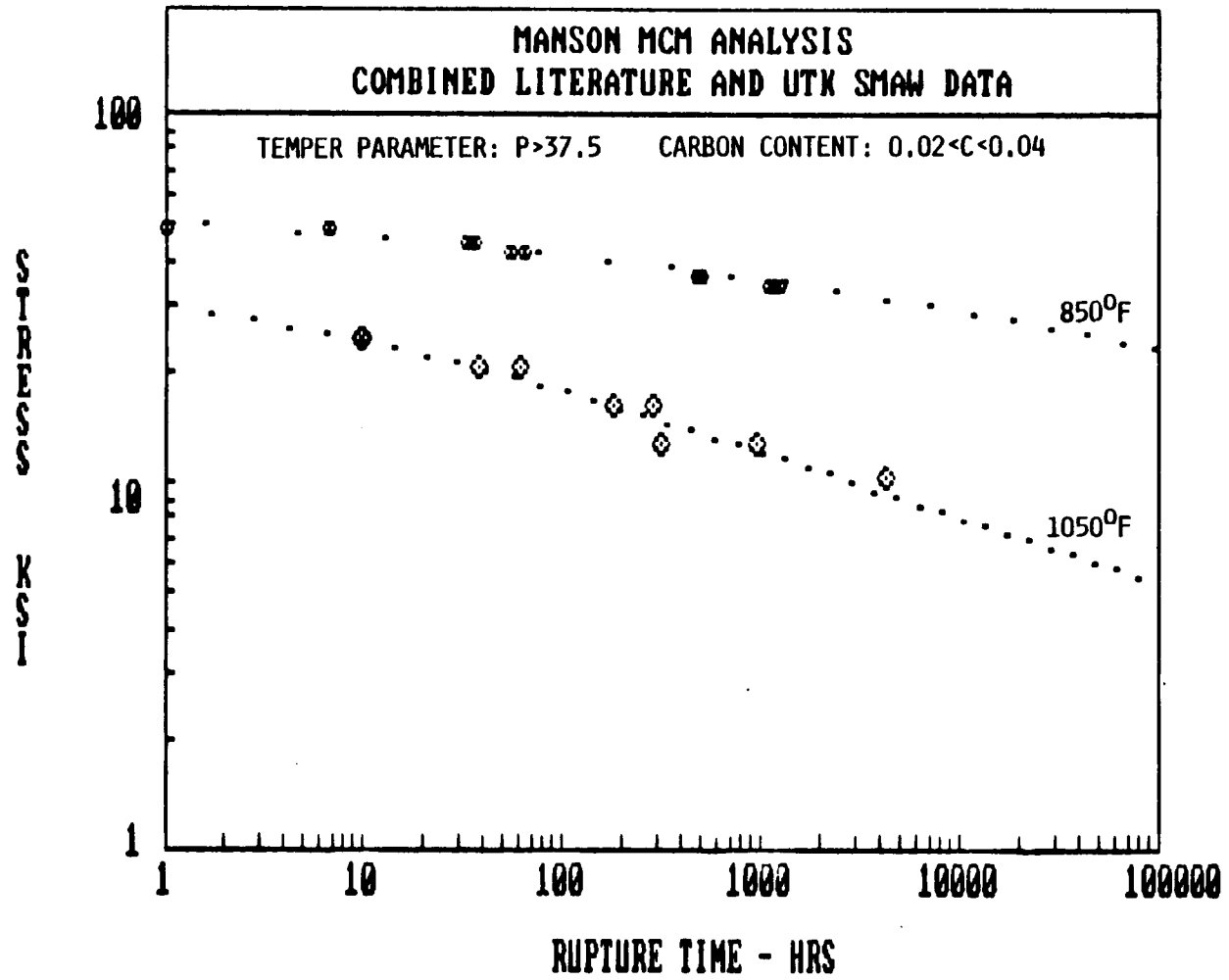


Figure A89. Manson MCM analysis of PWHT 2-1/4Cr-1Mo SMA weld metal (P>37.5, 0.02<C<0.04) at 850 and 1050°F as determined from combined literature and UTK data.

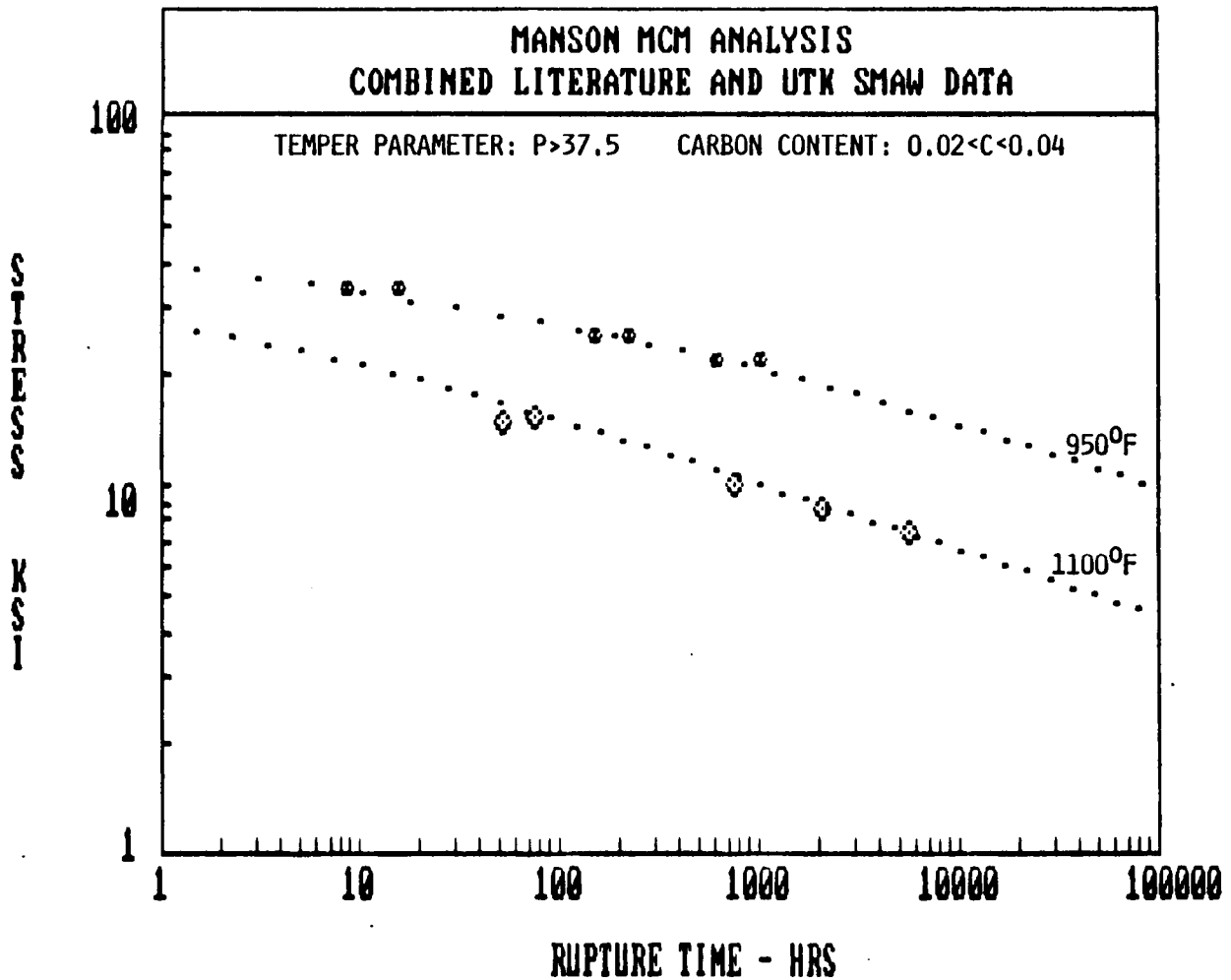


Figure A90. Manson MCM analysis of PWHT 2-1/4Cr-1Mo SMA weld metal (P>37.5, 0.02<C<0.04) at 950 and 1100°F as determined from combined literature and UTK data.

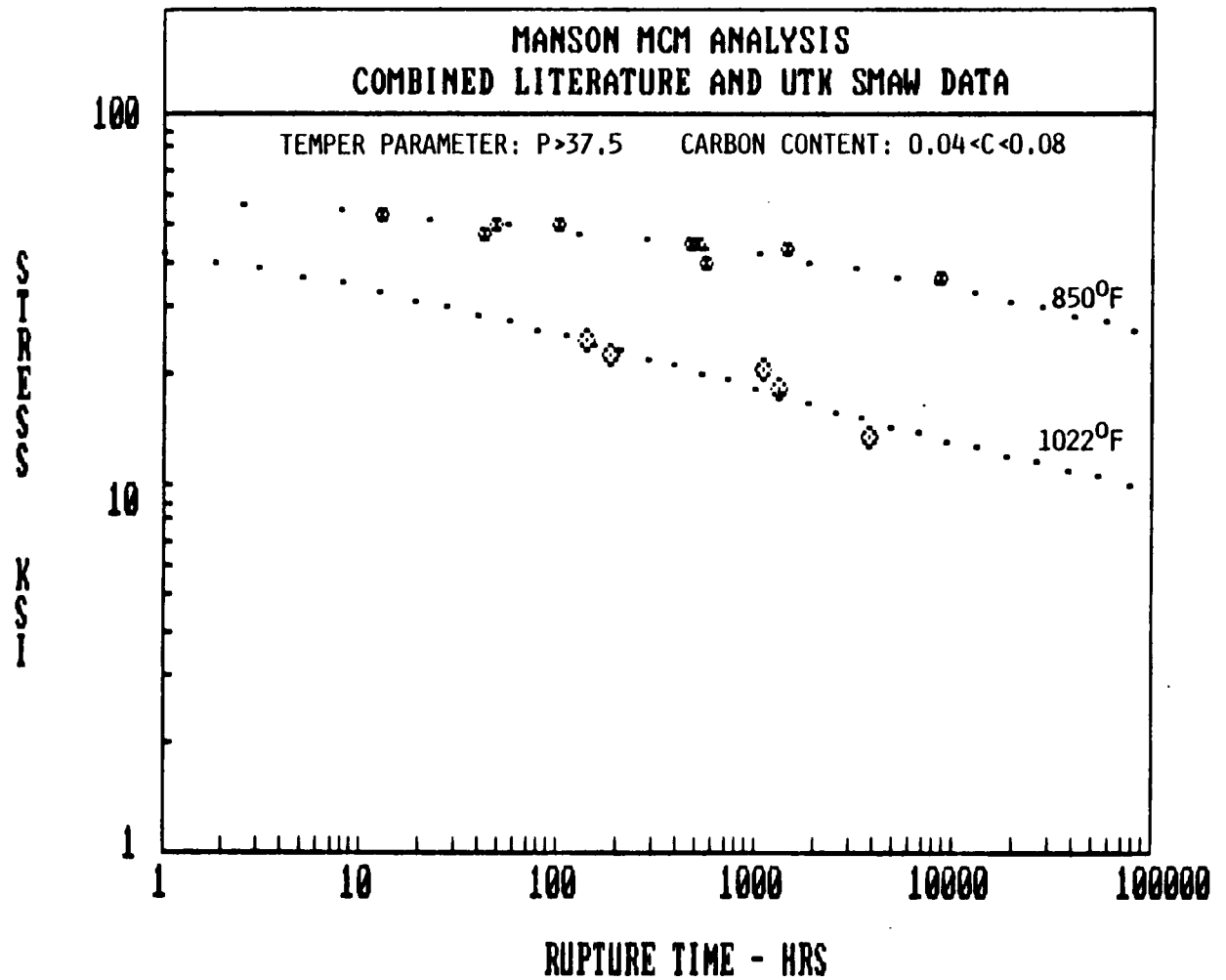


Figure A91. Manson MCM analysis of PWHT 2-1/4Cr-1Mo SMA weld metal (P>37.5, 0.04<C<0.08) at 850 and 1022°F as determined from combined literature and UTK data.

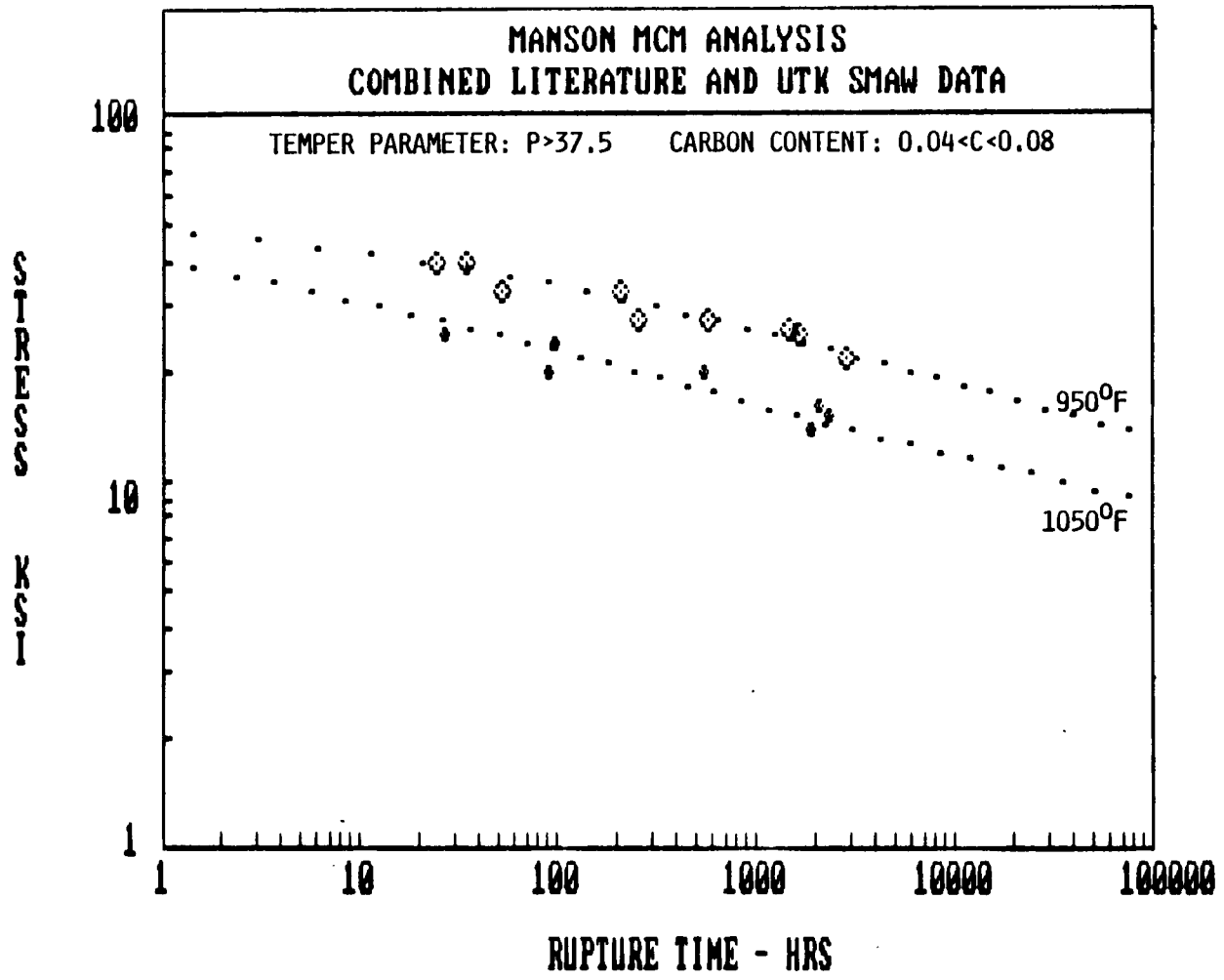


Figure A92. Manson MCM analysis of PWHT 2-1/4Cr-1Mo SMA weld metal (P>37.5, 0.04<C<0.08) at 950 and 1050°F as determined from combined literature and UTK data.

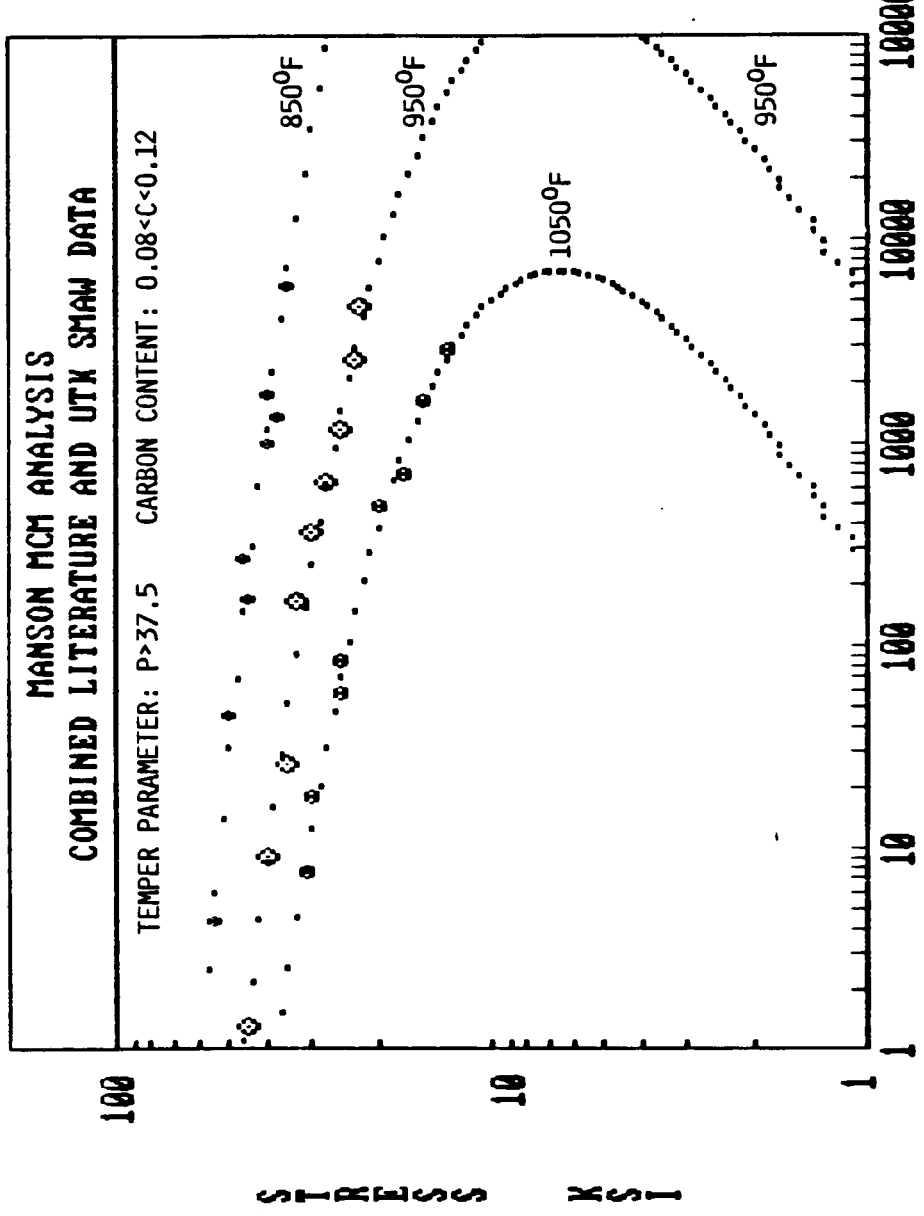


Figure A93. Manson MCM analysis of PWHT 2-1/4Cr-1Mo SMA weld metal (P>37.5, 0.08<C<0.12) at 850, 950, and 1050°F as determined from combined literature and UTK data.

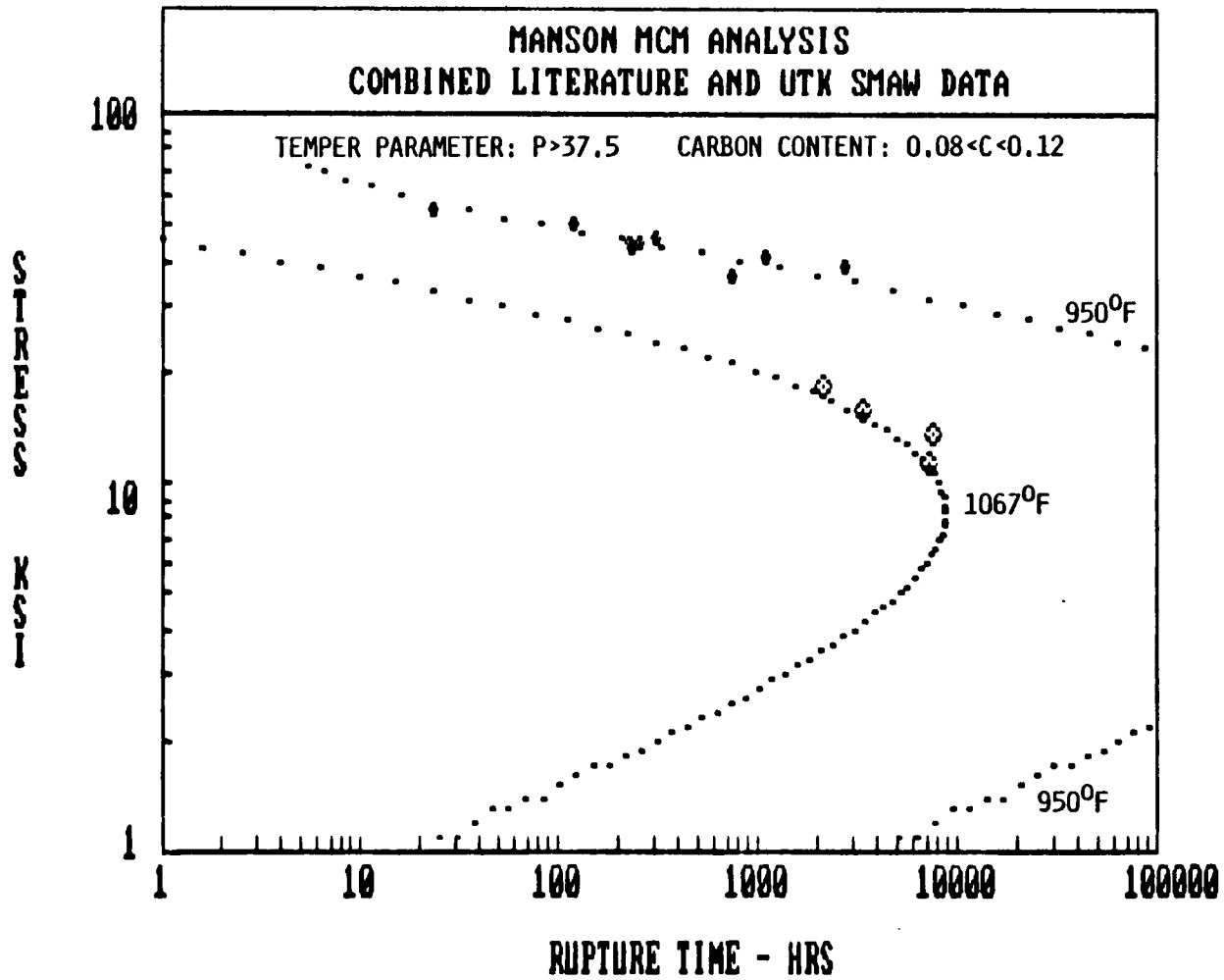


Figure A94. Manson MCM analysis of PWHT 2-1/4Cr-1Mo SMA weld metal (P>37.5, 0.08<C<0.12) at 950 and 1067°F as determined by combined literature and UTK data.

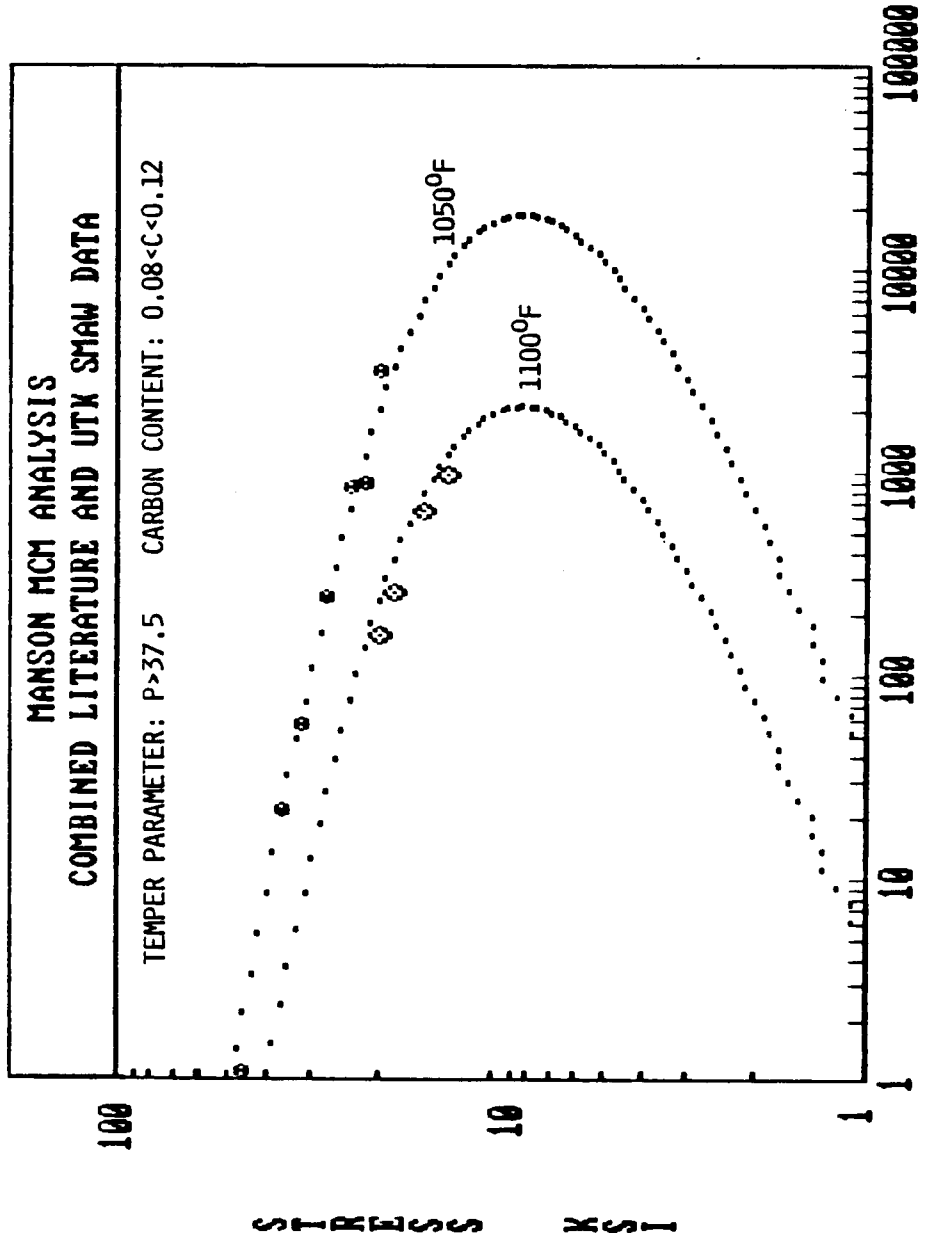


Figure A95. Manson MCM analysis of PWHT 2-1/4Cr-1Mo weld metal (P>37.5, 0.08<C<0.12) at 1050 and 1100°F as determined for combined literature and UTK data.

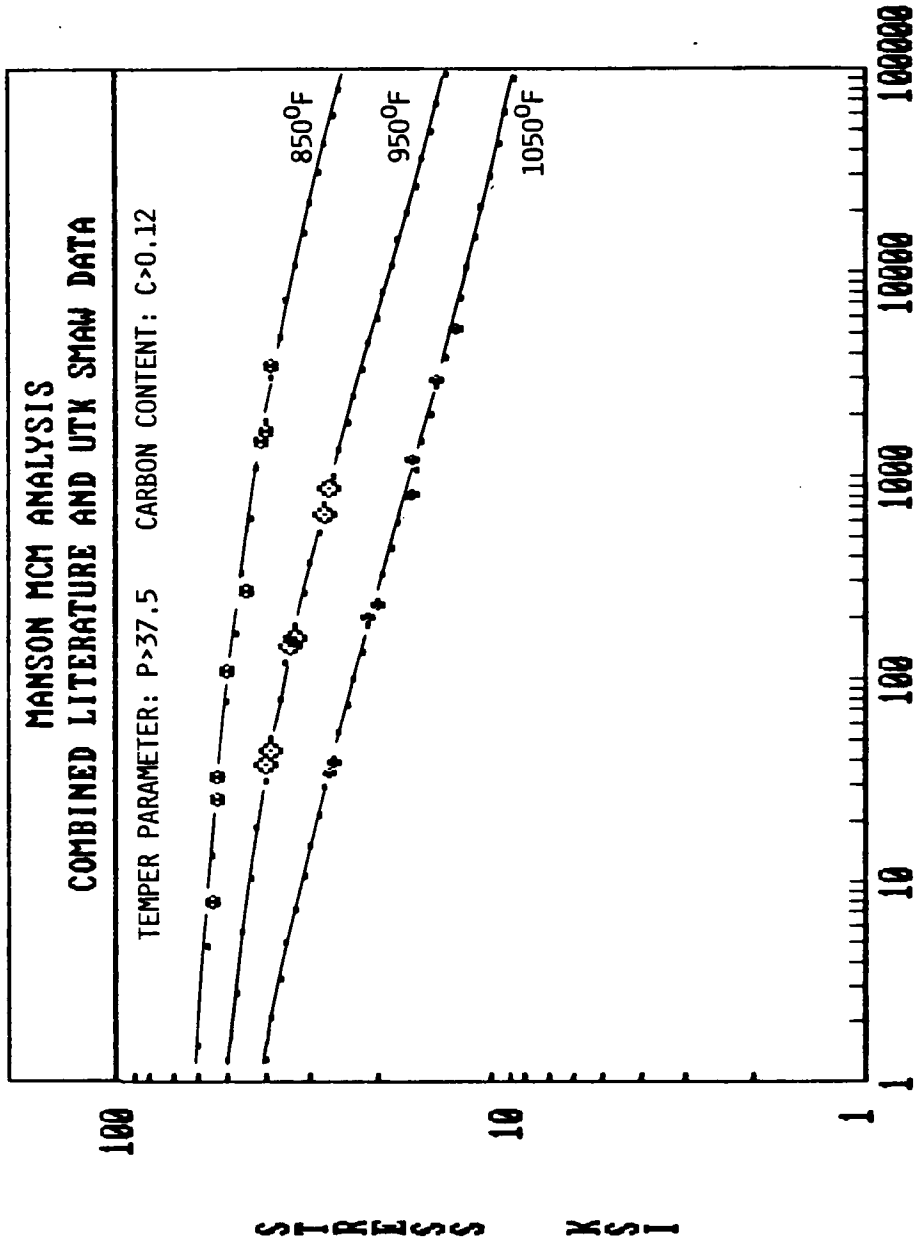


Figure A96. Manson MCM analysis of PWHT 2-1/4Cr-1Mo weld metal (P>37.5, C>0.12) at 850, 950, and 1050°F as determined from combined literature and UTK data.

APPENDIX B

STRESS RUPTURE DATA

The rupture data presented below are in the form of computer printouts from various data files. Besides listing the rupture data, these printouts also contain information on test temperature, PWHT, welding process, carbon content, and tempering parameter. All heats of data are identified with respect to the reference from which they were taken. Data obtained from UTK testing are identified using the composition descriptors employed in the text of the thesis.

Figure B1 gives an example of the rupture data format for the literature data. The first line contains all of the information which describes the heat of weld metal. The value at "A" is a file line number and is unrelated to the substance of the file. At location "C" is the number of rupture data points obtained at the test temperature given at location "B." These data points appear in the lines immediately below the main information line. At "D," the source of the data is given. The PWHT associated with the weld metal heat appears at "E" and is given in terms of a temperature and time schedule. All temperatures are in F^{o} while the times are given in hours. The welding process employed in depositing the weld metal is identified in "F." The acronyms used are in agreement with those designated by the American Welding Society. The use of "UK" at location "F" indicates that the deposition process is not specified in the literature. The carbon content of the weld metal in weight percent is given in "G." At location "H," the value of the temper

```
 A   B    C     D              E          F     G        H
 ↓   ↓    ↓     ↓              ↓          ↓     ↓        ↓
001 850   7   REF 101 PWHT 1300F/25HR   SAW  C=0.12  P=37.7
002 56.5  8.5
003 56.6  15.0
004 50.2  82.1
005 50.2  214.9
006 45.5  739.5
007 45.5  1351.2
008 42.4  7832.5
009 950  10
010 49.6  2.5
011 46.3  13.0
012 46.3  26.4
013 40.7  46.1
014 37.8  108.7
015 37.8  293.6
016 33.3  462.1
017 33.3  497.2
018 32.5  728.9
019 29.7  1893.5
020 1050 9
021 37.8  3.2
022 37.8  3.5
023 34.1  8.3
024 34.1  14.2
025 26.5  98.7
026 26.5  132.9
027 21.1  754.4
028 21.1  867.2
029 17.1  2940.7
STOP
     ↑    ↑
     I    J
```

Figure B1. Example of stress rupture data format.

parameter which characterizes the PWHT is given. The individual stresses and rupture times appear at positions "I" and "J" respectively. Stresses are given in KSI while the rupture times are in hours. Finally, the end of the data for each heat of weld metal is designated by a "stop" label.

The format employed in listing the UTK rupture data is almost identical to that used for the literature data. The only deviation occurs at position "D." Instead of giving a reference number to identify the source of the data, a descriptor is used which identifies the weld metal by its carbon range. The weld metal class may be determined by examining the PWHT specified in "E." Class 2 weld metals are associated with a PWHT of 1300^{o}F/25 hrs. while Class 3 material is PWHT 1175^{o}F/25.5 hrs.

The stress rupture data analyzed in this program are presented in two figures. Figure B2 lists the rupture data from the literature. The UTK rupture data appear in Figure B3.

```
001 850  7  REF 101 PWHT 1300F/25HR  SAW  C=0.12  P=37.7
002 56.5  8.5
003 56.6  15.0
004 50.2  82.1
005 50.2  214.9
006 45.5  739.5
007 45.5  1351.2
008 42.4  7832.5
009 950  10
010 49.6  2.5
011 46.3  13.0
012 46.3  26.4
013 40.7  46.1
014 37.8  108.7
015 37.8  293.6
016 33.3  462.1
017 33.3  497.2
018 32.5  728.9
019 29.7  1893.5
020 1050 9
021 37.8  3.2
022 37.8  3.5
023 34.1  8.3
024 34.1  14.2
025 26.5  98.7
026 26.5  132.9
027 21.1  754.4
028 21.1  867.2
029 17.1  2940.7
STOP
030 1022 4  REF 73  PWHT 1202F/12HR  SAW  C=0.07  P=35.0
031 24.7  1024.0
032 20.2  3478.0
033 15.7  7272.0
034 13.5  10536.0
STOP
035 1067 1  REF 73  PWHT 1292F/4HR  SAW  C=0.05  P=36.1
036 11.2  3900.0
037 1112 1
038 11.2  1320.0
STOP
039 1067 1  REF 73  PWHT 1292F/12HR  SAW  C=0.05  P=36.9
040 11.2  2600.0
STOP
041 1112 2  REF 73  PWHT 1274F/2HR  SAW  C=?  P=35.2
042 22.4  82.0
043 17.9  452.0
STOP
044 1112 5  REF 73  PWHT 1274F/4HR  SAW  C=0.08  P=35.7
045 22.5  49.0
046 18.0  145.0
047 13.5  319.0
048 9.0  1942.0
```

Figure B2. Literature stress rupture data.

```
049 6.8   7402.0
STOP
050 1112 4  REF 73  PWHT 1274F/4HR   SAW  C=0.07  P=35.7
051 18.0  220.0
052 13.5  1112.0
053 9.0   2491.0
054 6.8   12768.0
STOP
055 1022 4  REF 73  PWHT 1292F/8HR   SAW  C=0.08  P=36.6
056 22.5  595.0
057 18.0  2494.0
058 15.8  5472.0
059 13.5  12072.0
STOP
060 1022 3  REF 73  PWHT 1202F/12HR  SAW  C=0.10  P=35.0
061 20.3  2669.0
062 15.8  7248.0
063 13.5  17640.0
STOP
064 1022 5  REF 73  PWHT 1328F/3.5HR SAW  C=0.03  P=36.7
065 28.5  33.0
066 21.3  470.0
067 20.0  1040.0
068 18.7  1440.0
069 15.7  4700.0
STOP
070 1022 5  REF 73  PWHT 1292F/24HR  GMAW C=0.06  P=37.5
071 27.0  50.0
072 22.5  130.0
073 18.0  712.0
074 15.7  1990.0
075 13.5  6900.0
STOP
076 1067 2  REF 73  PWHT 1292F/12HR  GMAW C=0.08  P=36.9
077 24.7  434.0
078 20.2  1237.0
STOP
079 850  4  REF 71  PWHT 1300F/1HR   GTAW C=0.035 P=35.2
080 65.0  5.0
081 64.0  14.7
082 62.0  123.4
083 60.0  1487.9
084 950  3
085 45.0  24.5
086 40.0  118.4
087 35.0  1293.8
088 1050 4
089 35.0  7.6
090 25.0  148.9
091 20.0  723.9
092 18.0  990.1
STOP
093 850  4  REF 71  PWHT 1300F/1HR   GTAW C=0.11  P=35.2
094 75.0  8.0
```

Figure B2 (continued)

```
095 70.0  72.2
096 65.0  497.5
097 63.0  801.3
098 950  4
099 55.0  31.3
100 45.0  247.1
101 40.0  862.6
102 40.0  680.7
103 1050 3
104 40.0  14.5
105 30.0  137.0
106 20.0  2017.2
STOP
107 1000 2  REF 102 PWHT 1350F/1HR   UK   C=0.08  P=36.2
108 25.0  1118.0
109 20.0  2134.0
STOP
110 1100 4  REF 102 PWHT 1350F/1HR   UK   C=0.04  P=36.2
111 15.0  217.0
112 10.0  1441.0
113 7.5   3840.0
114 7.0   5162.0
STOP
115 1000 2  REF 102 PWHT 1350F/2HR   UK   C=0.12  P=36.7
116 50.0  11.0
117 45.0  12.0
118 1050 3
119 40.0  17.0
120 35.0  26.0
121 30.0  62.0
122 1100 2
123 30.0  19.0
124 25.0  50.0
125 1200 3
126 20.0  22.0
127 15.0  89.0
128 12.0  202.0
STOP
129 750  3  REF 13  PWHT 1125F/24HR  SMAW C=0.14  P=33.9
130 75.0  471.0
131 70.0  847.0
132 65.0  4480.0
133 850  5
134 70.0  29.0
135 60.0  264.0
136 55.0  1351.0
137 50.0  3356.0
138 47.0  8727.0
139 950  5
140 50.0  92.0
141 45.0  139.0
142 40.0  1225.0
143 37.5  2591.0
144 34.0  4967.0
```

Figure B2 (continued)

```
STOP
145 850  6  REF 13  PWHT 1075F/6HR   SMAW C=0.073 P=31.9
146 105.0 91.0
147 100.0 1130.0
148 95.0  213.0
149 95.0  611.0
150 90.0  1832.0
151 80.0  4696.0
152 900  8
153 80.0  444.0
154 75.0  349.0
155 70.0  1107.0
156 65.0  2970.0
157 55.0  3534.0
158 50.0  3921.0
159 50.0  4705.0
160 45.0  6558.0
STOP
161 800  5  REF 54  PWHT 1075F/4HR   SAW  C=0.08  P=31.6
162 110.0 8.0
163 106.0 3068.0
164 103.0 9299.0
165 95.0  16946.0
166 90.0  18341.0
167 850  3
168 90.0  2794.0
169 85.0  4163.0
170 80.0  8263.0
171 900  4
172 65.0  2650.0
173 60.0  2862.0
174 55.0  4001.0
175 50.0  6764.0
STOP
176 850  5  REF 71  PWHT 1300F/1HR   GTAW C=0.003 P=35.2
177 55.0  0.6
178 50.0  19.4
179 47.5  88.3
180 45.0  245.0
181 43.0  658.9
182 950  3
183 39.0  22.8
184 35.0  94.4
185 31.0  590.2
186 1050 3
187 30.0  11.2
188 20.0  182.0
189 15.0  2244.1
STOP
190 900  7  REF 103 PWHT 1275F/20HR  SMAW C=0.063 P=37.0
191 69.9  0.5
192 54.0  48.1
193 50.0  111.7
194 48.0  185.9
```

Figure B2 (continued)

```
195 45.0  474.2
196 44.0  619.5
197 42.5  1043.7
198 1050 2
199 29.0  156.7
200 20.0  1185.1
STOP
201 1050 4  REF 70  PWHT 1275F/?HR   SMAW C=0.038 P=?
202 32.0  83.0
203 30.0  192.0
204 26.0  625.0
205 23.5  1105.0
206 1100 2
207 27.0  125.0
208 22.0  595.0
209 1200 2
210 15.0  117.0
211 10.0  517.0
STOP
212 1050 1  REF 70  PWHT 1275F/?HR   SMAW C=0.040 P=?
213 30.0  225.0
214 1100 1
215 19.0  1268.0
216 1150 1
217 13.0  957.0
218 1200 1
219 11.0  334.0
STOP
220 1050 5  REF 70  PWHT 1275F/?HR   SMAW C=0.103 P=?
221 32.0  132.0
222 30.0  213.0
223 27.0  456.0
224 24.0  678.0
225 22.0  1797.0
226 1100 3
227 27.0  171.0
228 22.0  564.0
229 18.0  1033.0
230 1200 2
231 15.0  87.0
232 12.0  242.0
STOP
233 1100 5  REF 104 PWHT 1350F/12HR  SMAW C=0.036 P=38.2
234 15.0  75.7
235 14.7  52.5
236 10.0  767.1
237 8.5   2069.0
238 7.5   5647.0
STOP
239 1100 5  REF 104 PWHT 1250F/12HR  SMAW C=0.036 P=36.0
240 15.0  314.5
241 10.0  2262.0
242 9.0   4506.0
243 8.0   9346.5
```

Figure B2 (continued)

```
244 7.6   12987.5
STOP
245 1100 4  REF 104 PWHT 1350F/12HR  SAW  C=0.09  P=38.2
246 15.0  146.5
247 10.0  1513.5
248 8.0   5588.0
249 7.0   10770.0
STOP
250 1100 5  REF 104 PWHT 1250F/12HR  SAW  C=0.09  P=36.0
251 15.0  492.0
252 12.5  1166.5
253 9.0   4915.0
254 8.0   7799.5
255 7.0   15109.5
STOP
256 1067 5  REF 105 PWHT 1250F/3HR   SMAW C=0.08  P=35.0
257 26.8  783.0
258 22.4  1804.0
259 17.9  6219.0
260 14.6  12426.0
261 12.3  20864.0
STOP
267 1100 4  REF 102 PWHT 1350F/1HR   UK   C=?     P=36.2
268 28.0  5.0
269 25.0  10.0
270 20.0  102.0
271 15.0  512.0
STOP
272 1100 4  REF 102 PWHT 1350F/1HR   UK   C=0.11  P=36.2
273 20.0  159.0
274 18.0  257.0
275 15.0  639.0
276 13.0  982.0
STOP
277 1050 4  REF 106 PWHT 1220F/3HR   SMAW C=0.08  P=34.4
278 20.2  2944.0
279 17.9  2732.0
280 15.7  9081.0
281 13.4  14577.0
282 1100 3
283 13.4  4214.0
284 11.2  10248.0
285 9.0   28713.0
286 1022 4
287 22.4  2506.0
288 20.2  3576.0
289 17.9  5016.0
290 15.7  7877.0
STOP
291 1022 6  REF 107 PWHT 1337F/2HR   SMAW C=0.06  P=36.5
292 28.4  452.0
293 17.6  5257.0
294 11.4  15989.0
295 28.3  562.0
```

Figure B2 (continued)

```
296 17.8  4801.0
297 11.3  18377.0
STOP
298 1000 3  REF 102 PWHT 1350F/2HR   UK   C=0.08  P=36.7
299 30.0  110.0
300 26.0  1080.0
301 22.0  1583.0
302 1100 3
303 20.0  96.0
304 18.0  134.0
305 15.0  1493.0
STOP
306 1050 3  REF 102 PWHT 1325F/?HR   UK   C=0.10  P=?
307 30.0  351.0
308 25.0  306.0
309 20.0  1070.0
STOP
310 1050 2  REF 102 PWHT 1325F/?HR   UK   C=0.075 P=?
311 33.0  49.0
312 24.0  660.0
STOP
313 1000 5  REF 102 PWHT 1350F/?HR   UK   C=?     P=?
314 35.0  31.5
315 30.0  104.0
316 25.0  390.0
317 20.0  1450.0
318 18.0  5500.0
STOP
319 1022 4  REF 73  PWHT 1292F/20HR  SMAW C=0.05  P=37.3
320 27.0  46.0
321 22.5  355.0
322 18.0  1376.0
323 13.5  2740.0
STOP
324 1022 3  REF 73  PWHT 1292F/44HR  SMAW C=0.05  P=37.9
325 22.5  188.0
326 18.0  1324.0
327 13.5  3771.0
STOP
328 1022 5  REF 73  PWHT 1292F/8HR   SAW  C=0.06  P=36.6
329 27.0  115.0
330 22.5  1150.0
331 18.0  1965.0
332 13.5  2976.0
333 9.0   27510.0
STOP
334 1022 4  REF 73  PWHT 1292F/20HR  SAW  C=0.06  P=37.3
335 22.5  218.0
336 18.0  1669.0
337 13.5  7813.0
338 9.0   28806.0
STOP
339 1022 4  REF 73  PWHT 1292F/44HR  SAW  C=0.06  P=37.9
340 22.5  236.0
```

Figure B2 (continued)

```
341 18.0  507.0
342 13.5  3196.0
343 9.0   22248.0
STOP
344 1100 3  REF 108 PWHT 1350F/2HR   UK   C=0.08  P=36.7
345 20.0  96.0
346 18.0  134.0
347 15.0  1493.0
STOP
348 1067 4  REF 106 PWHT 1283F/3HR   SMAW C=0.088 P=35.7
349 18.0  2122.0
350 15.7  3400.0
351 13.5  7524.0
352 11.2  7184.0
STOP
353 1058 4  REF 73  PWHT 1275F/2HR   SMAW C=0.08  P=35.2
354 27.0  348.0
355 22.5  978.0
356 18.0  3961.0
357 13.5  13343.0
358 1112 4
359 22.5  226.0
360 18.0  591.0
361 13.5  2941.0
362 9.0   10224.0
STOP
363 1112 3  REF 73  PWHT 1292F/4HR   SMAW C=0.07  P=36.1
364 11.2  4400.0
365 11.2  5800.0
366 11.2  2100.0
STOP
367 1112 1  REF 73  PWHT 1292F/32HR  SMAW C=0.07  P=37.7
368 11.2  3100.0
STOP
369 1022 2  REF 73  PWHT 1292F/44HR  SMAW C=0.06  P=37.9
370 24.7  141.0
371 20.2  1098.0
STOP
372 850  7  REF 109 PWHT 1300F/25HR  GTAW C=0.069 P=37.7
373  52.0 20.9
374 42.0  253.4
375 40.0  463.9
376 36.0  2300.4
377 43.0  428.8
378 53.0  39.3
379 45.0  85.9
380 950  7
381 35.0  51.2
382 31.0  148.2
383 26.0  565.0
384 32.0  104.5
385 37.0  13.9
386 22.0  1264.3
387 41.5  4.5
```

Figure B2 (continued)

```
388 1050 7
389 23.0  31.0
390 29.3  8.7
391 19.9  92.8
392 18.0  66.9
393 18.0  83.2
394 16.0  408.4
395 13.0  5155.6
STOP
396 950  5  REF 110 PWHT 1300F/25HR  EBW  C=0.11  P=37.7
397 38.0  61.0
398 32.0  683.4
399 30.0  973.2
400 35.0  146.0
401 30.0  1000.4
STOP
402 950  4  REF 110 PWHT 1300F/25HR  EBW  C=0.12  P=37.7
403 38.0  40.2
404 30.0  346.2
405 25.0  2528.6
STOP
406 950  6  REF 110 PWHT 1300F/25HR  EBW  C=0.12  P=37.7
407 44.0  60.3
408 40.0  162.2
409 38.0  81.9
410 33.0  288.0
411 30.0  1633.9
412 30.0  1218.4
STOP
```

Figure B2 (continued)

```
800 850  10  0.02-0.03C WELD METAL  PWHT 1300F/25HR  C=0.024  P=37.7
801 36.6  505.1
802 48.8  6.8
803 44.7  36.0
804 42.2  55.0
805 42.4  64.8
806 48.8  1.0
807 36.6  479.5
808 44.7  32.9
809 34.0  1104.8
810 34.0  1240.0
811 950  7
812 41.5  0.1
813 33.7  15.7
814 25.6  224.5
815 22.0  614.9
816 33.7  8.8
817 25.6  151.7
818 22.0  1029.4
819 1050 9
820 20.3  37.7
821 16.3  182.3
822 24.6  9.7
823 12.6  946.9
824 16.3  289.5
825 24.6  10.0
826 20.3  61.4
827 10.2  4237.4
828 12.6  319.5
STOP
829 850  9  0.04-0.05C WELD METAL  PWHT 1300F/25HR  C=0.045  P=37.7
830 45.0  463.1
831 43.7  1457.9
832 50.0  49.2
833 45.0  508.0
834 50.0  101.4
835 40.0  566.6
836 53.0  12.8
837 48.0  42.8
838 36.0  8647.1
839 950  9
840 33.0  209.0
841 40.0  34.6
842 28.0  259.0
843 25.0  1672.9
844 40.0  24.7
845 28.0  579.0
846 33.0  53.0
847 22.0  2867.2
848 26.0  1462.4
849 1050 7
850 24.9  27.0
851 20.0  91.8
852 15.0  2324.8
```

Figure B3. UTK stress rupture data.

```
853 20.0  552.0
854 24.0  97.7
855 16.0  2099.5
856 14.0  1885.6
STOP
857 850  8  0.08-0.09C WELD METAL  PWHT 1300F/25HR  C=0.091  P=37.7
858 55.0  4.4
859 50.0  45.3
860 40.0  1002.9
861 45.0  170.7
862 40.0  1720.8
863 37.0  1361.8
864 46.0  267.7
865 35.0  5871.4
866 950  9
867 44.0  1.3
868 35.0  26.2
869 40.0  9.1
870 33.0  166.5
871 30.0  360.1
872 28.0  639.6
873 25.0  1178.6
874 23.0  2589.6
875 22.2  4654.6
876 1050 8
877 20.0  495.4
878 17.0  707.6
879 25.0  85.5
880 30.0  18.4
881 15.0  1605.9
882 25.0  59.1
883 31.0  7.5
884 13.0  2863.8
STOP
885 850  8  0.12-0.13C WELD METAL  PWHT 1300F/25HR  C=0.13  P=37.7
886 50.0  108.8
887 45.0  269.4
888 40.0  1657.6
889 55.0  8.0
890 54.0  26.0
891 41.0  1473.4
892 53.0  33.3
893 38.0  3473.9
894 950  6
895 38.0  44.2
896 33.0  157.1
897 28.0  640.6
898 40.0  38.3
899 34.0  145.9
900 27.0  870.4
901 1050 8
902 26.0  39.0
903 20.0  227.8
904 16.0  1195.5
905 14.0  2959.2
906 27.0  34.7
907 21.0  198.6
908 16.0  819.5
909 12.4  5224.6
STOP
```

Figure B3 (continued)

```
910 950  9  0.08-0.09C WELD METAL  PWHT 1175F/25.5HR  C=0.091  P=35.0
911 38.0  2755.6
912 43.0  237.1
913 45.0  231.2
914 44.0  259.4
915 46.0  311.1
916 50.0  121.5
917 41.0  1088.5
918 55.0  23.7
919 36.0  747.1
920 1050 7
921 46.0  1.1
922 36.0  21.8
923 28.0  243.9
924 20.0  3135.9
925 24.0  855.1
926 22.0  900.8
927 32.0  57.0
STOP
```

Figure B3 (continued)

VITA

Stephen Kelley was born in Baltimore, Maryland in 1950, the first of four children, to Loy and Ruth Kelley. He grew up and attended school in the Baltimore suburbs. Upon graduation from high school, he went to the University of Maryland where he earned his B. S. in physics. He was soon drafted into the Army after getting his degree and served for three years in an Army Corps of Engineers research laboratory. Steve worked for 5 1/2 years in industry as a production engineeer before entering the University of Tennessee to obtain an M. S. in metallurgical engineering. He is now working in industry, applying his knowledge of metallurgy and welding.